NASA CONTRACTOR REPORT

NASA CR-66727-1

NASA CR-66727-1

TITAN/MARS HARD LANDER

Volume I

1400 lb Capsule System Design Study

Prepared by
GENERAL ELECTRIC
RE-ENTRY SYSTEMS
for Langley Research Center

6 JANUARY 1969

NATIONAL AERONAUTICS AND SPACE ADMINISTRATION–WASHINGTON, D. C.

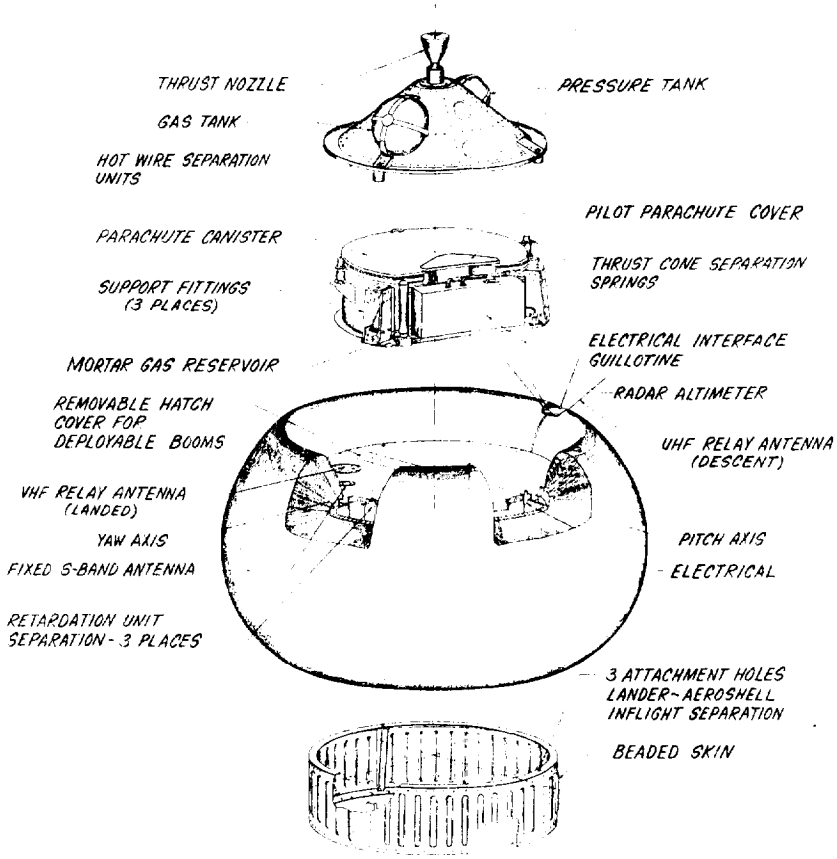

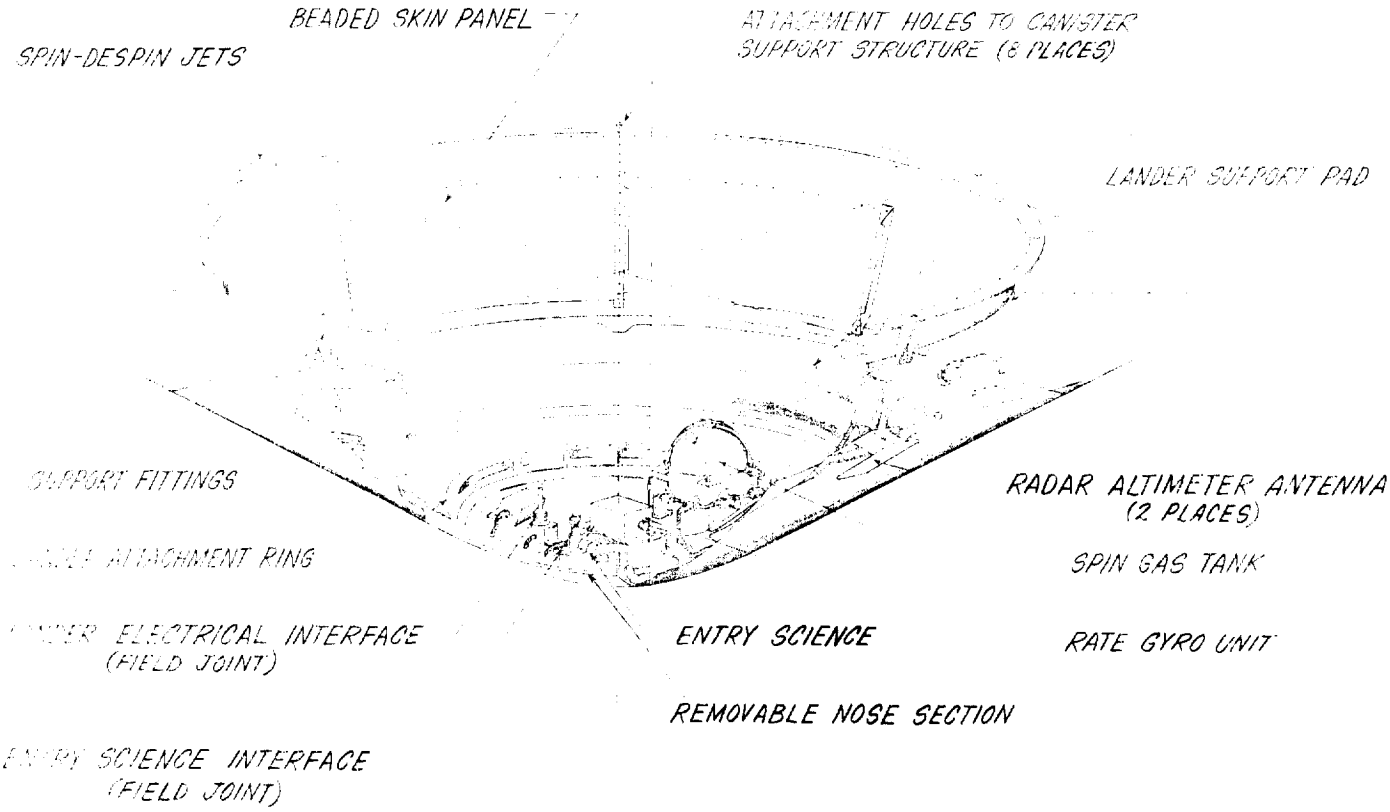

FOLDOUT FRAME 1

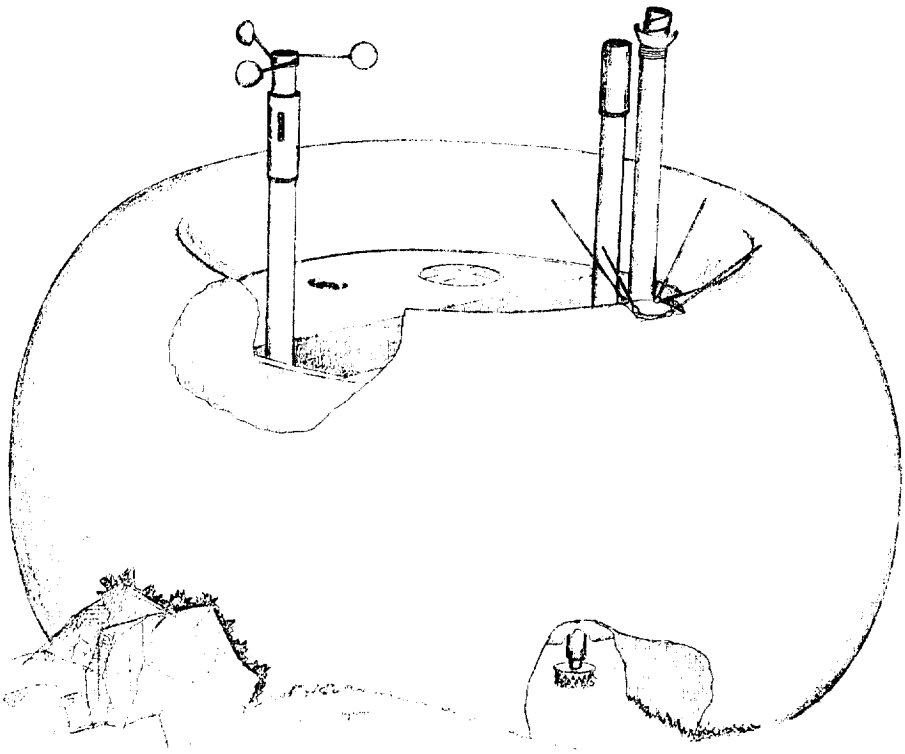

LANDED CONFIGURATION

FOLDOUT FRAME 2

NASA CR-66727-1

TITAN/MARS HARD LANDER

Volume I

1400 LB CAPSULE SYSTEM DESIGN STUDY

Distribution of this report is provided in the interest of information exchange. Responsibility for the contents resides in the author or organization that prepared it.

Issued by Originator as General Electric Document No. 68SD7041 (Vol. I, Books 1 and 2)

PREPARED UNDER CONTRACT NO. NAS 1-8098 BY

GENERAL ELECTRIC
RE-ENTRY SYSTEMS
3198 Chestnut Street, Philadelphia, Pa. 19101

FOR
LANGLEY RESEARCH CENTER

NATIONAL AERONAUTICS & SPACE ADMINISTRATION

FOREWORD

This report consists of three books prepared for the Langley Research Center of NASA by the Re-entry Systems Organization of the General Electric Company.

This work has been prepared under Contract No. NAS 1-8098, Mars Hard Lander Capsule Study. The first written report was submitted on July 31, 1968 and has been assigned NASA CR number 66678. The second report describes work accomplished during the contract extension period since that date.

The three books in this report contain the following information:

Volume I - Design study of a Mars 1973 Mission 1400 lb Hard Lander. This design contains approximately 60 lb of science instruments (exclusive of power, telemetry and supporting equipments) and in conjunction with a Flyby Support Module, relays 30 million bits of imagery data. About one hundred thousand bits of life detection, geological and meteorological data are transmitted direct to Earth over a 3 day period. Broad analysis and specific design investigations have led to the conclusion that this is a completely practical design approach to meet all objectives of early Mars exploration.

Volume II - Feasibility study of Autonomous Hard Lander Capsules suitable for Mars 1973 missions. This study has considered an autonomous Capsule which is essentially a self-contained landing system. The mission was analyzed and hardware identified to enable the Capsule to perform all functions from booster separation to the end of the surface mission. It is concluded that this approach is not the optimum way to fulfill early Mars exploration objectives and should not be continued at this time.

Volume III - Summary cost and schedule of feasible implementation plans for Hard Landers in 1973.

TABLE OF CONTENTS

Section				Page
FOREWORD				ii
1	SUMMARY			1-1
2	MISSION REQUIREMENTS AND CONSTRAINTS			2-1
	2.1	Mission Objective		2-1
	2.2	NASA/LRC Guidelines		2-1
3	MISSION DEFINITION			3-1
	3.1	Science Measurements		3-2
		3.1.1	Introduction	3-2
		3.1.2	Atmospheric Measurements	3-2
		3.1.3	Other Measurements	3-11
		3.1.4	Operations and Sequencing	3-15
		3.1.5	References	3-17
	3.2	Reference Mission		3-18
		3.2.1	Launch and Arrival Configurations	3-18
		3.2.2	Entry Path Angle Dispersion	3-19
		3.2.3	Definition of Reference Entry Trajectories	3-23
		3.2.4	Definition of Tangential Deflection Velocity	3-24
		3.2.5	Reference Mission Design Summary	3-24
	3.3	Retardation Design Rationale		3-38
		3.3.1	Retardation Design Rationale for 1400 lb Lander	3-38
		3.3.2	Design Approach for Statistically Defined Environment	3-47
		3.3.3	References	3-50
	3.4	Mission Profile		3-51
		3.4.1	Summary of Mission Sequence	3-51
		3.4.2	Checkout Sequence	3-57
		3.4.3	Command Sequence	3-58
4	SPACECRAFT SYSTEM DESIGN SUMMARY			4-1
	4.1	Overall Spacecraft System Description		4-1
	4.2	Flight Capsule Design Summary		4-2
	4.3	Support Module Design Summary		4-33
5	FLIGHT CAPSULE SYSTEMS			5-1
	5.1	Science		5-1
		5.1.1	Lander Science Instruments	5-1
		5.1.2	Entry Science	5-28
		5.1.3	References	5-31

TABLE OF CONTENTS (Cont'd)

Section		Page
5.2	Telecommunications	5-32
5.2.1	Telecommunications Subsystem	5-32
5.2.2	Description of Operation	5-38
5.2.3	Data Handling Subsystem	5-43
5.2.4	Relay Link	5-55
5.2.5	Direct Link	5-78
5.2.6	Radar for Deceleration Events	5-108
5.2.7	References	5-115
5.3	Electrical Power and Distribution (EP&D)	5-116
5.3.1	Power Subsystem	5-116
5.3.2	Initiation Subsystem	5-131
5.3.3	Distribution Equipment	5-142
5.3.4	Battery Supporting Data	5-142
5.4	Computer and Sequencer	5-157
5.4.1	Functional Requirements	5-157
5.4.2	Baseline Implementation	5-157
5.4.3	Telemetry Data Storage	5-176
5.4.4	Logical Description	5-177
5.4.5	Operational Conditions	5-184
5.5	Environmental Control Subsystem	5-186
5.5.1	Lander Thermal Control Design	5-186
5.5.2	Requirements and Constraints	5-186
5.5.3	Design Solution	5-188
5.5.4	Pre-entry Environmental Control	5-200
5.6	Landed Equipment Container	5-203
5.6.1	Subsystem Description	5-203
5.6.2	Structural Design	5-203
5.6.3	Lander Packaging Studies	5-219
5.6.4	Deployment Studies	5-228
5.7	Impact Limiter	5-234
5.7.1	Requirements and Design Constraints	5-234
5.7.2	Impact Limiter Description	5-236
5.7.3	Effects on Design Due to Variations in Design Conditions	5-240
5.7.4	Materials Considerations, Balsa vs Honeycomb	5-245
5.7.5	Shaping Approach for a Minimum Weight Impact Limiter	5-250
5.7.6	Fabrication	5-250
5.7.7	Impact Limiter Configuration Studies	5-253
5.7.8	References	5-255

TABLE OF CONTENTS (Cont'd)

Section		Page
5.8	Parachute Subsystem	5-257
5.8.1	Subsystem Requirements	5-257
5.8.2	Design Trade-offs	5-257
5.8.3	Subsystem Description	5-260
5.8.4	Subsystem Design	5-264
5.8.5	Subsystem Performance	5-267
5.8.6	Component Selection	5-271
5.8.7	Reference	5-275
5.9	Aeroshell	5-276
5.9.1	Requirements and Constraints	5-276
5.9.2	Structural Design	5-276
5.9.3	Structural Aeroshell Development Status	5-301
5.9.4	Heat Shield Design	5-304
5.9.5	Heat Shield Development	5-313
5.9.6	References	5-314
5.10	De-orbit Propulsion	5-315
5.10.1	Requirements	5-315
5.10.2	System Description	5-315
5.10.3	System Comparison	5-322
5.11	Attitude Control	5-324
5.11.1	System Requirements	5-324
5.11.2	System Performance	5-325
5.11.3	Component Selection	5-335
5.11.4	Development Status	5-336
5.12	Canister and Adapter	5-337
5.12.1	Canister Design Requirements	5-337
5.12.2	Canister Structural Design Analysis	5-338
5.12.3	Pressure and Venting Subsystem Requirements	5-344
5.12.4	Pressure and Venting Subsystem Description	5-345
5.12.5	Adapter Structural Design Requirements	5-351
5.12.6	Adapter Structural Design Description	5-351
5.13	Separation	5-354
5.13.1	Canister Separation	5-354
5.13.2	Capsule Separation	5-358
5.13.3	Thrust Cone Separation	5-358
5.13.4	Aeroshell Separation	5-358
5.13.5	Parachute Separation	5-359
5.13.6	Separation Components	5-359

TABLE OF CONTENTS (Cont'd)

Section			Page
6	SUPPORT MODULE SUBSYSTEMS		6-1
	6.1	Engineering Mechanics	6-1
		6.1.1 Structure Subsystem	6-1
		6.1.2 Temperature Control Subsystem	6-2
		6.1.3 Mechanical Devices Subsystem	6-2
		6.1.4 Pyrotechnic Subsystem	6-3
		6.1.5 Cabling Subsystem	6-3
	6.2	Propulsion Subsystem	6-4
		6.2.1 Requirements	6-4
		6.2.2 Functional Description	6-4
		6.2.3 Comparison to Mariner '69	6-7
	6.3	Guidance and Control Subsystem	6-9
		6.3.1 Central Computer and Sequencer	6-9
		6.3.2 Attitude Control	6-13
	6.4	Power Subsystem	6-18
		6.4.1 Functional Description	6-18
		6.4.2 Modifications to '73	6-20
		6.4.3 Power Profiles and Allocations	6-20
		6.4.4 Subsystem Characteristics	6-23
	6.5	Telecommunications Subsystem	6-24
		6.5.1 Radio Frequency Subsystem	6-24
		6.5.2 Command Subsystem	6-28
		6.5.3 Flight Telemetry Subsytem	6-31
		6.5.4 Data Storage Subsystem	6-34
		6.5.5 Relay Subsystem	6-35
7	MISSION ASSURANCE		7-1
	7.1	Criticality and Risk	7-1
	7.2	Risk	7-3
	7.3	Reliability Estimate Analysis (REA)	7-7
	7.4	Summary	7-9

LIST OF ILLUSTRATIONS

Figure		Page
3.1-1	Turbulent Flow Base Pressure Correlation	3-8
3.1-2	Diurnal Variation of Surface Temperature on the Martian Equator at Perihelion	3-10
3.1-3	Temperature Versus Time at the Equator of Mars at the Surface and at Z-0.5 Meters (Neubauer - 1960)	3-10
3.2.1-1	Basic Mission Planning Chart	3-20
3.2.4-1	ΔV_T Tangential Velocity Determination	3-25
3.2.5-1	1400 lb Mars Hard Lander Capsule Reference Mission Arrival Configuration	3-26
3.2.5-2	Downrange Dispersions (Atmosphere and Entry Path Angle Variations)	3-28
3.2.5-3	Capsule Altitude, Mach Number, and Velocity vs Time	3-31
3.2.5-4	Capsule Deceleration and Dynamic Pressure vs Time	3-32
3.2.5-5	Relay Communication Parameters	3-33
3.2.5-6	Relay Communication after Landing	3-35
3.2.5-7	Communication after Landing - Geometry	3-37
3.3-1	Influence of Elevation Uncertainties on Altitude of Parachute Deployment (MIN Atmosphere)	3-39
3.3-2	Influence of Elevation Uncertainties on Altitude of Parachute Deployment (MEAN Atmosphere)	3-40
3.3-3	Effect of Entry Path Angle on Mach 2 Altitude (MIN Atmosphere)	3-41
3.3.1-1	Effect of Rock Size on Limiter Weight	3-44
3.3.1-2	Terminal Velocity Constraint on Ballistic Coefficient	3-45
3.3.1-3	Lander/Parachute Descent Velocity Trade-off	3-46
3.3.2-1	Sample Probability Density Function for Entry Angle	3-48
3.3.2-2	Optimization Logic	3-49
3.3.2-3	Format of Results	3-50
3.4-1	Sequence of Events	3-52
4.1-1	Selected Launch Vehicle Configuration	4-3
4.1-2	Launch Configuration Study	4-5
4.1-3	Adapter/Canister Study	4-6
4.1-4	Sterilization Canister	4-7
4.1-5	Spacecraft Configuration	4-8
4.2-1	Flight Capsule Inboard Profile	4-9
4.2-2	Separated Flight Capsule Assembly	4-11
4.2-3	Aeroshell	4-13
4.2-4	Parachute Deployment Sequence	4-16

LIST OF ILLUSTRATIONS (Continued)

Figure		Page
4.2-5	Retardation Subsystem	4-17
4.2-6	Impact Conditions	4-19
4.2-7	Lander Deployment Configuration	4-20
4.2-8	Lander Packaging Concept	4-22
4.2-9	Lander Packaging	4-23
4.2-10	Mass Properties Reference Axes	4-26
4.2-11	Electrical System Block Diagram	4-30
4.3-1	Support Module, Simplified Block Diagram	4-35
5.1-1	High and Low Speed Cameras	5-5
5.1-2	Gas Chromatograph - Mass Spectrometer Flow Chart	5-8
5.1-3	BBRC Hardened Wolf Trap Concept	5-13
5.1-4	Elimination of Stress Concentration by Uniform Loading	5-17
5.1-5	Elimination of "Billiard Ball" Action	5-18
5.1-6	Using the Breakwire as an Initiator	5-19
5.1-7	Increased Land Bearing Area and Shaft Stiffness	5-20
5.1-8	GE Water Vapor Detection System	5-23
5.1-9	Contoured Surface Silicone Avalanche Detector	5-23
5.1-10	Rotary Potentiometer Clinometer	5-28
5.2-1	Telecommunication System Block Diagram	5-34
5.2-2	Data Collection and Transmission Profile	5-39
5.2-3	Data Handling System, Functional Block Diagram	5-45
5.2-4	Approximation Converter, Block Diagram	5-49
5.2-5	Counter Convertor, Block Diagram	5-49
5.2-6	Typical High Level Analog Multiplexer	5-50
5.2-7	Data Control Unit, Block Diagram	5-53
5.2-8	Data Control Unit, Timing Diagram	5-54
5.2-9	Relay Link Subsystem	5-57
5.2-10	Landed Relay Performance	5-58
5.2-11	Spectra for FSK of Separate Oscillators	5-62
5.2-12	Entry Link Multipath Degradation and Net Margin	5-64
5.2-13	Entry Antenna (Four Whips) Pattern	5-66
5.2-14	Lander 400 MHz Antenna Pattern	5-66
5.2-15	400 MHz Transmitter, Block Diagram	5-67
5.2-16	Bit Sync Scheme for Split Phase Signals	5-68
5.2-17	Correlation Function for Split Phase Signals	5-69
5.2-18	Performance of Wide-band FSK with Multipath Interference	5-72
5.2-19	Multipath Parameters	5-74
5.2-20	Alternate Entry Data Collection Scheme	5-77
5.2-21	Earth and Sun Visibility from Landing Site	5-79
5.2-22	Direct Link Subsystem	5-80

LIST OF ILLUSTRATIONS (Continued)

Figure		Page
5.2-23	Celestial Sphere for 10° N Latitude Landing Site	5-82
5.2-24	Earth Elevation from 10° North Latitude, 2/7/74	5-82
5.2-25	Pattern of Vertically Oriented Antenna	5-85
5.2-26	Pattern of Body-Fixed Antennas	5-86
5.2-27	Antenna Configurations	5-87
5.2-28	Alternate Antenna Systems	5-88
5.2-29	Maximum Acquisition Sweep Rate	5-90
5.2-30	16 Watt Solid State Power Amplifier	5-91
5.2-31	R-F Switching Modes	5-93
5.2-32	Signal Reduction Resulting from Interference	5-94
5.2-33	Transponder Functional Diagram	5-96
5.2-34	Command Modulator (Functional)	5-99
5.2-35	Command Waveforms	5-100
5.2-36	Command Detector	5-101
5.2-37	Program Control	5-103
5.2-38	Altitude Marking Radar, Functional Block Diagram	5-109
5.2-39	Geometry of AMR Return Signal	5-109
5.2-40	Aeroshell Radar Antenna Pattern	5-111
5.2-41	Roll Pattern Radar Antenna on Aeroshell	5-112
5.2-42	E and H Plane Patterns of Antenna on Vehicle Body	5-113
5.3-1	1400 lb Lander Power Profile	5-119
5.3-2	Points of Power Use	5-120
5.3-3	Power Subsystem Block Diagram	5-123
5.3-4	Comparison of Voltage Conversion Approaches	5-128
5.3-5	Capacitor Discharge Circuit	5-133
5.3-6	Thermal Battery Circuit	5-133
5.3-7	Comparison Between Capacitor Discharge and Thermal Battery Pyrotechnic Initiation Equipment	5-135
5.3-8	Typical Hot-wire Inflight Disconnect	5-137
5.3-9	Initiation Subsystem	5-140
5.3-10	1400 lb Lander Grounding Diagram	5-143
5.3-11	EP&D Subsystem Block Diagram	5-145
5.3-12	Battery Design	5-149
5.3-13	Battery, Model N3HT, and Individual Cell	5-150
5.3-14	Power vs Volume	5-153
5.3-15	Power vs Weight	5-154
5.3-16	Demand Factor vs Weight	5-155
5.3-17	Demand Factor vs Volume	5-156
5.4-1	Computer and Sequencer, Block Diagram	5-172
5.4-2	Computer and Sequencer, Functional Diagram	5-179
5.4-3	Telemetry Memory Capacity for Worst Case Trajectory	5-182

LIST OF ILLUSTRATIONS (Continued)

Figure		Page
5.5-1	Atmospheric and Surface Temperatures vs Time on Surface after Sunrise	5-187
5.5-2	Equilibrium Component Temperature without Power Profile - without Heater Power Control (Voltage Regulator, Data Handling Processor)	5-190
5.5-3	Equilibrium Component Temperature with Power Profile - without Heater Power Control (Data Handling Processor, Power Controller, Lander Programmer)	5-191
5.5-4	Equilibrium Component Temperature with Power Profile - without Heater Power Control (Operational Battery, Voltage Regulator, Memory Unit)	5-192
5.5-5	Equilibrium Component Temperature with Power Profile - without Heater Power Control (Transponder Exciter, Command Decoder)	5-193
5.5-6	Transmitter Thermal Storage Weight vs Transmission Time	5-194
5.5-7	Equilibrium Component Temperature with Power Profile and Heater Power Control (Memory Unit)	5-195
5.5-8	Equilibrium Component Temperature with Power Profile and Heater Power Control (Voltage Regulator)	5-196
5.5-9	Daily Average Heater Power Requirements vs Allowable Temperature for Selected Group of Lander Components	5-197
5.5-10	Battery Weight Allowances for Thermal Control vs Component Allowable Temperature	5-198
5.5-11	S-band Antenna Temperature Profile	5-199
5.5-12	1400 lb Cruise Module Heater Power vs Insulation Thickness	5-202
5.6-1	Lander Assembly	5-205
5.6-2	Lander Component Arrangement	5-207
5.6-3	S-band Vertical Antenna	5-209
5.6-4	Lander Structure Detail	5-211
5.6-5	Lander Impact Angle	5-214
5.6-6	Bending Moment for Container Structure at $\theta = 30^{\circ}$	5-215
5.6-7	Minimum Container Cross Section	5-218
5.6-8	Lander Packaging Concept	5-220
5.6-9	Alternate Packaging Concept	5-221
5.6-10	Conventional Packaged Scheme, Zones and Packing Densities	5-222
5.6-11	Alternative Packaged Scheme, Zones and Packing Densities	5-223
5.6-12	Central Bay	5-224
5.6-13	Component Sub-chassis	5-227
5.6-14	Block Diagram - Vertically Oriented Antenna	5-231
5.6-15	Dual Axis Gravity Sensing Unit	5-232
5.6-16	Gravity Sensing Electrolytic Transducer	5-233

LIST OF ILLUSTRATIONS (Continued)

Figure		Page
5.7-1	Design Conditions	5-235
5.7-2	Impact Limiter Details	5-237
5.7-3	Area Variation with Stroke	5-239
5.7-4	Limiter Weight Due to Rock Clearance	5-241
5.7-5	Effect of Sway on Limiter Weight	5-243
5.7-6	Effect of g-Level Variation	5-244
5.7-7	Materials Specific Energy	5-246
5.7-8	Materials Crushing Stress	5-247
5.7-9	Materials Thickness (Stroke) Efficiency	5-248
5.7-10	Materials Obliquity Effects	5-249
5.7-11	Post Test Photograph of GE-RS Phenolic Fiberglass Honeycomb Impact Limiter Model	5-252
5.8.2-1	Variation of Ratio of Filling Time to Diameter with Snatch Velocity	5-260
5.8.2-2	Parachute Weight Variation with Dynamic Pressure	5-261
5.8.2-3	Opening Force for Reefed Parachute	5-262
5.8.3-1	Parachute Subsystem Deployment Sequence	5-263
5.8.4-1	Effect of Mach No. on Trailing Drogue Drag	5-265
5.8.4-2	Effect of Forebody Drag on Trailing Drogue Drag	5-266
5.8.4-3	Pilot Thermal Cover Ejection Study - Mach 2, 10 kft, q = 20 psf	5-267
5.8.5-1	Pilot Deployment Trajectory Study in Minimum Density Atmosphere	5-269
5.8.5-2	Main Parachute Trajectory in Minimum Density Atmosphere	5-272
5.8.6-1	Retardation Subsystem Hardware Arrangement	5-273
5.9-1	Axial Deflection vs Radial Distance	5-279
5.9-2	Axial Bending Moment (M_x) vs Radial Distance	5-279
5.9-3	Shell Transverse Shear vs Radial Distance	5-280
5.9-4	Meridional In-plane Load vs Radial Distance	5-280
5.9-5	Axial Honeycomb Facing Stress vs Radial Distance	5-281
5.9-6	Critical Aeroshell Dimensions	5-282
5.9-7	Aeroshell Entry Loads, Temperature, and Margin of Safety - Entry Condition No. 7	5-284
5.9-8	Aeroshell Entry Loads, Temperature, and Margin of Safety - Entry Condition No. 3	5-285
5.9-9	Allowable Strength of 7075-T6 after 500 hr at 300°F (Sterilization)	5-286
5.9-10	Aeroshell Entry Stresses, Entry Condition No. 7, Outer Facing, Outboard of Payload	5-288
5.9-11	Aeroshell Entry Stresses, Entry Condition No. 7, Inner Facing, Outboard of Payload	5-289

LIST OF ILLUSTRATIONS (Continued)

Figure		Page
5.9-12	Aeroshell Entry Stresses, Entry Condition No. 7, Outer Facing, Inboard of Payload	5-290
5.9-13	Aeroshell Entry Stresses, Entry Condition No. 7, Inner Facing, Inboard of Payload	5-291
5.9-14	Aeroshell Entry Stresses, Entry Condition No. 3, Outer Facing, Outboard of Payload	5-292
5.9-15	Aeroshell Entry Stresses, Entry Condition No. 3, Inner Facing, Outboard of Payload	5-293
5.9-16	Aeroshell Entry Stresses, Entry Condition No. 3, Outer Facing, Inboard of Payload	5-294
5.9-17	Aeroshell Entry Stresses, Entry Condition No. 3, Inboard Facing, Inboard of Payload	5-295
5.9-18	Aeroshell Entry Margin of Safety, Entry Condition No. 7	5-296
5.9-19	Aeroshell Entry Margin of Safety, Entry Condition No. 3	5-297
5.9-20	Typical Stress Distributor in Z-type Stiffener Rings	5-299
5.9-21	Aeroshell Alternate Designs	5-300
5.9-22	Cold Wall Convective and Radiative Heat Flux Histories for Thermal Design Trajectory	5-307
5.9-23	Hot Wall Heat Flux Histories for Thermal Design Trajectory	5-308
5.9-24	Heat Shield Thickness Requirements	5-309
5.9-25	Hyperthermal Arc Test - ESM 1004AP	5-310
5.9-26	Surface and Backface Temperature Histories	5-311
5.9-27	Temperature Gradients Through the Shield	5-312
5.10.2-1	MM '69 Propulsion Subsystem Schematic	5-316
5.10.2-2	Solid Propellant System	5-320
5.11.2-1	Spin, De-spin, Roll Rate Control Subsystem (Propulsion - Cold Gas Reaction Control)	5-328
5.11.2-2	Δ V Orientation Error	5-331
5.12-1	Sterilization Canister	5-339
5.12-2	Aeroshell/Canister Dynamic Excursion Clearance	5-341
5.12-3	Canister Separation Joint	5-342
5.12-4	Required Ring Inertia for Stability as a Function of Critical Load	5-343
5.12-5	Pressure and Venting Subsystem, Functional Schematic, Sterilization Configuration	5-346
5.12-6	Pressure-Time Profiles for P&V Subsystem	5-349
5.13-1	Sequence of Separation Events	5-355
5.13.1-1	Hot-wire Separation Nut	5-357
5.13.1-2	Hot-wire Tension Bolt	5-357
5.13.2-1	Correction to Capsule Tip-off Rate as a Function of Support Module to Capsule Mass Ratio	5-359

LIST OF ILLUSTRATIONS (Continued)

Figure		Page
5.13.6-1	Capsule Ejection Adjustable Spring Assembly	5-362
6.2.2-1	Mariner '69 Propulsion Subsystem Schematic	6-5
6.2.2-2	Orbiting Support Module Propulsion Subsystem Schematic	6-6
6.3.1-1	Coded Command Word Formats	6-10
6.3.1-2	CC&S Functional Block Diagram - Mars '73	6-11
6.3.2-1	Attitude Control Functional Block Diagram	6-15
6.4.1-1	Power Subsystem Functional Block Diagram	6-19
6.5.1-1	Mariner Mars '71 Radio Subsystem Block Diagram	6-25
6.5.2-1	Mars '73 FCS Block Diagram	6-30
6.5.3-1	Flight Telemetry Subsystem Block Diagram	6-32
6.5.5-1	Relay Subsystem Block Diagram	6-36
6.5.5-2	Synchronization Loops, 7 kbps and 1.1 kbps	6-37
6.5.5-3	Relay Antenna - Turnstile Over Ground Plane	6-38
6.5.5-4	Relay Antenna Pattern	6-38
7.1-1	Mission Value Profile 1400 lb Capsule Mission	7-2
7.1-2	Mission Functional Flow Diagram	7-5

LIST OF TABLES

Table		Page
3.1-1	Entry Science Payload	3-3
3.1-2	Surface Science Payload	3-5
3.1-3	Atmospheric Measurement Accuracies Comparison	3-6
3.1-4	Surface Science Sequencing	3-16
3.2.1-1	Arrival Configurations	3-21
3.2.5-1	Reference Mission Summary	3-27
3.2.5-2	Entry Trajectories, Atmosphere and Entry Path Angle Dispersion	3-30
3.2.5-3	Relay After Landing	3-34
3.3.1-1	Retardation Parameters	3-43
3.3.2-1	Discrete Distributions	3-49
3.3.2-2	Parachute Deployment Success Probability	3-50
4.2-1	Weight Summary, 1400 lb Capsule System	4-25
4.2-2	Mission Sequence Mass Properties	4-27
4.3-1	Weight Summary, Support Module	4-40
5.1-1	Lander Instrument Development Status	5-2
5.1-2	Typical Camera Specifications	5-6
5.1-3	Mass Spectrometer Comparison	5-11
5.1-4	BBRC Wolf Trap Conceptual Design Evaluated in Terms of GE-RS Design Criteria	5-14
5.1-5	Basic Features for Structural Integrity	5-15
5.2-1	Capsule Communication Requirements	5-33
5.2-2	Definition of Telemetry Modes	5-36
5.2-3	Definition of Data Modes	5-37
5.2-4	Physical Characteristics	5-40
5.2-5	Entry Science Data Requirements	5-43
5.2-6	Landed Science (Non-Imaging) Data Requirements	5-44
5.2-7	Summary of Telemetry and Data Mode Requirements as a Function of Mission Phase	5-46
5.2-8	Conversion Techniques	5-51
5.2-9	Interface Signals Between Data Handling Subsystem and Memory	5-52
5.2-10	Data Collection and Transmission Summary	5-56
5.2-11	Relay (Landed) Design Control Table	5-59
5.2-12	Entry Link Design Control Table	5-63
5.2-13	Relay Link Bit Sync Performance	5-70

LIST OF TABLES (Continued)

Table		Page
5.2-14	Multipath Degradation Computation	5-75
5.2-15	Relay (Landed) Design Control Table - Low Bit Rate	5-76
5.2-16	Time from End of Blackout to Landing	5-77
5.2-17	Circulator Switch Positions	5-78
5.2-18	Landed Communication Geometry	5-83
5.2-19	Performance Characteristics of 20 Watt TWT Amplifier	5-92
5.2-20	Design Control Table, Data Transmission 50 BPS, Vertically Oriented Antenna, 20 Watt, 210 Ft DSNA	5-105
5.2-21	Design Control Table, Data Transmission, 5 BPS, Fixed Antenna, 20 Watt, 210 Ft DSNA	5-106
5.2-22	Design Control Table, Command 1 BPS, 85 Foot, 100 KW, Fixed Antenna	5-107
5.2-23	Functional Parameters	5-114
5.2-24	Physical Parameters	5-114
5.3-1	Load Profile	5-118
5.3-2	Battery Energy Calculation	5-122
5.3-3	Power Subsystem Characteristics	5-130
5.3-4	Initiation Power Requirements	5-132
5.3-5	Summary of Initiation Requirements	5-136
5.3-6	Evaluation of Hot-wire Release	5-138
5.3-7	Initiation Subsystem Hardware Characteristics Summary	5-141
5.3-8	Measured Data on the Sterilized Silver-Zinc Secondary Experimental Batteries	5-151
5.4-1	Command Abbreviations	5-158
5.4-2	Mars Hard Lander Sequence of Commands	5-159
5.4-3	Computer and Sequencer Real Time Commands	5-175
5.6-1	Accelerations	5-217
5.6-2	Comparison of Installed Gross Packaging Densities	5-219
5.6-3	Weight Growth Histories - From Design Configuration Freeze to Flight Date	5-226
5.8.2-1	Parachute Recovery System Techniques	5-258
5.8.2-2	Parachute Weights, 1400 lb Capsule	5-529
5.8.4-1	Parachute Description, 1400 lb Capsule	5-264

LIST OF TABLES (Continued)

Table		Page
5.8.5-1	Pilot Parachute Deployment Trajectory Study Parameters	5-268
5.8.5-2	Main Parachute Reefing Optimization Design Parameters	5-270
5.8.5-3	Parachute Trajectory Parameters, 1400 lb Capsule	5-270
5.9-1	Maximum Entry Deceleration Loads	5-276
5.9-2	Honeycomb Facing Material Comparison	5-277
5.9-3	Weight Comparison of Honeycomb vs Ring Stiffened Aeroshell	5-299
5.9-4	Thermophysical Properties of ESM Materials	5-306
5.10.2-1	Subsystem Detailed Weight Breakdown	5-317
5.10.2-2	Nominal Performance Summary	5-318
5.10.2-3	Solid Propellant Motor Data	5-321
5.10.3-1	Cost Comparison (in millions of dollars)	5-322
5.11.1-1	Vehicle Characteristics and Design Factors	5-324
5.11.2-1	Significant Parameters	5-329
5.11.2-2	Expected Error Sources	5-332
5.12-1	Canister/Adapter Limit Design Loads	5-340
5.12-2	Structural Analysis of Forward Canister Loads	5-341
5.12-3	P&V Subsystem Component Summary	5-350
5.13.6-1	Separation Mechanism Summary	5-360
5.13.6-2	Spring Data	5-361
6.2.2-1	Propulsion Subsystem Weight Breakdown	6-7
6.2.2-2	RS 14 Engineer Data Summary	6-8
6.4.3-1	Subsystem Power Allocation	6-21
6.4.3-2	Abbreviations	6-22
6.4.3-3	Nominal Flight Phases and Cross Power Requirements	6-22
6.4.4-1	Power Subsystem Requirements	6-23
6.5.1-1	Radio Modes	6-27
6.5.3-1	Time Between Samples (sec)	6-33
7.2-1	High Risk Components	7-8
7.2-2	Components Probability of Failure	7-8

LIST OF TABLES (Continued)

Table		Page
7.3-1	Mission Success Probability	7-9
7.3-2	Failure Rate Data Source	7-10

1. SUMMARY

1. SUMMARY

As part of the Hard Lander studies performed for the NASA Langley Research Center, General Electric was assigned a task of evaluating a 1400 lb Flight Capsule with a Hard Lander. This 1400 lb Flight Capsule, in conjunction with a relay Support Module, is to be transferred to the planet Mars in 1973 on a flyby trajectory by a Titan IIIC Launch Vehicle. The baseline Support Module used in the study is a minimum Mariner '69 configuration which weighs 659 lb. The Flight Capsule is designed for a direct entry mission based on a nominal path angle of 21° and worst case cumulative environments for the entry aeroshell and landing conditions. A radar altimeter is used to deploy the parachute and the Lander is designed for impact at 100 fps in the surface environments prescribed by NASA/LRC.

This design study shows that this is a significant mission which provides under worst case design conditions:

1. 3×10^7 bits of landed imaging data over the flyby relay link
2. 2.5×10^5 bits of life detection and meteorology data on an S-band direct link
3. 2.5×10^5 bits of entry science on a UHF relay link independent of landing success.

This significant data return is performed with a 661 lb Lander which delivers to the surface instruments for (1) molecular analysis, (2) life detection, (3) surface visual characterization of the landing site, and (4) meteorology. The measurements are transmitted on a battery powered relay and direct link back to Earth for a period of 3 days without regenerated power. This mission can be performed with a high degree of confidence because the Hard Lander incorporates a passive landing system which is readily adaptive to great variations and uncertainties in the nature of the environments.

The Hard Lander is shown to experience considerably lower landing loads than were previously believed possible as a result of greater understanding of the impact limiter system. Also, hardened instrument design criteria, used in the design of military space programs, were applied to verify that no unusual design problems did, in fact, exist for the proposed science and component group. Component packaging studies were performed in consort with the hardened component studies to provide the design rationale for an integrated Lander package which provides packaging flexibility for the experimenter.

The 1400 lb Flight Capsule (1332.0 lb with contingency), has an estimated program cost of $133.2 million based on manufacture of 5.5 equivalent Flight Capsule systems with two flight models and a compatibility model retrofitted as a spare.

If the Hard Lander program begins in the third quarter of calendar year 1969, adequate time exists to develop, demonstrate, and build a passive Flight Capsule of this nature.

The additional Support Module requirements for a '69 minimum Mariner orbiting relay are described (1157 lb). Launch Vehicle and Spacecraft adapter design studies are summarized which show that slightly more than 200 lb of adapter structure is required to provide simple attachment to the Titan IIIC transtage. This adapter configuration provides a clean interface at the Support Module interface, for either a flyby or orbiter Support Module.

The report begins with a statement of the design study constraints (Section 2). The mission definition is then described (Section 3), with consideration of the entry and retardation worst case design rationale (3.3) and the design rationale for landed surface operations (3.4). The entire Spacecraft system is summarized in Section 4. The remaining Sections, 5, 6 and 7, provide the detailed subsystem background for Section 4.

2. MISSION REQUIREMENTS AND CONSTRAINTS

2. MISSION REQUIREMENTS AND CONSTRAINTS

2.1 MISSION OBJECTIVE

The primary objective of the Mars '73 mission is to obtain scientific data which will significantly increase knowledge of the Mars atmosphere and surface with particular emphasis on providing indications of the possibility of Mars supporting life.

Entry Science Objectives

The entry science objectives consist of (1) determination of atmospheric composition and (2) determination of atmospheric structure.

Surface Science Objectives

The surface science objectives are organized into priorities:

1 -
- Visually characterize the landing site
- Determine atmospheric composition
- Search for organic compounds
- Direct search for biology
- Search for atmospheric water
- Search for subsurface water.

2 -
- Determine atmospheric pressure
- Determine atmospheric temperature
- Determine wind velocity.

The science payload defined in table 2.1-1 represents the NASA/LRC contractual requirement. It is typical of the complement of scientific measurements which will eventually be selected for the '73 mission.

2.2 NASA/LRC GUIDELINES

The following is extracted from the Statement of Work defining this study. "The study shall consider a 1400 pound Direct Entry flight capsule with a no-science flyby. The capsule maximum diameter should not exceed thirteen (13) feet in diameter. This particular design will identify overall weights and derive a resulting science payload weight."

"Modified Guidelines

A. Launch vehicle to be T-III-C.

B. Two spacecraft to be launched.

C. Mode of delivery shall be direct entry.

D. Entry and surface science are of a higher priority than orbital science.

E. Minimum lander lifetime on the surface shall be three days.

F. Minimum data return shall be 10^7 bits. Data compression techniques may be feasible to reduce the number of bits to be transmitted to Earth.

G. Entry data must be obtained independent of landing success.

H. Minimum time-of-arrival separation shall be 10 days to allow preliminary analysis of the entry data and surface science data from the first lander before second lander entry is committed.

I. The existing DSN net of three 85' and one 210' antenna facilities can be used. An additional 210' antenna may also be assumed.

J. Minimum launch period to be 30 days.

K. Minimum launch window to be two hours.

L. Available launch azimuth range to be 45°-115°.

M. For the Mars '73 mission, the probability that Mars will be contaminated shall not exceed 4×10^{-5}.

N. An orbiter or support module may be used to support the lander during cruise and to provide relay communications.

O. Data return goal is 10^8 bits.

P. It shall be a goal that the lander be designed to have a 90-day lifetime with the use of regenerated power.

Q. Science Payload - The science payload defined in table 2.1-1 represents a highly desirable complement of scientific measurements for the Mars '73 mission. It is anticipated that because of the present economic constraints for the '73 mission, the entire instrument complement cannot be accommodated, necessitating that the payload be considered a shopping

list. To be able to realistically utilize the defined payload, it shall be assumed that within the entry and surface groups the experiments are given in an order of priority. The specific instruments and their associated characteristics are defined to provide continuity for subsequent studies and should not be considered a final payload selection for the '73 mission. Similarly, it can be anticipated that future planning activities and design studies will result in modifications to the payload both in the instrument selection and the specified characteristics."

TABLE 2.1-1 NASA/LRC EXPERIMENT LIST

ENTRY				
OBJECTIVE	INSTRUMENT	POWER, WATTS	WEIGHT, LBS.	DATA, BITS
ATMOSPHERIC STRUCTURE	CAPACITANCE DIAPHRAGM	3	3	2×10^4
	PLAT. RESISTANCE THERMOMETER	1	1	10^4
	ACCELEROMETER TRIAD	4	4	10^5
ATMOSPHERIC COMPOSITION	MASS SPECTROMETER	8 AVG., 11 PEAK	8	6×10^4
H_2O VAPOR	Al_2O_3 HYGROMETER	1	2	5×10^3
SURFACE				
IMAGERY	FACSIMILE	10	5	10^7
ATMOSPHERIC COMP./ORGANIC COMPOUNDS	GCMS/ PYROLYSIS	35 W/PYROLYSIS 20 GCMS ONLY	16 (INCLUDES 8 FOR ENTRY)	10^5
BIOLOGY	HYBRID (MULTI-CELL) LIFE DETECTION	10	8	10^3
	SOIL SAMPLER	10	8(2)	10^2
ATMOSPHERIC H_2O	Al_2O_3 HYGROMETER	1	1	10^3
SUBSURFACE H_2O	Al_2O_3 HYGROMETER W/PROBE	5	1(3)	10^3
ATMOSPHERIC TEMPERATURE	PLAT. RESISTANCE THERMOMETER	.5	1	10^3
ATMOSPHERIC PRESSURE	CAPACITANCE DIAPHRAGM	1.4	1	10^3
WIND VELOCITY	CUP ANEMOMETER	2.2	2	10^3

3. MISSION DEFINITION

3. MISSION DEFINITION

This section defines all mission-related aspects of the 1400 lb Lander Capsule design which are the inputs for the system and subsystem design.

Section 3.1 defines the science package for atmospheric and other measurements and the surface imaging requirements. The basis for this definition is the list of desired instruments supplied by NASA/LRC as part of the Mission Guidelines and Constraints (Section 2.0). Weights, data rates, and total data returns are identified for the various instruments; accuracy requirements are also listed and compared with the NASA/LRC specifications.

The mission is defined in terms of Spacecraft and Capsule trajectories in Section 3.2. Based on the requirements of minimum launch energy and a thirty day launch period, appropriate combinations of launch and arrival data are identified. A specific set of launch and arrival dates is chosen to serve as the basis for the complete definition of a Reference Mission.

The rationale which is followed in the design of the entry and retardation systems is provided in Section 3.3. Because of the lack of a complete statistical description of the environment, this design is necessarily a "worst case" design. However, an outline is presented of a study toward a design method based on the assessment of the probability of success. A few examples are given to show how such probabilistic considerations may influence the design.

Finally, the sequence of events and landed operations are defined in Section 3.4.

3.1 SCIENCE MEASUREMENTS

3.1.1 INTRODUCTION

Using the NASA/LRC experiment list, the goal of the study was to select suitable instrument hardware, combine these instruments physically and functionally into an integrated science payload, and demonstrate that the Capsule design can fully accommodate this payload.

During the study, the accuracy requirements on the measurements suggested by NASA/LRC were translated into instrument selections and the mission profile, during which the science measurements would be made, was defined. On the basis of available information on instrument characteristics and the environment in which the measurements would be made, anticipated accuracies were predicted and compared to the NASA/LRC goals.

A summary of the science instruments and their interfaces is presented in tables 3.1-1 (for entry measurements) and 3.1-2 (for surface measurements). The instruments were selected on the basis of accuracy and reliability per unit power and weight.

The status of instrument development, sterilization and hardening was also evaluated. Approaches for hardening the more complex instruments such as life detectors were developed. The results are discussed in detail in Section 5.1.

3.1.2 ATMOSPHERIC MEASUREMENTS

The entry measurements include altitude profiles of temperature, pressure, and density and the gas composition of the well-mixed atmosphere.

NASA/LRC's requirements are typically expressed as percentages of the reading at a given altitude or time. In order to determine the accuracy and resolution requirements for the instruments, these requirements must be converted to another form since (1) complete altitude profiles generally require different ranges of sensitivity, and (2) magnitudes, rather than relative percentages, facilitate an evaluation for the various atmospheres specified.

Table 3.1-3 compares the NASA/LRC requirement, the conversion and the expected accuracy of the instruments selected.

In establishing the magnitudes for the required accuracy, sensor performance has been taken into consideration. Sensors typically have errors that are constant and not proportional to their measurement. This characteristic does not permit sensors to meet, in general, accuracies expressed as constant percentages relative to the measured values. To minimize this problem, the altitude profiles have been divided into several altitude regimes where the quoted accuracies do not exceed 20 percent of the smallest measurement that will occur for the MIN atmosphere model.

The requirements for composition measurements in table 3.1-3 are identical to the NASA/LRC objectives with the exception of the resolution requirement for water detection which is set at 1 part/billion to reflect the seemingly low concentration of water in the Martian atmosphere. This represents the best capability that probably could be made available for the 1973 mission.

TABLE 3.1-1. ENTRY SCIENCE PAYLOAD

Instrument (Lander)	Weight (lb)	Volume	Power Req'mts (watts)	Location	Sampling Schedule	Data Format
Mass spectrometer	1 (ducting only)	Detector in surface science package	7	Included in GCMS surface package. Same MS used for entry and surface measurements	Initiates near Mach 5. Terminates at impact	50 (8) bit words per sample (2 sec scan, 8 sec readout) 50 bits/sec readout
Resistance thermometer	0.5 each	1 in. dia. x 2 in. long	1 each	Two on base of vehicle	Initiates at Mach 5. Terminates at impact	1 sensor output channel 1 sample/sec
Variable capacitor pressure trans-ducers	0.5 each	2 in. dia. x 2 in. long	1 each	Two on base of vehicle	Initiates at beginning of entry. Terminates at impact	1 sensor output channels 1 sample/sec
Tri-axial accelerometer (1 Dual Scale)	2	2.8 x 1.8 x 2 in.	4	Located at body c.g. with one axis aligned to vehicle vertical axis	Initiates at beginning of entry. Terminates impact	8 bits/sample/axis 10 samples/sec 72 bits/sec total Automatic scale switching
Water vapor detector	1 (ducting only)	Detector located in surface science package	N/A	Ducting located same as mass spectrometer ducting	Initiates near Mach 5. Terminates at impact	1 sample/15 sec 2 seven bit (parallel) channels 1 eleven bit (parallel) channels

TABLE 3.1-1. ENTRY SCIENCE PAYLOAD (Concluded)

Instrument (Aeroshell)	Weight (lb)	Volume	Power Req'mts (watts)	Location	Sampling Schedule	Data Format
Stagnation temperature transducer (1)	0.5	1 in. dia. x 2 in. long	1	See test	Initiates at beginning of entry. Terminates at aeroshell ejection	1 sensor output 1 sample/sec
Stagnation Region pressure transducer (4)	0.5 each	2 in. dia. x 2 in. long each	1	Behind nose of aeroshell (See text)	Initiates at beginning of entry. Terminates at aeroshell ejection	1 sensor output 1 sample/sec

TABLE 3.1-2. SURFACE SCIENCE PAYLOAD

Objective	Instrument	Unit Weight (lb)	Volume	Power (watts)	Location	Data Profile
Imagery	Facsimile (2)	2.5 each	1 to 2 in. dia. X 9 to 12 in. long each	6-10	One on each of two booms deployed above Lander	Flexible to meet maximum transmission capability of Lander. Period from 1 sec to 8 hr per picture. Total bits 10^7 to 10^8.
Atmospheric Comp/Organic Compounds	GCMS/ Pyrolysis	16.0	600 in.^{3}	20 + 35 (Pyrolizer)	Internal to Lander	Calibrate = 1 kbits Atm. Run = 0.4 kbits Soil Run = 40 kbits 1st Run Total = 41.5 kbits Repeat atmosphere and soil runs at least twice.
Life Detection	Wolf Trap	8	9 × 9 × 9 in.	1.5 (average)		Sample every 20 min 49 bits/ sample, 10^4 bits total
Soil Sampling	Sampler	6		10		200 bits total
Subsurface Water Detection	Al_2O_3 Hygrometer	1	20 in.^{3}	1	Mounted internal to Lander	1 sample/min for 20 min when pyrolizer on. 25 bits/ sample.
Atmospheric Water Detection	Al_2O_3 Hygrometer	1	20 in.^{3}	1	Mounted internal to Lander	1 sample/20 min 2.7 kbits total
Atmospheric Temperature	Plat. Res. Thermometer (2)	0.5 each	1 in. dia. X 2 in. long each	1 each	One on each camera boom	1 sample/20 min, 1% accuracy 2 channels, 7 bits each, 1.5 kbits total
Atmospheric Pressure	Capacitance Diaphragm (2)	0.7 each	2 in. dia. X 2 in. long each	1 each	Internal near skin of Lander	1 sample/20 min, 2 channels 7 bits each, 1.5 kbits total
Wind Velocity	Cup Anemometer (2)	2.0 each		0.5 each	One on each camera boom	3 samples/hr, 4 channels, 7 bits each, 28 bits/sample, 6 kbits total.
Lander Attitude	Clinometer (2)	1.3	2 in. dia.	3	Two internal to Lander mounted with long dimension parallel to vertical axis of Lander.	1 sample/6 hr, 2 channels, 7 kbits each, 200 bits total.

TABLE 3.1-3. ATMOSPHERIC MEASUREMENT ACCURACIES COMPARISON

Parameter	NASA/LRC Requirements		Converted Requirements			Hard Lander Accuracy Capability Prediction		Comments
	Accuracy Objective	Altitude Range	Area of Interest	Resolution	Accuracy			
			Altitude Profile			Supersonic	Subsonic	
Pressure Profile	± 5%	0-60 km	0-20 km 20-40 km 40-60 km	5×10^{-1} mb/5km 1×10^{-2} mb/5km 2×10^{-4} mb/5km	$\pm 5 \times 10^{-2}$mb $\pm 1 \times 10^{-3}$mb $\pm 2 \times 10^{-5}$mb	± 10%	< +5%	Supersonic measurements will be difficult to improve over 10% accuracy. Subsonic measurements can improve to ± 2% if an altimeter is used to provide an altitude base.
			Altitude Profile			Supersonic	Subsonic	
Temperature Profile	± 2%	0-60 km	0-20 km 20-60 km	2°K/km 2°K/km	$\pm 5^{o}$K $\pm 5^{o}$K	± 10%	< ± 2%	Error predictions are based upon analytical relationships being identified that remove raw heating of sensor and angle-of-attack effects. Analysis techniques may be aided by pre-flight simulation testing of prototype vehicles.
			Altitude Profile			Pre Chute	Post Chute	
Density Profile	± 5%	0-60 km	0-20 km 20-40 km 40-60 km	2×10^{-6}g/cm^3/5 km 6×10^{-8}g/cm^3/5 km 1×10^{-9}g/cm^3/5 km	$\pm 2 \times 10^{-7}$g/cm^3 $\pm 6 \times 10^{-9}$g/cm^3 $\pm 1 \times 10^{-10}$g/cm^3	± 5%	< ± 5%	Predictions based upon results of Experiment Simulation Techniques.
Atmospheric Composition	± 10%	50 km		1 Mass Unit (Water 1 part per billion)	± 5% if 50% of total ± 10% if 50% of total.	< ± 10%		Detection of minor constituents down to 10^{-11} torr partial pressure is expected. Mass resolution of 1 AMU for continuous scan system from 10-60 AMU is possible. Amplitude resolution of each mass number should be 1-2%.
Magnitude of Wind Velocity	± 5 m/sec	Surface	Winds Altitude Profile Surface Magnitude	 2 m/sec/km - - -	 ± 5 m/sec ± 5 m/sec	~ 1 m/sec		Accuracy will be strongly dependent upon Reynolds number and location of sensor relative to local perturbations on atmosphere motion. Accuracy of time measurements is limiting item in electronics.
Wind Direction	± 10°	Surface	Surface Direction	—	± 10°	< ± 10°		Accuracy will depend upon wind direction and have finest values when wind is aligned to one axis of sensor.
Atmospheric Moisture	None	< 50 km	—	1 part per billion	—	± 5% for concentration > 1 ppm		Accuracy is a function of pumping system and time available for counting.

The analysis of an experiment's accuracy included the consideration of: (1) errors due to discrepancies between local and ambient values (resulting from flow effects, etc.), (2) instrument errors, (3) telemetry errors, and (4) data analysis errors inherent in the methods.

In the case of ambient temperature, direct measurements during supersonic flight are impossible, and the determination of local ambient conditions must rely on post-flight analysis. Present indications, based on Earth flight experience, are that measurements made in the stagnation region can be reliably analyzed for ambient values and that the results should be good to about ± 5 to 10 percent. Such accuracies are anticipated provided there is adequate data on ratio of specific heats, angle-of-attack, and velocity.

Ambient temperature measurements during subsonic flight are subjected to less severe perturbations and as a result should show significant improvement in accuracy. Without the benefit of detailed subsonic data for temperature measurements made at the Capsule base, estimates of the accuracies are in the area of ± 2 percent if flow heating effects can be ignored. The evaluation of the anticipated accuracies in subsonic temperature measurements are made using the Experiment Simulation Techniques described below and in detail in ref. 3.1-1.

The measurement of pressure involves the same situation regarding the perturbations during supersonic flight and the current ability to correct for these effects. A significant difference is that considerable Earth flight test data (ref. 3.1-2) indicates that base pressure readings can be useful at high Mach numbers for determining ambient pressures. A typical correction curve based on such data is shown in fig. 3.1-1 (ref. 3.1-3). However, until more ground test data is available, the anticipated accuracies for both stagnation and base measurements are estimated to be ±10 to 15 percent if adequate knowledge of the entry atmosphere and flight conditions exist.

Base pressure readings during subsonic flight are also subject to the same type of corrections. Again the generation of reliable correction curves appears feasible with sufficient preflight testing. The accuracies in pressure-altitude profiles that can be expected, if such curves are assumed to be available, have been established with the use of the Experiment Simulation Techniques.

In the supersonic (pre-parachute) regime, density is derived from triaxial accelerometer data. The experiment simulation computer code has been applied to this technique. On the basis of the results obtained and taking into account further refinements involving iterative methods, it is anticipated that accuracies of 5 percent can be achieved (ref. 3.1-4). In the subsonic (post-parachute) regime, density is derived from measured pressure and temperature data. Parametric studies employing Experiment Simulation were conducted for this case. The results indicate that agreement with the true densities within ± 5 percent can be achieved if sampling intervals below 2 sec are used.

The term "Experiment Simulation" mentioned above refers to a method by which the data from an experiment is mathematically simulated, analyzed, and interpreted before the experiment is actually conducted. By evaluating the effect of various changes in the type

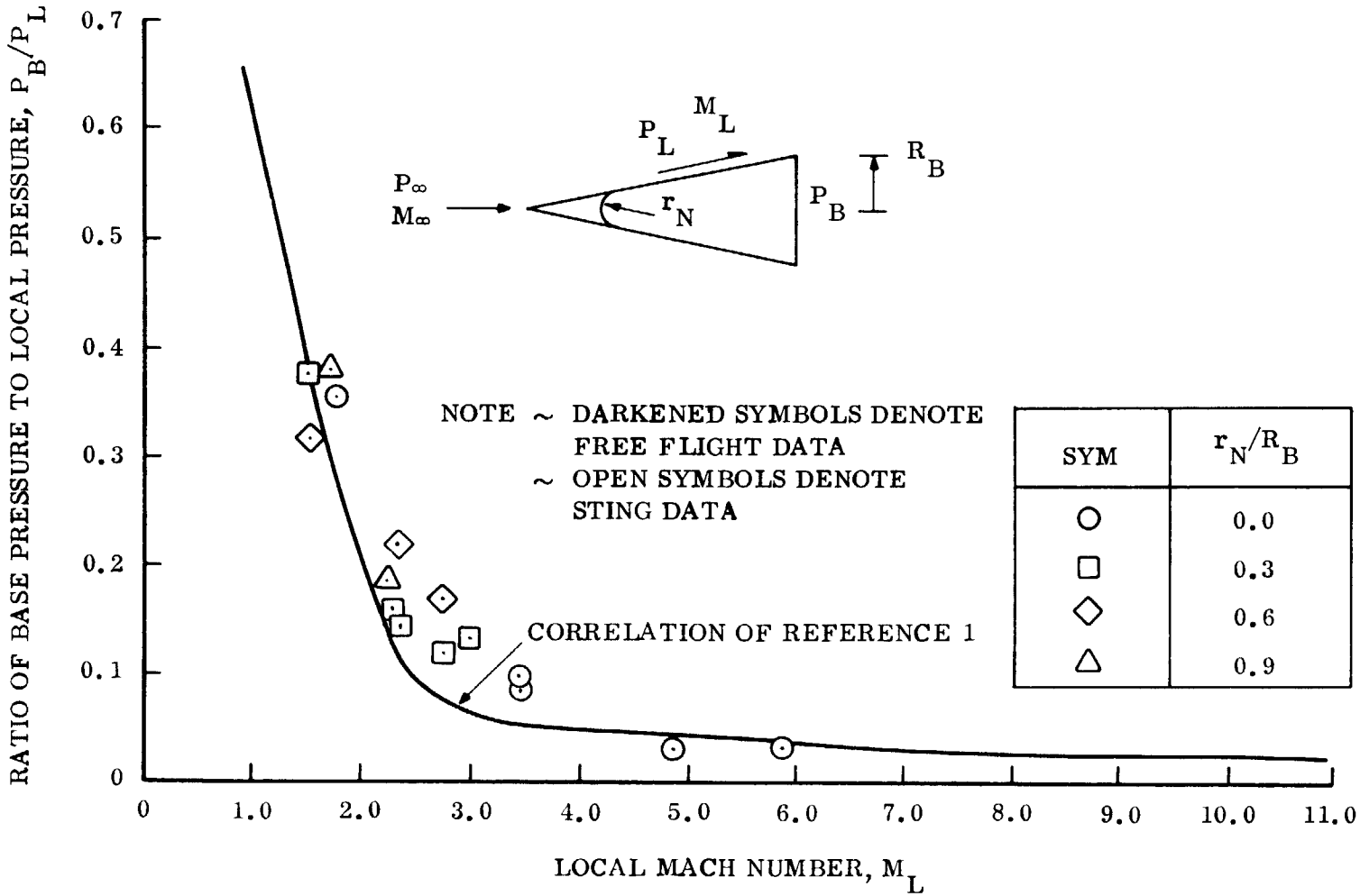

Figure 3.1-1. Turbulent Flow Base Pressure Correlation

of data considered, the experiment design, instrumentation properties, and analysis techniques used, the actual experiment can be optimized for these factors. The technique was used to evaluate parametrically the achievable experiment accuracy as a function of ballistic coefficient, sampling rate, sensor accuracy, atmospheric model, trajectory type, and subsystem errors. The study was limited primarily to the subsonic regime and clearly demonstrated that mean molecular weight and the altitude profiles of pressure, temperature, and density could be obtained from pressure and temperature data alone.

The computer programs which have been developed generate ideal data, add expected errors to produce simulated raw data, and perform the required data analysis to produce automatic plots of the resulting atmospheric profiles and errors (deviations from nominal). By applying an averaging technique to the mass of data obtained in the parametric study, the required sampling rates for desired accuracy is established.

On the basis of the more recent observed data and theoretical analyses, the most probable temperature variation at the surface of Mars near its equator, is given in fig. 3.1-2 (ref. 3.1-5). The prediction of this variation is assumed valid for all the models and a measurement resolution of $2^{o}K$/hour with a $\pm 5^{o}K$ accuracy should be adequate to verify the actual variation. Several investigators (ref. 3.1-6) anticipate the near-surface diurnal variation in temperature to differ markedly from the surface variations. In fact, recent theoretical studies on the subject (ref. 3.1-6) indicate the maximum near-surface (0.5 meters altitude) temperature will be $30^{o}K$ to $50^{o}K$ less than the maximum surface temperature. The situation is summarized in fig. 3.1-3, where it can also be noted that the temperature resolution and accuracy requirements in table 3.1-3 are adequate to detect the near-surface diurnal variation.

The measurement of temperature on the surface of Mars will be a difficult task. Until the relationships between true atmospheric temperature and equilibrium temperature of the resistance element can be defined, any attempts to evaluate the accuracy of this measurement must be directed at the ability of the system to measure the temperature of the transducer's sensitive element only. Resistance thermometers can faithfully measure the temperature of their sensitive element to accuracies of 0.1 percent or better. The errors encountered in telemetering this data will swamp out this error and the result will be a system error equal to the digitization error. At best, the resolution of temperature to $\pm 3^{o}K$ will be possible with a telemetry system capable of 1 percent analog-to-digital conversions. The accuracy of this measurement cannot be defined at this time.

The lack of observational data on pressure and density variations makes the establishment of their resolution requirements very speculative. The diurnal variation for pressure has been estimated to be on the order of 0.2 millibar, which for the MIN atmosphere is a 4 percent change and for the MAX atmosphere is a 1 percent change.

No attempt has been made to estimate the diurnal variation of density since its variation should be quite small ($\sim$ 1 percent) and no direct density measurement is currently planned. The accuracy requirement on pressure is consistent with NASA/LRC objective ($\pm$ 5 percent of value at known time) if the requirement is to be met for the lowest surface pressure models.

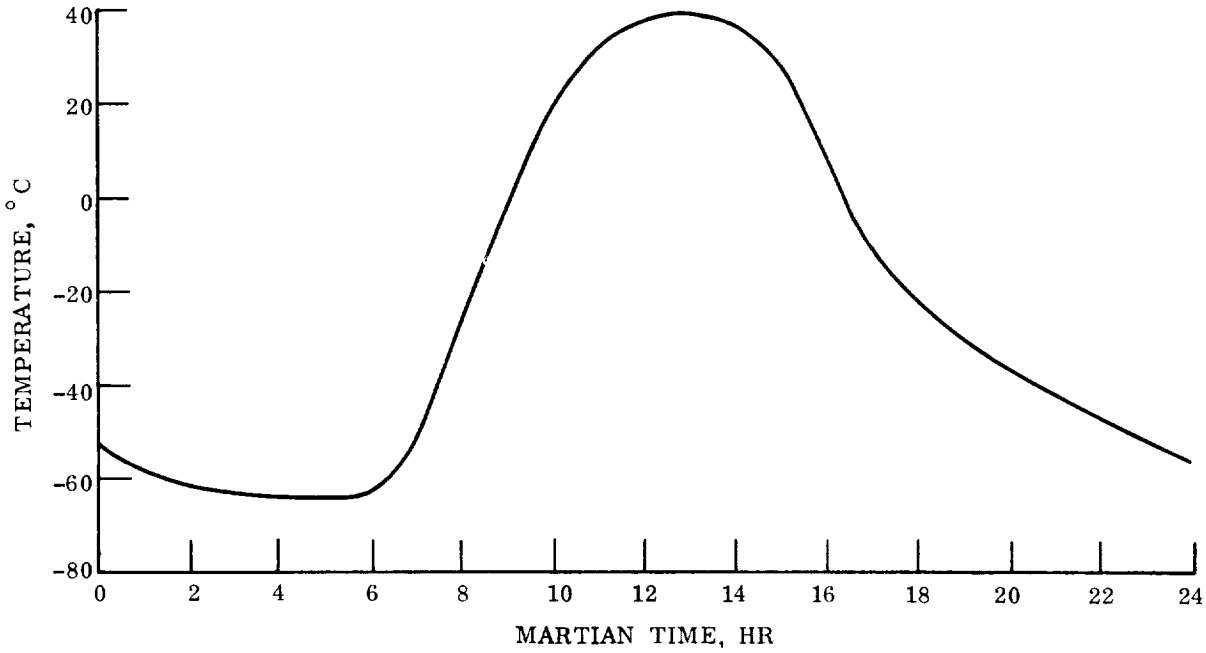

Figure 3.1-2. Diurnal Variation of Surface Temperature on the Martian Equator at Perihelion

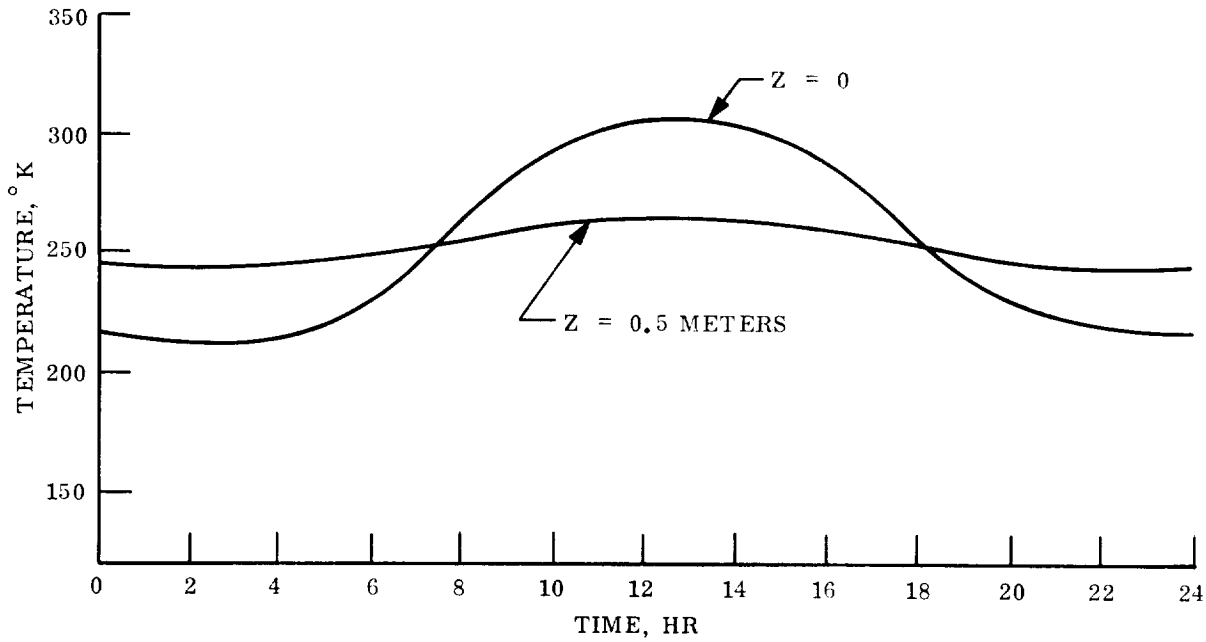

Figure 3.1-3. Temperature Versus Time at the Equator of Mars at the Surface and at Z - 0.5 Meters (Neubauer - 1960)

The accuracy to which the atmospheric pressure on the surface of Mars can be measured is dependent upon the following error sources:

1. Perturbation of the atmospheric flow over the Lander and the resultant deviation from the free stream pressure at the pressure sensor port.

2. Errors inherent in the pressure transducer itself.

3. Errors resulting from the digitization process in the telemetry system.

The first of these sources is impossible to predict at present due to the lack of information about the Martian atmosphere. Errors generated in the sensor itself can probably be kept below 0.25 percent following calibration to remove bias and non-linearity contributions. The random telemetry drop-outs can produce very significant errors if the number of statistical samples is small; however, when the same function is measured many times in a short period of time (so as to minimize variation of the parameter during the sampling period) this error becomes negligible. The digitization error for the pressure transducer will be approximately 1 percent. Taking the root sum square of these errors it appears that a 2 percent measurement may be possible if the first error source can be kept below $\sim$ 1.5 percent. Assuming the pressure transducer has a full scale of 25 mb, the best resolution possible will then be $\approx$ 0.25 mb (one digital level) and the accuracy will be $\approx$ 0.5 mb.

The only other atmospheric parameter that could show distinct diurnal characteristics is the local wind field which could be significantly affected by the solar thermal flux. Although statistically adequate data cannot be obtained in a 24 to 48 hr period, the engineering value of providing preliminary data on the apparent magnitude of steady-state wind conditions and their variability is very high. The detection of steady or gust wind conditions in the vicinity of 150 to 200 ft/sec would help verify the necessity for concern on the gust-loading problem for touch-down dynamics of future Landers. The lack of observational data makes all estimates highly speculative. Therefore the NASA/LRC objectives for accuracy have been used directly while the resolution requirement comes from the vertical wind gradient of 2 ft/sec/1000 ft specified in the model atmospheres.

3.1.3 OTHER MEASUREMENTS

3.1.3.1 Surface Imaging

Initial imaging missions of the Martian surface will most likely be concerned with Lander site topography and geomorphology. Imaging requirements therefore consist of panoramic sweeps at moderate spatial resolutions supplemented by periods of acquisition at higher spatial resolutions with attendant reduced fields of view. A geological model is established by combining this total set of pictures. Images are without peer in their ability to indicate visible landforms, relative roles of land building and destructive process (e.g., tectonic versus erosional processes), to define sizes, shapes and relative positions of objects of interest. To be useful geologically, the images must cover a substantial spatial resolution range, preferably with nested fields. Field experience gained indicates that the highest resolution ought to correspond to that of the human eye at a distance of about 2 meters; i.e., a ground resolution of 1 mm.

Although the contribution of imaging reconnaissance to life detection on Mars is likely to be of an indirect nature, the results will undoubtedly center on the establishment of the role certain unusual environmental conditions play in the development of life forms. Such unusual conditions are thought to exist in the areas of high reflectivity at the boundaries of the Martian polar caps and especially within the dark areas, maria such as Syrtis Major (a likely candidate for a Lander site on the first mission) which exhibit seasonal changes. Currently these changes (known as the wave of darkening) can be interpreted either as a biological phenomena or as a seasonal transport of dust between the highlands and the lowlands. On the basis of available evidence no preference can be attached to either theory. An imaging reconnaissance may resolve this problem.

The imaging will be performed by two boom-mounted facsimile camera sets which are described in detail in Section 5.1. The facsimile cameras have a limiting angular resolution that is fixed by the design of the imaging optics. For this mission the two selected angular fields of view are 0.1° and 0.01°. The Hard Lander can assume any one of a wide variety of landed positions on the planet, each of which can result in a different distance between the lens and nearest object. Typical figures for the smallest linear element corresponding to the angular fields of view of 0.1° and 0.01° are 2.5 mm and 0.25 mm, respectively. The identification of an object with these dimensions will depend on its shape; those that are long and thin, such that they are one linear resolution element in width and at least four such elements in length, will be resolved provided they have enough contrast with the background. Objects that are square or round will not be resolved unless their linear dimensions are at least twice that of the minimum resolvable ground resolution. Based on assumed clear conditions, it will be possible to resolve long thin objects that are at least 4 mm by 12 mm, or round or square shaped objects that are 8 mm in width or in diameter with a 0.1° IFOV, and objects of one tenth these dimensions with a 0.01° IFOV.

The presence of a thick dust cloud could conceivably result in such a high degree of scattering that photographic resolution could be impaired both by motion of the scattering cloud and by a reduction in contrast. A reduction in resolution may also occur at very low light levels, such as may occur in the shadow of the Lander. The data given assumes a high contrast ratio in the subject. Details of the performance of the camera in low illumination situations are not available, but will undoubtedly be affected by the speed at which the scanning is carried out.

From scientific considerations the illumination from the Sun is ideal at a large zenith angle in a low scattering atmosphere. This results in a large range in phase angle (angle between source, subject, and camera), and enables the illuminated subject to be more easily identified through its photometric properties. Concurrently, from the standpoint of the engineering requirements, this presents to the photoimaging sensor a wide signal dynamic range, a requirement that is not easily accommodated in all detectors. In the reference mission for this study the landing point is about 30° from the terminator and the Sun is therefore at a zenith angle of 60°. In this situation the illumination in the absence of scattering is, in the main, ideal for determining local topography from the shadows cast, creates a wide signal dynamic range and a large difference in phase angle. In addition, it throws long shadows of the Lander which may reduce the information content in the high resolution domain. Alternatively, if there is a strongly scattering region in the atmosphere, better photographic illumination is obtained when the Sun is at zenith angles of between 30° and 60°.

3.1.3.2 Molecular Analysis

The gas chromatograph-mass spectrometer combination is a powerful tool for use in the analysis of the chemical composition of the Martain lithosphere and atmosphere. Many or all of the following objectives may be attained, depending, of course, on the complexity and versatility built into the instrument.

1. Accurately determine the constituency of the atmosphere (probably comprised of simple molecules, such as CO_2, N_2, H_2O, A, NH_3, CH_4, NO_2, or others).

2. Determine the typical composition and nature of organic and biologically significant molecules in the atmosphere and surface, including but not restricted to the following:

   a. Amino acids

   b. Odd-carbon-number normal hydrocarbons

   c. Even-carbon-number fatty acids

   d. Steroids and their derivatives

   e. Polypeptides

   f. Porphyrin rings.

The gas chromatograph-mass spectrometer is particularly suited to detect molecular order, which is significant to biological studies. Many compounds associated with life are also found in fossils.

The first Lander missions should probably concentrate on analyzing the organic compounds due to major interests in biological studies. Rigorous inorganic chemical studies may be pursued on later missions.

The water detectors should be integrated with the gas chromatograph-mass spectrometer in order that the same air and soil sampling and preparation devices may be utilized by all instruments requiring them. A sensitive water detector will supplement mass spectrometer data not only in identifying air and soil moisture, but also in detecting water pyrolyzed from hydrates and possibly other chemical reactions.

Analysis of biologically significant compounds suggests the desirability of analyzing atomic or molecular weights from unity to at least a few hundred. Lightweight flyable mass spectrometers with unit atomic mass resolution capabilities from one to 150 can be made available for the 1973 Lander mission. Virtually all atmospheric molecular compounds will fall within this range. The simpler biologically associated organic compounds (amino acids, numerous pyrolysis products, etc.) also have molecular weights less than 150. It may be feasible to include a second mass spectrometer covering the molecular weight range from

about 100 to several hundred, perhaps as high as 1000 units. The latter spectrometer should determine moleuclar weights to accuracies of a few units in the higher molecular weight ranges. This is within the state-of-the-art and would enhance the value of the scientific mission. Additional weight requirements will be minimal, perhaps between 1 and 2 lb at most. The complexity of the device increases as heavier mass units are analyzed. Detailed studies must eventually specify the types of organic molecules which shall be analyzed in the microcolumns.

The instruments are summarized in table 3.1-2, and a detailed description including hardening, sterilization, and development status is presented in Section 5.1.

3.1.3.3 Life Detection

No single "life detection" technique has yet been identified which will determine with certainty whether life exists outside the terrestrial biosphere. Greater confidence may be placed in our judgment concerning the existence of extraterrestrial life as the amount of correlative information increases. Among the several approaches under consideration (for example, visual imaging, analyses for specific compounds and metabolic products, study of transfer and conversion of energy, observation of growth and reproduction, etc.) the weight-limited Hard Lander science payload under consideration in this report will include an integrated scientific attack on the following problems:

1. Does life exist on Mars?

2. If life does not presently exist on Mars, did it ever exist?

3. If life has never existed there, what factors are present which suggest life may be formed at some future time?

The proposed payload will provide insights far beyond an attempted answer to question 1 above. It is indeed possible that Martian microorganisms (if they exist) may not respond to terrestrial life detection techniques. The gas chromatograph-mass spectrometer may prove to be the most important "life detector" aboard since it will be capable of analyzing air and soil samples for several of the basic constituents present in the microenvironment.

Medium and high resolution TV cameras will define prominent features in the macrostructure of the environment. Atmospheric temperature and pressure measurements will further elucidate the physical characteristics of the environment relevant to biological problems.

It is hoped that the proposed biological life detectors will detect life, if Martian life exists and responds favorably to a terrestrial model. However, a negative result from life detector instruments may not lead to any conclusions following analysis of the results of the integrated mission. (It must also be noted that a positive result from Wolf Trap and/or Gulliver does not state with certainty that life exists; several potential ambiguities have been identified.) Instrumentation, hardening and sterilization problems are discussed in Section 5.1.

3.1.4 OPERATIONS AND SEQUENCING

To conserve weight and space, portions of the science payload have been functionally integrated. The mass spectrometer and the water detector are used during both entry and surface operations. This requires the addition of appropriate ducting and valves.

The sequence of operation is shown in table 3.1-4. The sequence is divided into two basic phases.

The first is the relay phase which occurs immediately after touchdown during the flyby of the Support Module. During this phase, imaging is performed and multiple samples of atmospheric data are taken.

The second is the direct link phase. During this period, meteorological data is sampled every 20 min as shown, and the other detectors are operated.

Soil sampling is initiated immediately, on the premise that the total science payload should be exercised as soon as practicable. Power and data transmission profiles are based upon this sequence.

Soil samples will be acquired, processed, and injected into the pyrolyzer and life detector. The pyrolyzer will feed the gas chromatograph and the subsurface water detector. The mass spectrometer will analyze the output of the gas chromatograph columns, every time a gas peak appears at the exit of a column. This mode of operation is preferred over a continuous sampling of the gas chromatograph/mass spectrometer since it conserves data bits. The molecular analysis of the soil may consist of several stages. First the pyrolyzer temperature is raised gradually to about 150°C, to vaporize more volatile molecules, such as water. Then a second run is made with the pyrolyzer going gradually up to 700°C to vaporize the remaining molecules of interest. The complete molecular analysis will be repeated twice as limited by telemetry and power constraints.

If a Wolf Trap life detector is used, the chambers containing the soil samples would be sampled every twenty minutes for amount of light scattered by the chamber contents. Note that the culture chambers, which may contain water, remain sealed until the first series of water detection measurements have been completed.

Soil sample acquisition, processing, and analysis is a series operation but relative timing is flexible. Also, the time when the sequence is done can be varied to optimize thermal balance and power subsystem loading. For example, the pyrolyzer requires up to 35 watts of power, and it may be desirable to operate it at night for system thermal balance purposes.

If the clinometer is used to detect seismic activity in addition to determining Lander attitude, repeated sampling over longer time periods would be desirable.

TABLE 3.1-4. SURFACE SCIENCE SEQUENCING

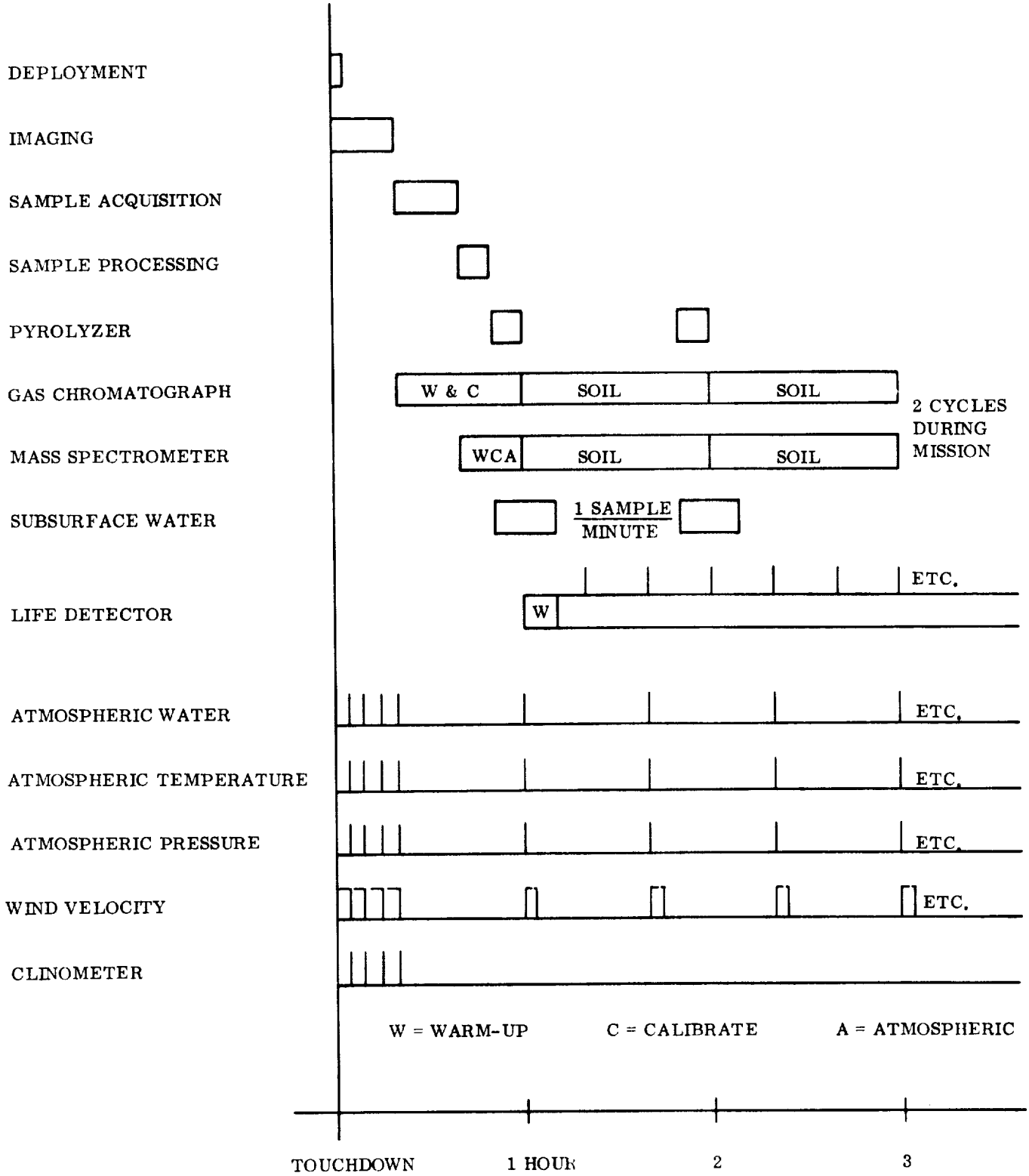

3.1.5 REFERENCES

3.1-1 "Mars Hard Lander Capsule Study," NASA CR-66678-2, Vol. II. Prepared by General Electric for NASA Langley Research Center, 31 July 1968.

3.1-2 "Correlation of Available Flight Test Base Pressure Data", General Electric Company, Re-entry Systems, November 29, 1967.

3.1-3 "Evaluation of Base Pressure Characteristics for Planetary Entry Configurations", General Electric Company, Re-entry Systems, Technical Brief, November 10, 1967.

3.1-4 "Synthesis Techniques for Experiments in Planetary Atmospheres", S.O. Smith, P. DeVries, R.J. Homsey; AIAA Paper No. 68-155; January 22, 1968.

3.1-5 Hess, D.S. and Pounder, E., "Voyager Environmental Predictions Document", SE003BB001-1B28, NASA-JPL, Oct., 1966.

3.1-6 Neubauer, F.M., "Thermal Convection in the Martian Atmosphere", Journal of Geophysical Research, Vol. 71, p. 2419, May 15, 1966.

3.2 REFERENCE MISSION

The various parts of the Reference Missions are defined in Sections 3.2.1 through 3.2.4; a summary of the Reference Missions and detailed design data for entry trajectories and post-landing relay communications are presented in Section 3.2.5.

The design of the Reference Mission begins with the identification of launch and arrival periods; this is done mainly on the basis of requiring minimum launch energy and a 30 day launch period. Next, the nominal entry path angle is derived from the path angle dispersion and the skip-out limit. The principal input here is the assumption of a 50 km (1-sigma) impact parameter error; the result is a nominal entry path angle of 21.0°, and a maximum (3-sigma) path angle equal to 24.5°.

The entry Capsule ballistic coefficient, equal to 11.5 lb/ft^2, is determined by the maximum path angle by requiring that Mach 2 altitude in the MIN atmosphere, when entering with the maximum path angle, is not lower than 10 kft. The basis for this altitude is the requirement that terminal velocity be reached at a landing altitude of 6 kft, with 4 kft required for the parachute to slow down from deployment velocity to terminal velocity. The parachute is sized for a terminal velocity equal to 100 ft/sec in the MIN atmosphere. The definition of entry Capsule ballistic coefficient and parachute makes the entry times known for all cases of entry trajectories to be considered (three atmospheres and three entry path angles).

Finally, to complete the definition of the reference mission, the Capsule deflection velocity is determined. The normal component is determined by the entry path angle; the tangential component determines where the Support Module will be in relation to the Lander at the time of landing. The tangential component is chosen such that the Support Module will be rising at 45° elevation not earlier than 150 sec after landing in order to always obtain a 45° to 45° communication pass. The design case for this condition is the case of MAX atmosphere with maximum entry path angle.

According to usually accepted terminology, the term "Spacecraft" refers to the Capsule and Support Module before separation. After separation there are two vehicles, the Support Module and the Capsule. The term "Lander" is here used only when referring to the vehicle after landing.

3.2.1 LAUNCH AND ARRIVAL CONFIGURATIONS

The requirements which determine the combinations of launch and arrival dates to be considered for the 1400 lb Capsule mission are:

1. minimum launch energy
2. 30 day launch period
3. 1 day separation of arrival times of two missions
4. declination of launch asymptote must be less than 35°.

These requirements lead to the mission points identified by the shaded area on fig. 3.2.1-1. This area is bounded by lines of constant arrival dates of 1 January and 15 February 1974; further, on the left, by the line of declination of launch asymptote equal to 35°, and on the right by the line of launch energy equal to 16.2 km^2/sec^2. Some important mission parameters are listed in table 3.2.1-1 for the four corner points of this area. These parameters are:

1. launch date
2. arrival date
3. twice launch energy per unit mass, C_3, km^2/sec^2
4. approach velocity, V_∞, km/sec
5. flight time, T_F, days
6. communication distance, R_c, km.

Also listed are the angles which identify the positions of Sun, Earth, Canopus, approach asymptote and Mars' North polar axis in two coordinate systems, the impact parameter coordinate system and a Mars equatorial system. The nomenclature is defined in the table. (Note that the terms "right ascension" and "declination", which properly refer only to the Earth equatorial system, are here used in relation to the Mars Equator.)

Table 3.2.1-1 lists also the same parameters for the mission point which is chosen as the reference, for further mission definition; this point is indicated by a cross in fig. 3.2.1-1.

3.2.2 ENTRY PATH ANGLE DISPERSION

The selection of the mission point as defined in the previous section allows the computation of entry path angle dispersion and, in particular, the determination of the nominal and maximum entry path angles. The entry path angle dispersion is based on the following assumptions:

impact parameter error, $dB = 50$ km (1σ)

deflection velocity error, $d\Delta V = 0.25$ percent (1σ)

deflection pointing error, $d\phi = 0.6°$ (1σ)

The dispersion is conveniently expressed by the linear error analysis

$$d(\cos \gamma_E) = C_1 \frac{dB}{B} + C_2 \frac{d\Delta V}{\Delta V} + C_3 \, d\phi$$

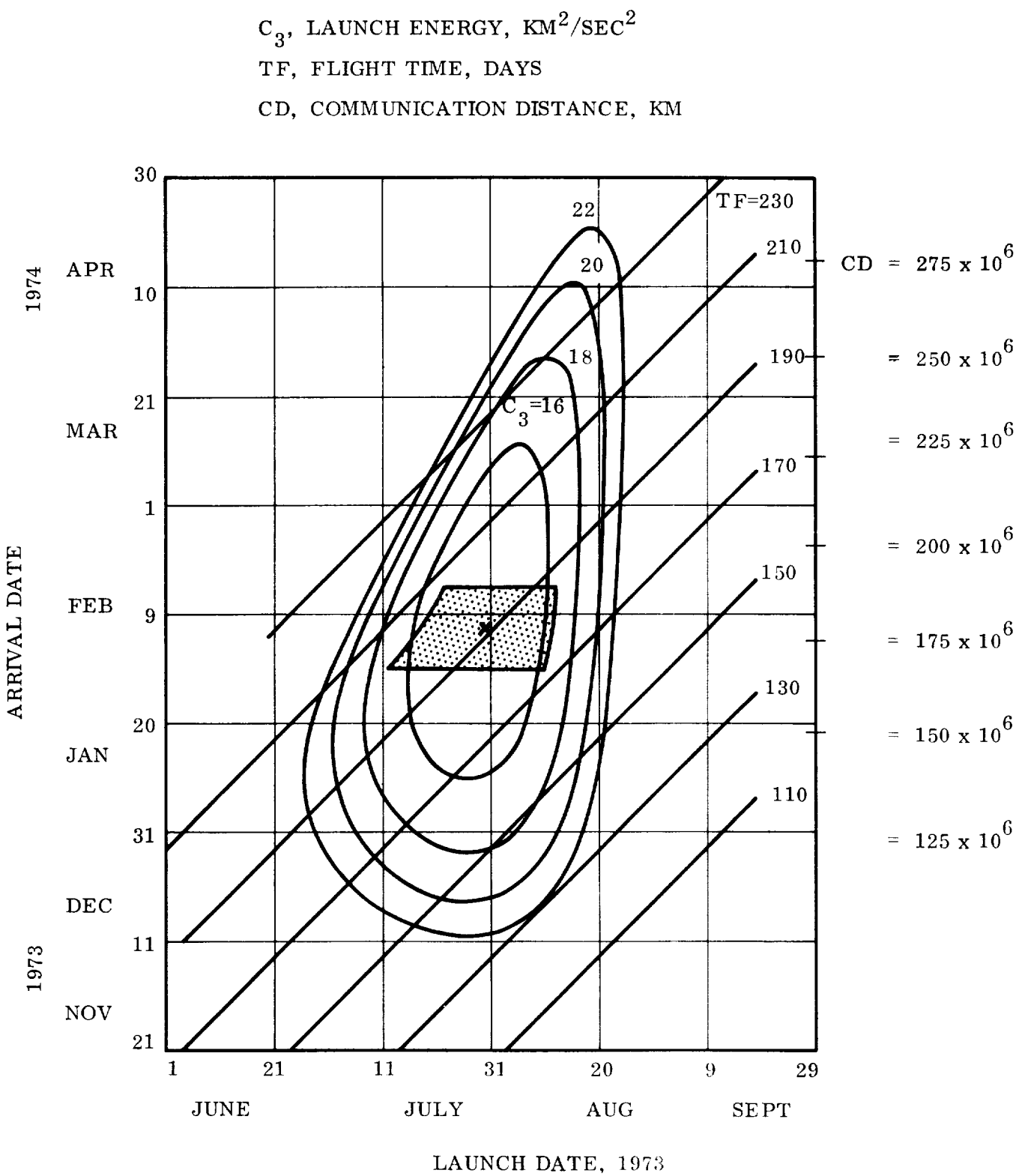

Figure 3.2.1-1. Basic Mission Planning Chart

TABLE 3.2.1-1. ARRIVAL CONFIGURATIONS

		1	2	3	4	5
	Launch Date	7-14-73	7-24-73	8-11-73	8-9-73	7-30-73
	Arrival Date	1-30-74	2-13-74	2-15-74	2-1-74	2-7-74
	C_3 (Km^2/sec^2)	16.383	14.901	16.152	15.964	14.462
	V_∞ (Km/sec)	3.194	2.908	2.834	3.216	3.003
	T_F (days)	200	204	188	176	192
	R_C (Km x 10^6)	167.2	187.5	190.6	170.3	179.7
RST Coordinate System	ξ_S (ZAP angle)	129.59	123.27	127.13	137.27	130.50
	η_S	24.40	21.28	17.54	20.09	21.19
	ξ_E	152.91	149.08	156.20	162.30	156.39
	η_E	77.68	65.38	62.50	88.11	74.39
	ξ_C	59.69	57.76	64.11	66.93	62.56
	η_C	104.88	105.17	103.90	103.18	104.04
	ξ_N	95.83	97.75	91.65	89.17	93.21
	η_N	-72.60	-72.42	-71.74	-70.84	-71.59
Equatorial Coordinate System	α_S	-0.99	5.34	6.22	-0.08	2.64
	δ_S	-1.65	1.17	1.57	-1.23	-.03
	α_E	-37.21	-30.28	-29.27	-36.24	-33.28
	δ_E	-17.63	-15.16	-14.77	-17.30	-16.27
	α_C	123.88	123.88	123.88	123.88	123.88
	δ_C	-65.41	-65.41	-65.41	-65.41	-65.41
	α_A	129.09	128.78	133.33	137.19	133.22
	δ_A	-5.83	-7.75	-1.65	0.83	-3.21

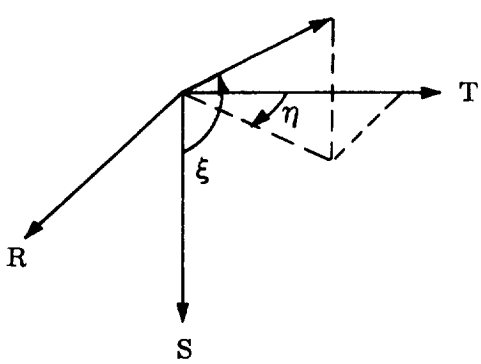

S axis is along approach asymptote direction
R, T axes are in impact parameter plane
T axis is parallel to ecliptic

α = "right ascension" } With respect to
δ = "declination" } MARS equator

Subscripts: S - Sun
E - Earth
C - Canopus
N - Mars North Pole
A - Approach asymptote

where

$$C_1 = \frac{V_\infty B}{R_E V_E}\left(1 + \frac{\Delta V_t}{V_{BS}}\right)$$

$$C_2 = -\left[\frac{V_\infty B}{R_E V_E} - \cos\gamma_E\right] = -0.1931$$

$$C_3 = \left[\frac{V_\infty B}{R_E V_E}\left(1 + \frac{\Delta V_T}{V_{BS}}\right) - \cos\gamma_E\right] + \frac{V_\infty B}{R_E V_E}\,\frac{\Delta V_n}{V_{BS}} = 0.2678$$

and

V_∞, approach velocity = 3.003 km/sec

B, impact parameter = 7803.7 km

R_E, entry radius = 3630 km (800 kft altitude)

V_E, entry velocity = 5.730 km/sec

V_{BS}, Spacecraft velocity at deflection = 3.054 km/sec

R_S, distance Mars to separation point = 274,390 km (at 24 hr before periapse passage)

γ_E, entry path angle = 21°

ΔV_n, deflection velocity normal to Spacecraft velocity = 15.3 m/sec

ΔV_t, deflection velocity parallel to Spacecraft velocity = 20 m/sec

ϕ, angle between deflection velocity and ΔV_n = 52.58°

ΔV, total deflection velocity = 25.2 m/sec.

Inasmuch as this analysis depends on the values of γ_E, ΔV_n and ΔV_t, these numbers are actually the result of an iterative process. The nominal path angle is the end result of this analysis, because it is obtained by adding the dispersion to the skip-out limit; furthermore, the normal deflection velocity, ΔV_n, is directly related to the nominal entry path angle, while the tangential velocity component, ΔV_t, is chosen to provide a specific position of the Support Module with respect to the landing site at the time of landing (this depends on the entry time, which in turn depends on the path

angle, the vehicle ballistic coefficient, the parachute and the atmosphere). The numbers shown here represent the end result of the iteration; the choice of ΔV_t, the vehicle ballistic coefficient, and the parachute is explained in Sections 3.2.3 and 3.2.4.

The result of the entry path angle dispersion analysis is, in terms of 3-sigma values,

minimum path angle = 16.85°

(this "skip-out" angle is actually the vacuum graze path angle at 800 kft, for approach velocity equal to 3 km/sec)

nominal path angle = 21°

maximum path angle = 24.53°

(Note that the nonlinearity in the dependence of entry path angle on impact parameter is taken care of by expressing the error analysis in terms of the cosine of the path angle.)

3.2.3 DEFINITION OF REFERENCE ENTRY TRAJECTORIES

The allowable entry Capsule ballistic coefficient is related to the maximum entry path angle through the following considerations.

First, it is assumed that the parachute will be deployed on a signal derived from an altimeter. Second, the parachute must not be deployed at a Mach number greater than two. Third, it is required that if the Capsule comes in over a plateau as high as 6 kft, terminal velocity will be reached at that altitude. The vertical distance required to reach terminal velocity (at 6 kft) in the MIN atmosphere (NASA/LRC atmosphere model, May 1968) is 4 kft; the altimeter setting is thus 4 kft. The lowest Mach two alitude occurs on a trajectory entering the MIN atmosphere with the maximum entry path angle, which is 24.5° according to the dispersion analysis. For this condition the Mach 2 altitude is 10 kft,(i.e., 6 kft plateau altitude and 4 kft altimeter setting) if the vehicle ballistic coefficient is 11.5 lb/ft^2 or 0.357 slug/ft^2. If the terminal velocity is to be 100 ft/sec (at the plateau altitude of 6 kft), the ballistic coefficient of the Capsule parachute combination is 0.427 lb/ft^2 or 0.0133 slug/ft^2 (this is $\rho V_t^2/2g$, with $\rho = 3.23 \times 10^{-5}$ slug/ft^3, the density of MIN atmosphere at 6 kft; V_t = 100 ft/sec the terminal velocity; and g = 12.2 ft/sec^2).

In summary, the Lander entry trajectories are thus determined by the following conditions:

1. Entry Capsule ballistic coefficient = 0.357 slug/ft^2 (the hypersonic drag coefficient is 1.46, for a 60° sphere/cone configuration)

2. Parachute is released according to an altimeter setting of 4 kft, and the parachute ballistic coefficient is 0.0133 slug/ft^2

3. Entry path angles to be considered are 16.85, 21 and 24.53°

4. Atmospheric models to be used are the MIN, MEAN, and MAX models (NASA/LRC, May 1968).

The purpose of computing entry trajectories, to be presented in detail in Section 3.2.5, is mainly to determine the relay communication conditions at landing and after landing. The Lander will therefore be assumed to land at zero altitude, even though the parachute was sized for a landing at 6 kft altitude. The landing at zero altitude represents a more critical condition for the relay communication.

3.2.4 DEFINITION OF TANGENTIAL DEFLECTION VELOCITY

For any given approach velocity, the component of the deflection velocity normal to the Spacecraft velocity is mostly determined by the desired entry path angle; it is also slightly dependent on the tangential component. The tangential component is determined such that a specific condition for the relay communication at the time of landing is obtained. This condition is the following: considering the total range of entry path angles (from 16.8 to 24.5°) and the total range of atmospheres, a 45° to 45° relay communication pass must be obtained, beginning at least 150 sec after landing. It has previously been shown that the 45° to 45° pass presents a near optimum compromise between the length of the pass and the greatest communication distance, in order to receive the maximum number of bits. The combination of MAX atmosphere with maximum entry path angle yields the earliest time at which the Support Module is rising at 45°, so that this is the "design case". The required tangential deflection velocity depends mostly on the time from entry to landing; this dependence is shown in fig. 3.2.4-1, in which the Support Module elevation at landing is shown as a function of the time from entry to landing and the tangential deflection component. The entry time for the "design case" is 322 sec; to this is added 150 sec for deployment of equipment, and from fig. 3.2.4-1 it follows that the tangential velocity component is 20 m/sec, assuming deflection at 24 hr before periapse passage. The normal velocity component for an entry path angle equal to 21° is then 15.3 m/sec. (The Support Module elevation at landing also depends on the central angle from entry to landing; this angle is about 9° for the "design case" and fig. 3.2.4-1 is drawn for that value.) The total deflection velocity is 25.2 m/sec and is directed at an angle equal to 52.58° with respect to the local horizontal.

3.2.5 REFERENCE MISSION DESIGN SUMMARY

3.2.5.1 Pre-entry and Entry Design Data

Except for the detailed computation of entry trajectories and post-landing relay communication geometry, the reference mission is completely defined by Sections 3.2.1 through 3.2.4. A summary of important mission parameters is given in table 3.2.5-1. The arrival configuration is illustrated in fig. 3.2.5-1, which shows a projection in the

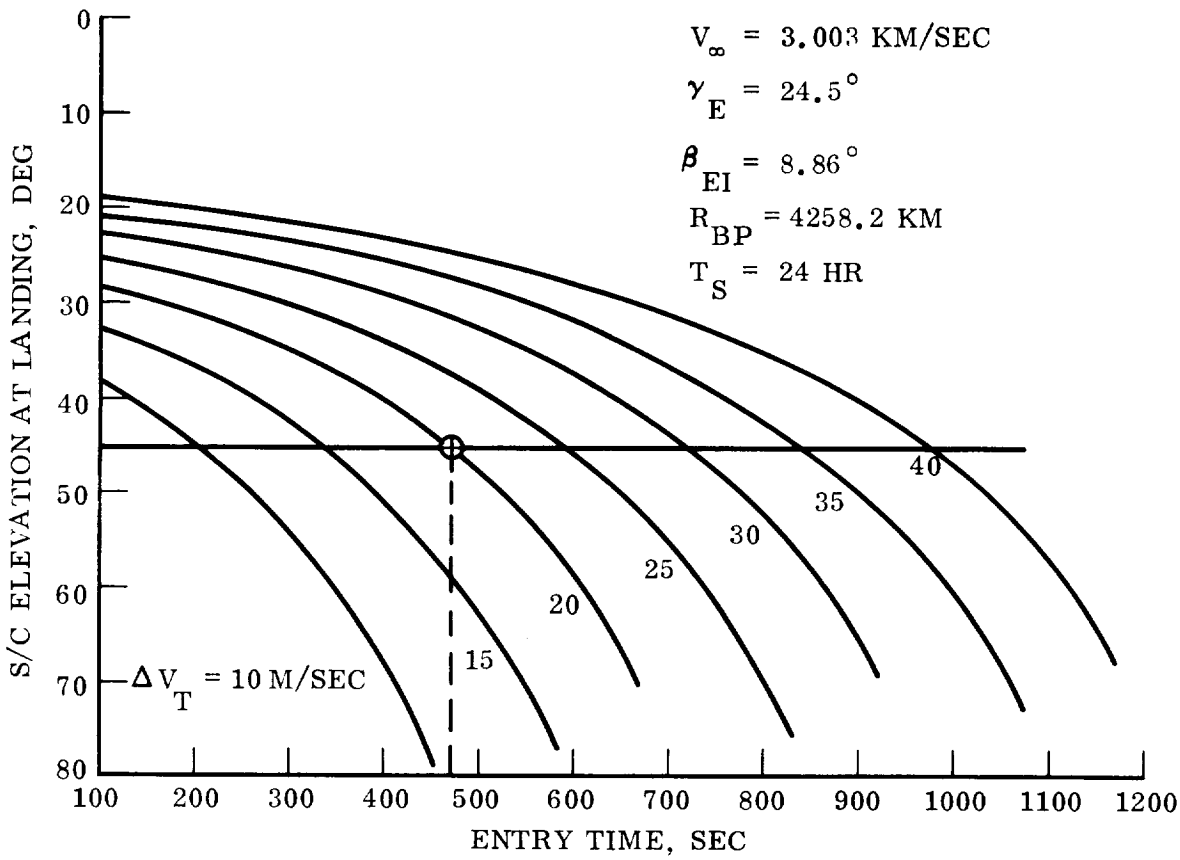

Figure 3.2.4-1. ΔV_T Tangential Velocity Determination

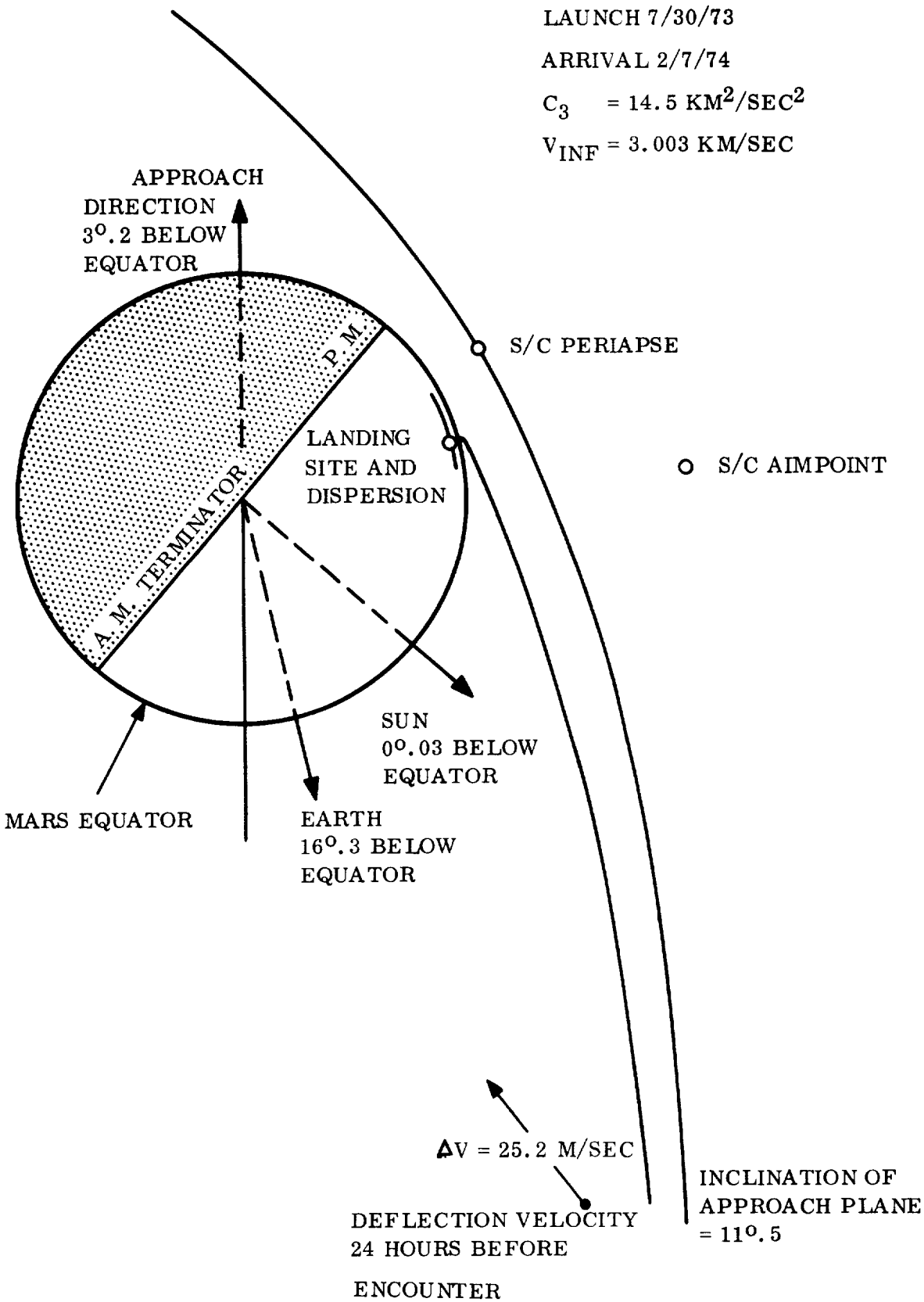

Figure 3.2.5-1. 1400 lb Mars Hard Lander Capsule Reference Mission Arrival Configuration

Mars equatorial plane. The nominal Support Module and Capsule trajectories are indicated approximately; their plane is actually inclined to the equator at an angle equal to 11.5°. More detail about the entry and landing configuration is shown in fig. 3.2.5-2; this figure shows, in the trajectory plane, the Support Module and Capsule positions at landing for the nominal case (with MEAN atmosphere) and the two extreme cases of dispersion (minimum path angle with MIN atmosphere and maximum path angle with MAX atmosphere).

TABLE 3.2.5-1. REFERENCE MISSION SUMMARY

Transfer	
Launch	July 30, 1973
Arrival	February 7, 1974
Flight time	192 days
Launch energy	14.462 km^2/sec^2
Communication distance	179.7×10^6 km
Approach velocity	3.003 km/sec
ZAP angle	130.50°
Approach, Entry	
Approach	Posigrade
Separation Velocity	25.2 m/sec (24 hr before periapse passage)
Approach hyperbola periapse altitude	1000 km
Entry path angle	21°
Entry velocity	18,772 ft/sec
Inclination of approach plane	11.536°
Landing latitude	10° N
Sun angle at landing	57.5°
Dispersions (3σ)	
Entry path angle	16.8 - 21.0 - 24.5°
Periapse altitude	1128 - 1000 - 872°
Downrange, MIN atmosphere	800 - 0 - 450 km
MAX atmosphere	630 - 0 - 420 km
All atmospheres	830 - 0 - 480 km
Cross range	±80 km

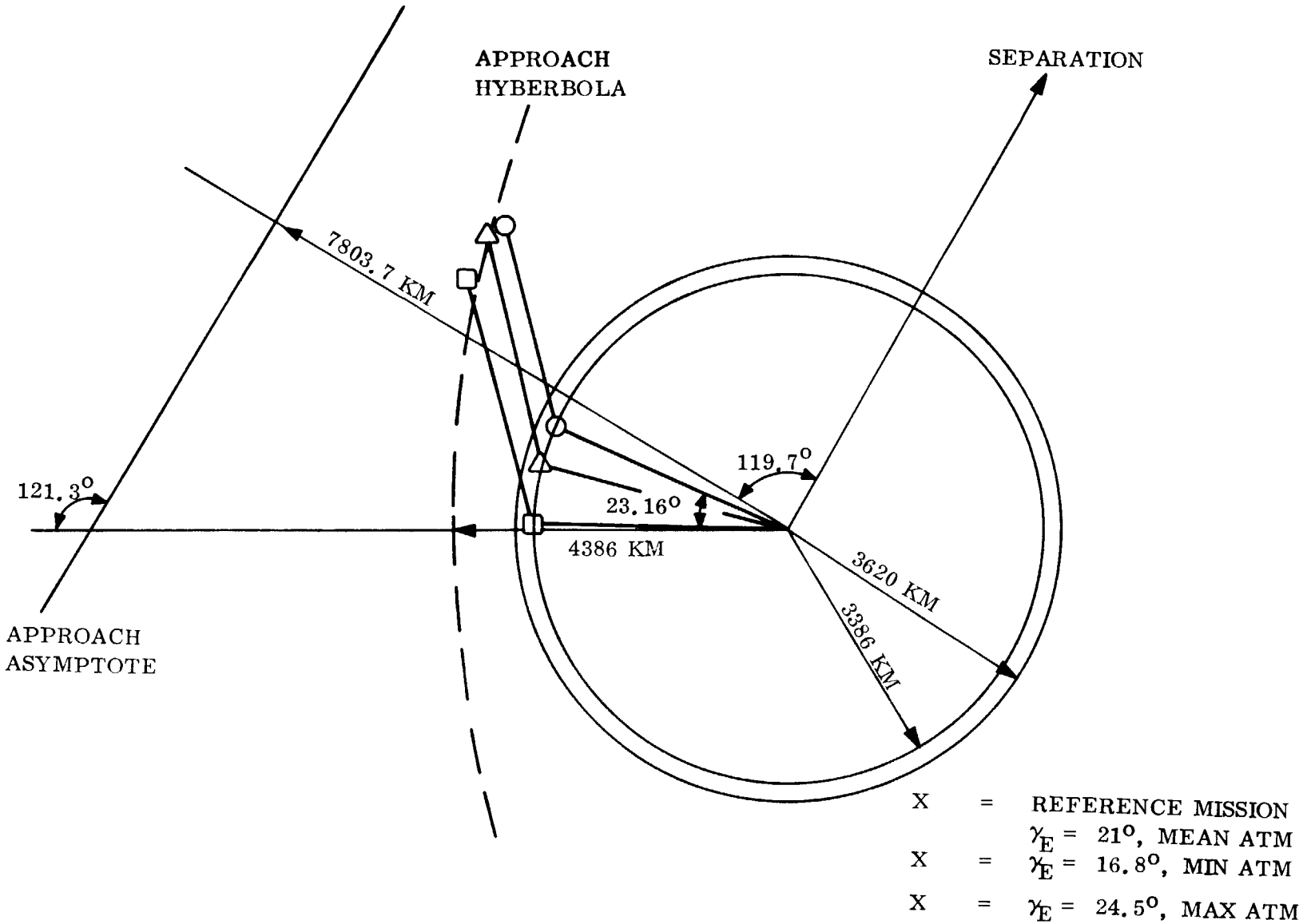

Figure 3.2.5-2. Downrange Dispersions (Atmosphere and Entry Path Angle Variations)

Capsule entry trajectories have been computed for the three atmosphere models, MIN, MEAN, and MAX, and for three approach conditions. The three approach conditions are the nominal, resulting in entry path angle equal to 21.0°, and two extreme dispersion cases, resulting in the minimum (16.8°) and maximum (24.5°) entry path angles. A number of important Capsule trajectory parameters are listed for all nine cases in table 3.2.5-2. In addition, some parameters are shown as functions of time in figs. 3.2.5-3 through 3.2.5-5 for the case of nominal path angle and MEAN atmosphere. Complete data for all nine trajectories are available in PIR 8860-PE-186.

The parameters shown in figs. 3.2.5-3 through -5 are:

3.2.5-3	Capsule altitude, km Mach number Capsule velocity, km/sec
3.2.5-4	Deceleration, Earth g's Dynamic pressure, lb/ft^2
3.2.5-5	Support Module to Capsule communication distance, km Support Module to Capsule range rate, km/sec Support Module elevation above landing horizon.

3.2.5.2 Post Landing Trajectory Design Data

The tangential component of the deflection velocity has been designed to make a 45° to 45° relay communication pass available, beginning not sooner than 150 sec after landing. Of the nine cases to be considered (three atmospheres and three entry path angles), the case with MAX atmosphere and maximum path angle has the Support Module rising at 45° elevation at the earliest time; this is the design case. In all other cases the Support Module rises at 45° elevation at a later time; in particular, the latest time is 432 sec after landing in the case of MIN atmosphere and minimum entry path angle.

The pertinent data is listed for all nine cases in table 3.2.5-3; this table shows the Support Module elevation and the communication range at landing and at 150 sec after landing; also the times (after landing) at which the Support Module is seen rising and setting at 45° elevation, and the range at those times. The elevation and range are shown as functions of time after landing for the specific case of MEAN atmosphere and nominal (21.0°) path angle in fig. 3.2.5-6; for the other eight cases the curves are nearly the same, but displaced in time forward or backward. The complete set of graphs is available in PIR 8860-PE-186.

TABLE 3.2.5-2. ENTRY TRAJECTORIES, ATMOSPHERE AND ENTRY PATH ANGLE DISPERSIONS

Atmosphere	Min	Min	Min	Mean	Mean	Mean	Max	Max	Max
Entry Path Angle, deg	16.8	21	24.5	16.8	21	24.5	16.8	21	24.5
Impact Parameter, km	7953.7	7803.7	7653.7	7953.7	7803.7	7653.7	7953.7	7803.7	7653.7
Approach Hyperbola Periapse Alt., km	1128.5	1000	872.2	1128.5	1000	872.2	1128.5	1000	872.2
Entry Velocity, ft/sec	18772	18772	18772	18772	18772	18772	18772	18772	18772
Time, Entry to Landing, sec	370	242	194	387	278	232	455	366	322
Central Angle, Separation to Entry, deg	97.60	91.63	86.69	97.60	91.63	86.69	97.60	91.63	86.69
Central Angle, Separation to Landing, deg	117.89	104.42	96.80	115.89	103.89	96.52	113.41	102.79	95.78
Per Angle at Landing, deg	-1.78	-15.29	-22.93	-3.78	-15.82	-23.22	-6.27	-16.92	-24.46
Support Module Elevation at Landing, deg	14.66	23.77	29.42	18.13	25.74	31.11	25.00	31.47	36.22
Range to Support Module at Landing, km	3255	3331	3350	3078	3141	3157	2626	2693	2722
Velocity at Landing, ft/sec	89.7	89.9	89.8	94.3	94.3	94.3	76.3	76.3	76.3
Mach No. at Parachute Deployment	0.92	0.92	1.15	0.77	0.75	0.75	0.49	0.50	0.50

Parachute Deployment at $h = 4000$ ft

Reference Mission: $V_\infty = 3.003$ km/sec, $\Delta V_T = 20$ m/sec, $\Delta V_N = 15.3$ m/sec,

$\gamma_E = 21^\circ$, $\gamma_{E\,max} = 24.5^\circ$, $\gamma_{E\,min} = 16.8^\circ$, $T_S = 24$ hr

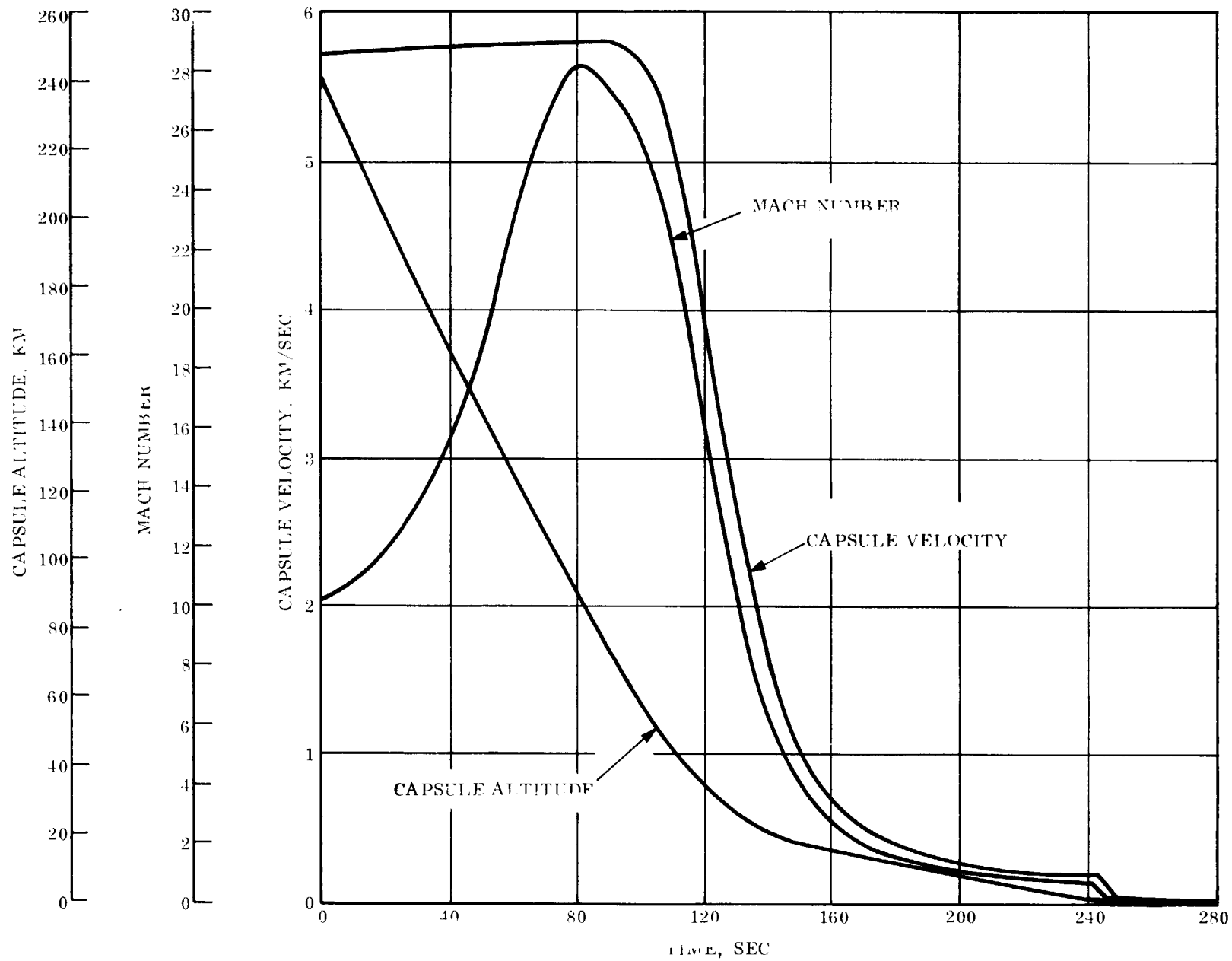

Figure 3. 2. 5-3. Capsule Altitude, Mach Number, and Velocity vs Time

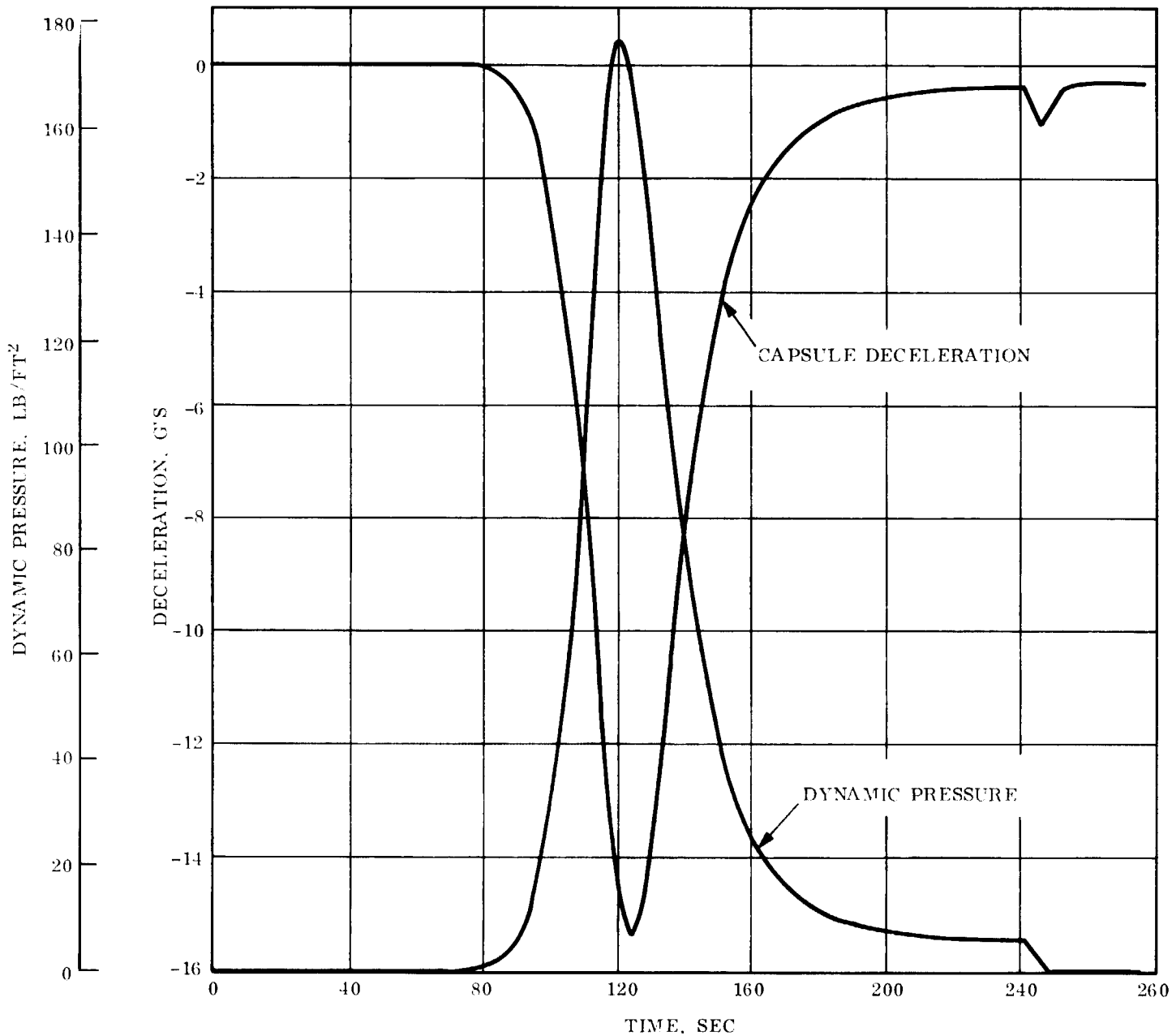

Figure 3. 2. 5-4. Capsule Deceleration and Dynamic Pressure vs Time

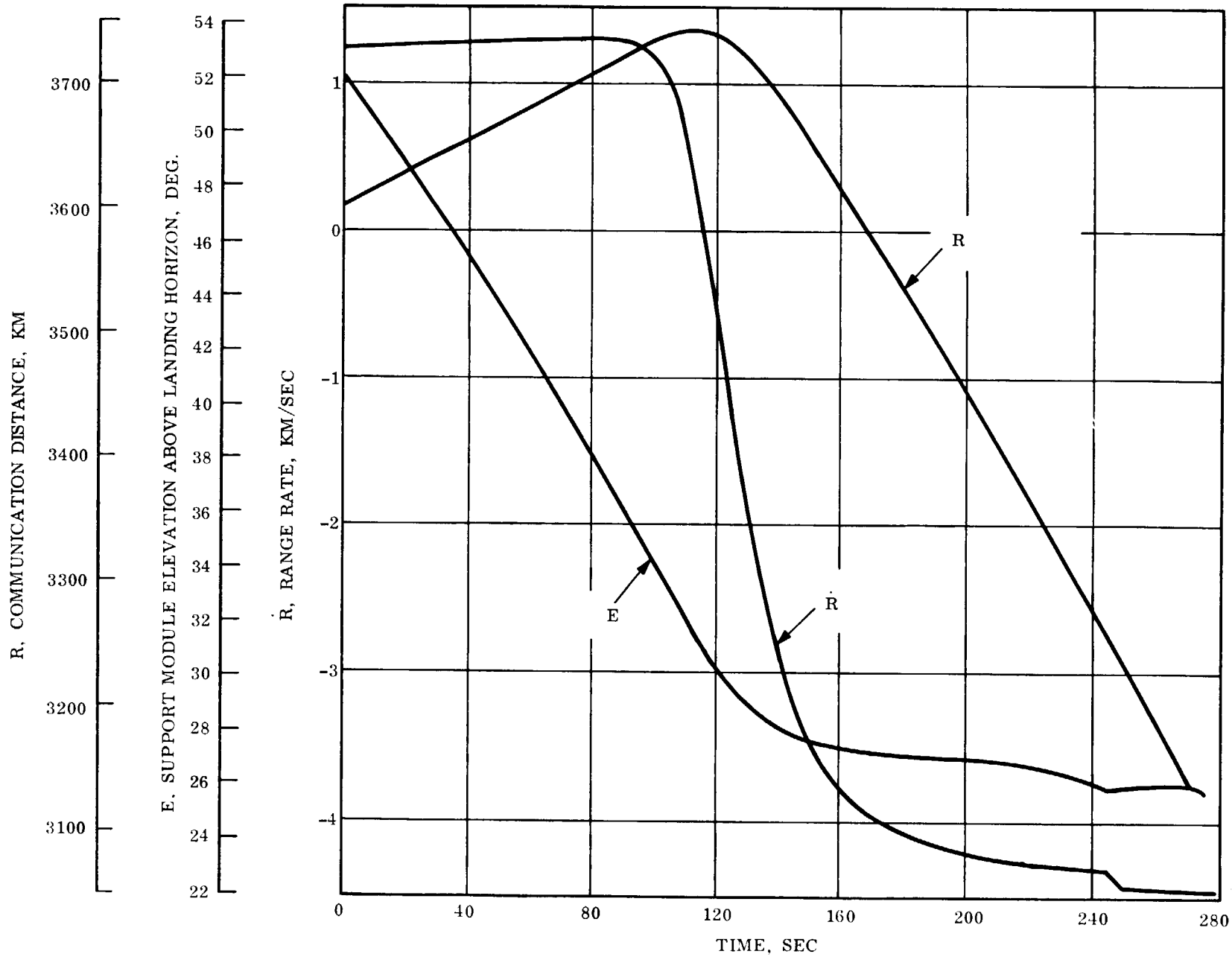

Figure 3. 2. 5-5. Relay Communication Parameters

TABLE 3.2.5-3. RELAY AFTER LANDING

Atmosphere Entry Path Angle, Deg.	Min. 16.8	Min. 21	Min. 24.5	Mean 16.8	Mean 21	Mean 24.5	Max. 16.8	Max. 21	Max. 24.85
E at landing	14.7	23.8	29.4	18.1	25.7	31.1	25.0	31.5	36.2
R_{BC} at landing	3255	3331	3350	3078	3141	3157	2626	2693	2722
E, 150 seconds after landing	20.8	29.0	34.3	24.9	31.8	36.8	34.5	39.9	45.0
R_{BC}, 150 seconds after landing	2616	2690	2700	2433	2505	2522	2000	2073	2100
t, at E = 45° rising	432	390	332	380	335	285	253	260	160
R_{BC}, at E = 45° rising	1510	1730	1940	1580	1760	1960	1630	1830	2060
t, at E = 45° setting	870	820	788	820	767	748	698	660	640
R_{BC}, at E = 45° setting	1570	1270	1170	1540	1290	1170	1490	1280	1180

E = elevation of Support Module above Lander horizon (deg.)

R_{BC} = range from Lander to Support Module (km)

t = time elapsed after landing (secs)

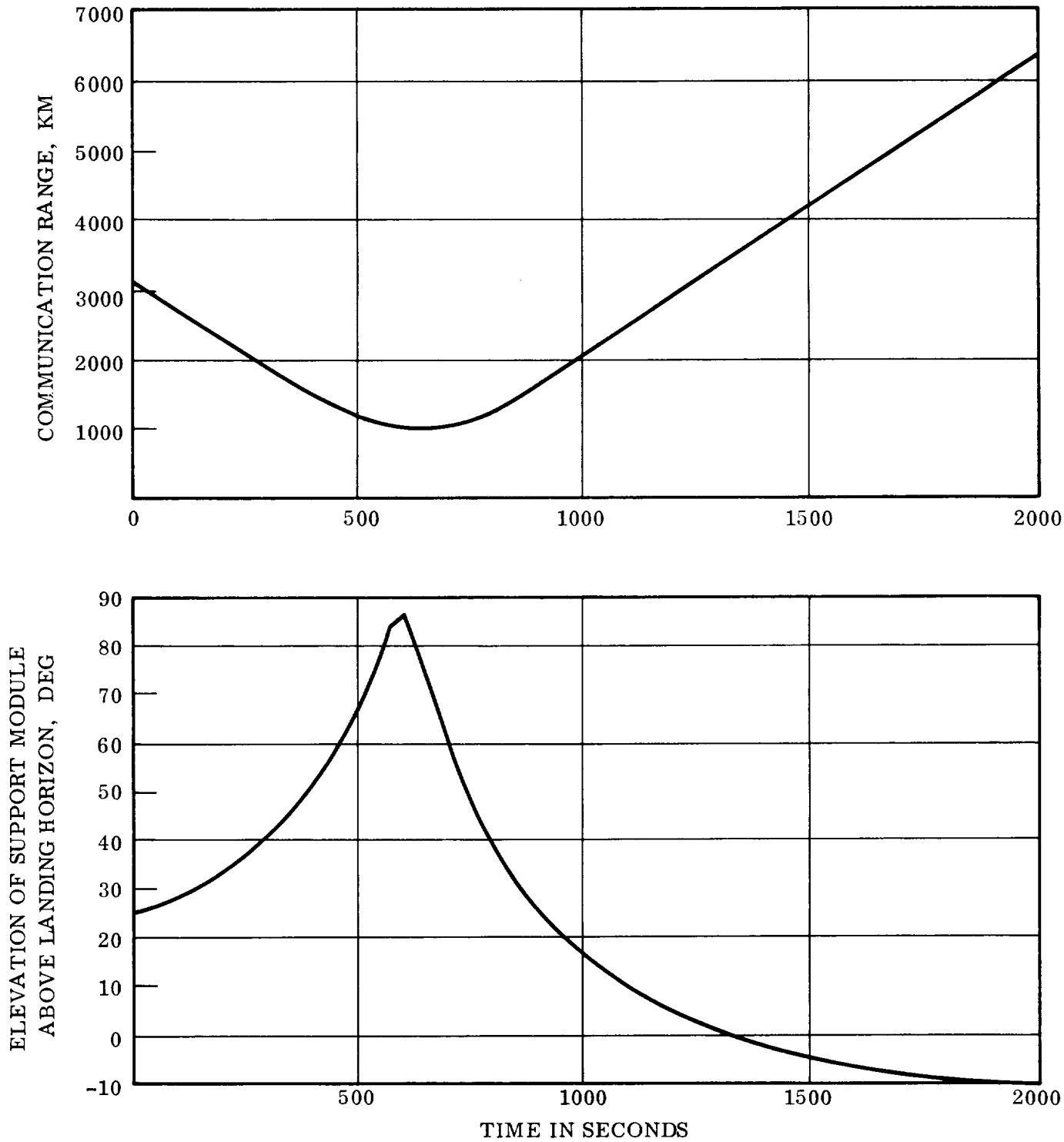

Figure 3.2.5-6. Relay Communication after Landing

The Support Module elevations and ranges are also shown in fig. 3.2.5-7; this diagram contains the times after landing at which the Support Module reaches elevations of 15, 34, 45 and 90°. It is of interest to observe how the pattern for the three entry path angles in the MAX atmosphere is maintained, but displaced to the right, for the MEAN and MIN atmospheres. This displacement is due to the longer entry times and causes the Support Module to be at only 14.7° elevation at the time of landing in the case of MIN atmosphere and minimum path angle. Therefore, if dispersion analysis is to include the range of atmospheres, there may be a possibility of having no relay communication at the time of landing. On the other hand, if it is thought that the Martian atmosphere will be better known in 1973 than it is now, the dispersion analysis need not consider a range of atmospheres. The tangential component of deflection velocity can then be designed for a particular atmosphere, and the pattern of Support Module elevation can be made to look like the pattern for MAX atmosphere in fig. 3.2.5-7. Due to the entry path angle dispersion, the Support Module elevation at landing need then not vary more than from 36.2 to 25°, so that a high probability is obtained for having relay communication at landing (in addition to having the 45 to 45° pass).

PARACHUTE DEPLOYED AT 4000 FT ALTITUDE

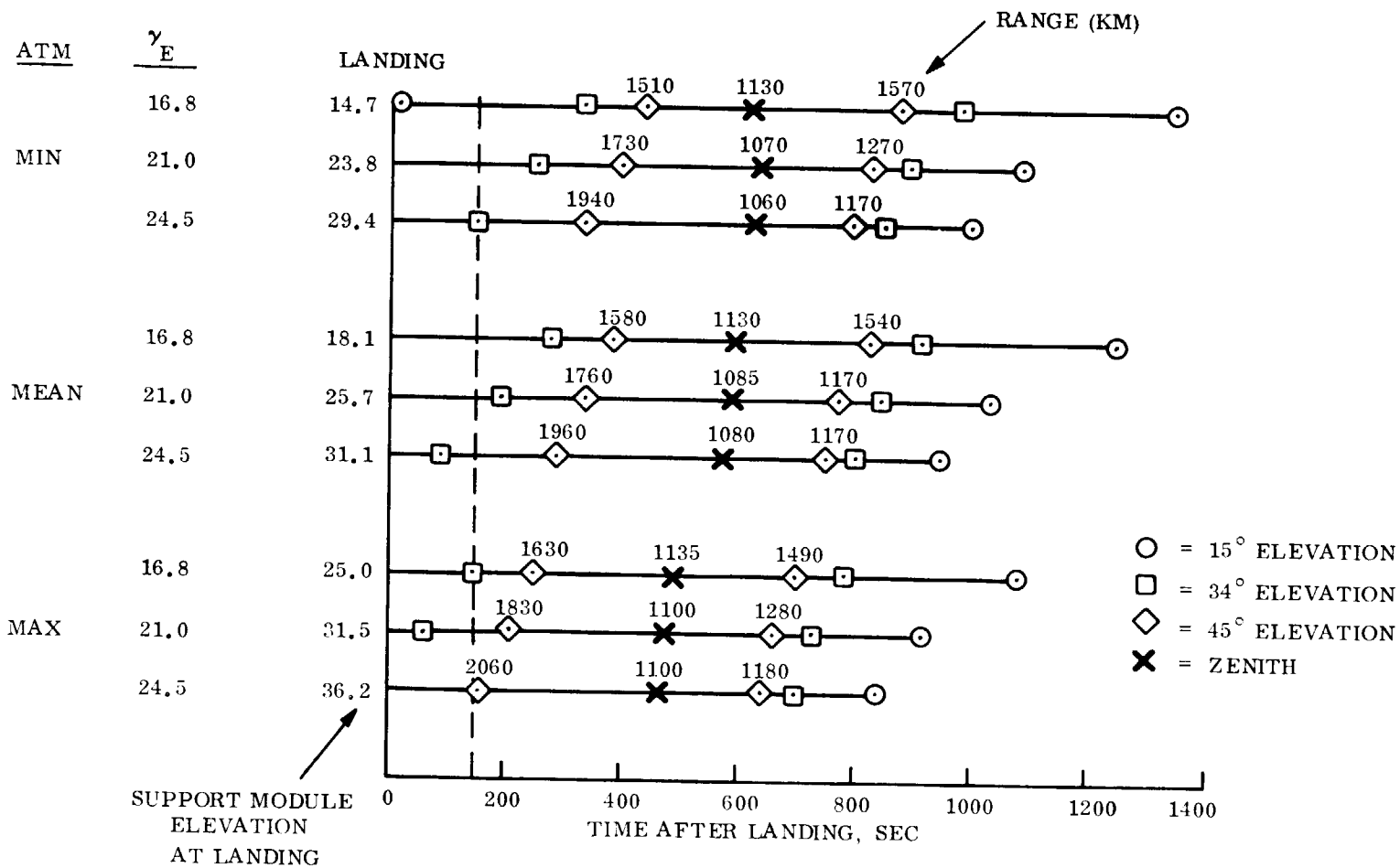

Figure 3. 2. 5-7. Communication after Landing - Geometry

3.3 RETARDATION DESIGN RATIONALE

The current state of knowledge of the Martian environment reflects significant uncertainties in parameters critical to retardation design. Accordingly, statistical models which attempt to represent the state of uncertainty of the environment, for use in the design process (refs. 3.3-1 and 3.3-2). Methods for the use of statistically defined environments in design evolution, especially when the effects of various parameters interact strongly, are not well established. The most direct approach, and the one adopted for design of the 1400 lb Lander, is to select a representative "worst case" value of each environmental parameter and then configure a design which can endure simultaneous occurrence of all parameters at these values. Depending on how realistically these design parameter values are chosen, the resulting design is likely to be conservative with respect to the probability of encountering an environment which precludes mission success. On the other hand, such an approach does not necessarily produce a weight-efficient design as it does not properly accout for the fact that the simultaneous occurrence of "worst case" values of all parameters is very improbable -- furthermore, the fact that one parameter exceeds its "worst case" value does not necessarily imply failure, as the mission may be saved by favorable values of other parameters. If one is overly zealous in identifying design conditions, the payload can be substantially reduced. An example of this is indicated by fig. 3.3-1, which illustrates trajectories into the minimum atmosphere specified by ref. 3.3-2 for an entry angle typical of the worst (from a retardation standpoint) that can occur. The dashed lines superimposed on this plot at particular altitudes represent the probability the local surface elevation will exceed that value -- for example, the line labeled 10 percent indicates the local elevation will exceed 13 kft with probability 0.1. These probability levels were obtained by assuming a uniform distribution of the density for each bar in the surface elevation histogram of ref. 3.3-2.

Thus, if an altimeter is set to deploy a parachute at a reading of 4 kft from an entry vehicle with a ballistic parameter of 10 lb/ft^2, there is about a 20 percent chance that the parachute will be deployed at a Mach number greater than two. Note that this 0.2 is not a total probability; it merely represents a conditional probability based on the minimum atmosphere and 25° entry path angle. If this conditional probability is required to be a very low value such as 0.01, the ballistic parameter would have to be reduced to about 6 lb/ft^2. For a fixed "all up" Capsule weight, this would be an extreme penalty as Capsule diameter would have to be increased at a considerable cost in aeroshell and bio-barrier weight. Note that the occurrence of parachute deployment above Mach 2 is of negligible probability, given the mean atmosphere (fig. 3.3-2). Furthermore, even with the minimum atmosphere, the problem tends to disappear as the entry angle becomes smaller than 25° (fig. 3.3-3).

3.3.1 RETARDATION DESIGN RATIONALE FOR 1400 LB LANDER

A point to be emphasized is that design environments can be chosen which compound margins of safety to a degree which precludes a useful mission. For preliminary design of the Hard Lander, a balance was sought between payload weight and probability of success, a consideration which required selection of certain design environments at values which have non-negligible probability of being exceeded. The result is that one can identify certain low probability combinations of environments for which the design is marginal. In particular,

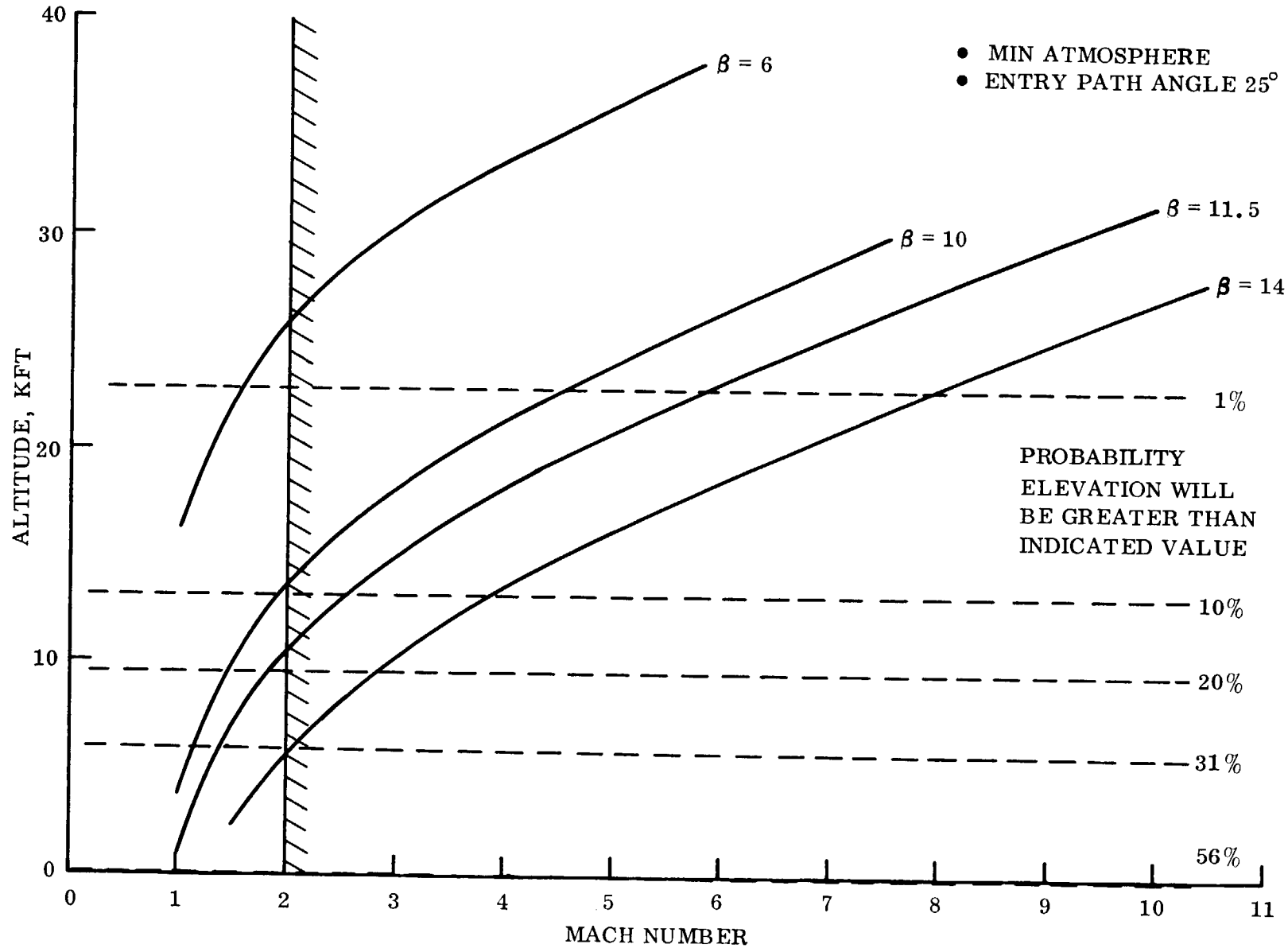

Figure 3.3-1. Influence of Elevation Uncertainties on Altitude of Parachute Deployment (MIN Atmosphere)

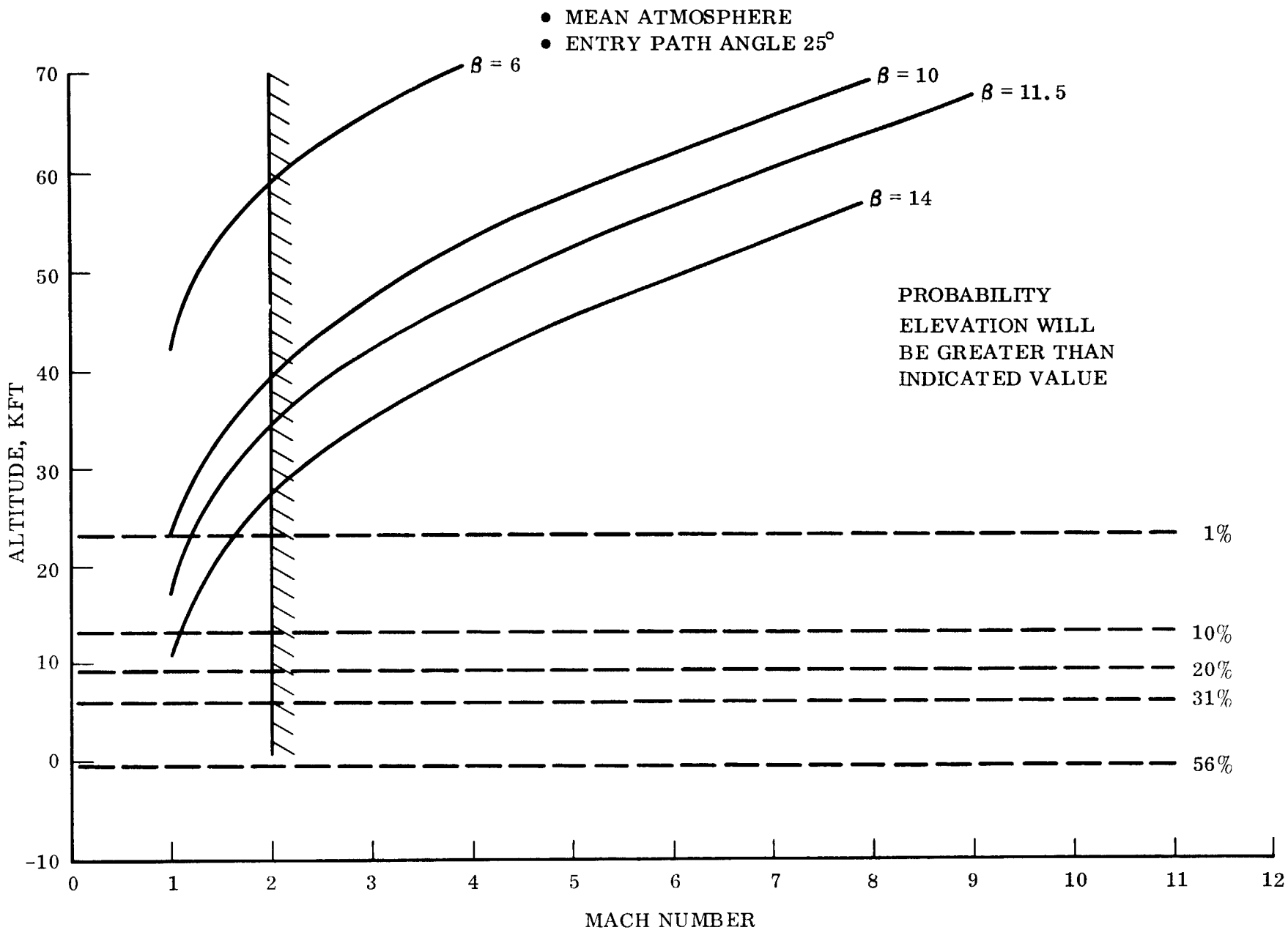

Figure 3.3.-2. Influence of Elevation Uncertainties on Altitude of Parachute Deployment (MEAN Atmosphere)

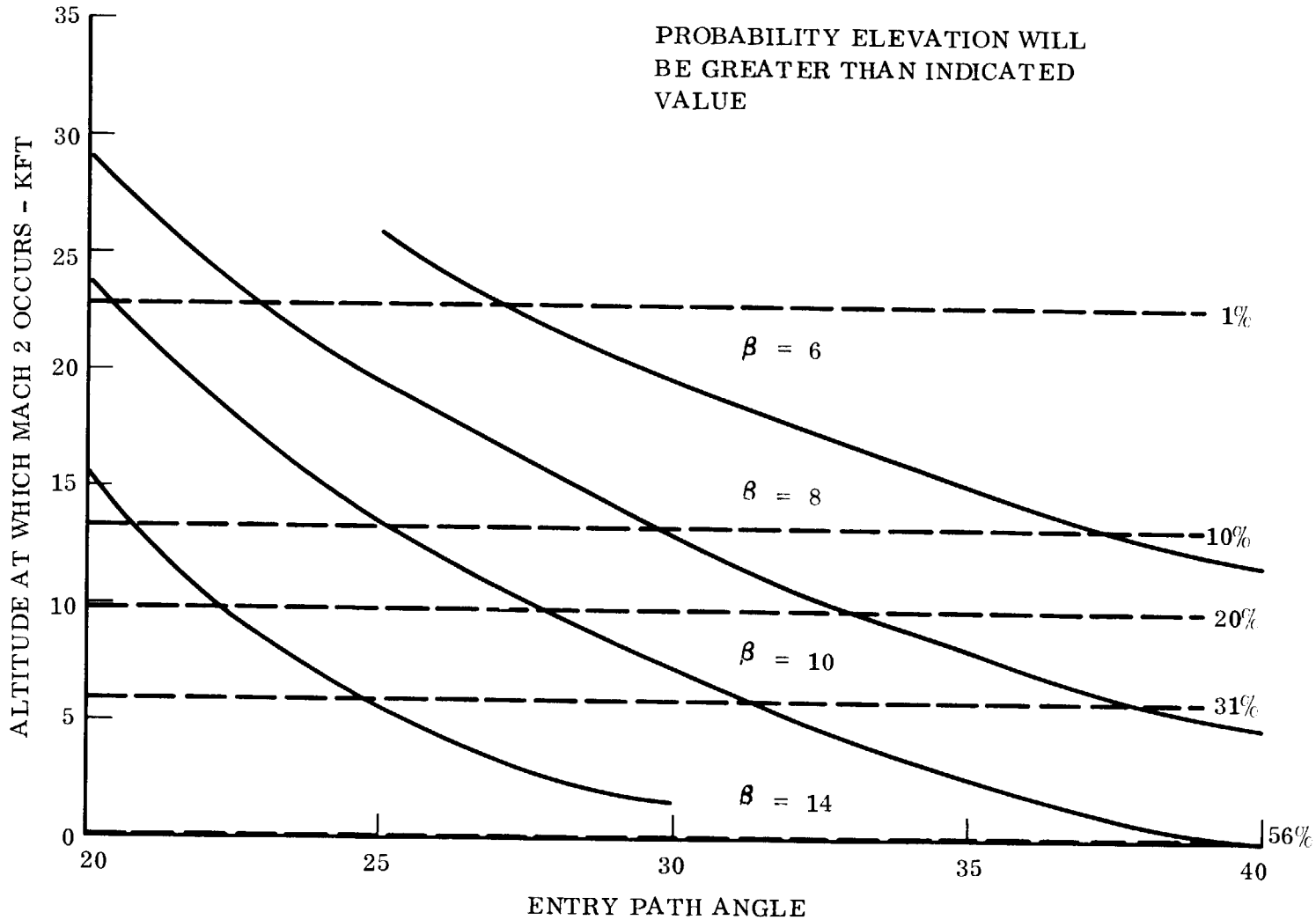

Figure 3.3-3. Effect of Entry Path Angle on Mach 2 Altitude (MIN Atmosphere)

the design environments which were selected at somewhat less than worst case levels are landing elevation, surface slopes, and rock size.

The design landing elevation was selected at 6 kft; according to ref. 3.3-2, the probability of landing at a higher elevation is approximately 0.3. However, this will cause difficulty only with certain relatively improbable combinations of atmosphere and entry path angle. Using a statistical design approach which is being developed (Section 3.3.2) to handle probabilistic environments, the probability that the 1400 lb Lander design will achieve Mach 2 before parachute deployment was found to be greater than 0.96 (assuming the three design atmospheres to be equally likely).

The design surface slope was selected to be 20°; according to ref. 3.3-2, the probability of a greater slope is approximately 0.05. Again, this does not represent a failure probability as the limiter is designed for a ±40° parachute sway angle (resulting from a worst case gust of wind) which adds directly to the surface slope in establishing the limiter design. Simultaneous occurrence of surface slopes greater than 20° and near maximum parachute sway angle in such a direction that effects are additive is very improbable.

The design rock size was selected to be 5 in. diameter. Assuming that the Mars landing site is similar to the Surveyor I site on the Moon, there will be approximately 10 rocks of larger size in each 100 square meters of surface area. With a Lander area of about one square meter, it can be argued that the probability of initial impact on a rock larger than 5 in. is approximately 0.1. As before, this does not represent a failure probability. Generally, failure will occur only if high impact velocity on an unyielding surface also occurs due to simultaneous occurence of a low density atmosphere, high velocity winds, and a hard surface. Fig. 3.3.1-1 indicates the cost of designing the impact attenuator for larger surface rocks.

With the exception of the environmental parameters discussed above, the 1400 lb Lander can tolerate other parameters at realistic "worst case" values extracted from ref. 3.3-2. A summary of important design oriented parameters is given in table 3.3.1-1.

The maximum Entry Capsule ballistic coefficient can be related to the parachute/Lander descent velocity as shown in fig. 3.3.1-2. The parachute/Lander descent velocity also links the parachute and impact limiter designs. Therefore, the selection of this descent velocity defines the limiter, parachute and aeroshell design requirements. The descent velocity is selected on the basis of a trade-off of the parachute and limiter subsystem weights as shown by fig. 3.3.1-3. This figure indicates that the minimum combined weight of parachute and limiter is obtained for a descent velocity of about 100 fps. This velocity has been selected as the design value for the 1400 lb Capsule. From fig. 3.3.1-2, a maximum Entry Capsule ballistic coefficient of 11.5 psf is obtained for the 100 fps descent velocity, assuming an altimeter setting of 4 kft and landing at 6 kft altitude. The entry retardation and impact limiter discussions which follow are based upon these design specifications, i.e., V_D = 100 fps and β_{MAX} = 11.5 psf.

TABLE 3.3.1-1. RETARDATION PARAMETERS

Constraint	Value	Remarks
Atmosphere	Langley defined minimum	Defined in ref. 3.3-2.
Maximum entry angle	25°	Based on 50 km (1σ) impact parameter error and realistic deflection maneuver errors.
Entry velocity	5.74 km/sec	Corresponds to July 30, 1973 launch and February 7, 1974 arrival. Design is insensitive to small changes.
Ballistic parameter	11.5 psf	
Maximum parachute sway angle	$\pm 40^{\circ}$ (with zero rate)	Based on multi-degree-of-freedom motion analysis with worst case gust.
Parachute diameter	67 ft	
Maximum parachute deployment velocity	Mach 2	Guideline based on Planetary Entry Parachute Program
Parachute deployment altitude	4 kft	
Maximum elevation of landing site	6 kft	Langley direction
Maximum surface wind speed	118 ft/sec	Vernal equinox in northern hemisphere (ref 3.3-2).
Maximum surface slope	20°	
Maximum impact deceleration	1000 Earth g's	
Surface bearing strength	Unyielding	
Maximum rock diameter	5 in.	

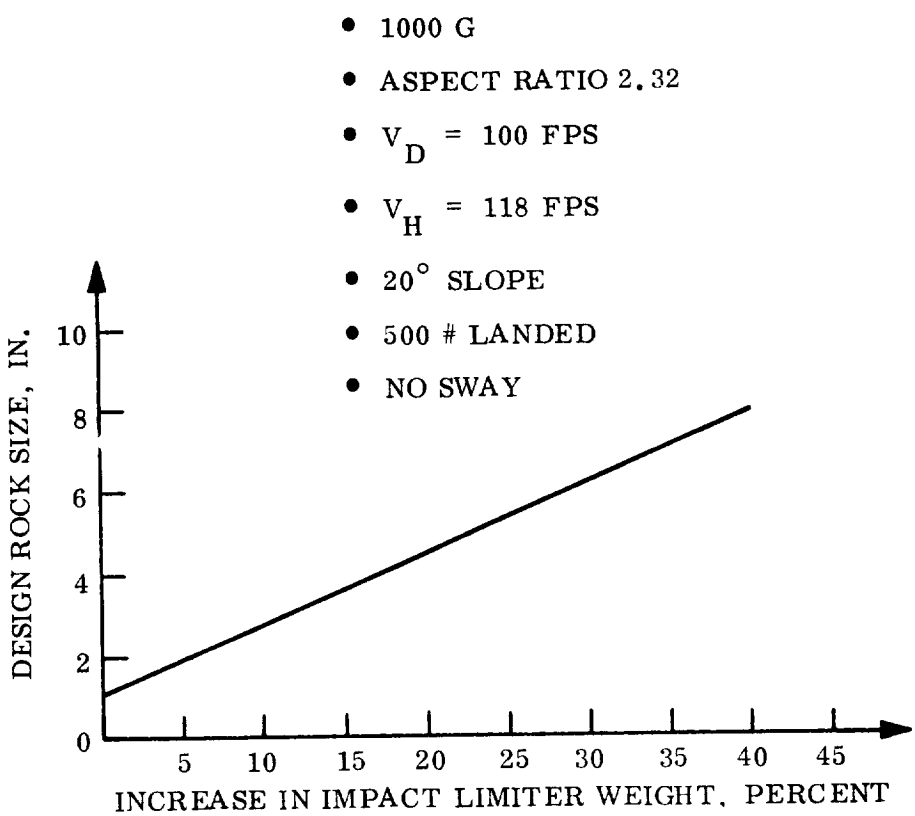

Figure 3.3.1-1. Effect of Rock Size on Limiter Weight

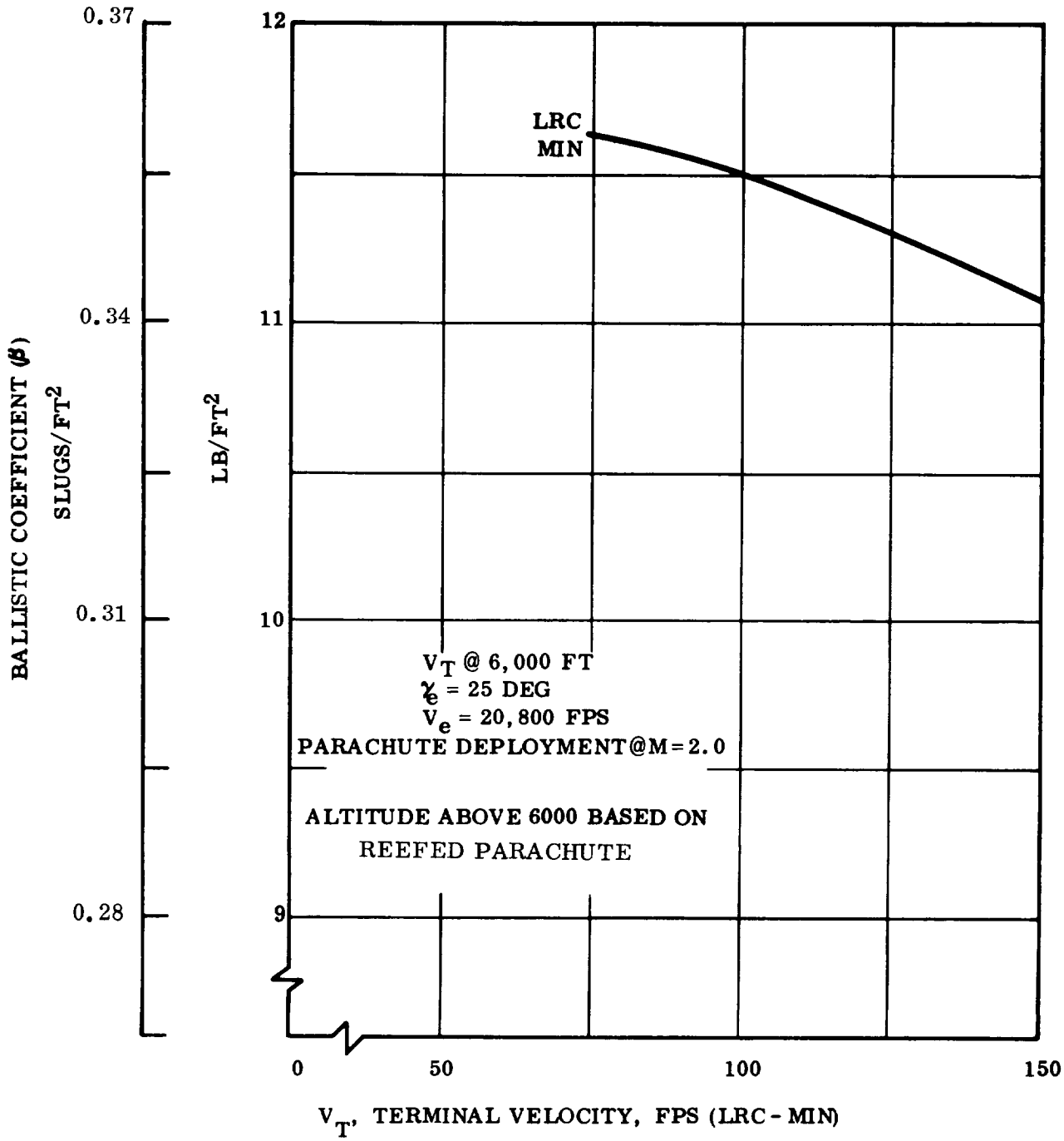

Figure 3.3.1-2. Terminal Velocity Constraint on Ballistic Coefficient

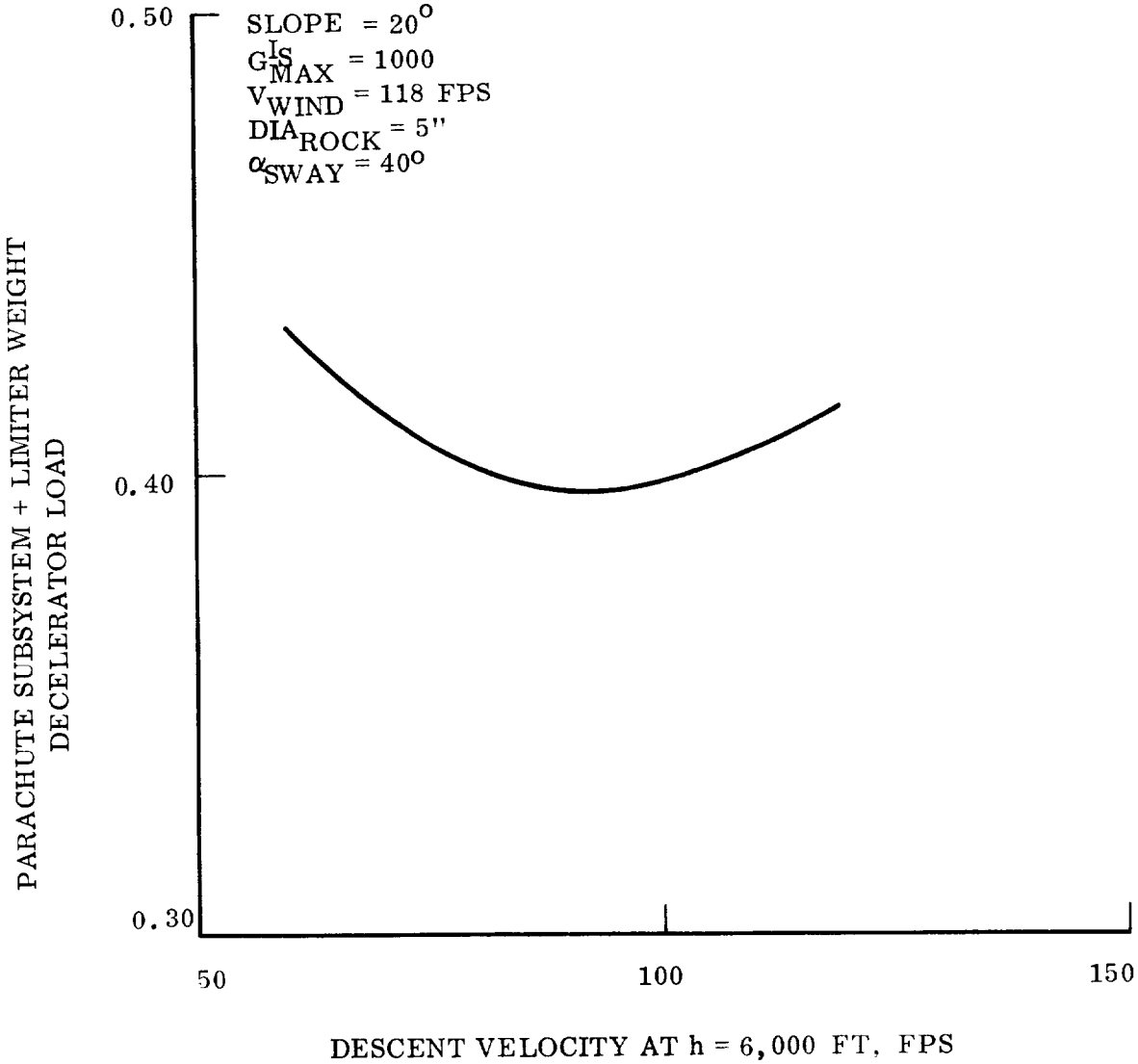

Figure 3.3.1-3. Lander/Parachute Descent Velocity Trade-off

3.3.2 DESIGN APPROACH FOR STATISTICALLY DEFINED ENVIRONMENT

In order to evaluate the effect of interacting environmental parameters on the overall probability of successful entry and landing retardation, an effort was established to develop a technique useful for design for a statistically defined environment. This section discusses this technique as it will be applied in the near future to the overall retardation design of a Mars Hard Lander.

3.3.2.1 Description of Environment

The mathematical technique identified for design performance evaluations requires discrete approximations to continuous distributions. The environmental parameters which have been identified as significant to the overall retardation design are:

1. Atmosphere
2. Entry angle
3. Hypersonic drag coefficient
4. Local terrain altitude
5. Parachute drag coefficient
6. Wind velocity
7. Surface slopes
8. Surface bearing strength
9. Parachute sway angle
10. Rock size.

Discrete distributions for each of these parameters will be developed based on refs. 3.3-1 and -2, plus additional estimates where required. As an example, several specific atmospheric models will be identified together with an estimated occurrence probability for each; the sum of the occurrence probabilities will be one. With regard to entry angle, a sample density function is shown in fig. 3.3.2-1. Similar density functions must be generated for the other parameters.

3.3.2.2 Description of Design

A Mars entry vehicle can be considered to consist of the aeroshell, parachute, impact limiter, and payload. The weight of these four subsystems will add up to an entry weight consistent with the 1973 opportunity. Furthermore, specification of the weight distribution among these subsystems together with a parachute deployment altimeter setting

permits a first order evaluation of system performance, given a specific environment. Performance of a specific system (specified by weight distribution and parachute deployment altitude) is then evaluated for all possible combinations of environmental parameters and weighted by the probability of occurrence of each combination. The measure of success of a specific system is the probability that deceleration of the payload does not exceed a specified level (e.g., 1,000 Earth gravitational units).

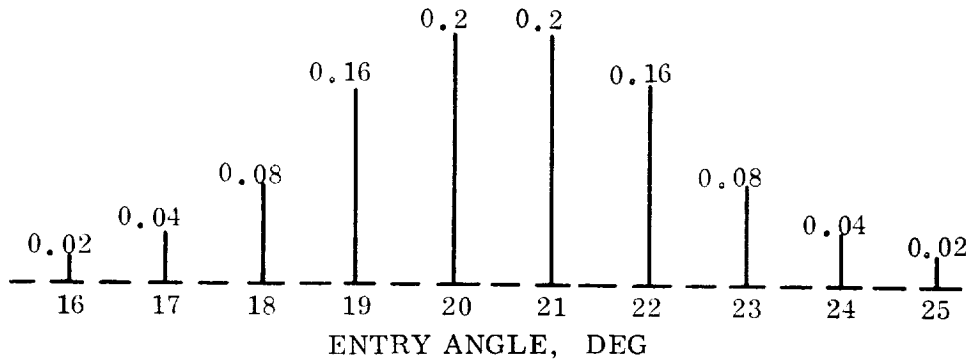

Figure 3.3.2-1. Sample Probability Density Function for Entry Angle

The logic used to identify an "optimum" system is illustrated by fig. 3.3.2-2; the type of result to be obtained by such a study is illustrated by fig. 3.3.2-3.

3.3.2.3 Example of Design Evaluation With Statistically Defined Environment

Part of the computer program (POSE-Probability of Success Evaluation) which will be used to optimize the Hard Lander retardation subsystems is complete and has been used to evaluate the probability that the 1400 lb Lander design will deploy the parachute at Mach 2 or below. This evaluation considered the effects of entry path angle, hypersonic drag coefficient uncertainty, atmosphere, and landing site elevation on probability of parachute deployment below Mach 2. Table 3.3.2-1 lists the discrete distributions of entry path angle and landing site altitude which were used. Variations in the drag coefficient were taken to be ± 5 percent (3σ) which produces a very small effect on Mach 2 altitudes compared to entry angle uncertainties; for this study, the effect was included in the entry angle statistics by spreading the 3σ entry angle values 0.2^{o}. The entry velocity was held at 5.74 km/sec. Two different sets of probabilities of occurrence were assigned to the three atmospheres - 0.33, 0.34, 0.33 and 0.1, 0.8, 0.1 for the MIN, MEAN, and MAX atmospheres, respectively. Table 3.3.2-2 summarizes the results.

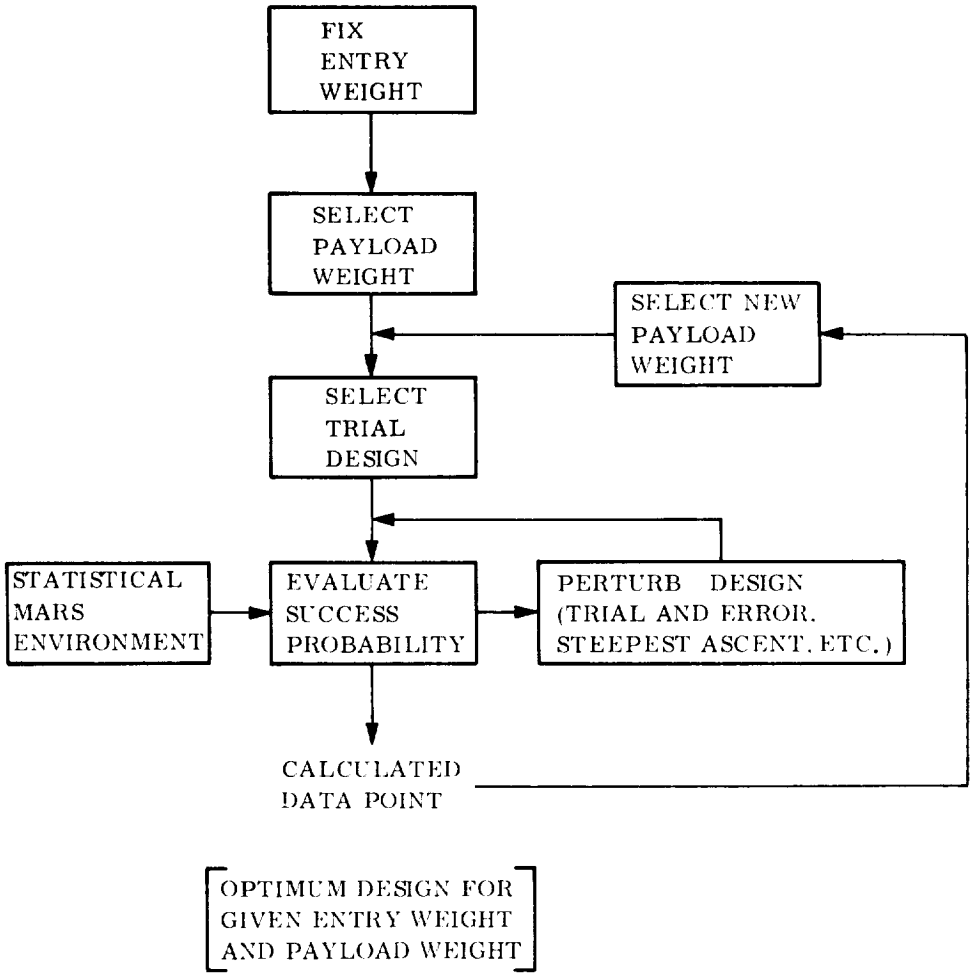

Figure 3.3.2-2. Optimization Logic

TABLE 3.3.2-1. DISCRETE DISTRIBUTIONS

	Value	Probability
Path Angle	16.37°	0.0026
	20°	0.2474
	21°	0.5
	22°	0.2
	24°	0.0474
	24.87°	0.0026
Elevation	8.5 km	0.01
	5.5	0.09
	2.5	0.29
	-0.5	0.51
	-3.5	0.1

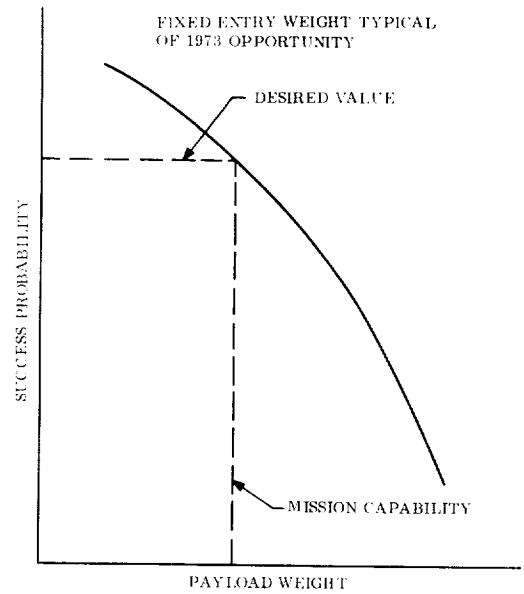

Figure 3.3.2-3. Format of Results

TABLE 3.3.2-2. PARACHUTE DEPLOYMENT SUCCESS PROBABILITY

Case	Deployment Altitude (kft)	Ballistic Parameter (psf)	Atmosphere Probability of Occurrence			Success Probability (%)
			MAX	MEAN	MIN	
1	4	11.5	0.33	0.34	0.33	0.962
2	4	10	0.33	0.34	0.33	0.974
3	10	11.5	0.33	0.34	0.33	0.895
4	4	11.5	0.1	0.8	0.1	0.989
5	4	10	0.1	0.8	0.1	0.992
6	10	11.5	0.1	0.8	0.1	0.968
7	4	8	0.1	0.8	0.1	0.999

3.3.3 REFERENCES

1. Voyager Environmental Standards, Voyager Project Office, NASA, September 25, 1967.

2. Mars Engineering Model Parameters for Mission and Design Studies (Preliminary Draft), Langley Research Center, NASA, May, 1968.

3.4 MISSION PROFILE

This section describes the mission sequence of events.

3.4.1 SUMMARY OF MISSION SEQUENCE

The Mars Hard Lander mission is divided into the following 11 phases:

1. Pre-launch
2. Launch and Injection
3. Interplanetary Cruise
4. Midcourse Maneuvers
5. Capsule Separation
6. Capsule Path Deflection
7. Capsule Cruise to Planet
8. Atmospheric Entry
9. Terminal Descent
10. Initial Landed Operations
11. Daily Landed Operations

The major events of the mission are depicted in fig. 3.4-1. The Pre-launch phase is the period when final checkout is performed and on-board stored commands are inserted.

During the Launch and Injection, Interplanetary Cruise and Midcourse Maneuver phases the Capsule is inactive except for periodic diagnostic checks which are performed through the Support Module telemetry system. Power is provided by the Support Module.

The Separation phase is defined as including all events required to effect separation of the Capsule from the Support Module. This phase starts 10 days prior to actual separation. Most of this time is required to charge the Capsule batteries,which are carried in a semi-charged state. After battery charging a detailed check out of the Capsule is performed using the Support Module command and telemetry systems.

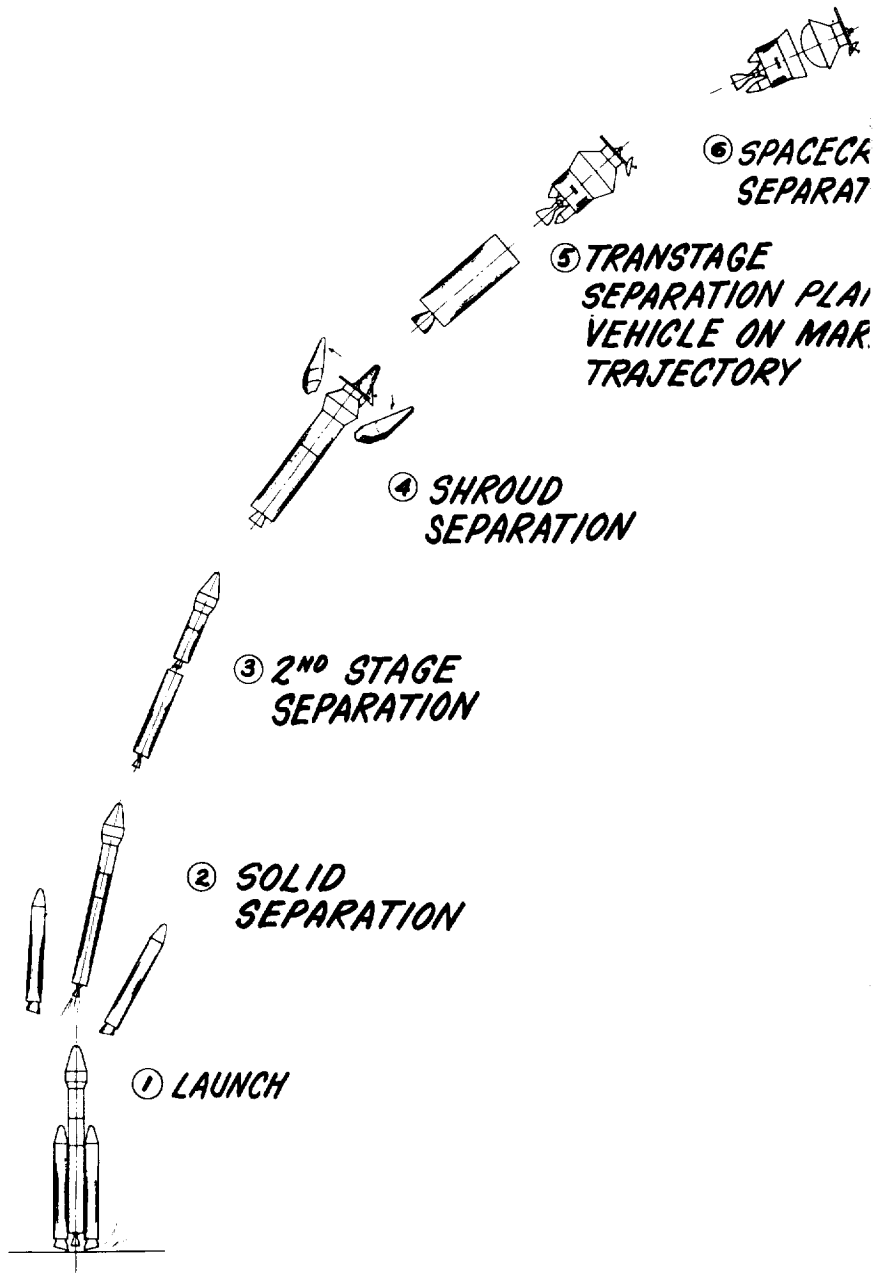

FOLDOUT FRAME 1

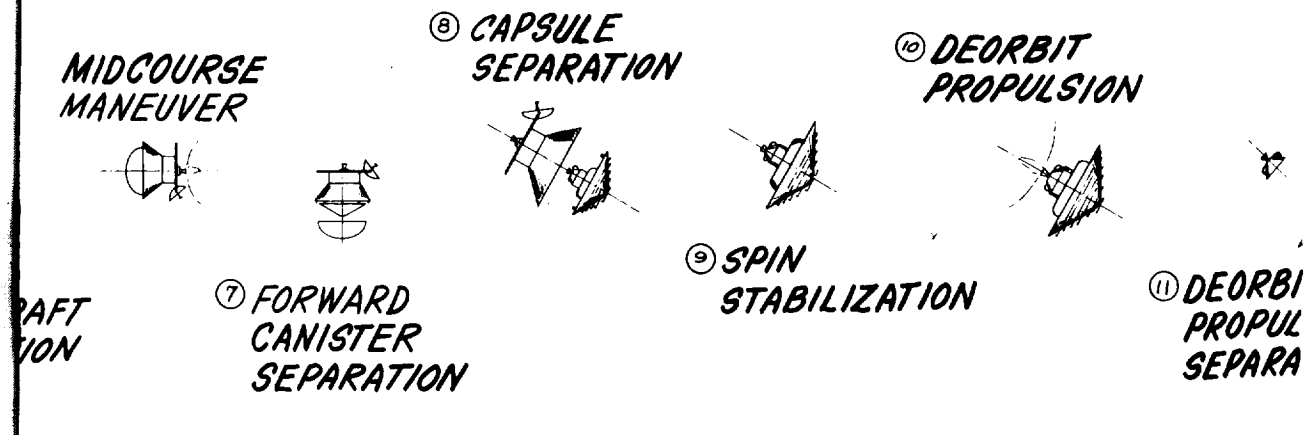

	TIME	EVENT	DESCRIPTION
1.	T_L 0	Launch	Booster function
2.	T_L + 1 min 59 sec	Solid stage separation	Booster function
3.	T_L + 4 min 15 sec	2nd stage separation	Booster function
	T_L + 4 min 30 sec	Pressurization and venting cycle	Relieve internal pressure and maintain steriliza
4.	T_L + 4 min 40 sec	Shroud separation	Booster function
5.	T_L + 7 min 50 sec	Transtage separation	Booster function
6.	T_L + 17 min	Spacecraft separation	Spacecraft function
7.	T_O - 1.5 hr	Canister forward section separation	Hot-wire nut and spring separation
	T_O - 1.4 hr	Capsule orientation	Spacecraft maneuvers to Capsule separation atti
	T_O - 0.1 hr	Switch to internal Lander power	Line contactor switches power source
8.	T_O (T + 193 days)	Capsule separates from Command Module	Hot-wire IFD; electrical separation Hot-wire nut and spring mechanical separation
9.	T_O + 0.5 sec	Spin stabilization	Initiation pulse to normally closed explosive val· Spin-up to 25 rpm
10.	T_O + 30 min	De-orbit propulsion	Initiation pulse to normally closed explosive val· Termination pulse to normally open explosive va
11.	T_O + 32 min	Thrust cone separation	Hot-wire IFD; electrical separation Hot-wire nut and spring mechanical separation
12.	T_O + 24 hr 12.3 min	Entry, de-spin and aerodynamic deceleration	De-spin initiation and system turn-on
13.	4,000 ft	Parachute deployment	Mortar eject pyro initiation
14.	4,000 ft + 4 sec	Aeroshell separation	Hot-wire IFD; electrical separation Hot-wire nut and spring mechanical separation
15.	150 ft	Parachute separation	Guillotine electrical separation Hot-wire nut parachute and container separation
16.	0. ft	Impact	Lander initiates Landed operations after 2.5 mir delay

OPERATIONAL FLIGHT SEQUENCE FROM LAUNCH TO IMPACT

FOLDOUT FRAME 2

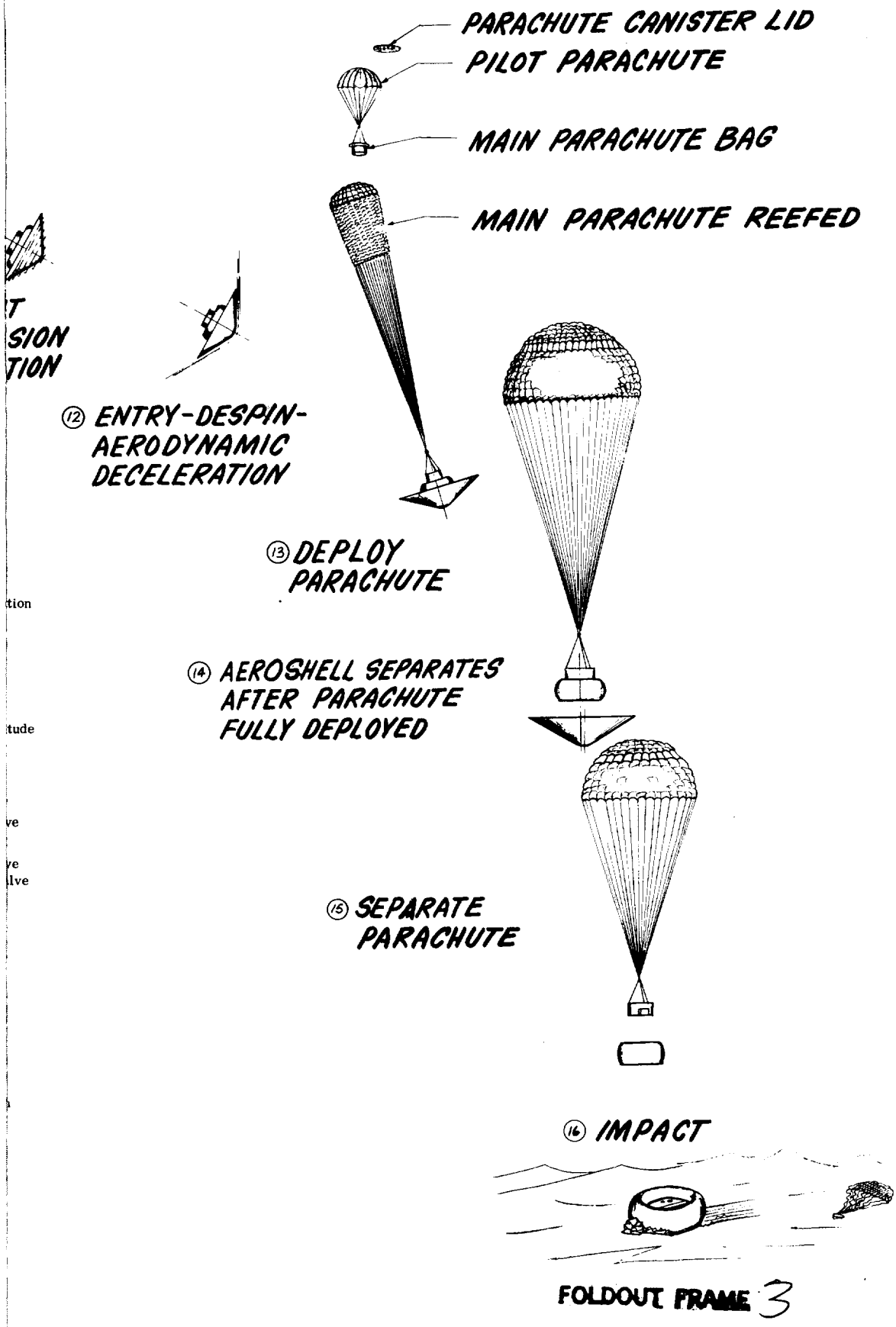

Figure 3.4-1. Sequence of Events

The Capsule is separated from the Support Module 24 hr before entry. This choice is not particularly critical. In general, however, late separations increase the path deflection impulse requirements, whereas early separations increase the electrical energy (battery) that must be carried for the longer cruise. Late separations also offer the possibility of improved estimation of the impact parameter and consequently narrower entry corridor. This advantage however, begins to appear not before 6 hr before periapsis passage. This appears to be too late to be useful.

Prior to Capsule separation the forward portion of the biological canister is released. The Support Module is then maneuvered to the position required for applying the path deflection impulse. The correctness of the achieved position is verified by ground interpretation of telemetry. Sufficient time is allowed between start of maneuver and separation for verification and possible correction of error while still separating at the nominal time.

The Capsule Path Deflection phase begins with separation. When this occurs the Capsule is spun up to provide stabilization during thrusting of the path deflection rocket motor. Spin-up is initiated very quickly after separation to prevent a buildup of errors in the pointing of the rocket motor as a result of tip-off rates caused by the separation device. This time, however, must be long enought to assure that separation has in fact occurred before spin-up is initiated. The sources of error of the thrust maneuver and their magnitude are shown in Section 5.11.

Initiation of rocket engine ignition, to effect flight path deflection, is delayed for 30 min after separation. This time is believed adequate to increase Support Module to Capsule distance sufficiently to preclude rocket exhaust from contaminating the Support Module. The particular time chosen is not critical. However, short times increase the probability of rocket exhaust impingement, whereas long times increase Capsule electrical energy requirements.

After rocket engine operation, which takes approximately 2 min, the propulsion system assembly (also called thrust cone assembly) is separated.

The Capsule Cruise phase begins at this point and continues for 24 hr and 12 min, until entry. During this time Capsule systems are shut down except for hourly 1 min intervals when diagnostic telemetry is transmitted. The frequency of sampling is an arbitrary compromise between frequent sampling to obtain meaningful diagnostic data and less frequent sampling in an attempt to conserve electrical energy which translates to battery weight. Six min prior to nominal entry, Capsule systems are turned on.

The entry phase consists of atmospheric entry with the aeroshell reducing Capsule velocity and atmospheric entry measurements being made.

The Terminal Descent Phase beings at 4 kft above the terrain. This altitude is sensed by a radar altimeter which provides a signal to deploy the parachute. The aeroshell is released about 4 sec later. Finally, at 150 ft above the ground the Lander is released from the parachute and it falls to the surface.

During the preceding two phases most commands for system operation are generated from sensed physical conditions rather than from a time base. For example, roll control to zero speed is enabled when 0.1 g deceleration is sensed. Parachute deployment and subsequent separation of the parachute is initiated on altitude. Physical parameters rather than time are employed because uncertainty in time of events is too large to be meaningful. These time uncertainties arise from time of flight errors while in heliocentric transit; from impact parameter (miss distance) errors; and from variations in the prediction of the atmospheric model.

Upon landing and coming to rest, the Lander begins its ground operations. These are separated into two phases. The first lasts about 20 min while the second about 2-1/2 days to end of mission.

Initial landed operations is the phase immediately after touchdown during which data transmission is by means of a relay link through the Support Module. The Support Module will be visible from the Capsule for a period of at least 401 sec sometime during a 22 min time span. The uncertainty in mutual visibility time is a result of entry angle dispersion and atmospheric uncertainty. All data is therefore transmitted in 401 sec and the transmission repeated for a total of three times. In this manner, at least one of the transmissions will occur while the Support Module is in view.

Photo imaging constitutes the bulk of data collection and transmission at this time. Some environmental and engineering diagnostic data is also transmitted.

The events comprised in this phase include equipment deployment, sequential picture taking, other scientific and engineering measurements, and transmission. The phase ends with the termination of photo imaging and relay transmission.

Since transmission at this time is at a rate of 70 kbps, the sequencing of the picture taking must be carefully planned to reduce wasteful transmission. At the present time the sequence is one in which the position and resolution setting of camera 2 is changed while camera 1 is taking a picture. The order is then reversed. The sequence, which is time based, is commanded by the computer and sequencer. The sequence is performed at increments of 1 sec, although if appropriate these could be made at fractional second increments.

During daily landed operations, soil is sampled to determine composition, water content, and life. Atmospheric measurements are also made. These data are stored and subsequently transmitted by the direct link to Earth.

The instrument sampling frequency is a compromise between the desire to obtain a significant quantity of data and the data storage, electrical energy, and data transmission rate limitations of the Lander. The daily measurement cycle includes one 2 hr and 40 min soil experiment. This consists of water detection, gas chromatograph, and mass spectrometer experiments. These experiments are performed with the soil heated to two different temperatures. The life detection experiment and atmospheric measurements are sampled every 20 min during the daily cycle. Details of these measurements are discussed in Section 5.1.

Direct link transmission takes place at 17-1/2 hr after touchdown. Beyond this the events are essentially repeated with 20 min atmospheric samplings and one Earth test per day.

The command receiver is turned on 16-1/2 hr after touchdown when the Earth comes into view and shut off at 18-1/2 hr after touchdown. In this manner direct commands may be executed if Capsule state must be changed.

3.4.2 CHECKOUT SEQUENCE

An in-flight checkout of the Capsule system is conducted prior to separation from the Support Module. Such a checkout may be performed by the computer and sequencer with a stored program or by the direct link command link. Both methods have certain merits as well as disadvantages. Table 3.4-1 implies that the checkout is performed manually by means of the Support Module command and telemetry system by showing it as a single event.

On the other hand, only 2 hr are indicated for the checkout. Such a short time is possible only with an automated checkout sequence. When a checkout program is determined and its method of implementation decided upon, its details will be shown on the list of commands.

In developing the in-flight checkout sequence the following basic twofold rationale will be employed:

1. The checkout sequence should demonstrate the degree of readiness of all systems (Capsule, Support Module, DSN, etc.) to perform.

2. The checkout should be oriented toward procedural and hardware alternatives. That is, the existence of an option should form the technical basis for checkout sequence priorities. An example would be science instrument checkout, and the option, possibly, could be reallocation of communication capability to "up" instruments at the expense of "down" instruments.

In performing the checkout sequence:

1. Telemetry sensors needed for operation are used, rather than checkout sensors, as a general rule. Deductions can be made as to the readiness and operability of Capsule systems. An example would be monitoring of voltages, state switches and quiescent dark currents associated with the image equipment electronics. If all were proper, especially dark levels, a deduction that the hardware was probably ready for operation would be justified.

2. The commands required for nominal operation are used to set up the in-flight check. Separate commands and flying stimulator equipment, for the purpose of in-flight checkout, will generally not be used. To implement the in-flight checkout, those ground commands which are required for nominal mission operation would be used. For example, the mass spectrometer instrument, part of the entry science, would be turned on in the attempt to get a telemetered readout showing an exclusive nitrogen environment (the canister being pressurized with sterile nitrogen).

The in-flight checkout sequences used should be selected for the degree to which they will support the mission. When a mission phase is considered which has alternative and back-up modes, the in-flight checkout sequence should be capable of giving some clue as to probability of a backup mode operating when a primary mode is in doubt because of some trouble. If, for example, prior to landing, some trouble is indicated in a particular telemetry mode, or with a particular landed science instrument, the sequence should be designed to assist in selecting a preferred alternate cycle of science operation and read back.

Every mission phase has some associated degree of option, even if only the decision to abort the mission.

3.4.3 COMMAND SEQUENCE

A list of commands has been generated for the entire mission. This list defines the sequence of commands and the time at which these commands are issued based on a nominal reference mission (defined in Section 3.2). This command list is presented in table 5.4-2 of Section 5.4 (Computer and Sequencer).

4. SPACECRAFT SYSTEM DESIGN SUMMARY

4. SPACECRAFT SYSTEM DESIGN SUMMARY

This section provides a summary description of the total 1973 Mars Spacecraft which consists of the Flight Capsule, the Support Module, and the necessary adapters for mating these two elements to each other and to the Launch Vehicle.

4.1 OVERALL SPACECRAFT SYSTEM DESCRIPTION

The preferred launch configuration for the spacecraft is shown in fig. 4.1-1 with the Flight Capsule mounted beneath the Support Module. Several alternatives were studied to arrive at this configuration and are shown in fig. 4.1-2. The major variables treated were mounting to the Launch Vehicle shroud vs a separate adapter, and mounting of the Support Module above or below the Flight Capsule.

Mounting to the Launch Vehicle shroud incurred a weight penalty, and appeared undesirable from an interface standpoint. Discussions with Martin-Marietta confirmed this view and that approach was abandoned. Mounting of the Support Module above the Flight Capsule provides a much cleaner interface between the two systems, and the preferred design was selected for that reason.

As can be seen in fig. 4.1-1, launch loads are carried through two adapter sections which are mated through a load carrying section of the sterilization canister. Several alternate arrangements for the canister/adapter, shown in fig. 4.1-3, were studied. They vary in the degree of integration between the canister and adapter structure. The preferred approach was selected primarily because of ground operation considerations. The aft dome of the canister can be removed and tests conducted with Capsule and Support Module mated with free access to the Lander during these tests.

The selected canister design is shown in greater detail in fig. 4.1-4. The canister is 115 in. in diameter to contain the 108 in. aeroshell. The load carrying portion of the canister is 14 in. high and is a triangular-shaped torque box structure, supporting the Entry Capsule system from its inside edge and transmitting the load through torsional shear to the eight support fittings mounted on the outer surface. The toroidal-shaped section is then capped forward and aft by dome-type covers to complete the sterilization canister.

The forward canister is a hemispherically shaped minimum gauge aluminum shell making a tangent at its maximum diameter through a quarter torus section. The aft canister is hemispherically shaped and is structurally sized for the internal pressure of 1.0 psig. This dictates the same minimum gauge aluminum as was selected for the forward canister.

The internal pressure is controlled to a differential of 0.5 to 1 psi during and after sterilization and during the powered flight phase. The pressure and venting system includes a 0.3 micron filter and a manually operated fill valve for purging and sterilization procedures.

The Spacecraft adapter is 123.2 in. in diameter, and packages in an 11 ft shroud. The Spacecraft adapter transmits the boost phase loads from the Spacecraft to the Launch Vehicle. The adapter is a semi-monocoque conical frustum, consisting of aluminum alloy skins, two interface rings and an intermediate ring, with eight major longerons running from the Transtage interface to the Spacecraft separation plane. Electrical and mechanical interfaces are provided at each end of the adapter. The adapter also contains the Spacecraft separation devices.

The Support Module Adapter is a lightweight "W" truss, extending from the interface ring of the sterilization canister up to the lower face of the Support Module. It functions to transmit the boost loads from the Support Module to the Flight Capsule support section and to provide mechanical support between the Support Module and Flight Capsule during mission cruise.

The vertical height would be approximately 22 in. depending on the final dome height of the aft sterilization canister. The 16 truss tubes of 1-1/2 in. diameter, 0.035 wall aluminum alloy tubes, interfaced with the Support Module octagon longerons and with the eight "bath tub" fittings, mounted externally around the reinforced sterilization canister. Attachment at each end would be by eight tension shear bolts. A separation joint, similar to the Mariner '69, could be readily incorporated at the Support Module interface.

The Spacecraft in the cruise configuration is shown in fig. 4.1-5. This configuration assumes the use of a fixed solar array on the Support Module. Alternatives are discussed in Section 4.3.

4.2 FLIGHT CAPSULE

An inboard profile of the 1400 lb Flight Capsule is shown in fig. 4.2-1. An exploded view of the major physical elements of the Lander are shown in fig. 4.2-2.

Capsule Separation and Deflection

During the cruise portion of the mission, the Capsule is relatively dormant with the exception of diagnostic engineering data. Just prior to Capsule separation from the Support Module, the canister is vented to relieve the internal pressure. The V-band is then released, allowing four springs to separate the forward portion of the canister at 2.5 ft/sec.

The Support Module orients the Capsule to the proper attitude for firing of the deflection engine. The Capsule is then released and spring separated at 1.5 ft/sec. from the aft portion of the canister. Remaining with the canister is the pressure and venting equipment used to maintain internal pressure between 0.5 and 1.0 psig throughout the ground and launch phase. Also, electrical equipment which is used in the Capsule/Support Module interface remains with the canister. This includes both power and telecommunication equipment.

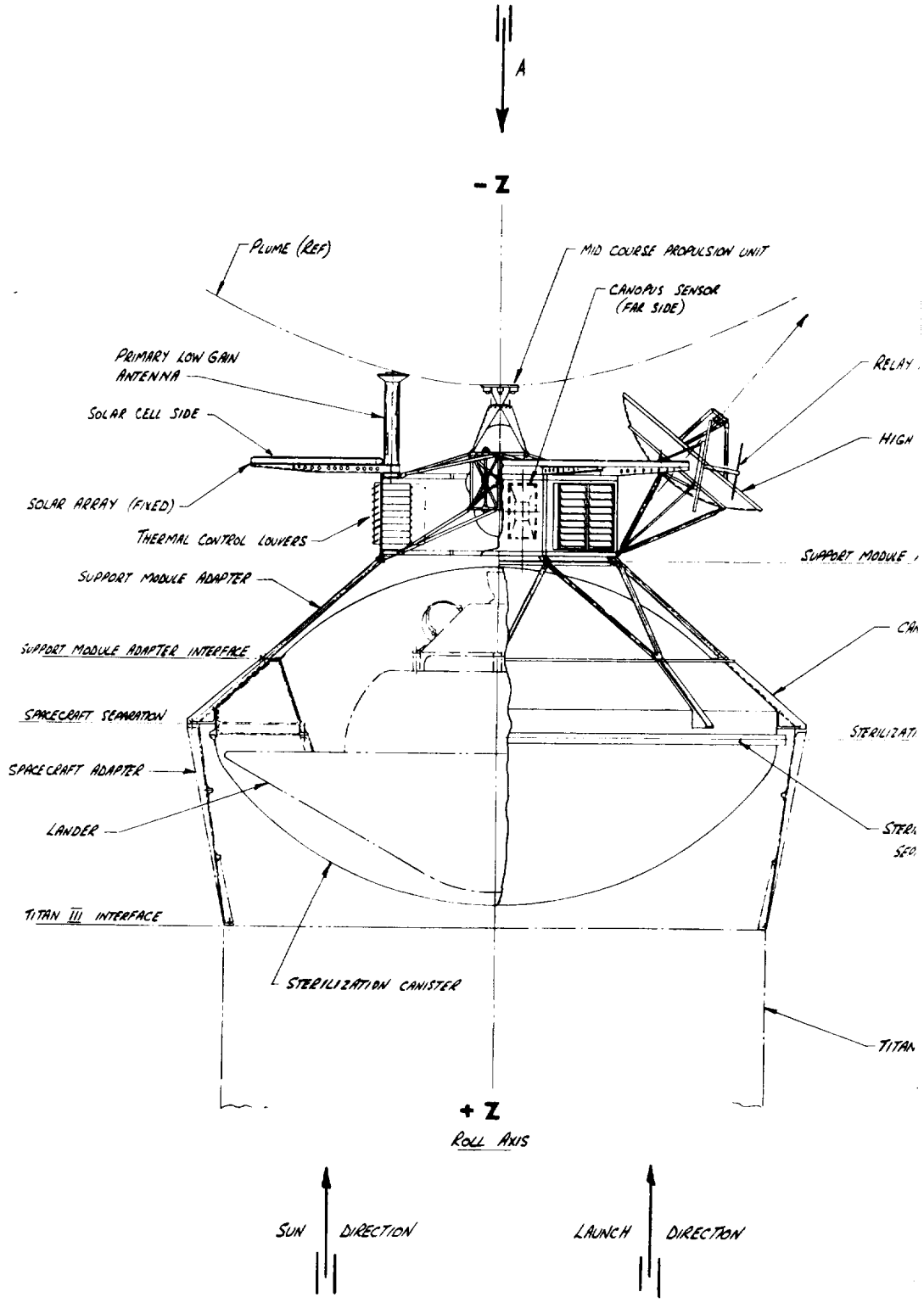

FOLDOUT FRAME 1

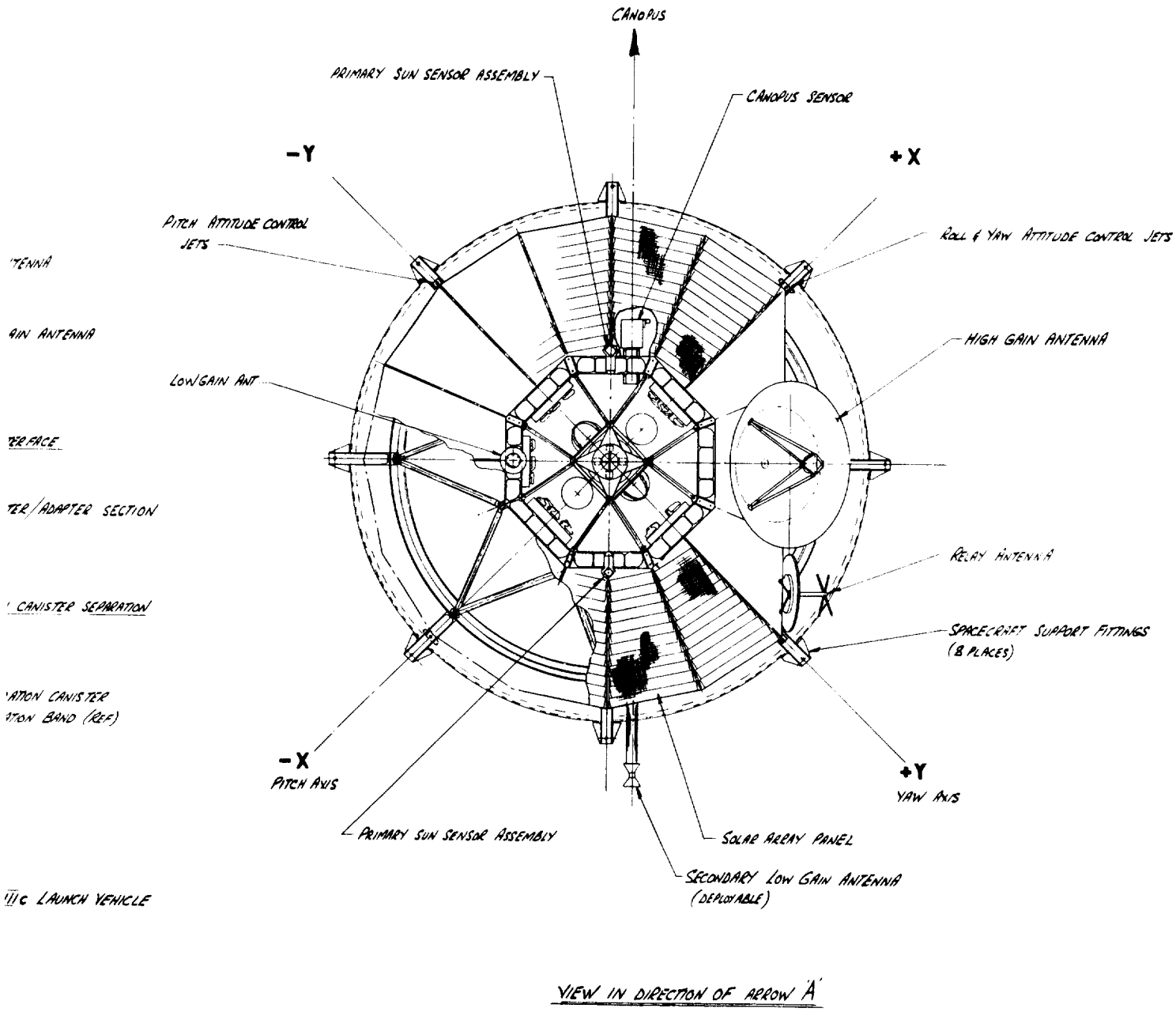

FOLDOUT FRAME 2

Figure 4.1-1. Selected Launch Vehicle Configuration

- SHROUD SEPARATION
- SUPPORT MODULE INTERFACE
- LOAD PATHS

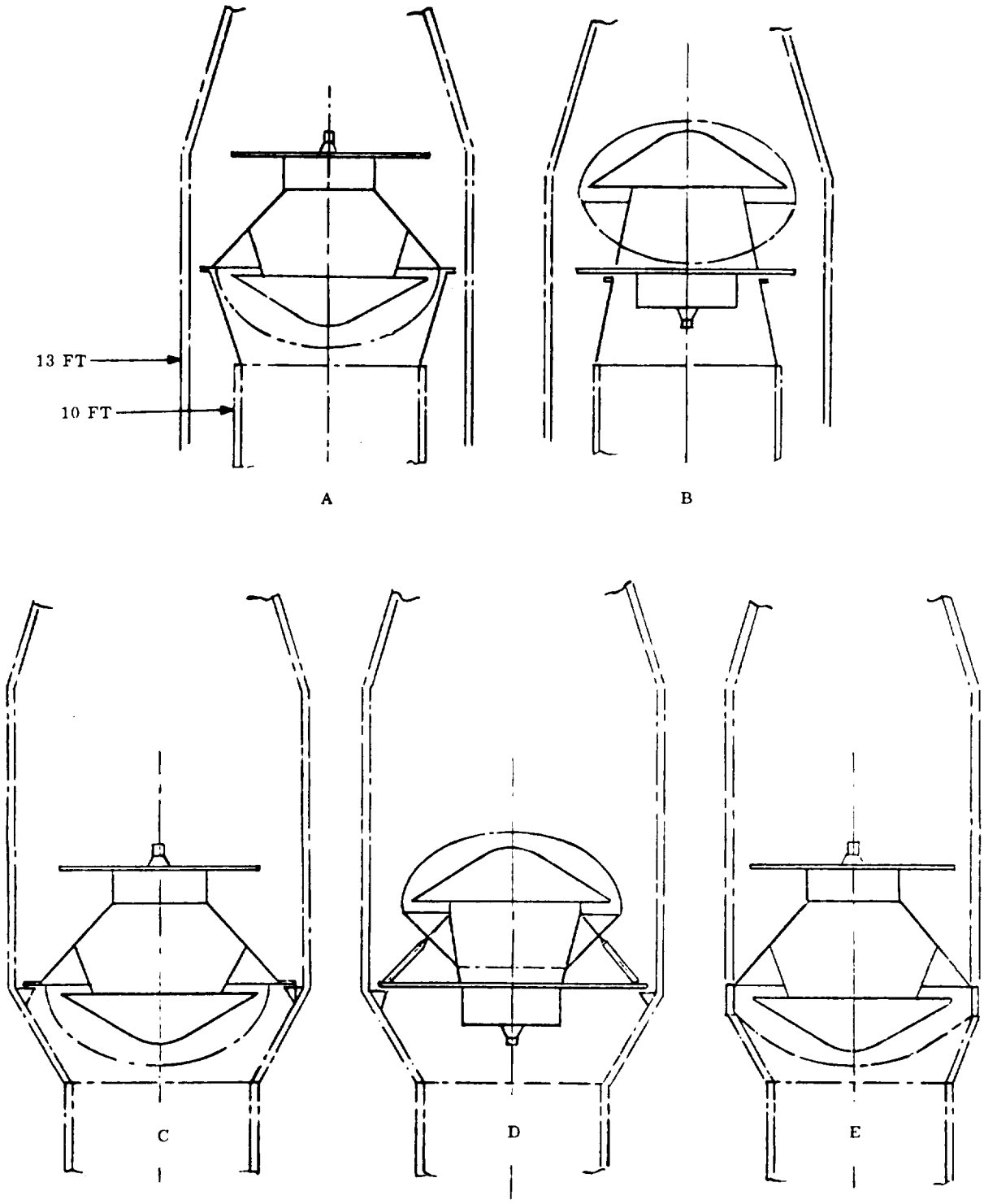

Figure 4. 1-2. Launch Configuration Study

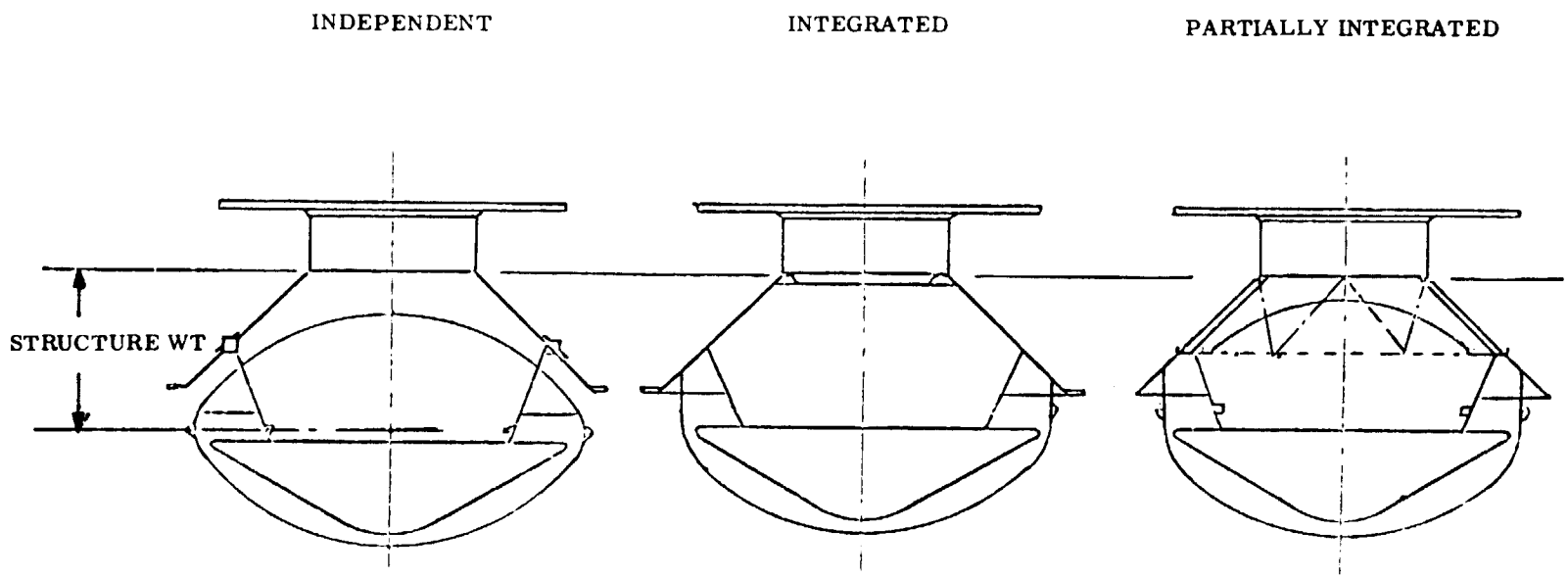

Figure 4.1-3. Adapter/Canister Study

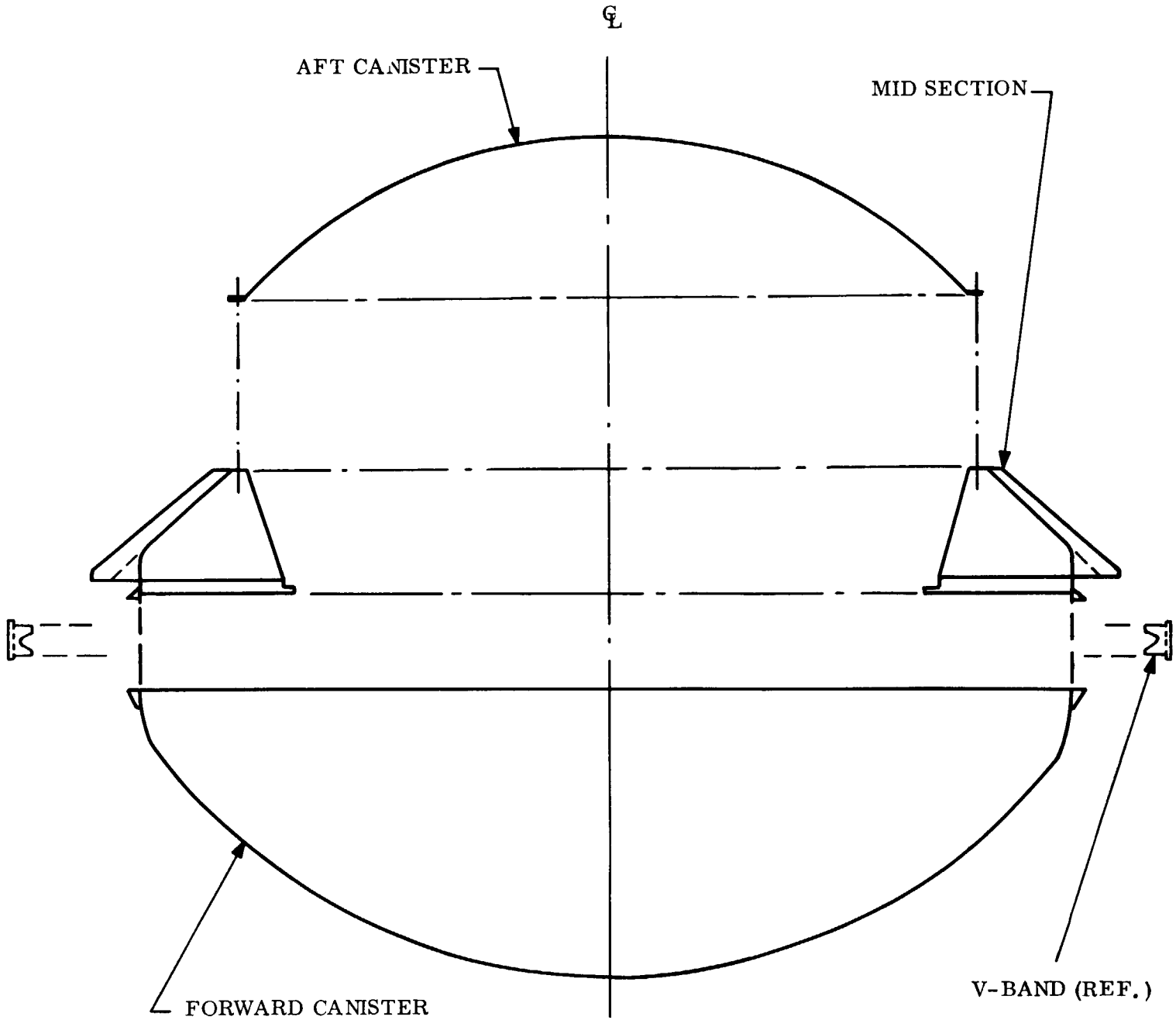

Figure 4.1-4. Sterilization Canister

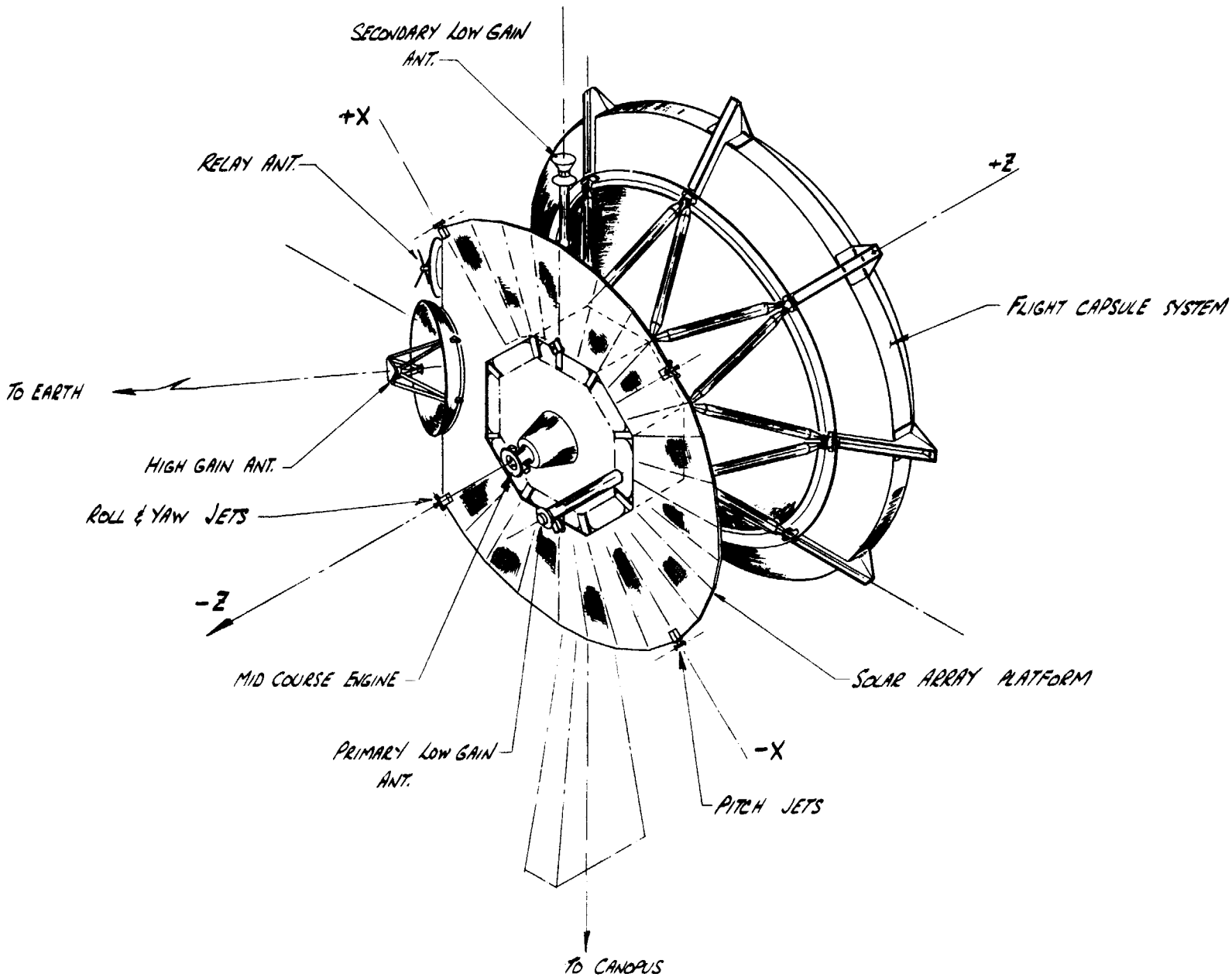

Figure 4.1-5. Spacecraft Configuration

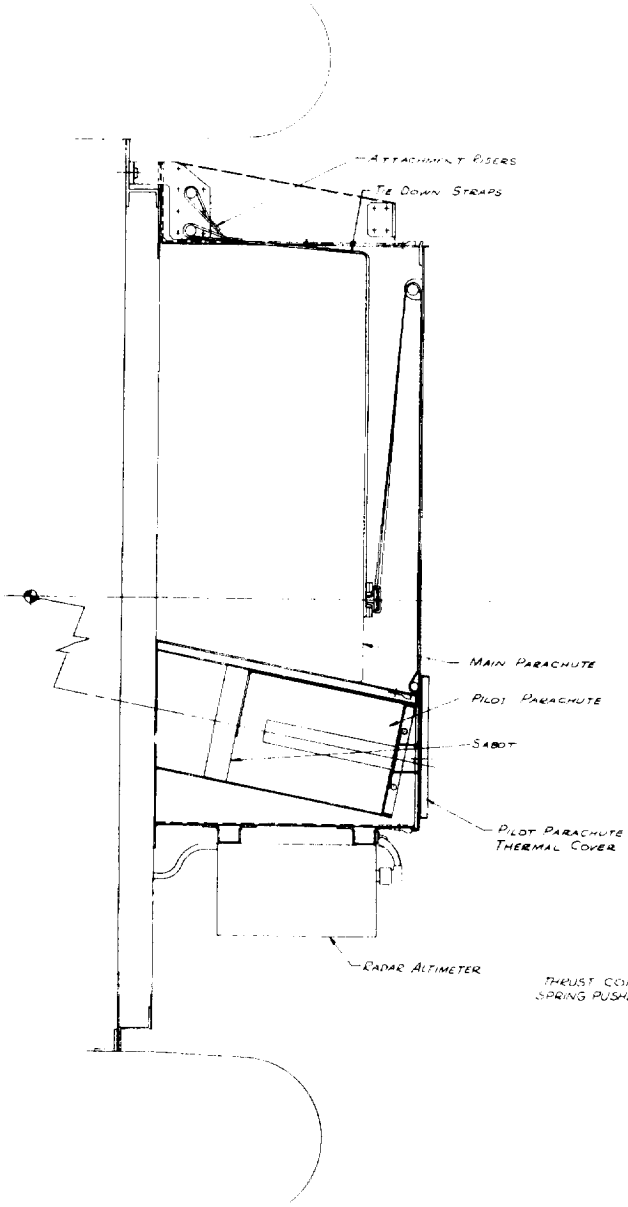

Section F-F
Scale 1/2

Section E-E

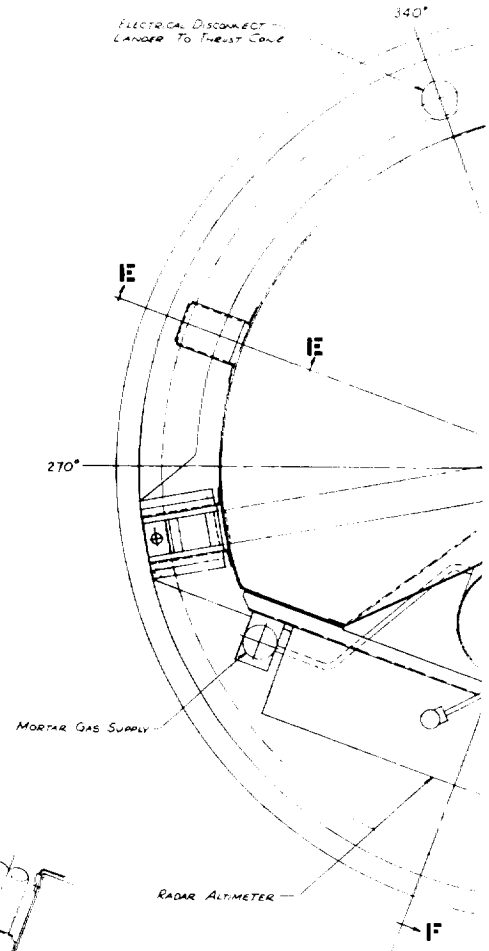

FOLDOUT FRAME 1

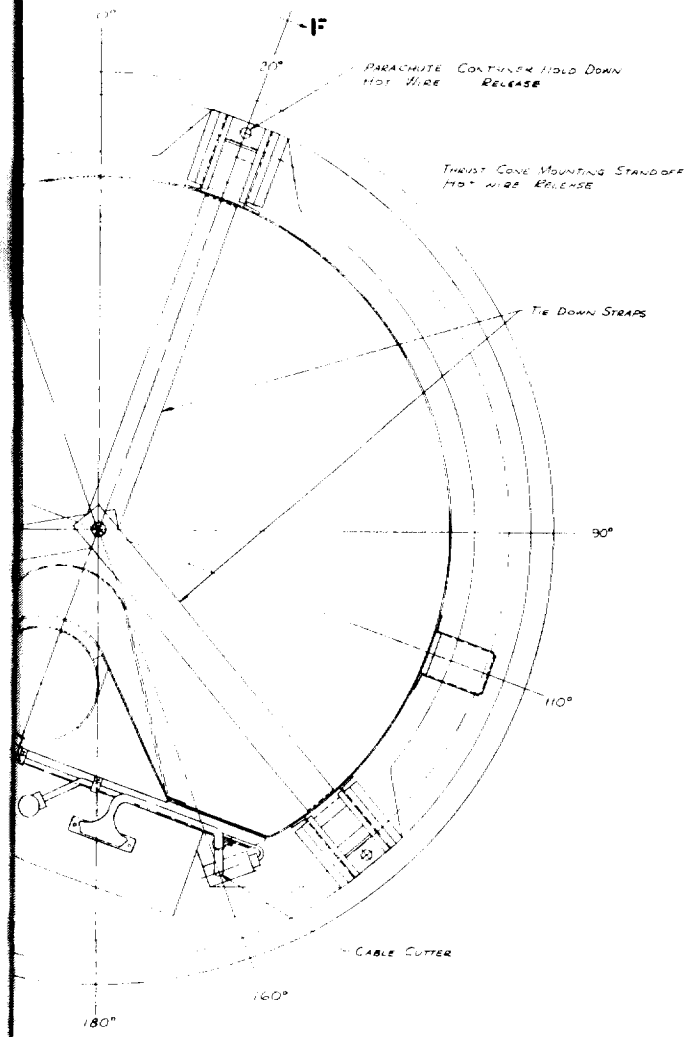

SECTION 13-13
SCALE 1/2

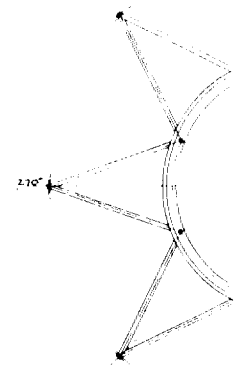

FOLDOUT FRAME 2

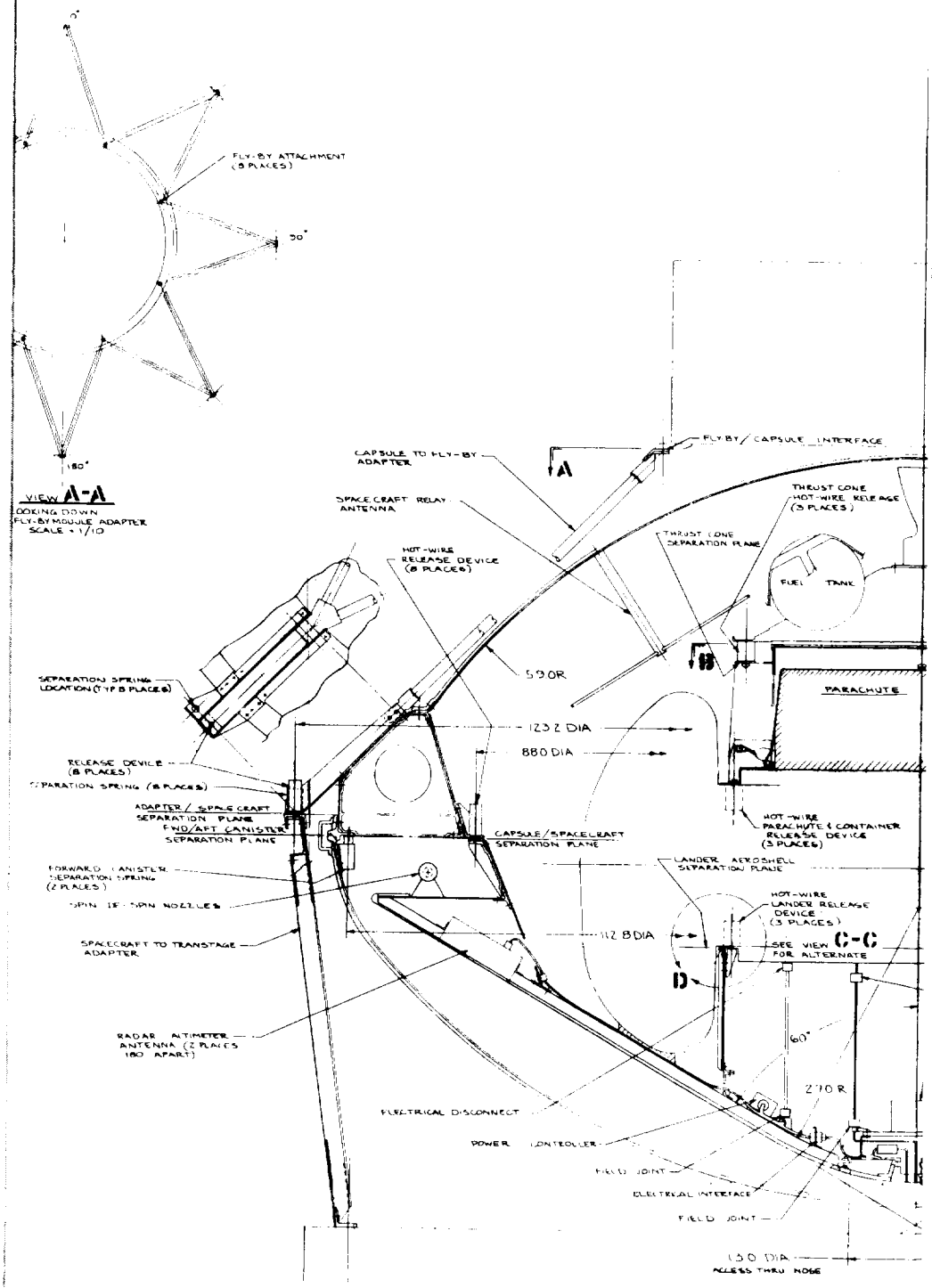

FOLDOUT FRAME 3

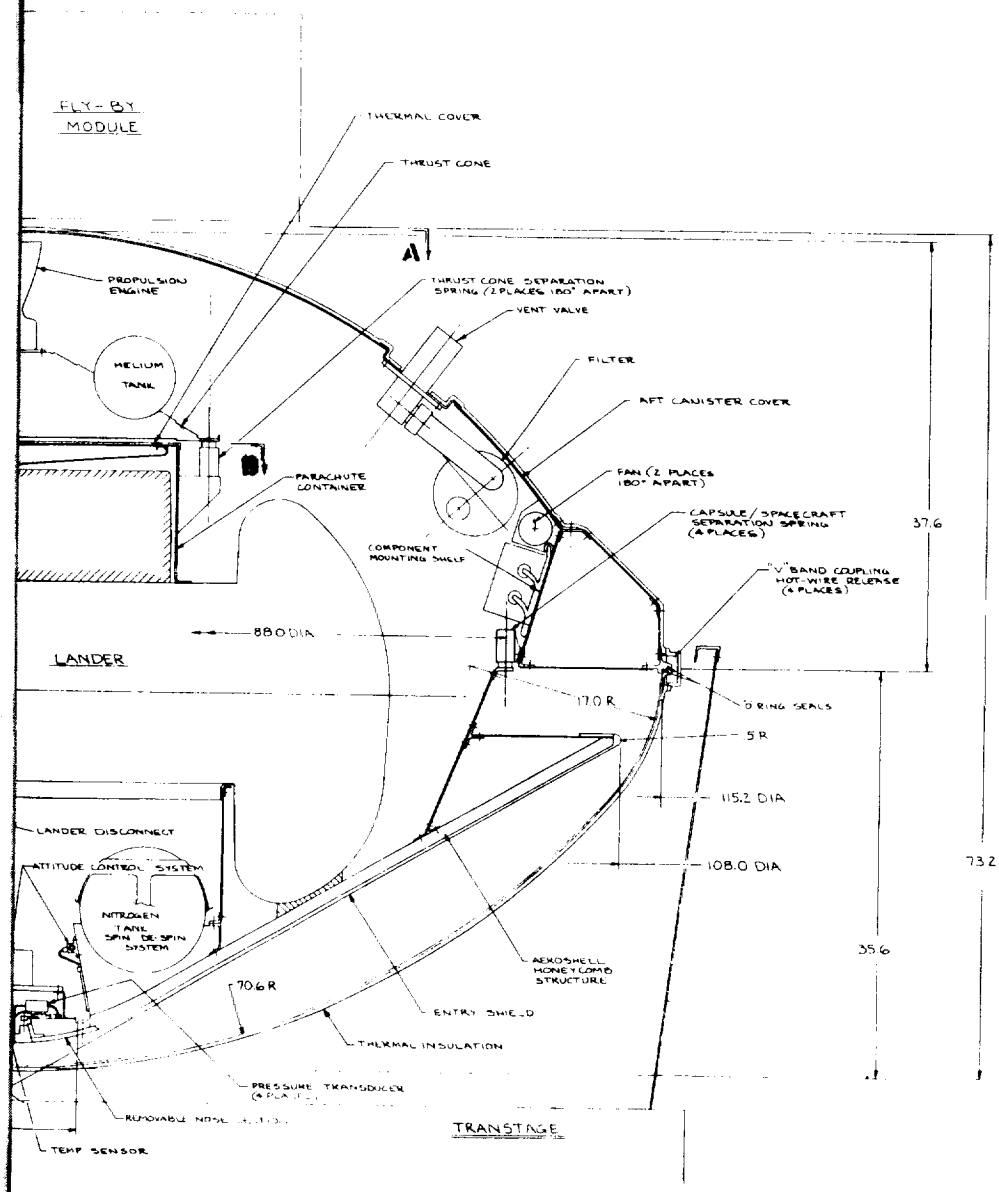

FOLDOUT FRAME 4

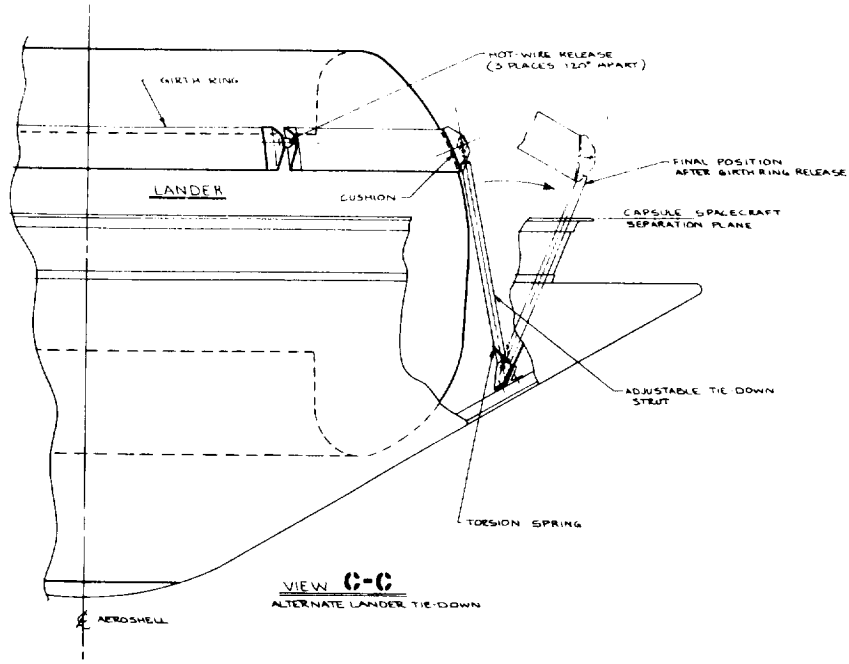

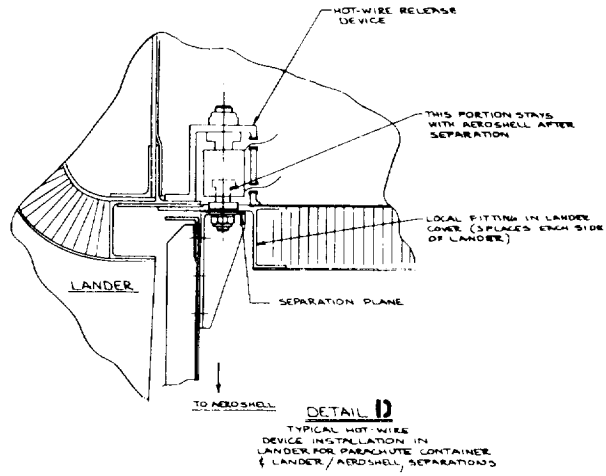

Figure 4.2-1. Flight Capsule Inboard Profile

FOLDOUT FRAME 5

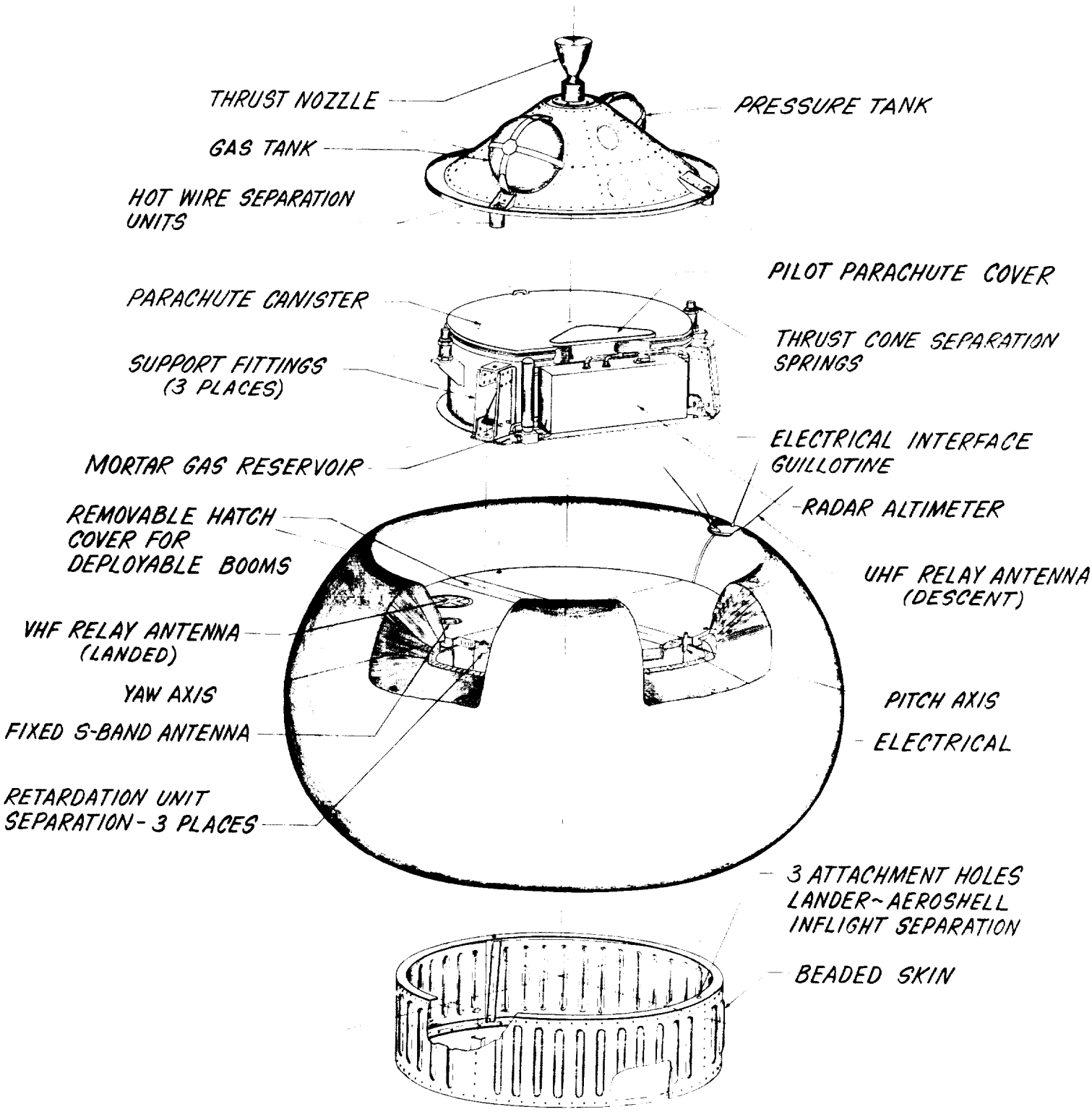

Figure 4. 2-2. Separated Flight Capsule Assembly

The Flight Capsule is spun up to 25 rpm 1/2 sec after separation from the Support Module to provide stability during firing of the deflection engine. The Spin Subsystem utilizes a single rate gyro, relatively simple electronics, and a cold gas (nitrogen) reaction control system which are all mounted on the aeroshell. The spin stabilization is maintained during the 24 hr free flight period so that the angle-of-attack at entry is less than 40°.

At separation, the Capsule maintains communication with the Support Module by means of the UHF relay link. 50 watts of r-f power is transmitted over a turnstile antenna to transmit engineering diagnostic data at 1100 bps. A modified Mariner '69 Propulsion Subsystem has been selected to perform the Capsule deflection propulsive maneuver. This propulsion subsystem was designed by JPL as a modular assembly using anhydrous hydrazine as the liquid mono-propellant, providing 50 lb of vacuum thrust. It has a capability of imparting a velocity increment of approximately 30 meters/sec to a 1,100 lb vehicle.

Modifications to the propellant bladder, tanks, pressure regulator, and electrical harness may be required to enable the Propulsion Subsystem to survive the terminal heat sterilization requirements.

The Mariner '69 Propulsion Subsystem was selected for this mission primarily on the basis of cost and that it is a flight proven system. The tradeoffs considered, reasons for selection, and a detailed design description, including a weight and performance summary, are presented in paragraph 5.10 of this report.

The empty thrust cone is separated after the deflection maneuver is completed. Four hot-wire tension bolts similar to those used on the canister V-band are used for attachment and separation. Compression springs identical to the ones used on the canister impart a separation velocity of 2.0 fps to the thrust cone. The spent propulsion equipment and thrust structure are jettisoned and the Capsule spin rate reduced to 5 rpm before entry.

After the deflection impulse and thrust cone separation, the relay communication is turned off to conserve battery power. During the Capsule cruise to the planet, it is turned on once per hour to transmit a short burst of diagnostic data.

Entry

The aeroshell, shown in fig. 4.2-3, is a blunt sphere-cone vehicle with a bluntness ratio (R_N/R_B) of 0.5. The spherically shaped nose has a radius of 27 in., making a tangent with a cone frustum of 60° half angle and base diameter 108 in. The ballistic parameter at entry is 11.5 lb/ft^2.

The aeroshell structure is an aluminum honeycomb shell with a core thickness of 1.0 in. and 7075-T6 facing sheets 0.012 in. thick to form a total shell thickness of 1.024 in. The aft end of the aeroshell has a torque box ring structure made of

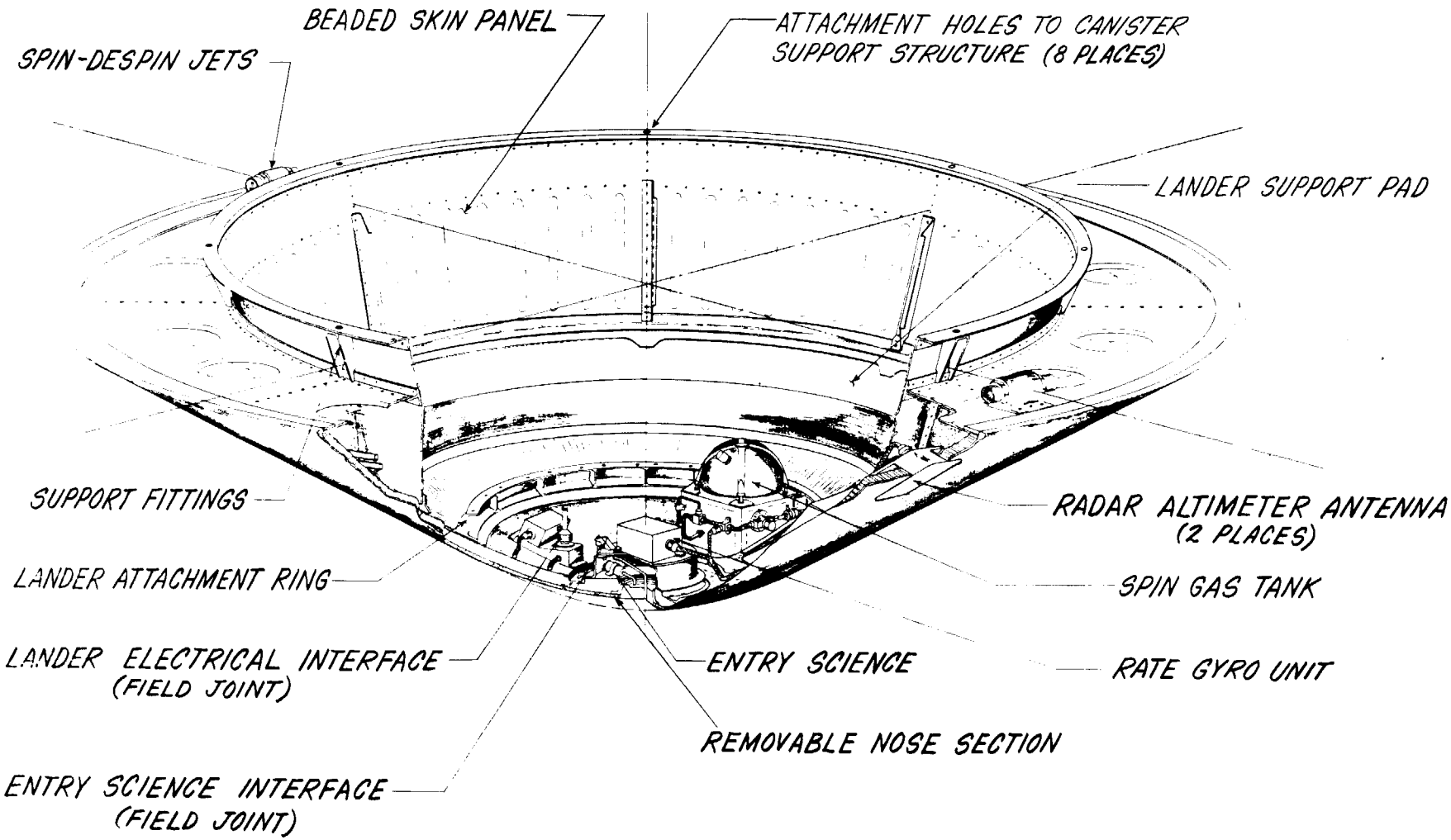

Figure 4. 2-3 Aeroshell

webs and rings with periodic ribs to provide internal stiffness. An extension of the conical longitudinal web of the torque box provides the structural connection between the aeroshell and the canister. Separation of the aeroshell from the canister occurs at the aft end of this conical extension and serves as the load path for the separation forces. The combined spin, de-spin, and roll control nozzles are mounted on the aft web of the torque box.

A removable nose section is bolted into the aeroshell. It consists of an aluminum honeycomb substructure covered with thermal protection except for the nose tip, which is a beryllium heat sink mounting for the pressure sensors, temperature sensors, and air intake for the mass spectrometer. Also located in the nose are the electronics, rate gyros, and nitrogen tank for the attitude control system. The maximum deceleration trajectory (24.75° - MIN atmosphere) and the maximum heating trajectory (16.5° - MAX atmosphere) override all other powered flight, space flight, and ground handling load conditions for aeroshell design. The maximum deceleration trajectory imposes the maximum load (29.5 g's) on the aeroshell structure, and the lowest temperature rise. The maximum heating trajectory imposes the maximum structural temperatures and maximum temperature differential between the outer and inner facings of the honeycomb shell with a lower loading of 8.2 g's.

The aluminum honeycomb shell material was selected for its competitive weight, ease of fabrication and lower cost than other types of structure. The aeroshell design approach is discussed further in Section 5.9.

The Lander is attached to the aeroshell by an aluminum sheet metal cylinder located immediately below the Lander flat pack instrument container. The Lander impact attenuator rests in a phenolic glass honeycomb saddle, which has a teflon lining between it and the Lander to eliminate the possibility that the Lander may adhere to the saddle during the long space flight. The Lander/Aeroshell separation plane is located at the bottom of the flat pack equipment container. Separation is accomplished by three release devices.

The heat shield is a low density charring ablator soft bonded to the aluminum honeycomb structure with 10 mils of RTV-560. Density of this ESM 1004 AP heat shield material is 35 lb per cubic ft. The heat shield thickness distribution varies from 0.37 in. in the stagnation region to 0.29 in. at the end of the frustum. To protect against the possibility of backface heating around the edge of the entry vehicle, the exposed aeroshell structure at the base and inboard on the vehicle is coated with ESM 1004 AP, which results in a total heat shield weight of 115 lb. A high emissivity coating is adequate protection for the remainder of the afterbody. The heat shield material is designed to be fabricated in panel sections of approximately 10 ft^2, joined by circumferential scarf joints (45° angle) with a thermal control coating wherever possible.

The entry science payload consists of three platinum resistance thermometers, two mounted on the Capsule base and one on the aeroshell in the stagnation region; six variable capacitance pressure transducers, two on the Capsule base and four

in the stagnation region; and a dual-scale tri-axial accelerometer at the Capsule's center-of-gravity. A mass spectrometer and a water vapor detector which are part of the surface science payload are also used to determine atmospheric composition during entry. The stagnation temperature is used for the supersonic part of the flight while base temperature is used for the subsonic region, primarily during parachute descent, and can reliably be related to the ambient value. The base pressure measurements are used for both supersonic and subsonic flight while the stagnation values are used primarily to determine angle-of-attack, but also serve as backup to the base measurements. Density in the supersonic regime is determined from the accelerometer data. In the subsonic regime density it is obtained from the pressure and temperature by a data analysis technique which also provides a value for the mean molecular weight.

During entry, data is transmitted continuously at 1100 bps. The entry science data is transmitted in real time and also delayed by 70 sec. This provides assurance of receiving data that is acquired during the communication blackout period of entry.

To insure aerodynamic stability at low velocities, the roll rate of the vehicle is controlled to less than 17 rpm. This is accomplished by the same pneumatic system that provides the spin/de-spin function.

Two radar altimeter antennas are located near the aft end of the aeroshell as shown in fig. 4.2-3. At an altitude of 4000 ft above the local terrain, a signal from the radar altimeter is used to initiate the parachute retardation phase.

Parachute Retardation and Landing

The parachute deployment sequence is shown in fig. 4.2-4. The signal to fire the pilot parachute mortar at 4000 ft above the local surface is received from the radar altimeter. The pilot parachute extracts and deploys the main parachute compartment cover and the main parachute. The main parachute is deployed reefed, and is disreefed by pyrotechnic reefing line cutters after a short time delay. At the time of disreefing, the aeroshell will be released and allowed to freefall.

The parachute system is shown in fig. 4.2-5. A pilot parachute thermal cover secures the pilot parachute pack in the mortar. The pilot parachute riser is attached to the main cover at two points and forms a securing tuck bight with the tie-down straps that anchor the main parachute. During pilot parachute deployment of the main parachute, the pilot riser tuck bight is pulled out, releasing the tie-down straps and freeing the main parachute bag handles to deploy the main parachute. A detailed design description is provided in Section 5.8 of this report.

The pilot parachute mortar, the mortar ejection gas supply, and the electrical disconnect are located inside the parachute compartment in the area where the main parachute pack is recessed. The radar altimeter is mounted on the outside of the parachute compartment wall.

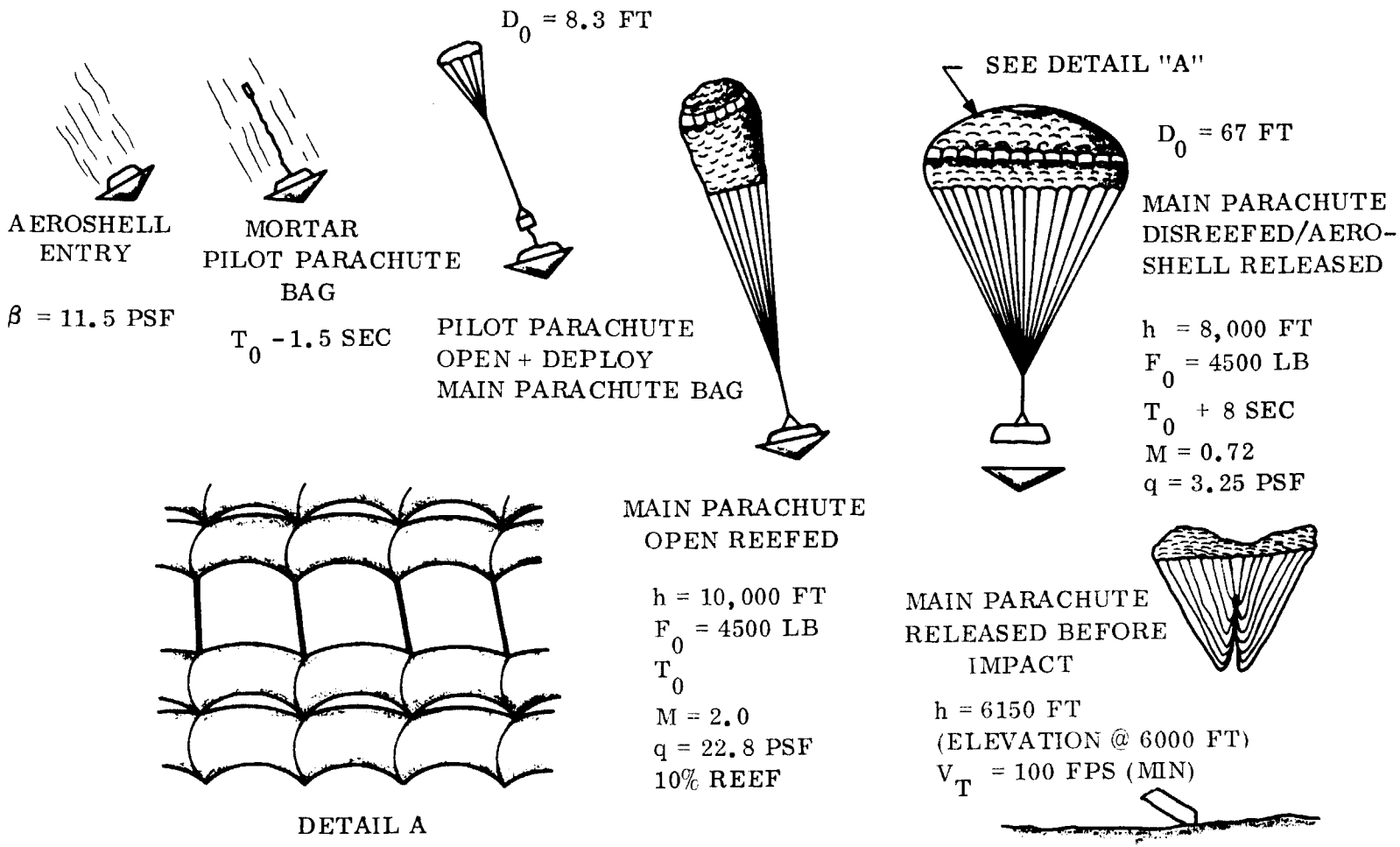

Figure 4.2-4. Parachute Deployment Sequence

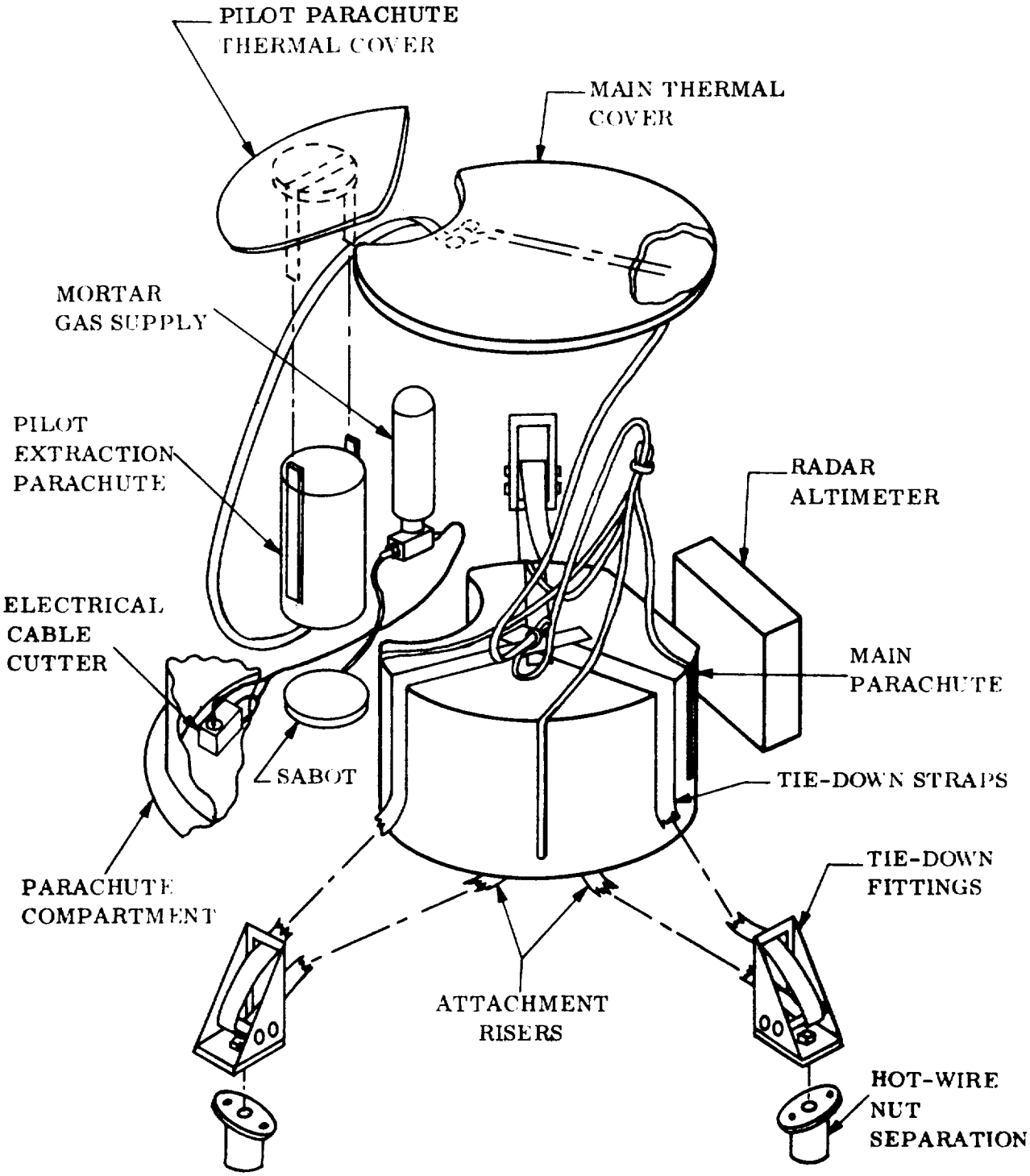

Figure 4. 2-5. Retardation Subsystem Hardware Arrangement

At 100 ft above the surface, the parachute release signal is received from the radar altimeter and the explosive separation nuts fire. The released main parachute removes the parachute compartment and all of the hardware attached to it. The Lander surface, where the retardation subsystem equipment was mounted, is now clean for landing.

The impact limiter is designed to insure less than 1000 g shock to the equipment container under the landing conditions shown in fig. 4.2-6. The limiter is constructed of phenolic fiberglass honeycomb blocks oriented such that the cells are roughly parallel to the stroke direction. The blocks are bonded to the equipment container and to each other by a film adhesive which foams during curing to provide secure attachment. Sufficient honeycomb is provided for primary impact under the adverse conditions shown in fig. 4.2-6, and additional material on the upper surface absorbs secondary impacts due to bounce should the lander overturn. The design allows for coming to rest in either a "heads" or "tails" attitude.

Landed Operation

Immediately after landing, cameras, the wind measuring instrument, and an S-band antenna are deployed to yield the landed configuration shown in fig. 4.2-7. These devices can be deployed in either direction. The proper direction is determined by a gravity sensor after the Lander comes to rest.

At 150 sec after landing, pictures are taken with the facsimile cameras and the data is transmitted over the relay link to the Support Module. UHF antennas are located on each face of the equipment container and the appropriate one is selected by means of the gravity sensor previously mentioned. With an r-f power output of 50 watts, under worst case entry and landing conditions a data rate of 70 kbps can be sustained for a minimum of 400 sec as the Support Module passes overhead. This 2.8×10^7 bits of data is stored on board the Support Module for later transmission to Earth.

In addition to the facsimile cameras, surface science instruments include a gas chromatograph/mass spectrometer, a life detector, atmospheric and subsurface moisture detectors, temperature, pressure and wind velocity sensors. Measurements are made with these instruments in accordance with the sequence described in Section 3.0 and data is stored in the Lander.

Approximately 17 hr after landing, the Earth will pass near the Lander zenith. During this time period, stored and real time data can be transmitted directly to Earth over an S-band link. The S-band antenna shown in fig. 4.2-7 is vertically oriented by means of a local vertical sensor and drive motors. For a nominal landing site at 10° north latitude and the sub-Earth point at 17° south latitude, the half beam width of this antenna must be slightly greater than 27° to insure that the Earth will pass through the beam as Mars rotates. The antenna gain achievable is 6 dB. Using the 20 watt high shock TWT that has been developed, the data rate

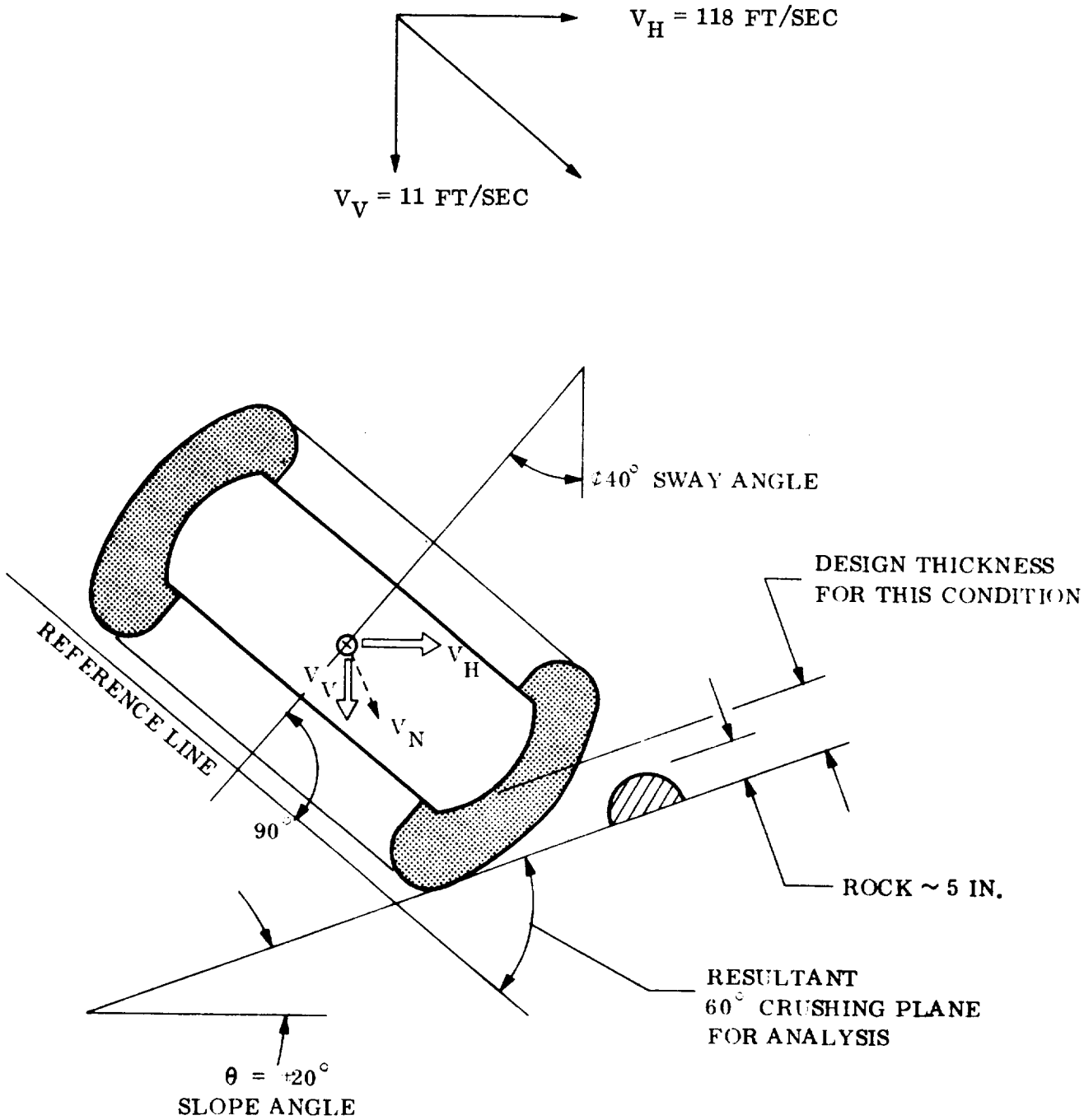

Figure 4.2-6. Design Conditions

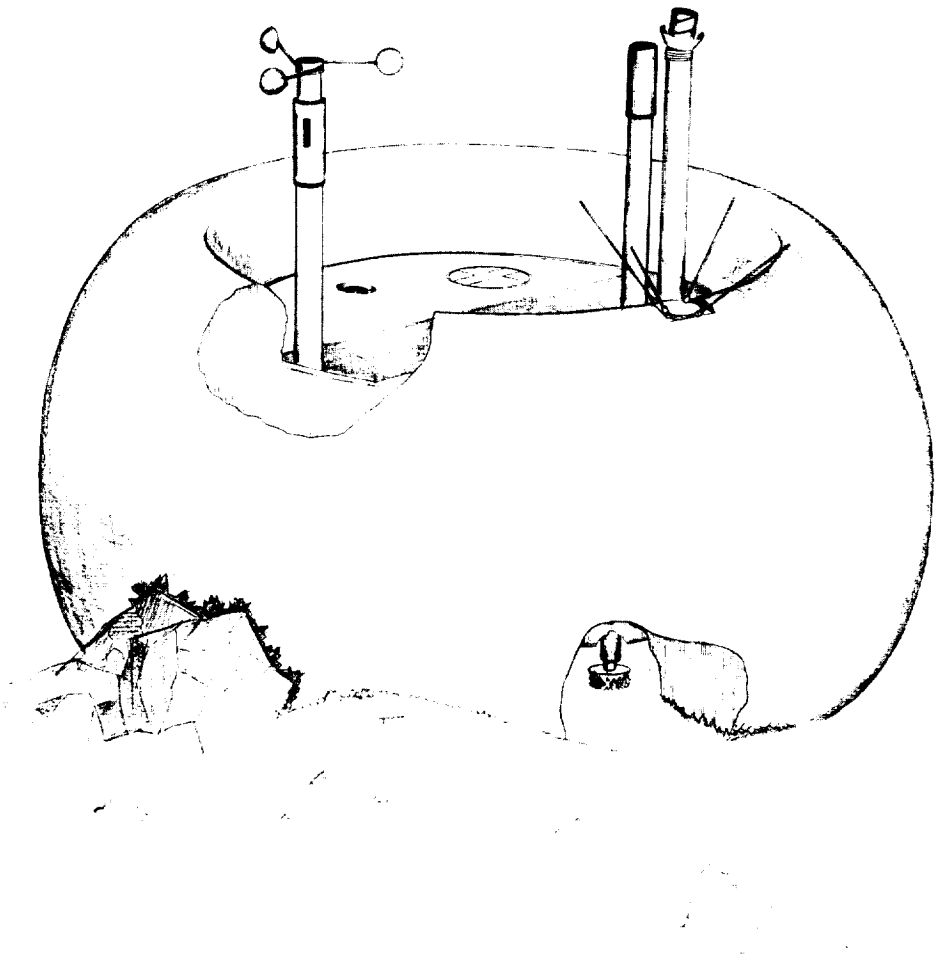

LANDED CONFIGURATION

Figure 4.2-7. Lander Deployment Configuration

achieved with the 210 ft receiving antenna is 50 bps. A data transmission interval of approximately 1500 sec can be accommodated with the available power to yield 75 kbits of data per day.

The vertically oriented S-band antenna is backed up by a body fixed antenna. The beamwidth of the fixed antenna is much wider than the vertically oriented one to accommodate 20° surface slopes and 12° of asymmetry in the honeycomb crush-up. With the fixed antenna, a data rate of 5 bps can be achieved.

Ground commands can be received through the body fixed antenna. Command capability is provided to allow alteration of pre-programmed sequences during the mission. Normal control of the mission sequence is accomplished by the Computer and Sequencer. It is a programmable device with sufficient capacity to control all events from Capsule separation to end of mission.

Power for the three day landed mission is provided by a silver-zinc battery. A single battery is provided to accommodate the entry phase as well as the landed operation.

The science instruments and supporting subsystems are arranged within the cylindrical container as shown in figs. 4.2-8 and -9. A system of bays was designed to provide room for weight and volumetric growth for all equipments and also provide a maximum of design and schedule flexibility for the science instruments. Most of the support subsystems are modularized to permit packaging in a high density zone next to the container rim while science components are located in less dense compartments. The deployable equipment, including cameras, wind velocity sensor, and Earth link antenna are located in a central bay with ample space for deployment clearances and growth. This bay, which is the full width and depth of the Lander payload container, allows the instruments and antenna to be mounted on short spring-loaded swinging booms for deployment. The wind velocity sensor requires secondary spring-loaded arms, which unfold at right angles to a spring-loaded extension of the camera booms when the booms are deployed. Deployment of equipment from this bay is substantially automatic following selection and jettison of the bay door on the uppermost and exposed side of the Lander. Low and high resolution cameras are provided on each of the two booms and, hence, provide some redundancy although both are required to obtain the specified view angles under adverse conditions of orientation.

Thermal control, primarily an insulation problem, is achieved by the use of honeycomb panels with fiberglass core for the outer shell of the Lander container. The honeycomb cells are filled with insulation. In addition, thick layers of foam are used on exposed surfaces, such as the sidewalls of the camera bay. Batteries are maintained at a proper temperature by a combination of heat dissipation from other components and electric heaters.

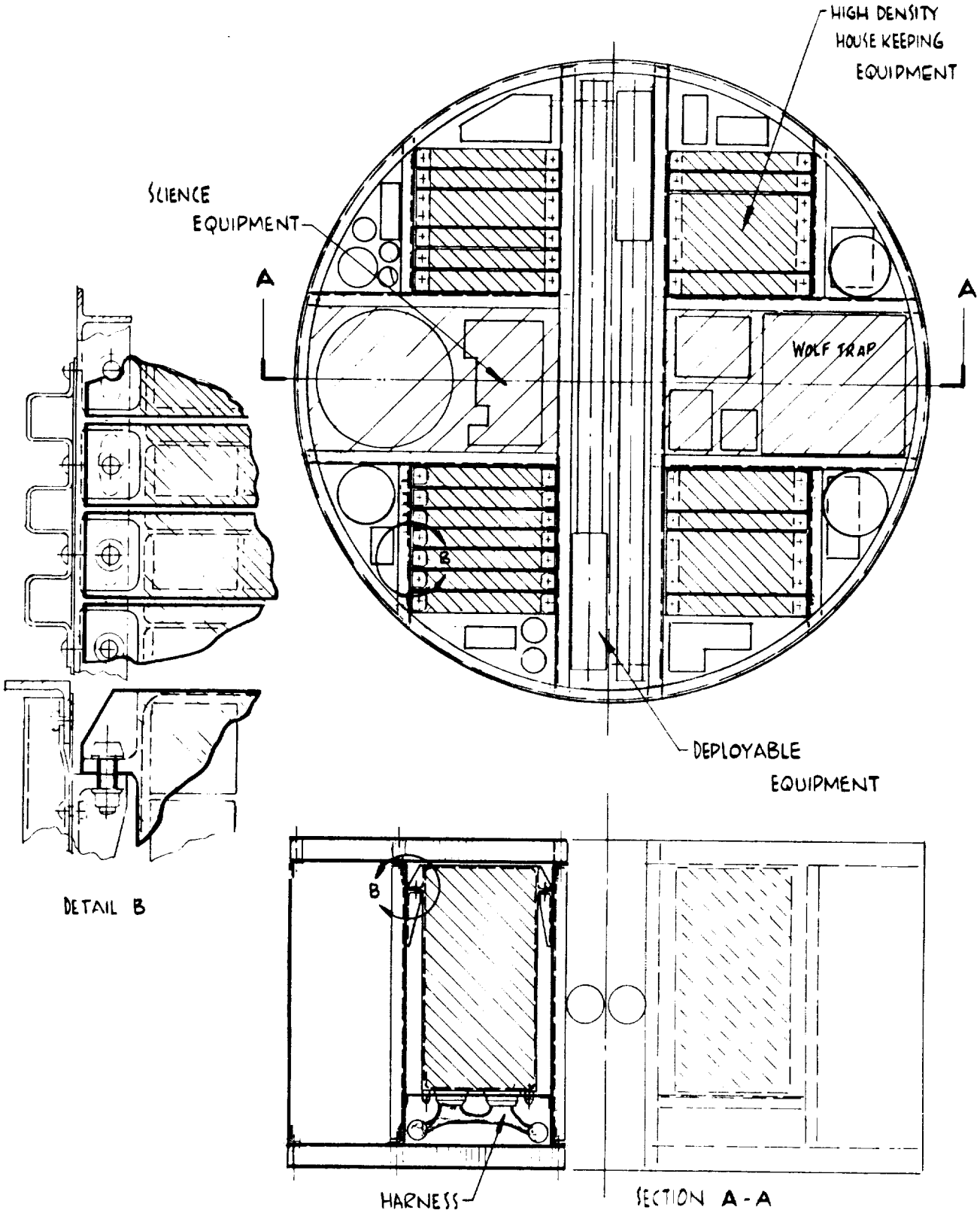

Figure 4.2-8. Lander Packaging Concept

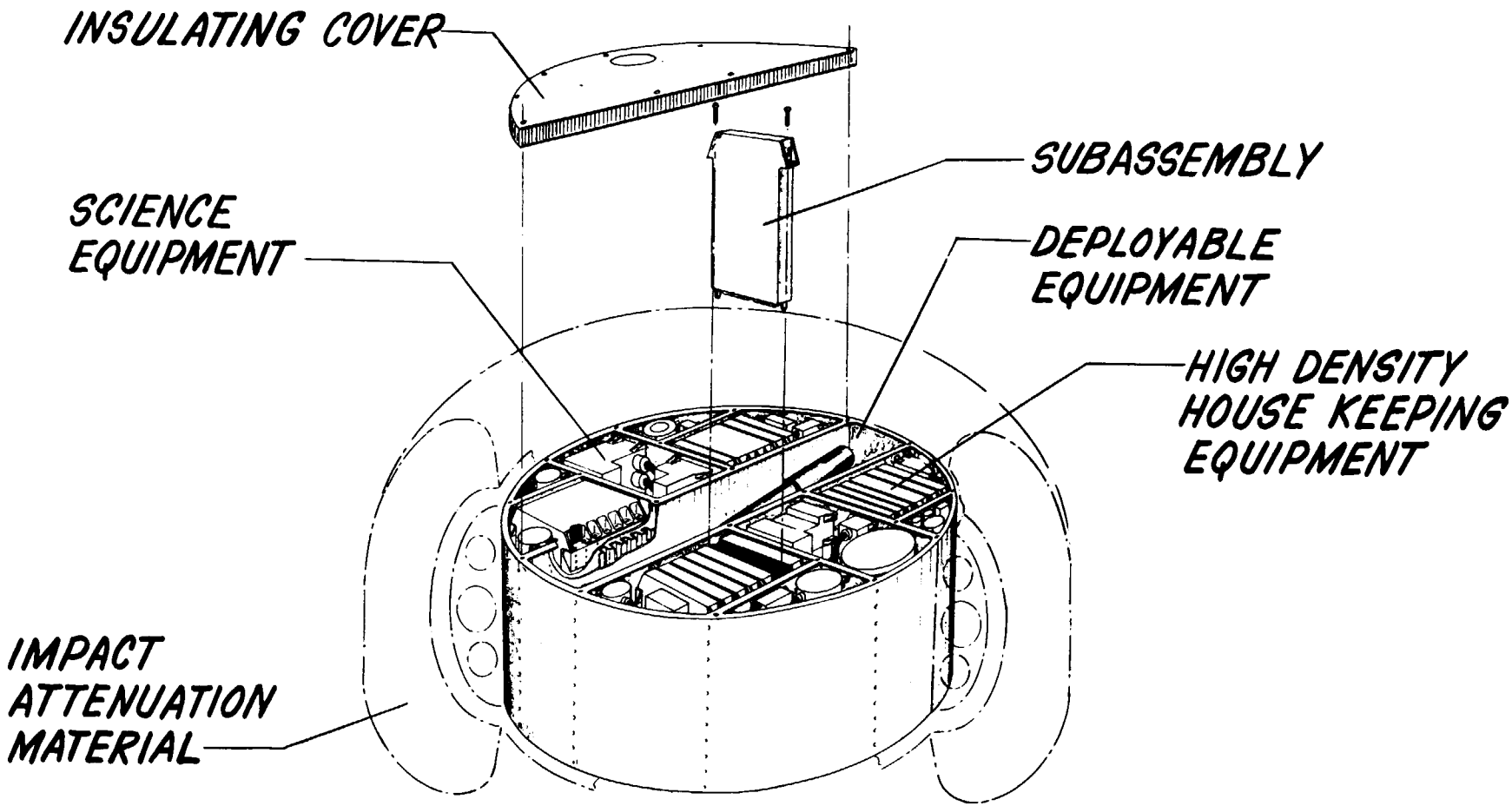

Figure 4.2-9. Lander Packaging

Mass Properties Summary

The weight summary for the 1400 lb Flight Capsule system is listed in table 4.2-1, which shows a total Capsule weight of 1332 lb, not including growth. The Launch weight, which includes in addition to the Capsule a Support Module, a Capsule-to-Support Module adapter, and a Spacecraft adapter, is 2201 lb. The mass properties, including both weights and mass moments of inertia, are listed in table 4.2-2. The mass properties reference axes are defined in fig. 4.2-10.

Electrical System Block Diagram

Fig. 4.2-11 presents the electrical system block diagram for the Flight Capsule. The layout defines where a component is first used in the flight sequence and to which subsystem it is assigned.

TABLE 4.2-1. WEIGHT SUMMARY, 1400 LB CAPSULE SYSTEM

Lander System	661.1
Structure (est.)	175.6
Science	60.0
Telecommunications	50.8
Electrical Equipment (separation, power and distribution)	116.7
Computer and Sequencing	13.0
Environmental Control	25.0
Attenuation	220.0
Retardation System	96.5
Main Parachute	52.0
Pilot Parachute	3.0
Containers and Covers	18.0
Fixed Equipment	8.5
Radar Altimeter	15.0
Aeroshell System	266.0
Structure (Shell)	54.1
Structure (Internal)	56.8
Heat Shield	115.0
Entry Science	2.5
Electrical Power and Distribution	8.1
Telecommunications	5.5
Attitude Control	24.0
Thrust Cone	58.4
Propulsion System	48.5
Electrical Equipment (separation, power and distribution)	9.9
Canister	249.9
Structure (est.)	162.8
Electrical Equipment (instrumentation, power and distribution)	30.2
Pressure and Venting	15.3
Thermal Control	15.0
Separation System	26.6
*Total Capsule Weight	1331.9
Capsule-to-Support Module Adapter	30.0
Support Module	659.0
Spacecraft-to-Transtage Adapter (est.)	180.0
*Total Launch Weight	2200.9

*This does not include growth factor

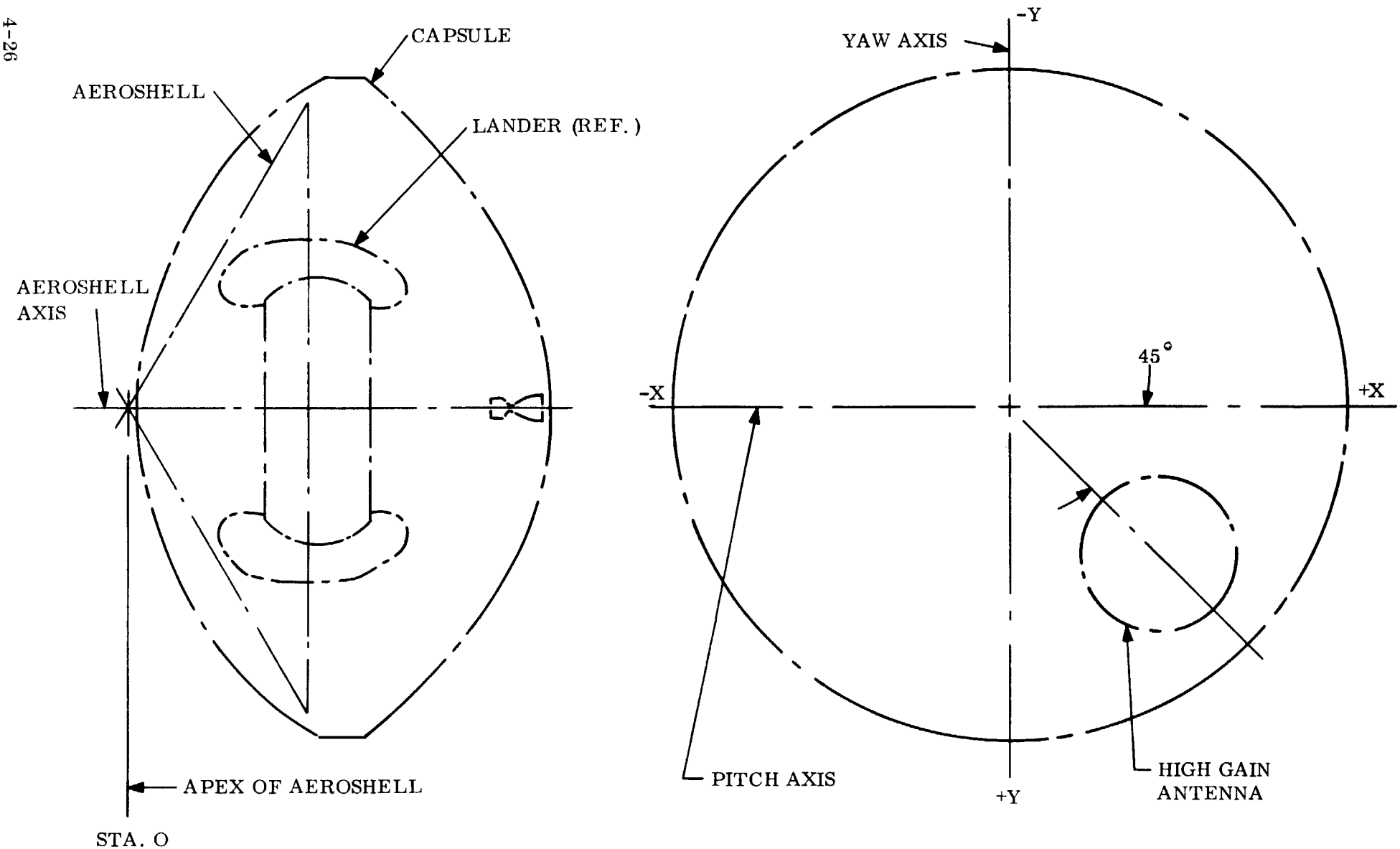

Figure 4.2-10. Mass Properties Reference Axes

TABLE 4.2-2. MISSION SEQUENCE MASS PROPERTIES

	Weight (lb)	Center-of-Gravity			**Mass Moments of Inertia (slug/ft^2)		
		*Roll	***Pitch	***Yaw	Roll	Pitch	Yaw
All up weight less shroud system	2200.9	50.9	-0.1	0.2	487.5	579.7	579.6
less spacecraft to Transtage adapter	-180.0	19.5	0	0	2.5	2.2	2.2
Spacecraft separated weight	2020.9	53.7	-0.1	0.3	354.3	472.9	472.8
less forward canister	-57.5	27.0	0	0	31.0	14.0	14.0
Spacecraft less forward canister	1963.4	54.5	-0.2	0.3	323.2	448.9	448.8
less flyby support module, Capsule to flyby adapter, and aft canister with V-band assembly	-881.4	79.5	0	0	176.9	131.3	131.3
Separated Capsule weight	1082.0	34.2	-0.3	0.5	146.2	106.9	106.8
less thrust cone	-58.4	64.5	0	0	0.8	0.5	0.5
Entry weight	1023.6	32.5	-0.3	0.5	145.4	94.2	94.1
less aeroshell	-266.0	22.0	0	0	89.0	50.0	50.0
Decelerator load	757.6	36.1	-0.4	0.7	56.5	35.6	35.5
less retardation system	-96.5	49.5	0	0	2.5	2.2	2.2
Lander	661.1	34.2	-0.5	0.8	54.0	29.1	29.0

*Distance from apex of aeroshell **Taken about the center-of-gravity

***The pitch and yaw center-of-gravity locations are approximate values; in a detail design program these values could be controlled by proper packaging so that the center-of-gravity will not be greater than 0.1 in. from the roll axis.

PRESSURIZATION AND VENTING SUBSYSTEM

ELECTRICAL INTERFACE EQUIPMENT

TELE-COMMUNICATIONS SUBSYSTEM

ELECTRICAL POWER AND DISTRIBUTION SUBSYSTEM

SEPARATION AND RETARDATION SUBSYSTEM

COMPUTER AND SEQUENCER SUBSYSTEM

THERMAL CONTR SUBSYSTEM

ATTITUDE CONTROL SUBSYSTEM

SCIENTIFIC PAYLOAD SUBSYSTEM

Figure 4.2-11. Electrical System Block Diagram (1 of 2)

FOLDOUT FRAME 1

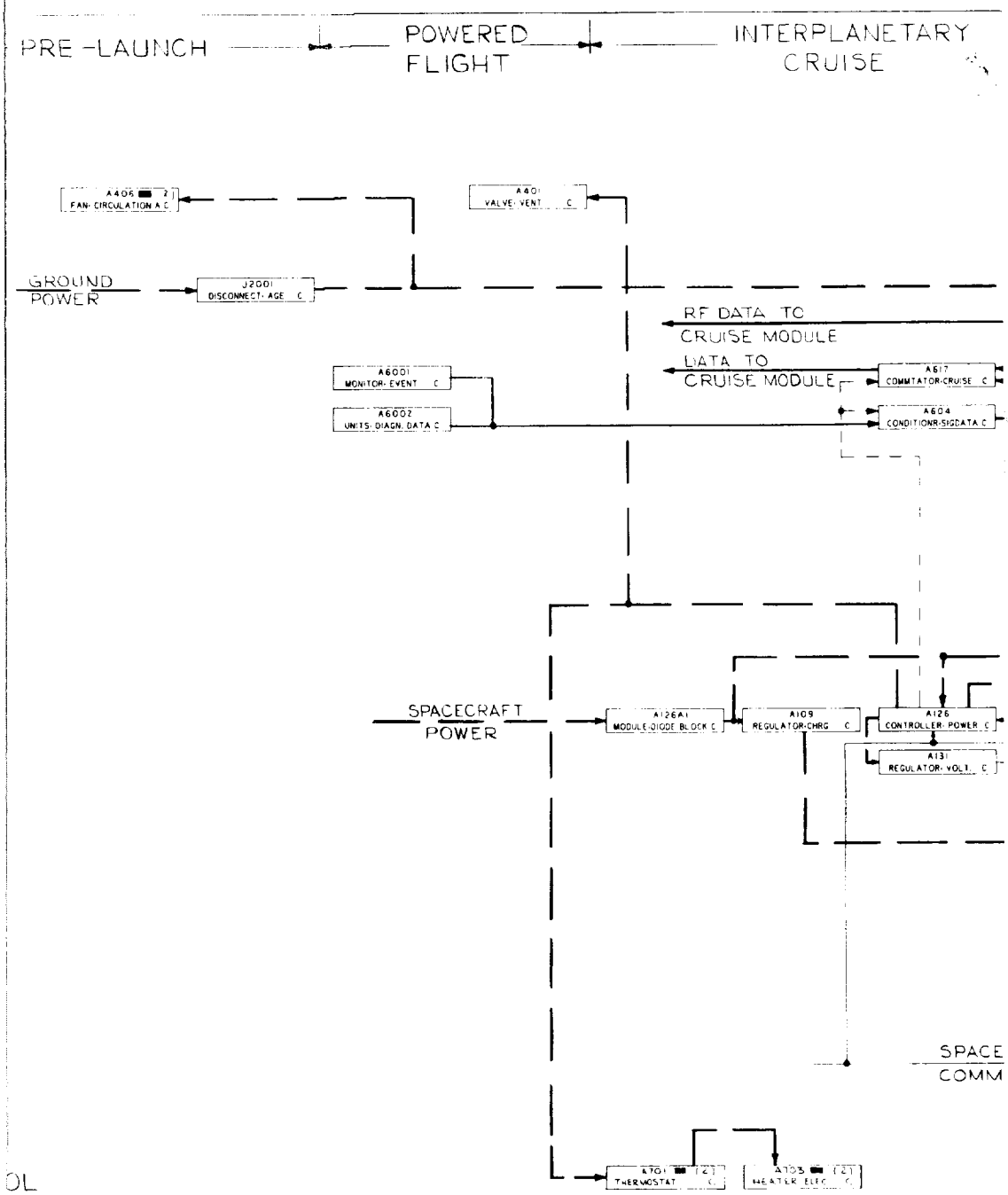

OL

NOTES:

1. SINGLE LINE DIAGRAM FORMAT IS USED FOR CLARITY. NOTE THAT INDIVIDUAL LINE MAY CARRY MULTIPLE FUNCTIONS.
2. ELECTRICAL REF DESIGNATOR ASSIGNMENTS SHOWN IN ACCORDANCE WITH MIL STD 16 B.
3. THIS DIAGRAM ILLUSTRATES FUNCTIONAL OPERATION. THE SUBSYSTEMS ARE SHOWN FROM TOP TO BOTTOM IN SEQUENCE OF USE. THE EQUIPMENT IS SHOWN FROM LEFT TO RIGHT IN THE ORDER OF FIRST FUNCTIONAL OPERATION IN SEPARATED FLIGHT.

LEGEND:

AD
UN
RE
SIG
DA
✳ UN

PRE-LAUNCH — POWERED FLIGHT — INTERPLANETARY CRUIS

FOLDOUT FRAME 2

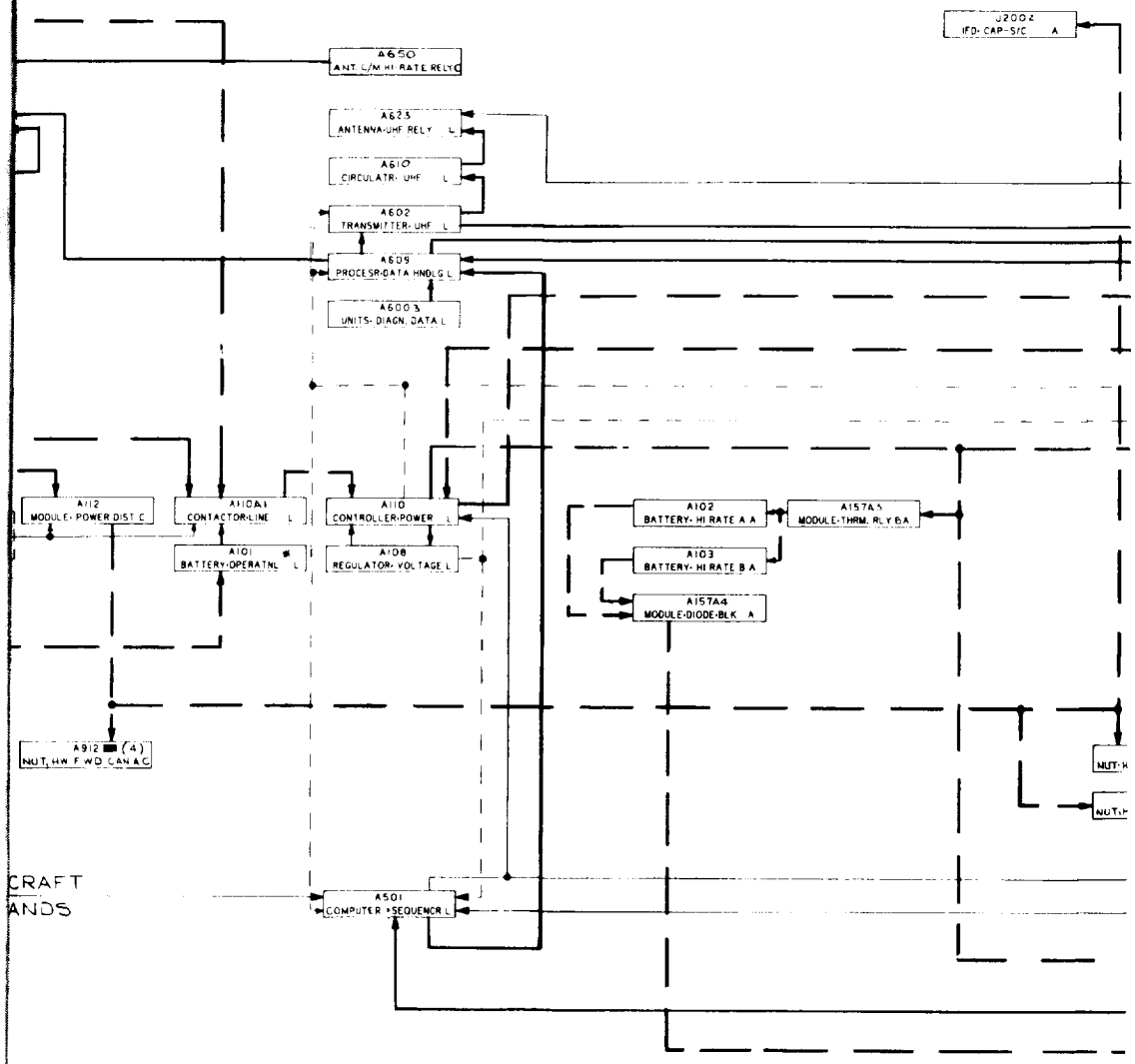

CRAFT
ANDS

DITIONAL UNITS NOT SHOWN
REGULATED POWER FLOW
GULATED POWER FLOW
GNAL PATH
TA PATH
IT CONTAINS INTERNAL HEATER

LOCATION CODE:

A – AEROSHELL
C – CANISTER (AFT LOCATED)
G – GROUND EQUIPMENT
L – LANDER
T – THRUSTCONE

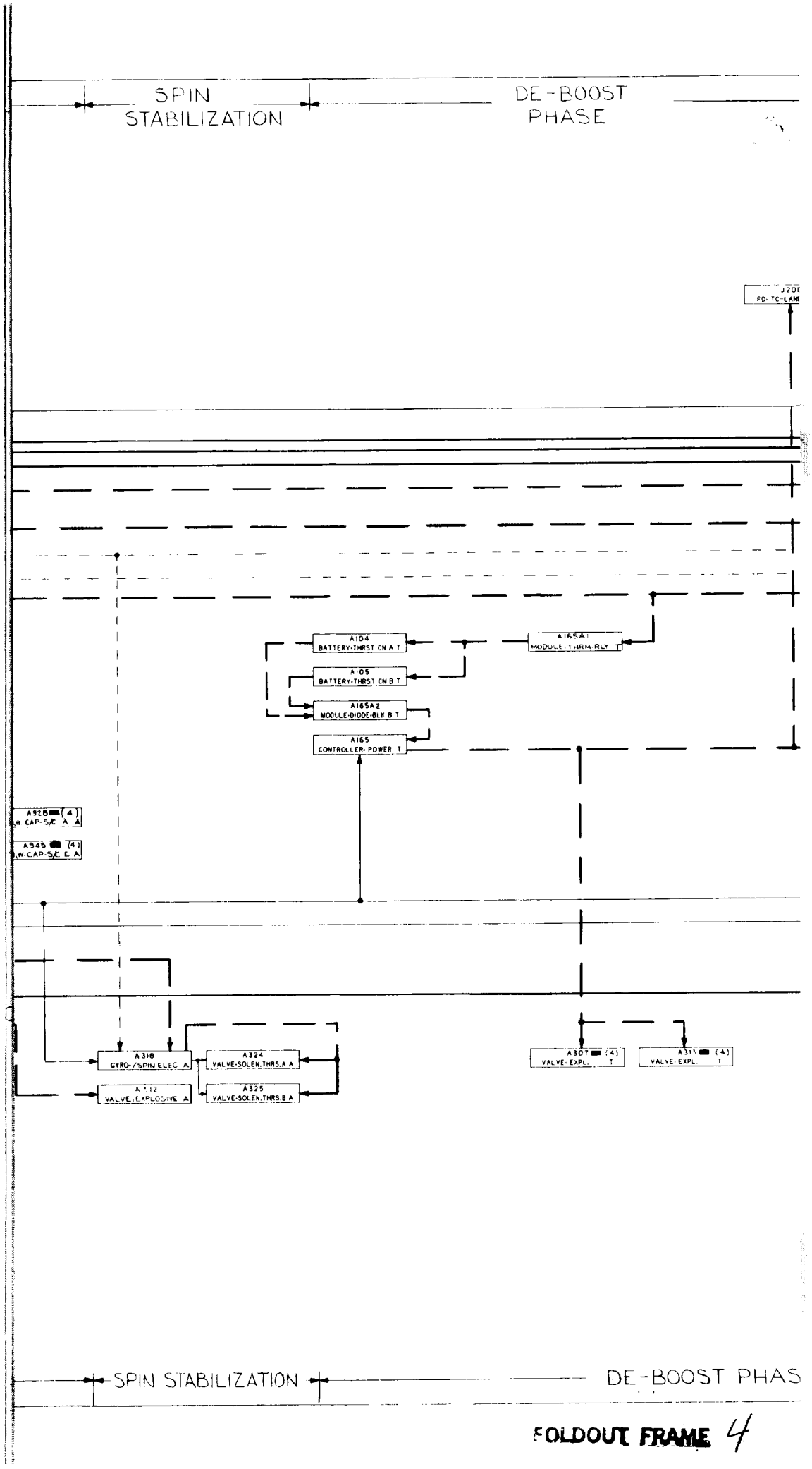

FOLDOUT FRAME 4

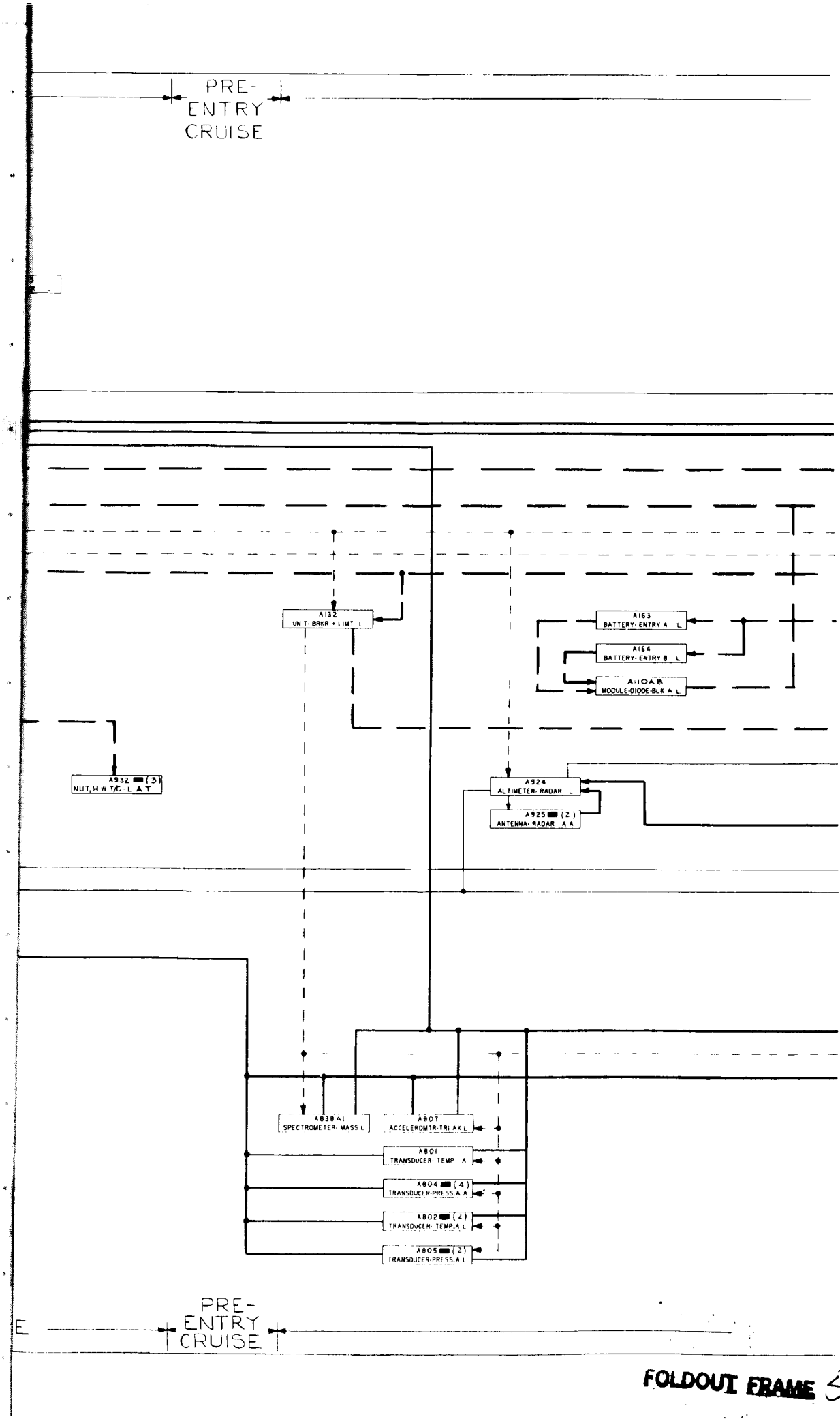

FOLDOUT FRAME 5

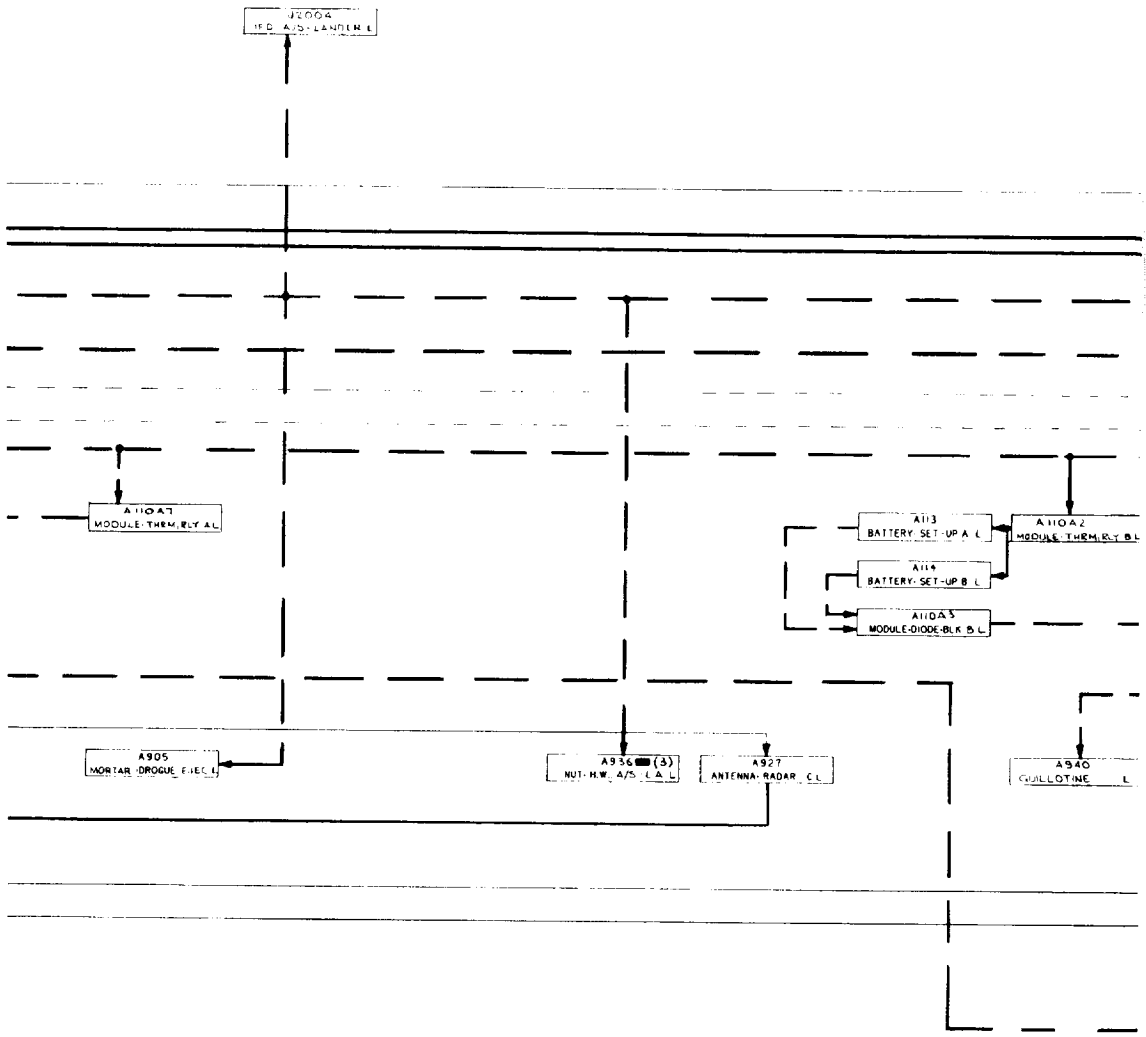

FOLDOUT FRAME

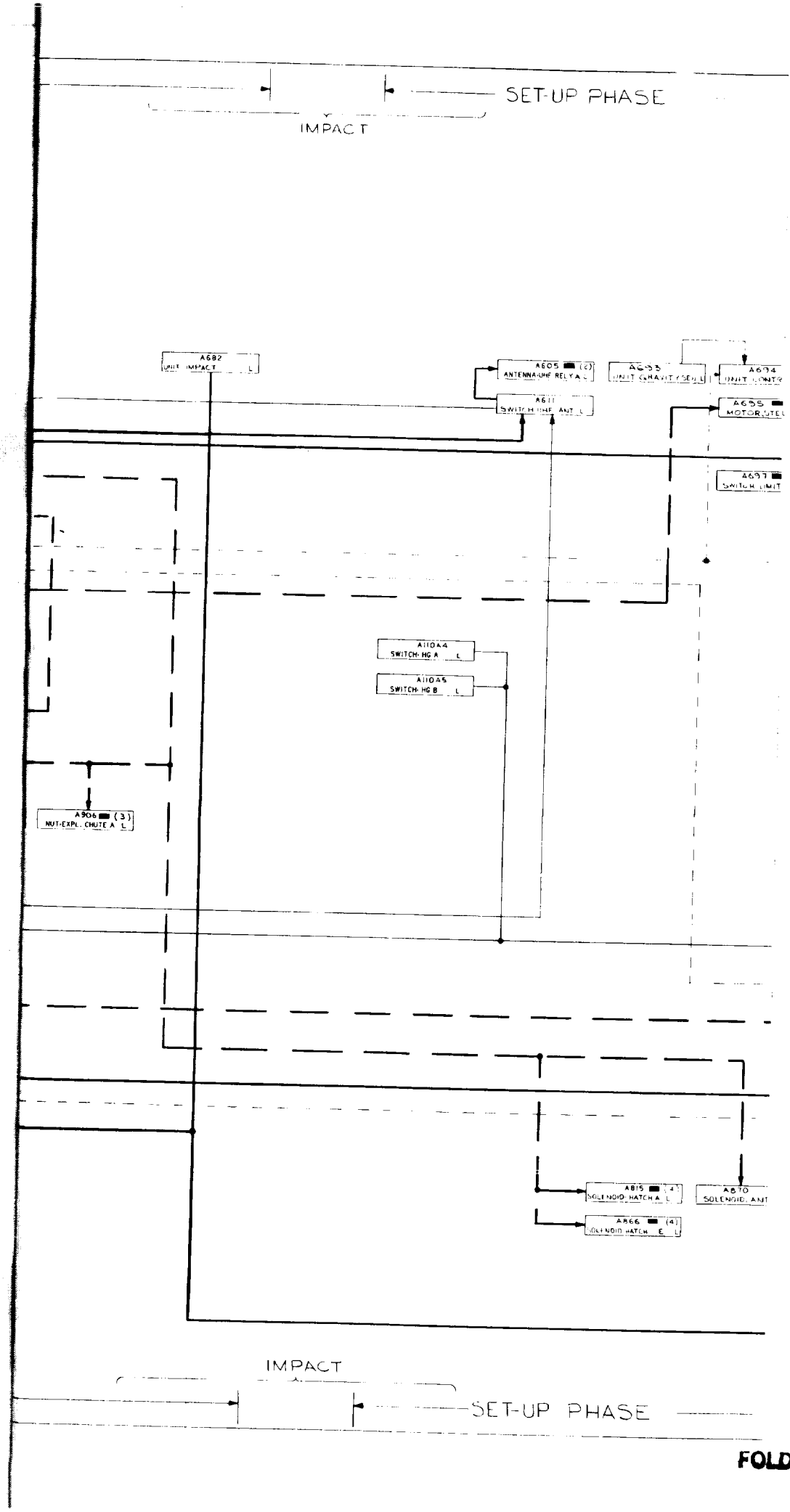

FOLDOUT FRAME 2

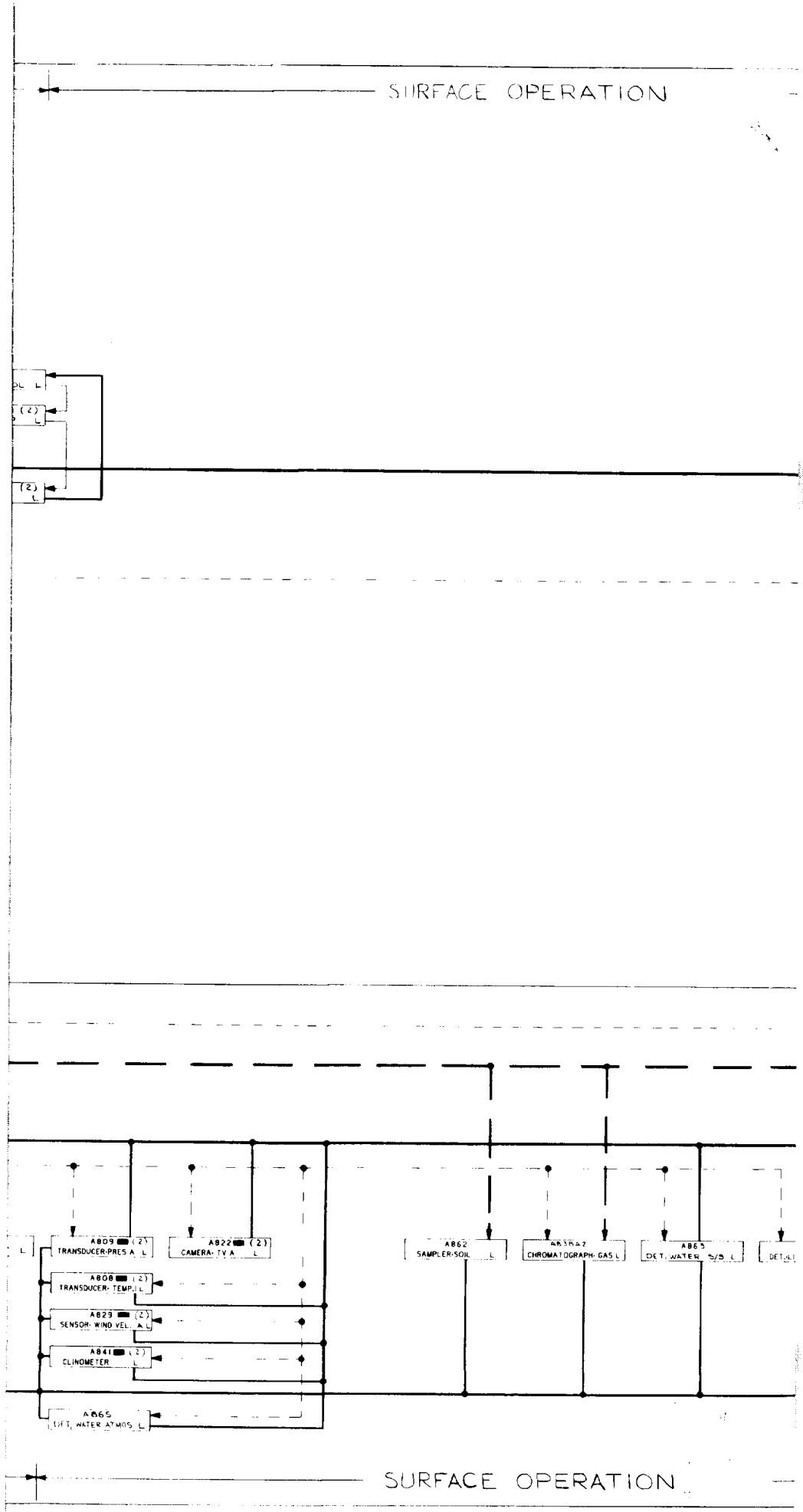

FOLDOUT FRAME 3

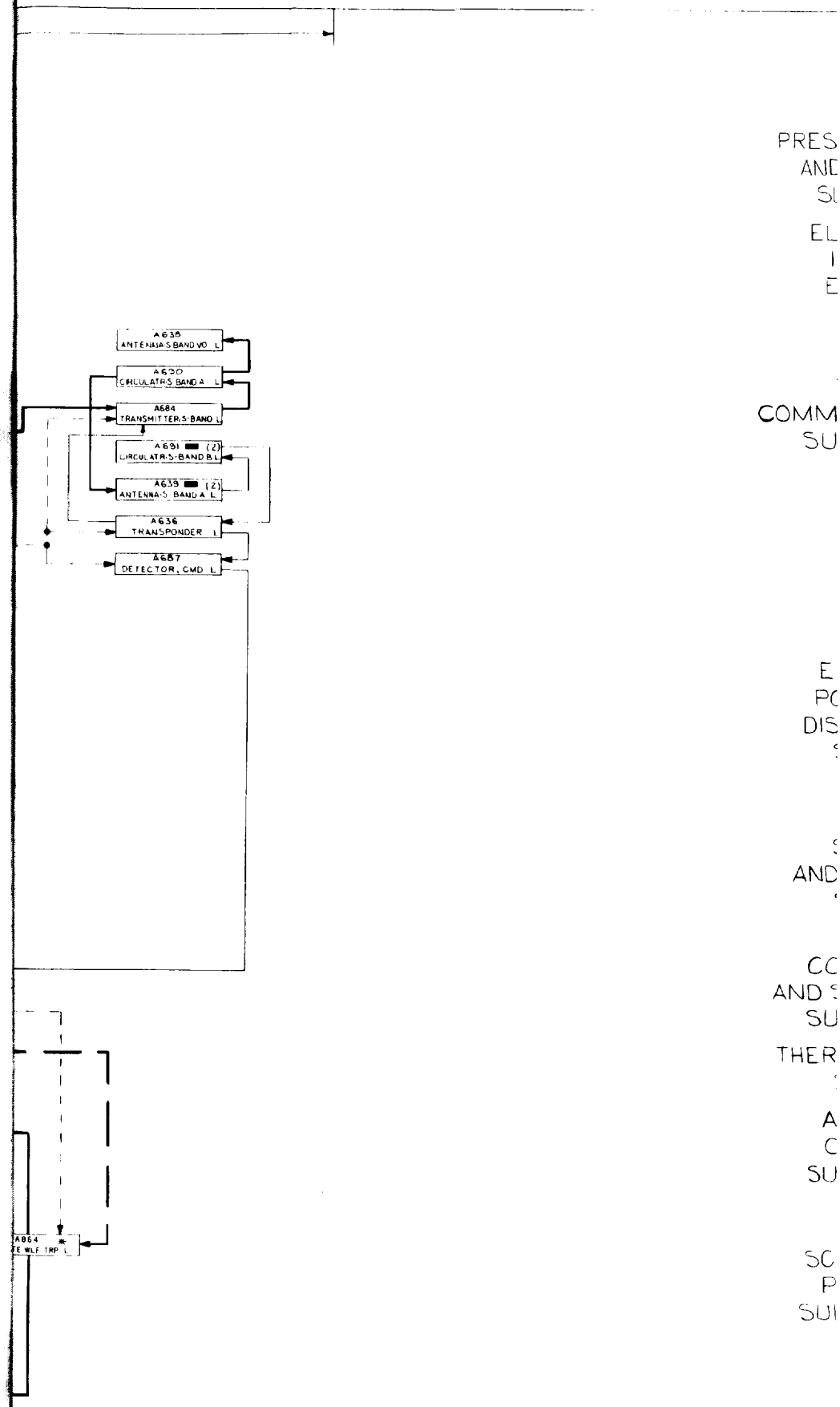

PRES
AND
SU

EL
I
E

COMM
SU

E
PO
DIS

AND

CO
AND
SU
THER

A
C
SU

SC
P
SUI

FOLDOUT FRAME 4

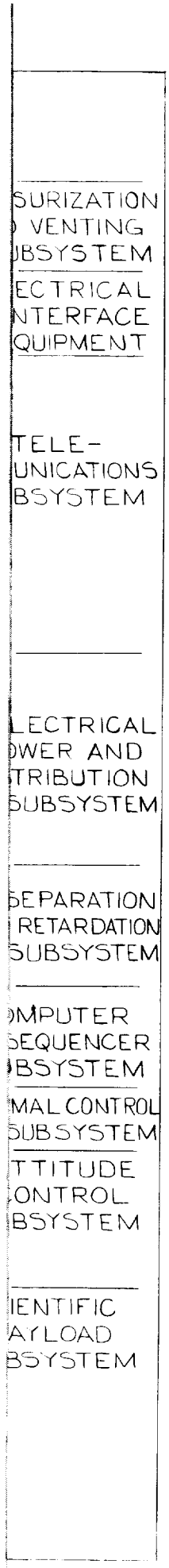

Figure 4.2-11. Electrical System Block Diagram (2 of 2)

FOLDOUT FRAME

4.3 SUPPORT MODULE DESIGN SUMMARY

The primary purpose of a Support Module is to serve as a relay station for the return of entry and post-impact imagery from the Flight Capsule to Earth. Fulfilling requirements for this relay function implies the need for Attitude Control and Power Subsystems as well as the obvious Relay and Radio Subsystems. In addition, the Support Module can support the Flight Capsule by assuming all other cruise functions which are not required by the separated Capsule, e.g., cruise phase telemetry and command, midcourse propulsion, etc.

During the cruise phase, the Support Module:

1. Provides attitude control for collection of solar power and reorients to arbitrary attitudes and attitude hold conditions during engine firing

2. Provides propulsion for midcourse velocity corrections

3. Provides mechanisms for Launch Vehicle separation and maneuver antenna deployment

4. Provides telemetry link for monitoring Spacecraft performance, including Capsule status

5. Provides command and sequencing functions for the Spacecraft, including the Flight Capsule

6. Provides power for Spacecraft, including Capsule heater and battery charging power.

During the encounter phase, the Support Module:

1. Provides power and a real time telemetry link to Earth to check out the Flight Capsule before separation

2. Maneuvers the Flight Capsule to its separation attitude

3. Provides attitude control to point the fixed Flight Capsule and Earth link antenna to establish and maintain data links

4. Receives and stores the pre-entry, entry and post-impact imagery data from the Capsule and Lander

5. Transmits to Earth the stored data.

The Support Module is essentially a stripped down version of the Mariner '69 Spacecraft using Mariner '69 flight proven hardware and techniques throughout the mission. The Mariner '69 Scan Platform, Science, and Data Automation System have been deleted. The deployable solar array panels of Mariner '69 have been replaced by a fixed array of smaller area to reflect reduced power requirements. The midcourse propulsion engine has been

moved to the roll axis and its propellant tankage increased to reflect the heavier combined weight of Support Module and Flight Capsule. A new maneuver antenna has been added to enable verification of maneuver attitude, and to supplement the low gain antenna at increased ranges. The digital tape recorder and telemetry subsystem have been modified to reflect new data rates; a second recorder has been added for redundancy. Structure weight and cable weights have been reduced significantly in the course of these modifications. Other subsystems are virtually unchanged from Mariner '69.

Following separation from the Launch Vehicle, the Spacecraft (Support Module plus Flight Capsule) acquires and locks on to the Sun and Canopus, which are its attitude references during the lengthy cruise phase. During this phase, engineering data showing Support Module and Flight Capsule status is sent via the telemetry link at 33-1/3 bps. Power is furnished by the solar array and is supplied to the various subsystems, including heater power to the Flight Capsule. About 10 days after launch, a midcourse velocity correction is commanded. The Spacecraft is reoriented to an arbitrary attitude to point the midcourse engine; the attitude is held while the engine fires to impart the desired velocity. During the maneuver sequence, power is supplied by battery and the telemetry link is maintained via the maneuver antenna. Following the correction, the Spacecraft automatically reacquires the Sun and Canopus, and the cruise mode of operation is reestablished. A few days before encounter, a second maneuver and midcourse correction takes place.

Sometime before Flight Capsule separation, Flight Capsule checkout begins. All Capsule subsystems which can be activated practically, undergo a complete status checkout. Flight Capsule telemetry data is sent to Earth in real time at 1100 bps via the Support Module telemetry system.

About 24 hr before encounter, the Spacecraft is maneuvered to the Flight Capsule separation attitude. After Capsule separation, the Support Module reacquires the Sun and Canopus.

From time of Flight Capsule deflection to entry, a data rate of 1100 bps is relayed from the Flight Capsule to the Support Module to Earth. During entry and until after landing, the 1100 bps data relay link is maintained and the data is stored on board the Support Module. The data rate is then increased to 70 kbps, allowing real time imaging data to be transmitted and stored on the Support Module. The Support Module later transmits the stored data to Earth at a convenient time as it flies by the planet.

A block diagram of the Support Module is shown in fig. 4.3-1.

Both a flyby and an orbiting Support Module have been considered during this study. Major emphasis was placed on the flyby design because it is lighter and it meets the primary mission requirement, which is to deliver a Lander to the Martian surface. Succeeding sections of this report are generally concerned only with the flyby design; however, a brief summary of an orbiting Support Module design is given here.

The primary advantage of an orbiting Support Module would be the ability to establish a relay station for obtaining more imagery data from the Lander. At each periapsis passage, the Lander/Orbiter relay link could be reestablished by ground command and a new series of

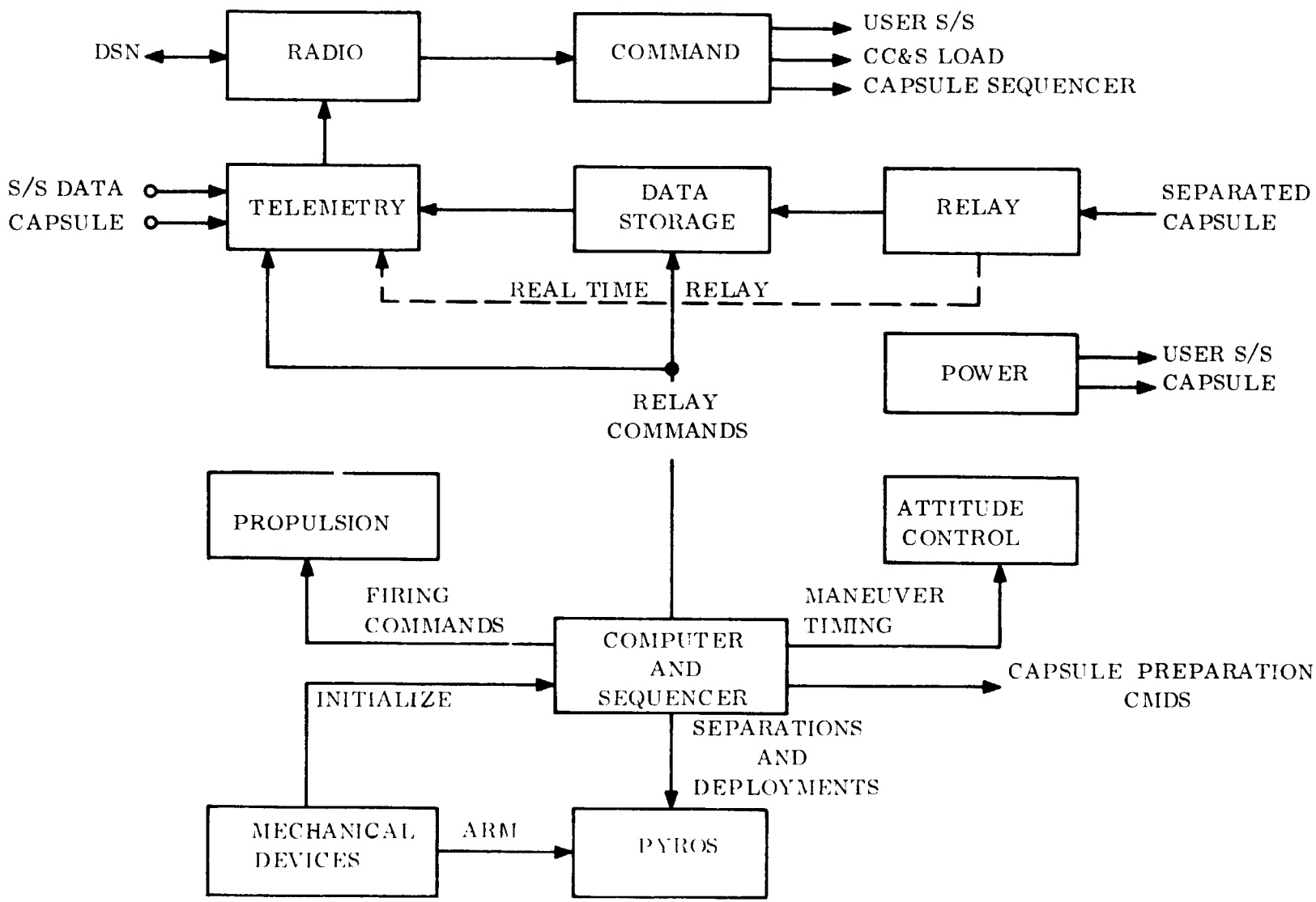

Figure 4.3-1. Support Module, Simplified Block Diagram

pictures could be obtained. In addition, a Mariner '69 TV Subsystem might be added to one of the empty bays on the Support Module octagon. At periapsis passage, the Support Module could be reoriented to point the TV camera at the planet and obtain orbital pictures of the planet.

The major penalty for an orbiting Support Module is the need for a larger propulsion system. The Rocketdyne RS14 bipropellant engine would replace the Mariner '69 monopropellant engine. The new engine and propellant required for orbit insertion weighs 565 lb as compared to the 82 lb of the flyby system.

Additional significant penalties occur in other subsystems. Solar array area must be increased to maintain required power for the increasing Sun-Spacecraft distance and added subsystems, such as the TV. This may require a deployable array. More extensive redesign of the attitude control autopilot is required since the RS14 engine must be gimballed because the vanes of Mariner '69 engine cannot tolerate the high temperature exhaust. The high power mode (20W) of the radio system or a lower data rate would compensate for the greater communication distances.

These changes place the orbiting Support Module beyond the capability of the Titan IIIC, and would probably require the Titan Centaur. However, weight estimates and propulsion requirements have been included in the succeeding sections in the event that a bigger launch vehicle is used for this mission.

Configuration Summary

The preferred configuration of the Mars '73 Spacecraft is shown in fig. 4.1-1. Although the Support Module contains many of the Mariner '69 subsystems, and is functionally almost identical, its outward appearance has changed significantly. The most obvious change is the deletion of the deployable solar array panels. Because of the reduction in required power with the deletion of science, scan platform, etc., a fixed solar array was selected since it could provide the area required. The array provides 50 ft^2 of solar cells compared to the 83 ft^2 of the Mariner '69.

Another significant change is the movement of the Mariner '69 bay-mounted propulsion system to a position on the Support Module roll axis. This engine is used during the midcourse corrections. The engine is unchanged — only its location and tank volume is changed. The propellant tanks are located in the octagon.

The Mariner '69 scan platform has also been deleted. The octagon configuration has been retained for housing the electronics subsystems although two of the bays are empty. Thermal control louvers are used on each of the bays to maintain bay temperatures.

The high gain antenna is unchanged from Mariner '69 but has been relocated to avoid the propulsion plume. The low gain antenna has been shortened and relocated for the same reason. A deployable maneuver antenna has been added to provide downlink coverage during maneuvers. Two new relay antennas have also been added.

The secondary Sun sensor assembly of the Attitude Control Subsystem has been relocated to avoid blockage by the Capsule. The attitude control jets have been relocated due to deletion of solar panels. (They were mounted at the tips of the panels on Mariner '69.)

Engineering Mechanics Design Summary

Engineering mechanics consists of the structure, temperature control, mechanical devices, pyrotechnic, and cabling subsystems. The baseline designs for these five subsystems are the Mariner '69 subsystems. Modifications are required to each subsystem because of the elimination of deployable solar panels, planet scan platform, and all science experiments. These modifications and associated weight changes are discussed in detail in Section 6.1 of this report.

The Mariner '69 octagon is maintained as the primary structure; however, only six of the eight bays are used. Changes to the upper and lower rings and superstructure are required to accommodate the above listed eliminations, a new fixed solar array, a fixed high gain antenna, deployable maneuvering and low gain antennas, and remounting the Propulsion Subsystem on the roll axis. The overall weight of the structure subsystem is reduced to 158 lb.

The temperature control, mechanical devices, pyrotechnic, and cabling subsystems have all been modified to accommodate the changes as listed above, causing reductions in weights to 26, 11.1, 10, and 57.9 lb, respectively.

Propulsion Design Summary

The Propulsion Subsystem that conforms to the requirements for the flyby Support Module is a modified Mariner '69 subsystem. It employs anhydrous hydrazine as the liquid monopropellant, a 50 lb vacuum thrust engine, and weighs approximately 82 lb, of which 53 lb is usable propellant. The structural arrangement, as designed by JPL, will be modified to some extent because the Propulsion Subsystem will be mounted on the roll axis instead of on the side of the octagon.

The orbiting Support Module requirements dictate a new Propulsion Subsystem. It employs a bipropellant engine with nitrogen tetroxide and mono-methyl hydrazine as the propellants, and provides 316 lb of vacuum thrust. The total subsystem weighs 565 lb with 428 lb of propellant.

Both the flyby and orbiting Support Module Propulsion Subsystems are described in detail in Section 6.2 of this report.

Guidance and Control Design Summary

The Attitude Control Subsystem acquires and stabilizes the Spacecraft to the Sun and Canopus, maneuvers the Spacecraft to any spatial attitude for subsequent propulsive velocity increments, and maintains vehicle attitude and stability during engine firings. Comprising the subsystem are Sun sensors, the Canopus sensor, the gyro control unit, attitude control electronics, cold gas system, and engine vane actuators. For Mars '73, the view of the Mariner '69

secondary Sun sensors located on the positive roll side of the octagon is blocked by the Flight Capsule and the sensors require relocation. The autopilot electronics will undoubtedly be changed to accommodate the different dynamic characteristics of the '73 Spacecraft.

The central computer and sequencer (CC&S) is a special purpose digital processor which generates and distributes on-board commands so that the Spacecraft can perform its mission automatically. Functions controllable by the CC&S include initial stabilization and maneuvers and engine firings. The CC&S consists of a reprogrammable computer and a maneuver sequencer. Computer reprogramming is accomplished via coded commands through the Flight Command Subsystem. The maneuver sequencer functions as a redundant source of critical maneuver and burn timing commands. Readout of the CC&S may be accomplished via the Flight Telemetry Subsystem for ground verification of the contents of the computer memory. The 128-word Mariner '69 memory is sufficiently large that minimal ground reprogramming is anticipated to conduct a nominal '73 mission automatically, and therefore the Mariner '69 CC&S appears adequate for '73.

Power Design Summary

The Power Subsystem provides a central supply of power to operate the electrical equipment onboard the Spacecraft and switching and control functions for the effective management and distribution of the power. Power is derived from a fixed solar array with a total area of about 50 ft^2. Stored power is provided via a rechargeable battery. Principal power distribution is a-c: viz., 50 volts rms, 2400 Hz, square wave. Also available are three-phase 400 Hz and unregulated d-c at 25 to 50 volts. In addition to the array and battery, the Power Subsystem includes two redundant boost regulators, two redundant 2400 Hz inverters and clocks, a 400 Hz inverter, battery charging circuitry and boost mode sensing and control electronics to prevent undesired array/battery sharing when the Spacecraft is Sun oriented.

Telecommunications Design Summary

Four subsystems classically comprise the planetary telecommunication group: radio, command, telemetry, and data storage. The addition of the Flight Capsule System in '73 adds a newcomer to this group, the Relay Subsystem.

The keystone of the telecommunications is the Radio Frequency Subsystem, which is functionally responsible for S-band reception from and transmission to the stations of the Deep Space Instrumentation Facility, detection and demodulation of the signal received at the Spacecraft, coherent frequency translation of the uplink-signal for subsequent downlink transmission, and modulation of the downlink carrier. Comprising the subsystem are three antennas (high gain, primary low gain, and maneuver gain), two redundant 20/10 watt TWT power amplifiers and exciters, a phase tracking receiver, and associated switching and isolation. Except for the maneuver antenna and its switches, the components are identical to Mariner '69. The high gain antenna is a prime focus paraboloid with a diameter of 40 in. and a nose gain of 25.5 dB. It is a fixed antenna with HPBW of 6.5°. The low gain antenna is similar to that used on Mariner '69 and '71. It is pointed along the negative roll axis, and its pattern is symmetrical about the axis, with a peak gain of 7.5 dB and a 3 dB beamwidth of 80°. The maneuver antenna is oriented such that its toroidal shaped pattern lies in a plane parallel to the Spacecraft roll/pitch plane. It has a gain of 4.5 dB and a beamwidth of 50°.

Switching is arranged so that transmission can occur on any antenna, while reception can only occur on either the low gain or maneuver antennas. The high gain antenna is employed principally for high data rate transmission to Earth, the low gain for communications when the Spacecraft is in conventional Sun orientations, and the maneuver antenna for uplink commands and downlink telemetry when the Spacecraft is in a maneuver attitude, or beyond the range of low gain antenna.

The Flight Command Subsystem operates on subcarriers from the Radio Subsystem, demodulates and decodes the command information, and issues commands to the applicable subsystems of the Support Module and to the Flight Capsule. The subsystem employs two types of commands:

1. Direct commands, which are single, discrete switch closures, and are used by the majority of subsystems and the Flight Capsule

2. Coded commands, which are binary data streams, sent to the CC&S for updating information stored therein.

The Command Subsystem consists of a command detector and a command decoder.

The Flight Telemetry Subsystem conditions, encodes, and multiplexes Spacecraft engineering data. Two modulated data channels are sent to the Radio Subsystem, a high rate channel and a low rate channel. The high rate channel is employed for imagery and entry data from the Data Storage Subsystem and pre-separation Flight Capsule checkout data from the Relay Subsystems. Stored data is transmitted at 4050 bps to the 210 ft dish; Flight Capsule checkout data is transmitted in real time at 1100 bps to the 210 ft antenna. Spacecraft engineering data (including Capsule status during cruise phase) is transmitted at either 8-1/3 or 33-1/3 bps on the low rate channel.

The Data Storage Subsystem (DSS) consists of a new digital tape recorder (DTR) which can store 3×10^7 bits.

The Relay Subsystem accepts data from the separated Flight Capsule during Capsule cruise and entry, and from the Lander during post-impact operation, and routes it to the DSS for delayed transmission to Earth. Relayed data is recieved on a 400 MHz carrier at 1100 bps during entry, and at 70 kbps after landing. Reception for cruise/entry (1100 bps) and post-impact (70 kbps) is accomplished by separate relay antennas. Each is a turnstile over a ground plane with a gain of +4 dB on axis and +3 dB at $\pm 55^\circ$ off axis. The antenna outputs proceed through separate receiver and FSK demodulators prior to routing the DSS. The Relay Subsystem is entirely new for Mars '73 Capsule mission.

Mass Properties

The weights of the '73 Support Module were developed by establishing the detailed weight of each component. The weight summary in table 4.3-1 shows the subsystem weights of the

Flyby Support Module configuration in which the Mariner '69 Propulsion System design is used. Also shown is the weight summary of an Orbiting Support Module, where a single R4d engine characterizes the Propulsion System. For comparison purposes, Mariner '69 weights are also listed.

TABLE 4.3-1. SUPPORT MODULE, WEIGHT SUMMARY

Subsystem	Mariner '69 Weight (lb)	Flyby Support Module (lb)	Orbiting Support Module (lb)
Structure	203.0	158.0	158.0
Radio Frequency	56.0	60.0	60.0
Command	8.0	8.0	8.0
Relay	—	5.0	5.0
Power	120.5	101.0	115.0
Central Computer and Sequencer	24.0	24.0	24.0
Flight Telemetry	21.5	21.5	21.5
Attitude Control	62.2	62.0	62.0
Pyrotechnics	11.0	10.2	11.0
Cabling	67.2	57.9	57.9
Propulsion	46.5	82.0	565.0
Temperature Control	29.0	25.8	25.8
Devices	63.1	9.6	9.6
Data Storage	37.2	34.0	34.0
Data Automation	13.8	—	—
Scan Control	19.8	—	—
Ultraviolet Spectrometer	34.6	—	—
Television	46.8	—	—
Infrared Spectrometer	38.5	—	—
Infrared Radiometer	7.5	—	—
Total System Weight	910.2	659.0	1156.8

5. FLIGHT CAPSULE SYSTEMS

5. FLIGHT CAPSULE SYSTEMS

5.1 SCIENCE

5.1.1 LANDER SCIENCE INSTRUMENTS

5.1.1.1 Summary

Studies of the Lander science instruments were necessitated in order to determine the development status of each with respect to 1973 Hard Lander mission requirements. The following points were considered: (1) hardenability to a 2500 'g' impact loading for a few msec, (2) sterilizability (135° C for 96 hr), (3) reasonable weight, power, and volume requirements, and (4) reasonable mechanical, thermal, and electrical interface requirements upon the rest of the system. Those instruments not currently suitable for the Lander mission were further analyzed to determine what modifications are required to qualify them, and whether it is reasonable to expect completion of design, construction, and testing programs within strict time constraints.

After surveying the development status of each type of instrument identified in table 3.1-2, it became evident that none met all the criteria listed above. However, it was established that only the hardenability requirement constitutes a major problem - fortunately, not insoluble - for most of the instruments. In addition, relatively major engineering efforts are required to develop certain instruments or portions of them (e.g., soil sampler, gas chromatograph, an integrated life detector, and the clinometer). Table 5.1-1 describes and summarizes the approximate status for each of the instruments.

Additional problems are identified in the following sections where background information is presented. Sterilizability constitutes a relatively minor problem for several instruments. The purpose of this study was to scope the magnitude of instrument development and integration problems and determine whether solutions were forthcoming without excessive expenditures of time and money. That this is the situation has been demonstrated.

5.1.1.2 Facsimile Cameras

One camera package will be mounted on each of two booms. Each integrated package will contain a high and low resolution camera. Fig. 5.1-1 shows two camera designs and the elements that each contains. Neither of the two versions shown contain the azimuthal drive motor. The high speed version has a 5-sided mirror that rotates unidirectionally; the preferred video rate for this version is not well defined and can be from 10 kHz to 100 kHz depending on circumstances. The incident light passes through the window and is reflected from the mirror onto the silicon cell detector. The solid state amplifier amplifies the resulting electrical signal to +5v maximum, the output signal leads from the camera housing carry this signal to the processing electronics. The slow speed version (that can take up to 4 hr for a full panoramic

TABLE 5.1-1
LANDER INSTRUMENT DEVELOPMENT STATUS

Primary Instrument	Current Hardening Status (Units: g-loading)	Relative Engineering Effort Required For Development, Integration and Flight Qualification	Remarks
Facsimile Camera	3500	Continuing effort required	Successfully tested at high g-loading
Gas Chromatograph-Mass Spectometer	Few hundred (estimate)	Major effort	Integrated instrument not tested; chromatograph components tested to 10,000g; magnetic sector mass spectometer tested to 400 g
Life Detector (Wolf Trap, New Design)	Not yet constructed	Major effort	Conceptual design
Water Vapor Detector (Al_2O_3)	Few hundred	Major effort	Major problems anticipated in removing terrestrial water contamination from Lander system
Wind Velocity Sensors (Cup Anemometer)	Hardened for CSAD Program at JPL	Relatively minor effort	Hardening cups and erectable boom reasonably straightforward

TABLE 5.1-1 (CONT)
LANDER INSTRUMENT DEVELOPMENT STATUS

Primary Instrument	Current Hardening Status (Units: g-loading)	Relative Engineering Effort Required For Development, Integration and Flight Qualification	Remarks
Pressure Transducer (Capacitance Diaphragm)	2500	Minor effort	Problems anticipated during sterilization; may have to recalibrate following sterilization
Temperature Transducer (Platinum Resistance Thermometer)	1000	Minor effort	Use of a non-platinum material may be desired
Soil Sampler	Not tested	Major effort	Design not yet specified,
Clinometer	Not yet constructed	Moderate effort	Conceptual design
Alternate Instruments			
3 DQ Mass Spectrometer	Not yet constructed	Major effort	Currently in laboratory and commercial development stage
Life Detection (Gulliver)	50 or 100, not tested	Moderate effort	Design of ejection mechanism required

TABLE 5.1-1 (CONCLUDED)
LANDER INSTRUMENT DEVELOPMENT STATUS

Primary Instrument	Current Hardening Status (Units: g-loading)	Relative Engineering Effort Required For Development, Integration and Flight Qualification	Remarks
Wind Velocity Sensor (Sonic Anemometer)	Not tested	Major effort	Operational reliability improvement required design of boom and erection mechanism
Water Detector (Tritiated CaH_2)	Not yet constructed	Major effort	Development and testing stage removal of terrestial water contamination

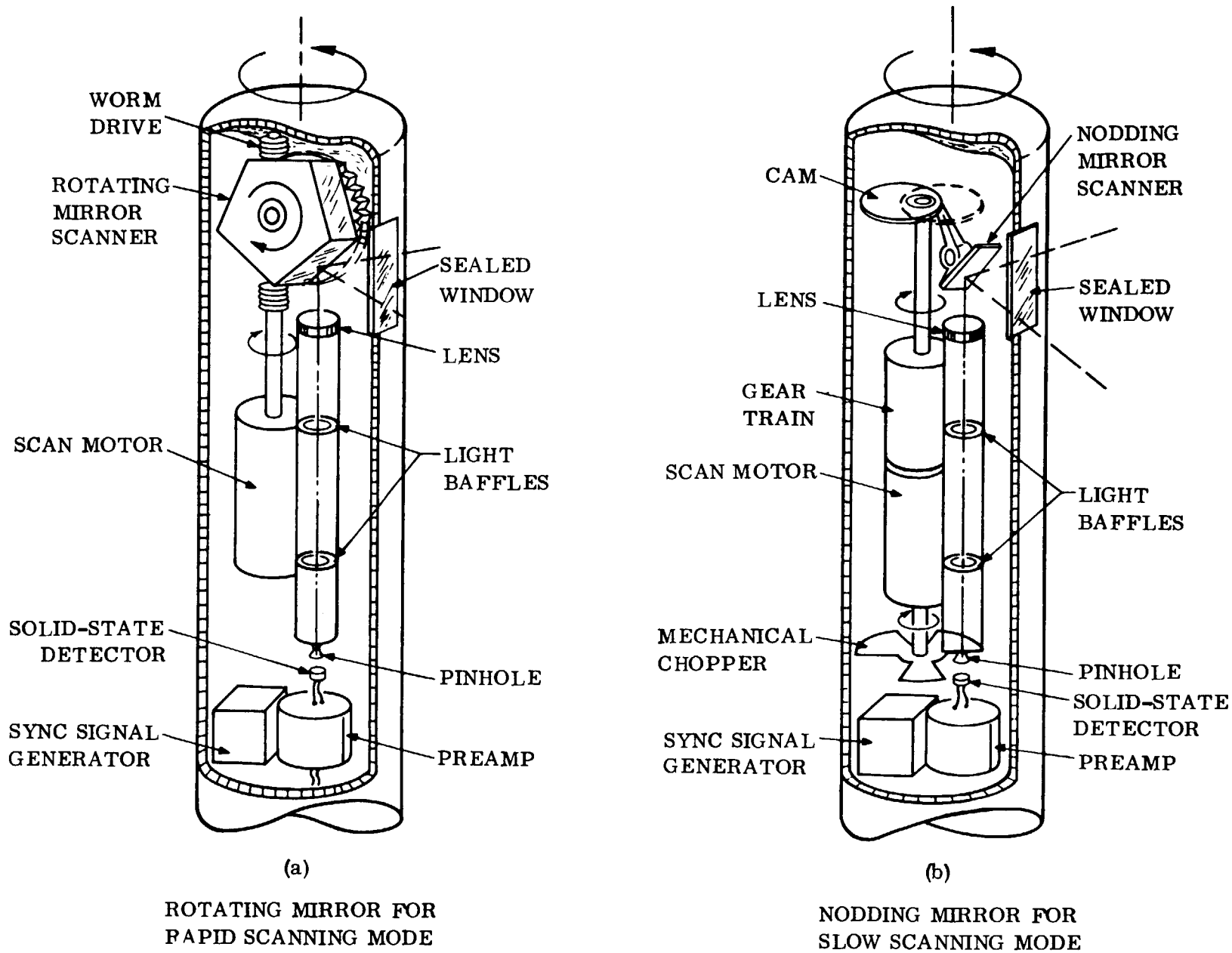

Figure 5.1-1. High and Low Speed Cameras

TABLE 5.1-2. TYPICAL CAMERA SPECIFICATIONS

Model Identification	CM	SL	NP	SS	SM
Special Feature	small size small power	rugged	high speed	adjustable performance	high resolution
Field of view	9° x 360°	50° x 360°	25° x 360°	10° x 10° to 90° x 360°	1° x 1°
Resolution	0.1 in. @6 ft	0.1 in. @6 ft	1 in. @100 ft	0.1 in. @1 ft to 0.1 in. @ 60 ft	1 micron @ 3/4 in.
Frame time	1/2 min	7 min	2-1/2 sec	30 sec to 10 hr	1 sec
Sensitivity range	0.1-1000 ft-L	0.3-3000 ft-L	1.5000 ft-L	0.001-5000 ft-L	10-10,000 ft-L
Size	1 in. dia x 6 in. long	1.5 in. dia x 10 in. long	2.5 in. dia 11 in. long	3 in. dia x 18 in. long	3 in. dia x 15 in. long
Weight	0.4 lb	3.5 lb	5.5 lb	6.5 lb	6 lb
Power	1 W	10 W	150 W	15 W	4W
Temperature (of the environment)	-10° F to $+150^\circ$ F	-40° F to $+180^\circ$ F	-10° F to $+125^\circ$ F	-45° F to $+145^\circ$ F	-45° F to $+145^\circ$ F
Pressure (external)	1 ATM	10^{-9} Torr	1000 psi	1 mb	1 mb
Shock and Vibration	1000 g	3500 g	100 g	300 g	50 g

sweep) has a nodding mirror activated by a cam. The light beam is deflected via this mirror onto the silicon cell after being chopped by a small light chopper placed in front of the cell. This latter addition enables the same basic amplifier to be used for both the high speed and low speed versions. The dimensions of the camera unit that contains all the mechanical drive mechanisms and all the electronics for the video and synchronizing signals varies with the full design specification; normally, however, these will be between 1 and 3 in. in diameter and between 6 and 16 in. long. Total weights of the cameras as described can again vary from 1/2 to 6-1/2 lb (See table 5.1-2).

The photoimaging sequence is programmed to take four low resolution pictures in a format containing 1.75×10^5 resolution elements; the frame limits are variable; the present extremes are $70^\circ \times 25^\circ$ and $50^\circ \times 35^\circ$. Each of the low resolution frames has nested within it a high resolution frame of $5^\circ \times 5^\circ$ and containing 2.5×10^5 resolution elements. The four frames are taken in four directions that are mutually at right angles. The combination of the aforementioned resolution elements of 1.75×10^5 (low resolution) and 2.5×10^5 (high resolution), four frames, and a 6-bit gray level results in a total imaging data load of 1.02×10^7 bits. If telemetry permits more data bits, an attempt will be made to complete the panorama by taking frames in additional directions.

The hardened camera system is at a relatively advanced stage of development. Additional design and testing is required. Optical alignment following impact is critically important. Hardenable and erectable booms must be designed and integrated into the vehicle.

5.1.1.3 Gas Chromatograph-Mass Spectrometer

This system is required to identify many volatile inorganic and organic materials in the Martian atmosphere and soil. A flow chart is shown in fig. 5.1-2.

There are two modes of operation. In the first mode, atmospheric gases will be fed directly to the mass spectrometer and there identified and measured.

In the second mode, a soil sample is placed in the pyrolizer oven. There it is heated and vapors are released to enter a chamber where they are held. After a sufficient vapor sample has been acquired the pyrolizer valve is closed and an inert gas (e.g., helium) carries the vapor through the chamber and chromatograph columns, selective interactions occur between various components of the sample and the column packing material, causing component velocities through the columns to differ. Different components thus leave the column at different times. Samples may have to be routed through several colunms to achieve complete separation. At the outlet of the gas chromatograph column a thermal conductivity detector determines when a sample emerges and its quantity. Knowledge of the delay time for known substances allows identification, particularly when a known calibration material is also processed.

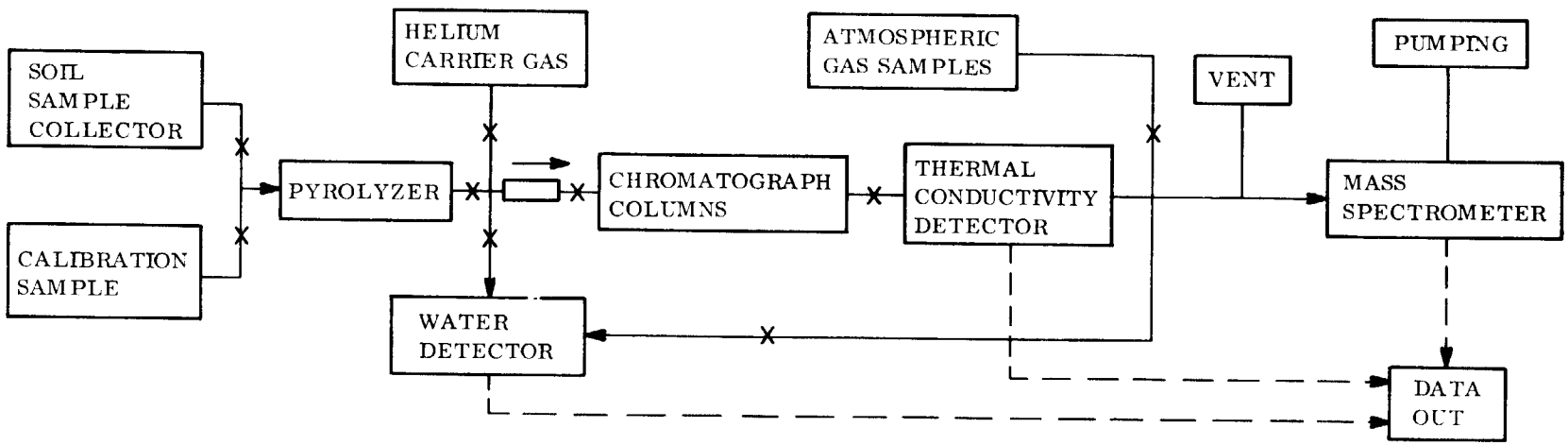

Figure 5.1-2. Gas Chromatograph-Mass Spectrometer Flow Chart

Supplementary analyses can be accomplished with a very sensitive water detector shown in fig. 5.1-2 and described in para. 5.1.1.5.

The sample leaving the thermal conductivity detector would then be sampled by a controlled leak for analysis by a mass spectrometer. An ion source would ionize and to some degree break up the molecules of the vapor sample. These ions would then be accelerated in an electrostatic field and be separated by charge-to-mass ratio through bending in electrostatic and magnetic fields. (Other mechanisms for separation are available but are not considered here because of their early stage of development.) These separated ions are then detected with accuracies of one atomic mass within the lower mass ranges.

The gas chromatograph recommended for this application is a very light and simple unit comprised of only a small oven (pyrolyzer), valving, a system temperature control, the carrier gas and regulator, a few microcolumns, a power supply, and logic sequences that are usable with the mass spectrometer. A thermal conductivity detector may be used or may be omitted since sensing can be accomplished with the mass spectrometer.

Recent work has reduced the gas unit chromatograph to very small size and weight; probability of its inclusion on a hard Mars Lander is thus enhanced. A development effort is required for bracing the entire unit (components have been hardened in at least one study) and integrating the soil acquisition device, the mass spectrometer, and water vapor detector. The very sensitive water detector will supplement mass spectrometer data. In case different ions with the same molecular weight, (e.g., H_2O, NH_2D (ammonia) CH_2D_2 (methane)) are present, the water detector will identify the water component with more certainty.

The drawbacks to such a system are the critical ion optics and magnet alignment, the weight of the magnet, the vacuum pump requirement, and the difficulty of analyzing light gases and heavy molecules in the same apparatus due to the great differences in their radii of curvature. The alignment and weight problems can be solved by miniaturization and adequate bracing, but analysis of both heavy (> 150 Amu) and light (< 50) molecules is likely to require two different instruments. Depending upon resolution requirements, the heavy molecule analyzer will probably be larger and heavier than the light molecule analyzer. Due to severe weight constraints imposed upon the Lander system, it may be necessary to restrict the atomic weight range to relatively light weight atoms and molecules if a magnetic sector device is chosen.

The recent introduction of a cold cathode ion source has resulted in improved prospects for hardening the magnetic sector mass spectrometer, as well as reduced power requirements. Units have been tested to 400 g's, and can be designed to withstand higher loadings.

Gas chromatograph components have been hardened to 10^4 g's. However, complete units designed to withstand g-loadings of the order of 2500 g's have not been constructed. According to several independent sources, hardening a complete gas

chromatograph-mass spectrometer system is within the state-of-the-art.

Units similar to those used in gas chromatographs and mass spectrometers have been sterilized. Assuming proper design, system sterilization will be straightforward.

Small lightweight gas chromatographs have been developed for use with a mass spectrometer. Several companies have done work on relatively complex units. Overall status for a flyable instrument is one of advanced development.

Magnetic sector mass spectrometers of the required size and weight have been constructed. Flyable units are available with 400 g capability. Advanced development status exists for higher 'g' units. Table 5.1-3 compares three candidate types of mass spectrometer.

A new, very promising mass spectrometer design is being developed by the General Electric Research and Development Center. This device, the Three Dimensional Quadruple (3DQ) mass spectrometer, has the advantage of being a very small monolithic unit easily braced for high 'g' shocks. It requires very little power and its total weight is below that of comparable spectrometers.

There are no critical optics or magnetic field needed since separation occurs through selective storage of a given charge to mass ratio. The frequency and amplitude of an r-f signal applied to the storage electrode along with a dc voltage determine which charge to mass ratio is stored. The sensitivity because of this storage feature is very high and allows analysis of very low pressure gases ($< 10^{-10}$ mm Hg).

Analysis of a different range of charge-to-mass ratio can be made with the same electronics by changing the scale of the electronics. Thus, the range of 2 to 50 amu and the range of 40 to 1000 amu can be covered with the simple addition of another electrode configuration weighing a few ounces and an expanded power capability for the oscillator. A fixed frequency crystal controlled oscillator with a stepped voltage amplitude of 25 to 1 would fit both requirements.

Due to its small mass and unitized construction, hardening to 2500 g's should not constitute a major problem. Sterilization will be straightforward.

The 3DQ mass spectrometer is in an early stage of development. Models have been built for various government laboratories and are now being developed for commercial application.

5.1.1.4 Life Detector

The detection of life of an unknown type in an unknown environment presents a major challenge. Success in this venture will more probably occur if carefully defined and integrated experiments are conducted. Several approaches to the problem involve the search for physiological evidence of life, including the detection of growth, reproduction, or metabolic activities. The "Wolf Trap" measures microbiological growth.

TABLE 5.1-3 MASS SPECTROMETER COMPARISON

Characteristic	Quadrupole Mass Spectrometer	Magnetic Sector Mass Spectrometer	Three-Dimensional-Quadrupole Mass Spectrometer	Comments
AMU RANGE RESOUTION	ALL ARE COMPARABLE			
WEIGHT (lb)	8	8	UNDER 5	
POWER (watts)	10	3.5	UNDER 3	
SIZE (in.^{3})	300	300	UNDER 70	10 in. LENGTH IS NECESSARY FOR SEVERAL DESIGNS
PUMPING	LN_2 SORPTION PUMP 4 LITER/SEC ION PUMP		0.15 LITER/SEC ION PUMP	
FLIGHT PROVEN	YES	YES	NO	
STERILIZABLE	YES	YES	YES	
HARDENED	400 g	400 g	NO	
DETECTION OF HEAVY MOLECULES	PROHIBITIVE COST IN POWER	PRACTICABLE BUT REQUIRES LARGER OR MORE MASSIVE INSTRUMENT PLUS MORE POWER	PRACTICABLE AT MODEST COST IN POWER OR SLIGHT ADDED WEIGHT	3DQ REQUIRES MUCH SMALLER SAMPLES

"Gulliver" detects reproduction and/or metabolism by identifying the formation of radioactive CO_2 from C^{14}-labeled substrates. The metabolic uptake of radioactive and phosphate are additional observables. A very sensitive and rapid means of identifying the presence of organisms involves the observation of intracellular ATP (adenosive triphosphate) through bioluminescent techniques.

Chemical evidence of life may be obtained by gas chromatographic-mass spectrometric analyses. Another very important chemical means is that of optical rotation activity. The source of optical rotation of plane polarized light may be proteins, nucleic acids, or nucleotides. Additional methods for detecting extraterrestrial life have been suggested.

Several of these techniques may be integrated into a single instrument (e.g., the Automated Microbial Metabolism Laboratory (AMML)-proposed by Dr. Gilbert V. Levin, of Biospherics Research, Inc., Washington, D.C., and the Multivator-proposed by Dr. Joshua Ledenberg of Stanford University).

Two of the life detection techniques which have advanced engineering status have been studied as typical examples to determine whether they may be integrated into a Hard Lander. These are the Wolf Trap and Gulliver, both of which have been described in the literature (refs. 5.1-1 through 5.1-4).

The Wolf Trap utilizes nephelometric (light scattering) techniques to observe the increase in density of microorganisms due to growth. Ball Brothers Research Corporation (BBRC) of Boulder, Colorado completed a conceptual study for a small lightweight version of Wolf Trap which will withstand an impact loading of 2500 g's for a few msec.

An informal design review of the new concept was conducted at BBRC on October 3, 1968. The improved design occupies a cylinder 8.187 in. long and 3.15 in. in diameter and is estimated to weigh approximately 1.5 lb. This design represents a significant advancement over the earlier engineering model which measured 9 x 9 x 9 in. and weighed approximately 10 lb. The new conceptual design contains all of the salient features of the original engineering model with the exception of ph probes and the sample acquisition device. A schematic of the design is presented in fig. 5.1-3, which is intended only for the purpose of illustrating the functional characteristics of the concept. The complete details will be published by Ball Brothers Research Corporation and released under the authority of Dr. Wolf Vishniac, the principal investigator for the Wolf Trap.

In general, the BBRC conceptual design contains most of the basic features necessary for structural integrity under high impact shock conditions. These are listed in table 5.1-4, which presents an evaluation of the key elements in the BBRC conceptual design for high shock capability. Three questionable features were found to exist. These were in the valves and pistons, optics, and mounting portions of the design. Recommendations for improvements in these areas have been communicated to BBRC and several are being incorporated into a revised design. Table 5.1-5 summarizes

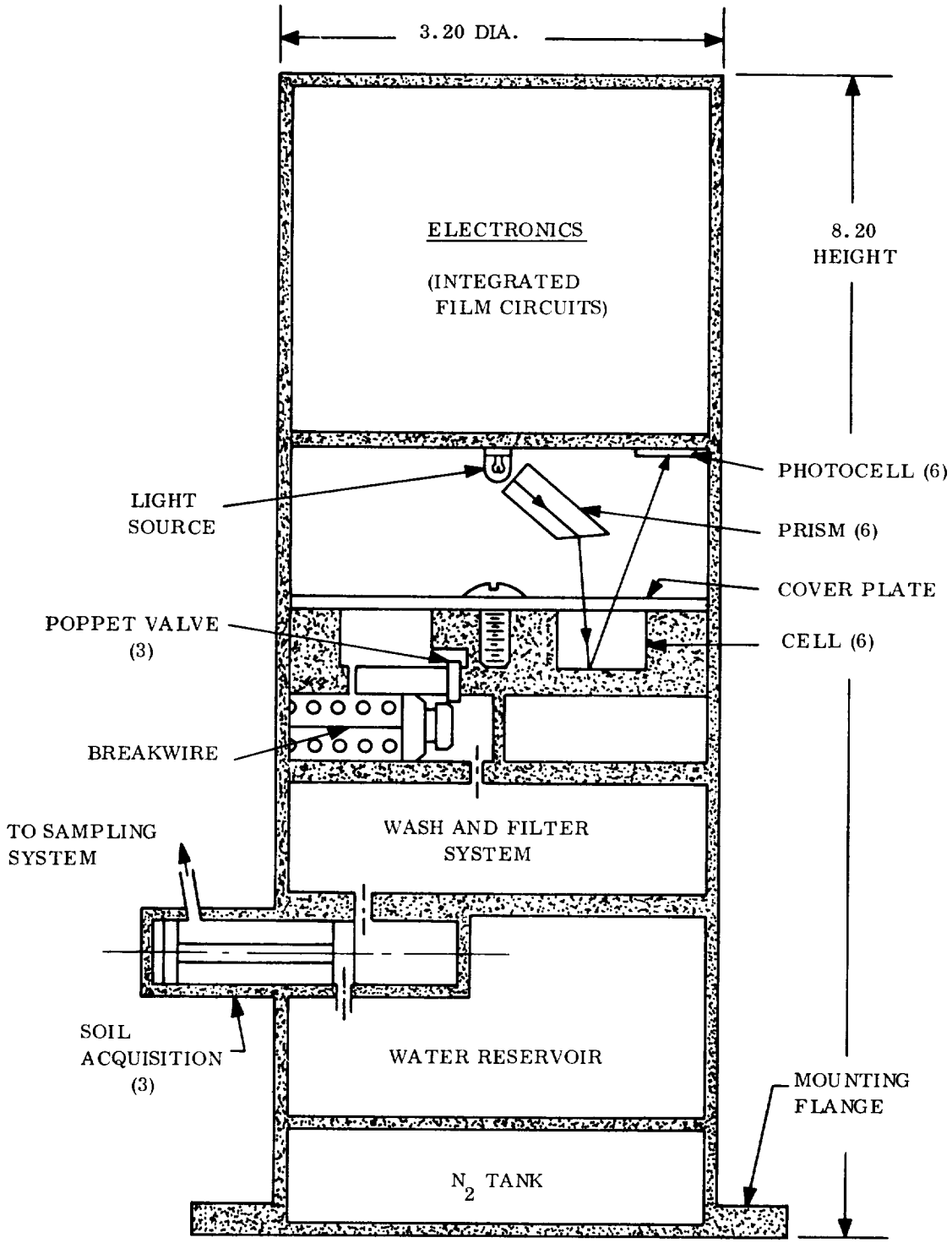

(SCHEMATIC - NOT TO SCALE)

Figure 5.1-3. BBRC Hardened Wolf Trap Concept

TABLE 5.1-4. BBRC WOLF TRAP CONCEPTUAL DESIGN EVALUATED IN TERMS OF GE-RS SHOCK DESIGN CRITERIA

CRITERION / DESIGN ELEMENT	RELATIVE MOTION	BALANCING	FREQUENCIES	"BILLIARD BALL"	DAMPING	PRELOADING	STIFFNESS AND MINIATURIZATION	IMPEDANCE MISMATCHING	STRESS CONCENTRATION: AREA CHANGES	BRITTLE MATERIALS	LOAD PATHS
SIZE AND WEIGHT			M				M				
UNITIZED ASSY.	M	M	M				M		M		
VALVES, PISTONS	?		?	?		M	?		?	M	?
OPTICS	M	M	M	M	?		M	?	M	?	?
ELECTRONICS	M		M	M	M		M	M	M		M
MOUNTING	?		?						?	M	?

KEY: M - MEETS CRITERIA

? - QUESTIONABLE AREA

BLANK - NOT APPLICABLE

TABLE 5.1-5

BASIC FEATURES FOR STRUCTURAL INTEGRITY

1.	Small size and weight
	8.187 in. long x 3.15 in. diameter — 1.5 lb
2.	Unitized assembly
	Machined from cylinder of titanium
	High strength to weight
	Rigidized design
	High natural frequency
	Absence of cantilevers, brackets, etc.
	Fluid passages integral part of design
	Tubing, connections, sealing, eliminated
3.	Simplified fluid transport system
	Valve pistons are mechanically captive
	Preloaded springs used for energy sources
	Bellows replaced by N_2 operated piston
4.	Simplified lens system over original design
	Single prism for directing light to each cell
	High strength glass
5.	Non-critical orientation
	Closed system after soil acquisition
	Operates in any orientation
6.	Hardened electronics
	Solid state light detector
	Solid state integrated circuits
	Hybrid film circuits

the desirable features found in the BBRC design, including the General Electric recommendations.

Figs. 5.1-4, through -7 illustrate some of the recommended design changes to the mounting structure, nutrient poppet valve, breakwire/plunger and acquisition plunger. The recommended design changes will greatly improve the shock resistance without seriously affecting the weight of the system. Two of the more serious design defects observed in the BBRC concept center around the plunger device shown in figs. 5.1-5 and -6. Fig. 5.1-5 shows the BBRC concept which utilized a plunger to disengage a spring-loaded poppet valve which allows the water sample to pass into the nutrient cells. This approach is undesirable because of the possibility of "billiard ball" action during the high impact shock condition, which could result in premature plunger engagement, poppet valve distortion and subsequent jamming, or structural failure of the plunger preload tension wire. The GE-proposed design change utilizes an internal porting design which eliminates the poppet valve. The breakwire tension device is replaced by a structurally superior tension rod held in place by a split collet as shown in fig. 5.1-6. In this arrangement, the breakwire serves only to keep the collet in position. When the breakwire is activated, the tapered head will separate the collet, allowing the compressed spring to move the plunger.

The electronics, housed within the titanium cylinder, will be composed of thick film integrated and hybrid circuits. No significant problems can be foreseen in impact-hardening the circuitry.

In summary, the BBRC conceptual design of Wolf Trap contains most of the features required to withstand the high impact shock expected in the Mars' 73 Hard Lander. Several design features which appear to contain potential problems have been evaluated, and design improvements recommended. These design improvements are minor in nature and are being considered by BBRC.

The new concept for the hardened Wolf Trap can be sterilized in dry heat at 145° C for 24 hr without significant problems.

It has already been noted that the hardened Wolf Trap is in conceptual design. BBRC states that designs can be completed and models built, tested, and delivered for flight qualification testing within two years following the receipt of a contract.

The second life detection reviewed for hardenability was the "in sites" model of Gulliver (ref. 5.1-3).

Gulliver detects bacterial reproduction and/or metabolism by identifying the formation of radioactive CO_2 from C^{14}-labeled liquid or solid substrates such as formate, glucose, lactate, glycine, or other nutrients. Growth or reproduction is indicated by an exponential increase in the counting rate of the radioactive gas. If metabolism occurs without growth or reproduction, the count rate also increases. The count rate curve of the test is calibrated against one obtained from a bacterial growth chamber in which an inhibitor of growth has been introduced.

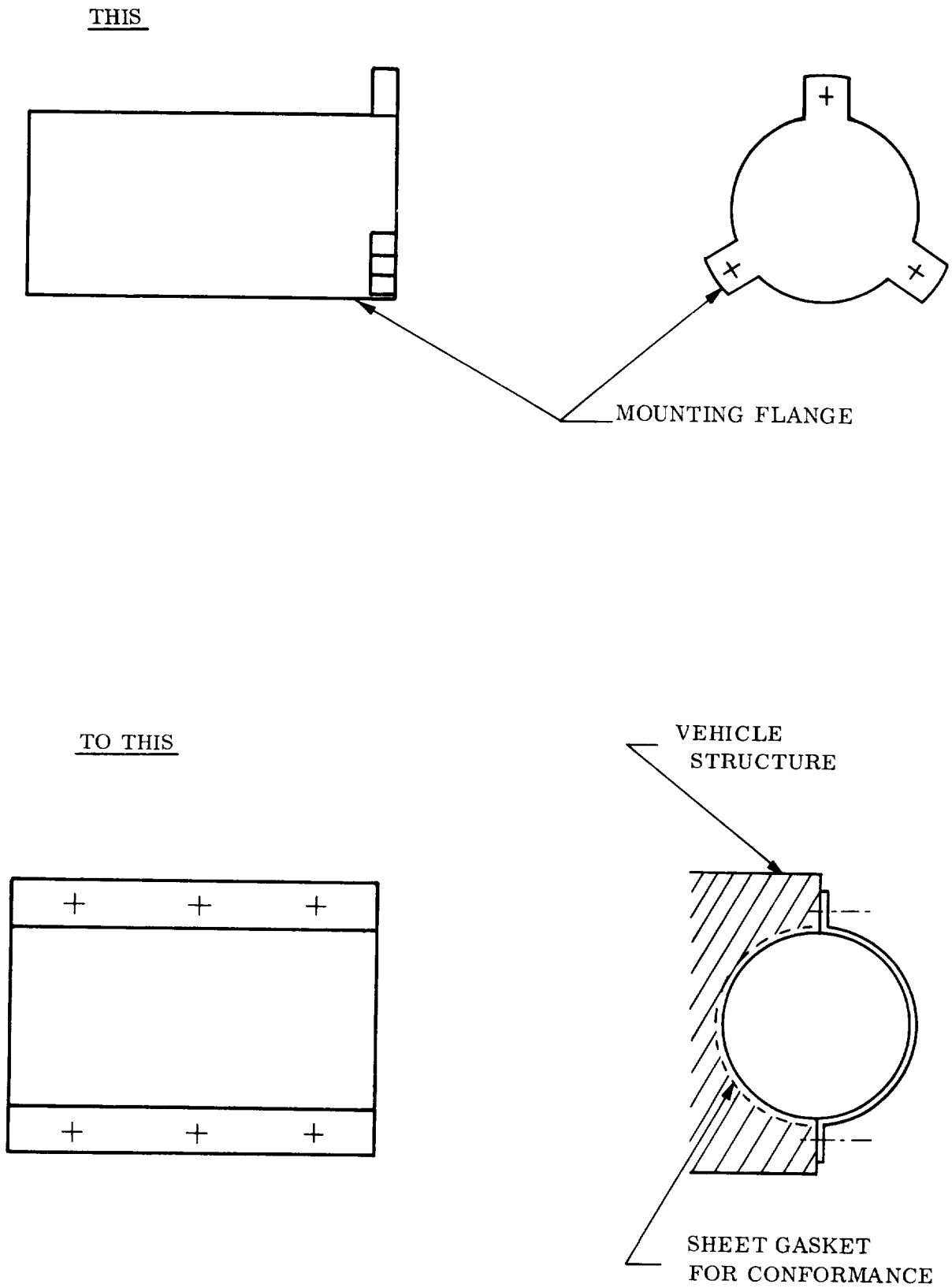

Figure 5.1-4. Elimination of Stress Concentration by Uniform Loading

THIS

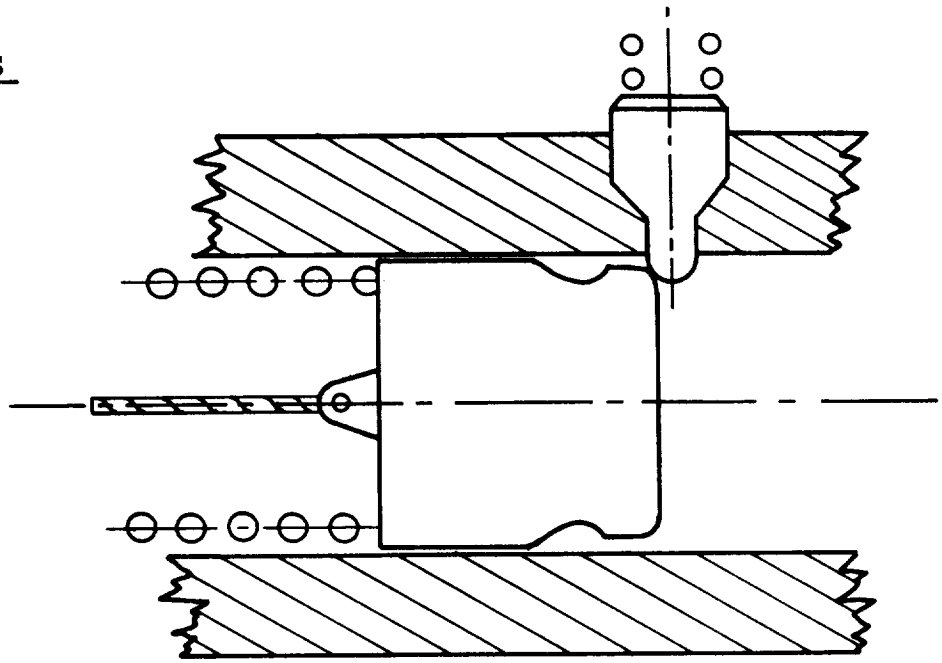

TO THIS

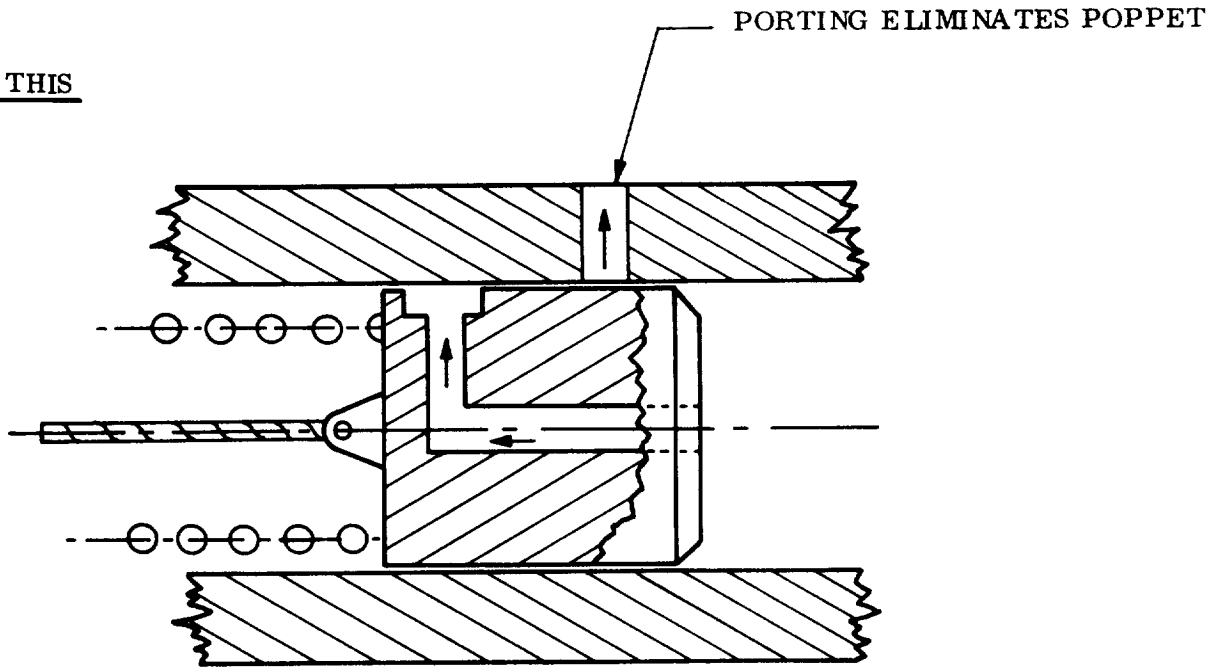

Figure 5.1-5. Elimination of "Billiard Ball" Action

THIS

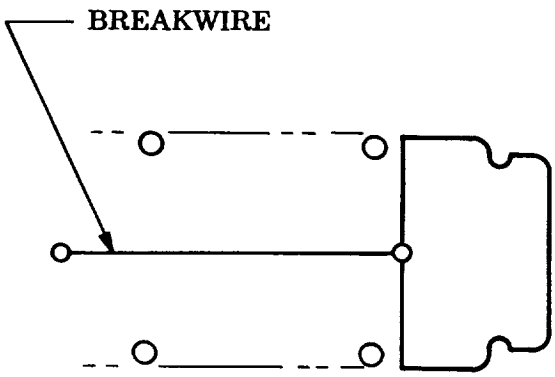

BREAKWIRE IN TENSION

TO THIS

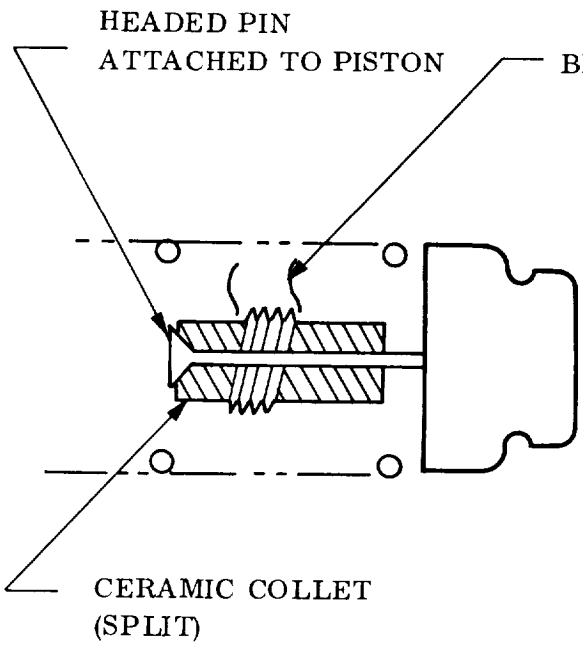

PISTON RETAINED BY
CERAMIC HELD IN POSITION
BY BREAKWIRE

Figure 5.1-6. Using the Breakwire as an Initiator

THIS

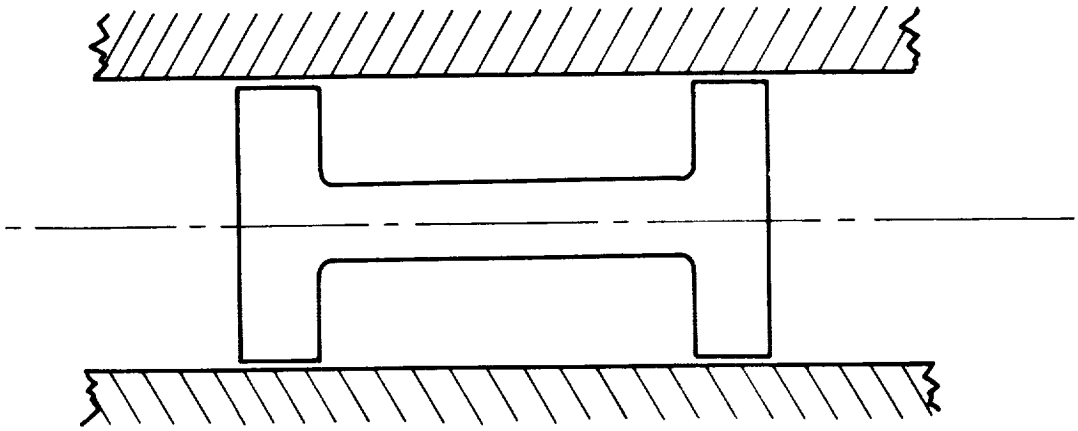

TO THIS

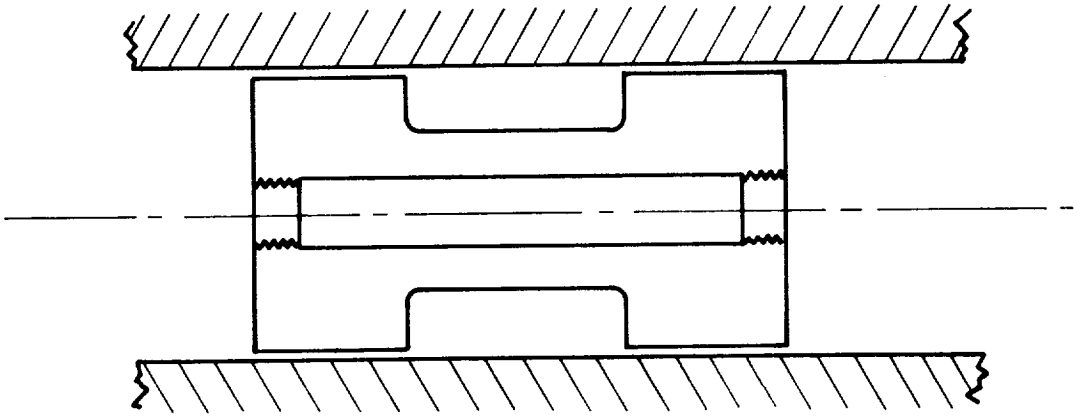

Figure 5.1-7. Increased Land Bearing Area and Shaft Stiffness

The small (3 in. x 1.25 in. diameter, 3 ounce weight) Gulliver Capsule is ejected from the Lander by a compressed spring or pyrotechnic device. An umbilical cord is connected with the Lander for data transmission. The module erects itself on landing. Pliable bellows on the bottom portion rest on the planetary surface to confine the radioactive broth which is released at the proper time. If microbiota are present and will grow in the broth provided to release $C^{14}O_2$, a geiger counter located in the top portion of the module will detect it. The geiger counter is not located in direct line of sight to the broth on the planetary surface. It will detect the radioactive gas which rises in the module.

Gulliver can be designed to withstand an impact loading of 2500 g's. It is sterilizable, and the unhardened design is in an advanced state of engineering development.

5.1.1.5 Water Vapor Detector

Of the several water detection techniques available, two are currently under consideration for use in the Hard Lander. These meet the subsystem constraints, including low weight, and low power requirements, high sensitivity to water, and little or no interaction with other atmospheric or surface components. The first method to be discussed involves the Al_2O_3 hygrometer which is distinguished by its simplicity and light weight. The second technique utilizes tritiated calcium hydride and is characterized by its extreme sensitivity to the detection of very small concentrations of water vapor. The water detection will supplement data from the mass spectrometer.

Either water detector will be integrated with the gas chromatograph-mass spectrometer. The same atmospheric sampling unit will serve both the mass spectrometer and water detector. If the Al_2O_3 hygrometer is chosen, it is tentatively recommended that two units be included in the payload. One of these would observe atmospheric gases only; the other would detect water from the outgassing soil and pyrolysis products. It is conceivable that the amount of water introduced into the analytical units from one of the sources may be different from the other source. If water vapor concentrations in the Martian environment are extremely low, any relatively large concentration may unduly influence the accuracy of succeeding readings from the second source. It is important that the Lander should be degassed of water vapor prior to launch so that it will not serve as a source of water contamination.

The desirability of performing several atmospheric measurements is due to the need to improve the measurement statistics as well as observe the duirnal humidity changes and the effects of the freeze-thaw phenomena in the nearby soil.

It is anticipated that fresh samples of atmospheric gases will be analyzed on each succeeding occasion the experiment is performed. However, it is presently believed that subsurface soil will be collected on only one occasion and delivered into a hopper from which samples will be removed when required for appropriate experiment. Therefore, all analytical studies will be performed on different portions of the first- and only-sample delivered into the central hopper. It is therefore required that the sample introduced into the hopper not be contaminated with any terrestrial materials.

Water and the honeycomb phenolic glass crush-up material appear to be the greatest problems.

Water will be stored in only one experiment currently under consideration (Wolf Trap). All valving must be designed so that no vapor leaks at any time into the Lander or its surroundings. As one precaution against leaks, the first atmospheric and subsurface water determinations will be initiated prior to the time the water container in Wolf Trap is opened and nutrient, soil and water mixing begin.

The Al_2O_3 hygrometer consists of of a thin gold layer deposited on a porous Al_2O_3 layer atop an anodized aluminum plate. The two plates of a capacitor are formed by the aluminum plate and gold layer, separated by the Al_2O_3 insulator. The impedance characteristics vary as water vapor penetrates the gold layer and changes the resistance of the Al_2O_3 as water is absorbed within it. Sensor impedance is measured by an impedance bridge.

The Al_2O_3 sensor structurally consists of an aluminum plate attached inside a small case. Electrical contacts are made to a simple electrical circuit.

Solutions to hardening and sterilization problems appear to be relatively straightforward.

An alternate experiment involves a very sensitive water vapor detection system which has been developed by General Electric. It is based on the reaction of water with tritium, and the determination of water vapor is translated to the measurement of tritium levels. See fig. 5.1-8.

A contoured avalanche semiconductor radiation detector is used to sense the tritium level. (fig. 5.1-9). The detector amplifier and read-out are entirely solid state, and one version has been flight rated. Detection efficiencies of better than 70 percent for 10KeV electrons have been measured at Goddard, with backgrounds of less than 0.5 cpm, and the feasibility of determining tritium in the gas phase has been demonstrated at General Electric.

During operation the sampling system delivers gas at a given temperature, pressure and flow rate to the detection tube inlet. A flow rate of about 3 cm^3/min will yield a system response time of one min. The gas is passed through heated tubing and fed to a cylindrical bed of tritium labeled CaH_2 operating at about the same temperature as the tubing. The quantity of tritium released is directly proportional to the amount of water vapor in the gas stream. The tritium concentration is determined in the known gas volume, and this is directly related to the water concentration in the gas stream. Operation can be either intermittent or continuous.

The sampling system is an important factor in limiting system sensitivity and response. Experiments at General Electric have shown that for water vapor concentrations below about 10 ppm, ordinary materials of construction do have a significant effect on system response and sensitivity. Water sorption and desorption is apparently

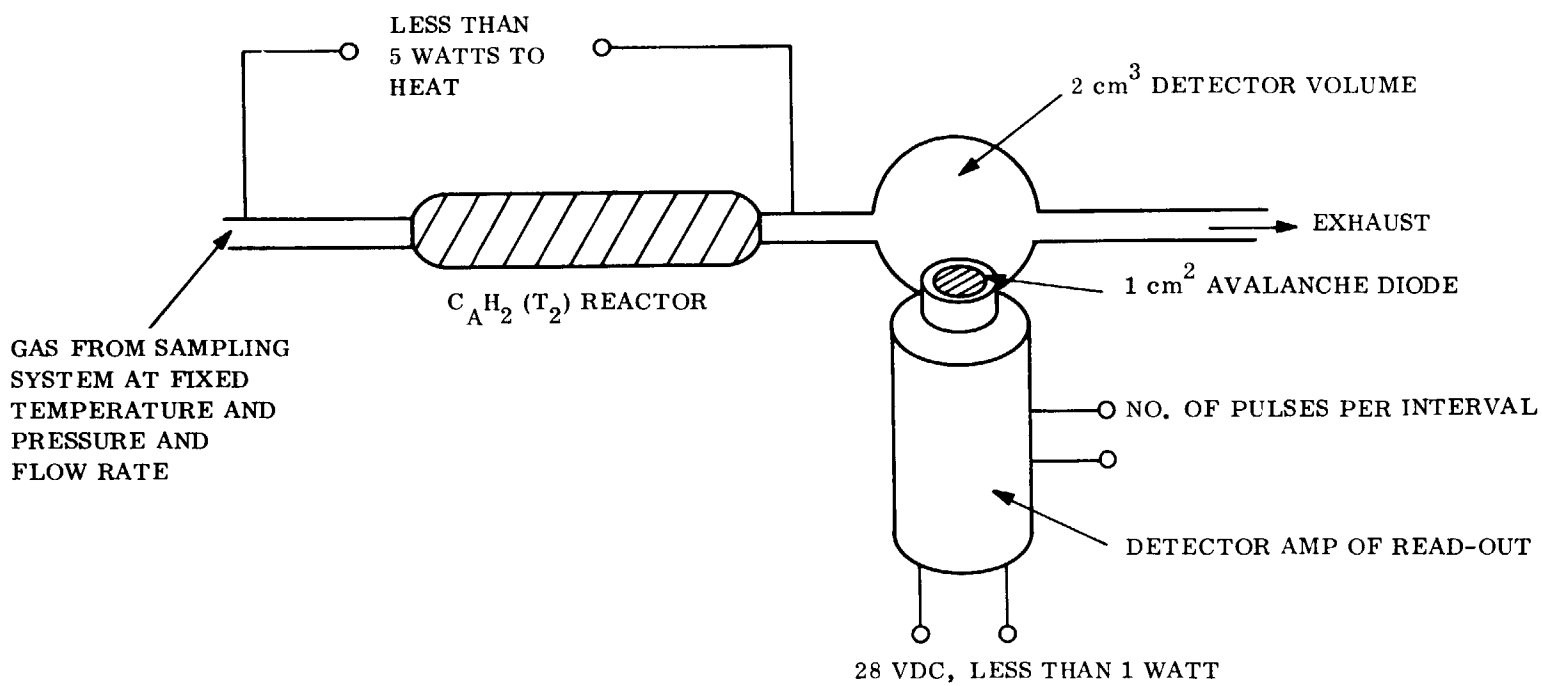

Figure 5.1-8. GE Water Vapor Detection System

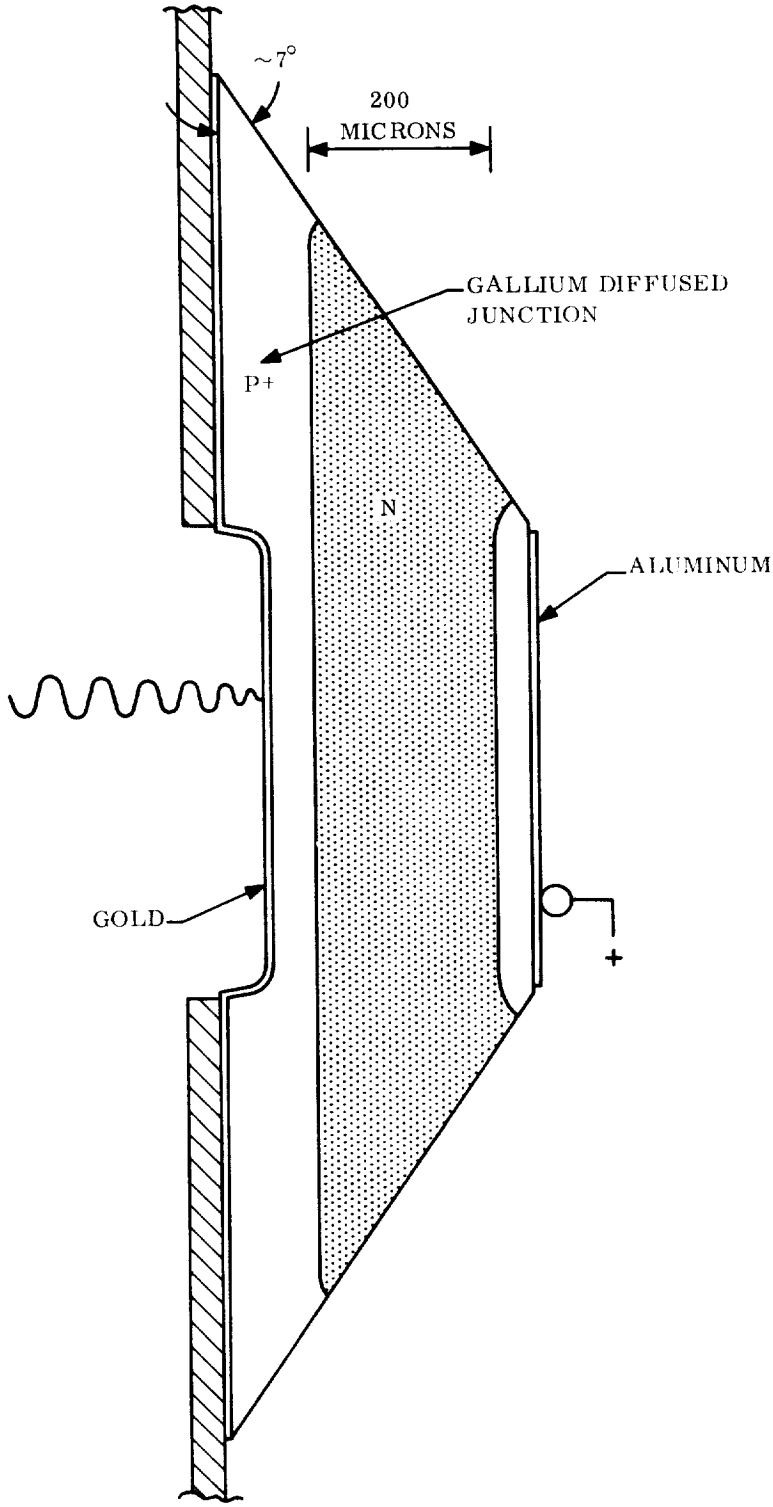

Figure 5.1-9. Contoured Surface Silicone Avalanche Detector

controlling, and experiments are currently under way or planned to select optimum materials and operating conditions. Past work at General Electric has established criteria for materials selection and shown temperature to be a crucial operating parameter while total operating pressure is not a factor.

Expected water detection sensitivity based on current laboratory experimentation is in the range of 1 - 10 ppb. Response time requirements can have a strong influence on precision at the lower water concentration. Inaccuracies in the determination of the gas density in the detector volume are reflected directly in calculation of water concentration.

Labeled CaH_2 has been heated to 180° C for days without any measurable effect. The detector and its electronics have operated continuously at temperatures exceeding 100° C ambient. On this basis, no harmful effects of repeated exposure to a dry heat sterilization cycle are anticipated.

5.1.1.6 Wind Velocity Sensor

Both rotational and aerovane anemometers are among the types of wind velocity sensors which have been considered. Rotational anemometers usually have three, four or more cups rotating in a horizontal plane and attached to a vertical shaft. Aerovane types are designed with a helical propeller mounted in front of a vane which identifies wind direction. In both types, a linear relation exists between fluid velocity and rotational speed regardless of fluid density or pressure over a wide dynamic range (about five decades). It has been shown by Professor G. L. Gill of the University of Michigan that given instruments maintain their linear calibration whether operating in water, air at one atmosphere, or air at pressures of a very few millibars in a low pressure wind tunnel. At low atmospheric pressures (approximating the anticipated seven millibar surface pressure on Mars) a longer period of time is required for the sensor to reach its proper rotational speed due to wind slippage.

Cup anemometers have been recommended for use because of their simplicity of design, high reliability, light weight, low power requirements, and due to the fact that dust will not adversely affect their accuracy. Lubrication of moving parts in the tenuous Martian atmosphere will have to be investigated, but will not constitute a major problem. However, problems may exist in measuring low velocity winds due to the very small dynamic fluid pressures. Wind direction cannot be accurately measured with an aerovane at low velocities for the same reason.

In the absence of definitive studies it is suggested that the wind velocity sensor should ideally be mounted at a height above the vehicle equal to the height of the vehicle above ground. However, future studies might indicate that turbulence due to the presence of the vehicle in the windstream would extend to a distance less than one vehicle diameter above the upper surface. Mechanical weight and other constraints (e.g., the field of view of the TV cameras) may require the sensor to be mounted within a foot or so of the upper Lander surface. Effects due to turbulence can be studied and, to some extent, be "calibrated out."

A three-cup anemometer suitable for use on the Lander may have arm lengths of about 3 in. (measured to the center of the cup). The cups (hemispheres) will have diameters of about 1 in. The weight of an unhardened version is estimated to be about 2 lb. The revolution rate of the cups may be easily measured by capacitance changes or other well known techniques. It appears that tachometric methods should not be employed on Mars. While operating, the electronics will probably require less than 0.5 watts.

Wind velocities during established time intervals may be integrated in order to derive an average velocity. Both peak and instantaneous velocities may also be measured.

JPL has successfully conducted hardening studies, and experiments on cup anemometers for the CSAD program. Careful packaging is essential in the Hard Lander to prohibit cantilever action in the arms and boom. Uniform loading will remove this problem.

No problem will exist in sterilizing the instrument.

An additional wind velocity sensor should be noted. The sonic type has significant promise and was described briefly in the previous Hard Lander Study report. (ref. 3.1-1)

5.1.1.7 Pressure Transducers

A variable capacitance pressure transducer monitors ambient pressure. The device detects pressure differences between the two sides of a diaphragm mounted between nearly rigid capacitor plates. Deflection of the diaphragm causes capacitance changes which are measured by a simple electronic circuit. The direction and magnitude of the capacitance difference is calibrated in terms of pressure differentials.

The instrument samples pressure every 20 min during the diurnal cycle. Under normal circumstances this frequency may not be necessary but, as a result of the lower atmospheric pressure on Mars, the time constant for atmospheric changes may be shorter than on Earth. If a pressure change accompanying or preceding a sudden large atmospheric event occurs, a sample rate geared to the anticipated most rapid change is chosen.

Although the instrument has not been sterilized at 135°C, it appears that a high pressure buildup may occur in one of the cells. It would have to be determined whether the unit would be damaged or lose its calibration.

5.1.1.8 Temperature Transducers

A platinum resistance thermometer serves as a temperature transducer. Temperature variations cause resistance changes which are sensed by a resistance bridge circuit and which, in turn, generate an output voltage. This voltage is proportional to the thermometer resistance.

The thermometer should be isolated from direct thermal contact with the Lander and with solar radiation. The Lander wind contact should also be minimized. Apart from interest in the maximum and minimum temperatures, major interest is centered upon the rate of change in the sunset and sunrise periods. One sample each 20 min during landed mission life has been chosen as a suitable time interval.

Platinum resistance thermometers may be hardened and sterilized without significant engineering problems.

5.1.1.9 Soil Sampler

The soil sampler is required to obtain and deliver subsurface soil to a hopper from which the Wolf Trap and gas chromatograph-mass spectrometer-water detector may secure specimens for analysis. Subsurface acquisition is desirable because a higher density of microorganisms is likely to be found due to absence of ultraviolet radiation. Moisture content is also probably higher. In addition, the retrieval of native surface materials contaminated with phenolic glass particles is to be avoided.

The sampler must be hardenable, sterilizable, and probably subject to baking and sealing prior to launch in order to eliminate contamination from terrestrial water. In order to prevent the killing of microorganisms the sampler must not develop high temperatures due to friction while digging.

Many sampler designs have been studied by JPL and industry, but none has been selected as a preferable design. General Electric considered a concept primarily to determine whether it is hardenable. The identification of this concept does not constitute a recommendation by General Electric that this is an optimum or desirable design.

In this concept a two-axis gimbaling system directs a drill in a downward direction, which is specified by the clinometer. A motor causes the drill to rotate and advance. Diagnostic data indicates whether the drill is penetrating the soil; if not, the drill may be retracted and redirected. It is not essential that the drill travel in the vertical direction. After the drill has penetrated the surface the outer portion will stop rotating, on command, and an inner, smaller diameter drill will continue drilling. Subsurface soil will be carried into a chamber in the upper part of the drill portion. The soil will then be mechanically lifted into a hopper from which it is distributed to specified science instruments.

Uniform loading within the Lander package will permit the device to withstand high g-loadings. Sterilization will be straightforward.

5.1.1.10 Clinometer

A commercially available clinometer with an electrical output indicative of angle has not been located. A method of making the measurement is shown in fig. 5.1-10. The potentiometer proposed for this purpose is a Bourns unit specially designed with a ceramic element and rulon bearings. Such pots have been tested to 2000 g's successfully. No sterilization problems are foreseen.

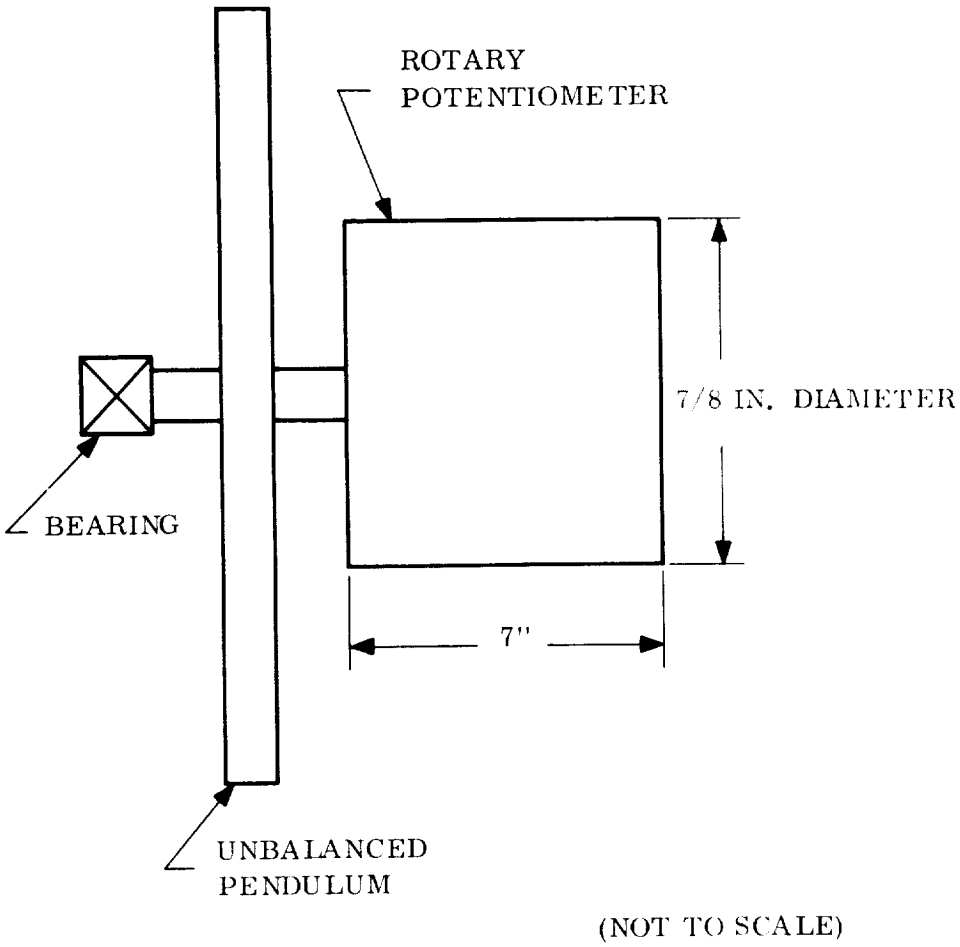

Figure 5.1-10. Rotary Potentiometer Clinometer

5.1.2 ENTRY SCIENCE

5.1.2.1 Temperature

Atmospheric temperature measurements during the entry phase are performed by three platinum resistance thermometers. These were selected because of their superior performance characteristics in the temperature regime of interest (100-300°K). Additionally, their excellent calibration stability provides a high confidence level in the ultimate measurement accuracy.

One thermometer is located in the stagnation region of the aeroshell and measures the stagnation temperature from the beginning of entry to the deployment of the parachute and separation of the aeroshell. The use of only stagnation readings in the higher Mach number altitude regime stems primarily from the extreme difficulty

in reliably interpreting temperature data at other points when extensive aeroshell heating and ablation occur. In addition to the effort required to design a sensor for optimum performance during Martian entry, extensive preflight testing will be required to evaluate and establish calibration curves for the sensor performance under the anticipated flow conditions. The data is necessary for the post-flight analysis to determine ambient temperatures.

The other two thermometers are located on the base of the Lander system and are used during the subsonic region of flight, primarily during parachute descent. Available data indicates that the correspondence between the measured base temperatures and the ambient values can be reliably predicted.

A resistance thermometer employs a temperature sensitive element to parametrically measure temperature by measurement of the element's electrical resistance. Platinum's excellent electrical stability over long periods of time and its high melting point, coupled with its extreme resistance to chemical deterioration lead to its use over extended temperature ranges. Accuracies of the order of 0.02 percent at 500°C are possible.

The characteristics of this instrument are shown in table 3.1-1.

5.1.2.2 Pressure

Variable capacitance pressure transducers located on the aeroshell and on the base of the entry system measure atmospheric pressure profiles. This type of instrument was chosen because of its demonstrated reliability, independence from other measurements, and the accuracy requirements of the measurements. During supersonic flight the primary measurements for determining the ambient values of pressure will be made at the vehicle base since correlation studies (ref. 5.1-5) indicate that a reliable correlation curve can be obtained. Measurements will also be made in the stagnation region where four pressure transducers will primarily provide data for determining vehicle angle-of-attack and will also serve as back-up devices for the base pressure transducer. These transducers are located just behind the heat shield and are exposed to the external environment via ducting leading through the beryllium cap of the heat shield. Preflight testing will be employed for establishing the measurement requirements and post-flight analysis.

The subsonic pressure measurements will also be made at the base of the vehicle and will be used with the corresponding temperature measurements to determine the altitude-time profile to impact.

The variable capacitance pressure transducer is a "referenced" type of instrument which senses a difference in pressure between the sample being measured and a reference carried in a hermetically sealed chamber. It determines the pressure by measuring the change in capacitance between a deflected diaphragm and one or more reference surfaces located near the diaphragm. Motion of the diaphragm causes changes in the capacitive reactance of one leg of an unbalanced capacitance bridge network. The resulting bridge output potential indicates the pressure difference between the reference chamber and the sample.

The characteristics of this instrument are given in table 3.1-1.

5.1.2.3 Density

The use of triaxial accelerometers at high Mach numbers provides for the indirect determination of density as a function of time. A single set mounted at the Capsule's c.g. is adequate for this function if the body motion undergoes small angle-of-attack oscillations. The determination of the Capsule's altitude-time profile using the same basic data imposes more stringent requirements and forces the use of at least two measurement ranges. In addition, the existence of large angles-of-attack, if they occur, will demand the use of off-axis rate gyros to establish angle-of-attack histories which would be needed to account for the variation of drag coefficient with angle-of-attack.

The body acceleration interpretation approach to density determination was chosen on the basis of weight, volume, and system compatibility considerations. By sampling at high rates, the body dynamics sensitivity of the evaluation is minimized.

The primary operating regime will be from the beginning of entry down to parachute deployment. Below this point, the acceleration data will have primary importance for engineering performance and only a secondary scientific value. In this latter region density is obtained from the measured pressure and temperature profiles. Use of this data also significantly reduces the bias error in the higher altitude accelerometer data.

It is anticipated that the atmospheric density profile may be reconstructed to within 5 percent by this technique, based on results of computerized experiment simulation.

Characteristics of the accelerometer are given in table 3.1-1.

5.1.2.4 Composition

The composition of the atmosphere during entry is determined by means of the mass spectrometer which has been described in the Surface Science section (5.1.1). Similarly, the water vapor detector is operative during both the entry and surface phases of the mission and has also been described in Section 5.1.1.

Subsonic pressure and temperature data serve as a back-up to the mass spectrometer since, with proper data analysis, it leads to determination of mean molecular weight.

5.1.3 REFERENCES

5.1-1 BIOLOGY AND THE EXPLORATION OF MARS, edited by Colin S. Pittendrigh, Wolf Vishniac and J. P. T. Pearman, Publication 1296, National Academy of Sciences and National Research Council, Washington, D.C. (1966).

5.1-2 EXTRATERRESTRIAL LIFE: AN ANTHOLOGY AND BIBLIOGRAPHY, Compiled by Elie A. Shneour and Eric A. Ottesen, Publication 1296A, National Academy of Sciences and National Research Council, Washington, D.C. (1966).

5.1-3 THE SEARCH FOR EXTRATERRESTRIAL LIFE, Vol. 22, ADVANCES IN THE ASTRONAUTICAL SCIENCES, James S. Hannahan, ed., Scholarly Publications (1967).

5.1-4 L. Ried, Jr., E. Lemberg, D. E. Buckendah, "Wolf Trap Mars Microbe Detection Device", Final Report by Ball Brothers Research Corporation, Boulder, Colorado. Prepared for University of Rochester, Contract No. NSG 209-AG1, 20 March 1967.

5.1-5 Correlation of Available Flight Test Base Pressure Data for Application on Planetary Entry Configurations, GE-RS Technical Brief.

5.2 TELECOMMUNICATIONS

The telecommunication system for the 1400 lb Lander/Capsule includes the Communication Subsystem, the Radar Altimeter Subsystem and the canister Data Handling Subsystem; the Relay Link, Direct Link, and Data Handling Subsystems comprise the Lander/Capsule Communication Subsystem. Following is a description of the subsystem and its operation and performance.

5.2.1 TELECOMMUNICATION SUBSYSTEM

5.2.1.1 General Requirements

The general requirements of the Telecommunication System are summarized in table 5.2-1. In addition to these functional requirements, a mission constraint requires that the entry data be transmitted prior to landing. Further, because the mission value is measured in terms of data returned, there is a need to design the Telecommunication System to return the maximum practicable amount of data. The communication performance is limited by the Capsule resources of weight and energy available for communication equipments. Further, the selection of the performance goals must also take into account the mission success probability.

The selected telecommunication approach is consistent with reasonable data return capability based on simple, proven components and techniques. A simplified block diagram is shown in fig. 5.2-1.

5.2.1.2 Overall Subsystem and Mission Description

Throughout the mission the subsystem collects engineering diagnostic and performance data. During interplanetary cruise this data is read out by the Support Module telemetry subsystem for transmission to Earth. After separation a relay link to the Support Module is used. A 1100 bps link is established during this time, using the 400 MHz, 50 watt transmitter and an array of four whip antennas on the Lander. Operation of this link is intermittent until the atmosphere entry and descent phases begin.

When the Lander encounters the atmosphere, data from the entry science instruments is multiplexed with the engineering data resulting in a 550 bps data collection rate. The combined data is transmitted in real time as well as after a 70 sec delay to eliminate loss of data caused by blackout. The real time and delayed data are interleaved to produce the 1100 bps transmission rate.

After landing and during the 2.5 min settling and setup time, engineering data is transmitted at the 1100 bps rate. Upon completion of the setup the same Lander transmission equipment is used to transmit data at a 70 kbps rate. The picture taking sequence is initiated by the Computer and Sequencer Subsystem (C&S) and transmission is continued for a period long enough to assure that the Support Module will have received a minimum of 2.8×10^7 bits of data corresponding to 12 medium

TABLE 5.2-1. CAPSULE COMMUNICATION REQUIREMENTS

Mission Phase / Function	Checkout	Launch to Capsule Separation	Separation	Capsule Cruise	Capsule Entry and Descent	Landed Operations
Telemetry	Checkout of equipment and modes via hardwire through Support Module	Provide engineering data to Support Module	Support checkout of Capsule subsystem. Provide data to Support Module on separation events	Transmit engineering data to Support Module	Transmit entry, engineering and science data to Support Module. Provide altitude information for parachute deployment and jettison and altitude reference	Transmit engineering imagery and landed science data to Support Module. Transmit landed science and engineering data to Earth
Command	Checkout via hardwire through Support Module	None	Receive updated separation commands prior to separation	None	None	Receive commands to control operations

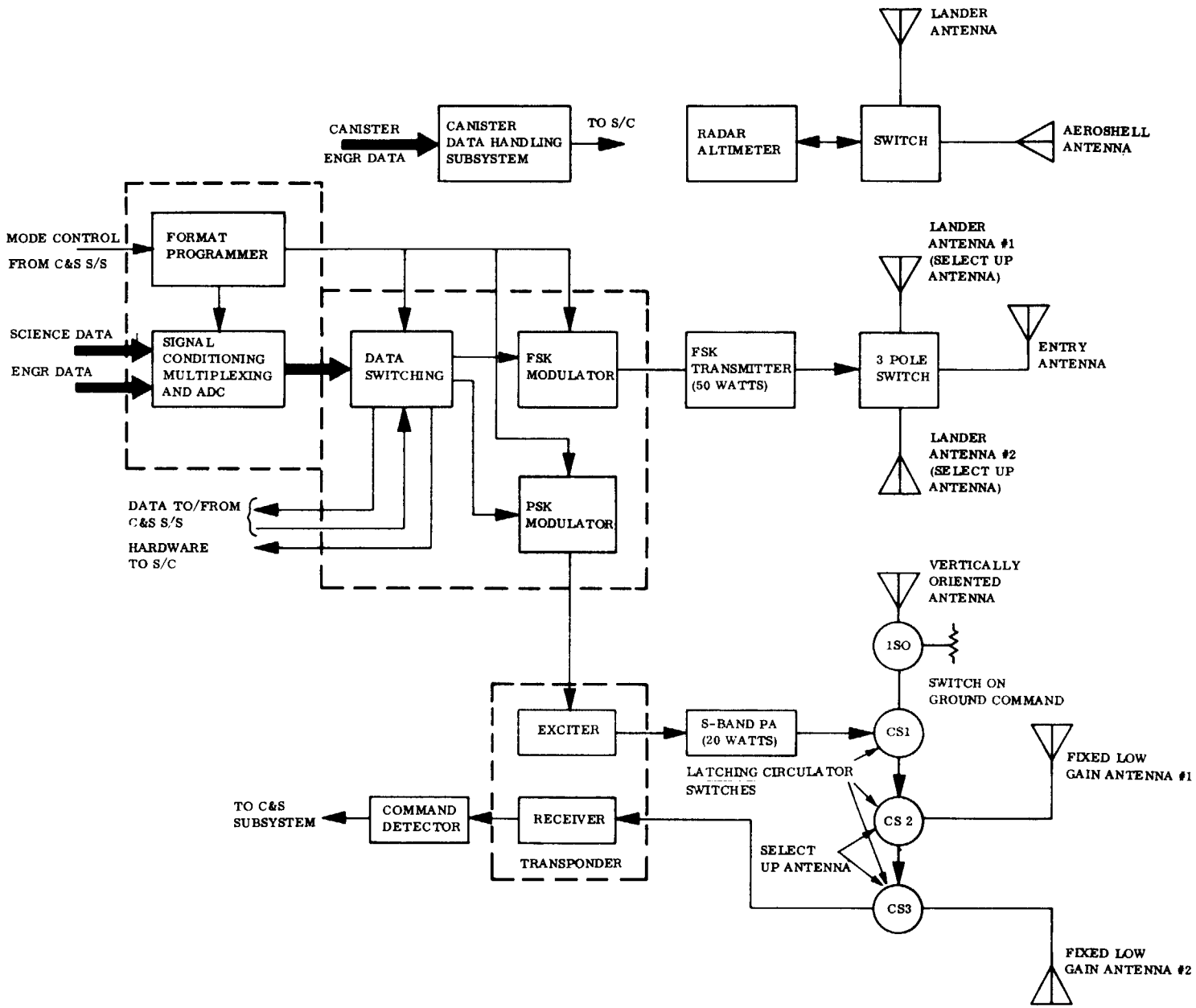

Figure 5.2-1. Telecommunication System Block Diagram

resolution and 12 low resolution pictures of the surface, plus landed engineering and science measurements and stored (entry) science and engineering data. The time of flight change induced at separation is designed to place the Support Module within range and line-of-sight for the required period. That is, the separation conditions cause the Lander to lead the Support Module such that, under the worst combinations of uncertainties of Lander descent time in the atmosphere and landing site dispersion, the Support Module will be no more than 45° above the horizon (rising) when the Lander is ready to transmit the imaging data.

After transmission of the imaging data to the Support Module, the S-band direct link to Earth becomes the prime Lander communication link. With a vertically oriented antenna and 20 watts of transmitted power, a 50 bps link is established for about a half hour per day for the remainder of the mission (210 ft DSN receiving antenna is required). This data comprises a surface composition experiment, life detection experiment, and instruments monitoring the atmosphere.

The subsystem also provides for command reception from Earth through a broad beam fixed antenna at a rate of 1 bps. This capability allows adjustments in Lander operations while on the surface. In addition to the 50 bps telemetry link, a backup link of 5 bps is available. The backup mode utilizes the broad beam antenna and is selected by Earth command.

The S-band transponder can also be used for two way doppler tracking of the Lander on the surface.

5.2.1.3 Subsystem Descriptions

5.2.1.3.1 Data Handling Subsystem

The Data Handling Subsystem provides the data encoding, multiplexing, and controls the data sequencing for the Lander/Capsule System from the time of the sterilization cycle through completion of the mission. In order to perform the variety of measurements required, a number of telemetry formats are needed. The nine telemetry modes used for format control are shown in table 5.2-2. The sources of the data in each mode is also shown.

In addition to the data collection function, the Data Handling Subsystem also controls the data transmission/storage. The data modes vary with the mission phase. These data modes are shown in table 5.2-3.

In the relay transmission modes, the Data Handling Subsystem provides a Manchester coded data stream to the UHF transmitter. In data mode #4 (50 bps), the data is block coded with the (32, 6) code and biphase modulates a square-wave subcarrier for transmission on the direct link. The 5 bps data mode #5 is a backup direct link mode and does not use coding.

TABLE 5.2-2. DEFINITION OF TELEMETRY MODES

Telemetry Mode	Measurement/Data Source
#1	Entry Engineering Landed Engineering #1 Landed Engineering #2 Post Landing Engineering Checkout Engineering
#2	Entry Engineering Entry Science Stored Data
#3	Post Landing Engineering Landed Engineering #1 Landed Engineering #2
#4	Imagery
#5	Mass Spectrometer Gas Chromatograph
#6	Life Detector Wind Velocity Atmospheric Water Atmospheric Temperature Atmospheric Pressure Clinometer Landed Engineering #1
#7	Life Detector Wind Velocity Atmospheric Water Atmospheric Temperature Atmospheric Pressure Clinometer Landed Engineering # 2
#8	Stored Data
#9	Subsurface Water

TABLE 5.2-3. DEFINITION OF DATA MODES

Mode	Data Transmission Rate
#1	Hardwire to Support Module
#2	1100 bps - Relay Transmission
#3	70 kbps - Relay Transmission
#4	50 bps - Direct Transmission
#5	5 bps - Direct Transmission
#6	Stored

The major interfaces for the Data Handling Subsystem are with the Relay Link, the Direct Link and the Computer and Sequencer Subsystems. The data stream for transmission is the only interface between the Data Handling Subsystem and the two radio subsystems. The commands for telemetry and data modes are received from the C&S. The data collected for storage is transferred from the Data Handling Subsystem to the C&S Subsystem. This stored data is later sent back to the Data Handling Subsystem for transmission.

5.2.1.3.2 Relay Link Subsystem

The Relay Link Subsystem consists of a 50 watt, FSK transmitter and an antenna system including the antenna switch and the entry and landed antennas. The major functional interface for this subsystem is with the Data Handling Subsystem. The transmitter is capable of operating at both the 1100 bps and 70 kbps data rates.

An array of four whip antennas comprise the entry antenna. The landed antenna is a fixed, tuned cross slot cavity. Two landed antennas are required to account for the uncertainty in Lander attitude, with the up antenna selected for use. The antennas and their locations on the Lander are shown in figs. 4.2-2 and -3.

5.2.1.3.3 Direct Link Subsystem

The Direct Link Subsystem provides the telemetry and command links for the post-relay phase of the mission. The subsystem contains a 20 watt S-band TWT amplifier, a transponder, a command detector, a vertically oriented antenna, fixed low gain antennas and an antenna selection switch. The data stream for transmission on the direct link to Earth is received from the Data Handling Subsystem. The detected command bits are fed to the C&S.

The telemetry link, with the vertically oriented antenna, transmits 50 bps. As a backup mode of operation, a 5 bps link which utilizes the fixed, broad beam command antenna is provided. The backup mode is selected by Earth command.

5.2.1.3.4 Radar Altimeter Subsystem

The Radar Altimeter Subsystem consists of the altimeter and two antenna subsystems, one on the aeroshell and the other on the Lander. The altimeter is turned on at entry and is used primarily for parachute deployment and jettison. The altimeter is jettisoned with the parachute in order to reduce the landing weight. In addition to its prime mission it provides altitude references measured as engineering data for use in data reduction.

5.2.1.3.5 Canister Data Handling Subsystem

The Canister Data Handling Subsystem is used to monitor the status and performance of the canister subsystems and the separation events. A multicoder is utilized to encode and time multiplex the data for transmission via hardwire to the Support Module Telemetry Subsystem.

5.2.1.4 Physical Characteristics and Development Status

Table 5.2-4 summarizes the physical characteristics and development status of the Telecommunication Subsystem. The key to development status is:

1. No modification required (off-the-shelf).
2. Modify (e.g., for high shock).
3. Redesign (basic equipment exists but redesign for new frequency, detection technique, etc.).
4. New design using established techniques.
5. New development (employs near future state-of-the-art techniques).

5.2.2 DESCRIPTION OF OPERATION

Fig. 5.2-2 is a profile of the data collection and transmission sequence for each of the telemetry and data modes of tables 5.2-2 and -3. A summary description of the Telecommunication System sequence of operation follows.

5.2.2.1 Interplanetary Cruise

In order to minimize the Support Module/Capsule interface lines, the multiplexer in the Lander is used during interplanetary cruise to multiplex the monitored Lander data points. The resulting serial data stream is clocked out to the Support Module Telemetry Subsystem with the Support Module sync signals. Similarly, a separate multiplexer and data converter is provided in the canister to monitor the Canister Subsystems.

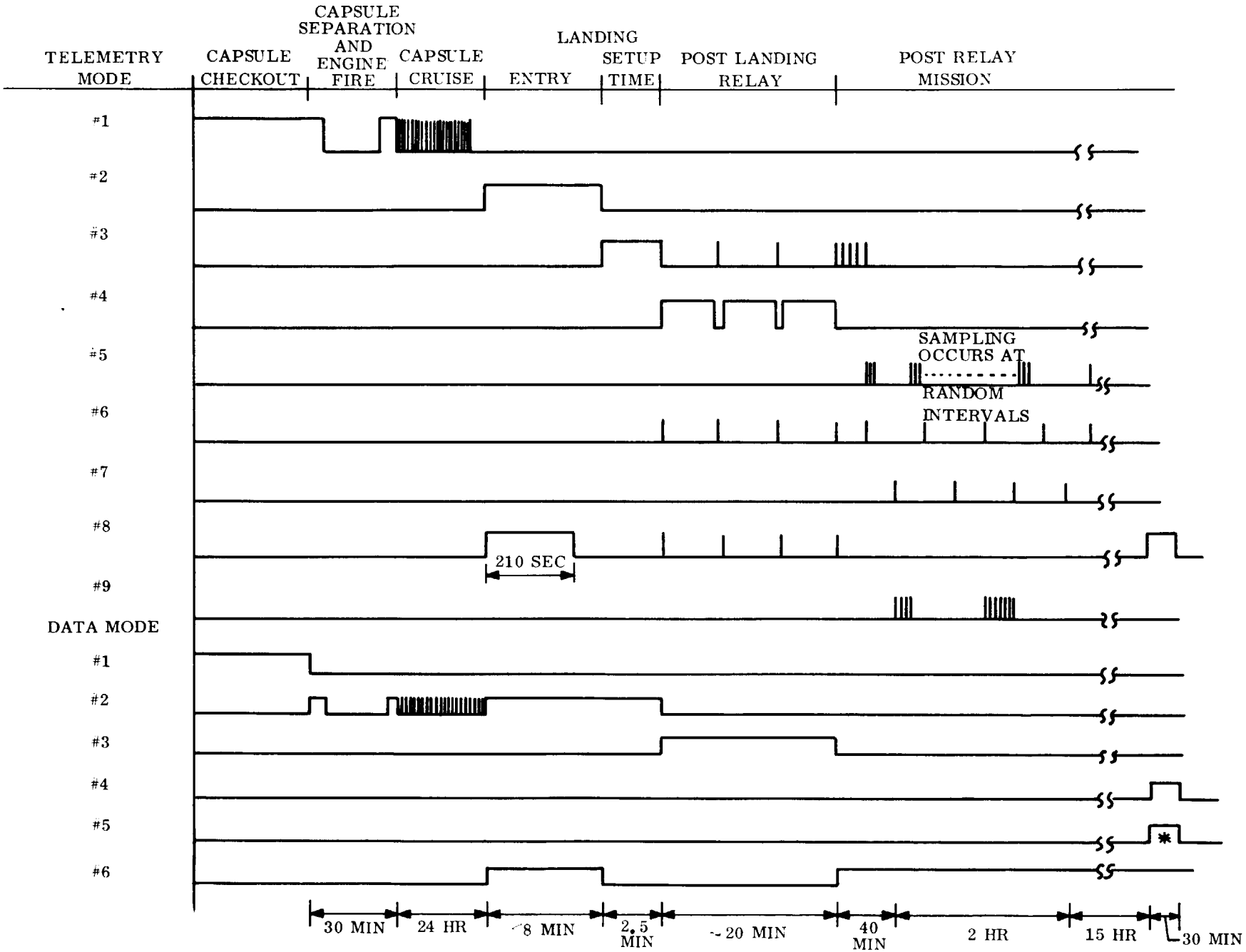

*BACKUP TO DATA MODE #4. SELECTED ON COMMAND.

Figure 5.2-2. Data Collection and Transmission Profile

TABLE 5.2-4. PHYSICAL CHARACTERISTICS

Component and Quantity	Size (in.)	Weight (Based on 1000 g's) (lb)	Power	Sterilizable (125° C)	Max Shock (present information)	Development Status	Remarks
UHF Transmitter (1)	30 in.^{3} 1.5 x 4 x 5	2.5	150w	yes	5,000 g's 0.5 ms	4	
UHF (Landed) Antenna (2)	8 dia. x 2	1	-	yes	700 g's 0.5 msec	4	2 required 1 will be used
UHF Circulator (1)	6 in.^{3} 2.5 x 2.5 x 1	0.4	-	yes	600 g's 0.5 ms	3	
UHF Antenna Switch (1)	4 in.^{3} 1.25 x 1.25 x 2.5	0.15	0.5 A @ 3.5V and 10 micro-A @ 28V	yes	3000 g's, 3 ms	1	
UHF (Entry) Antenna (1)		1.0			-		High shock not a requirement on this antenna
Data Handling Subsystem	336 in.^{3}	15	15 watts	yes	700 g's 0.5 ms		Power required during sampling and transmission periods only

TABLE 5.2-4. PHYSICAL CHARACTERISTICS (Concluded)

Component and Quantity	Size (in.)	Weight (Based on 1000 g's) (lb)	Power	Sterilizable (125° C)	Max Shock (present information)	Development Status	Remarks
Impact Measuring	2x3x4	1.6	3.6w				
Three Axis Impact Accelerometer				yes	10,000 g's	1	
Charge Amplifier(3)				yes	representative unit passed 2000 g test	1	3 required connected to accelerometer by coax cables
S-band P/A	300 in.^{3} 10x12x2.5	7	89w	yes	9600 g's	1	
S-band Antenna, fixed (2)	4 dia x 2	0.4	-	yes	-	4	2 required - 1 used
S-band Antenna, vertically oriented	4 dia x 4	0.5	-	yes	-	4	
S-band Latching Circulator (3)	2x2.5x1.25	0.7	pulse 2A, 28V, 1 ms	yes	600 g's, 5 ms	4	
Transponder	250 in.^{3}	10.0	8w	yes	240 g's	2	
Command Demodulator	153 in.^{3}	4	3.2w	yes	700 g's, 0.5 μsec	2	
Radar Altimeter	500 in.^{3}	15	20w	yes	-	3	High shock not a requirement
Aeroshell Antenna (Radar)	80	5.5	-	yes	-	3	
Lander Antenna (Radar)	18	0.5	-	yes	-	3	
Canister Data Handling Subsystem		7.5	-	yes	-	3	

5.2.2.2 Capsule Checkout

The Capsule checkout mode is initiated prior to separation to determine the status of the Capsule and its payload and to allow for corrective action if required.

The Lander and its payload are exercised under the control of the C&S. The UHF and S-band links are energized separately. A fixed sequence is transmitted and received by the relay receiver at the two UHF link data rates. The received sequence is detected at each rate, retransmitted by the Support Module in real time for the low rate and stored on the tape recorders for the high rate as it will be during the actual mission. The stored data is then read out to the DSN station to verify the complete data handling loop. An alternative which monitors the relay link operation but does not require data transmission and reception would be the direct readout of the Capsule Data Handling Subsystem to the Support Module Data Handling Subsystem.

Similarly, the status of the Canister Subsystem is checked prior to beginning the separation sequence via the Canister Data Handling Subsystem. At separation, the separation events are monitored.

5.2.2.3 Capsule Separation and Engine Fire

From Capsule separation to engire fire (approximately 30 min) the Capsule is transmitting at 1100 bps for a period of 5 min during spin-up and engine fire. Only engineering data is monitored. The received data on the Support Module is detected, transmitted in real time over the high rate channel, and stored for delayed transmission to Earth over the high data rate link.

5.2.2.4 Capsule Cruise

Capsule cruise lasts for approximately 24 hr. In order to conserve battery power and reduce the Support Module data storage requirement, the Capsule cruise data is read out in 2 min bursts at the 1100 bps data rate every hour during Capsule cruise. The received data on the Support Module is detected, transmitted in real time over the high rate channel, and stored for delayed transmission.

5.2.2.5 Capsule Entry

During entry, the data rate is maintained at 1100 bps. The entry science data collection rate requirements are shown in table 5.2-5. Assuming 175 bps for engineering data, the total data collection rate required is approximately 550 bps. For a blackout time of less than 70 sec, the storage required for data taken during blackout is less than 38.5 kbits. The time between end of blackout and impact is greater than 80 sec (see table 5.2-16). Therefore, in order to read out the delayed blackout data as well as real time data, the total data rate is 1100 bps. The time delayed data is transmitted during a period of 210 sec after entry. At this time, the memory ceases to accept data for time delay. In addition to the time delayed data, every fourth sample of the engineering and science instruments are stored for transmission after landing.

The radar altimeter is activated when atmospheric encounter is detected.

TABLE 5.2-5. ENTRY SCIENCE DATA REQUIREMENTS

	Sampling Rate (sec^{-1})	Bits/ Sample	No. of Channels	Bit Rate (bps)
Mass Spectrometer	1/10	8	50	40
Resistance Thermometer	1	9	2	18
Pressure Transducer	1	9	2	18
Tri-axial Accelerometer	10	8	3	240
Water Vapor Detector	1/15	7 11	2 1	1.67
Stagnation Temperature Transducer	1	9	1	9
Stagnation Pressure Transducer	1	9	4	36

5.2.2.6 Post Landing Relay

Upon landing, engineering data which monitors the deployment sequency and status of the Lander is read out at 1100 bps until completion of the setup period. Upon the completion of the setup period, the imaging data collection and transmission at 70 kbps begins. Engineering and landed science data and the stored entry data are transmitted between each complete set of 24 pictures. This process is repeated until three complete sets of imaging data and four sets of engineering landed science and stored entry data are read out (approximately 20 min). On the Support Module, the detected signal is stored for subsequent transmission.

5.2.2.7 Landed Phase

The landed science (non-imaging) data requirements are shown in table 5.2-6. Each day there are approximately 19 kbits of engineering data. These requirements take into account the short (18 hr) first day and the deletion of some measurements on the third day. The transmission rate is 50 bps using the vertically oriented antenna for a nominal period of 30 min, providing a total data return of 9×10^4 bits. If the backup mode (5bps) is required, the amount of data that can be returned is greatly reduced. Therefore, the scientific measurements of life detection and atmospheric measurements of telemetry modes 6 and 7 are stored in a separate section of the memory such that it can be transmitted first.

5.2.3 DATA HANDLING SUBSYSTEM

5.2.3.1 Introduction

The Data Handling Subsystem provides signal conditioning, encoding, time multiplexing and sequencing of the Lander's engineering and science data. Further, the Data Handling

TABLE 5.2-6. LANDED SCIENCE (NON-IMAGING) DATA REQUIREMENTS

	Sampling Rate	Bits/ Sample	No. of Channels
Life Detection	1/20 min	49	1
Water Detector - Atmospheric	1/20 min	25	1
Temperature - Atmospheric	1/20 min	7	2
Pressure - Atmospheric	1/20 min	7	2
Wind Velocity	1/20 min	7	4
Lander Attitude	1/20 min	7	2
Mass Spectrometer*	41.5 kbits — 1st day		
Gas Chromatograph*	40.2 kbits — 2nd day		
Water Detector - Soil	1/1 min**	25	1

*1st day includes calibration
- Mass spectrometer measures atmosphere once.
- Mass spectrometer and gas chromatograph measure soil composition during a 2-hr period.

**Measurement is made once each min for a 20-min period, each time the pyrolyzer is activated.

Subsystem, under command of the Computer and Sequencer Subsystem (C&S) controls the data collection, formatting and data transmission as a function of the mission phase from interplanetary cruise through the landed operations. The requirements upon the Data Handling Subsystem for telemetry and data modes as a function of the mission phase that were described in Sections 5.2.1 and 5.2.2 are summarized in table 5.2-7. In addition, during the pre-launch and interplanetary cruise phases, the subsystem operates in the same modes as in the Capsule checkout phase. This allows the data rate and collection interval to be controlled externally to the canister.

The functional block diagram of the Data Handling Subsystem is shown in fig. 5.2-3. The data imputs consist of high level and low level analog inputs and parallel digital inputs. An analog-to-digital converter is included to convert the analog signals to a digital code. A format programmer sets the operation of the unit and controls the various timing and multiplexing circuitry for each mode of operation. Each set of input data; i.e., entry science, entry engineering, imagery, etc, has its own multiplexer which is programmed into a

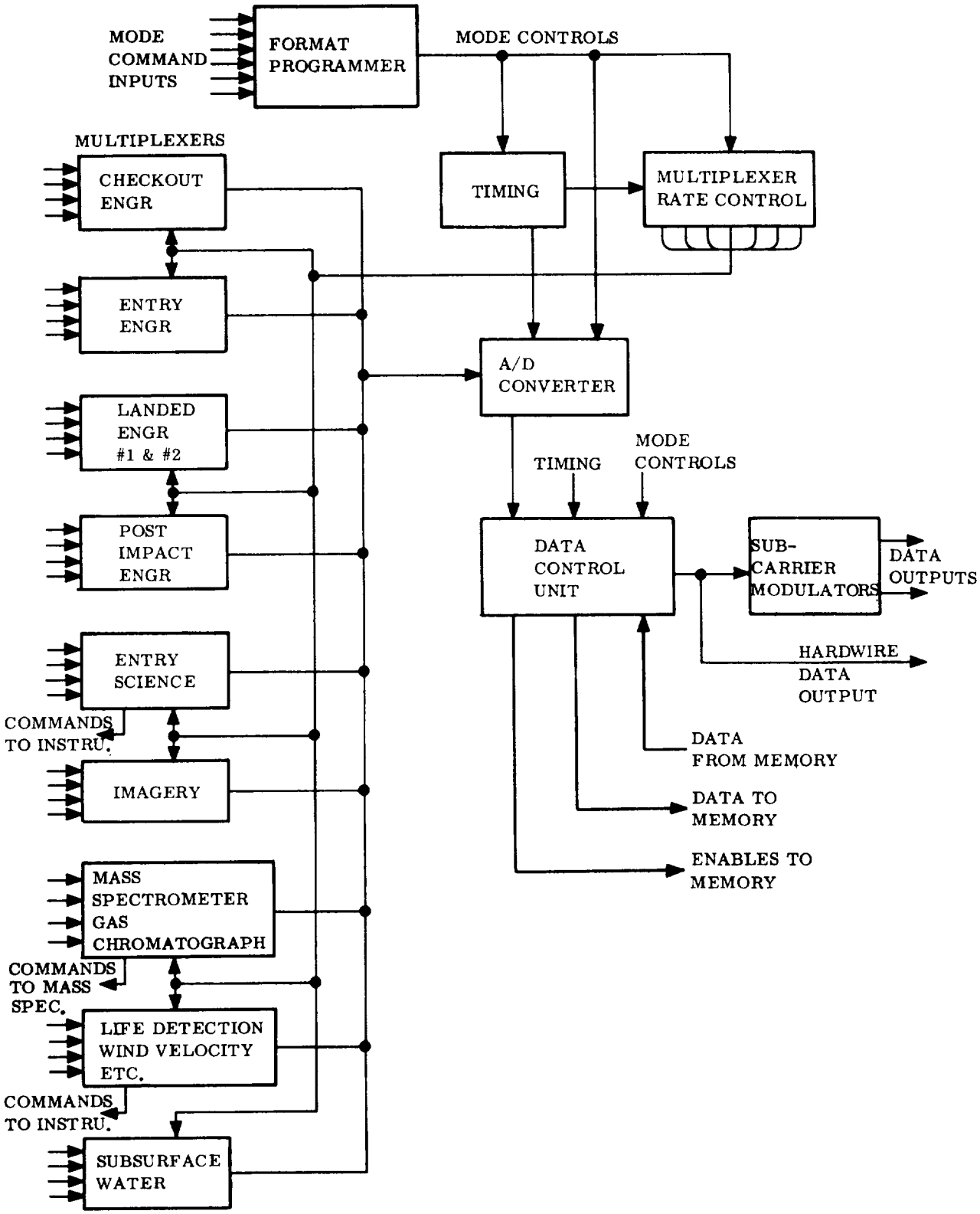

Figure 5.2-3. Data Handling System Functional Block Diagram

TABLE 5.2-7. SUMMARY OF TELEMETRY AND DATA MODE REQUIREMENTS AS A FUNCTION OF MISSION PHASE

Mission Phase	Telemetry Mode	Data Mode	Remarks
Capsule checkout	1	1	
Capsule separation and engine fire	1	2	Two transmission periods
Capsule cruise	1	2	Transmission and data collection every hr
Entry	2	2, 6	Real time and delayed data transmitted. Every fourth sample of entry data stored for transmission after landing
Setup time	3	2	
Post landing relay	3, 6, 8, 4	3	The sequence of modes is repeated three times, ending with 3, 6 and 8. Duration is approximately 20 min
Post relay data collection	3, 5, 6, 7, 9	6	TLM modes are repeated as data collection requirements dictate
Direct link transmission	8	4	Data mode No. 5 is a backup mode via low gain antenna

format providing the required sampling rate for each mode of operation. The multiplexed data is routed from the multiplexer sections and the A/D converter to either the memory or the subcarrier modulators. Frame synchronization and mode identification information is entered in the output data format in each mode. The output data signal is conditioned to the proper levels and form required by the transmitters for the various bit rates. A hardwire output signal is provided for ground checkout and to check the operation of the unit during and after sterilization.

5.2.3.2 Format Programmer

The format programmer is the heart of the Data Handling Subsystem. It accepts the mode control command pulses from the C&S and decodes the command pulses to control the proper sampling format, word length and bit rate for the mode of operation. The programmer utilizes majority logic to insure that the proper format is being enabled for the given mode. The outputs of the programmer are used by the other circuits as shown in the block diagram. The format programmer has the capability to select various word lengths within a given frame. In the entry mode science analog data requires conversion to 9 bit accuracy, while engineering inputs require only 7 bit accuracy and digital information inputs occur as 8 bit parallel words. If all data words were made 9 bits long, considerable frame space would be lost due to the unnecessary accuracy on some data. It is desired to obtain the maximum number of data samples within a given time period. Maximum utilization of the frame is obtained by segmenting each line of the frame into 9 bit, 8 bit and 7 bit sections, as shown below for a 16 word line.

1 2 3 4 5 6	7 8 9 10 11 12	13 14 15 16
9 bit words	8 bit words	7 bit words

The timing circuit provides the basic clock frequency and timing signals to control the multiplexers and A/D conversion. The basic clock frequency is 560 kHz and is generated by a crystal controlled multivibrator oscillator. The oscillator will be compensated for temperature and power variations to maintain a 0.01 percent bit rate accuracy over all operating conditions.

The basic clock frequency is divided by eight to provide the 70 kHz bit rate control signal for the A/D converter and the 70 kbps data rate. Additional countdown circuitry is programmed by the mode control signals to provide the bit rates of 1100 bps, 50 bps, and 5 bps.

5.2.3.3 Analog-to-Digital (A/D) Converter

The A/D converter utilized is a 9 bit successive approximations converter, which is programmable to convert to 7 bit accuracy also. The maximum conversion rate is 70 kbps. The block diagram of a successive approximation converter is shown in fig. 5.2-4.

Initially, the converter is set for a half scale comparison point and the result is used to set either a one quarter or three quarter comparison point. The result of each comparison is stored serially in the output register. This converter can be programmed from 9 bits to 7 bits simply by disabling the two least significant bits of the converter. No change in clock rate is required.

The converter design used provides a total conversion accuracy for a 9 bit conversion of ±0.25 percent of which ±0.1 percent is quantization error and ±0.15 percent is analog error.

Other methods of A/D conversion were considered and are outlined below:

In the Counter Conversion method a binary counter counts clock pulses and drives a digital to analog (D/A) converter. The voltage output of the D/A converter is compared to the analog input until a comparison is reached. The value in the counter is the binary equivalent of the analog input signal. The block diagram of the typical counter converter is shown in fig. 5.2-5.

The counter techniques require 2N-1 counts to accumulate in the word conversion time for a full scale input signal. For a 70 kHz bit rate in a 9 bit converter, a 4 MHz basic clock is needed.

In the sequencing conversion technique the analog input signal is compared to a reference voltage in successively decreasing powers of two. A comparator stage is required for each bit of conversion resolution. The converter is a series connection of the comparator stages. The results of each comparison are added to or subtracted from the analog input voltage and used as the input to the next consecutive stage. The speed of this conversion technique is high with bit rates of 1 MHz possible. This technique requires about 90 percent analog devices to implement, which makes it harder to hold a required accuracy over temperature changes.

Table 5.2-8 summarizes the characteristics of the three conversion techniques considered.

5.2.3.4 Multiplexer

The multiplexer rate control circuit generates word rate timing signals for the multiplexers. Mode select signals control the selection of the proper multiplexers for a given mode.

Each set of input data has an associated multiplexer to time division multiplex the analog and digital inputs associated with it. A typical high level analog input multiplexer is shown in fig. 5.2-6. Analog gating consists of MOS field effect transistors for both the high level and low level inputs, while the digital inputs are gated by integrated logic gates. The analog and digital gates are controlled by counters programmed to set the proper format. Two sets of input data, entry engineering and entry science, have two additional stages on the end of the multiplexer control counters. The purpose of these additional stages is to provide an output signal each fourth time the particular input gate matrix is being sampled. This signal is used to control data being sent to the memory unit for storage during entry.

The parallel digital data from the mass spectrometer is accepted on eight parallel lines with a command signal generated and sent to the spectrometer to step the data on the eight lines.

5.2.3.5 Data Control Unit

The data control unit accepts the serial PCM data from the A/D converter and routes this data between the output subcarrier modulators and the memory. During the entry mode real time data is sent to the memory to be delayed by 70 sec, then is interlaced with the real time data output word by word. Also, during this mode, every fourth sample of the same data is sent to the memory for storage and remains in storage until later mode. In other modes

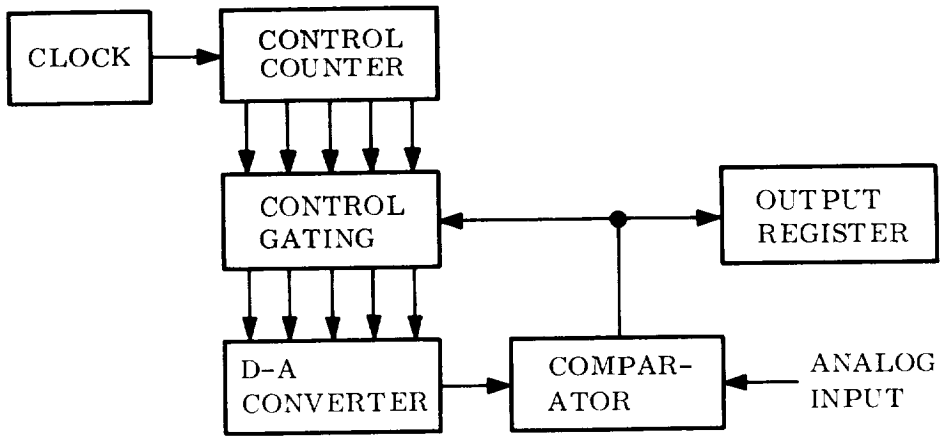

Figure 5.2-4. Approximation Converter, Block Diagram

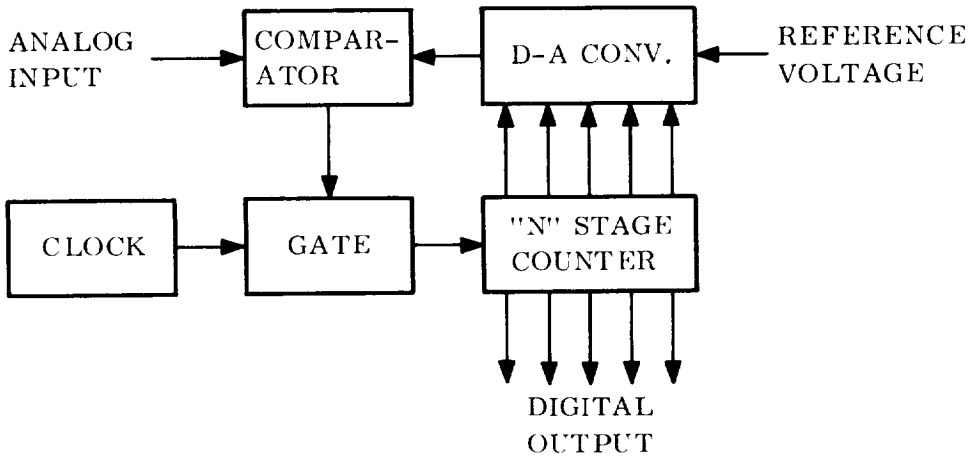

Figure 5.2-5. Counter Converter. Block Diagram

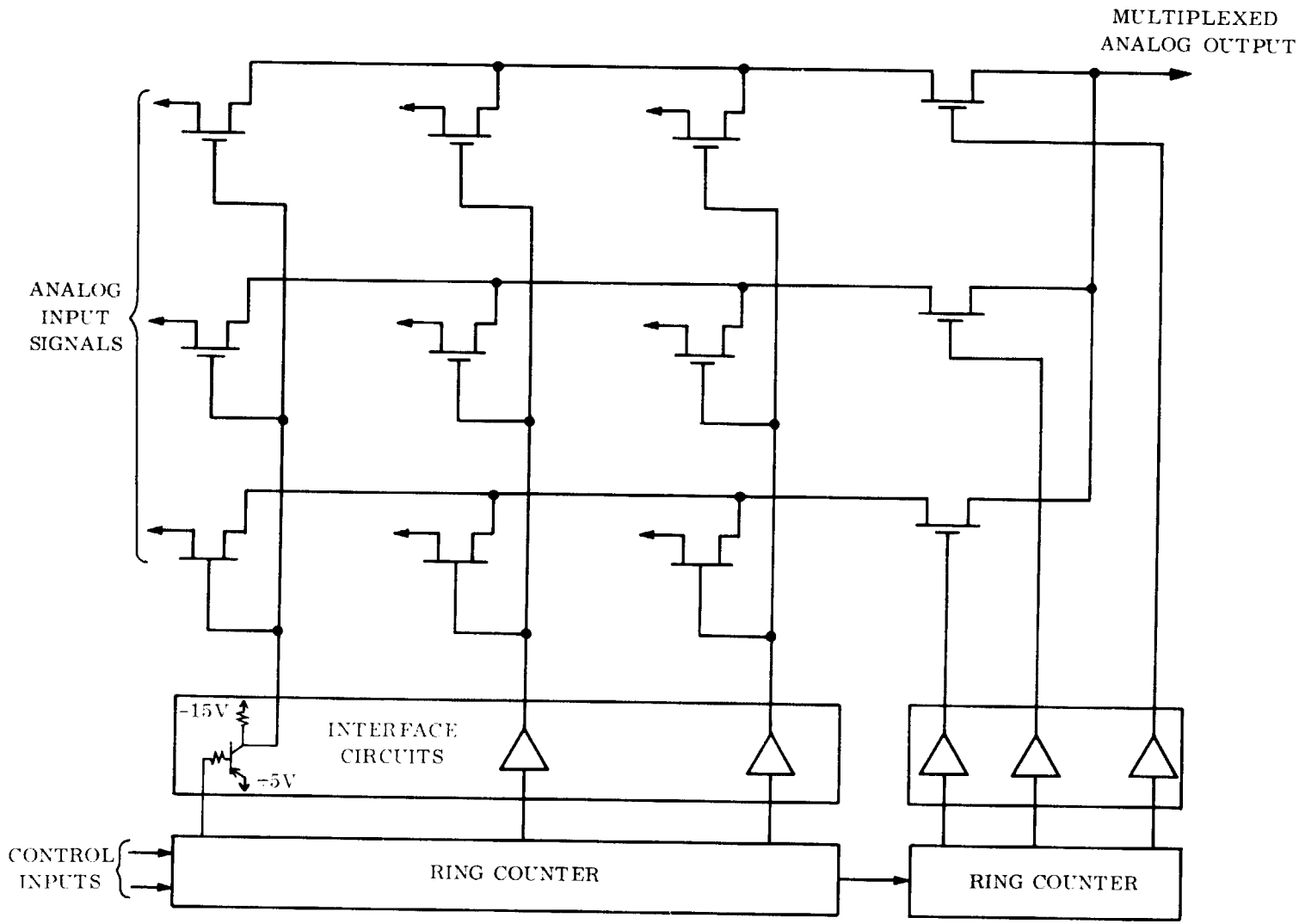

Figure 5.2-6. Typical High Level Analog Multiplexer

TABLE 5.2-8. CONVERSION TECHNIQUES

Technique	Speed	Percent Analog/Digital Devices	Relative Accuracy
Successive Approximation	Medium 200 kbps	50/50	High
Counter	Low 50 kbps	10/90	High
Sequencing	High 1 Mbps	90/10	Must be tailored to provide high accuracy

sampled data is sent as real time output, while some modes require data to be sampled periodically and stored in the memory, then transmitted as a complete group.

The interface signals between the data control unit and the memory are listed in table 5.2-9.

The functional block diagram of the data control unit is shown in fig. 5.2-7. Mode control commands and timing signals are received to set the proper operation, and control pulses and shift pulses are generated for the memory. The real time data from the converter enters through gate No. 1 and passes through to the real time data register. When data is also delayed, gate No. 1 is enabled to allow the data to pass through to the delaying portion of the memory. Selected segments of the data are sent to the memory for storage by enabled gate No. 2 when it is desired to store the data. An enable is generated for the duration of the time to tell the memory to delay and store. During the landed mode of operation after imagery, data is sampled and stored for later transmission. To accomplish this both gate No. 1 and gate No. 2 are enabled and an "enable" is generated to the memory to tell it to store the data. Another enable tags the engineering data to differentiate it from the science data during this mode, since the data is stored in different sections of memory. Outputting of the stored data in the memory is controlled by shift pulses and enables generated in this circuitry.

To interlace data word by word, two shift pulses, one of 550 bps (SP No. 1) and another of 1100 bps (SP No. 2) are required. The real time and delayed data are entered into their respective registers by the 550 bps shift pulse. Two additional shift pulses (SP No. 3 and SP No. 4) at the rate of 550/8 bps but 180° out of phase are generated and used to parallel shift data into the output register in groups of eight bits. The delayed data register contains four more stages than the real time register, which, along with the 180° phase difference of the shift pulses, allows the real time data and the delayed data to be interlaced word by word in the proper bit phasing. The data in the output register is shifted out at 1100 bps. A timing diagram is shown in fig. 5.2-8.

Frame synchronization and identification information is entered after the data has been delayed or stored. This is done so that synchronization patterns will only occur at the proper time. Also valuable space in the memory will not be used up with the frame synchronization

TABLE 5.2-9. INTERFACE SIGNALS BETWEEN DATA HANDLING SUBSYSTEM AND MEMORY

1. Delayed Entry Science Mode
    1. Enable (from Data Handling Subsystem to memory)
    2. Shift pulses, 550 bps (from Data Handling Subsystem)
    3. Data to memory
    4. Data from memory
2. Stored Entry Read In
    1. Enable (from Data Handling Subsystem - up during read in)
    2. Shift pulses
    3. Data to memory
3. Stored Entry Science Read Out
    1. Enable (from Data Handling Subsystem - up for time of read out)
    2. Shift pulses, 70 kbps (from Data Handling Subsystem)
    3. Data from memory
4. Landed Science Stored
    1. Enable
    2. Shift pulses (same line as stored entry science read in)
    3. Data to memory (same line as stored entry science read in)
5. Landed Science Read Out
    1. Enable
    2. Shift pulse (same line as stored entry science read out)
    3. Data from memory (same line as stored entry science read out)

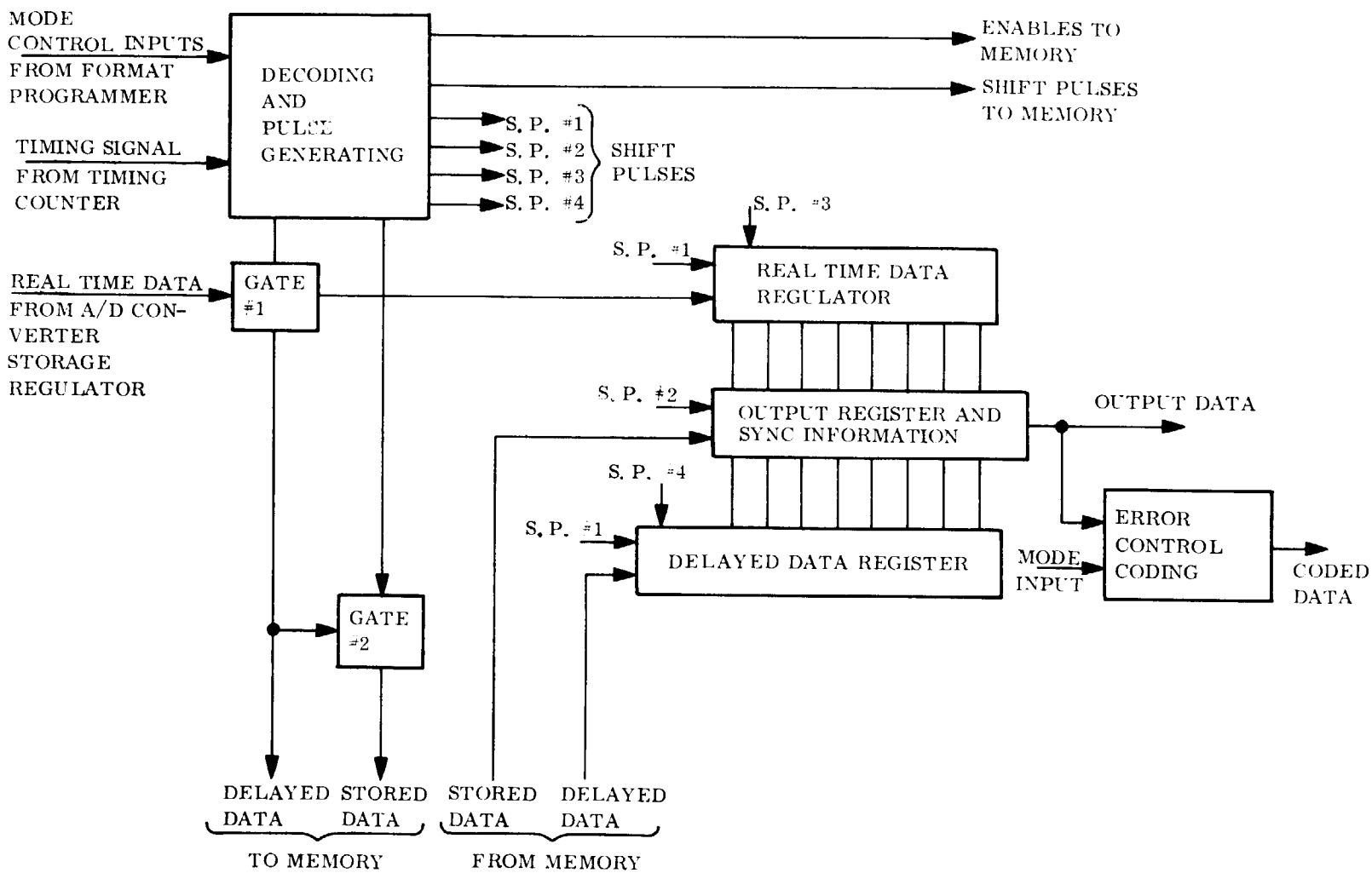

Figure 5.2-7. Data Control Unit, Block Diagram

pattern. During synchronization times the shift pulses to the memory will be cut off since there will be no data during these times.

The 50 bps direct link data signal is block coded using the (32,6) bi-orthogonal code, and the coded symbols biphase modulate a high frequency (e.g., 24 kHz) square wave subcarrier. The 5 bps data also modulates this subcarrier when this backup mode is used. The relay link data biphase modulates a square wave subcarrier having a frequency equal to the bit rate (1100 and 70,000 Hz), providing a Manchester coded (split-phase coded) signal to the transmitter.

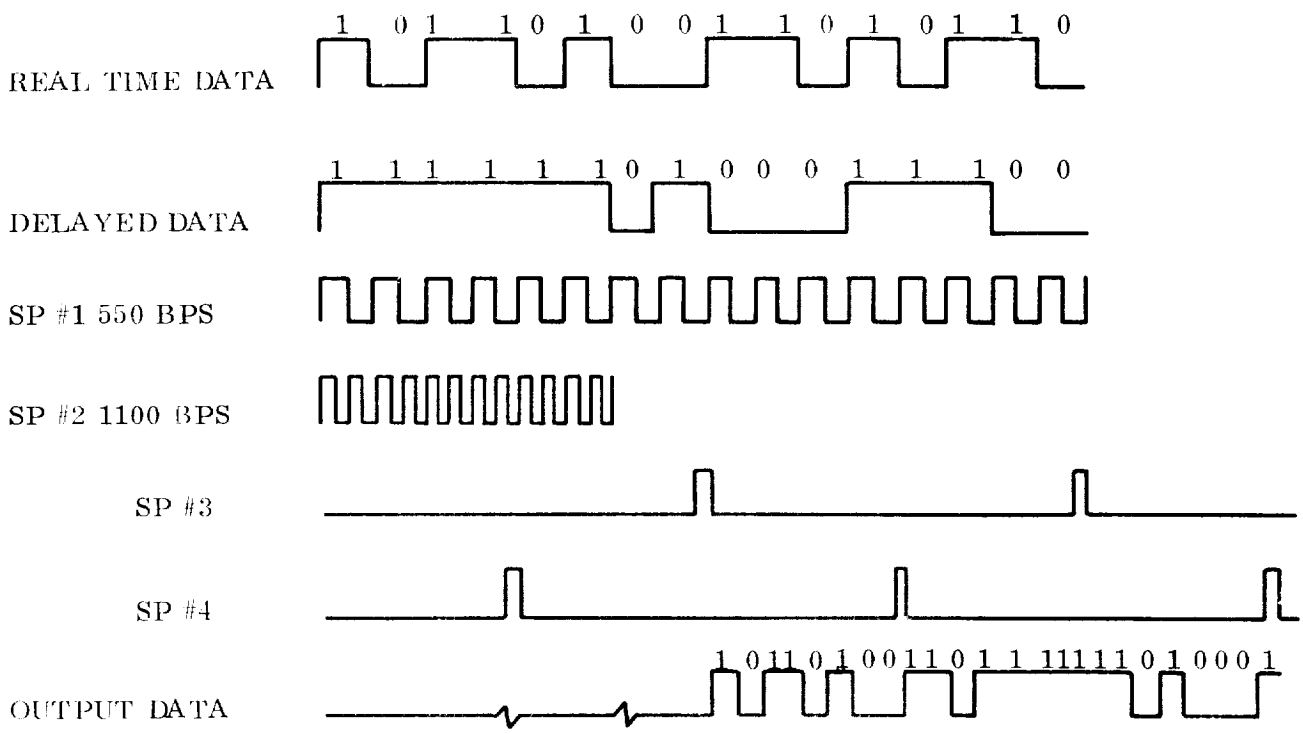

Figure 5.2-8. Data Control Unit, Timing Diagram

5.2.4 RELAY LINK

5.2.4.1 Introduction

The Relay Link Subsystem provides the most efficient means of obtaining entry data and landed imagery data. The link operates at a frequency of 400 MHz and has the capability to operate at data rates of 1100 bps and 70 kbps with Manchester coded data and a transmitter power of 50 watts.

The transmission rates for different mission phases are shown in table 5.2-10. The selected data rates were based upon the entry data requirements and upon the landed imagery mission. The 1100 bps data rate is used from Capsule separation through the settling and deployment period. The high data rate, 70 kbps, is used for transmission of the data during the imagery collection period.

A block diagram of the Relay Link Subsystem is shown in fig. 5.2-9. The subsystem consists of the 50 watt, 400 MHz transmitter, a modulator, power supply, antennas, and r-f switches. The transmitter is solid state and utilizes a modulator consisting of two independent crystal oscillators which are gated by the data train. The antennas used are physically small. The antenna used during entry consists of an array of four whips. For landed operation, the tuned crossed slot antenna, 8 in. diameter by 2 in. deep, is utilized. Each of the major components is discussed in detail.

5.2.4.2 Landed Relay Link Performance

The design control table for the landed relay link is shown in table 5.2-11. The values of transmit and receive antenna gain and range are used for reference purposes. Fig. 5.2-10 shows the margin over adverse tolerances for the landed relay link. The curves show the extreme cases of early and late turn-on requirements and the minimum communication time over adverse tolerances for 20° slopes and 12° crush-up tilt.

The data rate selection was made on the basis of obtaining the maximum data return for the selected antennas under the worst case situation of trajectory geometry and Lander tilt. Computer program TEL SEP 2 was utilized in this optimization. This computer program utilizes range, range rate, and direction of the line-of-sight referenced to both the Lander and Support Module as a function of time. These trajectory parameters and the transmit and receive antenna patterns, as well as the other parameters in the design control table, are used by the program to determine the data rate capability of the link. The data return is computed from the product of data rate and the time when the link margin is above threshold. The data rate which results in the maximum data return is then selected as the best data rate. This procedure is repeated for eight directions of tilt. The maximum data that can be returned with confidence is the least of these maximums, and the corresponding data rate is the optimum rate for the particular trajectory considered. This procedure is then repeated for each of the trajectories of interest to account for the uncertainties in the landing geometry. The final data rate is the one which results in the maximum

TABLE 5.2-10. DATA COLLECTION AND TRANSMISSION SUMMARY

Mission Phase	Data Collected	Data Stored	Transmission	Modulation
Interplanetary Cruise	All data collected and transmission performed by the Spacecraft			
Capsule Checkout	Engineering and science checkout data	---	via Spacecraft link	
Separation and Engine Fire	Separation Events Engineering data 1100 bps	---	Hardwire to Support Module from canister DHS and 1100 bps from Lander	FSK, UHF
Capsule Cruise	Engineering data 1100 bps	---	1100 bps (burst transmission) (once per hr)	FSK, UHF
Entry	Entry science 363 bps Engineering data 175 bps	Entry science and engineering data stored for 70 sec delay and every fourth instrument sample stored.	1100 bps (real time and delayed data)	FSK, UHF
Setup	Engineering - 1100 bps	---	1100 bps	FSK, UHF
Post Landing Relay	Sequential collection at 70 kbps of imaging data, engineering data, and stored entry data	---	70 kbps	FSK, UHF
Surface Operation	1st day Science - 48 kbits Engineering - 11 kbits 2nd day Science - 52 kbits Engineering - 19 kbits 3rd day Science -11 kbits Engineering - 19 kbits	All data stored	50 bps with 5 bps backup mode with reduced data.	PSK, S-band

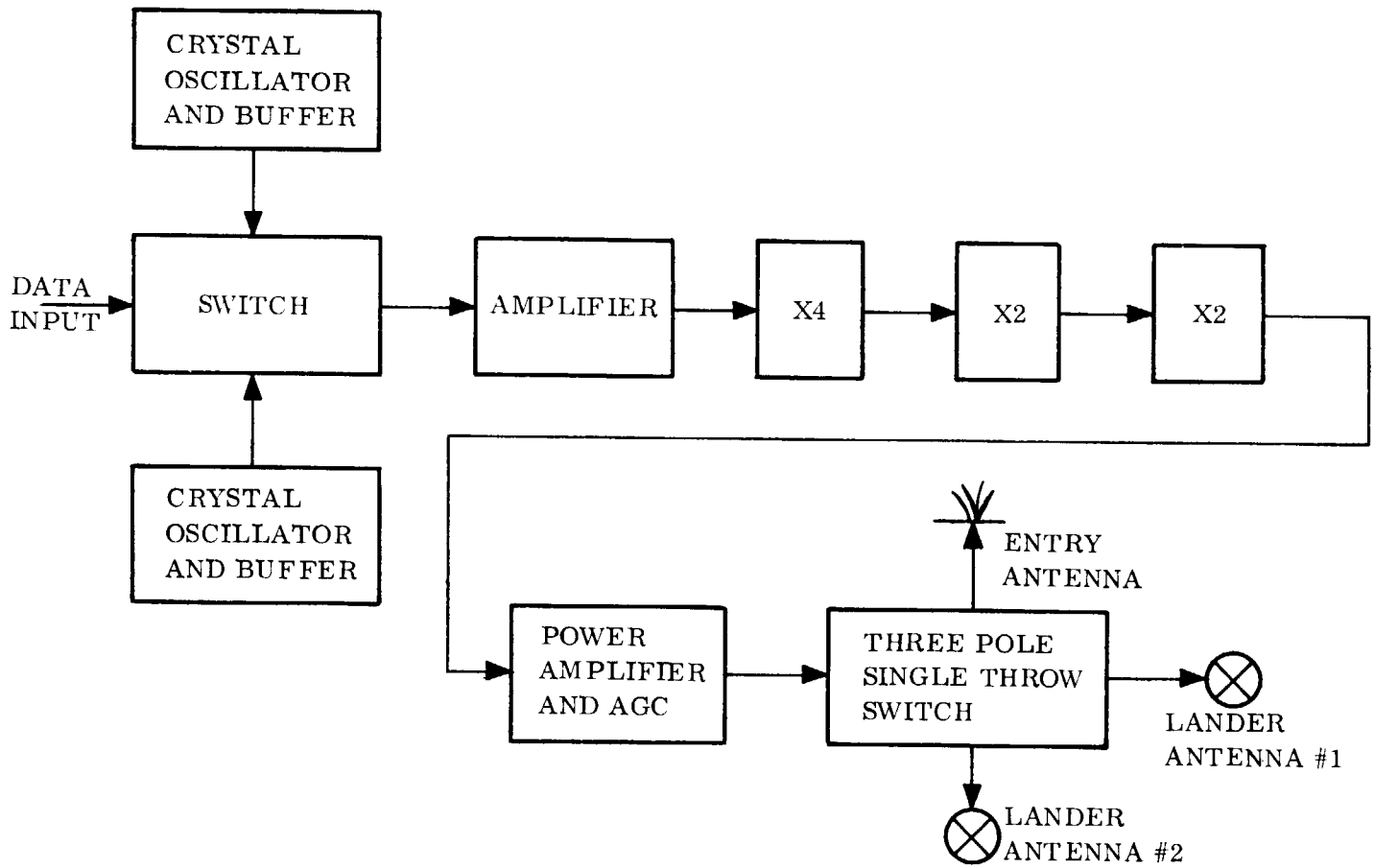

Figure 5.2-9. Relay Link Subsystem

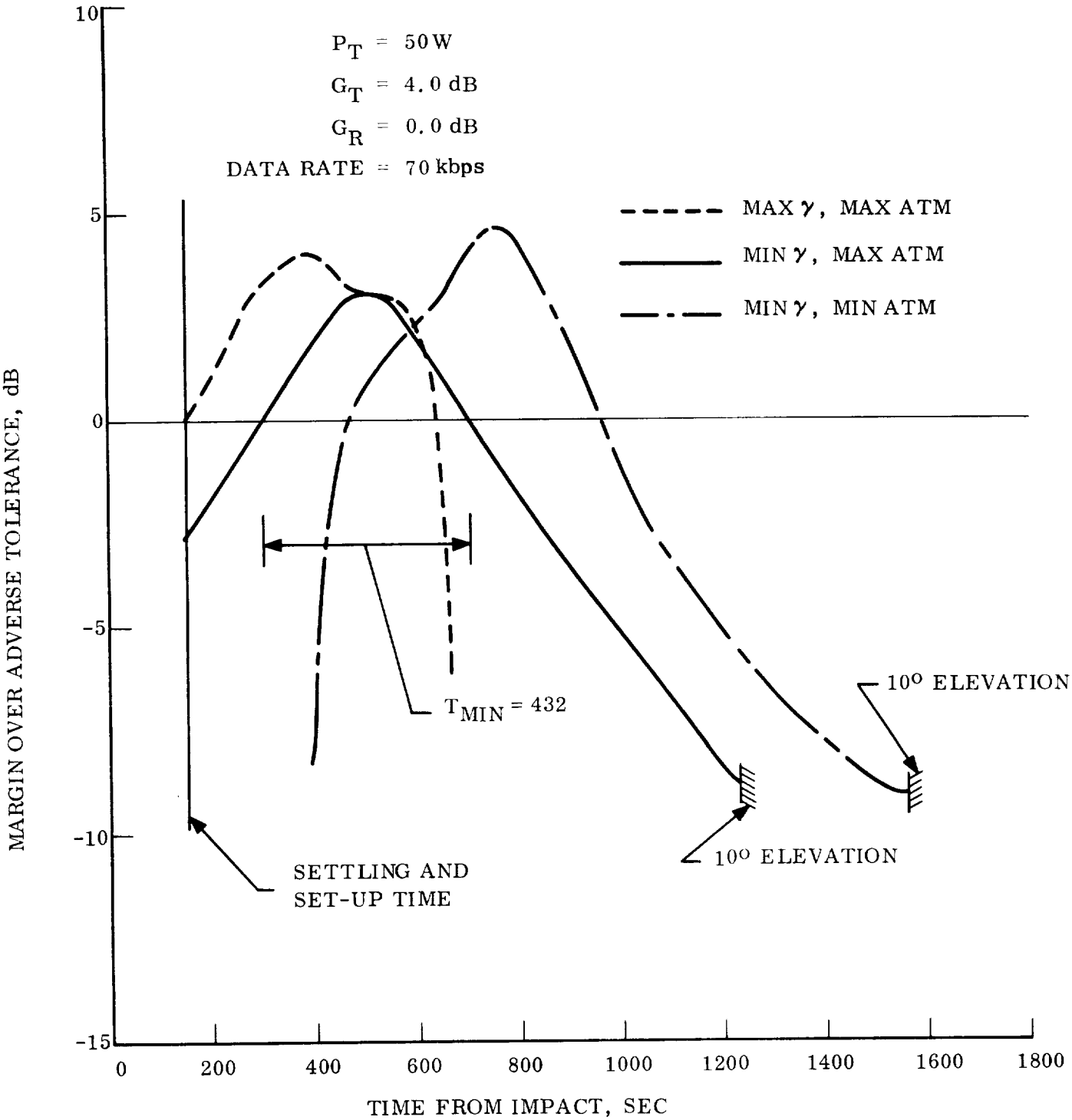

Figure 5.2-10. Landed Relay Performance

TABLE 5.2-11. RELAY (LANDED) DESIGN CONTROL TABLE

Parameter	Nominal Value	Adverse Tolerance
Modulation technique	FSK	--
Frequency (MHz)	400	
Transmitter power (watts)	50	
(dBm)	47.0	1.0
Transmit circuit loss	-1.5	0.4
Transmit antenna gain	4.0 (1)	0.5
Transmit antenna pointing loss	2.0 (1)	0.0
Reference range (km)	1000 (1)	
Space loss	-144.5	
Polarization loss	-1.0	0.5
Receiving antenna gain	4.0	0.5
Receiving antenna pointing loss	-4.0	0.0
Receiving circuit loss	-1.0	0.4
Total received power (S), dBm	-99.0	3.3
Effective noise temperature (^{o}K)	650°	
Receiver noise power spectral density (N/B)	-170.5	1.0
Data Power (dBm) S_D	-99.0	3.3
Bit rate, 1/T (bps/dB)	70k/48.5	--
Frequency uncertainty (kHz)	20.	--
I-F bandwidth (kHz)	300.0	--
Required S/N/B	60.0 (2)	2.0 (2)
Required ST/N/B	11.5 (2)	2.0 (2)
Threshold data power (dBm)	-110.5	3.0
Margin	11.5 (3)	6.3

(1) Reference values.

(2) Nominal signal-to-noise ratio used is theoretical value. 2 dB adverse tolerance is allowed to account for practical performance degradation, e.g., non-ideal bit sync.

(3) Margin based on reference values and nominal parameters.

data return for the trajectory which gives the smallest maximum. Additionally, the time that the transmitter must be on is also obtained from the program. As expected, the two extreme cases of impact parameter are the worst cases and are shown in fig. 5.2-10.

The resulting optimum data rate is 70 kbps. As shown in fig. 5.2-10, the minimum transmission time over adverse tolerance is about 402 sec. This gives approximately 2.8×10^7 bits of data. The overall mission has been designed such that the early turn-on occurs at the end of the expected settling and set-up period. The late turn-off is about 20 min from landing.

In the data handling subsystem, the NRZ data is bi-phase modulated (Manchester coded) on a square-wave subcarrier at the bit rate. This split phase data, frequency shift keys the transmitter. In the Support Module, the received signal is translated to i-f and amplified in a gain controlled amplifier. The two signalling frequencies are independently band-pass filtered and detected. The resulting signals are differenced to form the receiver baseband signal. The split phase coding causes a transition in each bit interval and allows a-c coupling of the detector outputs. This eliminates the unbalance due to noise that can occur in the output signal when the detector is direct-coupled. Such an unbalance can result from unequal gains or unequal predetection bandwidths in the two receiving channels. This unbalance can seriously affect the performance of the receiver, especially when the predetection SNR is low (ref. 5.2-1).

The baseband signal is fed into a bit sync detector which generates a squarewave subcarrier at frequency R_b to convert the split-phase difference signal back to the NRZ format. This signal is integrated in a matched filter and sampled to provide the data at the receiver output. The bit sync performance analysis, para 5.2.4.5, indicates bit sync acquisition time on the order of 1 msec and signal degradation due to bit sync jitter of about 0.1 dB. An allowance of 2 dB degradation from theoretical performance is shown in the design control table.

The separation between transmitted frequencies is chosen wide enough to limit adjacent channel interference to a tolerable level and yet the overall spectrum bandwidth must be less than the 2 MHz antenna bandwidth constraint. The two primary components of adjacent channel interference are (1) acceptance of the adjacent channel's main spectral lobes by the filter skirt and (2) secondary spectral lobes by the filter passband. The power spectral density for each channel with Manchester (split-phase) coded data, fig. 5.2-11 (a), is composed of a "carrier" component at the channel frequency and a continuous portion having a $\sin^4 x/x^2$ form. The filter bandwidth required to accept the signal main lobes is about four times the bit rate, i.e., $4R_b$. By using a frequency separation of $10R_b$, the secondary lobes of the interfering channel which are included in the passband, are down by 20.1 and 21.9 dB, respectively, indicating a signal-to-interference ratio of about 20 dB. Comparing this to the i-f signal-to-noise ratio of about 5.4 dB required to maintain the 4×10^{-3} bit error probability, indicates that secondary lobe interference will cause negligible degradation. Furthermore, since the separation to bandwidth (one sided) ratio is about 5:1,

filters having attenuations on the order of 60 dB of the adjacent channel frequency are easily realizable, indicating negligible main lobe interference.

Fig. 5.2-11(b) illustrates the combined power spectral density of the FSK signal. Based on a bit rate of 70 kbits/sec, 12 kHz combined transmitter and receiver frequency instability, and 8 kHz frequency uncertainty due to doppler, the filter bandwidth requirement is 300 kHz. This can be realized, for instance, using crystal filters with one percent bandwidth at an i-f frequency of 30 MHz.

5.2.4.3 Entry Link Performance

Entry data is transmitted via the same transmitter as the landed data but is received by a separate Support Module antenna and receiver which is optimized for the 1100 bps entry data rate. This approach, in lieu of utilizing the landed data receiver, increases the tolerance to multipath degradation. Table 5.2-12 is the design control table for the entry link and shows a margin over worst case tolerance of 23.8 dB for the reference range of 1000 km. To account for "black-out", data delayed by 70 sec is interleaved with real time data.

Entry link data is also split-phase (Manchester) coded and is recovered in a Support Module receiver in the same manner as described in para. 5.2.4.2. The bit sync analysis, para. 5.2.4.5, indicates an acquisition time on the order of 10 msec and signal degradation due to jitter of 0.5 dB. The entry link time shares the 400 MHz transmitter and, hence, has the same signal frequency separation as the landed link. However, the entry receiver bandwidth of 25 kHz is optimized for the 1100 bps data rate based on a frequency uncertainty due to combined oscillator instability and doppler shift of 20 kHz.

Fig. 5.2-12 shows the entry link margin over worst case adverse tolerances (excluding multipath degradation) for the worst case entry parameters - minimum density atmosphere model and minimum (3σ) entry angle. Also shown is the estimated degradation due to multipath. This is computed in para. 5.2.4.5, based on a -5 dB reflection coefficient. The fading is classified fast or slow and same-channel or cross-channel according to the relative delay and doppler shift between the direct and interfering path. (See para. 5.2.4.5 for details).

Initially, the fading is fast and there is little degradation. As the Lander decelerates and nears the surface, the fading becomes slow and same-channel. At the same time, the Lander attitude is such that antenna gains for the direct and specular reflection paths are nearly identical. These adverse effects combine at about 300 sec after entry to yield a net margin of 1.0 dB. Beyond this time the Lander approaches a near vertical descent which increases antenna pattern discrimination which decreases the multipath degradation.

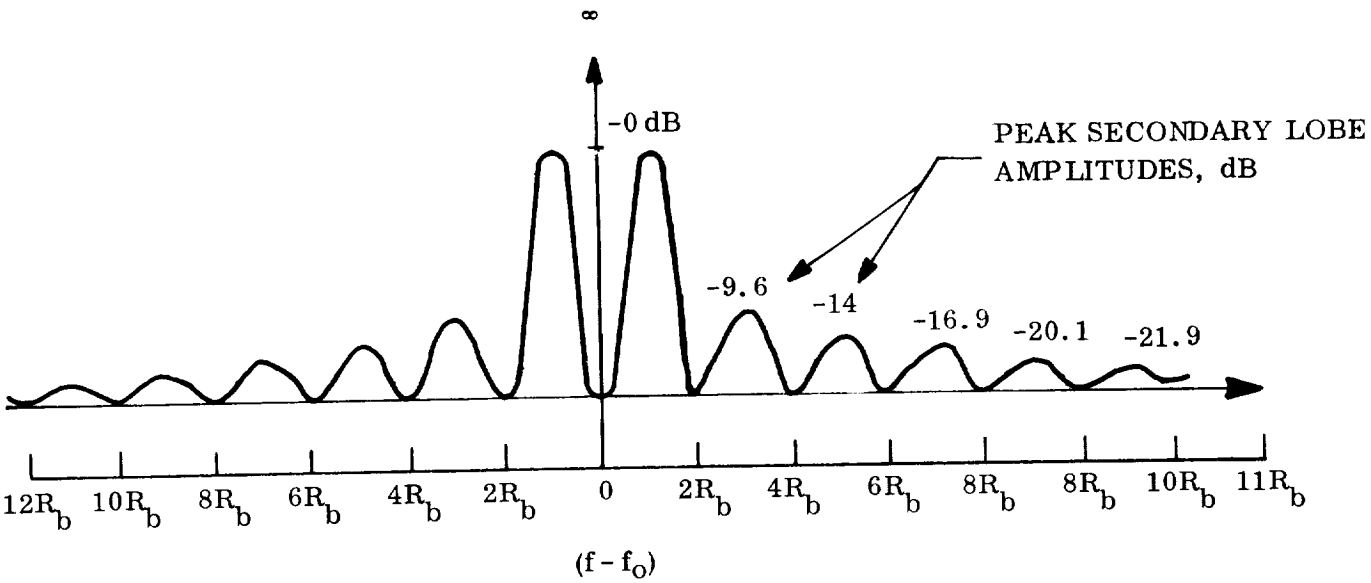

(a) Spectrum of Each Channel

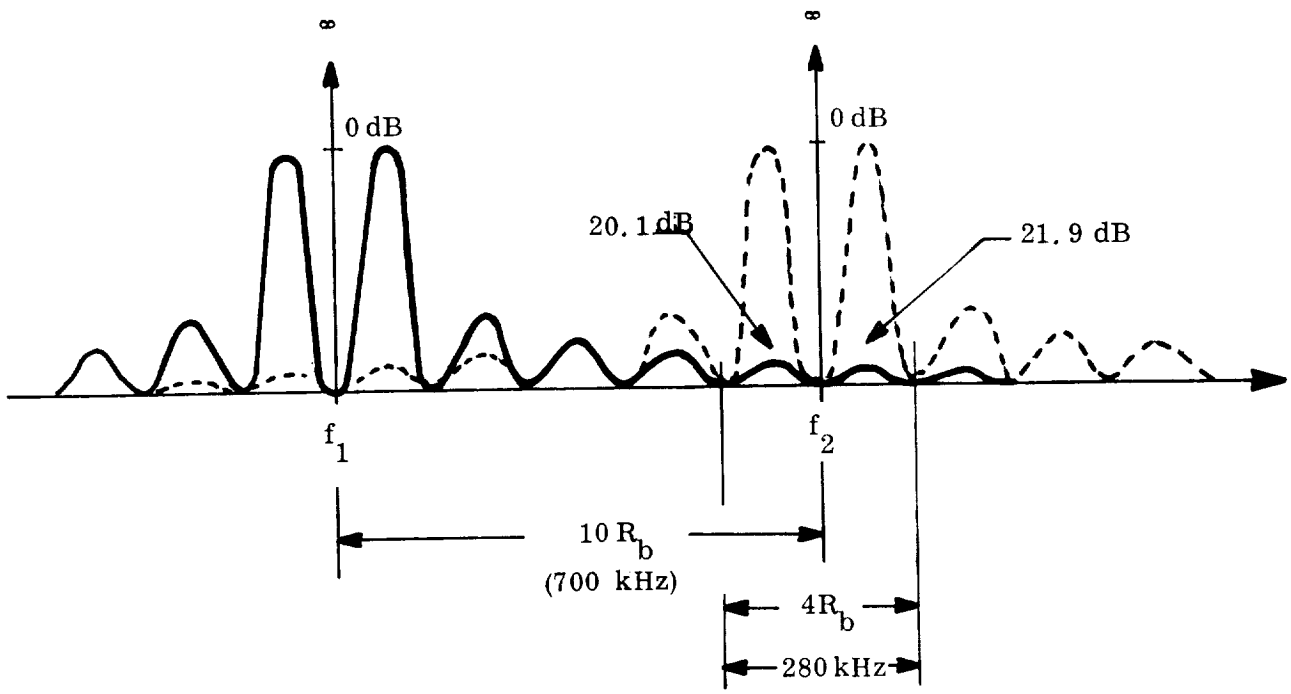

(b) Composite Spectrum

Figure 5.2-11. Spectra for FSK of Separate Oscillators

TABLE 5.2-12. ENTRY LINK DESIGN CONTROL TABLE

Parameter	Relay (entry) nominal	Adverse Tolerance
Modulation technique	FSK	--
Frequency (MHz)	400	
Transmitter power (watts)	50	
(dBm)	47.0	1.0
Transmit circuit loss	-1.5	0.4
Transmit antenna gain	2.0 (1)	0.5
Transmit antenna pointing loss	0.0	0.0
Reference range (km)	1000 (1)	
Space loss	-144.5	
Polarization loss	-1.0	0.5
Receiving antenna gain	4.0	0.5
Receiving antenna pointing loss	-1.0	0.0
Receiving circuit loss	-1.0	0.4
Total received power (S), dBm	-96.0	3.3
Effective noise temperature (^{o}K)	650°	
Receiver noise power spectral density (N/B)	-170.5	1.0
Data power (dBm) S_D	-96.0	3.3
Bit rate, 1/T (bps/dB)	1100/30.4	--
Frequency uncertainty (kHz)	20.	--
I-F bandwidth (kHz)	25.0	--
Required S/N/B	44.4 (2)	2.0 (2)
Required ST/N/B	14.0 (2)	2.0 (2)
Threshold data power (dBm)	-126.1	3.0
Margin	30.1 (3)	6.3

(1) Reference values.

(2) Nominal signal-to-noise ratio used is theoretical value. 2dB adverse tolerance is allowed to account for practical performance degradation.

(3) Margin for reference parameters excluding multipath degradation. Margin over worst case adverse tolerances is 30.1 - 6.3 = 23.8 dB.

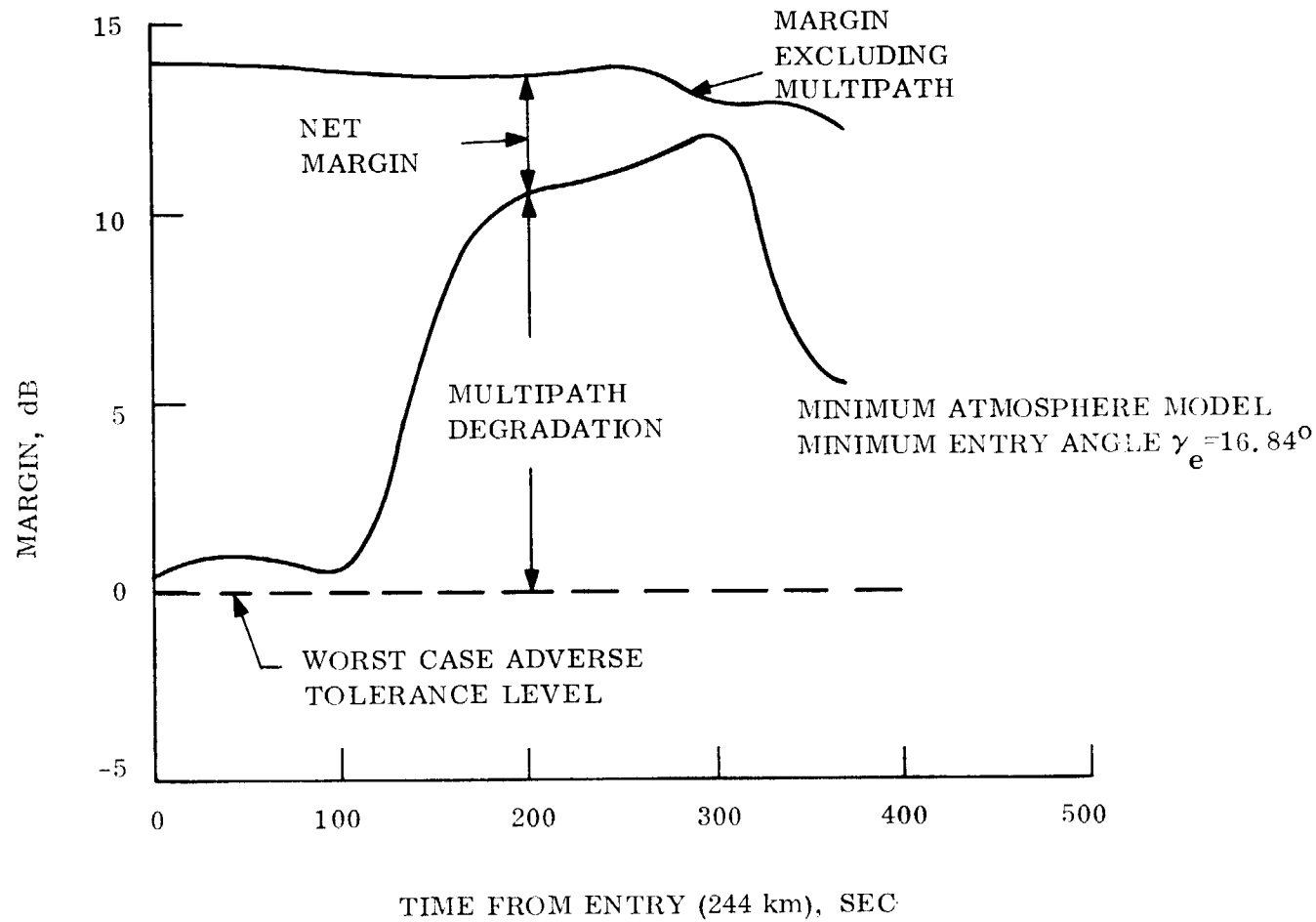

Figure 5.2-12. Entry Link Multipath Degradation and Net Margin

5.2.4.4 Equipment Description

5.2.4.4.1 Antennas

The entry antenna consists of an array of four whip antennas, each of which is 7.5 in. in length. The calculated pattern including the antenna efficiencies is shown in fig. 5.2-13. The exact spacing of the elements and the slope of the elements relative to the ground plane will be determined from actual pattern measurements on a model of the Lander/Capsule.

The configuration of the Lander 400 MHz antenna is that of a pill box 8 in. in diameter and 2 in. deep. The top surface of the box is flush with the vehicle outer surface and has two orthogonal slots, 2 in. wide and 8 in. long, dividing the top of the box into four quarters. The slots are tuned with capacitors to match the input and provide circular polarization. The bandwidth of this antenna is about 2 MHz. The pattern is shown in fig. 5.2-14. Since the Lander diameter is on the order of a wave length, the available ground plane is not large, indicating that the actual antenna pattern will vary somewhat from that shown.

5.2.4.4.2 400 MHz FSK Transmitter

A block diagram for the FSK transmitter is shown in fig. 5.2-15. The frequency shift keyed modulation is produced by switching between two stable crystal oscillators operating at 25.021875 MHz and 24.978125 MHz. Multiplying these signals by a factor of 16 produces transmitter output signals at 400.35 MHz and 399.65 MHz, respectively. The multiplier chain will be constructed at a low signal level in order that filtering and multiplier inefficiencies do not adversely affect the overall efficiency.

The power amplifier chain consists of amplifier stages to produce a total gain of about 47 dB; approximately 10 dB of this will be excess gain to be used for AGC. The final amplifier consists of two 2N5178's operating in push-pull; these transistors are each rated for 50 watts output at 500 MHz with a dissipation rating of 70 watts at 25°C.

The output power level of the transmitter will be controlled at 50 watts (+0, -1dB) through the temperature environment by means of an AGC circuit consisting of a detector for output sampling, a high gain amplifier, and a voltage variable attenuator located at the low level input to the 400 MHz power amplifier chain.

The transmitter oscillator stability will be 10 ppm over a temperature range of -40°C to +70°C with negligible warmup time at any temperature. Aging will be 1 ppm per year. The state of the art in temperature compensated crystal oscillators has reached a point where stabilities in the order of 1 ppm or better can be achieved for considerable periods of time. However, to account for degradation which may result from shock, such as deformation of the crystal structure or holder, a stability of 10 ppm is considered conservative.

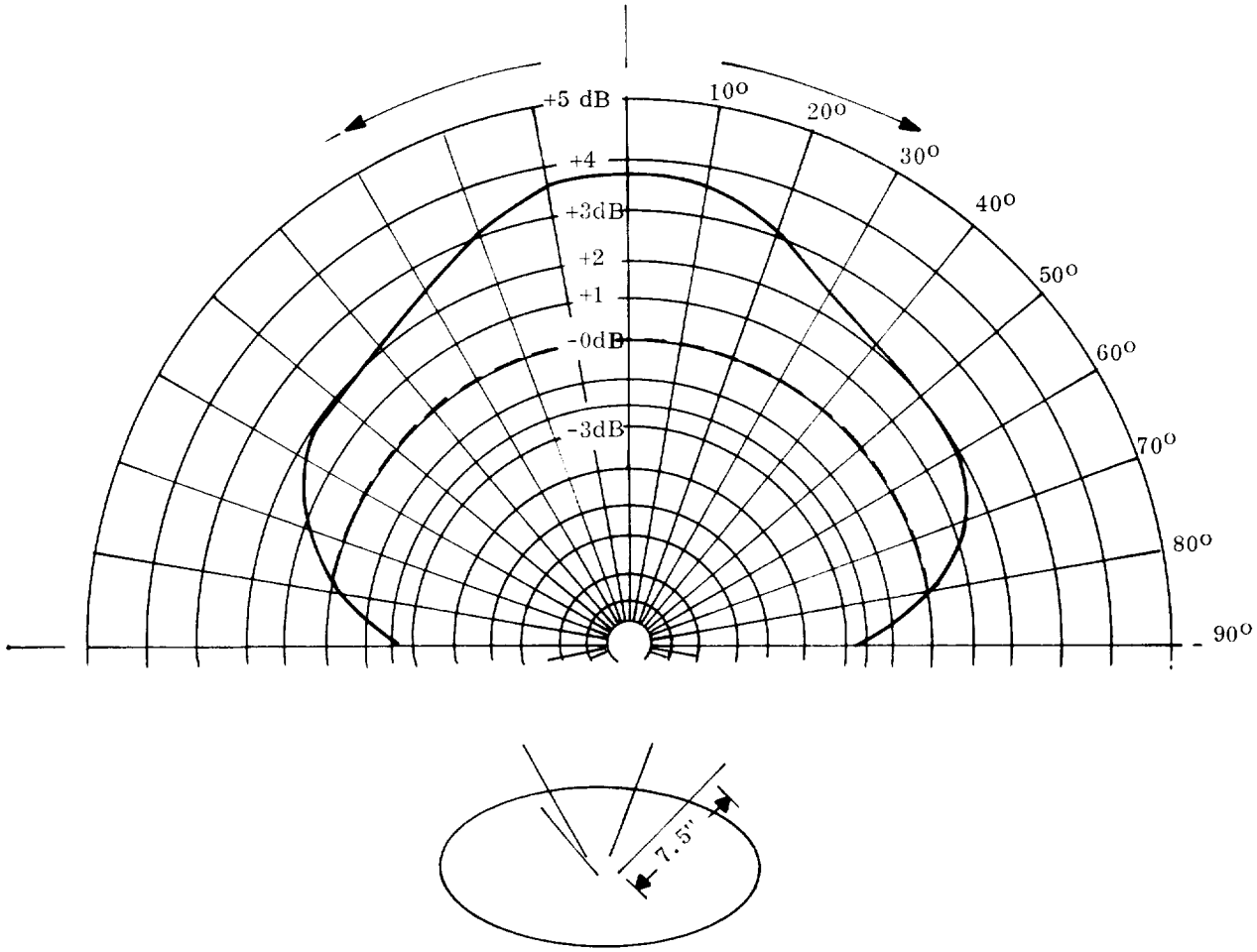

Figure 5.2-13. Fntry Antenna (Four Whips) Pattern

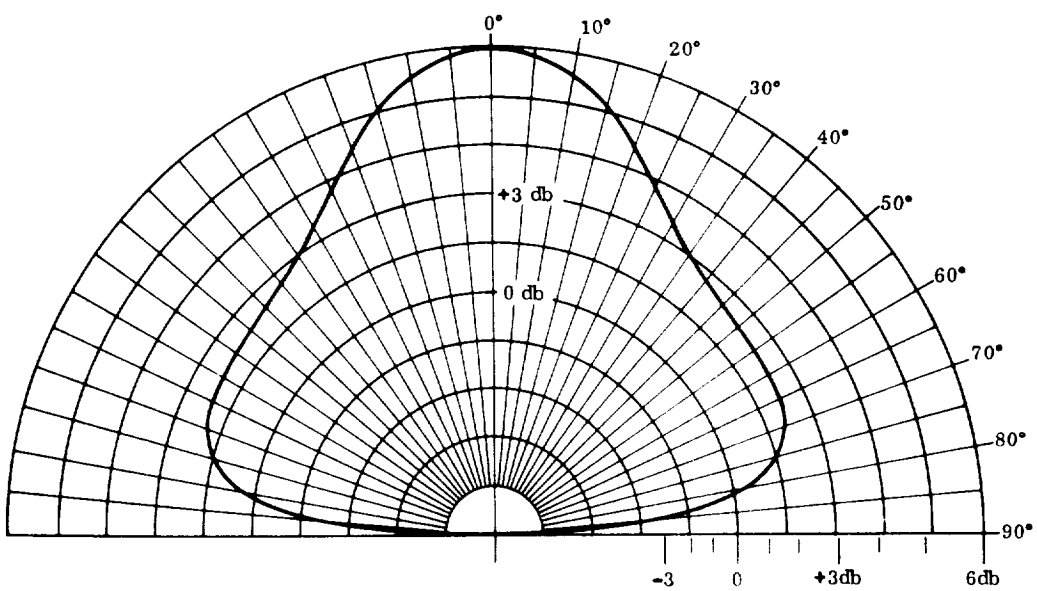

Includes polarization losses for circularly polarized receive antenna

Figure 5.2-14. Lander 400 MHz Antenna Pattern

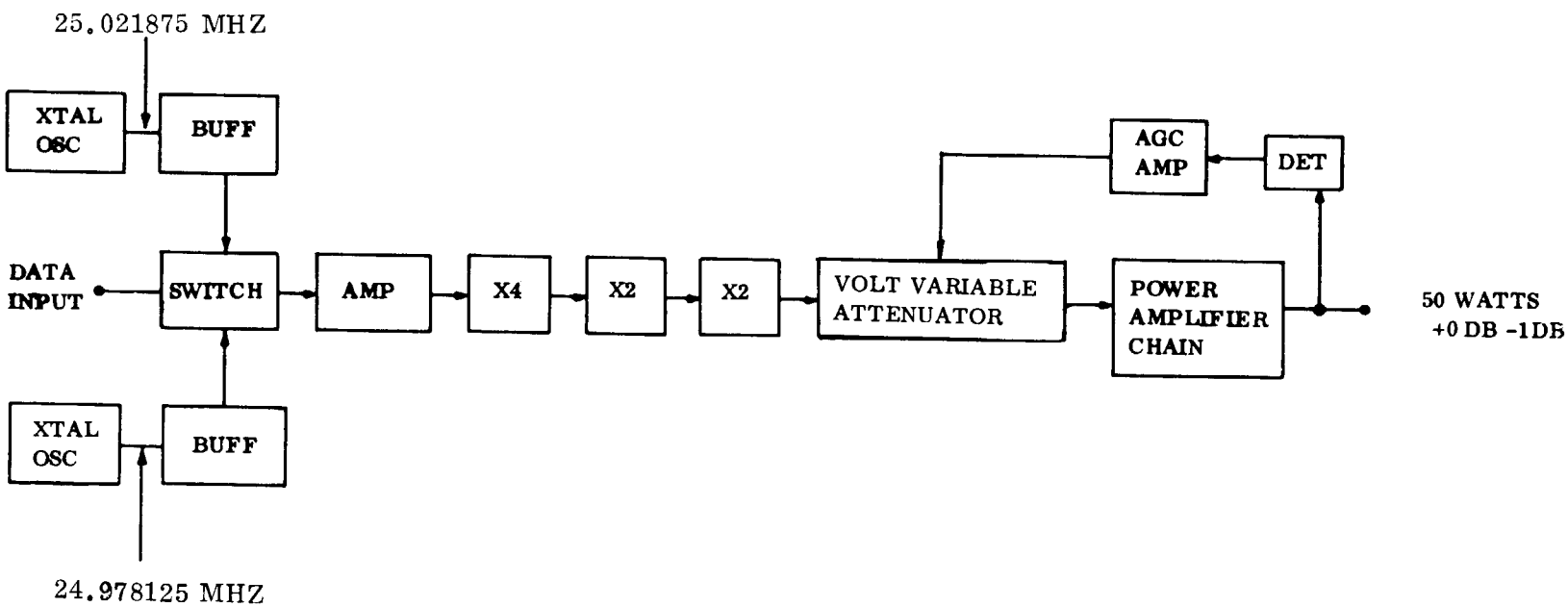

Figure 5.2-15. 400 MHz Transmitter, Block Diagram

No serious problems are anticipated in the sterilization of the transmitter or in the high shock levels expected. Several years ago GE-RS designed and constructed a VHF 50 watt transmitter which was successfully sterilized and subjected to multiple shock impacts at levels of 5000 g's for approximately 500 μsec. The transmitter was potted with Dow Corning XR-3700 silicon potting compound. (The complete results of these tests are reported in GE TIS 66SD2002 entitled "Fifty Watt Solid State FM Transmitter for Deep Space Communications," by Julius Shatas.)

5.2.4.4.3 RF Switch

The selection of the UHF antenna to be used at any given time is made by the antenna switch as shown in the block diagram, fig. 5.2-9. This solid state switch selects the appropriate antenna upon reception of a command from the C&S and power from the EP&D. A solid state switch is selected because of its reliability and potential to withstand the shock environment.

5.2.4.5 Design Studies

5.2.4.5.1 Bit Sync Performance

One means available for the unambiguous recovery of bit sync from a split phase signal is indicated in fig. 5.2-16 (ref. 5.2-2).

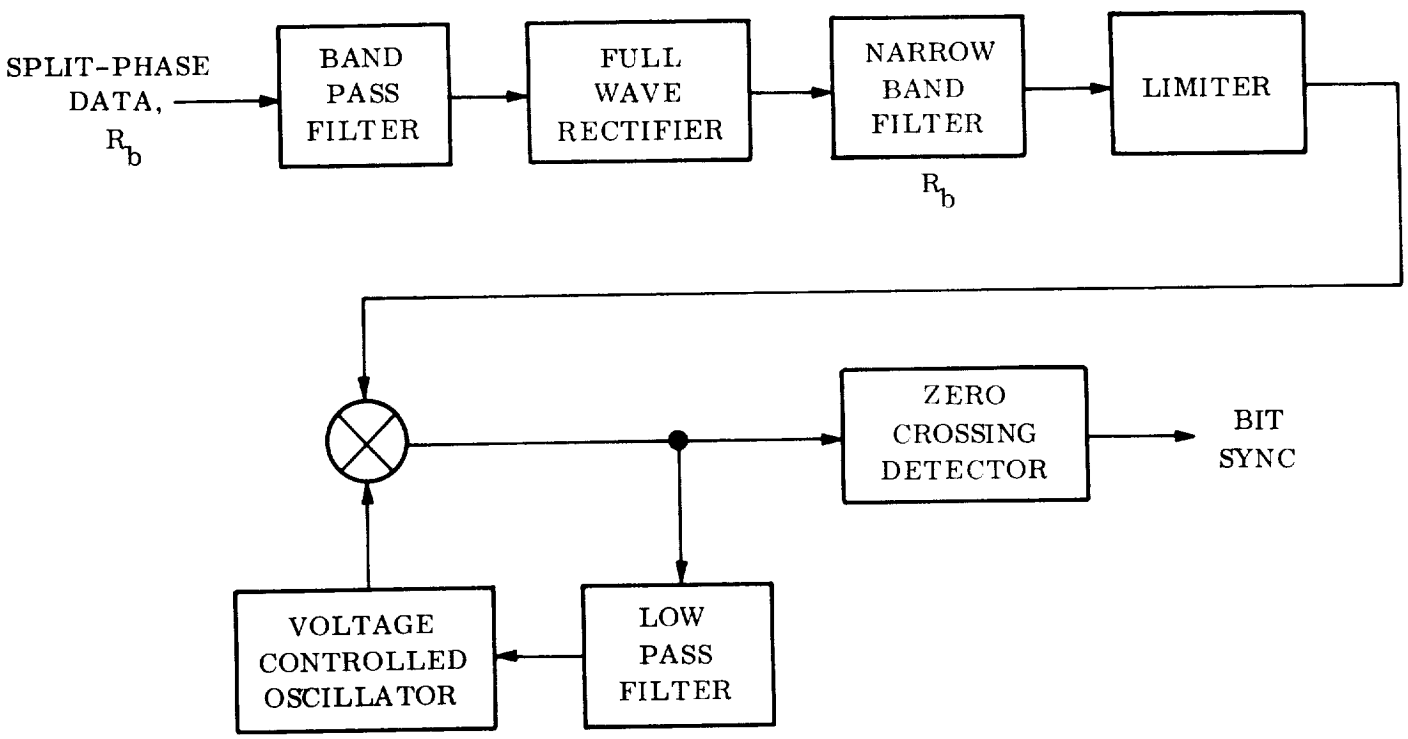

Figure 5.2-16. Bit Sync Scheme for Split Phase Signals

Errors in the derived bit sync phase reduce the effective signal-to-noise ratio due to non-ideal matched filter performance. This effect is estimated using the correlation function for split phase coded signals, fig. 5.2-17.

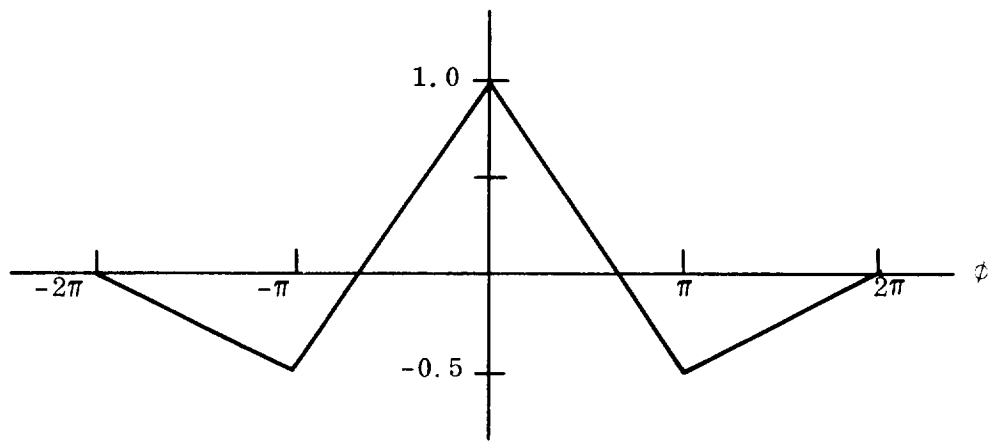

Figure 5.2-17. Correlation Function for Split Phase Signals

An estimate of signal power reduction (L_{SJ}) is obtained by evaluating the correlation function for a phase error equal to the rms bit sync phase jitter:

$$L_{SJ} \approx \left[1 - \frac{3\,\sigma_\theta}{2\,\pi} \right]^2$$

For high signal-to-noise ratios, the rms bit sync phase jitter is approximately

$$\sigma_\theta \approx \sqrt{\frac{1}{2\left(\frac{S}{N}\right)_{2B_{LO}}}} \quad \text{, radians}$$

where $\left(\frac{S}{N}\right)_{2B_{LO}}$ is the signal to noise ratio in the bit sync loop double sided noise bandwidth, $2B_{LO}$. This is given by Hackett, ref. 5.2-2, as

$$\left(\frac{S}{N}\right)_{2B_{LO}} = \frac{4\,(E/N_o)^2}{\pi^2\left[\left(1 + \frac{16}{\pi^2}\right)\frac{E}{N_o} + 2\right]} \cdot \left(\frac{R_b}{2B_{LO}}\right)$$

where E/N_0 is the received energy-to-noise power spectral density ratio. This relation assumes that the data is random, i.e., a one or zero is equally likely in any particular bit interval and each interval is independent of all other intervals.

Another important bit sync performance parameter is acquisition time. The acquisition time is dependent on the frequency uncertainty over which the phase lock loop (PLL) must acquire and the PLL parameters.

The frequency uncertainty is due to bit rate uncertainty and VCO instability. When the frequency uncertainty is small compared to the PLL bandwidth, the acquisition time is essentially determined by the PLL phase response time which is on the order of the reciprocal of the loop bandwidth.

The bit sync performance is estimated in table 5.2-13. The bit rate is crystal controlled and has very good stability. The VCO's are assumed to be of the L-C type with instabilities of 0.1 percent and 1.0 percent for the 70 kbps and 1100 bps data rates respectively. The resulting bit sync jitter losses do not exceed 0.5 dB.

TABLE 5.2-13. RELAY LINK BIT SYNC PERFORMANCE

Jitter Loss:					
Period	Bit Rate (bps)	$2B_{LO}$ (Hz)	E/N_o (1) (dB)	σ_θ (2) (deg)	Bit Sync Jitter Loss (dB)
Landed	70 k	1000	11.5	4	0.3
Entry	1100	100	14.0	6.4	0.2

Acquisition:					
Period	Bit Rate Instability (%)	VCO Instability (%)	Frequency Uncertainty (Hz)	Acquisition Time	
				(ms)	(bits)
Landed	0.01	0.1	77	1	70
Entry	0.01	1.0	11.1	10	11

(1) E/N_0 required for 4×10^{-3} bit error probability with 300 kHz and 25 kHz receiver bandwidths for 70 kbps and 1100 bps data rates, respectively.

(2) Assumes random data.

5.2.4.5.2 Multipath Degradation

During the descent phase, signals transmitted from the Lander may be reflected from the planetary surface before arriving at the Support Module receiver. These multipath signals may interfere with the desired signal which is received on the line-of-sight path from the Lander. Whether the resulting fading is fast or slow depends on the data rate and the doppler shift of the reflected signal relative to the line-of-sight (LOS) signal. If the relative doppler shift is large with respect to the data rate so that the composite received signal fluctuates rapidly within a bit interval, the fading is fast; if the amplitude of the composite signal can be considered constant during a bit interval, the fading is slow.

The effect of the time delay of the reflected signal on communication performance depends on the type of communication system used. In the present instance, a wideband binary FSK system is employed on the relay link. If the relative delay is much smaller than the bit interval, the interference appears in the same channel of the FSK receiver as the desired signal. This is termed "same channel interference". If the relative delay is comparable to, or longer than the bit interval, the interference and the desired signal can appear in opposite channels of the receiver. This is called "cross-channel interference".

The effect of power reflected from the planetary surface can be specified in terms of the signal to interference ratio as shown in fig. 5.2-18. When same channel interference occurs in the fast fading case, the performance is actually improved compared to the no fading case. When the fading is fast and cross channel interference occurs, some loss results but this loss is relatively small. The worst case loss condition is slow fading with same channel interference.

The interference level is a function of the surface reflectivity, the antenna pattern, and the vehicle surface geometry. A reasonable estimate of the worst case interference level is -5 dB when isotropic antenna patterns are assumed. This level has been determined from various analyses of Martian multipath. A treatment of the problem by GE (ref. 5.2-3) is based upon a rough surface model of the planet which is due to Beckman (ref. 5.2-4). Preliminary computations yield an interference level of -8 dB based upon an average power reflectivity of 7 percent as determined by radio astronomy (ref. 5-2-5). The radar observations indicate that the reflectivity of Mars can be as large as 13 percent in certain regions. This is twice the average value of 7 percent and results in the estimated -5 dB interference level.

Another analytical approach (ref. 5.2-6) gives maximum relative multipath levels of -4 dB for horizontal polarization and -8 dB for vertical polarization at 300 MHz. This analysis, based on a dry, rough surface, applies for a Lander altitude of 4.5 km and for reflection angles of up to 80°. The relative level is as low as -10 dB for horizontal polarization (at normal incidence and reflection) and -20 dB for vertical polarization (at the Brewster angle). Others (ref. 5.2-7) have computed a maximum relative multipath of -6 dB based on planet characteristics derived from 430 MHz radar observations.

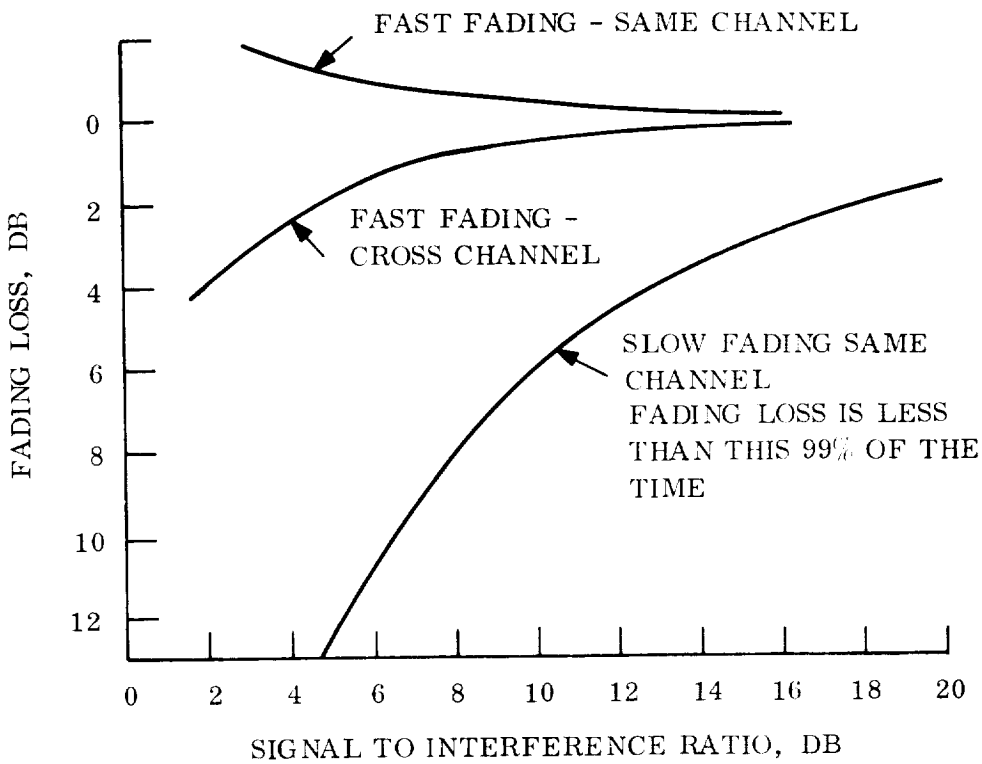

Figure 5.2-18. Performance of Wide-band FSK with Multipath Interference

Polarization of the reflected signal and the antenna directivity should reduce the level below -5 dB. The reflected signal will be elliptically polarized due to the difference in horizontal and vertical reflection coefficients of the surface at 400 MHz. In addition, any surface reflections from the antenna main beam will result in a reversed circular polarization at the orbital receiver. These polarization effects should further suppress the interfering signals.

The multipath parameters vary somewhat as a function of atmospheric model and entry angle and appear to be worst for the minimum (3σ) entry angle and the minimum density atmosphere. In this case the direct path range is maximum and the direct to interference path discrimination due to antenna pattern is minimum. The maximum interference level is expected to come from the vicinity of the specular reflection point (angle of incidence equal to angle of reflection). Fig. 5.2-19 shows the delay and doppler shift of the specular interference path relative to the direct path and the angle between each path and the antenna boresight axis. This data, the antenna pattern fig. 5.2-13, and the direct path parameters are used in table 5.2-14 to compute the interfering to direct received power ratio by modifying the -5 dB interference level by the ratio of interfering to direct path lengths and antenna gains. This result is then used in fig. 5.2-18 to compute the multipath degradation Whether the interference is classified fast or slow is based upon whether the relative doppler shift is greater than twice the bit rate (1100 bps during entry) or is less than the bit rate, respectively. It is classified cross-channel or same-channel when the

relative delay is greater than half a bit width or less than one quarter of a bit width respectively. (Because of split phase coding, a transition from one channel to the other occurs at the bit mid-point. Hence, a delay of more than hald a bit indicates cross channel interference.) In the intermediate delay and doppler regions, the performance degradation is estimated by interpolation between appropriate curves.

Table 5.2-14 shows the "margin" over worst case adverse link tolerances and the computed performance degradation due to multipath. Fig. 5.2-12 presents the results in graphical form. Initially the fading is fast and there is little degradation. As the Lander decelerates and nears the surface, the fading becomes slow and same channel. At the same time, the Lander attitude is such that antenna gains for the direct and specular paths are nearly identical. These adverse effects combine at about 300 sec after entry to yield a net margin of 1.0 dB. Beyond this time the Lander approaches a near vertical descent which increases antenna pattern discrimination and decreases multipath degradation.

5.2.4.5.3 Data Rate Considerations

Two approaches for the landed relay link were considered: the first approach maximum data return for the selected antenna, and a second approach to transmit at a 16.2 kbps data rate to minimize the changes to the spacecraft equipments.

The two major factors which are favorable to the lower data rate are:

1. The current Mariner tape recorders are capable of recording data at this rate

2. With a 50 in. diameter high gain antenna on the Support Module, the imagery data could be transmitted to Earth in real time. This would require a moderate change to the 40 in. diameter antenna used on Mariner '69.

An estimate of the data capacity at the lower rate is obtained as follows. Table 5.2-15, a design control table for the 16.2 kbps rate, shows a nominal margin of 17.6 dB, which is 6.1 dB above the nominal margin for the 70 kbps rate. The transmission time available is determined from fig. 5.2-11 as the minimum time that the margin shown in that figure exceeds -6.1 dB. The resulting data capacity is about 8×10^6 bits. By optimizing the Capsule time of flight change, the data return at this low rate could be increased to about 10^7 bits, which is significantly below the 2.8×10^7 bit capacity of 70 kbps. For the purposes of this study, the approach of maximizing the data return was selected.

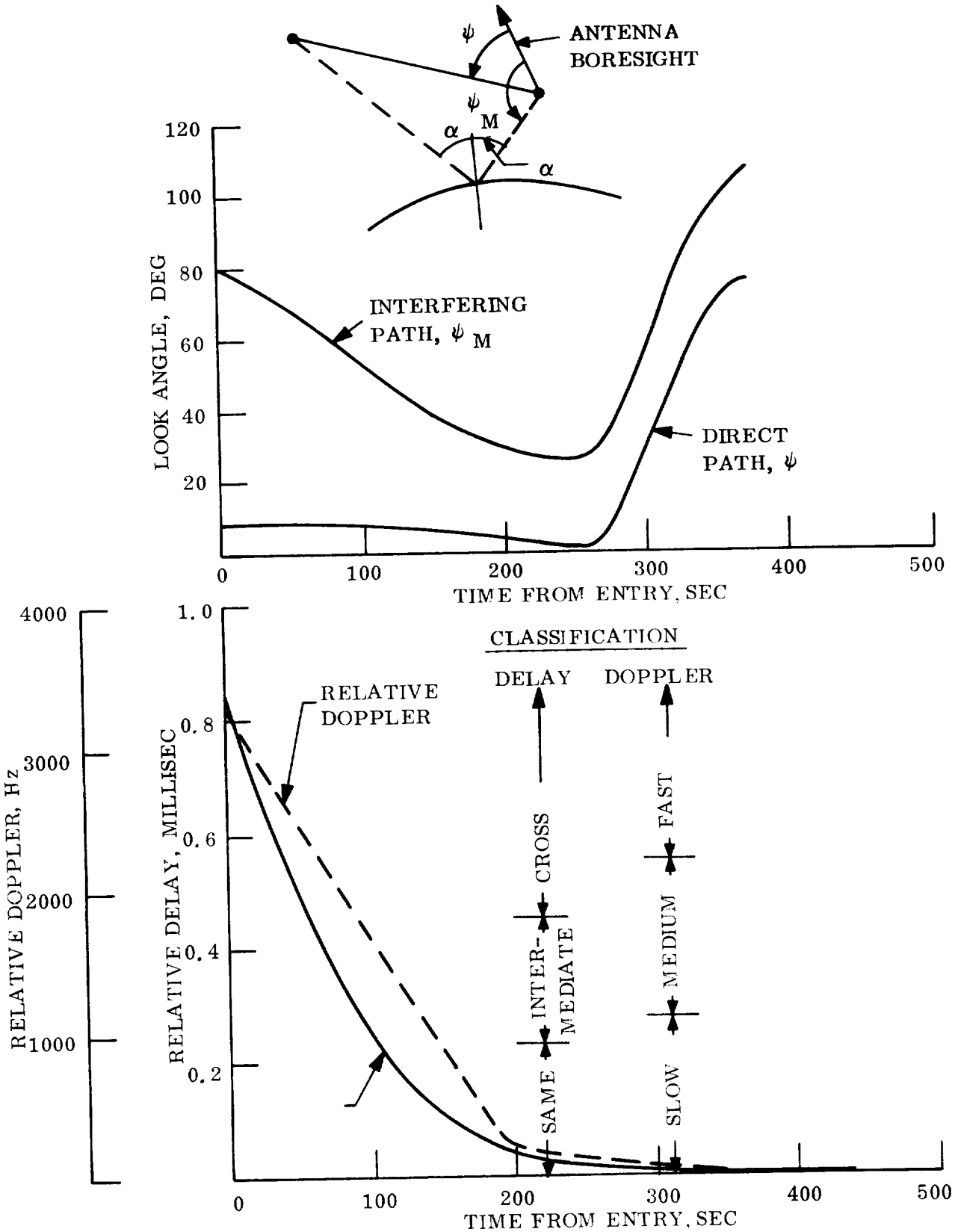

Figure 5.2-19. Multipath Parameters

TABLE 5.2-14 MULTIPATH DEGRADATION COMPUTATION

Time	Direct Path			Interfering Path		P_I/P_D (3) (dB)	Class (4)	Degradation (dB)
	Range (km)	Gain (dB)	Margin (dB)	Range (km)	Gain (dB)			
ref. (1)	1000	2.0	23.8 (2)	-	-	-	-	-
0	3669	3.5	14.0	3926	0.0	-9.1	FF/CI	0.5
50	3731	3.5	13.9	3882	1.5	-7.4	FF/CI	1.0
100	3794	3.5	13.8	3872	2.0	-6.7	FF/X	0.5
150	3858	3.5	13.6	3890	2.5	-6.1	X/SI	7.0
200	3894	3.5	13.5	3904	2.5	-6.0	SF/SI	10.5
250	3766	3.5	13.8	3772	2.8	-5.7	SF/SI	11.0
301	3561	2.3	13.0	3563	2.0	-5.3	SF/SI	12.0
341	3386	1.6	12.8	3386	-2.0	-8.6	SF/SI	7.0
370	3255	0.7	12.2	3255	-5.0	-10.7	SF/SI	5.5

(1) Reference conditions from entry design control table.

(2) Margin over worst case adverse tolerances for reference conditions.

(3) Ratio of interfering to direct received power.

(4) FF - Fast Fading; SF - Slow Fading; CI - Cross Channel Interference; SI - Same Channel Interference; X - Intermediate Cases

5.2.4.5.3 Entry Blackout

In the course of this study, it has been assumed that a blackout period; i.e., loss of communication during entry, will occur. The duration of this blackout period has been assumed to be 70 sec. As shown in table 5.2-16, the shortest length of time from end of blackout to impact is approximately 83 sec. Therefore, the use of a single 70 sec delay is sufficient to recover the data taken during the blackout period.

However, if the duration is determined to be longer than 83 sec, an alternate approach can be implemented in order to recover the data taken during the period prior to landing. The alternate approach is shown in fig. 5.2-20. It consists of two delay lengths. The advantage of this approach is that the data accumulated during blackout can be recovered in half the time of blackout duration. However, it requires that the data transmission rate be three times the data collection rate rather than twice as with the single delay.

TABLE 5.2-15 RELAY (LANDED) DESIGN CONTROL TABLE - LOW BIT RATE

Parameter	Nominal Value	Adverse Tolerance
Modulation technique	FSK	--
Frequency (MHz)	400	
Transmitter power (watts)	50	
(dBm)	47.0	1.0
Transmit circuit loss	-1.5	0.4
Transmit antenna gain	4.0(1)	0.5
Transmit antenna pointing loss	2.0(1)	0.0
Reference range (km)	1000(1)	
Space loss	-144.5	
Polarization loss	-1.0	0.5
Receiving antenna gain	4.0	0.5
Receiving antenna pointing loss	-4.0	0.0
Receiving circuit loss	-1.0	0.4
Total received power (S), dBm	-99.0	3.3
Effective noise temperature (°K)	650°	
Receiver noise power spectral density (N/B)	-170.5	1.0
Data power (dB m) S_D	-99.0	3.3
Bit rate, 1/T (bps/dB)	16.2K/42.1	--
Frequency uncertainty (KHz)	20.	--
I-F bandwidth (KHz)	35	--
Required S/N/B	53.9(2)	2.0(2)
Required ST/N/B	11.8(2)	2.0(2)
Threshold data power (dBm)	-116.6	3.0
Margin	17.6(3)	6.3

(1) Reference values.

(2) Nominal signal-to-noise ratio used is theoretical value. 2 dB adverse tolerance is allowed to account for practical performance degradation, e.g., non-ideal bit sync.

(3) Margin for Reference Values and Nominal Parameters.

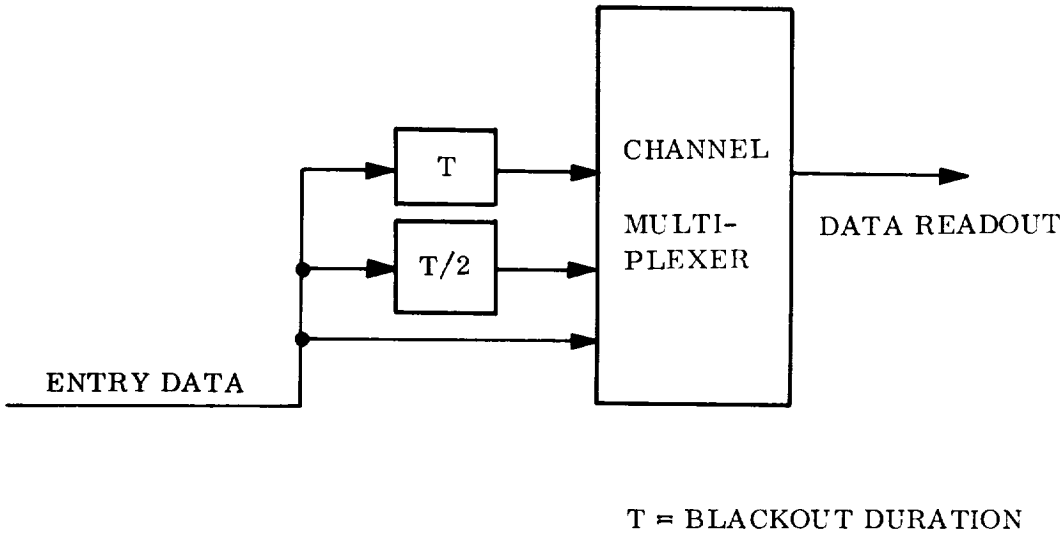

Figure 5.2-20. Alternate Entry Data Collection Scheme

TABLE 5.2-16. TIME FROM END OF BLACKOUT TO LANDING

Atmosphere	MIN	MIN	MIN	MEAN	MEAN	MEAN	MAX	MAX	MAX
γ_E	Min	Nom	Max	Min	Nom	Max	Min	Nom	Max
Time (sec)	162	105	83	201	149	126	295	250	246

5.2.5 DIRECT LINK

S-band direct links are used for communications between the Lander and the stations of the Deep Space Network (DSN). For the selected reference mission, landing occurs near the evening terminator. The visibility of the Earth and Sun from this site is depicted in fig. 5.2-21. Both the Earth and Sun are setting at landing. The line-of-sight to Earth is at a low elevation angle at landing and may even be below the horizon depending on the exact location within the landing footprint. Data transmission is therefore delayed until about 18 hr after impact when the line-of-sight to Earth is near maximum elevation. Transmission will be initiated by the C&S and will last for only 30 min, limited by the available battery energy. Transmission will be re-initiated on each succeeding day at the same relative time. Command capability is provided to allow altering the planned mission sequence and as a backup to on-board initiated events. The command receiver and detector operation are limited to a 2 hr period each day in order to conserve battery energy.

5.2.5.1 Functional Description

The Direct Link Subsystem, fig. 5.2-22, transmits Lander science and engineering data to the DSN and receives and detects ground commands. The primary transmitting antenna is a vertically oriented helix having a 3 dB beamwidth of 76°. This antenna is stored within the Lander until after impact. When the Lander comes to rest, the antenna mast is automatically deployed to the top side of the Lander, and the antenna is oriented to the local vertical. With the 20 watt TWT power amplifier, a data rate of 50 bps is transmitted to a 210 ft DSN antenna. Backing up the vertically oriented antenna are two broad beam antennas fixed to the top and bottom surfaces of the Lander. These antennas have a 3 dB beamwidth of about 120° and can support a data rate of 5 bps. After the Lander comes to rest, the r-f circulator switches are automatically switched to select the top antenna as indicated in table 5.2-17.

TABLE 5.2-17 - CIRCULATOR SWITCH POSITIONS

Circulator Switch \ Top Antenna	Antenna 1	Antenna 2
CS 2	CW	CCW
CS 3	CCW	CW

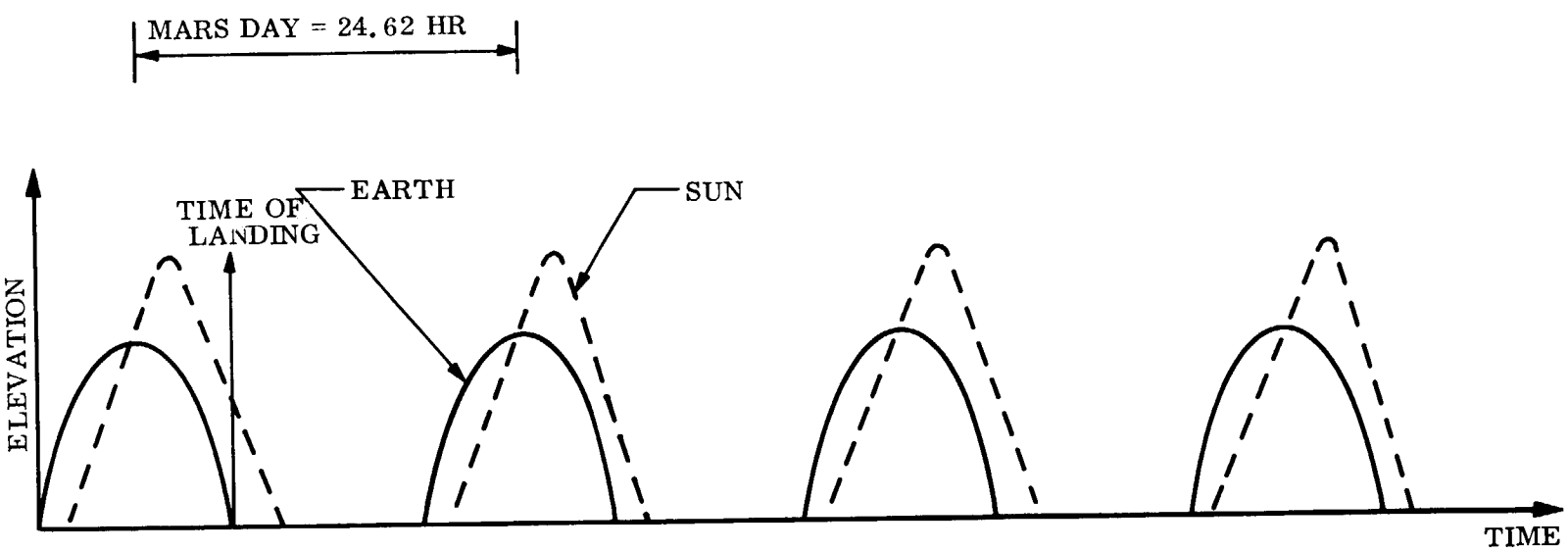

Figure 5.2-21. Earth and Sun Visibility from Landing Site

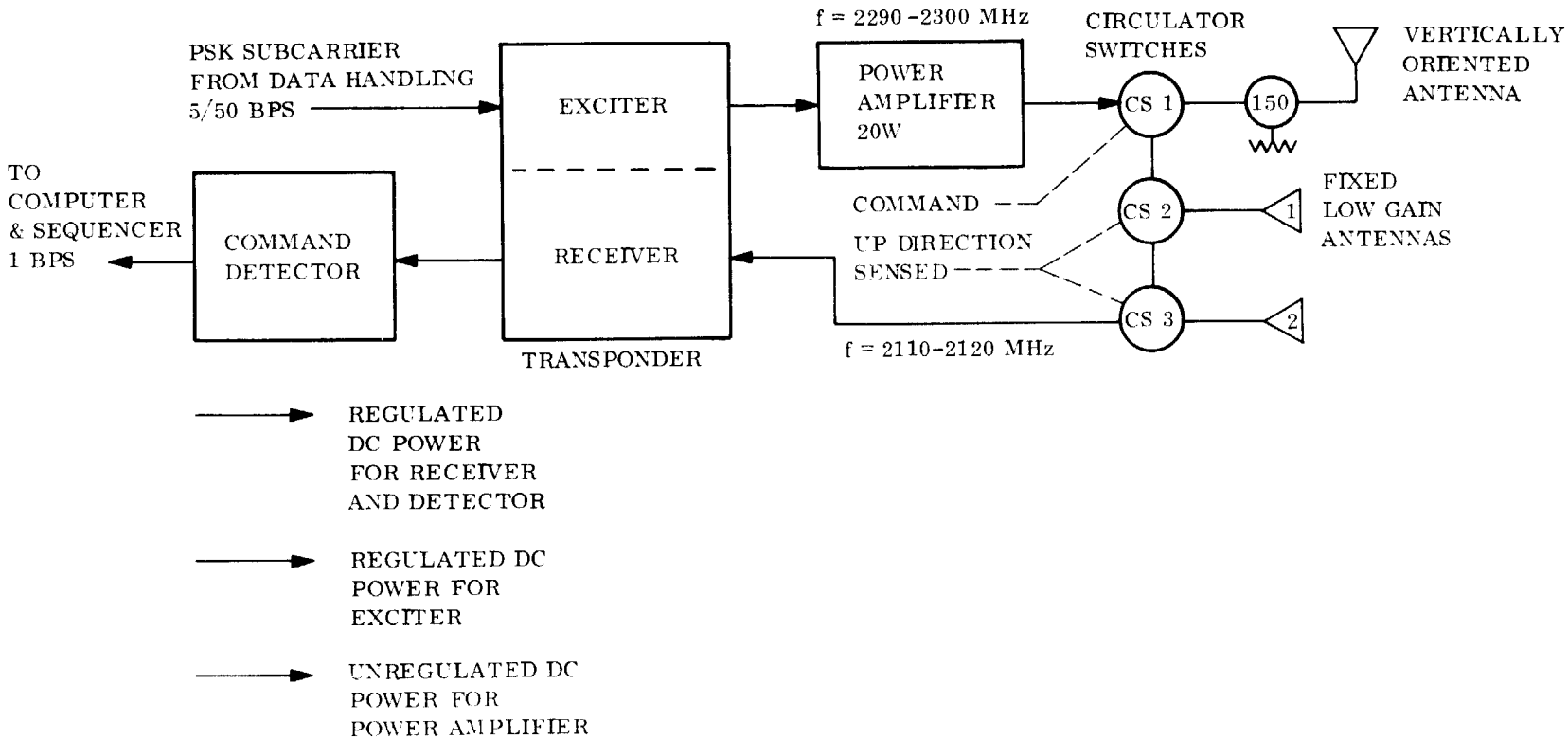

Figure 5.2-22. Direct Link Link Subsystem

Although the vertically oriented antenna is the primary transmitting antenna, the top fixed antenna is always used for reception. In order to transmit via the fixed antenna, ground command must be used to switch circulator switch 1 and select the 5 bps data rate. The command rate is 1 bps.

Both the command and telemetry links employ modulation and detection techniques that were developed for the Mariner Spacecraft. The telemetry link transmits binary coded data on a square wave subcarrier which phase modulates the S-band carrier. For the 50 bps data rate, error control coding is used to increase the data rate capability about two to one compared to an uncoded system. At the 5 bps data rate, coding is not used because system performance is principally limited by carrier and subcarrier detection rather than by data detection. The command modulation and detection scheme is the same as is used on Mariner '69. The data bi-phase modulates a sinusoidal subcarrier which is transmitted, together with the pseudo-noise (PN) sync signal, by phase modulating the up-link carrier. The phase lock receiver in the Lander serves as the command receiver and also functions as a coherent transponder to enable Doppler tracking of the Lander for position determination.

5.2.5.2 Component Description

In this section, the requirements for each of the major components of the Direct Link Subsystem are defined, and the implementation selected for each component is described. The components discussed are the antennas, power amplifier, r-f switching, the transponder, and the command detector.

5.2.5.2.1 Antennas

The beamwidth requirements of the antennas are set by the apparent track of the Earth through the sky at the landing site, and for the body fixed antennas, by the attitude of the Lander relative to the local horizontal. The major factors determining the communication geometry are listed in table 5.2-18. Fig. 5.2-23 shows the celestial sphere at the landing site of 10° North latitude on February 7, 1974. The intersection of the equatorial plane with the celestial sphere is inclined 10° to the Lander zenith direction, and since the declination of the Sun is 0°, the apparent path of the Sun on the celestial sphere lies in the equatorial plane. The Sun appears to make one complete traverse in the 24.62 hr Martian day. The Earth, which is at a declination of -17°, appears to move in a plane parallel to the equatorial plane but 17° below it. For these conditions, fig. 5.2-24 gives the elevation of the Earth as a function of time. The peak elevation of the Earth occurs when it is in the plane of the Lander meridian and is given by:

$$\theta_{max} = 90^\circ - |\lambda - \delta| = 63^\circ$$

where

λ = the Lander latitude

δ = the declination of the Earth

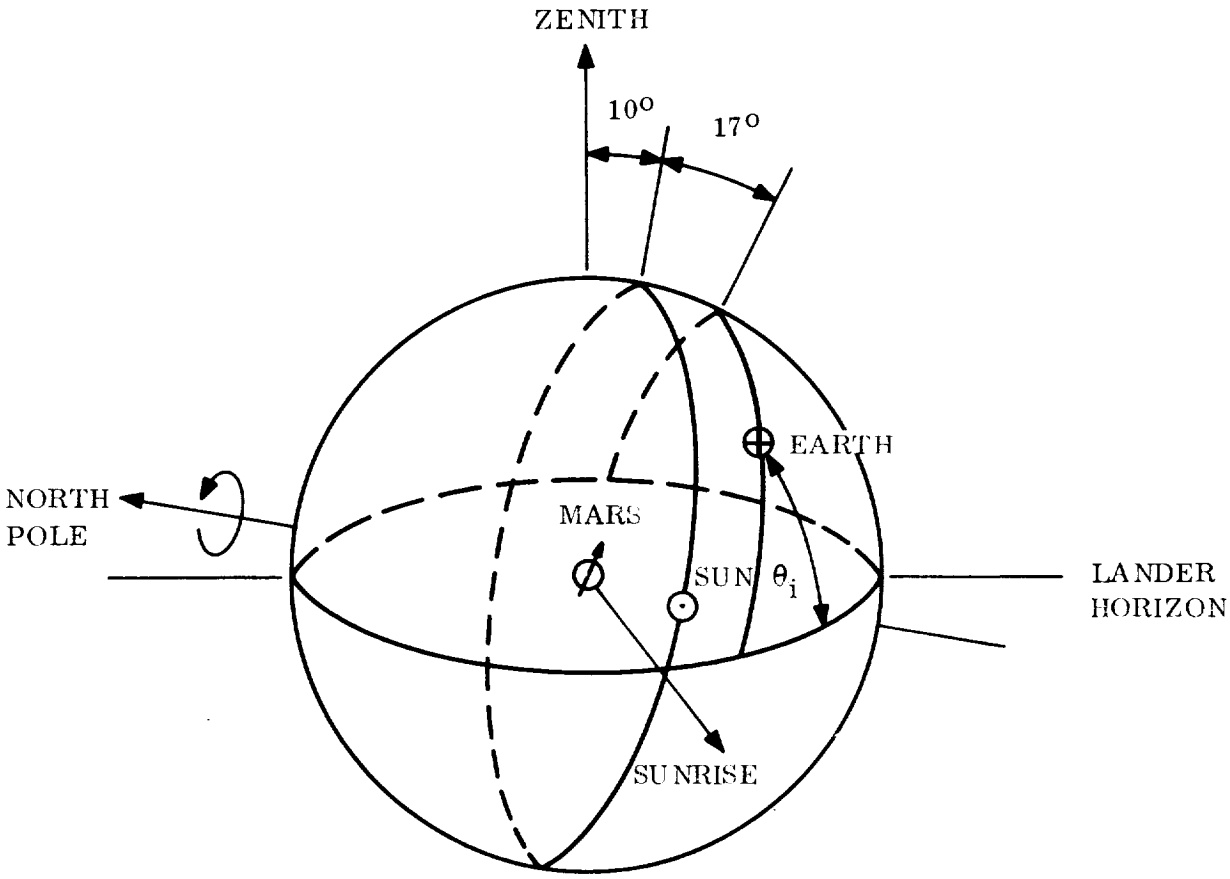

Figure 5.2-23. Celestial Sphere for 10° Latitude Landing Site

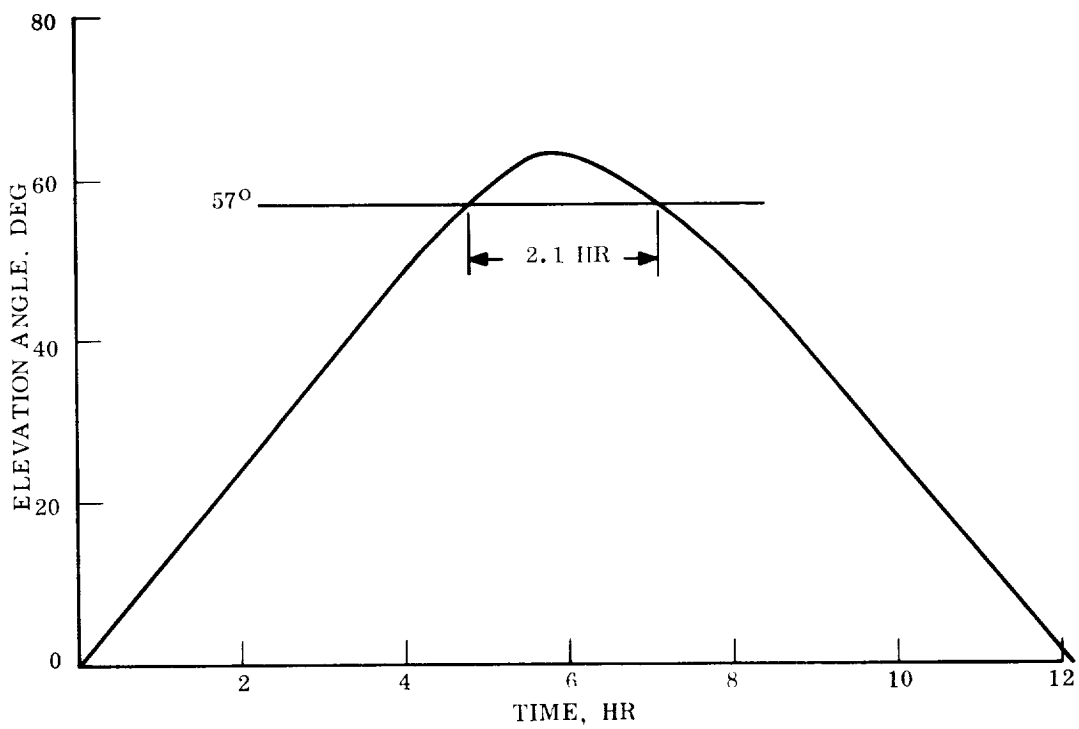

Figure 5.2-24. Earth Elevation from 10° North Latitude, 2/7/74

TABLE 5.2-18. LANDED COMMUNICATION GEOMETRY

Arrival date:	February 7, 1974 (reference)
Landing latitude:	Nominal 10° N
Latitude dispersion due to approach trajectory error:	
impact parameter magnitude:	10.5° N to 8.0° N
out-of-plane error:	± 1.5° (estimated)
Landing longitude dispersion:	21.8°
Declination of Earth:	17°
Declination of Sun:	0°
Landing attitude:	
maximum slope considered	20°
maximum tilt of Lander due to impact attenuation crush:	12°

In order to insure that the Earth passes through the antenna pattern within the 3 dB points, the beamwidth must be at least 2 (90-63) = 54° if the antenna is pointed exactly at the local vertical. A broader beam is required in order to provide a finite communication time. Further, the landing longitude dispersion (ΔL) must be taken into account if the initiation of tranmission is a fixed time from impact. Thus, for a 30 min communication period (T_c), the available communication time must be:

$$\tau_a = \frac{\Delta L}{360} \times T_{Mars} + T_c \quad \text{hr}$$

$$= 2.1 \text{ hr}$$

where T_{Mars} is the rotation period of Mars = 24.6 hr. As fig. 5.2-24 shows, the antenna pattern must come down to an elevation of 57°. Therefore, the beamwidth of a vertically oriented antenna must be 2 (90-57) = 66°. If an additional ±5° is allowed for landing latitude dispersion and errors in finding the local vertical, the beamwidth becomes 76°.

For a body fixed antenna, the required beamwidth must take into account the angle between the top face of the Lander and the local horizontal. For the assumed conditions of table 5.2-18, the minimum beamwidth becomes:

$$2\ \{|\lambda - \delta| + 32^\circ\} = 120^\circ$$

Helical antennas were selected for both the vertically oriented and body fixed antennas. A sketch of the antenna configuration and plots of the expected patterns are given in figs. 5.2-25 through -27. The antennas are mounted in conical cups which provide a minimum size ground plane and reduce the interference effects of nearby objects. The vertically oriented antenna is deployed from the Lander on a 2 ft mast. After being erected to the local vertical, no objects on the Lander are within the beam and the predicted pattern is expected to be achieved with little error. The body-fixed antennas, however, will have interfering objects within their beams, which will produce shadowing and reflections that distort the predicted pattern. The amount of degradation that will be produced must be evaluated experimentally. As long as the realized pattern gain is above 0 dB within the 80° cone centered on the zenith, and is above 0 dB over 95 percent of the entire 120° beamwidth, the degradation will be considered acceptable. If the degradation is greater than this, the antennas may have to be deployed above the Lander.

The vertically oriented antenna was selected for primary data transmission because it is simple in concept and provides significant antenna gain. Reliable mechanical deployment and means for driving the antenna to the vertical position must be provided, but the same basic mechanism designs required for the antenna are required for other devices on the Lander, such as the cameras. Thus, no unique problems must be solved to provide a rugged, reliable system. Alternate antenna schemes (fig. 5.2-28) that were considered but rejected were (a) multiple fixed antennas with a means to select the antenna most nearly pointing toward Earth, and (b) a retrodirective array. These systems trade simpler mechanisms for more complex circuitry.

If several fixed antennas are used, their patterns may be skewed with respect to each other so that the combined patterns cover the same 120° cone covered by the single fixed antenna. Each of these antennnas may have narrower beamwidths than tne single antenna, and hence, will provide a greater gain. If three antennas are used, the beamwidth can be 105°, affording a gain improvement of about 1 dB. If four are used, the beamwidth is about 84° and the gain improvement is 3 dB, which is about the same gain improvement achieved by using a vertically oriented antenna (BW = 76°). As more antennas are used, the gain of each increases. On the other hand, the weight and size of the antenna system increases (duplicate systems are needed on both the top and bottom sides of the Lander), the r-f switching becomes somewhat more complex and the switching losses may increase, partially offsetting the increased directive gain. Furthermore,

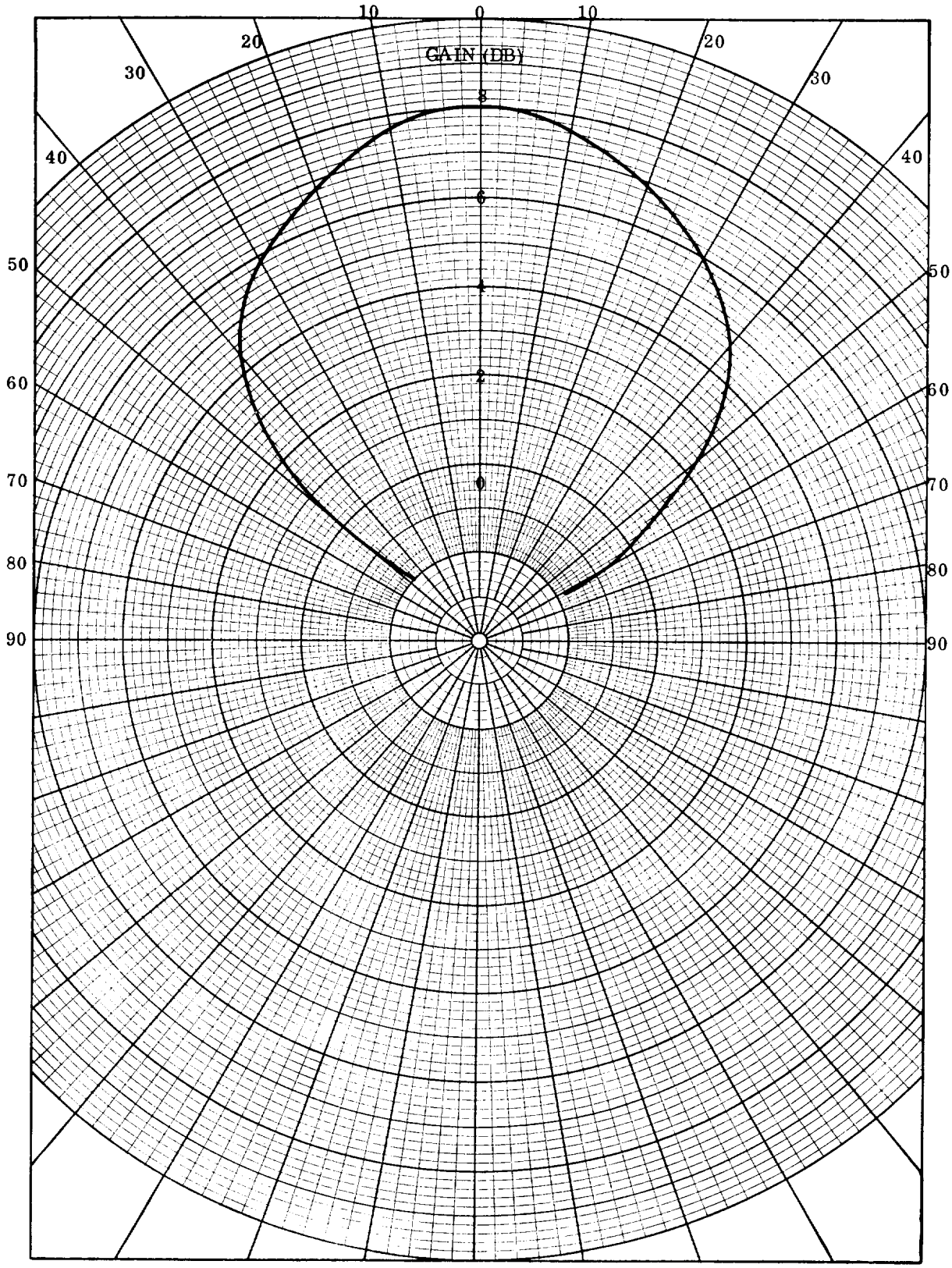

Figure 5.2-25. Pattern of Vertically Oriented Antenna

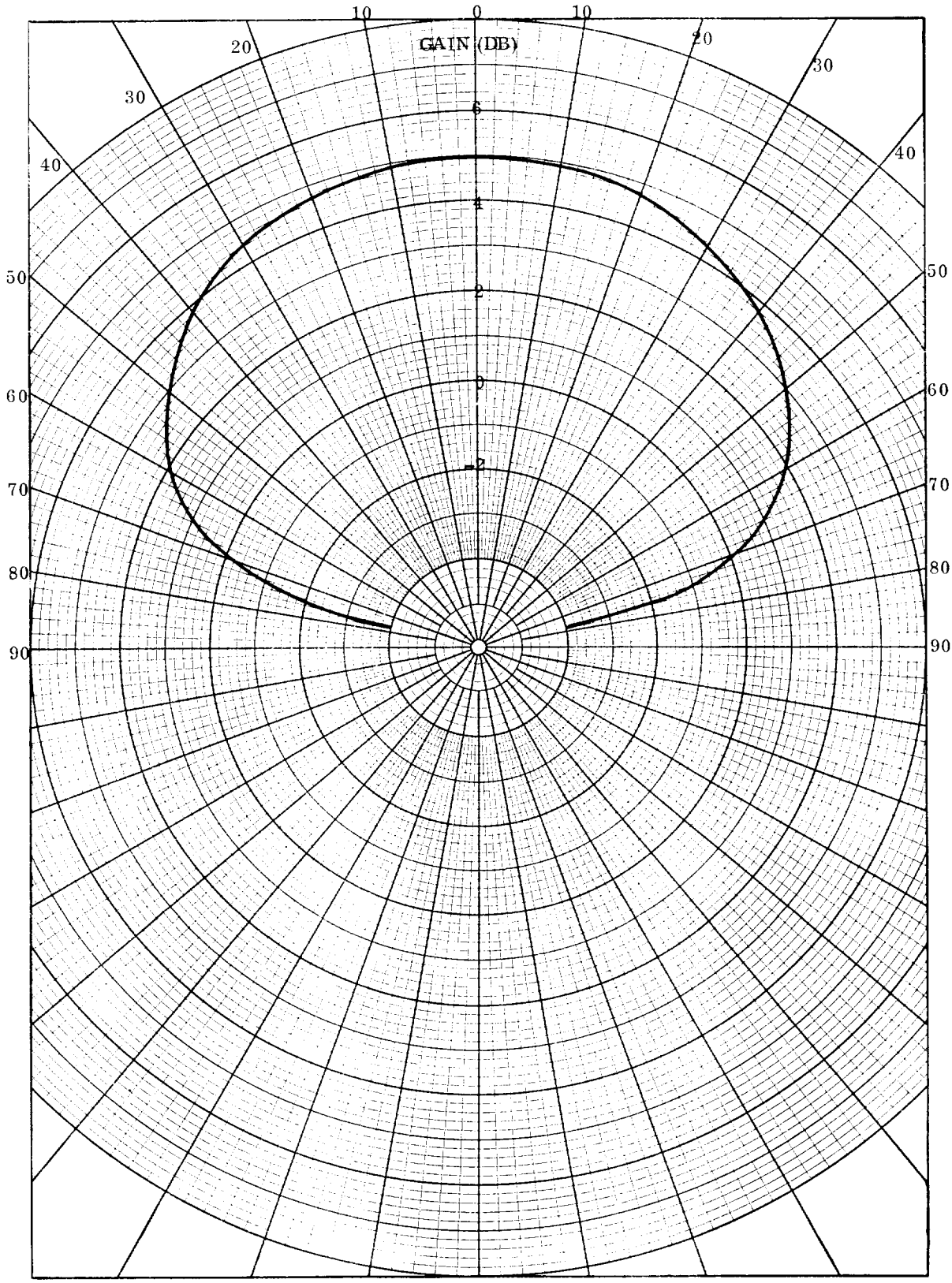

Figure 5.2-26. Pattern of Body-Fixed Antenna

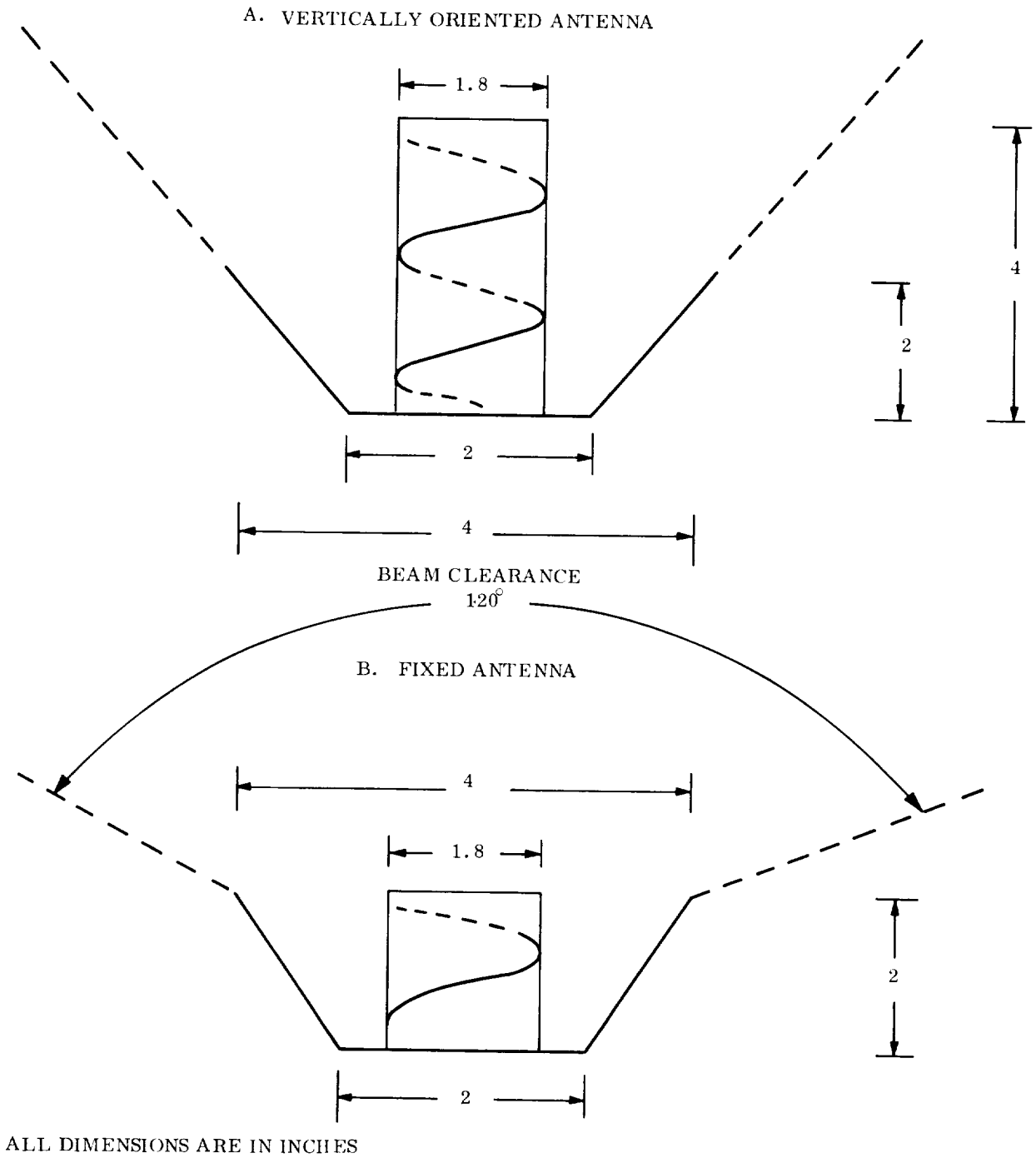

Figure 5.2-27. Antenna Configurations

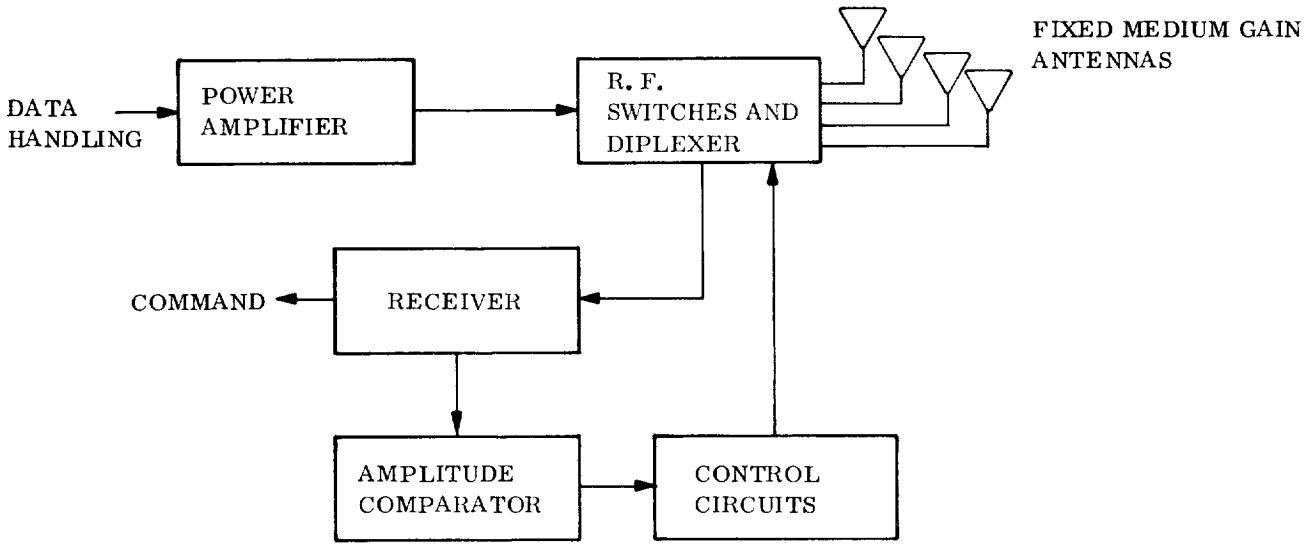

A. MULTIPLE FIXED ANTENNAS

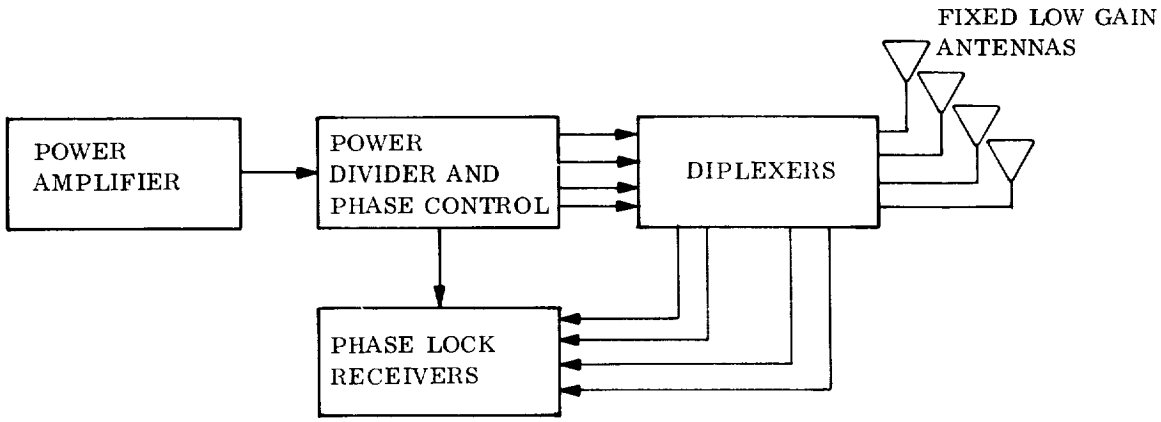

B. RETRODIRECTIVE ARRAY

Figure 5. 2-28. Alternate Antenna Systems

means must be provided for determining which of the multiple antennas is most nearly in the Earth direction during the communication period (more than one antenna may have to be used). The sensing system for determining the Earth direction may take several forms. One direct way is to switch the Lander receiver sequentially to each of the antennas as the ground station is transmitting, and to compare the received signal level from each, selecting the antenna that receives the strongest signal. Time must be allowed for the receiver to acquire the up-link carrier while it is connected to each antenna. Automatic frequency search and acquisition by the receiver may be used rather than using the "conventional" DSIF approach to simplify the ground operation problem. No up-link modulation would be applied during acquisition. Using the 85 ft antenna with the 100 kW transmitter, a sweep rate on the order of 200 Hz/sec could be used (fig. 5.2-29) since the received SNR is about 15 dB worst case referenced to the 20 Hz carrier loop bandwidth. Assuming a 50 kHz sweep range to account for the instability of the receiver VCO, the acquisition time is about 4 min, which is satisfactory for a small number of antennas. The principal advantage of this approach compared to the vertically oriented antenna is that the antennas can be fixed to the Lander, rather than having to be deployed and vertically oriented. The principal disadvantages are the reliance on the up-link operation and the more complex r-f switching and diplexing requirements.

An electrically steered array could be used to eliminate the steering motion although deployment might be required to avoid interference by cameras or other instruments. Either an interferometer system could be used to derive phase control signals for each antenna element, or a retrodirective array could be implemented. In either approach, multiple receivers are required in order to measure the direction of arrival of the signal from Earth. In addition, power dividers and phase shifters, which can be implemented in a compact form using strip line and diode phase shifter techniques, are needed. Again, a major factor in the decision not to use this approach is the dependence on the up-link operation, in addition to the added weight and power required for the additional receivers. However, if a very much higher data rate than 50 bps were clearly required, an electrically steered array would be an attractive possibility.

5.2.5.2.2 Power Amplifier

Both solid state and traveling wave tube (TWT) power amplifiers were considered for the Lander S-band transmitter. The TWT was selected principally because of the higher power efficiency it provides.

The power capability and gain of S-band transistors are continuously improving. Fig. 5.2-30 shows the design of a transistor power amplifier that provides a minimum output power of 16 watts at S-band. The transmitter is small and rugged and operates from low d-c voltages to minimize d-c breakdown possibilities. The d-c to r-f conversion efficiency, however, is only 12 percent. On the other hand, current TWT amplifiers

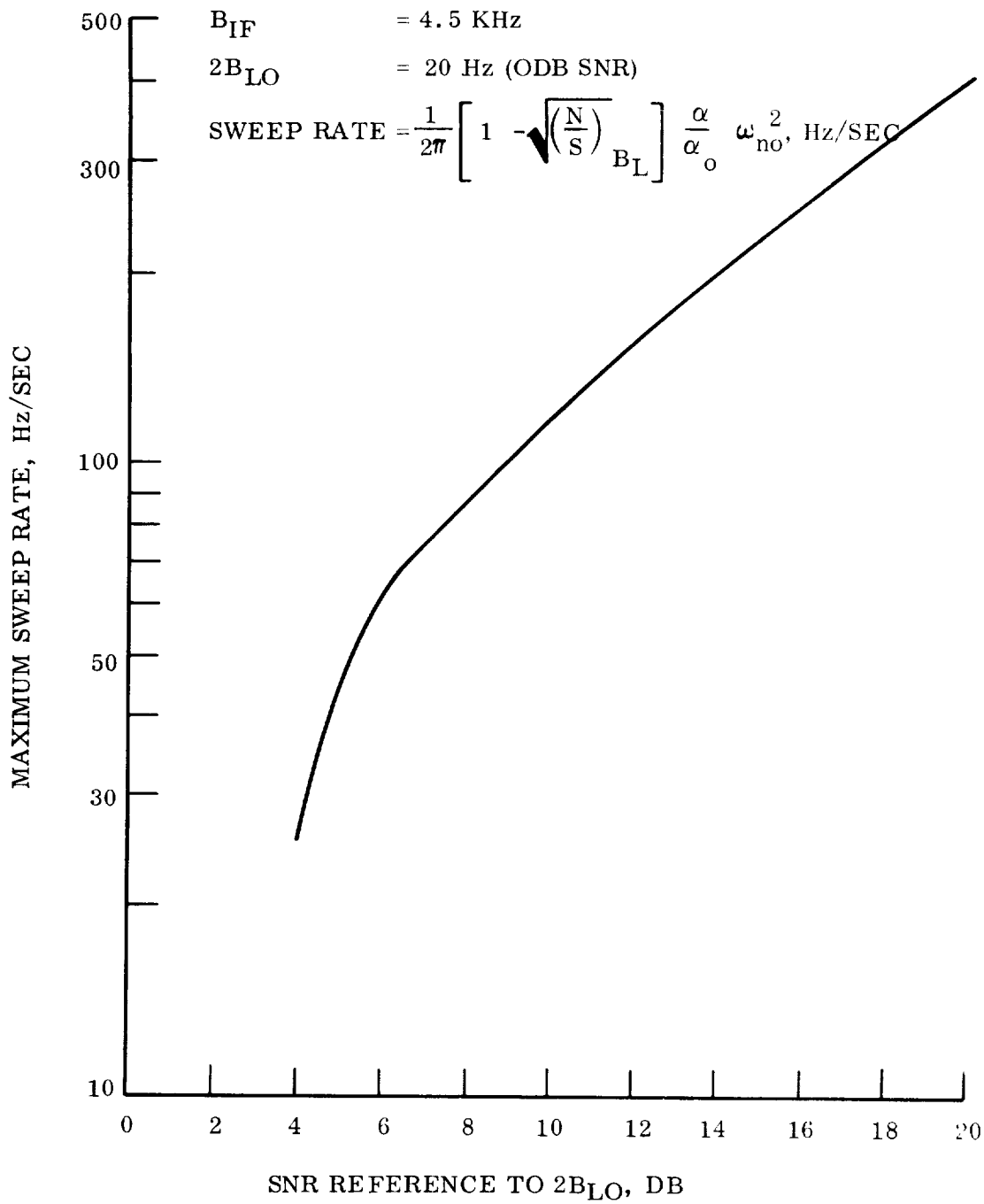

Figure 5.2-29. Maximum Acquisition Sweep Rate

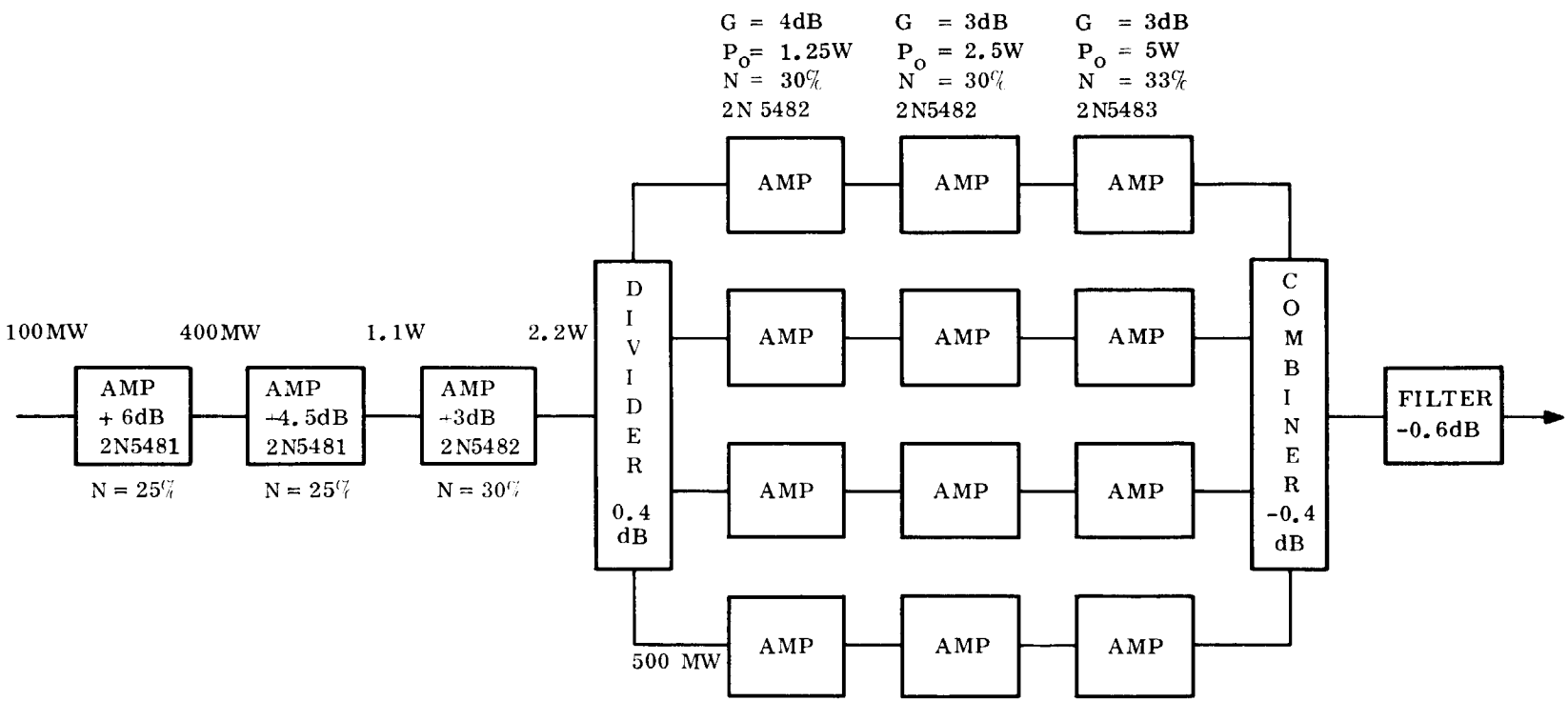

Figure 5.2-30. 16 Watt Solid State Power Amplifier

provide an efficiency of better than 20 percent, and current developments hold out the promise of tube efficiencies of better than 40 percent, which would lead to overall amplifier efficiencies, taking into account filter and power supply losses, of about 30 percent.

Under contract to JPL, Watkins-Johnson has developed a 20 watt TWT that has successfully been shock tested at 9600 g's with a 0.5 msec duration. This tube would provide an amplifier with an overall efficiency of 22.5 percent. Although further improvements in efficiency are possible, the current design is predicated on the use of this tube. The performance characteristics of the amplifier are given in table 5.2-19.

TABLE 5.2-19. PERFORMANCE CHARACTERISTICS OF 20 WATT TWT AMPLIFIER

Frequency	2.2 to 2.4 GHz
Duty Cycle	CW
Output Power	20 watts minimum
Saturated Gain	20 dB minimum
Bandwidth	10 MHz
Noise Figure	30 dB maximum
Phase Linearity	$\pm 2.5^{\circ}$ across passband

5.2.5.2.3 Switching

The switching of the transmitter and receiver to the vertically oriented and fixed antennas uses ferrite circulator switches, as shown in fig. 5.2-31. The r-f losses between the transmitter and receiver are based on the use of RG-142 cable, 0.1 dB loss for each connector, and losses of 0.5 dB and 0.8 dB for CS-1 and for CS-2 and CS-3, respectively, and 0.3 dB for the isolator.

Careful attention must be paid to achieving low VSWR through the system not only to minimize mismatch losses, but also to avoid sneak paths that will cause interference lobes in the antenna patterns. The isolator is included in the line to the vertically oriented antenna for this reason. In this system, reception on the low gain antennas may be interfered with by the signal received by the vertically oriented antenna if the isolator were absent. When receiving on fixed antenna #1, for example, the signal reaching

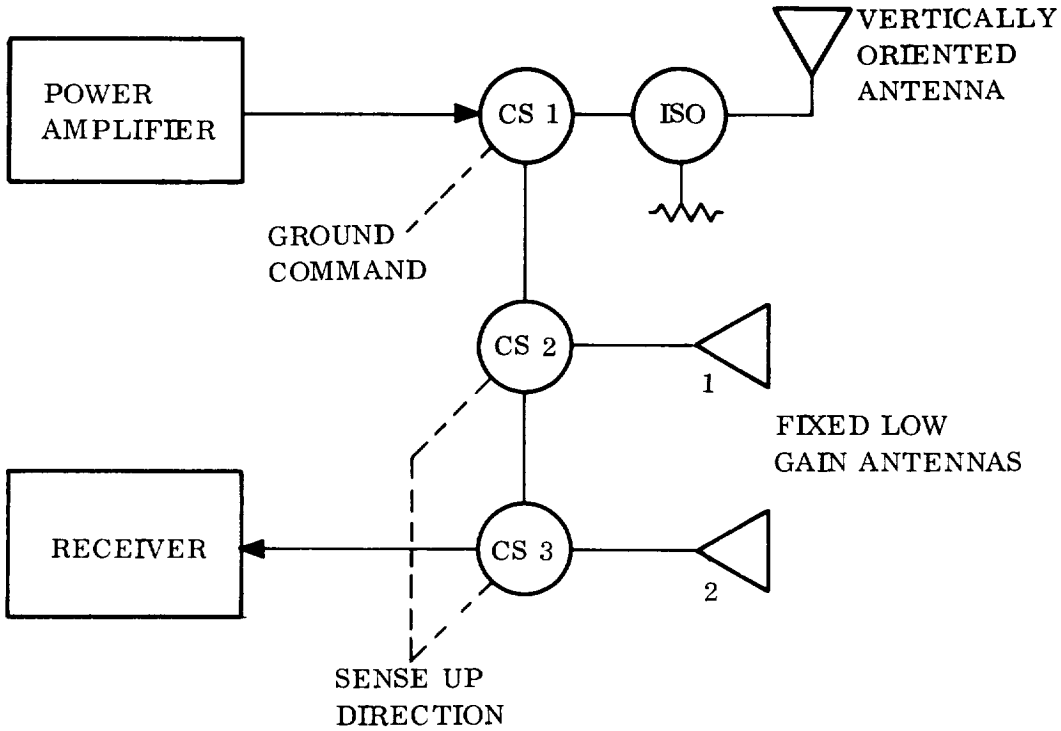

Transmitting Antenna	Receiving Antenna	Circulator Switch Positions*			Maximum RF Path Loss ~ dB	
		CS1	CS2	CS3	Transmit	Receive
Vertically Oriented	Fixed #1	CW	CW	CCW	1.9	1.1
Vertically Oriented	Fixed #2	CW	CCW	CW	1.9	1.5
Fixed #1	Fixed #1	CCW	CW	CCW	1.2	1.1
Fixed #2	Fixed #2	CCW	CCW	CW	1.6	1.5

*CW means low loss r-f path through switch is in clockwise direction. CCW is counter-clockwise.

Figure 5.2-31. R-F Switching Modes

the receiver from the vertically oriented antenna should be attenuated at least 20 dB by the reverse isolation of CS-2. However, if the VSWR looking into antenna #1 is 1.2 or greater, the reflected power reduces the effective isolation by 3 dB or more. The worst case effect of interference on the received signal is shown in fig. 5.2-32. By incorporating the isolator in the line to the vertically oriented antenna, the effective isolation is increased by 20 dB, so that the nominal isolation is 37 dB for a VSWR of 1.2. Even if the received level on the vertically oriented antenna is 5 dB above that on the fixed antenna, the maximum signal reduction is less than 0.2 dB.

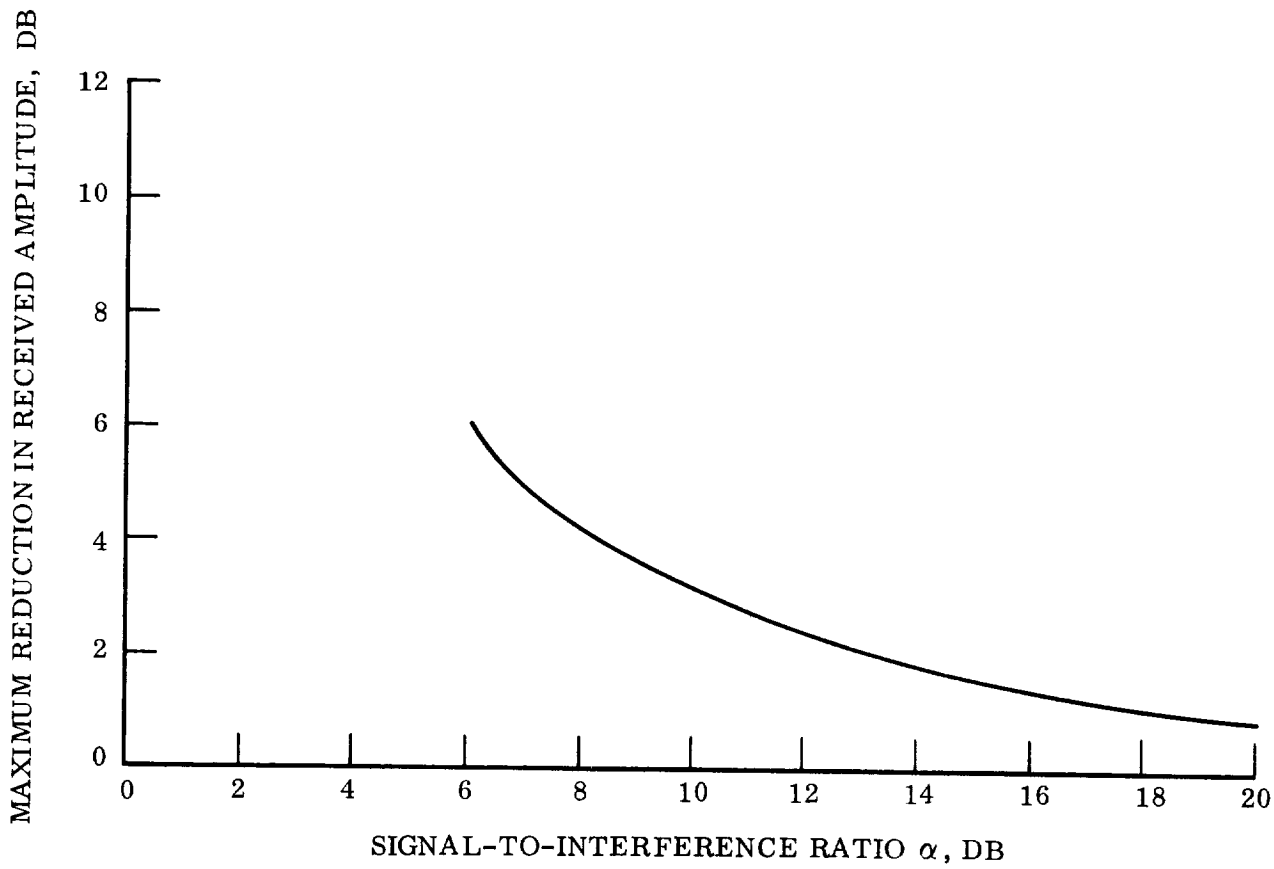

Figure 5.2-32. Signal Reduction Resulting from Interference

5.2.5.2.4 Transponder

The transponder consists of a phase lock receiver and a solid state exciter. The receiver demodulates the r-f signal and provides the command signal to the command detector. The exciter uses the receiver VCO or an auxiliary crystal oscillator as the S-band carrier reference. The carrier is phase modulated by the telemetry subcarrier from the Data Handling Subsystem, and is amplified to drive the TWT power amplifier.

The block diagram of the transponder is shown in fig. 5.2-33. A narrow band, low-loss preselector at the receiver input provides optimum matching into the first mixer. The S-band input signal mixes with the local oscillator in a balanced diode mixer. The mixer output is amplified in a preamplifier operating at approximately 47.8 MHz. The noise figure of the first mixer and preamplifier is typically 8 dB and the r-f to i-f conversion gain is 46 dB. The output of the preamplifier is applied to the gain controlled 47.8 MHz i-f amplifier and the second mixer which provides a conversion gain that is controllable over the range from +52 dB to -48 dB by the AGC voltage. The fixed-gain, second i-f amplifier contains a narrowband crystal filter at its input which limits the noise output to a 4.5 KHz passband at approximately 9.56 MHz. The module furnishes a linear output to the coherent amplitude detector (CAD), and a limited signal output to the carrier loop phase detector.

The receiver contains two carrier phase detectors that are similar in function, but which serve two purposes. When the carrier loop is in lock, the loop phase detector provides an output that is proportional to the phase difference between the received and the reference VCO signals. An error signal is produced at the output of the phase detector bridge whenever the input signal tends to lead or lag the locally generated reference signal in phase. This error signal is applied to the loop filter which filters out high frequency phase jitter. Low frequency signal components, including any drift of the center frequency, produce an error signal that is applied to the VCO, causing the phase of the locally generated signal to move toward the signal frequency.

The second detector, the coherent amplitude detector, provides an output that is proportional to the amplitude of the carrier signal. After suitable conditioning in the AGC d-c amplifier, the output of the amplitude detector is used to control the gain of the i-f amplifier. In both detectors, the bridge-reference signals are subjected to strong limiting (followed by tuned circuits) so that the detector output is dependent on the received signal characteristics only.

The voltage controlled oscillator can be deviated from its nominal frequency by the d-c voltage output of the loop filter applied to a voltage-variable capacitor in the oscillator series LC feedback loop. The VCO is the source for the phase detector reference signals, the first and second mixer injection, and the transmitter signal when suitably multiplied.

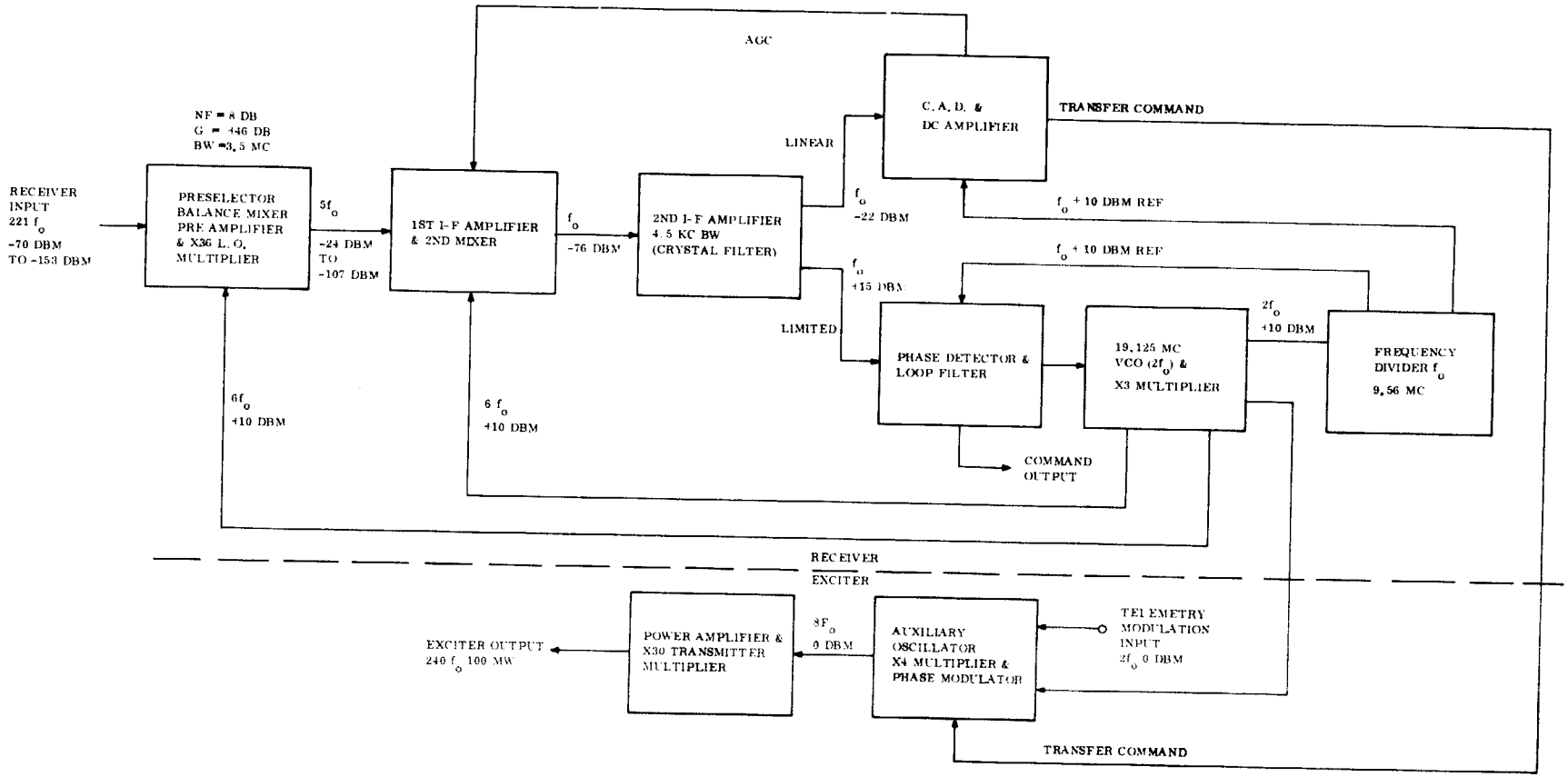

Figure 5.2-33. Transponder Functional Diagram

Command signals are demodulated to subcarrier baseband in the receiver carrier loop phase detector. The coherent amplitude detector provides information which operates a bistable multivibrator that transfers the transponder transmitter signal from an auxiliary oscillator to the VCO.

The exciter provides a stable S-band modulated carrier at a level which is suitable for driving the power amplifier. The exciter consists of an auxiliary oscillator module and a frequency multiplier module. The signal source for the carrier may be either the coherent receiver VCO or the stable self-contained auxiliary crystal oscillator. With no receiver input, the receiver voltage controlled oscillator would be subject to the fluctuations of an integrated noise output of a receiver operating without AGC and at a maximum gain. As a consequence, the receiver on Earth would see a signal that is undergoing phase and frequency variations which may exceed the tracking capability of the ground receiver. Hence, the transponder is equipped with an auxiliary crystal-controlled oscillator that is activated by the absence of receiver AGC voltage. This fixed frequency oscillator provides a relatively noise-free source on which the ground receiver can lock.

The exciter also contains the transmitter modulator which permits phase modulation of the carrier by preconditioned telemetry information. Down-link information is applied to the transponder transmitter in a phase modulator operating at 76.5 MHz. Modulation is accomplished by varying the tuning of a parallel-resonant circuit containing silicon voltage-variable capacitors. The instantaneous reactance of the circuit is controlled by the amplitude of the modulating signal. The modulated signal is multiplied by a factor of 30 to provide the transponder-transmitter output. An isolator at the output of the X30 multiplier prevents variations in load VSWR from detuning the final stage.

5.2.5.2.5 Command Detector

Commands may be transmitted to the Lander by any of the stations of the Deep Space Network, employing either the 85 ft or 210 ft antennas. In the ground station, the command data modulates the command subcarrier, which is added to the sync subcarrier, and the composite signal phase modulates the S-band carrier in the DSIF transmitter. The receiver in the Lander demodulates the S-band carrier and sends the composite subcarrier signal to the command detector.

A. Command Modulator

The command subcarrier signal that is transmitted to the Lander by modulating the S-band carrier has the following form:

$$e_c = (D \oplus f_D) \sin 2\pi f_s t + PN \oplus 2f_s$$

where

D = the NRZ command information bits, transmitted at the rate of 1 bps

f_D = square wave subcarrier with frequency equal to one-half the bit rate

f_s = sinusoidal data subcarrier frequency

PN = pseudo-noise sequence having the same characteristics as the Mariner PN Code

$2f_s$ = square wave sync subcarrier with a frequency of twice the data subcarrier frequency. There is one cycle of $2f_s$ per PN symbol.

A functional block diagram of the command modulator required at the DSIF stations is shown in fig. 5.2-34. The PN sync signal is generated by modulo-two summing the PN generator output and the $2f_s$ square wave. The sinusoidal data subcarrier, $\sin 2\pi f_s t$, is bi-phase modulated by a square wave signal, f_D, which is derived by counting down the bit sync pulses generated by the PN generator. The phase of $f_D \oplus f_s$ is normalized by setting the flip-flop each time a bit sync pulse occurs when f_s is negative. As a result, the phase of the modulated subcarrier, $f_D \sin 2\pi f_s t$, is explicitly established with respect to the phase of the PN sequence (bit) interval. This can be seen by inspection of the waveforms shown in fig. 5.2-35. For simplicity, a bit interval corresponding to a PN sequence of length 7 is assumed. The important phase relationships are the same for any odd-length PN sequence. Cases I and II show for either of the two possible phases of f_s which result from counting-down $2f_s$, the phase of $f_D \sin 2\pi f_s t$ is the same and is keyed to the PN sequence interval. This phase normalization is utilized in the Spacecraft command detector to resolve the phase ambiguity that results in the detection process. The normalized subcarrier is bi-phase modulated by the command data bits, and the resulting signal is linearly added to the sync waveform. The peak amplitudes of the data and sync subcarriers are selected to be equal.

B. Detector

The command detector selected is the Mariner '69 detector. The detector, fig. 5.2-36, generates a subcarrier reference for demodulating the command data subcarrier and delivers command bits to the program control unit. In addition, bit sync is derived from the sync subcarrier, and an out-of-lock indication is provided which inhibits decoding if the detector loses sync lock.

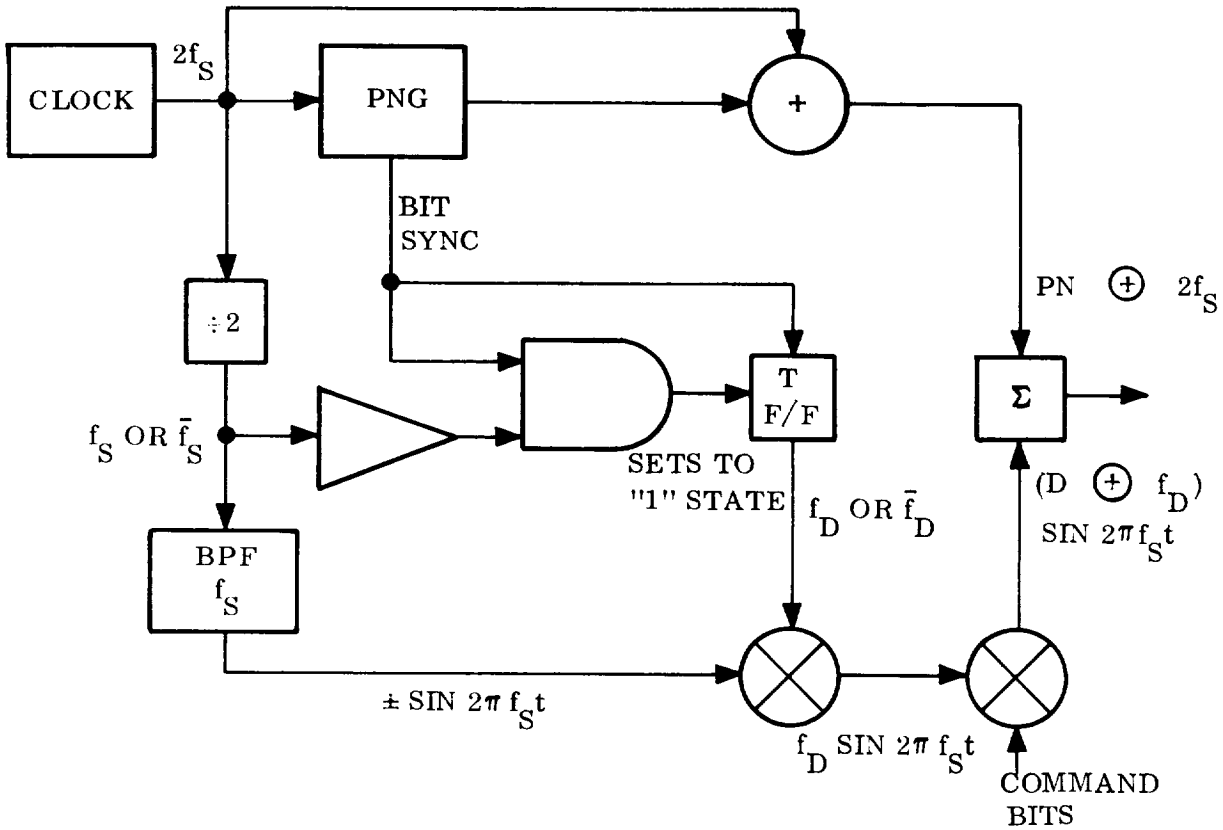

Figure 5.2-34. Command Modulator (Functional)

The sinusoidal command data subcarrier is separated from the sync subcarrier by the bandpass filter. The bi-phase modulated data subcarrier at frequency f_s is squared, and the fundamental component of the resulting signal waveform, $2f_s$, is detected by a phase lock loop. The VCO output drives the pseudo-noise generator (PNG) and is used to derive the subcarrier references used for demodulating both the data and sync subcarriers. To achieve synchronization of the detector PNG output with the input PN sequence on the sync subcarrier, the phase of the PNG is incremented one PN bit each second, under the control of the search logic. The correlation between the local and received PN sequences is measured, and when the correlation exceeds a selected threshold, the search is terminated. In order to determine the correlation, the incoming composite waveform is multiplied by PN $\oplus$ f_s. The output of the multiplier contains components resulting from the incoming data subcarrier as well as from the sync subcarrier. The component at $f_s\underline{/90^\circ}$, is filtered out and is multiplied by the locally generated $f_s\underline{/90^\circ}$. The average value of this product is measured by the matched filter and is proportional to the correlation between the local and incoming PN sequences. Note that the uncertainty in the phase of f_s, which results from counting down the subcarrier reference at $2f_s$ in order to obtain f_s and $f_s\underline{/90^\circ}$, does not affect the correlation process. The correlation is continuously tested, and, if the correlation drops below the desired value indicating loss of sync lock, the search is restarted. Loss of lock is also used to inhibit the decoding of the command data. Having achieved PN sync, the PNG state may be decoded to produce bit sync of the proper phase for matched filter detection of the command data bits.

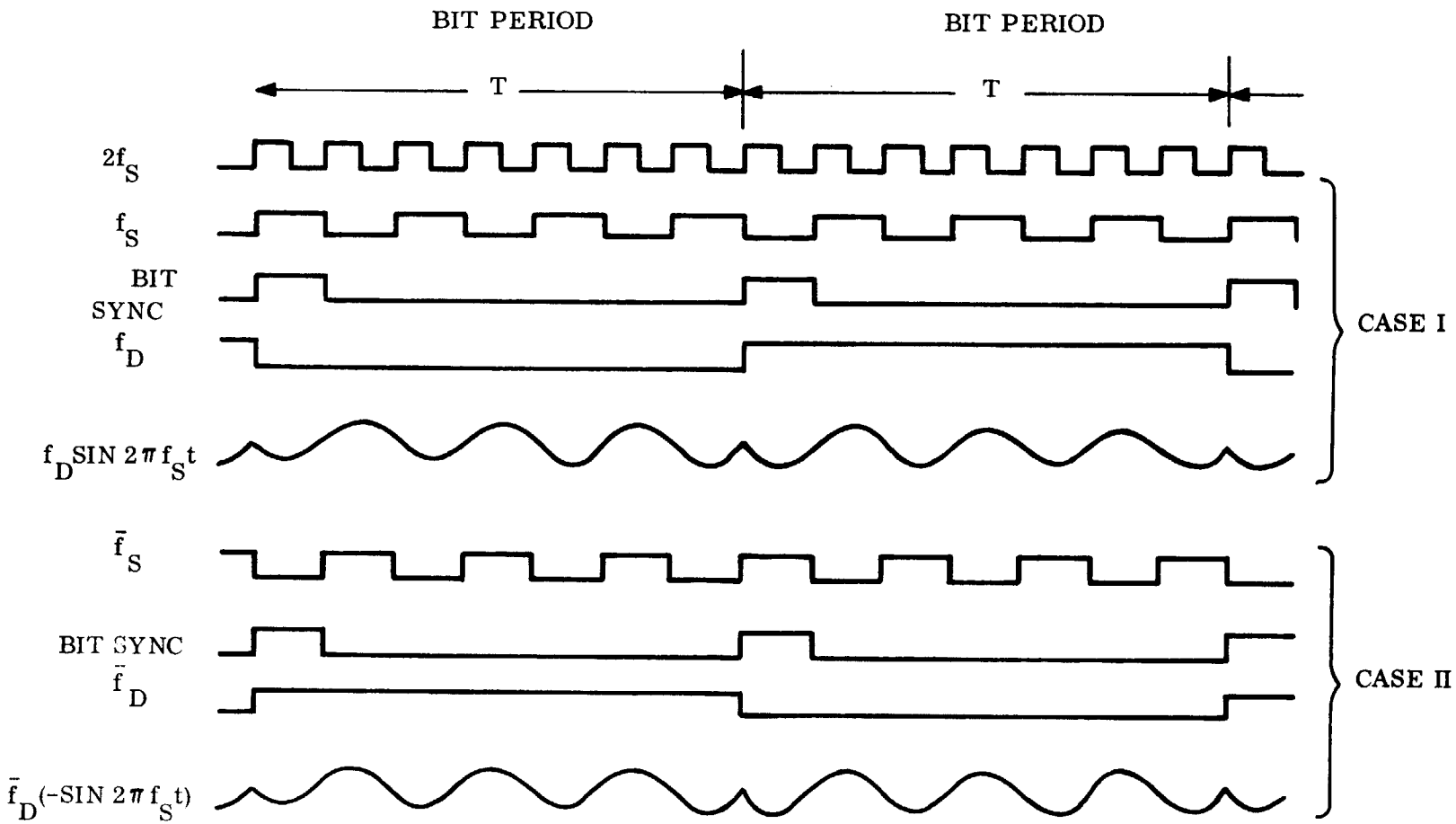

Figure 5.2-35. Command Waveforms

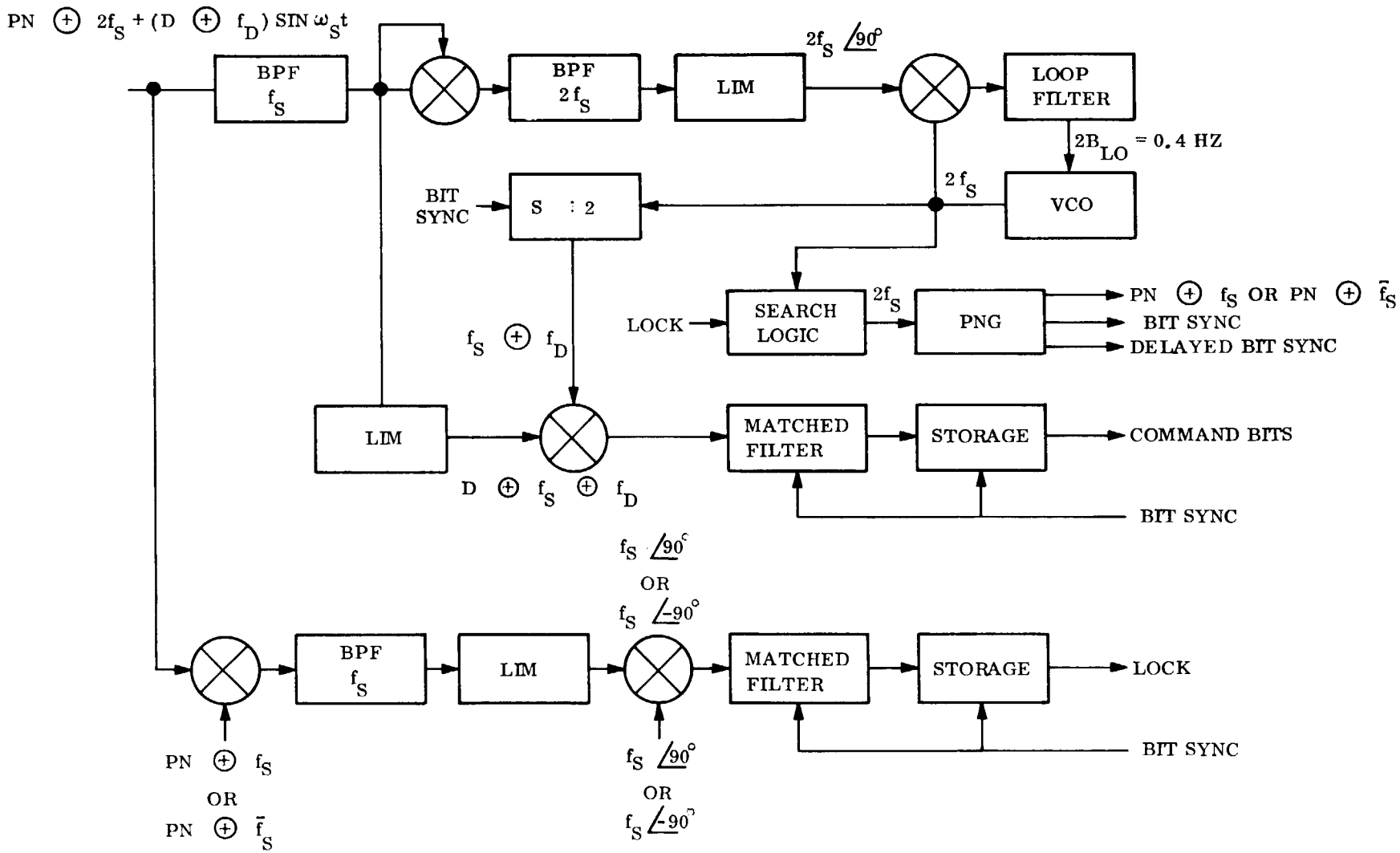

Figure 5.2-36. Command Detector

In order to demodulate the command data subcarrier, the VCO output at $2f_s$ is divided down to f_s by the flip-flop which is normalized by setting it each bit interval. The output of the flip-flop is $f_s \oplus f_D$ and is used for demodulating the data subcarrier. The data bits are matched filter detected.

C. Program Control

The program control (fig. 5.2-37) accepts the bit information from the detector along with bit sync and lock information. The program control provides sync, timing, and control pulses to the decoder in the C&S. An "out-of-lock" status indication from the detector inhibits the program control from processing the incoming binary information. After detector lock is established, the word sync detector looks for the word sync pattern. Upon recognition of word synchronization, bit synchronization and command data bits are transmitted to the decoder, and the inhibit signal is removed. The word sync detector is reset by an "end of word" pulse from the C&S.

The program control also directs the bit sync and detector lock signals to the Data Handling Subsystem for encoding into telemetry words that represent detector VCO frequency and the state of the detector lock signal.

5.2.5.3 System Performance

The system performance calculations are based on the methods described in a previous study (ref. 5.2-8). Design control tables for the two telemetry rates and for the command link are given in tables 5.2-20 to 5.2-22.

The direct links are designed to be compatible with the Deep Space Network. The efficient digital communications techniques developed by JPL for the Mariner spacecraft are applicable to the Lander telemetry and command links.

For the 50 bps telemetry link, the data is coded in order to reduce the signal energy to noise density ratio (E/N_o) required to meet the threshold bit error rate of 5×10^{-3}. The (32,6) block code being implemented by JPL for the Mariner '69 Spacecraft is used and provides a 3 dB improvement compared to an uncoded sytem. For the 5 bps link, coding is not used because, even with the use of the narrow bandwidth carrier phase lock loops being developed for the DSN (3 to 5 Hz), system performance is limited principally by the carrier channel, rather than by the data channel.

For the link calculations, the assumption has been made that the configuration of the 210 ft antenna at Goldstone used for Mariner '69 will also be used for this mission. Using the listen-only feed and restricting operations to times when the elevation of the line of sight to the Lander is above 20°, the receiving system temperature is a maximum of 28° K, which is one-half the worst case temperature for a standard system.

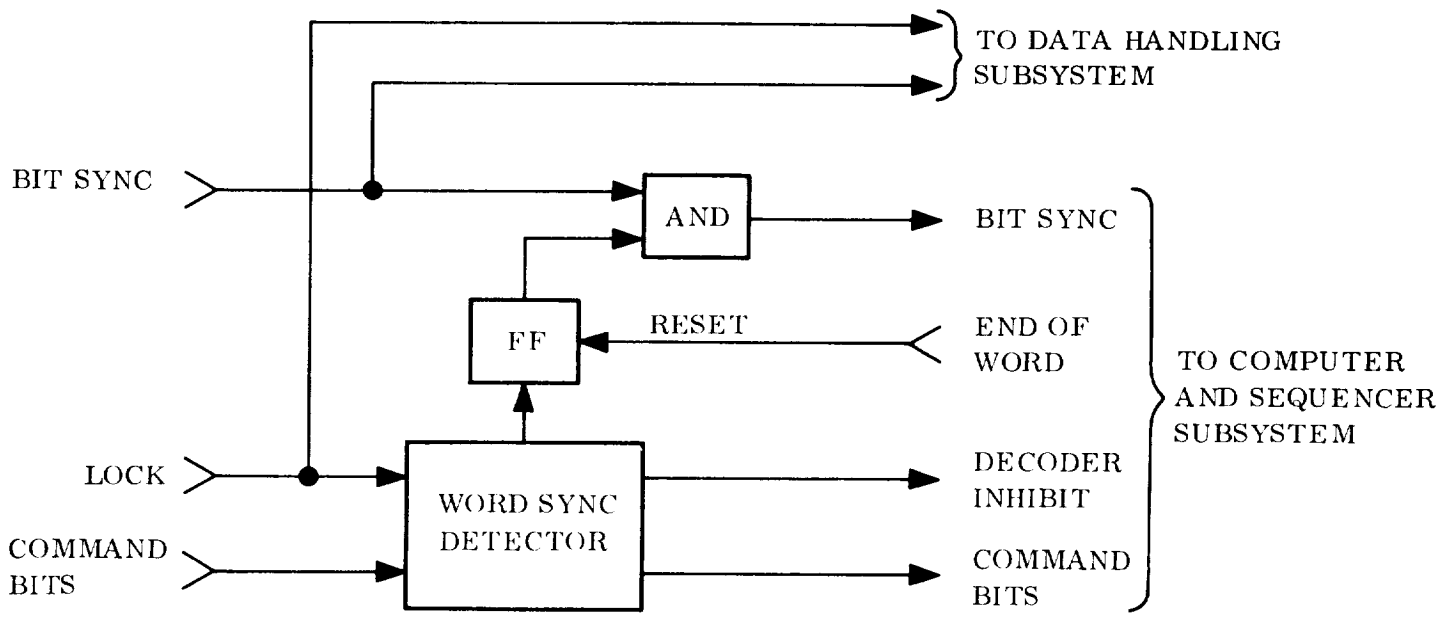

Figure 5.2-37. Program Control

The modulation indices are chosen to cause both the carrier channel and the data channel to threshold at the same received power level under worst case condition for each channel. The carrier channel threshold is set by the carrier phase lock loop bandwidth ($2B_{Lo}$) and the required signal-to-noise ratio (SNR) in that bandwidth. The data channel threshold is set by the data rate (R_b) and the ratio of data energy per bit to noise spectral density (E/N_o). As the modulation index is adjusted so that the carrier channel power is decreased, the power in the data channel increases, allowing a higher data rate to be achieved. However, as the SNR in the carrier loop is reduced, the VCO phase jitter is increased, thereby degrading the data channel performance. For the given set of values of carrier loop bandwidth and data rate, the modulation index which results in the best performance has been calculated. The bandwidth expansion of the DSN receiver with SNR was taken into account in calculating the jitter loss versus SNR in the loop. In determining the worst case modulation loss, the worst case E/N_o plus carrier jitter loss was used, with an eight percent modulation index tolerance. The worst case value of E/N_o (excluding carrier jitter losses) assumed is:

2.1 dB	E/N_o theoretical for 32,6 code, $P_e = 5 \times 10^{-3}$
0.3 dB	Filter loss
0.2 dB	Subcarrier and bit sync jitter loss
0.9 dB	Margin or additional E/N_o for data words of random length.
3.5 dB	

For the 5 bps link, the required data channel E/N_o was taken to be 7.4 dB based on the following assumptions:

Theoretical E/N_o for $P_e = 5 \times 10^{-3}$	5.2 dB
Filter loss	0.5 dB
Carrier jitter loss	0.8 dB
Subcarrier jitter loss	0.2 dB
Bit sync jitter loss	0.2 dB
Margin	0.5 dB
	7.4 dB

The time required for acquisition of the back-up 5 bps down-link signal using the fixed low gain antenna may be excessively long, using the 4 Hz carrier phase lock loop bandwith. The uncertainty in the down-link frequency due to aging, temperature uncertainty and shock induced shifts is expected to be less than five parts/million, resulting in a required frequency search width of about 10 kHz. Using the maximum permissible sweeprate (for 90 percent probability of acquisition) of 10 Hz/sec, the maximum acquisition period would be about 17 min. Since the down-link is only on for 30 min., pre-detection recording should be used to allow off-line acquisition. Alternately, the frequency uncertainty can be made negligibly small by operating in the coherent transponder mode, so that the down-link frequency is controlled by the DSN transmitter frequency. In order to minimize the detection degradation caused by jitter introduced by the noise in the transponder carrier phase lock loop, the 210 ft antenna must be used for transmission. This will degrade the 210 ft antenna receiving system temperature. Although hard data on the increase in system temperature is not available, the increase is expected to be less than 10° K, based upon analogy with the effect of diplexing on the temperature of the 85 ft antenna temperature (ref. 5.2-9). Such an increase will degrade the down-link performance by 1.3 dB. Since the worst case margin on the down-link is 1.5 dB, the nominal margin will exceed the maximum adverse tolerances by 0.2 dB, which is deemed adequate for this back-up link.

TABLE 5.2-20. DESIGN CONTROL TABLE, DATA TRANSMISSION 50 BPS, VERTICALLY ORIENTED ANTENNA, 20 WATT, 210 FT DSNA

		Nominal	Tolerances	
			Adverse	Favorable
1.	Transmitter Power 20W	43.5 dBm	0.5 dB	0.5 dB
2.	Transmitting Circuit Loss	-2.0 dB	0.4	0.0
3.	Transmitting Antenna Gain BW = 76°	8.0	0	0.5
4.	Transmitting Antenna Pointing Loss	-2.7	0.3	1.0
5.	Space Loss $R = 190 \times 10^6$ KM f = 2300 MHz	-264.9	-	-
6.	Polarization Loss	-0.1	0	0.1
7.	Receiving Antenna Gain	61.0	0	1.0
8.	Receiving Antenna Pointing Loss	-0.3	0	0.3
9.	Receiving Circuit Loss	0	0	0
10.	Total Received Power	-157.5 dBm	1.2	3.4
11.	Receiver Noise Density T = 28° K	-184.1 dBm	0	0
12.	Carrier Modulation Loss	-3.4 dB	0.7	0.6
13.	Received Carrier Power	-160.9 dBm	1.9	4.0
14.	Carrier Loop Bandwidth (12 Hz)	10.8 dB	-	-
15.	Required SNR (in $2B_{Lo}$)	10.0	-	-
16.	Threshold Carrier Power	-163.3 dBm	-	-
17.	Performance Margin	2.4	1.9	4.0
18.	Data Modulation Loss	-2.6 dB	0.6	0.5
19.	Received Data Power	-160.1 dBm	1.8	3.9
20.	Data Rate 50 bps	17.0 dB	0	0
21.	Required E/N_o $P_e^b = 5 \times 10^{-3}$	3.5	1.0	0.3
22.	Threshold Data Power	-163.6 dBm	1	0.3
23.	Performance Margin	3.5 dB	2.8	4.2

TABLE 5.2-21. DESIGN CONTROL TABLE, DATA TRANSMISSION 5 BPS, FIXED ANTENNA, 20 WATT, 210 FT DSNA

		Nominal	Tolerances	
			Adverse	Favorable
1.	Transmitter Power 20W	43.5 dBm	0.5 dB	0.5 dB
2.	Transmitting Circuit Loss	-1.2 dB	0.4	0
3.	Transmitting Antenna Gain	+3.0	0	2
4.	Transmitting Antenna Pointing Loss	-1.0	2	1
5.	Space Loss $R = 190 \times 10^6$ KM f = 2300 MHz	-264.9	-	-
6.	Polarization Loss	-0.1	0	0.1
7.	Receiving Antenna Gain	61.0	0	1.0
8.	Receiving Antenna Pointing Loss	-0.3	0	0.3
9.	Receiving Circuit Loss	0	0	0
10.	Total Received Power	-160.0 dBm	2.9	4.9
11.	Receiver Noise Density $T = 28^\circ K$	-184.1 dBm	0	0
12.	Carrier Modulation Loss	-1.9 dB	0.3	0.4
13.	Received Carrier Power	-161.9 dBm	3.2	5.3
14.	Carrier Loop Bandwidth (4 Hz)	6.0 dB	-	-
15.	Required SNR (in $2B_{Lo}$)	11.5 dB	-	-
16.	Threshold Carrier Power	-166.6 dBm	-	-
17.	Performance Margin	4.7 dB	3.2	5.3
18.	Data Modulation Loss	-4.6 dB	0.6	0.6
19.	Received Data Power	-164.6 dBm	3.5	5.5
20.	Data Rate 5 bps	7.0 dB	-	-
21.	Required E/N_o ($P_e^b = 5 \times 10^{-3}$)	7.4 dB	-	-
22.	Threshold Data Power	-169.7 dBm	-	-
23.	Performance Margin	5.1 dB	3.5	5.5

TABLE 5.2-22. DESIGN CONTROL TABLE, COMMAND 1 BPS, FIXED ANTENNA, 100 KW, 85 FT DSNA

		Nominal	Tolerances	
			Adverse	Favorable
1.	Transmitter Power 100 KW	+80.0 dBm	-	-
2.	Transmitting Circuit Loss	0 dB	0	0
3.	Transmitting Antenna Gain 85 FT	+51.0	0.5	1.0
4.	Transmitting Antenna Pointing Loss	-0.1	0	0.1
5.	Space Loss $R = 190 \times 10^6$ KM, f = 2115 MHz	-264.2	-	-
6.	Polarization Loss	-0.1	-	-
7.	Receiving Antenna Gain	3.0	0	2.0
8.	Receiving Antenna Pointing Loss	-1.0	2.0	1.0
9.	Receiving Circuit Loss	-1.2	0.3	0.1
10.	Total Received Power	-132.6 dBm	2.8	4.2
11.	Receiver Noise Density $T = 1750^\circ$ K	-166.2	0	0
12.	Carrier Modulation Loss	-0.9 dB	0.1	0.1
13.	Received Carrier Power	-133.5 dB	2.9	4.3
14.	Carrier Loop Bandwidth ($2B_{Lo}$)	13.0 dB	0.2	-
15.	Required SNR in $2B_{Lo}$	8.5	1.0	-
16.	Threshold Carrier Power	-144.7 dBm	1.2	-
17.	Performance Margin	11.2 dB	4.1	-
18.	Data Modulation Loss	-12.0 dB	0.4	-
19.	Received Data Power	-144.6 dBm	3.2	-
20.	Data Rate 1 BPS	0 dB	-	-
21.	Required E/N_o	11.3	-	-
22.	Threshold Data Power	-154.9 dBm	-	-
23.	Performance Margin	10.3 dB	3.2	-

5.2.6 RADAR FOR DECELERATION EVENTS

The function of the radar altimeter is to mark the altitude (4 kft) to deploy the Lander deceleration parachute and the altitude (150 ft) at which the parachute is separated from the Lander before touchdown. In addition to providing these essential marks, the radar provides a continuous altitude signal for correlation with atmospheric profile measurements.

5.2.6.1 Altitude Marking Radar (AMR) Description

The AMR is a non-coherent, pulse type radar which utilizes an early-late gate range tracking method. Fig. 5.2-38 shows the functional block diagram of the AMR. None of the redundancy is shown.

The transmitter, a triode oscillator operating at 1 GHz, is pulsed by the modulator with a pulse length which depends on altitude. Initially in Mode 1, the pulse length is 0.7μsec and remains so until about 5 kft altitude. Below 5 kft the pulse length is changed to 0.18μsec. This will give an accuracy of approximately 45 ft on the remaining ranges.

The duplexer is provided along with the proper gating to enable the use of one antenna for both transmission and reception.

After translation in frequency by the local oscillator the return signal is amplified, filtered, detected and enters the range tracking circuits. Because of the extent of the target and the width of the radar antenna pattern, the return is much wider than the transmitted signal; tracking of the leading edge of the return is desirable to determine altitude. To facilitate the early-late tracking approach, the target return is passed through a leading edge differentiator (delay line) whose output is a pulse of approximately the transmitted pulse width and whose position corresponds to the nearest point of the target return. Fig. 5.2-39 shows how the return pulse is formed. In this idealized diagram the timer intervals correspond to:

t_1 = time that leading edge of pulse hits the surface

t_2 = time that trailing edge of pulse hits the surface

During this time interval the reflected power increases linearly until the entire pulse illuminates the surface. The returned power then decreases from this level due to reflection from more distant points within the beam. If this pulse shape, appropriately delayed, is subtracted from the original, ideally one gets a non-zero output during the leading edge buildup with a negligible output (and the opposite polarity) for the trailing edge. The resulting narrow pulse is time discriminated in a split gate range tracker whose output controls the time position of the range gate.

The range gate is used to gate the preamplifier on at the proper range, enhancing the signal-to-noise ratio.

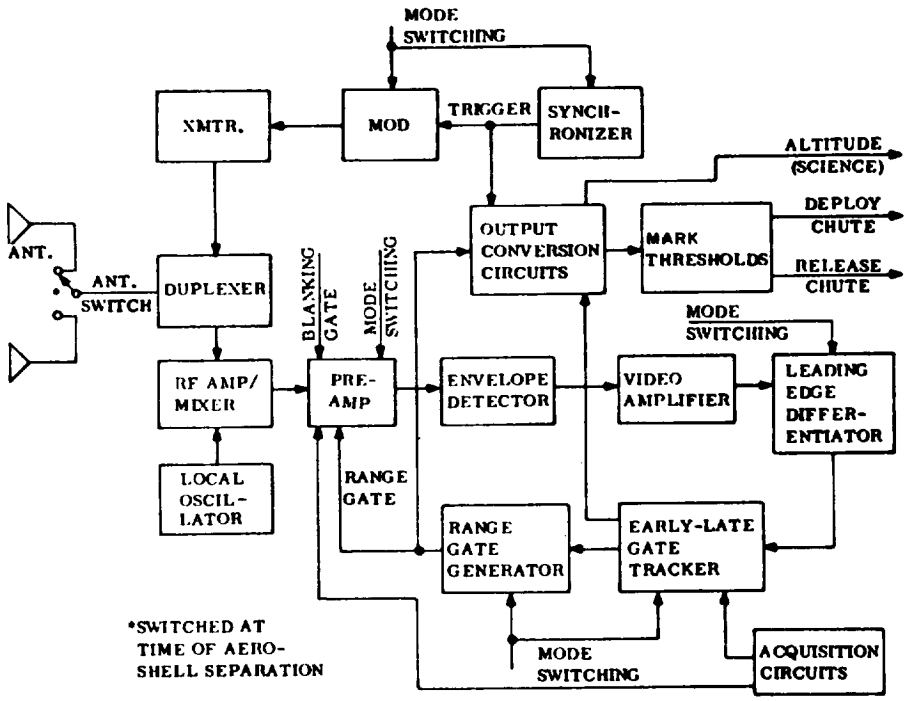

Figure 5.2-38. Altitude Marking Radar, Functional Block Diagram

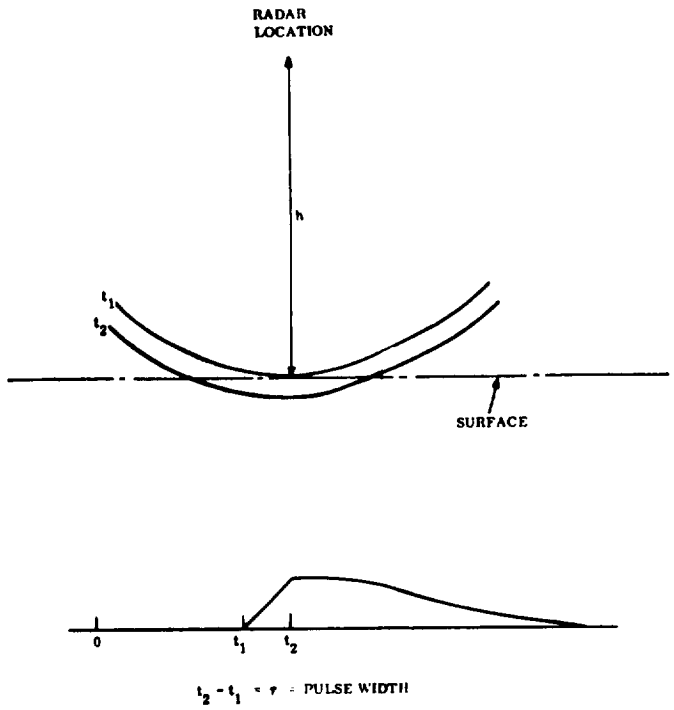

Figure 5.2-39. Geometry of AMR Return Signal

In the output conversion circuits, the time delay between the trigger and the range gate is determined and converted to an analog voltage to give continuous altitude signal.

5.2.6.2 Antennas

The AMR is used both prior to and after separation from the aeroshell. The attitude of the Lander varies over a wide range requiring a broad beam antenna to obtain signal returns for the expected orientations. This is accomplished by providing broad antenna patterns on both the aeroshell and the Lander.

The 1 GHz radar antenna system on the aeroshell will consist of a two antenna array. The two identical antennas will be located 180° apart on the shell on an 88 in. diameter. They will be fed in phase with equal amplitude signals from a hybrid. Each antenna, in turn, will be a single slot oriented with its long (8 in.) dimension along a cone element. The aeroshell 60° half-cone angle will inherently cause the peak amplitude of the individual antenna patterns to occur at an angle of 30° with respect to the vehicle axis. The combined pattern will be multi-lobed (see fig. 5.2-40). The gain, which is optimized for 85 to 35° (with respect to horizontal) flight path angle, will average 0 dB or greater over any cone of 10° half-angle within the range of angles from 5 to 65° with respect to nose-on (see fig. 5.2-41). Each antenna will be a cavity backed slot 2.5 in. deep, and and 8 x 2 in. quartz window will be required through the ablation shield to permit proper operation after the re-entry charring of the shield. The input VSWR will not exceed 3:1 for this antenna system for all ablation and re-entry plasma conditions. It will handle 50 watts of input power.

The antenna system on the body of the Lander for use after aeroshell separation will be a simple, single-slot located on the downward facing surface. The 6 x 1 in. slot will be backed by a 3 in. deep cavity. The pattern is linear polarized and has a major lobe with a gain of about 5 dB in the downward direction (see fig. 5.2-42). Everywhere within the required coverage angle (within 40° of the vehicle forward axis) the gain is +2 dB or greater. The input VSWR will be less than 1.5:1 for this antenna and it will handle 50 watts of power.

Switchover from one antenna to the other occurs at aeroshell separation and requires a signal from the computer and sequencer subsystem to shut down the transmitter, switch the antennas and repower the transmitter. The radar begins functioning again about 4 to 6 sec after aeroshell release. At this time the aeroshell will be near in range and must be discriminated against during the reacquisition of the desired target return. This is accomplished with a receiver blanking gate of 3-4μ sec duration effectively blanking out any target within 1500 to 2000 ft of the vehicle. This blanking gate is removed after the surface is reacquired and the normal range gate is functioning.

5.2.6.3 Parameters of the AMR

Tables 5.2-23 and -24 list the functional and physical parameters of the radar.

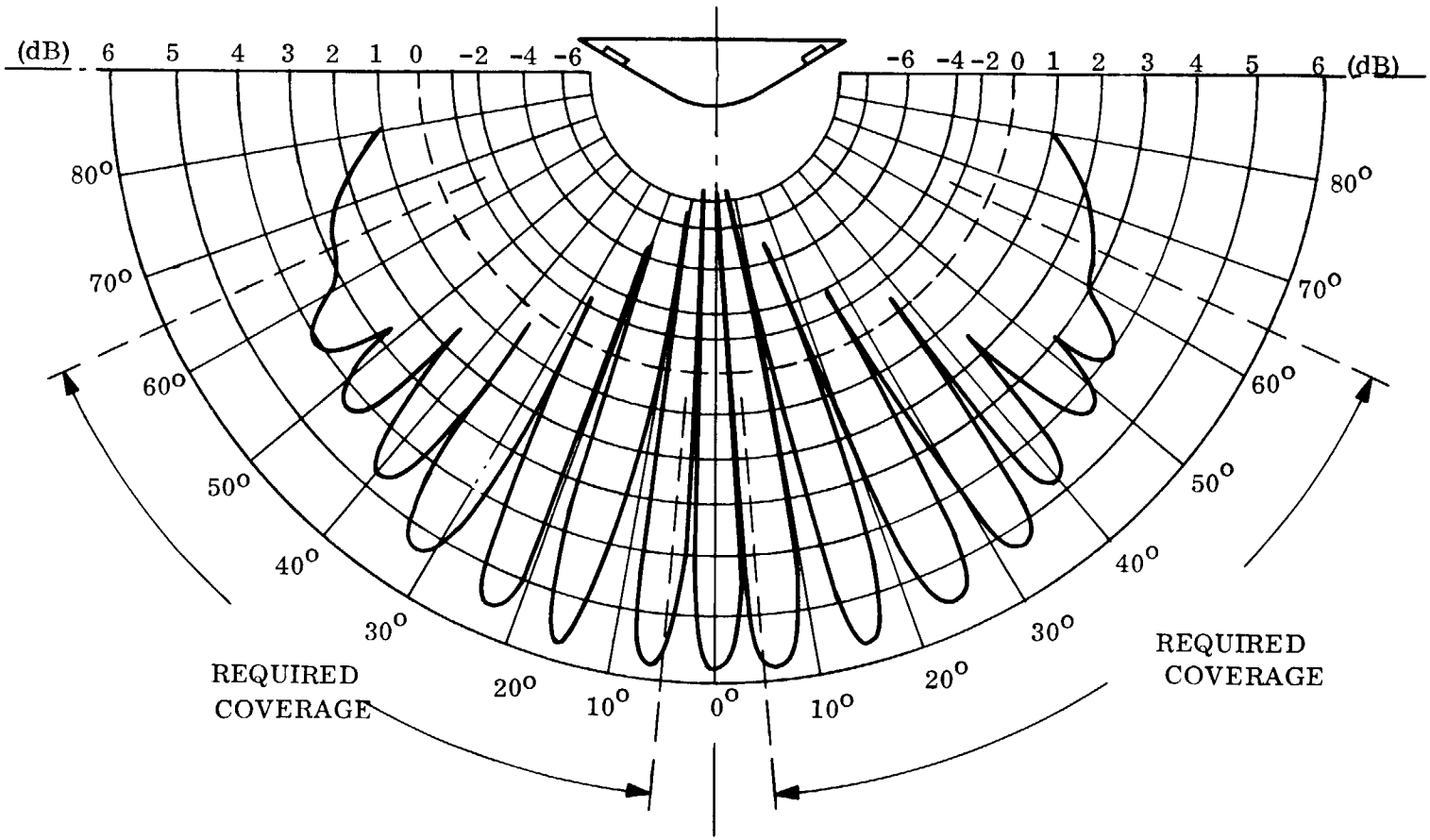

Figure 5.2-40. Aeroshell Radar Antenna Pattern

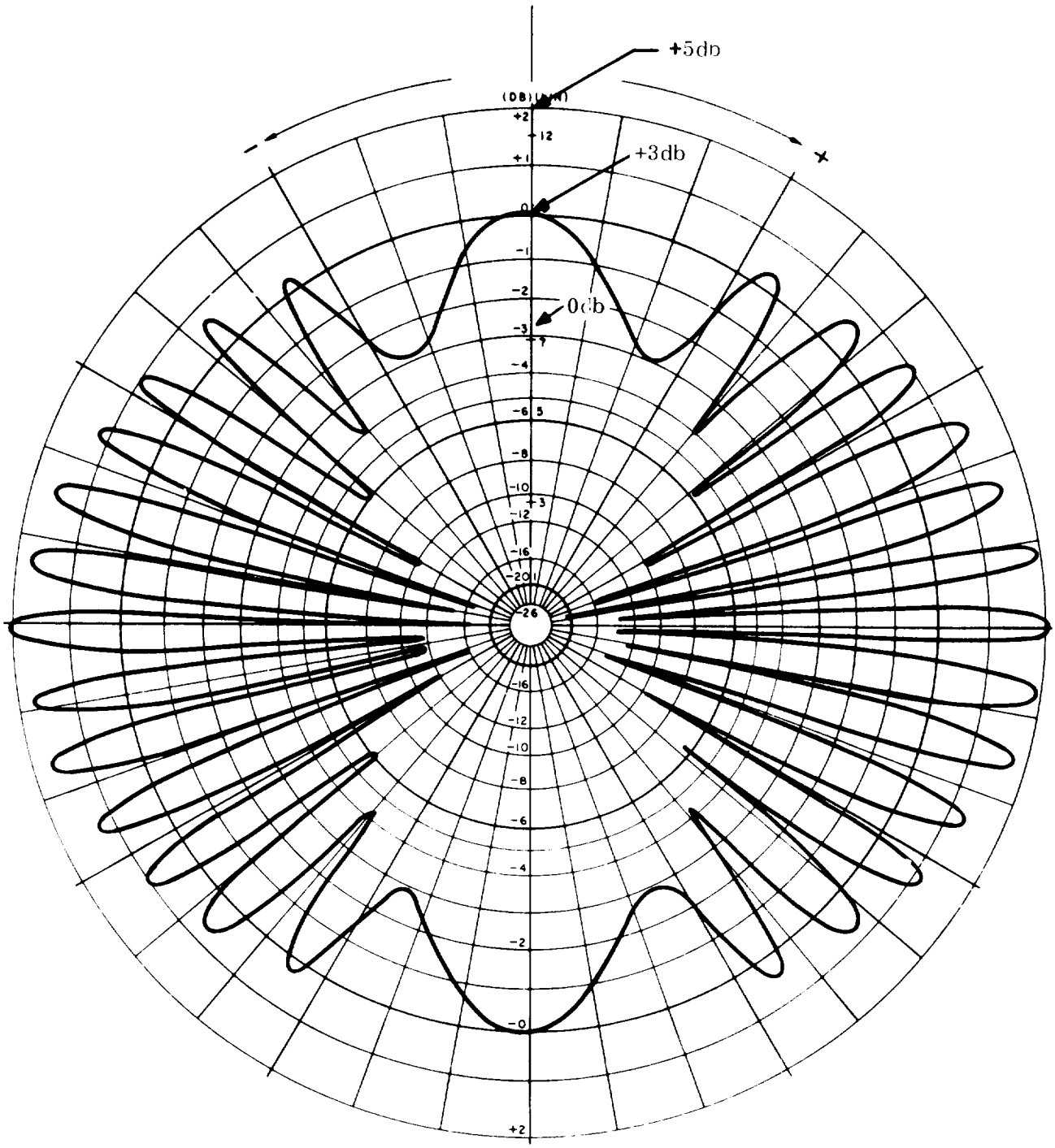

Figure 5.2-41. Roll Pattern Radar Antenna on Aeroshell

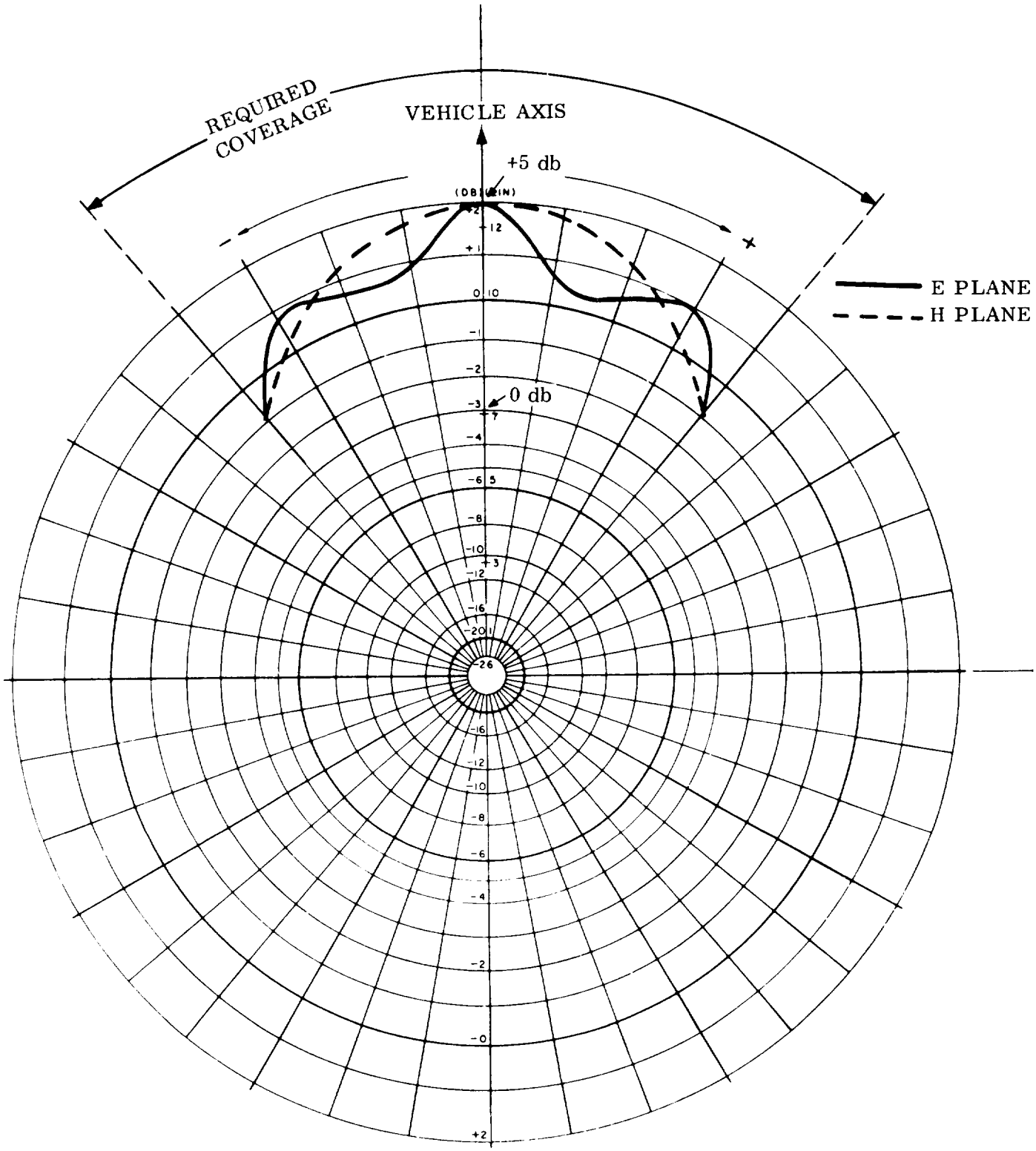

Figure 5.2-42. E and H Plane Patterns of Antenna on Vehicle Body

TABLE 5.2-23. FUNCTIONAL PARAMETERS

	Symbol	
Peak power	P	50 watts
Frequency	f	1.0 GHz
Wavelength	λ	0.3 meters
Antenna gain	G	0.0 dB
Pulse length	τ	0.7μsec (long range) 0.18μsec (short range)
Repetition frequency	PRF	1000 Hz
Noise figure	F	6 dB
System Losses	L	6 dB
I-F bandwidth	B	2.1 MHz (long range) 8.2 MHz (short range)
Acquisition sweep time	Taq	2 sec
Single pulse signal to noise	SNR(1)	+7.1 dB (long range @ 20,000 ft) 13.1 dB (short range @ 5000 ft)
Probability of detection single sweep	P_d	>0.95
Accuracy		1% ± 175 ft (long range) 1% ± 45 ft (short range)

(1) Surface reflectivity assumed to be -10.0 dB

TABLE 5.2-24. PHYSICAL PARAMETERS

Parameter	Value
Weight: (lb)	
Electronics	15
Lander antenna	0.5
Aeroshell antenna	5.5
Volume: (in.^{3})	
Electronics	500
Lander Antenna	18
Aeroshell Antenna	80
Power: (watts)	20

The calculation for SNR is based on the assumption that the surface reflectivity coefficient is $\sigma_o = -10.0$ dB.

$$SNR = \frac{\sigma_o P G^2 \lambda^2 C \tau}{64\pi^2 L H^3 R T_o F B}$$

where:

C = speed of light

k = Boltzmann's constant

T = 290^oK

Other symbols are defined in table 5.2-23.

5.2.7 REFERENCES

5.2-1. Sayer, T.C., Hackett, C.M., Jr., and Lash, J.A., "Performance of Noncoherent FSK Employing Post-Detection Integration", General Electric Company, TIS No. 66SD200, March, 1966.

5.2-2. Hackett, C.M., Jr., "A Bit-Sync Scheme for Manchester Signals", General Electric Company, TIS No. 66SD232, March, 1966.

5.2-3. K. Fong, "Statistical Theory on Propagation and Scattering of Electromagnetic Waves, Near a Planet", General Electric Company, Memo Report No. MO-67-1532, October, 1967.

5.2-4. P. Beckmann, "Scattering by Composite Rough Surfaces", Proc. IEEE, August, 1965, p. 1012.

5.2-5. R. B. Duce, et al (1965), Astronomical Journal, 72, p. 771.

5.2-6 A.B. Glenn, "Fading from Irregular Surfaces for Line-of-Sight Communications, IEEE Trans. on Aerospace and Electronic Systems, March, 1968.

5.2-7. Voyager Capsule Bus Study, McDonnell-Douglas, Report F694, Vol. II, Part B, 31 August 1967 (p. 5.5-10).

5.2-8 Mars Hard Lander Capsule Study, Volume III, Book 2 Capsule Parametric Study, NASA CR 66678-4, 31 July 1968, page 4-73.

5.2-9. Space Programs Summary, "The Deep Space Network," SPS-37-45, Volume III, p. 65, May 31, 1967, JPL.

5.3 ELECTRICAL POWER AND DISTRIBUTION (EP&D)

The EP&D Subsystem consists of the equipment associated with the source, conditioning, distribution and control of electrical power for the overall Flight Capsule. The load profile is periodically characterized by high current pulses for initiating hot-wire and pyrotechnic devices. In general, the equipment for supplying these pulses has been separated from the rest of the EP&D equipment in order to achieve adequate electrical isolation and to minimize weight. For these reasons these portions of the EP&D Subsystem are treated as separate functional entities and referred to hereafter as the Power Subsystem (serves all loads except specific high current pulses) and the Initiation Subsystem (handles hot-wire and pyrotechnic initiating pulses).

5.3.1 POWER SUBSYSTEM

5.3.1.1 Requirements

The principal requirements for the Power Subsystem are established by the load profile shown in table 5.3-1. This table lists the occurrence of the various Flight Capsule loads as a function of the Mission Sequence of Events described in Section 3.4.

The load profile spans a period from Flight Capsule separation through the cessation of direct communication about 70 hr after Lander touchdown on the Mars surface. Mission interval Nos. 1 to 22 are a direct time sequence of power demands through the completion of the gas chromatograph and mass spectrometer measurements. Except for intervals 5 and 6 and 23 to 26, the power demands shown exist continuously for the time length of each interval.

A 23 hr cruise period subsequent to thrust cone jettison is represented by intervals 5 and 6. Interval 5 represents the accumulation of 23 min of UHF transmission during this cruise period (one min of UHF transmission every hr). Interval 6 represents the remainder of this cruise period under standby conditions.

The lengths of intervals 14 to 22 are doubled to take account of two chromatograph/mass spectrometer cycles.

Interval 23 represents the demand during landed data sampling periods which occur for 2 sec every 20 min.

Interval 24 represents the demand during landed standby operation.

Interval 25 represents the demand during direct link data transmission. Three transmissions of 30 min each are accounted for.

Interval 26 makes allowance for 6 hr of command system operation.

A graphical representation of the loads is shown on fig. 5.3-1.

The loads in table 5.3-1 are listed in raw and regulated power categories. With the exception of the S-band transmitter the raw loads are those that could operate acceptably directly from battery power without the need for regulation. The S-band is

placed in the raw category since its estimated raw power level includes loss allowances for special voltage regulation.

The regulated load estimates are based on assuming that power is supplied to each load at several discrete regulated d-c voltage levels. In most cases these levels and their associated values of power have not been rigorously defined. Such information would be forthcoming from detailed design selection associated with each load. Nevertheless, the recognition of the need for multi-dc conversion is made to allocate appropriate loss allowances for this function.

Besides the raw and regulated loads, power must be supplied to the Initiation Subsystem for the actuation of secondary power sources. The energy content of such actuation pulses is extremely low and they have, therefore, not been included in the load profile. The specific actuation times are discussed in Section 5.3.2.

A lumped power allocation has been made for a large class of diagnostic and science sensors (temperature, pressure transducers, etc.) Power for these devices is contained within the allocation for the Data Handling Subsystem (DHS).

Along with the load profile, the locations to which power must be delivered constitute important constraints on the Power Subsystem design. Fig. 5.3-2 shows a block diagram which designates the points of power use for the principal equipment of the Flight Capsule. As shown, the bulk of the loads receive power from the internal power source while the canister loads specifically receive power from the Support Module Power Subsystem.

An important requirement regarding the Support Module interface is that the Flight Capsule Power Subsystem must be designed to accept any necessary power from the Support Module in the range of about 37 to 50 volts. This corresponds to the range of raw power availability from existing Mariner Spacecraft design under solar illuminated conditions.

Although this range may change as a result of specific Support Module implementation it is used as the basis for the Power Subsystem design description which follows.

TABLE 5.3-1. LOAD PROFILE

*Interval length doubled to take two chromatograph cycles into account.

Mission Interval No.		1	2	3	4	5	6	7	8	9	10	11	12	13	14	15	16	17	18	19	20	21	22	23	24	25	26
Datum		S	S	S	S	S	S	E	E	E	T	T	G	G	G	G	G	G	G	G	G	G	G	G	G	G	G
End Interval (hr., min.)		0+2	0+28	0+35	1+0	24+0	24+0	0-6	0+0	0+4	0+3	0+4	0+1	0+25	0+29	0+45	0+55	1+5	1+15	1+55	2+5	2+15	3+5				
Start Interval (hr., min.)		0+0	0+2	0+28	0+35	1+0	1+0	0-8	0-6	0+0	0+0	0+3	0+0	0+1	0+25	0+29	0+45	0+55	1+5	1+15	1+55	2+5	2+15				
Interval Length (hr., min.)		0+2	0+26	0+7	0+25	0+24	22+14	0+2	0+6	0+4	0+3	0+1	0+1	0+24	0+8*	0+32*	0+20*	0+20*	0+20*	0+80*	0+20*	0+20*	1+40*	0+20	66+42	1+30	6+10
Regulated Loads																											
Exciter	3																									3	
Receiver	5																										5
Command	3.2																										3.2
Data handling	15	15		15		15			15	15	15	15	15	15	15	15	15	15	15	15	15	15	15	15		15	
C&S - standby	2		2		2		2	2																	2		
operate	20	20		20		20			20	20	20	20	20	20	20	20	20	20	20	20	20	20	20	20		20	
Radar altimeter	20									20	20																
Spin control	5	5		5					5	5																	
Science:																											
Mass spectrometer	7								7	7	7	7					7	7	7	7	7	7	7				
Camera	10													10													
Gas chromatograph	13														13	13	13	13	13	13	13	13	13				
Atmospheric H_2O	5																							5			
Subsurface H_2O	5																	5	5		5	5		5			
Life detection	1.5																								1.5		
Soil sampler	10														10	10											
UHF Transmitter	143	143		143		143			143	143	143	143	143	143													
Totals		183	2	183	2	178	2	2	190	210	205	185	178	188	58	58	55	60	60	55	60	60	55	45	3.5	38	8.2
Raw loads																											
S-band transmitter	89																									89	
Pyrolizer	35																	35			35						
Antenna deployment	10														10												
Thermal control	2																								2		
Totals															10			35			35				2	89	

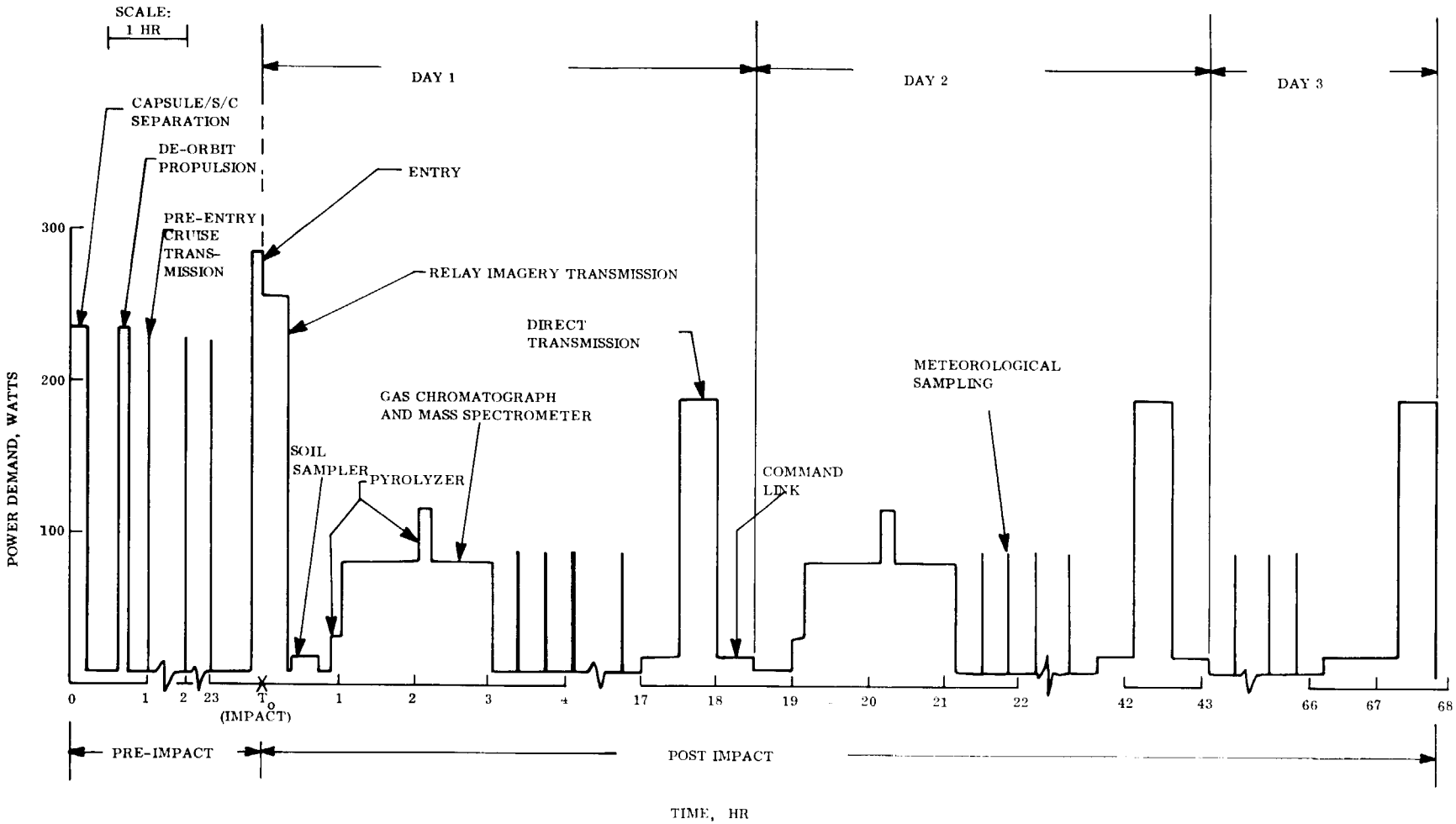

Figure 5.3-1. 1400 lb Lander Power Profile

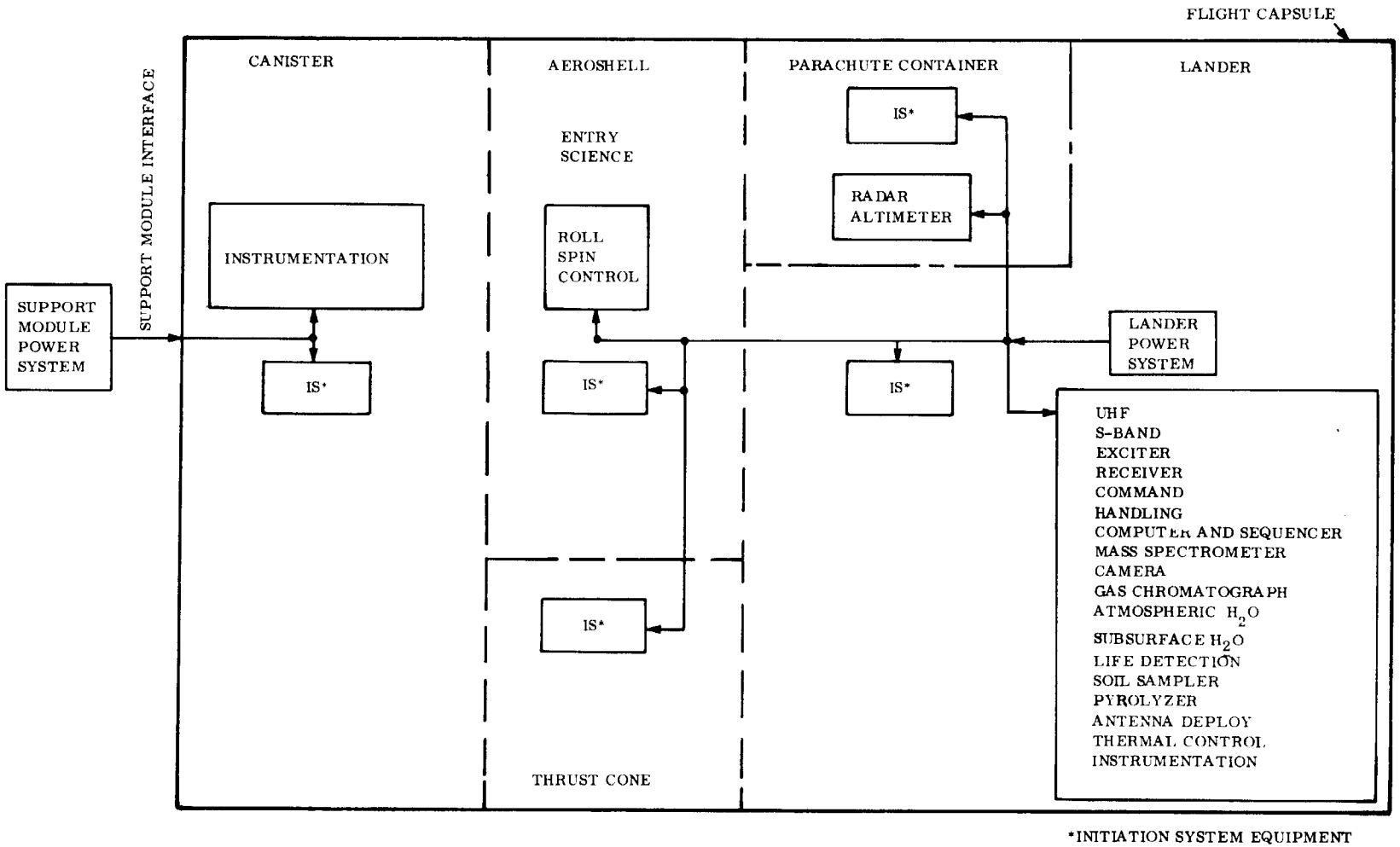

Figure 5.3-2. Points of Power Use

5.3.1.2 Power Subsystem Description

Although a solar array/battery regenerative arrangement would permit an extended landed mission, the 1400 lb weight limitation does not permit its inclusion along with the specified science payload.

A block diagram arrangement of the Power Subsystem is shown on fig. 5.3-3. The interface lines delineate the major Flight Capsule elements identifying EP&D equipment location. A single silver-zinc sterilizable battery is used with a nominal capacity of 2000 watt-hr. Taking various conditioning and standby losses into account this is deemed sufficient to complete operations through the completion of data transmission on the third day after landing.

The battery contains 20 series cells and supplies raw power at a nominal range of 25 to 32 volts. Some of the loads use this power directly but the bulk of the power is regulated and distributed to the various Flight Capsule elements, as shown, through two regulators. Regulator No. 1 supplies the low amount of power (2 watts) to the Computer and Sequencer (C&S) and for life detection instrumentation (1.5 watts) required during dormant standby modes of the mission. It operates continuously throughout the mission and is used to avoid the standby losses that would occur from the use of a single large regulator. Regulator No. 2 is designed to supply all other regulated load demands through centralized or individual voltage conversion units. The pros and cons of several alternative arrangements are discussed in a later paragraph.

Battery sizing is summarized in table 5.3-2, showing the net watt-hr demand up to any point in the mission. The factors used in this determination are as follows:

1. Regulator No. 1 and its associated conversion unit have a combined efficiency of 57 percent.

2. Regulator No. 2 has an efficiency of 90 percent, which is typical for series switching regulators. The UHF equipment operates directly from the regulated output since its load estimate is based on receiving power at a single regulated voltage level.

3. Conversion units operating from Regulator No. 2 have an efficiency of 83 percent.

4. In determining battery weight a contingency factor of 20 percent has been included. Battery energy density is taken to be 30 watt-hr/lb resulting in a battery weight of 65 lb.

Considered next is the question of whether the use of two batteries provides an overall weight advantage in that one of these could remain with the aeroshell at the time of its separation, thereby reducing battery weight in the Lander. By referring to table 5.3-2 the total battery energy required up to the time of aeroshell separation is 235 watt-hr (mission interval 9 on table 5.3-2).

TABLE 5.3-2. BATTERY ENERGY CALCULATION

Time Hours	0.03	0.43	0.12	0.42	0.40	22.23	0.03	0.1	0.07	0.05	0.02	0.02	0.40	0.14	0.54	0.34	0.34	0.34	1.32	0.34	0.34	1.66	0.34	66.7	1.5	6.0
Mission Interval No.	1	2	3	4	5	6	7	8	9	10	11	12	13	14	15	16	17	18	19	20	21	22	23	24	25	26
Regulator Demands																										
Converter Input (83% efficiency)	48.2		48.2		42.2			56.6	80.7	74.7	50.6	47.2	54.2	69.9	69.9	66.5	72.3	72.3	66.3	72.3	72.3	66.3	54.2		45.8	9.9
Regulation Input (90% efficiency)	53.5	3.5*	53.5	3.5*	46.8	3.5*	3.5*	62.8	89.6	82.9	56.2	46.8	60.2	77.6	77.6	73.6	80.3	80.3	73.6	80.3	80.3	73.6	60.2	6.14*	50.8	11.0
Battery Demand (watt-hours)	1.6	1.5	6.4	1.5	18.7	77.8	1.1	6.3	6.3	4.1	1.1	0.9	24.1	10.9	41.9	25.0	27.3	27.3	97.2	27.3	27.3	122.2	20.5	409.5	76.2	66
Regulation Input (90% efficiency) (UHF Transmitter)	159		159		159			159	159	159	159	159	159													
Battery Demand (watt-hours)	5.3		18.6		63.6			15.9	10.6	8.0	2.7	2.7	63.5													
Raw Demand																										
Input to Raw Demand														10			35			35					2	89
Battery Demand (watt-hours)														0.7			5.8			5.8					133.4	133.3
Total Battery Demands (watt-hours)	6.9	1.5	25.0	1.5	82.3	77.8	1.1	22.2	16.9	12.1	3.8	3.6	87.6	11.6	41.9	25.0	33.1	27.3	97.2	33.1	27.3	122.2	20.5	542.9	209.5	66.0
Cumulative Battery Demand (watt-hours)	6.9	8.4	33.4	34.9	117.2	195.0	196.1	218.3	235.2	247.3	251.1	[illegible]	412.4	359.9	395.8	420.8	453.9	481.2	578.4	611.5	638.8	761.0	781.5	1324.4	1533.9	1599.9

Total Mission Duration = 90.6 Hr. = 3.76 Days

Average Power = 21.19

Net Battery Energy Demand 1599.9 watt/hr

20% Contingency 1919.9 watt/hr

*Regulator @ 57% efficiency

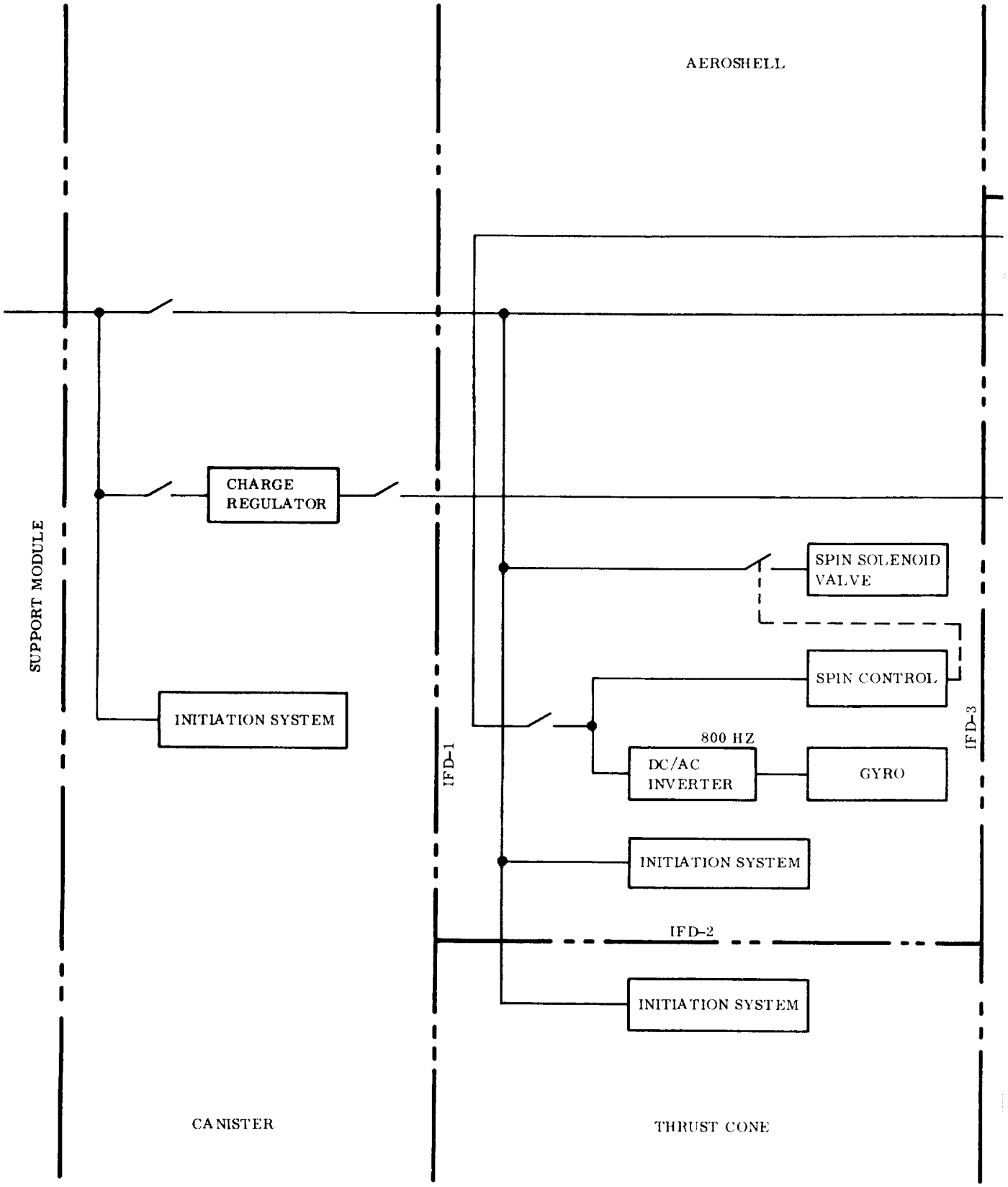

FOLDOUT FRAME 1

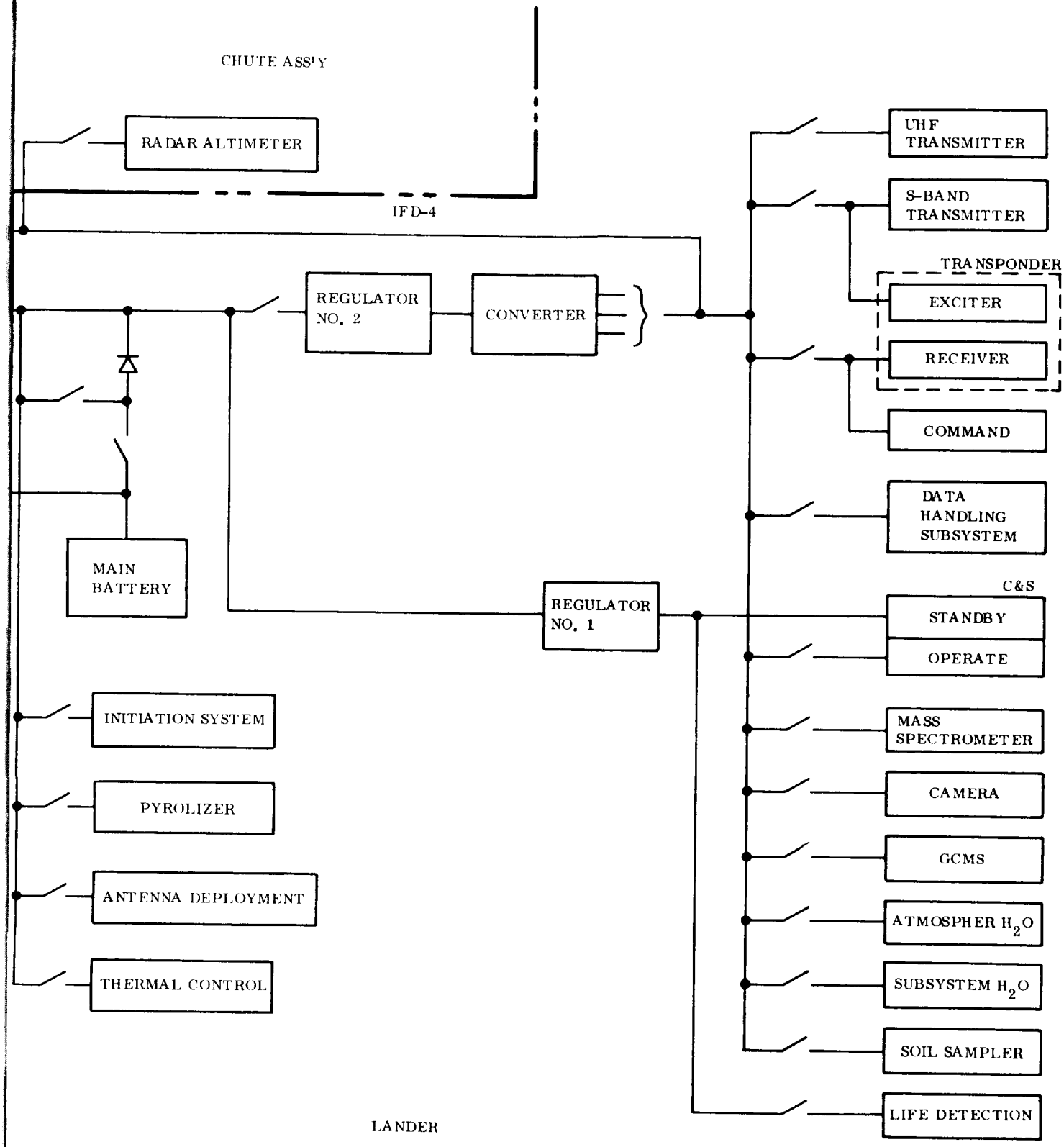

Figure 5.3-3. Power Subsystem Block Diagram

FOLDOUT FRAME 2

A separate aeroshell battery sized for this energy would weigh about 15 lb (16 watt-hr/lb for 8 to 10 ampere-hr batteries appears reasonable). The second battery would weigh about $\frac{(1600-235)}{30}$ = 46 lb based on a 30 watt-hr/lb rating, not including a contingency allowance. A single battery would weigh $\frac{1600}{30}$ = 54 lb. Required parachute and crush-up weight for delivered payload weight are approximately 0.08 and 0.3 lb, respectively per pound of landed payload. Thus the 9 lb Lander battery saving accounts for 0.72 lb of reduced parachute weight and 2.7 lb of reduced crush-up weight. Comparing the two approaches:

	Single battery approach	Two battery approach
Battery weight	54 lb	15 lb (Battery 1) 46 lb (Battery 2)
Net weight	54 lb	58.6 lb
Parachute savings	———	-0.72
Crush-up savings	———	-2.7

The two battery approach is heavier, justifying the use of a single battery.

The battery is kept in a semi-discharged state through interplanetary cruise until about 10 days before Capsule separation. The 2000 watt-hr capacity requires an appreciably high charging energy. This results from the charge to discharge voltage ratio (2.05/1.50 volts/cell) and a 90 percent ampere-hr efficiency. For the 2000 watt-hr battery the required charging energy is:

$$\frac{2.05 \times 2000}{1.50 \times 0.90} = 3000 \text{ watt-hr}$$

A 50 hour charging rate is considered to be the minimum allowable, consistent with maintaining proper cell balance; hence, 60 watts of power are needed from the Support Module for battery charging. If this level of power is unavailable from the Support Module it is possible to sequentially charge the battery in two halves, thus requiring 30 watts rather than 60. This does not involve any need for switching the two halves to a common ground point. Rather the charge regulator may be designed with a floating output which is switched from one battery section to the other. Whether this complication is necessary will depend upon the Support Module power capability.

With a charging voltage of 2.05 volts/cell the net charging voltage on the battery is 41 volts.

Based on estimates of the Mariner spacecraft raw power variations the Support Module voltage may be as low as 37 volts. It is therefore necessary to use a boost charge regulator to permit charging at 41 volts. Under such conditions it is not possible to have the battery on line assuming the use of the diode arrangement shown on the block diagram.

Once charging is completed,however, the battery may be switched on line with Support Module power still applied to the Capsule raw bus at the 37 volt level. There is no danger of discharge since the battery open circuit voltage is on the order of 32 to 36 volts and the diode is therefore back-biased. This method of coupling the battery to the Support Module voltage is useful in that the latter voltage may be applied up to the time of separation with an uninterrupted transition to battery power at the time of separation.

The general sequence of operation of the power system is as follows:

1. During interplanetary cruise the battery is maintained in a semi-discharged state to minimize electrochemical stress. The battery is isolated from the system by its output switch. Capsule power needs are supplied from the Support Module power system at a nominal voltage of 37 to 50 volts.

2. About 10 days before Capsule separation the battery is charged through the charge regulator located in the canister. Charging requires 60 watts of Support Module power and proceeds for a period of about 50 hr. If the Support Module cannot provide this level of power it is possible to sequentially charge upper and lower battery sections, in which case a 30 watt power level is used for a duration of 100 hours.

3. Twenty hours before the Support Module attitude maneuver associated with separation, checkout of the Lander is conducted using internal battery power. This proceeds for a 2 hr period at an estimated average power of 150 watts. This withdraws 300 watt-hr of battery energy.

4. Subsequent to checkout the battery is recharged over a 7.5 hr period at 60 watts or alternately for 15 hr at 30 watts (450 watt-hr are required because the battery watt-hr efficiency is about 67 percent). It may be necessary to isolate the battery during this recharge period if the Support Module power voltage is less than the charging voltage.

5. After recharge, Support Module power is applied continuously and supplies any necessary loads as long as they are not in excess of the Support Module capability. This continues up to the time of separation.

6. At separation the charge regulator remains with the canister and the separated Capsule operates on internal power. The various loads are energized through switch closures controlled by the C&S sequence. Permanent closure is made to the battery output switch, to avoid any possibility of contact chattering during the landing shock. Specific loads and any associated power conditioning equipment are jettisoned with specific separations in the mission: thrust cone separation, aeroshell separation and finally parachute container separation.

7. Upon landing, the C&S applies signals to switches which may have changed state due to the landing shock. The non-switched power input to the C&S and the permanent closure to the battery output switch assures that this can be accomplished.

8. The landed mission proceeds in accordance with the planned C&S sequence.

Returning to the relative merits of centralized or separate voltage conversion there are several methods that may be considered. These are shown on fig. 5.3-4 and described below:

1. Central Converter - The single regulator voltage supplies a multiple output central converter. Each output is distributed to the various loads. Power control switches are required for each voltage supplying each load.

2. Multiple Converter - Separate converters are used for each of the loads. With these converters physically located with their associated loads, power is distributed at a single regulated d-c level. Power control switches are located at each converter input.

3. Central d-c/a-c Inverter and Transformer-Rectifiers (T/R's) - A central d-c/a-c inverter distributes a-c power at a single voltage level and frequency. T/R's located at each load provide the necessary d-c levels. Input switches are required at each T/R.

A comparison of these approaches is shown on fig. 5.3-4. Battery and conversion weights were estimated for all three based on the mission load profile. The minor difference in battery weight results from the fact that partial load losses can be reduced for the multiple converter case, since each converter is matched for its particular load. The central inverter and T/R approach shows a slightly larger battery is needed because of additional transformer losses associated with the T/R's. The battery weight difference is somewhat counter-balanced by the converter weights so that the net weight difference is small.

In other respects the multiple converter approach provides the greatest number of design and interface advantages though there are important advantages to the other approaches as well.

The ultimate design will likely include features of all these approaches, depending to a large extent on detailed evaluation of the various loads. The science loads, for example, will likely entail design interfaces with various organizations. The use of an a-c bus for such users would reduce the necessity for continual checking to assure that the power consumption at given voltage levels did not exceed certain limits.

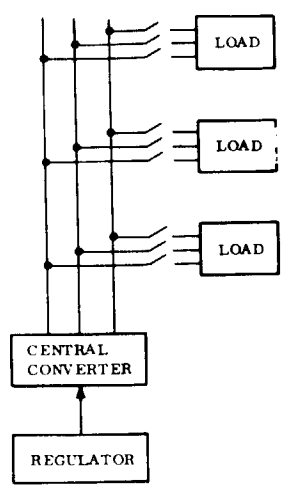

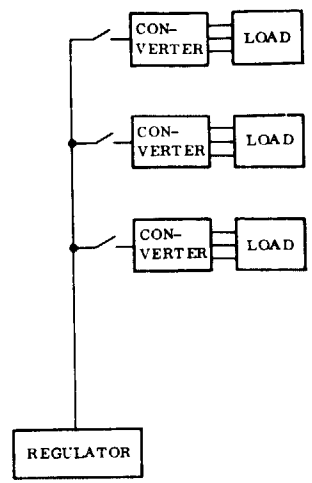

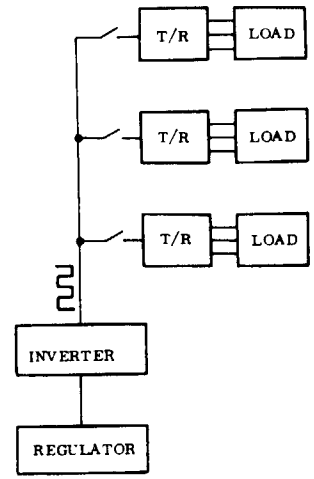

	Central Converter	Multiple Converter	Central Inverter and T/R's
Battery demand	1920 watt-hr	1875 watt-hr	1940 watt-hr
Relative Weight	Battery 65 Central Converter 3.0 (70 watt rating) 68.0 lb	Battery 63.5 Multiple Converters 5.0 (70 watt rating) 68.5 lb	Battery 65.6 Central Inverter 2.5 Transformer-rectifiers 2.5 (70 watt rating) 70.6 lb
Power Subsystem - user Interface:			
User voltage Selection	Fixed by central converter for all subsystems	Adjustable by converter design for each subsystem	Adjustable by each T/R design.
User power at specific voltages	Fixed by central converter design - user design change may require central converter design change.	Adjustable by converter design for each subsystem - user change only affects user converter.	Adjustable by T/R design for each subsystem - user change only affects user T/R.
Switch control	At each voltage at each load.	At each converter input	At each T/R input
Number of switching contacts	2 to 3 times N depending on number of voltages to each load	N	N
Harness weight	2 to 3 times W_H depending on number of voltages to each load.	W_H	W_H
Isolation	Load transients on any converter voltage is reflected to other loads - filters may be required.	Load transients buffered by each converter	Load transients buffered by each T/R
Harness faults	Buffered by converter - least jeopardy to battery	May require provisions in regulator to provide buffering.	Buffered by inverter - least jeopardy to battery
Design coordination	Unified power supply design; difficult energy management interface	User responsibility for power supply design could result in non-uniform design approaches; less difficult energy management interface	Unified power supply design; less difficult energy management interface.

Figure 5.3-4. Comparison of Voltage Conversion Approaches

5.3.1.3 Equipment Characteristics

The characteristics of the Power Subsystem equipment are summarized in table 5.3-3.

The battery design and the selection of suitable switching devices present the principal areas of concern relative to the power system equipment. The landing shock environment influences both of these types of equipment and the sterilization environment particularly influences the battery design.

Considerable information has been provided in previous reports regarding the status of sterilizable silver-zinc shock resistant batteries. The present situation is summarized as follows: Both GE (in cooperation with the Eagle-Picher Company) and other battery manufacturers have and are continuing to devote considerable attention to the development of suitable batteries. Prototype designs have been built and tested demonstrating that sterilizable shock resistant batteries can provide acceptable performance. In particular the GE/Eagle-Picher design indicated extensive life and cycle capability beyond those dictated by the Lander requirements though the particular battery sizes tested were relatively small (5 ampere-hr). In addition, small (5 ampere-hr) sterilizable batteries have been successfully integrated into a Lander design as demonstrated by the CSAD design pursued by JPL. Several large capacity designs, both shock and non-shock resistant, are being developed presently by several vendors. Thus there is an increasing body of data on which to base a design, though the step in going from small to large designs is by no means trivial. Section 5.3.4 presents an elaboration of the GE/Eagle-Picher and other efforts leading to the belief that a 30 watt-hr/lb battery of the necessary capacity can be achieved.

Electromechanical switching devices present possible problems of temporary disruption or permanent damage as a result of the landing shock. Temporary disruption can be overcome by applying reset signals from the C&S subsequent to landing and does not appear to be a serious problem. The question of permanent damage has been examined on several other programs faced with this problem. A variety of relays were tested as part of the GE Mk 12 program and suitable types were found that could withstand 1000 g's for 0.5 msec in all directions without damage. In discussions with JPL engineers, it was disclosed that relays for the CSAD program were tested to 2500 g's to a high degree of success. There was apparently some directional sensitivity, though the extent of this was not disclosed.

The use of solid state switches as an alternative may be attractive though there are several other problems which appear. First, they are sensitive to EMI and special steps would be necessary to minimize this effect. Second, they present a problem of electrical isolation in that the driving signal is related electrically to the voltage source being controlled. Third, they absorb small amounts of power in their off condition and would therefore result in a battery weight penalty.

TABLE 5.3-3. POWER SUBSYSTEM COMPONENT CHARACTERISTICS

Component	Function	Mounting Location	Weight (lb)	Volume (in.^{3})	Nature of Equipment
Charge Regulator (redundant)	Charge Lander battery	Aft canister	4.0	100	Electronics
Power Control Unit (redundant)	Distribution and power control	Aft canister	4.5	115	Switching and protective devices
Voltage Regulator/Converter	Regulate and condition battery power for Capsule loads	Lander	7.5	190	Electronics
Battery	Main power source	Lander	65.0	870	Electrochemical
Power Control Unit	Distribution and power control	Lander	10.0	250	Switching and protective devices

5.3.2 INITIATION SUBSYSTEM

5.3.2.1 Requirements

The Initiation Subsystem consists of devices and networks required for controlling, initiating, and accomplishing nonrepetitive events by hot-wire devices and electro-explosive devices. It powers the Mars Hard Lander functions of spacecraft separation, biobarrier separation, electrical inflight disconnect operations, thrust cone release, pneumatic line operations, aeroshell release, and deployment of various equipments. These requirements are shown in table 5.3-4.

5.3.2.2 Design Alternatives and Approach

The approach to Initiation Subsystem design is based upon certain interface rules and design constraints. These include:

1. Initiation circuits are not routed through inflight disconnectors.

2. Equipment shall be jettisoned as soon as possible after its function is completed.

3. Initiation circuitry shall be isolated by at least 1000 ohms from other subsystem equipment.

4. Short circuits or electrical faults in any initiator shall have no degrading influence on other subsystem functions or on subsequent initiations.

In the Titan/Mars vehicle studies two alternative initiation circuits have been utilized, namely capacitor-discharge and thermal batteries. These initiation circuits operate pyrotechnic and hot-wire initiation devices.

The capacitor-discharge approach has been shown in biobarrier/canister conceptual designs to fully meet the JPL interface approach. On the other hand, the entry vehicle and thrust cone conceptual designs show the thermal battery approach. This reflects the extensive success with thermal batteries in previous re-entry vehicles (over 850 batteries in consecutive space flights without a single failure).

Providing a technical basis for comparing and selecting initiation circuitry involves an evaluation of the weights and volumes for each alternative. (Reliability comparisons are postponed pending the availability of reliability numbers on sterilized capacitors). The objective is to provide trade-off data and determine which approach is lightest and/or smallest in the Lander and canister applications.

The capacitor-discharge approach is illustrated in fig. 5.3-5. The thermal battery is activated and brought to operating temperature in about 0.1 sec. The thermal relay module protects the operational battery during this activity. Upon receipt of a sequencing signal the power controller switches thermal battery power directly to the initiator through a paralleling blocking diode. The thermal battery remains in readiness for operating other initiators for approximately 1 to 3 min.

TABLE 5.3-4. INITIATION POWER REQUIREMENTS

Event	Device	Current Duration		Time Reference
		amps	msec	
1. Spacecraft Separation	HW	96	30	$T_1(T_L+17$ min)
2. Biobarrier Separation	HW	24	30	$T_2(T_4-1.5$ hr)
3. Canister/Lander IFD	HW	15.3	15	$T_3(T_4-0.1$ sec)
4. Canister/Aeroshell Release	HW	96	30	$T_4(T_L+193$ days)
5. A/C Propellant Open	EV	10	30	$T_5(T_4+0.5$ sec)
6. Deflection Motor Burn	EV	10	30	$T_6(T_5+30$ min)
7. Deflection Motor Cut-off	EV	10	30	$T_7(T_6+2$ min)
8. Thrust Cone/Lander IFD	HW	15.3	15	$T_8(T_7+3$ sec)
9. Thrust Cone Release	HW	24	30	$T_9(T_8+0.1$ sec)
10. Drogue Parachute Mortar	PY	30	30	$T_{10}(T_{11}-10$ sec)
11. Aeroshell/Lander Pneumatic Cut	PY	30	30	$T_{11}(T_4+23$ hr 46 min)
12. Aeroshell/Lander IFD	HW	15.3	15	$T_{12}(T_{11}+3$ sec)
13. Aeroshell/Lander Release	HW	18	30	$T_{13}(T_{12}+0.1$ sec)
14. Parachute/Altimeter IFD	P4	10	30	$T_{14}(T_{13}+30$ sec)
15. Parachute Container Tie-down Release	HW	12	30	$T_{15}(T_{14}+31$ sec)
16. Hatch Cover	HW	40	30	$T_{16}(T_{15}+2.5$ min)
17. Release Antenna	SOL	1	100	$T_{17}(T_{16}+10$ sec)

SYMBOLS

EV = Explosive valve
HW = Hot-wire release
PY = Pyrotechnic initiator
SOL = Solenoid

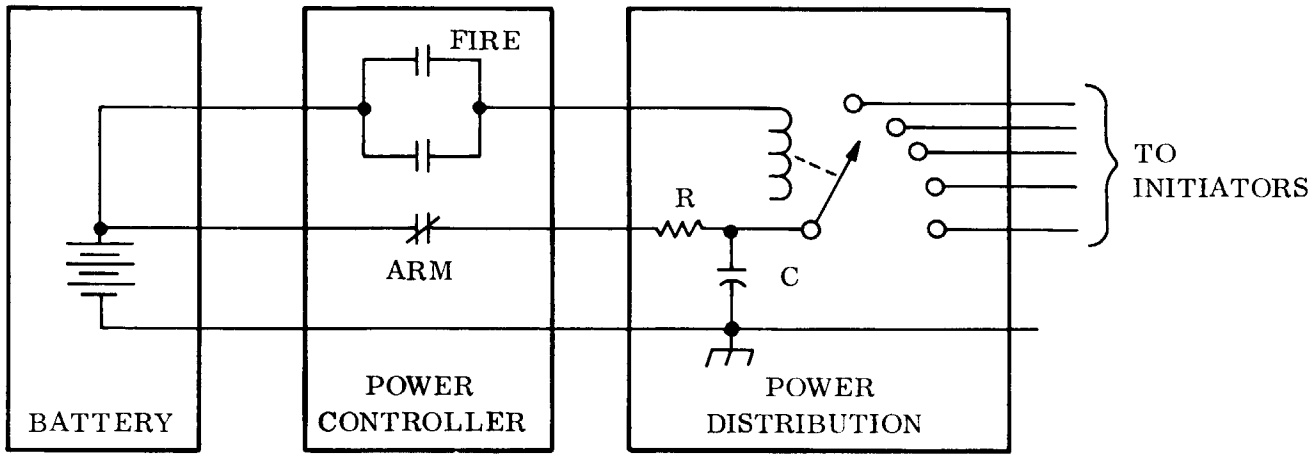

Figure 5.3-5. Capacitor Discharge Circuit

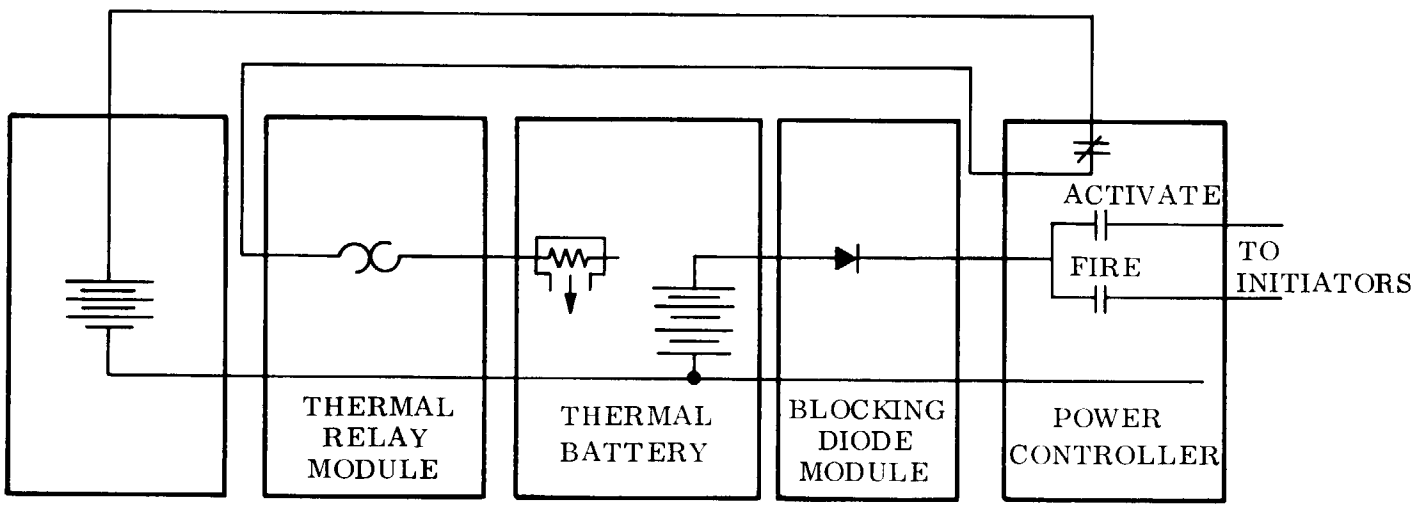

Figure 5.3-6. Thermal Battery Circuit

The two approaches have different operating modes as described above, leading to the study of different parameters for evaluation. Both cases require approximately the same sequencing and power control equipment. Hence, it is assumed that these equipments have no influence on the trade-off.

In the capacitor-discharge case, it is possible to separate the time of initiations sufficiently to permit full capacitor charging. This means that a single power distribution module in each section of the vehicle, i.e., canister, aeroshell, thrust cone or Lander, can be used to power all of the initiation equipment in that section. In this case, the size and power distribution module weight depends on the number of switch decks as determined by the number of initiators to be operated. Thus, the size and weights of the capacitor discharge equipment is evaluated as a function of the total number of initiators (pyro or hot-wire) in each particular section.

On the other hand, the thermal battery, once activated, can operate initiators one after the other at a 0.1 sec rate. That is, a single thermal battery could operate over 1000 initiators, provided the operations occurred in close time sequence. Since the thermal battery cools below operating temperature in a period of minutes, the number of thermal batteries required is dependent on time intervals in a mission when battery energy is needed. Thus, with thermal batteries it is advantageous to schedule as many initiations as possible into a minimum number of operate periods. Each such period has a 1 to 3 min duration and each will require a separate set of batteries. As a result, the size and weight of the thermal battery approach must be evaluated in terms of the number of operating time periods.

For purposes of comparison, a redundant approach is considered in both cases. The power distribution module will contain two capacitors, two resistors, two stepping switches and a connector. The thermal battery approach will involve two batteries, a diode isolation module and a dual-channel thermal relay module.

Figure 5.3-7 shows volume and weight as a function of operate periods and firing circuit number for the thermal battery and capacitor discharge approaches. To provide a basis for comparison, it is assumed that each thermal battery will furnish energy for at least two initiations per period of operation.

The illustration indicates that the cross-over occurs at two operate periods. Thus, when one or two sets (assumes reduncancy) of thermal batteries per vehicle section can satisfy all initiator requirements, the battery approach is smaller and lighter.

Table 5.3-5 summarizes the number of initiations and operate periods for the vehicle sections and indicates the design approach to implement each one.

This selection is based upon the assumption that energy for separation of the Spacecraft from the Transtage adapter is supplied by the Spacecraft. Another approach is for the Transtage to supply this separation power. In that case, the number of initiations on the canister section would be reduced to 14 and the operate periods would be reduced to two, indicating that the choice of a capacitor-discharge system should be re-evaluated. If a thermal battery is used, the weight savings would be about 1.2 lb.

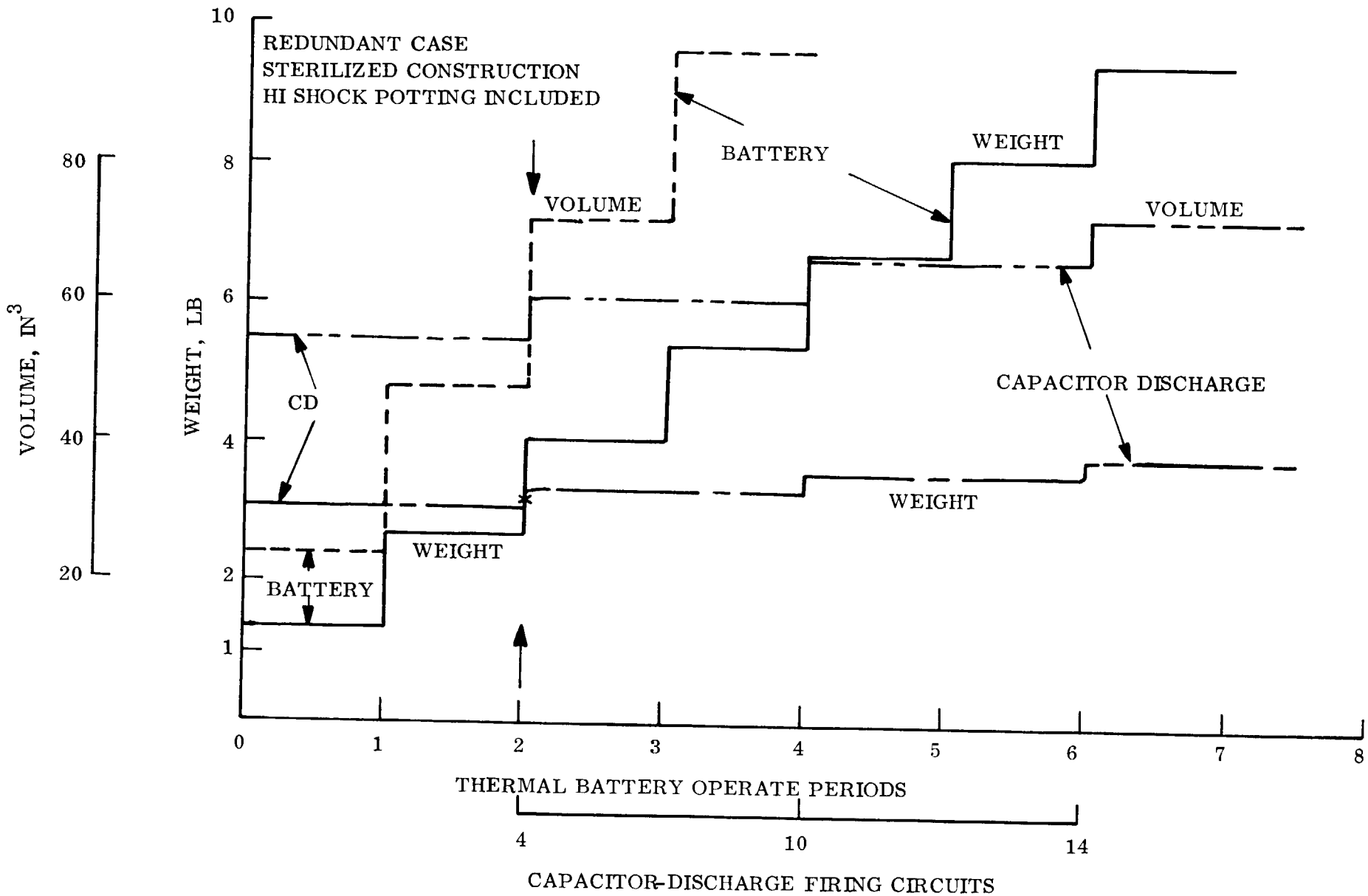

Figure 5.3-7. Comparison Between Capacitor Discharge and Thermal Battery Pyrotechnic Initiation Equipment

TABLE 5.3-5. SUMMARY OF INITIATION REQUIREMENTS

Vehicle Section	Number of Initiations	Operate Periods	Selected Approach
Canister	18	3	Capacitor-Discharge
Thrust Cone	14	1	Thermal Battery
Aeroshell	18	2	Thermal Battery
Lander	8	1	Thermal Battery

5.3.2.2.1 Actuation Devices

As shown in table 5.3-4, the Initiation Subsystem must drive a variety of different initiation devices in supporting the different subsystems. All the electrical inflight disconnects and many of the other release devices are constructed with hot-wire release collets. The hot-wire device provides unique safety and other advantages. An example, the inflight disconnect, will be described next.

The basic concept of hot-wire release involves a spring-loaded split collet which is held together by a wraparound stainless steel wire. The wire is fabricated with a chemically milled region of controlled cross-section. When an electrical current is applied, the wire heats in the limited cross section region, severs, and unwraps, allowing the collet to open. This permits the spring-driven release to operate. Fig. 5.3-8 illustrates the application to an inflight electrical disconnect. The hot-wire mechanism is shown in the upper part of the sketch. The cable enters from the left, is connected to the stainless steel wire wrapped around the ground collet. The spring-loaded shaft moves to the right on release, causing operation. Table 5.3-6 describes some advantages and disadvantages of the hot-wire approach.

GE has flown more than 25 hot-wire operated inflight disconnects with 100 percent flight operation success.

5.3.2.3 Initiation Subsystem Design Solution

Typical initiation circuitry and its operation are explained in para. 5.3.2.2 and figs. 5.3-5 and -6. The design solution is illustrated in fig. 5.3-9. The functioning of major subsystem components is presented in following paragraphs.

5.3.2.3.1 Canister Power Controller

The canister power controller switches power to the power distribution module controlling the flow of energy from the Support Module to be stored and used for initiation. Further, this controller switches power from the power distribution module to the proper initiator. The canister power controller contains two separate and complete channels for redundancy, arranged so that each channel is capable of completing the initiation function independently.

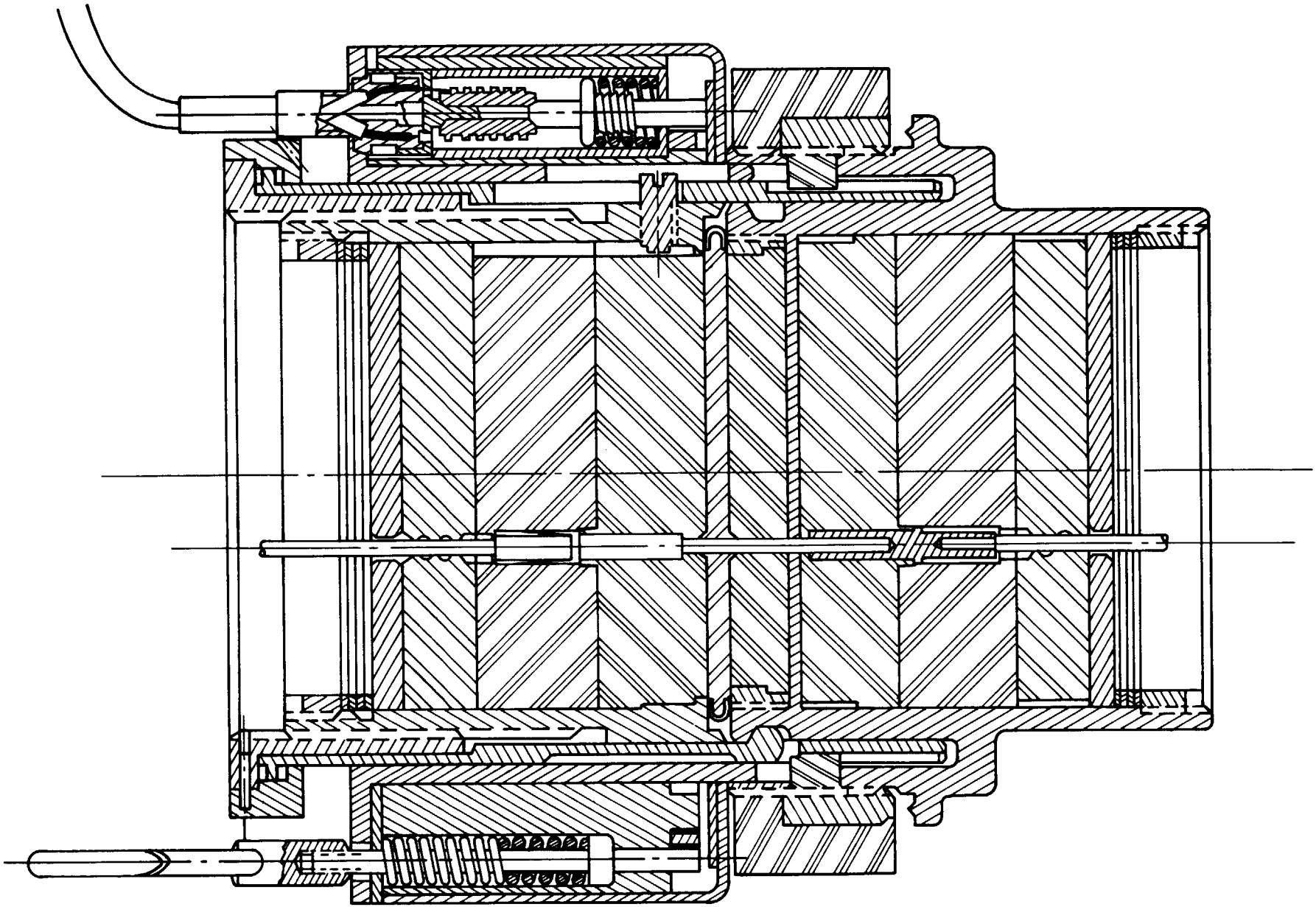

Figure 5.3-8. Typical Hot-wire Inflight Disconnect

TABLE 5.3-6. EVALUATION OF HOT-WIRE RELEASE

Advantages	Disadvantages
Non-hazardous operation	Initiation power and response time similar to pyrotechnic devices
Avoids bunker-storage and handling	Release energy limited to springs
Higher temperature capability (1000°F)	
Long term storage stability	
Resistant to humidity	
Lower i-f sensitivity	
Greater reliability[1]	
Hot-wire element easily replaced for test	
Avoids expensive test firing program	
High shock resistance (800 g's)	

1. Amicone, R.G.; Mackrell, B.R.; Sensitivity and Functioning Time Analysis of Connector Electrical/Electronmechanical Disconnect. Report of the Franklin Institute Research Laboratories, Number FC-1967, April 1967.

5.3.2.3.2 Canister Power Distribution Module

The canister power distribution module stores energy for initiation and switches this energy to the appropriate initiator cable. The module contains dual capacitors, switches and charging resistors to provide two completely independent channels for redundancy. The subsystem is armed when the power controller responds to commands from the Support Module C&S, sending power to charge the capacitors. Execution of initiation takes place when another Support Module command causes the switch to close to the appropriate initiator.

5.3.2.3.3 Thrust Cone Batteries and Diode

The thrust cone batteries power all thrust cone located equipment, avoiding the flow of initiation current through the inflight disconnect. Two separate redundant thermal batteries are used and connected through a diode blocking module so that either battery may provide full initiation power.

The thermal battery contains a molten salt electrolyte brought to operating temperature by heat paper which is ignited by redundant matches. This type battery provides an extremely high power density.

5.3.2.3.4 Thrust Cone Power Controller

The thrust cone power controller switches the initiator lines from the short circuited condition to the thrust cone battery for direct operation. The thrust cone programmer contains

redundant cross-linked initiation circuitry to assure full redundancy. Further, the power controller is equipped with a time delay circuit to assure that the electrical inflight disconnect operation occurs before mechanical parting.

5.3.2.3.5 High Rate, Entry, and Setup Batteries

The high rate battery provides aeroshell pulse initiation power immediately after separation, the entry battery provides initiation power for aeroshell release and parachute deployment activities and the setup battery powers the initiation events from parachute jettison through landed deployments. These batteries are identical to the thrust cone batteries described above. These batteries are switched by the Lander power controller.

5.3.2.3.6 Lander Power Controller and Thermal Relay Modules

The Lander power controller contains a separate section for initiation functions. This controller switches thermal battery power to the appropriate initiator lines. The activation of these thermal batteries is also controlled by this power controller. This activation provides the arming function.

5.3.2.4 Equipment Characteristics

The characteristics of the initiation system equipment are summarized in table 5.3-7.

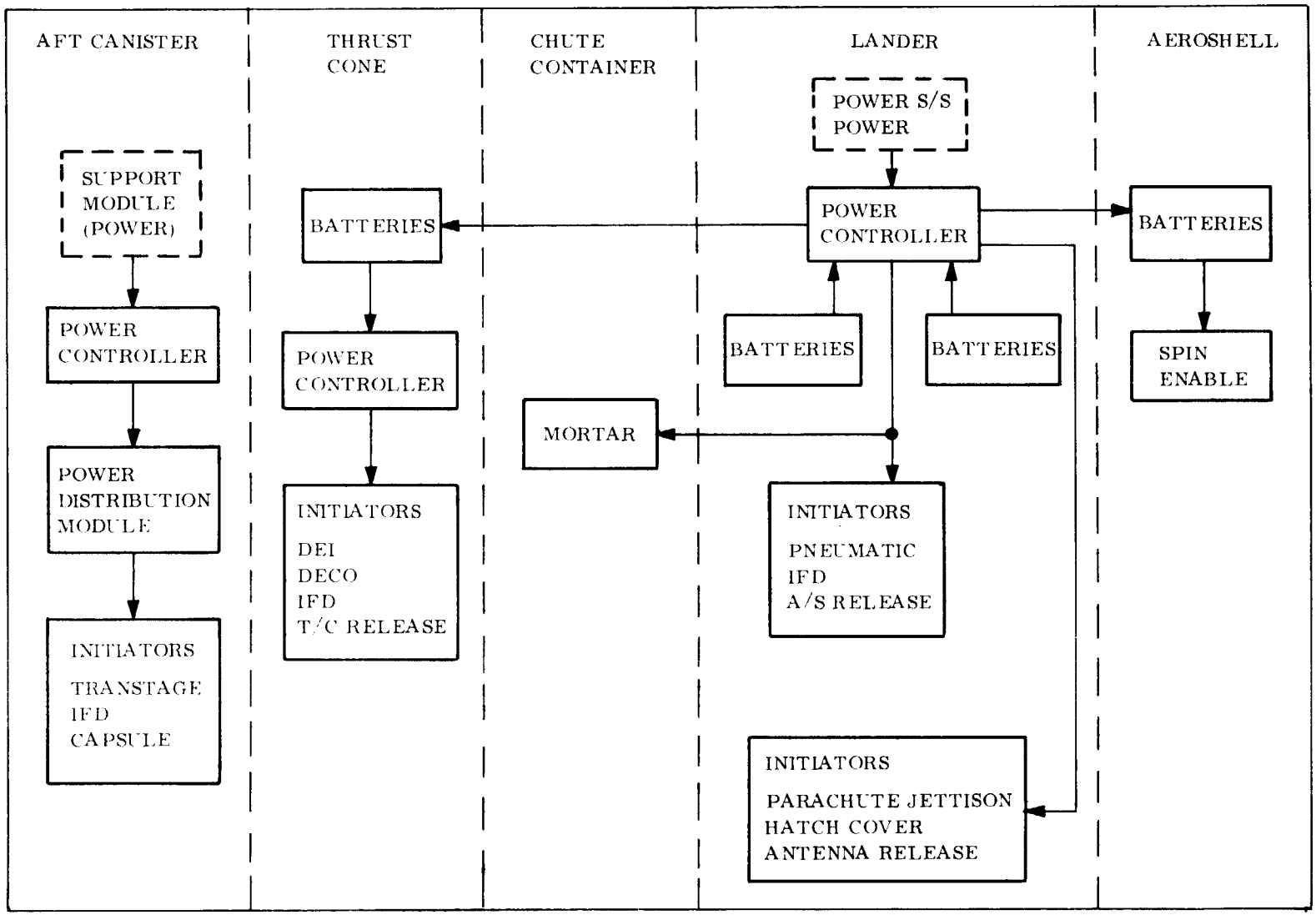

Figure 5.3-9. Initiation Subsystem

TABLE 5.3-7. INITIATION SUBSYSTEM HARDWARE CHARACTERISTICS SUMMARY

Component	Function	Name of Equipment	Mounting Location	Weight (lb)	Volume (in.^{3})
Power controller (initiation part)	Switch thermal battery power to initiators	Relay switches, analog time relay electronics, blocking diodes and thermal relays	Lander	5.4	18.8
Setup batteries	Provide pulse initiation power	Two thermal batteries	Lander	2.0	18.8
Entry batteries	Provide pulse initiation power	Two thermal batteries	Lander	2.0	18.8
High rate batteries	Provide pulse initiation power	Two thermal batteries	Aeroshell	2.0	18.8
Diode blocking module	Prevent reverse power flow	Redundant silicone semi-conductor diode	Aeroshell	0.2	5.6
Thermal relay module	Protect against faulted squib firing circuit	Bimetallic thermal switch	Aeroshell	0.2	6.8
Thrust cone battery	Provide pulse initiation power	Two thermal batteries	Thrust Cone	2.0	18.8
Power controller	Provide thermal battery power switching	Relay switches, analog time delay electronics, blocking diodes and thermal relay	Thrust Cone	2.2	25

5.3.3 DISTRIBUTION EQUIPMENT

The grounding diagram for the EP&D Subsystem is shown in fig. 5.3-10.

A block diagram showing the combined Power Subsystem and Initiation Subsystem is shown on fig. 5.3-11.

5.3.4 BATTERY SUPPORTING DATA

Four battery systems have been considered for this application. The application factors considered are listed below:

1. Sterilization	135°C - 96 hr
2. Activated life	10 months
3. Cycles	10
4. Discharge period	4 days

While these requirements must be satisfied, the highest power-to-weight and power-to-volume must be achieved.

5.3.4.1 Battery Selection

The major advantage of using the silver-cadmium or nickel-cadmium couple are their superior cycling characteristics over those of the silver-zinc couple. In this application where only a few cycles are required, the silver-zinc's higher theoretical power density makes this system an obvious choice. A variety of design approaches to overcome inherent sterilization and shock resistance problems have provided a wide range of performance characteristics from a number of sources. This data was analyzed before final selection was made and is described in this section.

Eight battery manufacturers or users were solicited to determine the state-of-the-art. The Yardney Corporation, Whittaker Corporation and Gould National had not made any progress into sterilization techniques. General Motors had been contracted by JPL to develop a system and provided a sterilized cell capable of 2 months wet life and 11 watt-hr/lb before the contract was terminated. Other work includes JPL/ESB, McDonnell/Douglas and GE-RS/Eagle Picher developments.

The McDonnell/Douglas work has been concentrated on a proprietory inorganic separator material. Sterilization has been successful and 11 watt-hr/lb is possible, although the high impedence separator makes the cells, temperature and current density (demand factor) sensitive. Because of the brittle nature of the inorganic membrane it was considered doubtful whether the design would survive high shocks.

✱ NOTE: GOOD GUIDANCE SIGNAL IS RELAY CLOSURE ISOLATED FROM BOOSTER CONTROLLED DRIVE COIL BY 10 MΩ.

✱ ✱ NOTE: CONTAINS OPERATIONAL 28V RETURN BUS

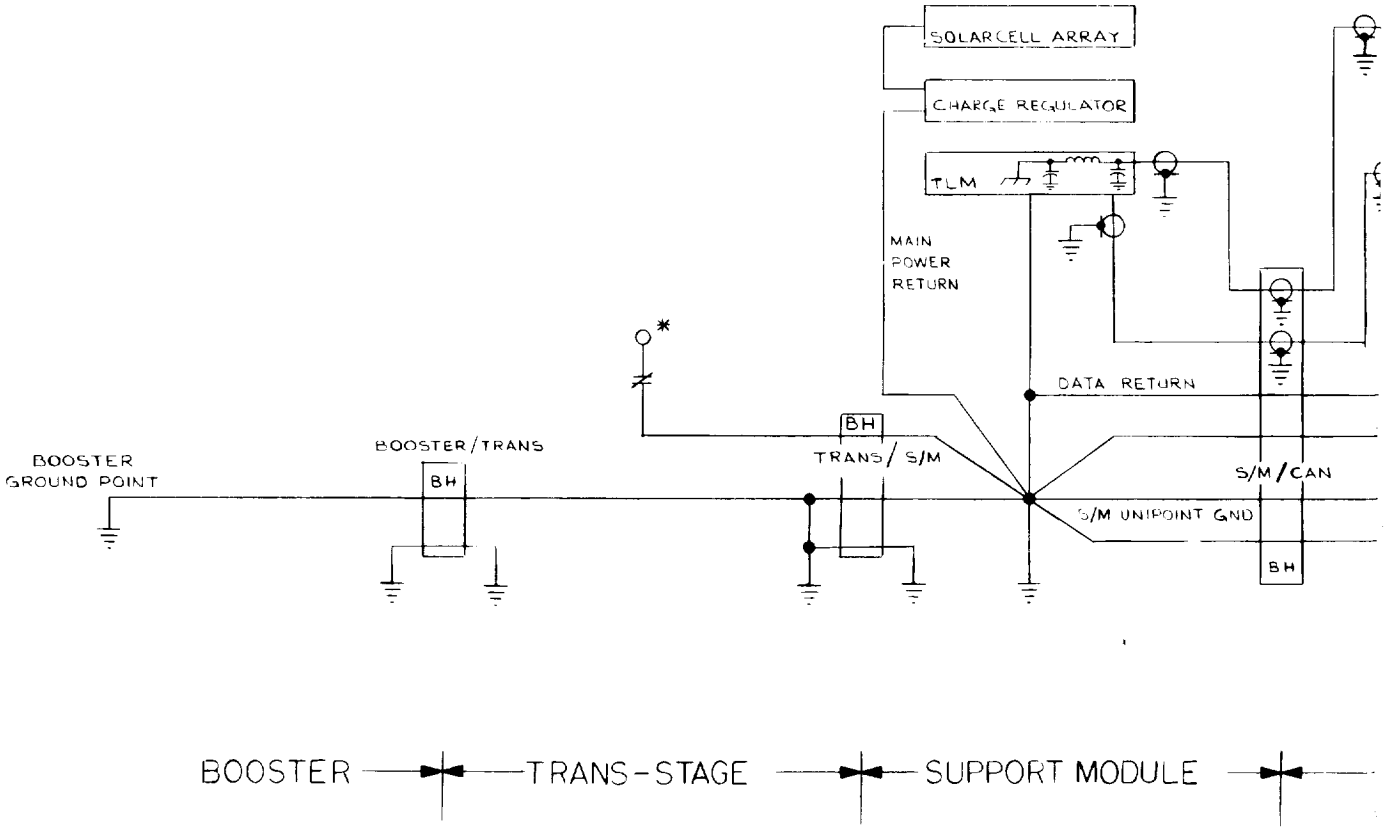

FOLDOUT FRAME 1

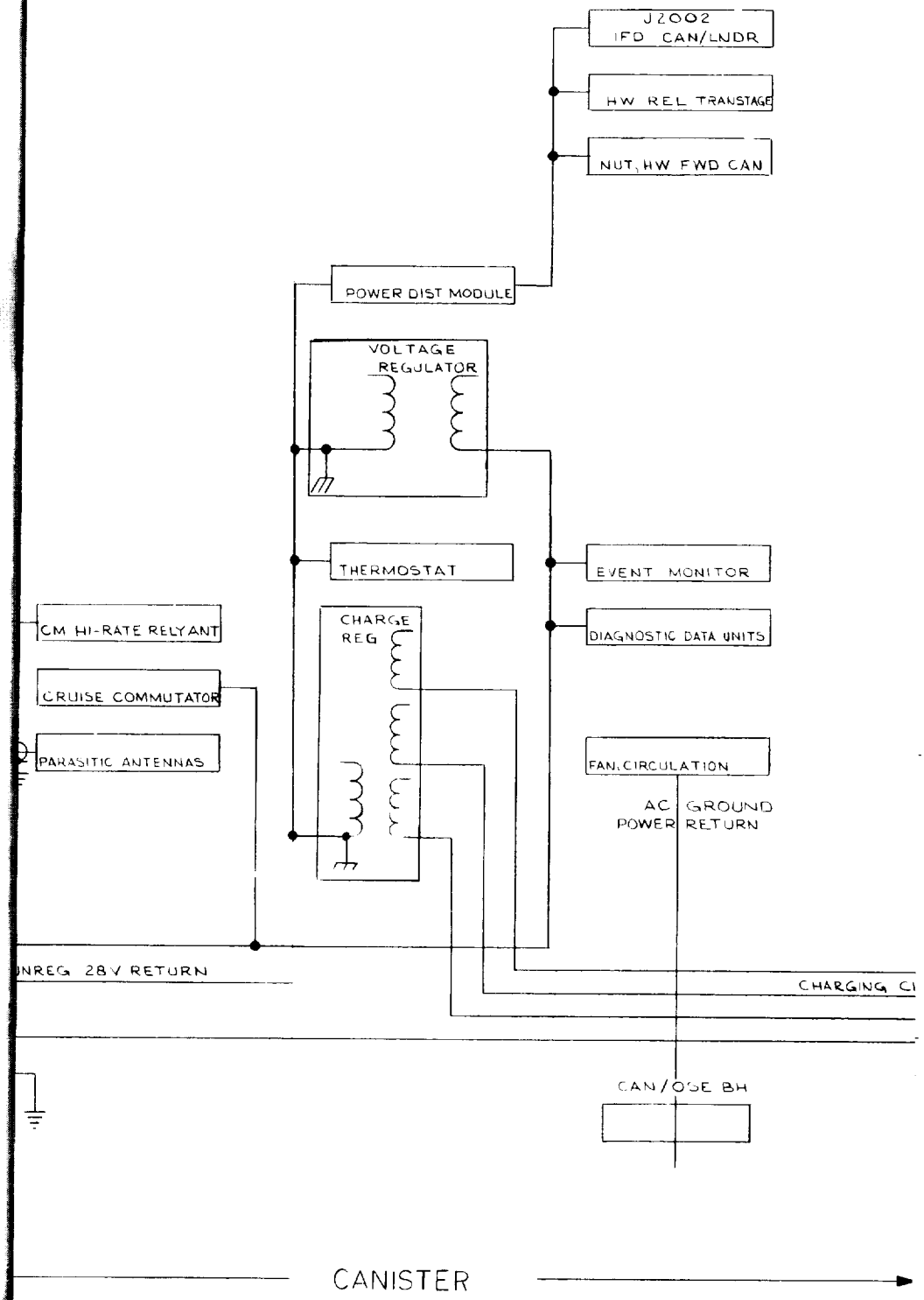

FOLDOUT FRAME 2

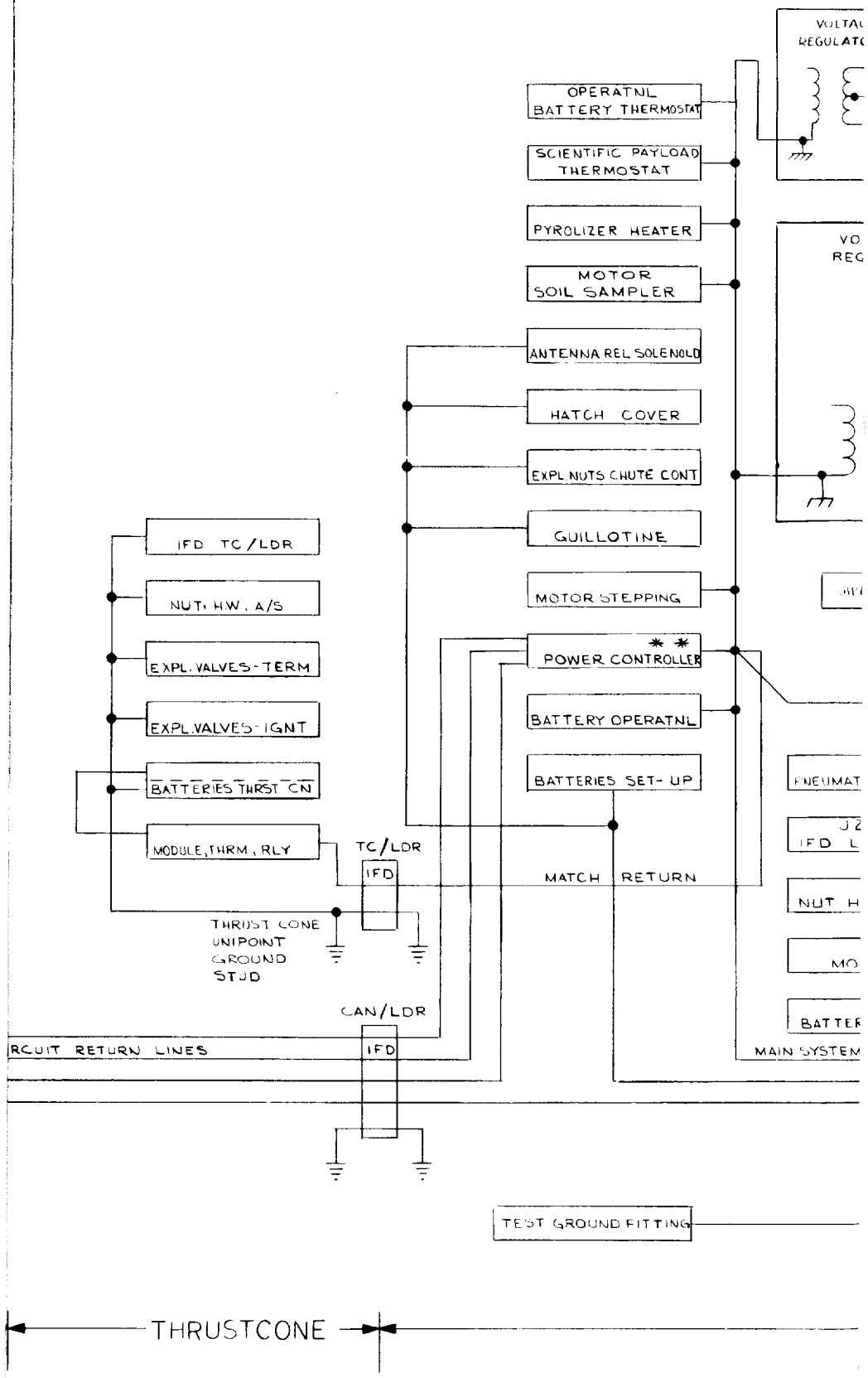

FOLDOUT FRAME 3

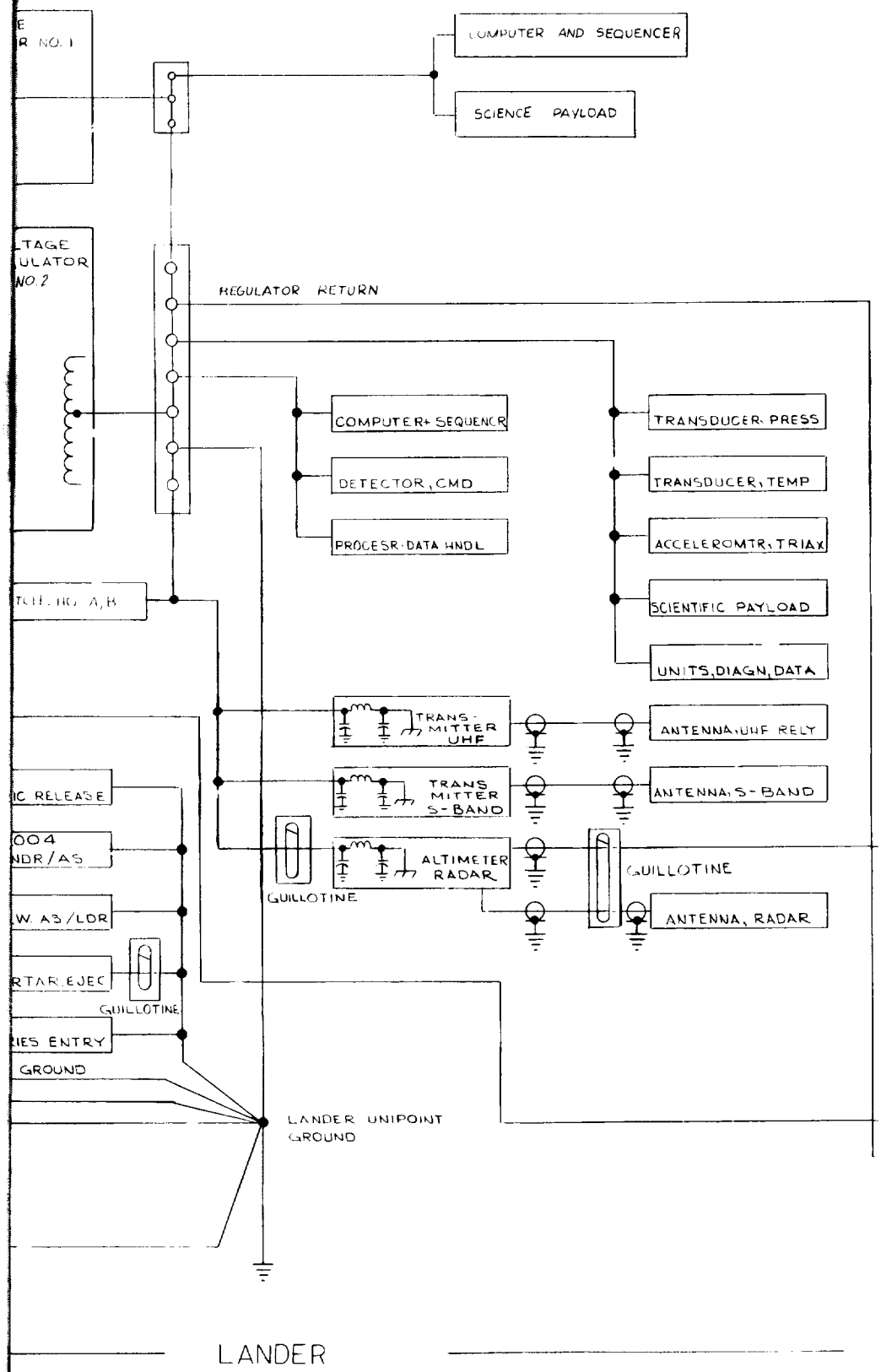

FOLDOUT FRAME 4

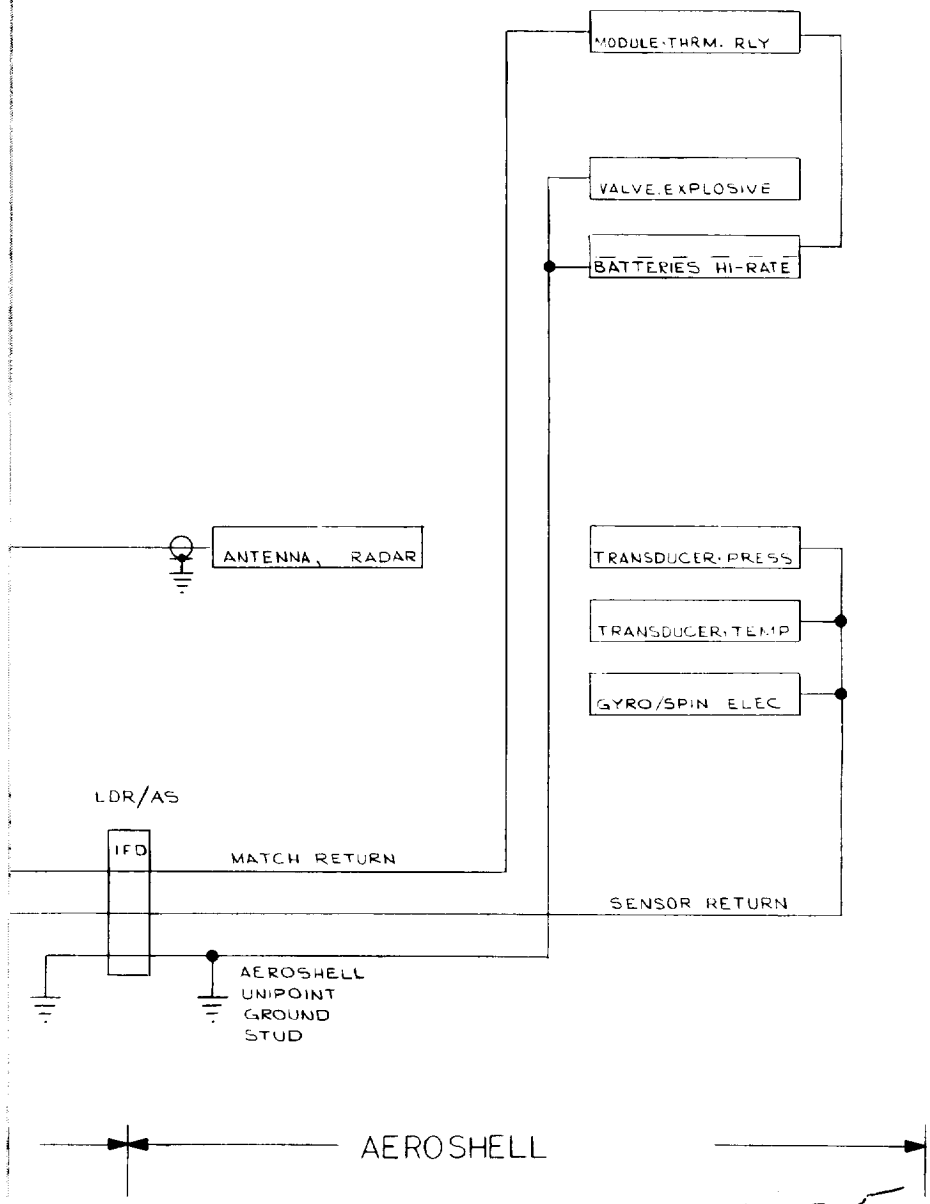

FOLDOUT FRAME 5

Figure 5.3-10. 1400 lb Lander Grounding Diagram

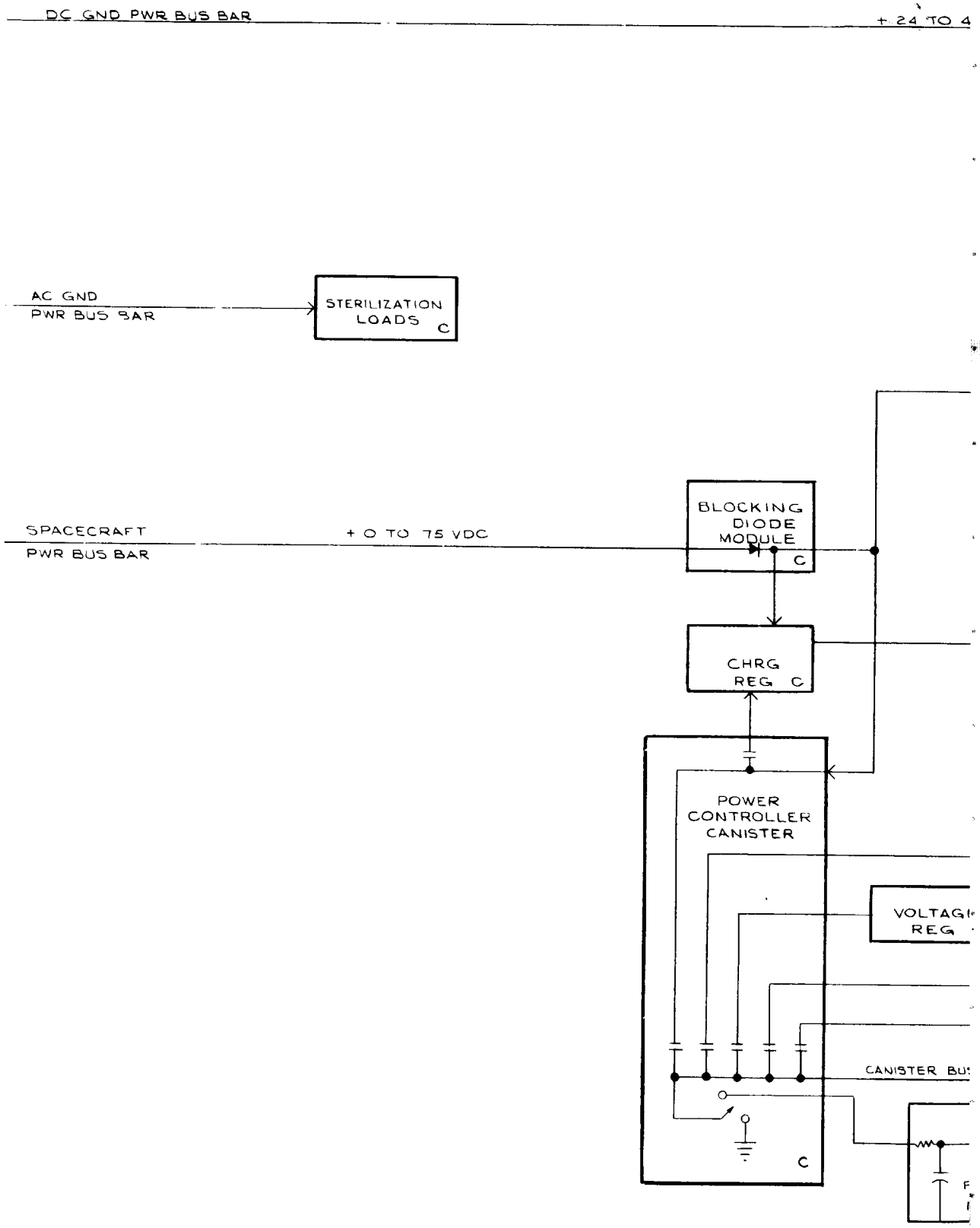

FOLDOUT FRAME 1

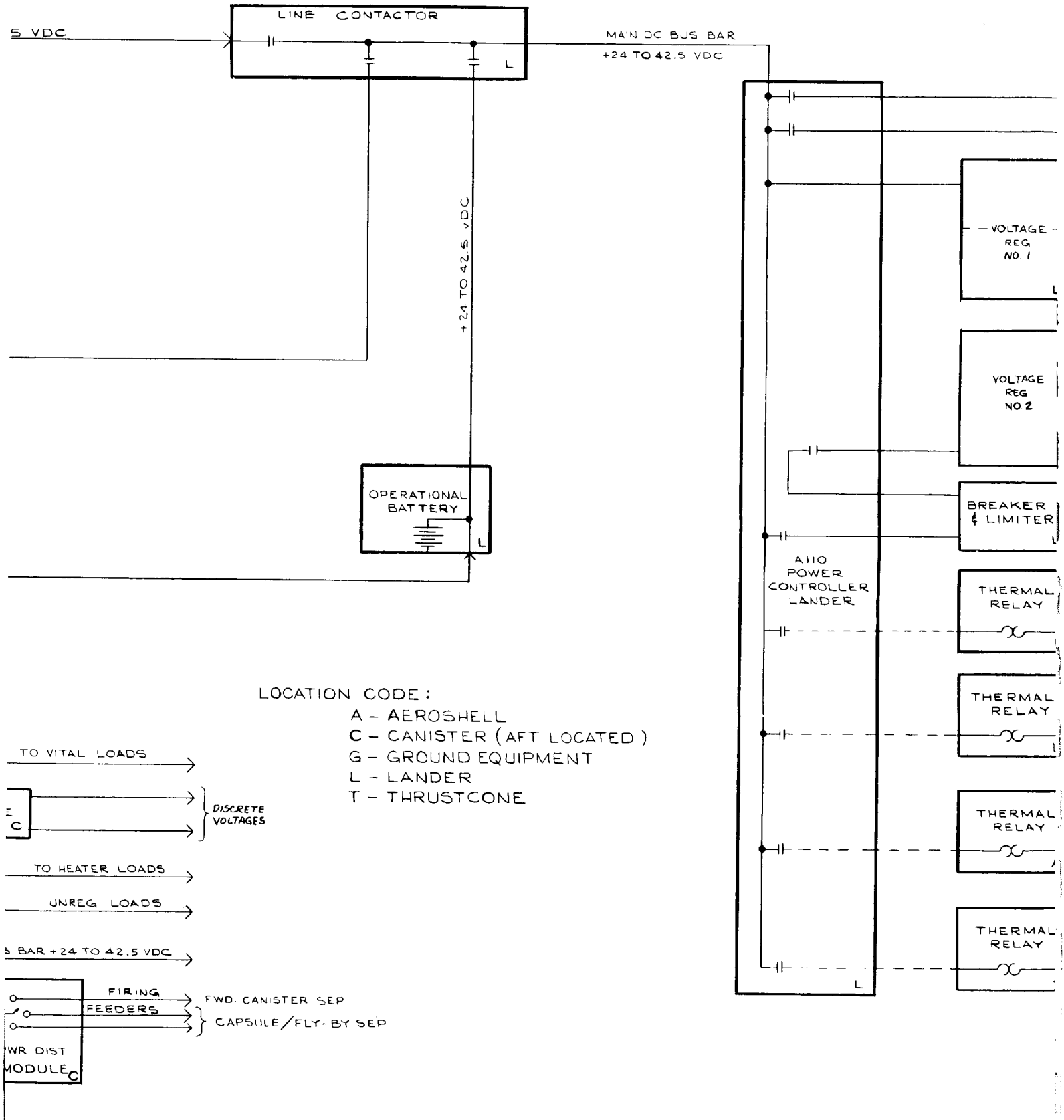

FOLDOUT FRAME 2

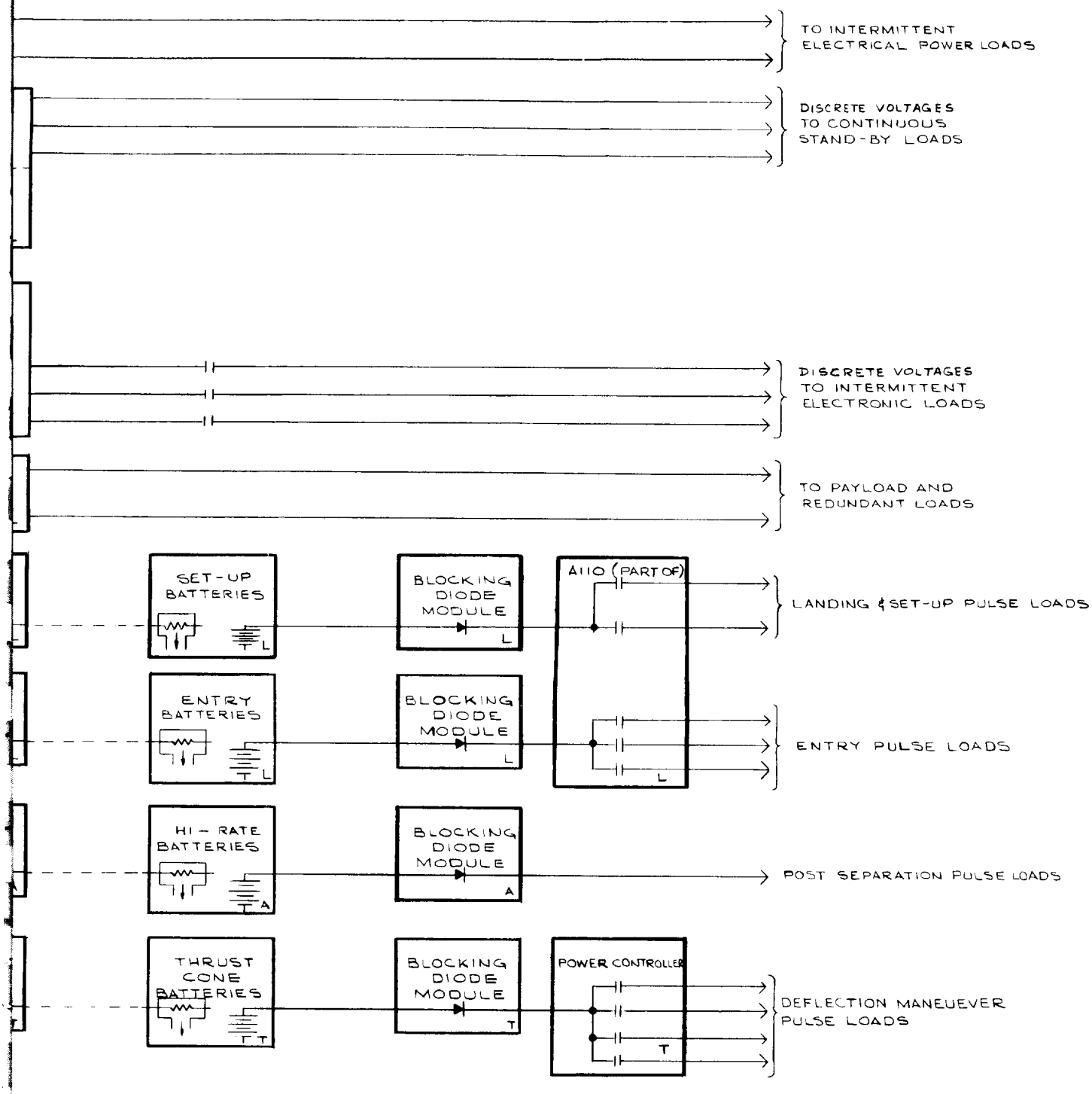

Figure 5.3-11. EP&D Subsystem Block Diagram

FOLDOUT FRAME 3

The JPL development contract with ESB and ESB-financed work has produced sterilized batteries with high shock resistance. Numerous types of separators are under consideration, most of which are irradiated cross linked polyethylenes with coboxalic grafts. RAI 116 and RAI 110 appear to be giving the best electrical performance. As in most vendor designs, the work is being performed on single cells. These cells have to be designed to withstand vapor pressures of the electrolyte during sterilization without distortion which considerably reduces the power-to-weight ratio. In spite of this disadvantage, power densities of 30 watt-hr/lb are envisaged and 9 watt-hr/lb achieved.

The ESB design includes support frames around each plate to increase rigidity on an otherwise floating plate. Shock applied in any direction causes the plate to move about the one fixed point which is the terminating sleeve. With low capacity cells and small light plates, high shock levels can be attained although some loss of active material must occur if any movement takes place. Obviously, with increased capacity cells, larger plate masses will cause deflection at lower g-levels unless the support frames are prohibitively large. ESB report E-5-68 shows that their design is shock limited and in larger batteries, i.e., 80 AH's, 200 g shock would be the maximum possible.

ESB has also been working on a remotely activated system containing dry charged plates. Exposure to elevated temperatures for prolonged periods reduces AgO to Ag_2O with a subsequent reduction in energy density. The loss is not prohibitive and is approximately 46 percent permitting energy densities of 15 watt-hr/lb in large capacity batteries. A further degradation can be expected if it is assumed that ESB's approach to the shock problem is similar to their secondary battery development. It is also apparent that a dry cell is more susceptible to shock than a wet cell.

General Electric and Eagle-Picher design engineers embarked on a preliminary development phase, with the major objective being to provide a shock resistant sterile battery with similar characteristics to standard units. With Eagle-Picher's conventional design and manufacturing processes, Biosatellite batteries weighing 135 lb and giving 14,000 watt-hr have been tested to 30 g's and 82 lb, 4,200 watt-hr batteries for Centaur at 500 g's. These batteries were not tested to the limit and clearly indicate that with the Eagle-Picher construction, higher shocks than those quoted in the ESB report can be achieved. To improve the shock resistance, it was further necessary to prevent the cell plates from moving and improve the binding strength of the negative plate. The manner in which this was done is described in General Electric report TIS 67SD337 and summarized later in this section. With the completely rigid cell pack that this design provides, very high shocks are believed feasible on batteries weighing 200 lb, a size far beyond that envisioned for the Mars Hard Lander.

To provide high power densities and be capable of sterilization it was apparent that single cell sterilization is not the best approach. A unique battery construction was devised which is also described in General Electric report TIS 67SD337 and summarized in this section.

A standard positive plate supported on a silver expanded grid was used in conjunction with a zinc oxide negative with approximately 2 percent polyethylene as a binder, mercuric oxide for long stand capability, and MnO_2 as an expander permitting improved redistribution during recharge.

The electrodes were separated by 0.002 in. polypropylene felt wrapped around each plate and six layers of modified Permion 307 Mn, "U" wrapped around the positive electrodes. The Permion separater was the type normally rejected by battery manufacturers screening tests because of excess porosity. Modification by soaking in permanganate and washing in oxalic acid increased the high temperature performance while reducing the pore size to a satisfactory level by filling the voids with MnO_2.

Polypropylene cases of normal thickness and fitted with relief valves were used* to house the cell packs and were bonded to the base of the cells. 45 percent KOH electrolyte was added.

Six such cells were connected in series and encapsulated in a stainless steel canister having an hermetically sealed lid. A water saturated pad was attached to the inside of the lid before sealing. See figs. 5.3-12 and 5.3-13.

Sterilized in this form, evaporation of electrolyte was prevented by the equalizing pressure of water vapor from the pad on the lid which kept the cell vents closed. The stainless steel can was designed to support the internal pressure, thus removing the need for heavy single cell design. Within the cell certain changes took place which provided a robustness for shock survival. Partial softening of the additives in the negative and the polypropylene felt provided some adherence of components across the whole cell pack. This in no way affected the performance of the semi-permeable membrane.

After sterilization in accordance with JPL Spec GMP-50436-O, SN-A and shocks of 2000-g six times in each axis, two batteries provided data that were used as the basis for the parametric study. One battery, stored in the charged state, exceeded 13 months life and another, which was stored in the discharged state for 10 months, still continues cycling after 34 months life. Table 5.3-8 gives performance data.

The battery that failed after 13 months was examined to determine the cause of failure and to investigate shock damage, if any. Failure was partially due to loss of hermetic seal in the battery case probably through a damaged glass-to-metal terminal. This loss caused some dehydration of the cells. Charged wet stand accelerated the normal electro-chemical degradation and migration of silver and zinc through the separators was extensive. The shock tests had no visible effect on the cells except for rippling of the folded edges of the separators. The resilience of the separator was sufficient to prevent fracture. GE TIS 67SD337 gives a complete analysis.

*Cells had relief valves to permit gassing into an hermetically sealed outer can.

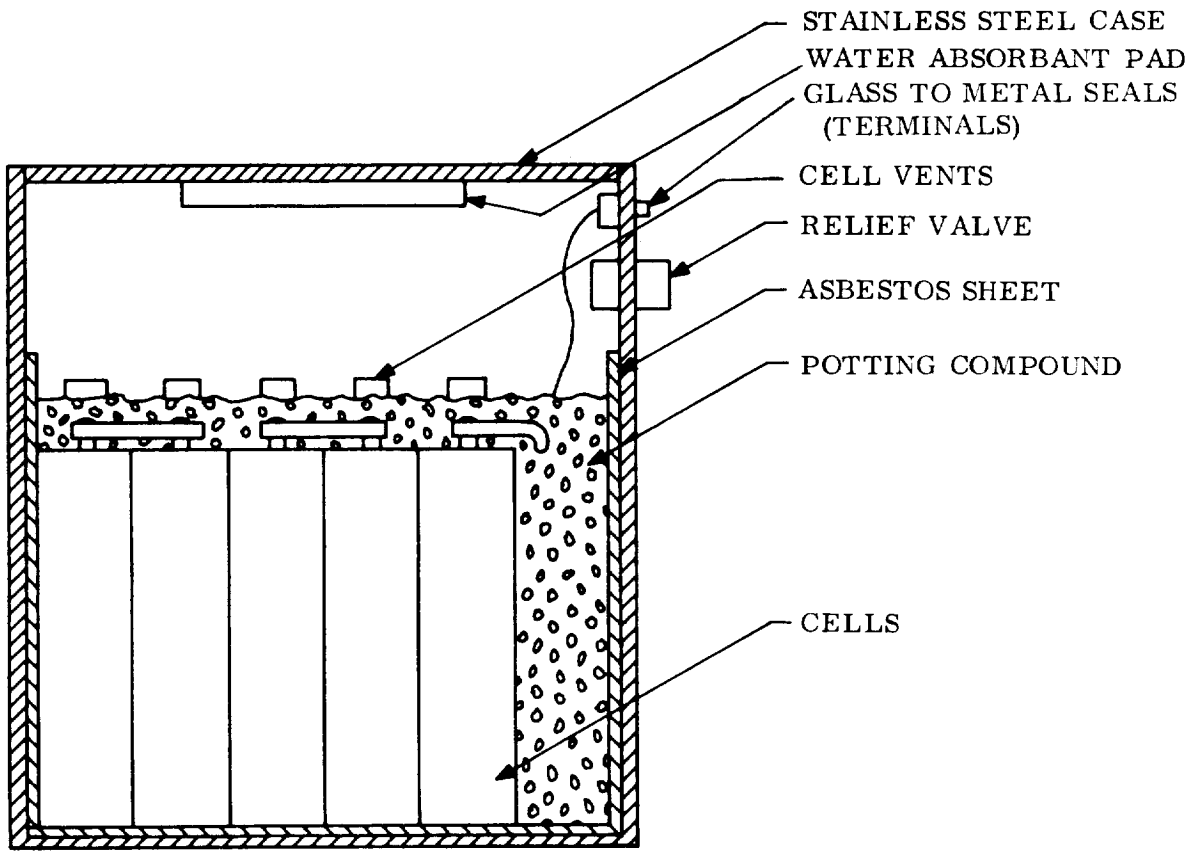

Figure 5.3-12 Battery Design

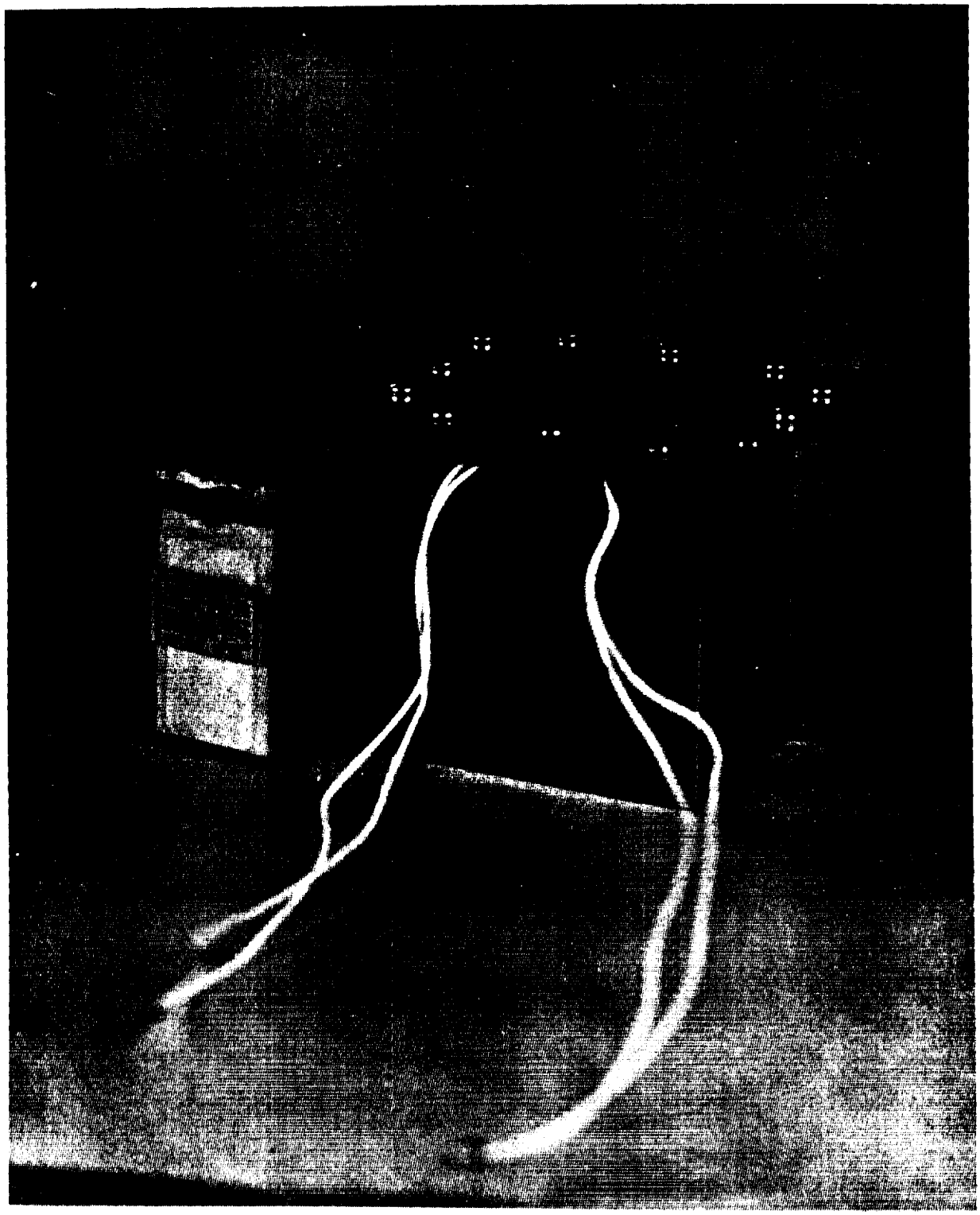

Figure 5.3-13. Battery, Model N3HT, and Individual Cell

TABLE 5.3-8. MEASURED DATA ON THE STERILIZED SILVER - ZINC SECONDARY EXPERIMENTAL BATTERIES

Wh/lb	Date	Stand Days	Charge MA	Gap AH	D/Charge Amps	Cap AH	Nom V	Cycle No.	Util Charge	Util Origin
40.2	10-1-65		500			11.5	8.4	1		- - -
34.2	10-1-65	2	500		2.5	9.66	8.5	2		83.5
39.4	12-14-65	7	500		2.5	10.75	8.8	3		93.5
41.4	1-9-67	25	500/100	12.0	2.5	11.25	8.82	4	93.8	98
38.1	4-4-67	83	500/100	8.4	2.5	10.54	8.7	5	126	92
37.3	4-12-67	7	500/100	10.55	2.5	10.2	8.77	6	96.8	89
38.2	4-20-67	3	500/100	10.54	2.5	10.4	8.8	7	98.6	90.5
34.8	4-26-67	5	500/100	9.7	2.5	9.5	8.8	8	98	82.7
36.4	5-4-67	7	500/100	9.7	2.5	10.0	8.75	9	103	87
34.6	5-15-67	10	500/100	10.07	2.5	9.5	8.73	10	88.7	82.7
34.2	5-23-67	7	500/100	8.78	2.5	9.4	8.74	11	99.5	81.8
30.2	5-31-67	2	500/100	9.57	2.5	8.4	8.6	12	88	73
30	6-8-67	1	500/100	8.8	2.5	8.3	8.7	13	94.4	72
29.4	6-14-67	1	500/100	8.8	2.5	8.14	8.67	14	92.5	71
27	6-21-67	1	500/100	8.0	2.5	7.75	8.68	15	97	67.4
26.8	7-19-67	21	500/100	8.2	Various	7.41	- -	16	90	64
26.5	7-28-67	2	500/100	9.3	Various	7.53	- -	17	81	66
26.1	9-12-67	41	500/100	7.31	Various	7.31	- -	18	100	63.5
25.3	10-20-67	31	500/100	7.82	2.5	7.32	8.65	19	94	63.8
21.5	12-7-67	5	500/100	5.44	2.5	6.0	8.6	20	111	52.2
23.5	1-2-68	30	500/100	6.31	2.5	6.55	8.6	21	102	57
25.2	3-11-68	18	500/100	7.5	2.5	7.06	8.6	22	94	61.5
24.8	5-6-68	2	500/100	7.88	0.5	6.94	8.6	23	88.1	60.2
14.4	5-13-68	1	1,.5,.1	2.82	0.5	4	8.6	24	142	35.0
21.5	5-14-68	1	1,.5,.1	5.73	0.5	6	8.6	25	113	52.1
19.85	5-15-68	1	1,.5,.1	5.97	0.5	5.55	8.6	26	93	48.3
19.65	5-16-68	1	1,.5,.1	6.0	0.5	5.5	8.6	27	91.5	48
19.65	5-17-68	1	1,.5,.1	5.28	0.5	5.5	8.6	28	104	48
18.4	5-20-68	1	1,.5,.1	5.09	0.5	5.15	8.6	29	101	45
17.9	5-21-68	1	1,.5,.1	5.02	0.5	5.0	8.6	30	96	43.5
17.55	5-22-68	1	1,.5,.1	4.88	0.5	4.9	8.6	31	100	42.7
17.3	5-23-68	1	1,.5,.1	4.77	0.5	4.85	8.6	32	102	42.2
22.6	5-24-68	1	1,.5,.1	7.58	0.5	6.3	8.6	33	83	50.9
18.3	5-28-68	1	1,.5,.1	5.19	0.5	5.1	8.6	34	98	44.3
17.6	5-29-68	1	1,.5,.1	4.96	0.5	4.9	8.6	35	99	42.7
17.2	5-31-68	1	1,.5,.1	4.67	0.5	4.8	8.6	36	101.5	41.7
16.85	6-5-68	1	1,.5,.1	4.81	0.5	4.7	8.6	37	97.5	40.9
17.2	6-3-68	1	1,.5,.1	4.81	0.5	4.82	8.6	38	100	41.9
15.9	6-6-68	1	1,.5,.1	4.61	0.5	4.45	8.6	39	92.5	38.8
19.8	6-7-68	1	500/100	6.03	0.5	5.55	8.6	40	92	48.2
22.2	6-14-68	1	500/100	9.43	0.5	6.2	8.6	41	65.6	54.0

The test data presented in this report shows that the GE-RS/Eagle-Picher design has adequate wet stand capability, cycle life and shock resistance.

This design concept appears to be more acceptable for Hard Lander vehicle designs than other alternatives in terms of weight, volume and shock resistance performance. In spite of 100 percent success on the cells and batteries, and high confidence in reproducibility, insufficient testing has been performed to offer reliability figures.

5.3.4.2 Selected Approach

At the present time and until more data is available to prove otherwise, the GE-RS/Eagle-Picher design has been selected for this vehicle design. Parametric data was evolved from the GE TIS Report No. 67SD337, and is detailed in the Mars Hard Lander Capsule study report No. NASA CR-66678-4. The parametrics included varying functions of mission duration, maximum temperature, minimum temperature, demand factor, wet stand life, cycles, shock, and vibration. By studying the effects of these parameters on each other, advantages to the battery were defined in this vehicle design. The two variables are power and demand factor and these are shown in figs. 5.3-14 to 5.3-17.

5.3.4.3 Battery Definition

On the basis of the empirical analysis and battery selection criteria the battery design was determined as follows:

1. Battery Type - Sterilizable silver-zinc batteries of the GE-RS/Eagle-Picher design.

2. Requirements -

Potential	24 to 33.5 volts
Average power	21.2 watts
Peak power	300 watts
Discharged duration cycles	90.6 hr
Charged activated wet stand	10 days

3. Environmental Conditions -

Minimum temperature	$50^{o}F$
Maximum temperature	$80^{o}F$
Shock level	2400 g's
Vibration level	10 g's

4. Physical Characteristics -

Total Weight	65 lb
Total Volume	870 in.^{3}
Number of cells	20

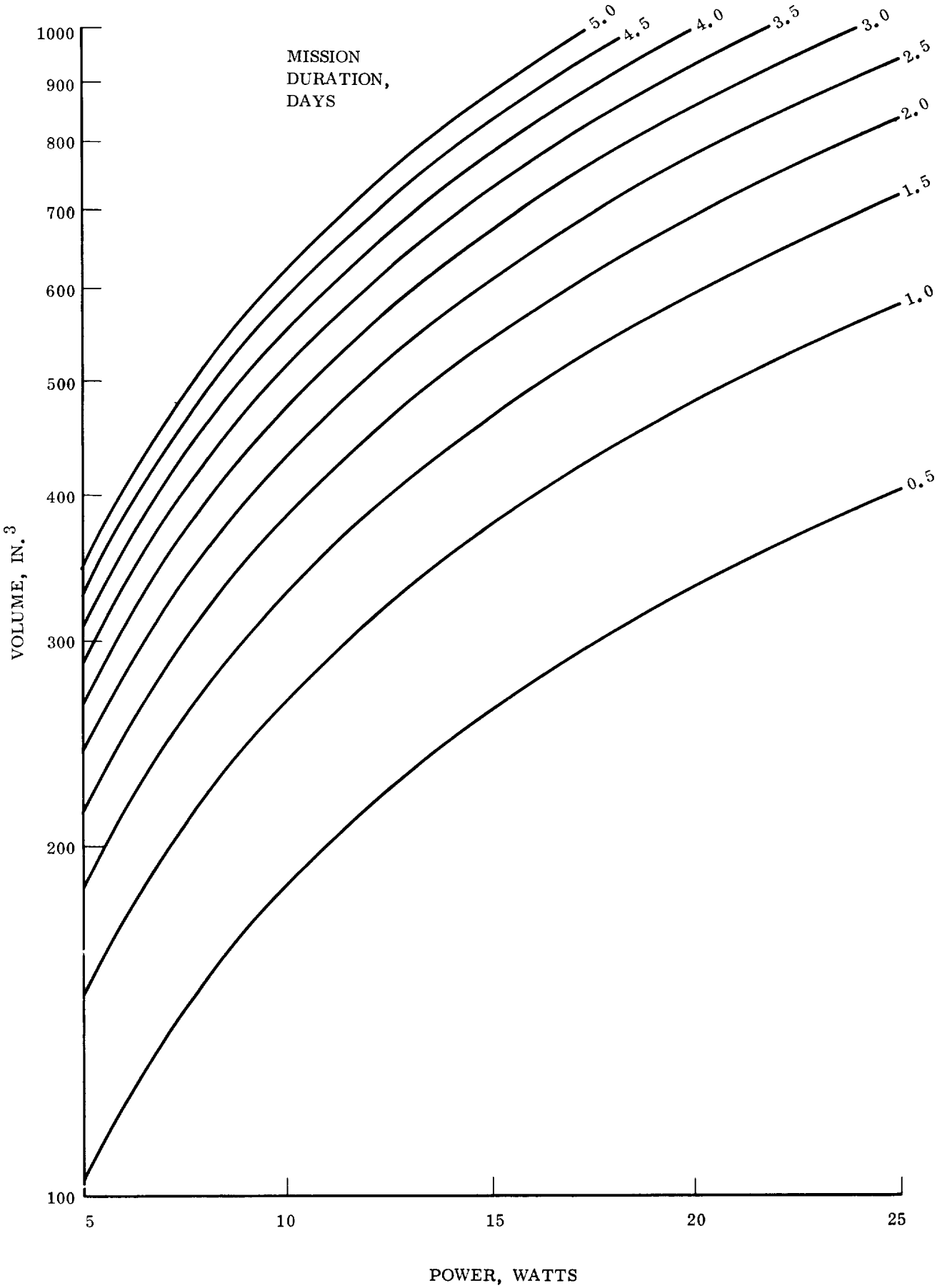

Figure 5.3-14. Power vs Volume

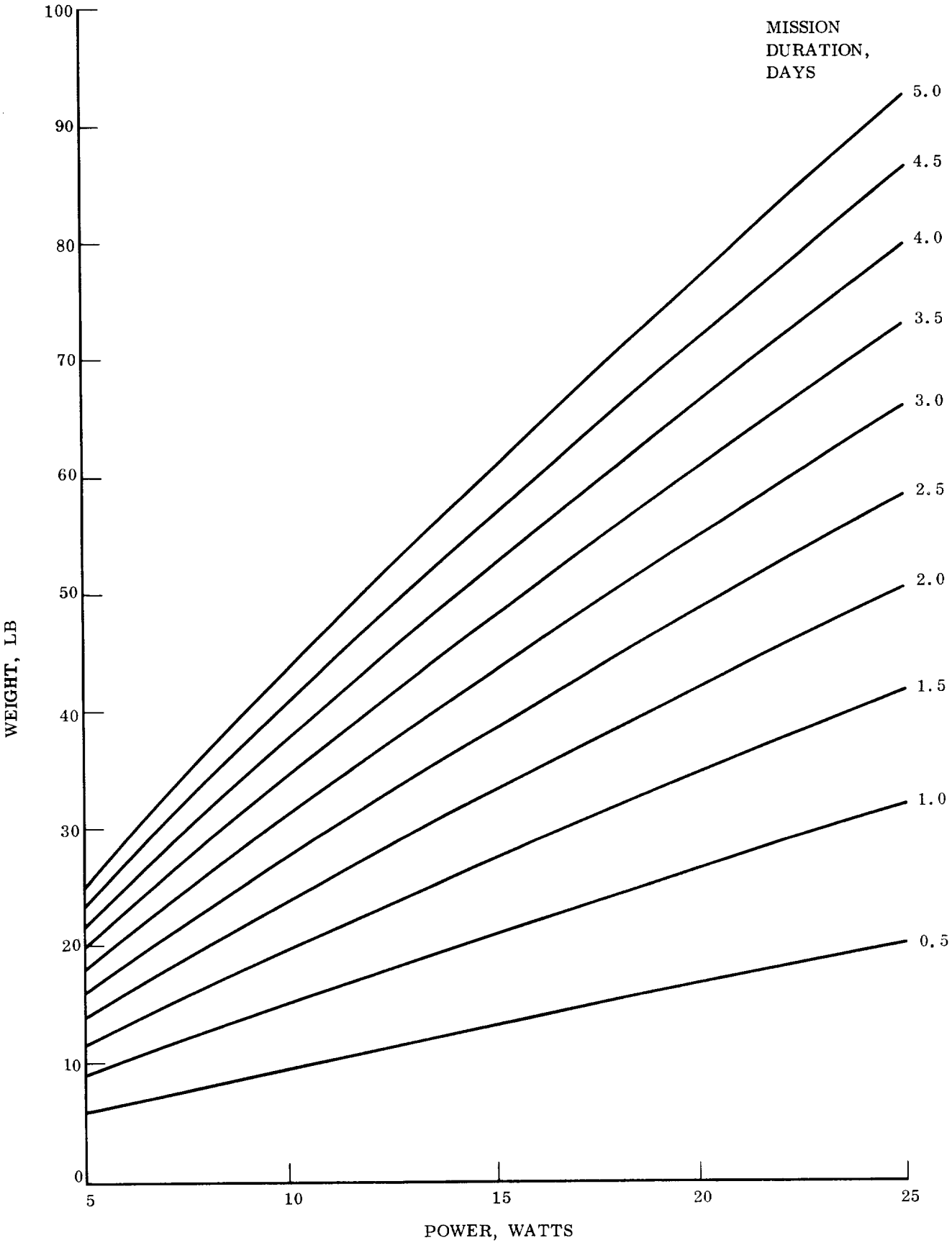

Figure 5.3-15. Power vs Weight

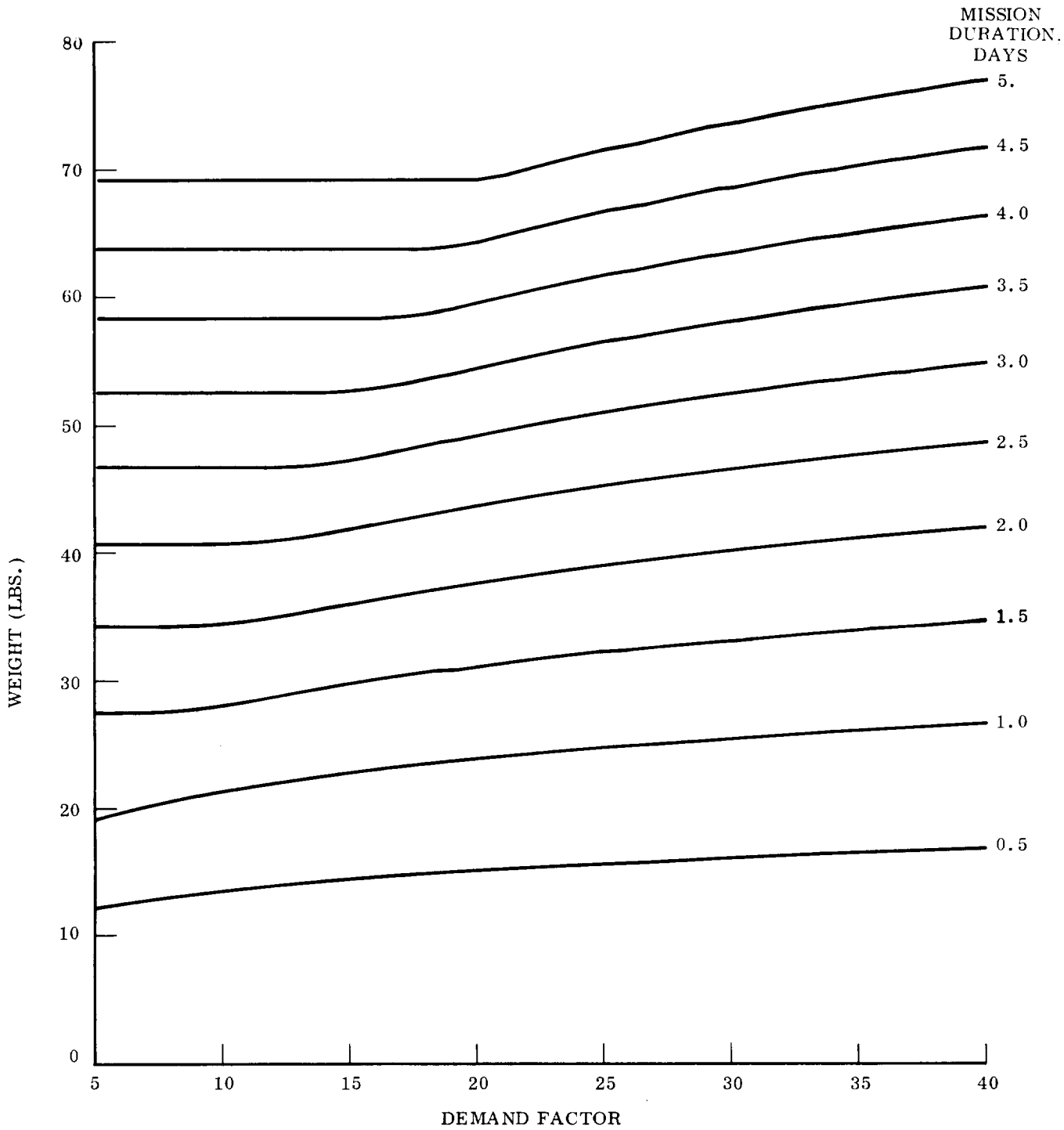

Figure 5.3-16. Demand Factor vs Weight

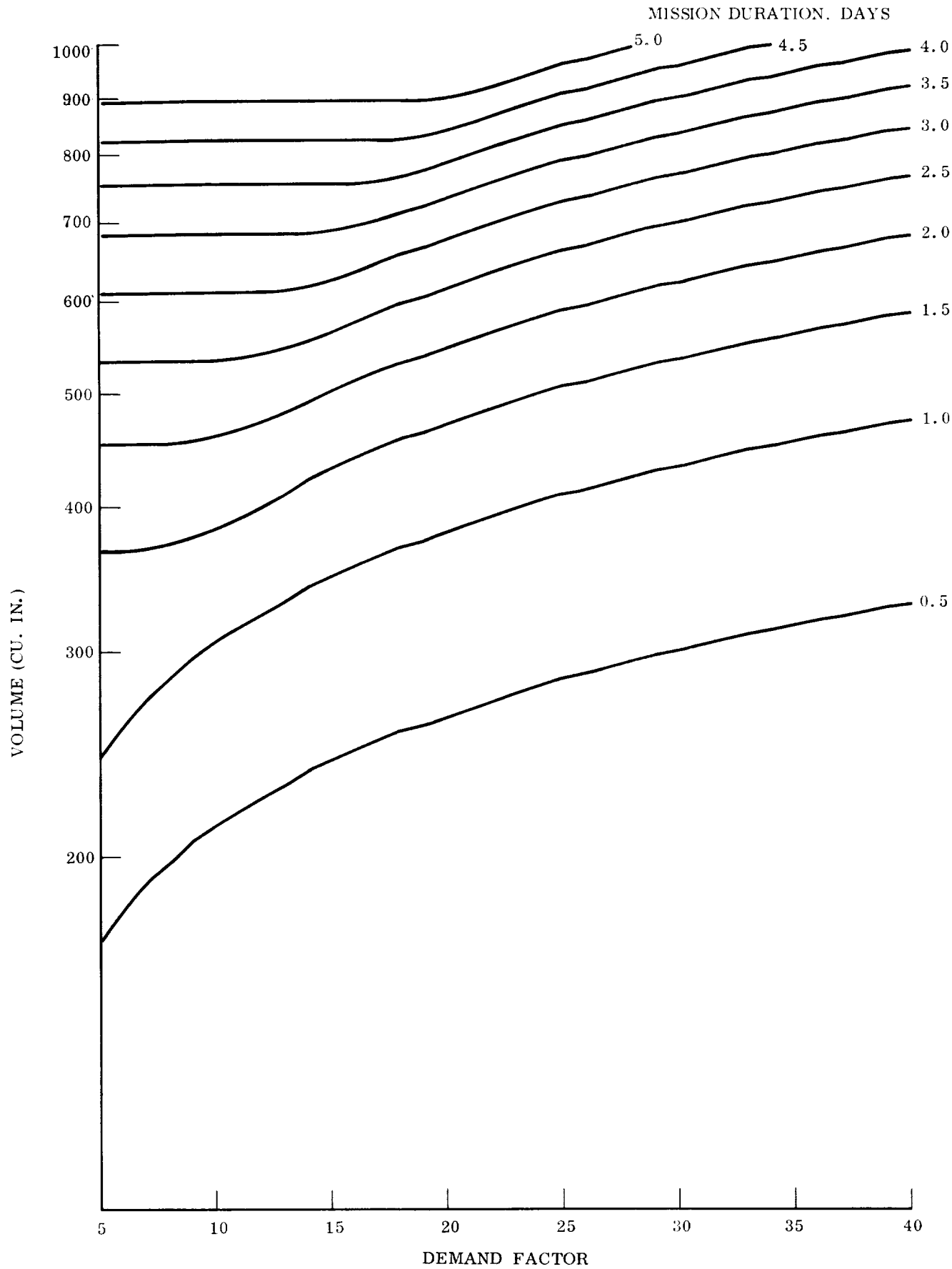

Figure 5.3-17. Demand Factor vs Volume

5.4 COMPUTER AND SEQUENCER

5.4.1 FUNCTIONAL REQUIREMENTS

The function of the Computer and Sequencer is to control the conduct of the Hard Lander mission after separation from the Support Module. This is accomplished by providing a sequence of commands to other subsystems to initiate a certain operation or to change the operating mode. The commands which the Computer and Sequencer must issue are given in table 5.4-2 with explanations listed in table 5.4-1.

In addition to its primary function of providing this command sequence, the Computer and Sequencer also;

1. Provides a command decoding capability which, in conjunction with the Lander or Support Module communication link, allows direct commands from Earth to the Lander. These commands can be used to update the stored sequence, or be used directly to effect a desired operation.

2. Provides memory capacity for storage of entry data, and storage of surface science data after landing.

5.4.2 BASELINE IMPLEMENTATION

5.4.2.1 General Concept

The Computer and Sequencer design, which is illustrated in fig. 5.4-1, utilizes a stored sequence of words in a random access memory which is capable of being updated at any time during the mission. The words are read out one at a time and operated upon. The operation involves decoding the two parts of the word - the time tag and the function tag. The function tag, when decoded, instructs the Computer and Sequencer as to which output to energize, or, in the case of special commands, which special mode of operation to enter. The time tag, when decoded, defines the actual time at which the function bits are to be executed. Each command in the sequence is referenced in time to the previous command. That is the time tag stores incremental or elapsed time between commands.

By storing incremental time, rather than storing large words with absolute time tags and comparing them against a continuously accumulating running clock, a considerable saving in memory size results. When the stored sequence of command words have been loaded into the memory the Computer and Sequencer may be initialized to the first memory location and started in one of two ways: by the receipt of a real time command through the command link, or by a discrete input from a physical event (such as separation from the Support Module). Once the sequence has been started at the first memory location, the Computer and Sequencer will automatically operate on each word in the memory, going to the next word when operation on the current word has been completed. Capability has been

Table 5.4-1 is a list of explanations for use with the command list.

TABLE 5.4-1. COMMAND ABREVIATIONS

Abbreviation	Command
CD	Command Decoder
CS	Computer and Sequencer
DHS	Data Handling System
DM	Data Mode
LCE	Launch Complex Equipment
N_2	Nitrogen
Orb CS	Orbiter (or Support Module) Computer and Sequencer
SS	Subsystem
TM	Telemetry Mode
Source	Prime Source of the Command
Dest	Destination of the Command
Bk up	Backup to the prime command source. Only immediately obvious ones are listed. Further study should reveal other backups.
( )	Times shown in parenthesis are the times at which events which are not controlled by the Computer and Sequencer occur.

TABLE 5.4-2. MARS HARD LANDER SEQUENCE OF COMMANDS

Item	Datum	hr	Time min	sec	Command	Source	Bk Up	Dest
Pre-launch								
	L	-24	----	----	Insert stored commands	LCE	None	CS
Launch-Injection								
Interplanetary Cruise								
Mid Course Maneuver								
Separation		(S)						
1	S	-240	00	----	Charge capsule battery	Orb CS	Orb CD	Power
2	S	- 25		----	Terminate charge	Orb CS	Orb CD	Power
3	S	- 25	----	----	Capsule checkout sequence	Orb CD	Orb CS	All SS
4	S	- 25	----	----	DHS to TM 1	OCD		DHS
5	S	- 25	----	----	DHS to DM 1	OCD		DHS
6	S	- 23	----	----	End Capsule checkout			
7	S	- 23	----	----	Remove Lander power	Orb CS	Orb CD	Orb power
8	S	- 23	----	----	Charge battery	Orb CS	Orb CD	Power

TABLE 5.4-2. MARS HARD LANDER SEQUENCE OF COMMANDS (Continued)

Item	Datum	Time hr	Time min	Time sec	Command	Source	Bk Up	Dest
9	S	- 08	----	----	Terminate battery charge	Orb CS	Orb CD	Power
10	S	- 04	02	----	Capsule CS to master sequence	Orb CD CS	Orb CS	Cap CS
11	S	- 04	00	----	Arm pyro	CS	Orb CD	Pyro (power)
12	S	- 04	00	____	Relieve canister pressure	CS	Orb CD	Power
13	S	- 01	-30	____	Separate forward canister	CS	Orb CD	Pyro
					Orbiter maneuvers to separation attitude			
14	S	(00	-20	----)	Attitude verified			
15	S	00	-03	----	Turn on Lander power (Seal Main contactor)			
					Spin control system (gyro and elec)	CS		Power
16					Data handling system	CS		Power
17	S	00	-03	----	DHS to mode TM 1	CS		DHS
18	S	00	-03	----	DHS to DM 1	CS		DHS
19	S	00	-03		Remove Orb power	CS		Power
20	S	00	-03	----	Enable separation	OCD		CS
21	S	00	00	----	Separate IFD -1	Orb CS		Pyro
22	S	00	00	----	Separate	Orb CS		Pyro
23	S	00	00	----	DHS to DM-2	CS		DHS
24	S	00	00	----	Turn on relay transmitter	CS	Sep. Sens.	Power

TABLE 5.4-2. MARS HARD LANDER SEQUENCE OF COMMANDS (Continued)

Item	Datum	Time hr	Time min	Time sec	Command	Source	Bk Up	Dest
Path Deflection								
25	S	00	00	00	Enable N_2 system	CS		Pyro
26	S	00	00	00.5	Spin rate command to 25 rpm	CS		Spin control
27	S	00	00	00.5	Enable valve power switches	CS		Power
28	S	00	00		Disable valve power switches	CS		Power
29	S	00	05	----	Turn off:			
30					DHS	CS		Power
31					Spin control system	CS		Power
32					Relay transmitter	CS		Power
33	S	00	05	----	CS to standby mode	CS		CS
34	S	00	28	----	CS to operate mode	CS		CS
35	S	00	28	----	Turn on:			
36					DHS	CS		Power
37					Spin control	CS		Power
38					Relay transmitter	CS		Power
39	S	00	28	----	DHS to TM 1	CS		DHS
40	S	00	28	----	DHS TO DM 2	CS		DHS
41	S	00	30	00	Engine ignition	CS		Pyro
42	S	(00	30	51)	Engine shut down (accelerometer)	SCS	CS (time)	Pyro
43	S	00	32	00.0	Separate IFD -2	CS		Pyro
44	S	00	32	00.0	Separate thrust cone	CS		Pyro

TABLE 5.4-2. MARS HARD LANDER SEQUENCE OF COMMANDS (Continued)

Item	Datum	Time hr	Time min	Time sec	Command	Source	Bk Up	Dest
45	S	00	35	----	Turn off:			
46					Spin control system	CS		Power
47					Data handling system	CS		Power
48					Relay transmitter	CS		Power
49	S	00	35	----	CS to Standby mode	CS		CS
Cruise								
50	S	01	00	----	CS to operate mode	CS		CS
51	S	01	00	----	Turn on:			
52					Data handling system	CS		Power
53					Relay transmitter	CS		Power
54		01	00	----	DHS to TM 1	CS		DHS
55	S	01	00	----	DHS to DM 2	CS		DHS
56	S	01	01	----	Turn off:			
57					Data handling system	CS		Power
58					Relay transmitter	CS		Power
59	S	01	01	----	CS to standby mode	CS		CS
					Repeat the above turn-on/turn-off cycle once every hour until entry. There will be a total of about 23 cycles.			
Entry	(E)							
60	E	00	-06	----	CS to operate mode	CS		CS

TABLE 5.4-2. MARS HARD LANDER SEQUENCE OF COMMANDS (Continued)

Item	Datum	Time hr	Time min	Time sec	Command	Source	Bk Up	Dest
61	E	00	-06	----	Turn on:			
62					Data handling system	CS		Power
63					Relay transmitter	CS		Power
64	E	00	-06	----	DHS to TM 1	CS		DHS
65	E	00	-06	----	DHS to DM 2	CS		DHS
66					Turn on:			
67	E	00	-06	----	Spin control	CS		Power
68	E	00	-06	----	Mass spectrometer	CS		Power
69	E	00	-06	----	Spin rate command to 0 rpm	CS		
70	E	00	-06	----	Enable g switch	CS		
71	E	00	-06	----	DHS to TM 2	CS	0.1g switch	DHS
72	S	(24	12	18)	Nominal entry time (E = 0)		0.1g switch	Power
73	E	00	00	----	Turn on radar altimeter	CS	0.1g switch	Power
74	E	(00 +	01	24)	Enable valve power switches (apply power)	0.1g switch	CS	Power
75	E	(0 +	02	28)	Enable mass spectrometer M5 (open stagnation port)	Altimeter		Power
Terminal		(T)						
76	E	(00 +	04	05)	Deploy parachute (mortar deploys pilot extraction parachute - 4000 ft altitude)	Radar		Power and CS
77	T Datum	00	00	----				

TABLE 5.4-2. MARS HARD LANDER SEQUENCE OF COMMANDS (Continued)

Item	Datum	Time hr	Time min	Time sec	Command	Source	Bk Up	Dest
77A	T	00	00 +	01	Turn off radar	CS		Power
78	T	00	00	----	Close Mass spec stagnation port	CS		Science
79	T	00	00	----	Open mass spectrometer base port	CS		Science
80	T	00	00	----	Disable valve power switches	CS		Power
81	T	00	00	----	Turn power off spin control	CS		Power
82	T	00	00	----	Switch to radar antenna on Lander	CS		Radar
83	T	(00	00	01.7)	Reefing line cutter fired			Pyro
84	T	(00	00	04.3)	Reefing line cutters cut			
85	T	00	00	05	Separate IFD -3 (Lander-aeroshell)	CS		Pyro
86	T	00	00	05	Separate aeroshell	CS 030		Pyro
87	T	(00	00	05.4)	Main parachute fully inflated			
88	T	00	00	06	Turn on radar	CS		Power
89	T	(00 +	00	07	Switch to Lander relay antenna	CS	CS	Radio
90	T	(00	00	32)	150 ft Altitude Sensed	CS		CS
91	T	(00 +	00	33)	Turn off power radar altimeter	CS		Power
92	T	00 +	00	33	Operate Guillotine	CS		Pyro
93	T	00 +	00	33	Separate parachute	CS		Pyro
94	T	(00 +	00	34)	Touchdown occurs - impact sensed			
95	T	(00 +	00	34)	DHS to TM 3	Impact sensor		DHS
Initial Landed Operations								
96	T change	(00 +	02	34)	Lander comes to rest - up direction sensed - landed operations begin	Mercury Switches		CS

TABLE 5.4-2. MARS HARD LANDER SEQUENCE OF COMMANDS (Continued)

Item	Datum	Time hr	min	sec	Command	Source	Bk Up	Dest
97	G	00	00	00	Apply power to:			
98					UHF transmitter	CS		Power
99					DHS	CS		Power
100	G	00	00	00	DHS to TM 3	CS		DHS
101	G	00	00	----	Turn off mass spectrometer	CS		Power
102	G	00	00	----	Switch to "up" relay antenna	CS		Radio
103	G	00	00	----	Release "up" hatch (cameras deploy)	CS		Pyro
104	G	00	00	05	Deploy down soil sampler	CS		Pyro
105	G	00	00	05	DHS to DM 3	CS		DHS
106	G	00	00	10	Release vertically oriented antenna	CS		Power
107	G	00	00	30	Turn on photo imagery	CS		Power
108	G	00	00	35	Camera 1 to position 1 low resolution	CS		Science
109	G	00	00	35	Camera 2 to position 1 low resolution	CS		Science
110	G	00	00	35.00	DHS to TM 3	CS		DHS
111	G	00	00	35.05	DHS to TM 6	CS		DHS
112	G	00	00	35.1	DHS to TM 8	CS		DHS
113	G	00	00	36.0	DHS to TM 4	CS		DHS
114	G	00	00	53.0	Start picture 1 on camera 1 (ends in 17 sec)	CS		Science

TABLE 5.4-2. MARS HARD LANDER SEQUENCE OF COMMANDS (Continued)

Item	Datum	Time hr	Time min	Time sec	Command	Source	Bk Up	Dest
115	G	00	01	10	Start picture 2 on camera 2	CS		Science
116	G	00	01	10	Camera 1 to position 1 high resolution	CS		Science
117	G	00	01	27	Start picture 3 on camera 1	CS		Science
118	G	00	01	27	Camera 2 to position 1 high resolution	CS		Science
119	G	00	01	44	Start picture 4 on camera 2	CS		Photo Imagery
120	G	00	01	44	Camera 1 to position 2 low resolution	CS		Photo Imagery
121	G	00	02	01	Start picture 5 on camera 1 (these commands continue for position 2 then 3, etc., until 6 positions have been covered by both cameras at both high and low resolution. There are a total of 48 commands).	CS Total of 48 commands		Photo Imagery
122	G	00	07	35	End picture 24	CS		Photo Imagery
123	G	00	07	35.00	DHS to TM 3	CS		DHS
124	G	00	07	35.05	DHS to TM 6	CS		DHS
125	G	00	07	35.10	DHS to TM 8	CS		DHS
126	G	00	07	36.00	DHS to TM 4 repeat picture taking sequence two more times for a total of three picture taking sequences end with:	CS		DHS

TABLE 5.4-2. MARS HARD LANDER SEQUENCE OF COMMANDS (Continued)

Item	Datum	Time hr	min	sec	Command	Source	Bk Up	Dest
127	G	00	21	53.00	DHS to TM 3	CS		DHS
128	G	00	21	53.05	DHS to TM 6	CS		DHS
129	G	00	21	53.10	DHS to TM 8	CS		DHS
Daily Ground Operations								
130	G	00	22	00	Turn off:			
131	G				UHF transmitter (relay)	CS		Power
132	G				Photo imagery	CS		Power
133	G	00	25	----	DHS to TM 3	CS		DHS
134	G	00	25	----	DHS to DM 6	CS		DHS
135	G	00	25	----	Turn on soil sampler	CS		Power
136	G	00	25	----	Turn on power to antenna control	CS		Power
137	G	00	25	----	Turn on gas chromatograph	CS		Power
138	G	00	25	----	Calibrate gas chromatograph	CS		DHS
139	G	00	30	----	DHS to TM 3	CS		DHS
140	G	00	30	----	DHS to DM 6	CS		DHS
141	G	00	30	----	Turn off power to antenna control	CS		Power
142	G	00	35	----	DHS to TM 3	CS		DHS
143	G	00	35	----	DHS to DM 6	CS		DHS
144	G	00	40	----	DHS to TM 3	CS		DHS
145	G	00	40	----	DHS to DM 6	CS		DHS
146	G	00	45	----	DHS to TM 3	CS		DHS
147	G	00	45	----	DHS to DM 6	CS		DHS

TABLE 5.4-2. MARS HARD LANDER SEQUENCE OF COMMANDS (Continued)

Item	Datum	Time hr	min	sec	Command	Source	Bk Up	Dest
148	G	00	45	----	Turn off power to soil sampler	CS		Power
149	G	00	45	----	Turn on mass spectrometer	CS		Power
150	G	00	45	----	Close base pressure port	CS		Power
151	G	00	45	----	Calibrate mass spectrometer	CS		Science
152	G	00	50	----	DHS to TM 3	CS		DHS
153	G	00	50	----	DHS to DM 6	CS		DHS
154	G	00	50	----	Open base pressure port	CS		Power
155	G	00	55	----	DHS to TM 3	CS		DHS
156	G	00	55	----	DHS to DM 6	CS		DHS
157	G	00	55	----	Close base pressure port	CS		Power
158	G	00	55	----	Open soil input valve	CS		Power
159	G	00	55	----	Turn on pyrolizer to low temperature	CS		Power
160	G	00	55	----	Turn on water detector	CS		Power
161	G	00	55	----	Open inlet valve water detector	CS		Power
162	G	00	55	----	DHS to TM 9	CS		DHS
163	G	00	55	----	DHS to DM 6	CS		DHS
					repeat lines 162 and 163 at 1 min intervals for 20 min			
164	G	01	05	----	Turn pyrolyzer off	CS		Power
165	G	01	05	----	Warm up life detector	CS		Power
166	G	01	15	----	Close inlet valve water detector	CS		Power
167	G	01	15	----	Turn power off - water detector	CS		Power

TABLE 5.4-2. MARS HARD LANDER SEQUENCE OF COMMANDS (Continued)

Item	Datum	Time hr	min	sec	Command	Source	Bk Up	Dest
168	G	01	55	----	Turn on pyrolizer high temperature	CS		Power
169	G	01	55	----	Turn on water detector	CS		Power
170	G	01	55	----	Open inlet valve water detector	CS		Power
171	G	01	55	----	DHS to TM 9	CS		DHS
172	G	01	55	----	DHS to DM 6	CS		DHS
					repeat lines 171 and 172 at 1 min intervals for 20 min			
173	G	02	05	----	Turn pyrolizer off	CS		Power
174	G	02	15	----	Close inlet valve water detector	CS		Power
175	G	02	15	----	Turn power off - water detector	CS		Power
176	G	02	20	----	DHS to TM 7	CS		DHS
177	G	02	20	----	DHS to DM 6	CS		DHS
178	G	02	45	----	DHS to TM 6	CS		DHS
179	G	02	45	----	DHS to DM 6	CS		DHS
180	G	03	05	----	Turn off:			
181	G				Mass spectrometer	CS		Power
182	G				Gas chromatograph	CS		Power
183	G	03	05	----	DHS to TM 7	CS		DHS
184	G	03	05	----	DHS to DM 6	CS		DHS
185	G	03	05	02	Turn off DHS	CS		Power
186	G	03	05	02	CS to standby mode	CS		CS
187	G	03	25	00	CS to operate	CS		CS

TABLE 5.4-2. MARS HARD LANDER SEQUENCE OF COMMANDS (Continued)

Item	Datum	Time hr	Time min	Time sec	Command	Source	Bk Up	Dest
188	G	03	25	00	Turn on DHS	CS		Power
189	G	03	25	00	DHS to TM 6	CS		DHS
190	G	03	25	00	DHS to DM 6	CS		DHS
191	G	03	25	02	Turn off DHS	CS		Power
192	G	03	25	02	CS to standby mode	CS		CS
193	G	03	45	00	CS to operate	CS		CS
194	G	03	45	00	Turn on DHS	CS		Power
195	G	03	45	00	DHS to TM 7	CS		DHS
196	G	03	45	00	DHS to DM 6	CS		DHS
197	G	03	45	02	Turn off DHS	CS		Power
198	G	03	45	02	CS to standby mode	CS		CS
					Events of line 193 to line 198, inclusive are repeated with a period of 20 min until:			
199	G	16	30	----	Turn on command receiver and detector	CS		Power
200	G	16	30	----	Turn on command decoder	CS		Power
201	G	17	15	----	CS to operate mode	CS		CS
202	G	17	15	----	Turn on DHS	CS		Power
203	G	17	15	----	Turn on S-band transmitter	CS		Power
204	G	17	15	----	DHS to TM 8	CS		DHS
205	G	17	15	----	DHS to DM 4	CS		DHS
206	G	17	45	----	Turn off S-band transmitter	CS		Power

TABLE 5.4-2. MARS HARD LANDER SEQUENCE OF COMMANDS (Continued)

Item	Datum	Time hr	Time min	Time sec	Command	Source	Bk Up	Dest
207	G	17	45	----	Turn off DHS	CS		Power
208	G	17	45	----	Switch S-band transmitter to fixed antenna	CS		Direct link SS
209	G	18	30	----	Turn off command decoder	CS		Power
210	G	18	30	----	Turn off command receiver	CS		Power
211	G	18	30	----	Switch S-band transmitter to vertically oriented antenna	CS		Direct link subsystem
212	G	18	30	----	Start the performance of the sequence beginning with line 137 and continue through line 211			
213	G	43	10	----	Start performance of the sequence beginning with line 187 and continue through line 212			
214	G	67	50	----	End of Mission			

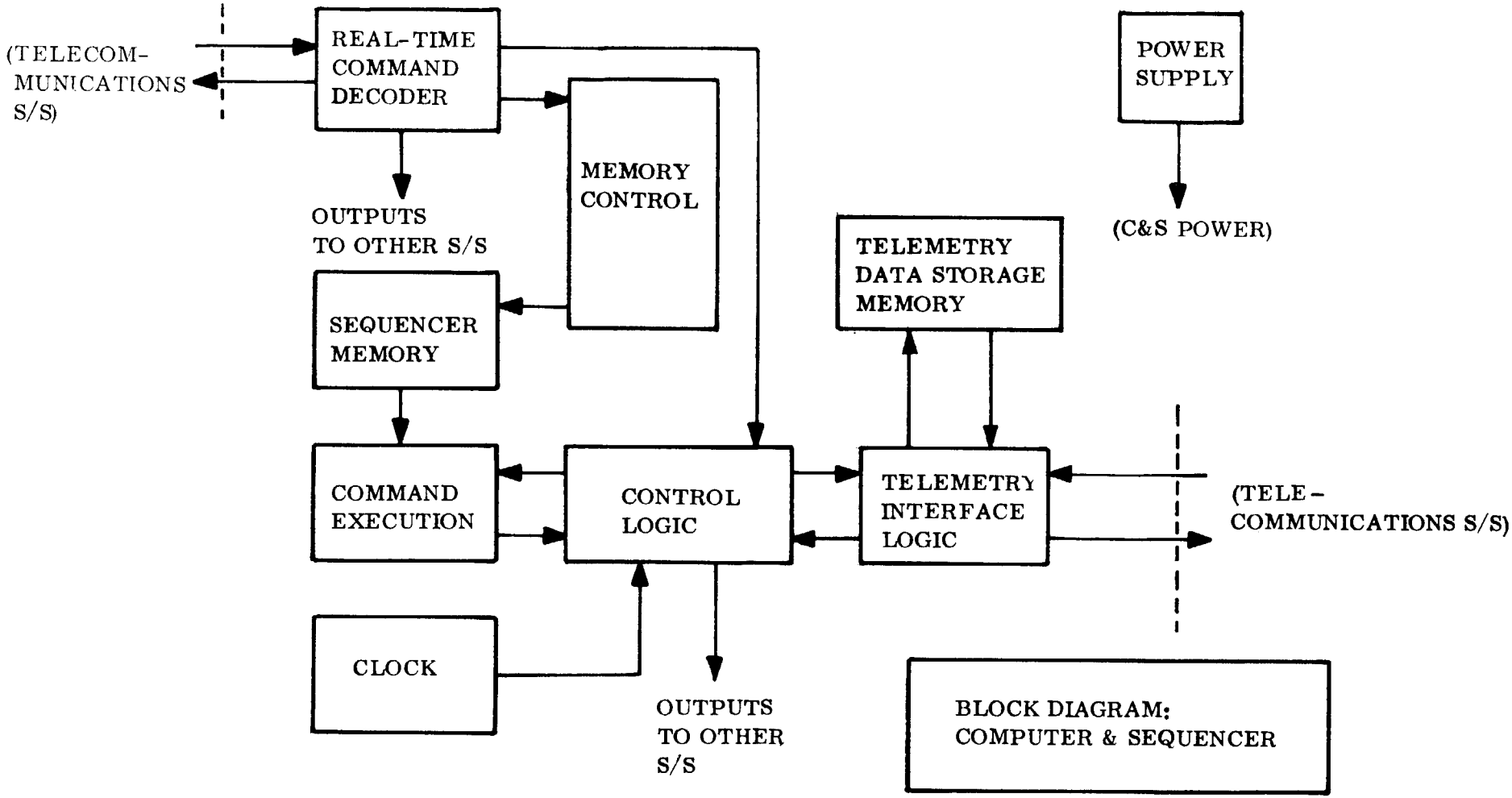

Figure 5.4-1. Computer and Sequencer Block Diagram

built in to permit the Earth to command the following: jumps to the next word, jumps back to the beginning of the memory, random access for memory updating. Special stored commands permit operation in special modes. These are explained in later paragraphs.

Real time Earth originated commands are decoded in the Computer and Sequencer. The major use of real time commands is to update the memory, however, selected other functions may also be performed.

The requirements of telemetry data buffering and data storage will be met by the use of a large telemetry data buffer memory and telemetry interface logic. The Computer and Sequencer will automatically provide a 70 sec delay for black-out data by means of this memory, and will store telemetry data during the entry phase of the mission and on the surface during landed operations. The Computer and Sequencer will provide synchronizing signals to the Telecommunications Subsystem for both read in and read out of data and the Telecommunications Subsystem will have access to the large memory for read in and read out purposes as required.

Emphasis has been placed on developing a design which would minimize power consumption while maintaining a reasonable degree of flexibility.

Several types of implementation are possible in designing the Computer and Sequencer. The most obvious approach is to have a continuously accumulating clock which starts at the beginning of the mission and runs to the end. Words stored in the memory would then have a time tag equal in number of bits to that of the clock. Each word could be uniquely defined in terms of time of mission. For this mission a time tag, for this technique, would be approximately 17 bits in length for a granularity of 1 sec. This takes up an inordinate amount of memory. An alternate approach was sought. The incremental counter approach for a stored program has been utilized on other programs and was proposed in the GE Voyager Preliminary Design. With this technique the time tags that are stored in memory are incremental time tags, and describe the time between the execution of the previous command and the command which they control.

The Computer and Sequencer contains a one pulse/sec clock. This clock is made available to a counter which is pre-set to the number contained in the time tag of the command word currently being operated upon. A counter is then released from the pre-set condition and allowed to count at 1 PPS until it is full. When it is full, the function bits of the command word are executed. The time tag is the command word, therefore, determines the time at which the execution of the current word will occur referenced to the previous word. The granularity of the system is 1 sec, which is sufficient to fulfill all requirements placed on the system. Using this approach, the time tag need only be 8 bits. This is a considerable saving in memory when compared with the 17 bit time tag for a continuously running absolute time system. The incremental counter philosophy was

therefore chosen for the baseline implementation. It is recognized that such an approach must be carefully reviewed in terms of reliability of operation, since the slippage in time of any command will influence the remaining commands. Techniques of reliability have been implemented to forestall any possible catastrophic operation along these lines. These are described in a later paragraph.

5.4.2.2 Stored Command Format

Commands stored in the Computer and Sequencer memory for the purpose of sequencing operations aboard the Lander will each consist of an 8-bit time tag and an 8-bit function tag. Normally, commands stored in the Computer and Sequencer memory will be decoded in real time, i.e., the single 16-bit command work will be operated upon, and its function will be performed according to the time tag contained in the word. These are called "normal stored commands" because they directly operate outputs of the Computer and Sequencer. Other types of stored commands are called "special stored commands". Special stored commands do not yield a function output immediately, but they are used internally to the Computer and Sequencer to cause it to go into special modes of operation.

Examples of special stored commands follow:

1. Extension - sometimes a time tag capability of 256 times 1 sec (the base counting rate) is not enough for an incremental time between commands. In such cases, a sequence of 2 commands stored in the memory is utilized to allow incremental times up to 16 hr. The first command in the series of 2 stored in the memory is a special stored command known as an "extension" command. The extension command, when decoded, causes the Computer and Sequencer to enter the extension mode. No output from the Computer and Sequencer occurs at this time. Then the second command in the series of two is loaded into the processor and is operated upon. The time tag in the second word is utilized as a number, n, which tells the Computer and Sequencer to cycle through the maximum 256 sec cyle, n times.

   When this has been done, the Computer and Sequencer decodes the function bits in the second word in the series (presently in the operation register). The indicated function is performed by providing a low-level output signal. With this method, two 16-bit words stored in the memory can extend the incremental time capability from 256 sec to up to 16 hr with granularity of 1 sec.

2. Wait for Discrete - the "wait for discrete" command stored in the memory is decoded and a flip-flop is set such that no further action takes place in the Computer and Sequencer until a discrete on a particular line is received from another subsystem. This feature can be used to reference any part of the sequence to an expected input discrete event.

3. Enter Loop - an "enter loop" command when operated upon, causes the Computer and Sequencer to go into a loop mode of operation. This type of operation is utilized

to perform repetitive functions. Rather than storing commands to perform these functions many times in the memory, a special sequence of commands is stored in the memory to cause the Computer and Sequencer to automatically loop through the required sequence a number of times. The first word stored in the memory in the special series, when decoded, tells the Computer and Sequencer to enter a particular loop mode. No output is given at this time. The next word in memory is then loaded into the processor section and the time tag bits of this word tell the Computer and Sequencer how many times to loop through the cycle. The function bits in this second word tell the Computer and Sequencer what function(s) to perform and what time to allow between the functions. The Computer and Sequencer will then perform the indicated functions n times where n is the number indicated by the time tag of this second word. This function is very similar to the incrementing function except that more capability is provided by means of the function bits in the second word.

5.4.2.3 Real Time Command Mode

The real time command mode for this system operates with the real time command link available, both from the Earth while the Capsule is on the surface of Mars, and from the Support Module while the Capsule is still attached. The real time command format is an 8-bit word. Data bits, shift pulses and a command enable signal will be provided as inputs to the Computer and Sequencer from the real time command link. The Computer and Sequencer will provide a real time decoding capability for an 8-bit word with up to 256 possible different outputs. Many of these outputs will be provided to external subsystems as low level output signals from the Computer and Sequencer. Several of the outputs, however, will be used internally to the Computer and Sequencer and are listed in table 5.4-3.

TABLE 5.4-3. COMPUTER AND SEQUENCER REAL TIME COMMANDS

Name	Function
Update Stored Time Tag	Change stored time tag in any memory location
Update Stored Time Tag and Function Bits	Change time tag and function bits in any memory location
Start the Sequence	Backup to initiation of sequence by on-board event.
Return to Location Zero	Stop automatic sequencing and restart at memory location zero
Skip to Next Word	Allows emergency bypass of any stored command
Enter Status Check Sequence	Initiates short fixed pattern of outputs to Lander Subsystems for status check
Stop Status Check Sequence	Aborts above sequence

Two of the real time commands are used for memory updating.

The first real time command uses a sequence of three 8-bit real time command words to update a time tag. The first 8-bit word indicates that a time tag update is to be performed, and therefore that two additional command words follow. The new time tag is then sent as the second 8-bit word. The Computer and Sequencer automatically stores the time tag and looks for the next word. The third and final word will give the memory address in which the new time tag should be inserted to complete the update. The second real time command uses a sequence of four 8-bit real time command words. The first word indicates that both the time tag and the function bits are to be updated, and that three additional words follow. Again, the second word is the updated time tag. The third word now contains the new function bits and the fourth and final word of the sequence is the memory address. Using this method of either three or four 8-bit real time command words, the time tag and the function bits of any random address in memory can be changed at will whenever commands can be received.

Other real time commands which are used internally to the Computer and Sequencer are also listed in table 5.4-3.

5.4.2.4 Reliability Considerations

Since the Computer and Sequencer is the major controlling function for Capsule events after separation from the Support Module during descent as well as on the surface of Mars, it is important that this device be as reliable as possible. To enhance the reliability of the Computer and Sequencer, counters and decoding registers have been made triply redundant with majority logic connected to their outputs. This means that when a word stored in memory is to be operated upon it will be placed in three identical registers and three sets of logic outputs will be supplied to a majority voting block of logic which will determine the correct time of execution for the command as well as the correct function. The price of this reliability enhancement is an increase in power consumption. Techniques of majority logic and triple redundancy have been used to enhance the reliability of command systems, digital computers, and general digital systems for many years and are well known and well documented. GE-RS used triply redundant majority logic in a similar application on a classified Satellite vehicle program in the design of a stored command programmer.

5.4.3 TELEMETRY DATA STORAGE

The Computer and Sequencer Subsystem provides the data storage capability for the telemetry data. The telemetry data is collected in nine different modes (see Section 5.2.2).

During entry, two modes of operation are required. The entry data is delayed for 70 sec and then transferred to the DHS for transmission by operating a portion of the memory as a delay line. Secondly, every fourth sample of the entry data is stored for transmission after landing.

Upon landing, the accumulated data is transmitted in real time.

The post relay phase again requires storage of data. Three separate sections of memory are required. The landed science data excluding the mass spectrometer and gas chromatograph is accumulated in one section and the engineering data in another. Both sets of data are transmitted under normal operation. However, when the 5 bps back-up link is used, only the science data is transmitted.

The mass spectrometer and gas chromatograph require the third area. In order to minimize the data that must be stored, the sampling of these two instruments is keyed to the gas chromatograph. The signals from the gas chromatograph occur randomly during the operating period, and hence do not conform to a fixed sampling format.

Each type of incoming telemetry data is identified as to type by the DHS so that it can be stored in the proper memory location. Each location is identified by the address of the first data word of each type. By using this technique, accessing data of a particular type is a simple matter, that involves reading out a particular portion of the telemetry data storage memory defined by the known address corresponding to the first stored word of the set of data.

5.4.4 LOGICAL DESCRIPTION

The Computer and Sequencer can be divided into the following nine major areas, as shown in the Block Diagram, fig. 5.4-1:

1. Clock
2. Real Time Command Decoder
3. Memory Control
4. Sequencer Memory
5. Command Execution
6. Control Logic
7. Telemetry Interface Control
8. Telemetry Data Storage
9. Power Supply

Further descriptions of the nine sections are given in the following paragraphs (refer to fig. 5.4-2, Functional Diagram).

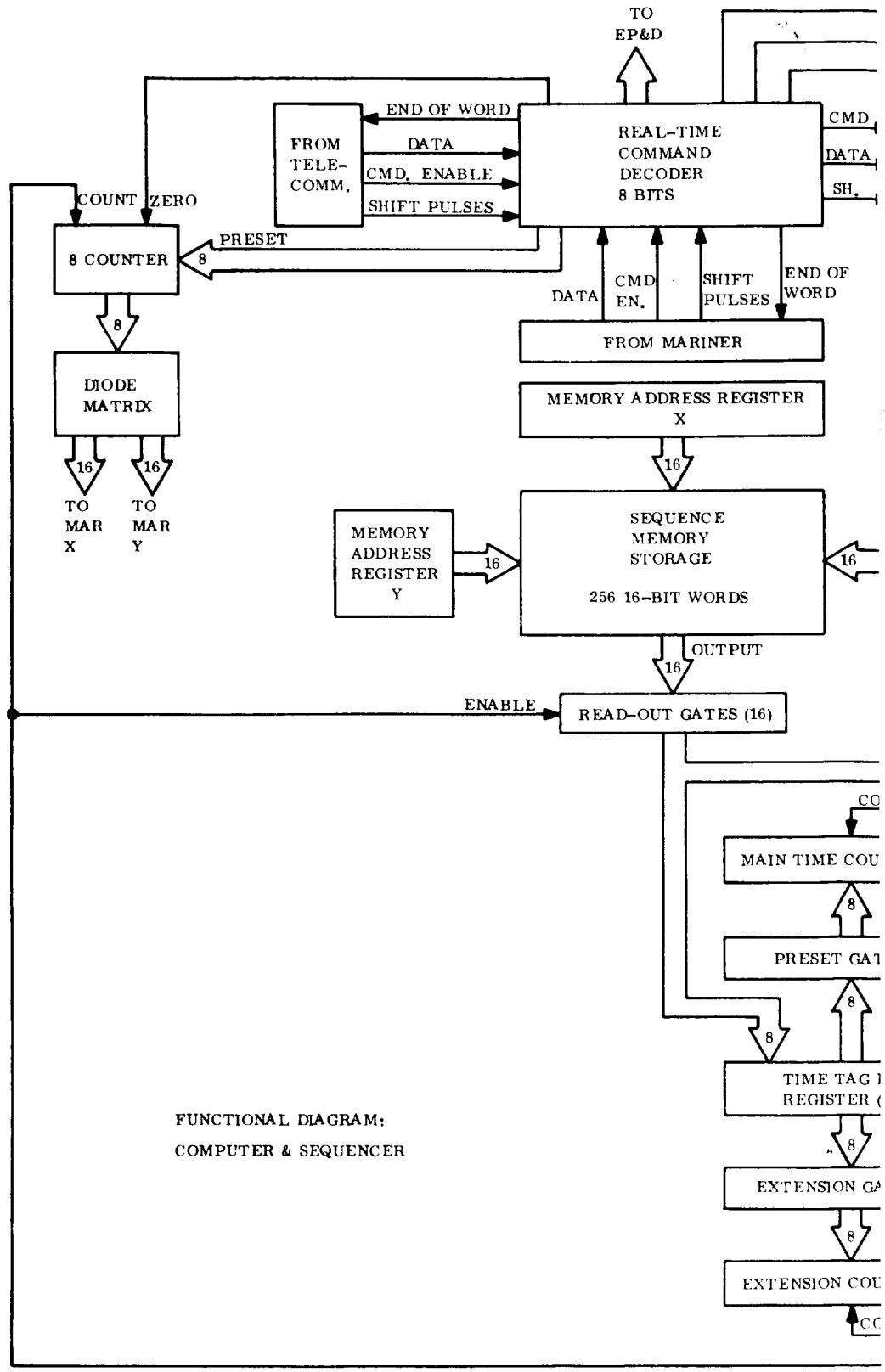

FUNCTIONAL DIAGRAM:
COMPUTER & SEQUENCER

FOLDOUT FRAME 1

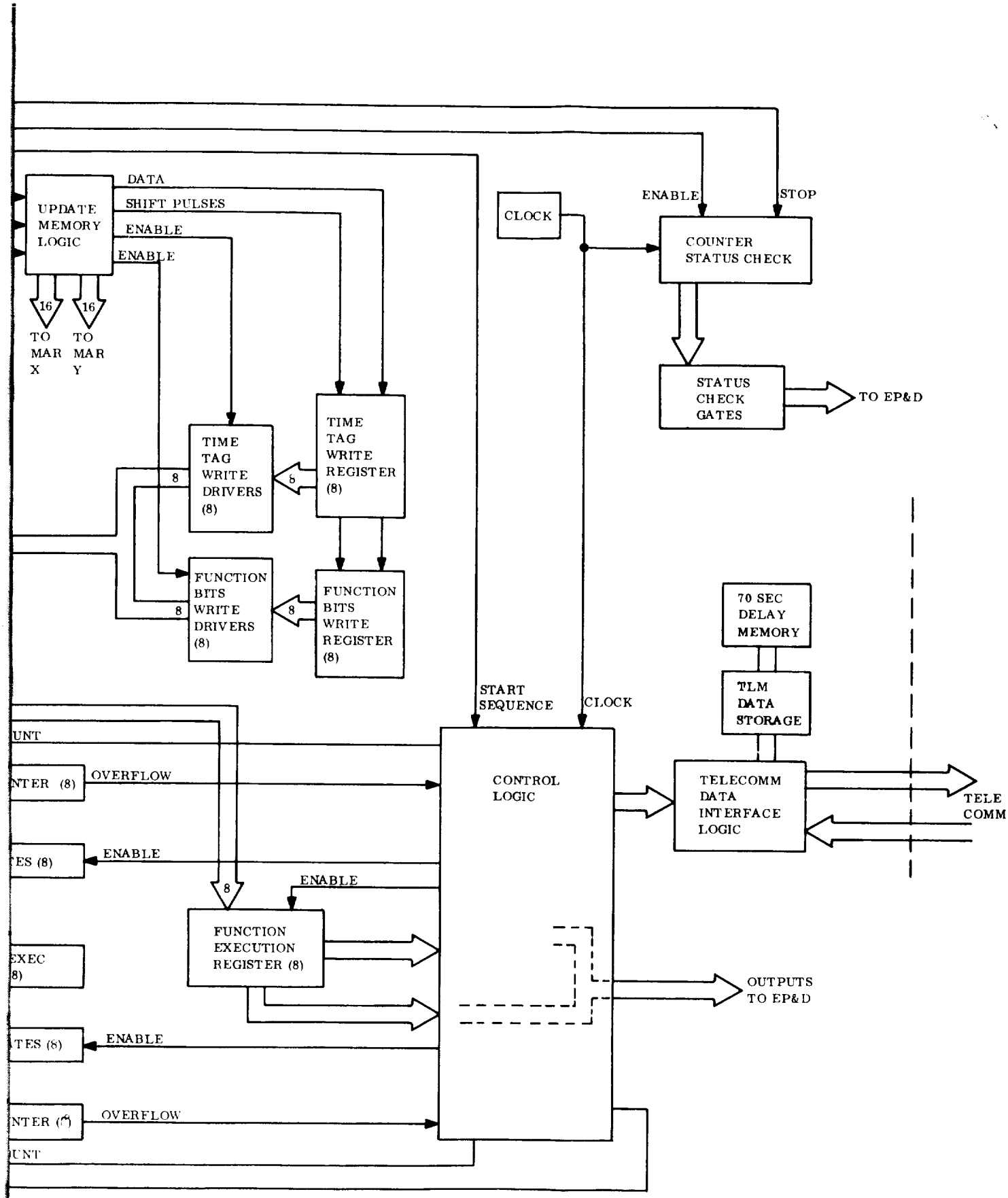

FOLDOUT FRAME 2

Figure 5.4-2. Computer and Sequencer Functional Diagram

5.4.4.1 Clock

The clock in the unit provides 1 pulse/sec output signals. A multiviorator circuit which is corrected for changes in temperature and voltage is used. A crystal controlled clock would require a basic crystal frequency at least 200 kHz or higher which would have to be counted down. The correction circuitry required for the free running oscillator is less than the countdown register would be.

5.4.4.2 Real-Time Command Decoder

The real time command decoder receives real time commands from the command detector in the Telecommunications Subsystem via r-f directly from the Earth to the Lander, and also interfaces with the Support Module command system to receive real time commands from that system before separation. The real time command decoder consists of an 8-bit shift register and decoding logic to provide the required outputs from the decoded commands. An enable, command bits, and sync pulses are received from the command detector. The command bits are shifted into the decoder register, and, when the word is completely read into the register, it is decoded and executed. If the detector loses lock during the receipt of the command, decoding is inhibited. Outputs from the real time command decoder are provided to other subsystems, or are used internally to the Computer and Sequencer for control and memory update functions.

5.4.4.3 Memory Control

Memory control is a block of logic and driver gates which accumulates incoming memory updating data, both time tag and function bits, recognizes the address to be updated and provides write signals to that address for the purpose of updating the contents. Memory control also contains x and y memory address registers used internally by the Computer and Sequencer for addressing memory locations sequentially in the read out of the stored program.

5.4.4.4 Sequencer Memory and Telemetry Data Memory

The sequencer memory is a 256 word 16-bit word memory for a total of 4,096 bits. It is a random access, non-destruct readout and non-volatile, and will retain its contents when power has been removed and re-applied. Memory size is determined by number of stored commands plus the requirements for the storage of blackout data and the entry science data. The command word sequence has been allotted 256 words of 16 bits each, since this size will contain the present estimate of mission required command words plus spares, and 256 is a convenient size from the standpoint of memory organization and updating address designation. Fig. 5.4-3 shows how the memory size required for telemetry is determined. The requirement to store blackout data at a rate of 550 bps for 70 sec means that 38,500 bits storage is required. In addition, entry data must be stored at one-fourth this rate for the duration of the worst case entry phase (455 sec) yielding an additional 62,560 bits storage. However, once 70 sec of blackout data has been accumulated, it is read out at the 550 bps rate for transmission and entry science data is read

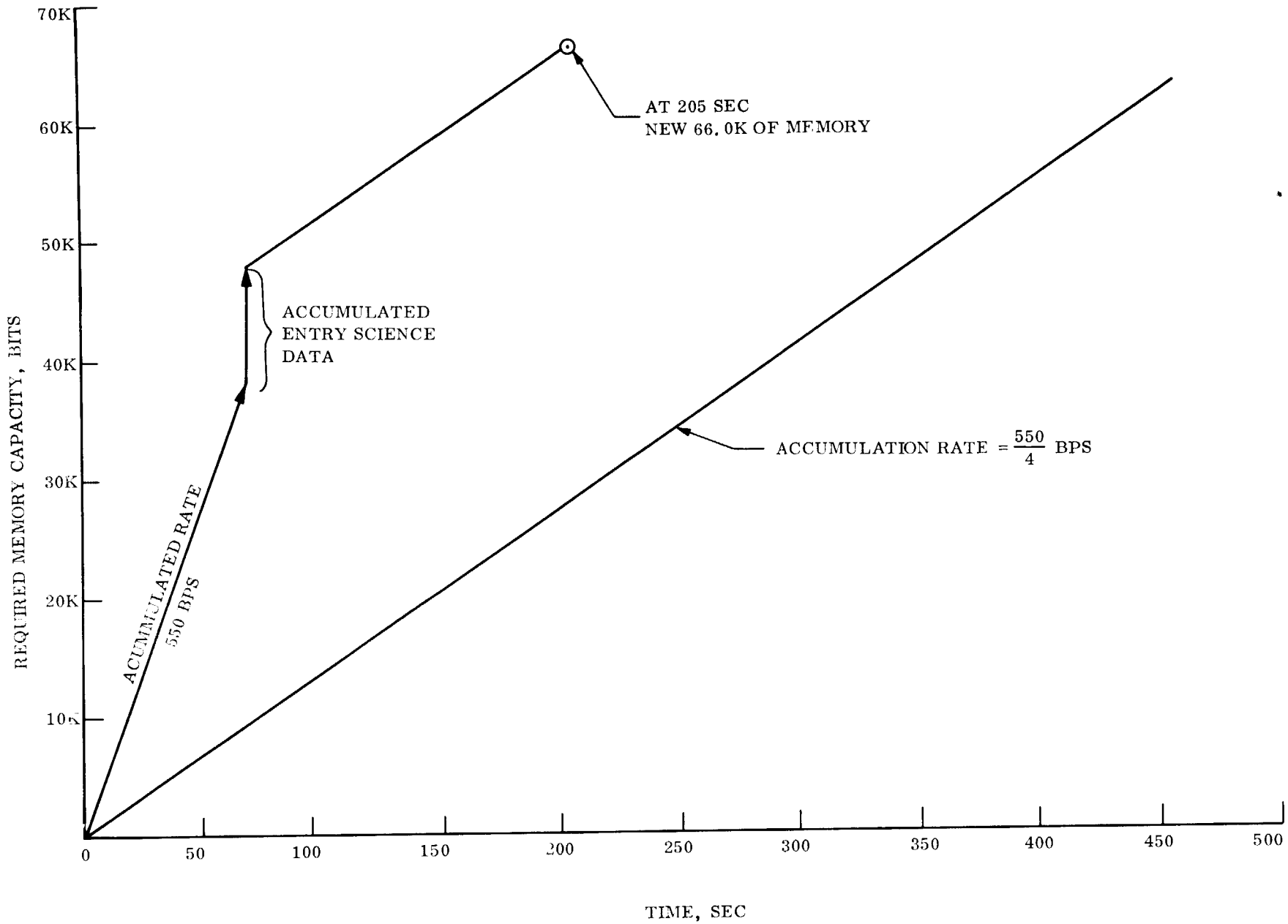

Figure 5.4-3. Telemetry Memory Capacity for Worst Case Trajectory

in its place. At the end of 210 sec the 70 sec delayed data input to the memory is terminated because blackout will have terminated even for the worst case trajectory. Therefore, as the figure shows, the storage requirement is 71,000 bits, a combination of the two lines on the figure. The storage capacity required for landed data is less than this, being about 68,000 bits.

The memory type used is a plated wire memory which is constructed using a small diameter conductive wire plated with a magnetic material. The advantages of the plated wire memory are:

1. The closed magnetic path of the magnetic material plated on the conductive wire makes the device insensitive to external magnetic fields.

2. The closed magnetic path allows NDRO since no self-demagnetization exists.

3. The lack of self-demagnetization allows the magnetic film to be made thicker than in a planar film memory giving larger output voltages.

The plated wire technique provides considerable size, weight and power savings over core type memories. Using presently available techniques the memory for both the sequencer and telemetry storage has the following characteristics:

Size	80 in.^{3}
Weight	5 lb
Power	4 watts

The above values include the electronics associated directly with the memory such as sense amplifier, timing and control, and address decoding. The memory cells plus the electronics associated with it are packaged as a subassembly.

5.4.4.5 Command Execution Logic

Command execution logic consists of two registers, one to contain function bits read out from the memory for a given command word. Counters are provided in the command execution logic which are pre-set to the number designated by the time tag register. The counter is enabled to count from its pre-set condition with a pulse/sec counting frequency which is supplied by the clock. Overflows of the counter are acted upon by the control logic described in a later paragraph. The function bit register is decoded by a set of gates similar to the decoding gates of the real time command decoder. The function bit execution gates are enabled by signals from the control logic section.

5.4.4.6 Control Logic

The control logic section synchronizes and controls the operation of the entire Computer and Sequencer. It receives a start input either from a discrete event such as physical separation from the Support Module or from a real time command. It selects the address of sequential words for read out purposes in the memory and also controls the actual read out process. It calls for a word from a location in memory to be operated upon and when the word has been operated upon it calls for the next word in the sequence. The control logic recognizes special stored commands when decoded and causes the Computer and Sequencer to enter special modes of operation described in other paragraphs. These include looping, waiting-for-discrete, and extension operation. The control logic also provides signals to the telemetry data storage and interface control sections.

5.4.4.7 Telemetry Interface Logic

The telemetry interface control logic provides synchronizing signals to the Telecommunications Subsystem and receives signals from the subsystem to read data in and out of the telemetry data storage memory.

5.4.4.8 Physcical Characteristics

The Computer and Sequencer will occupy 250 in.^{3} and will weigh 13 lb. It will consume 20 watts when fully active, and 2.0 watts in the dormant mode, when counting out long incremental times between command executions. The circuitry used for the Computer and Sequencer consists of integrated circuit elements for the logic circuits and piece part circuits for the telemetry interface signals. The electronic parts are mounted on multilayer printed circuit boards to obtain maximum packaging density. Four stage shift register integrated circuits are used in the design to obtain maximum package utilization.

5.4.5 OPERATIONAL CONSIDERATIONS

Some considerations for operation of the Computer and Sequencer Subsystem during the flight are described in the following paragraph.

The Computer and Sequencer provides a considerable amount of flexibility in that the stored program can be changed at any time during the mission, by means of real time commands sent from the Earth either directly to the Lander or through the Support Module command system. With this capability it is possible to change functions in a sequence, to change the time of execution of a given function, to rearrange a sequence or even to create an entirely new sequence and to cause the Computer and Sequencer to enter the entirely new sequence by means of a real time command. Changing the time of execution of the command is straightforward and requires sending a series of three real time commands of 8-bits each. Changing the function of a particular command is also straightforward and requires sending a series of four 8-bit real time commands.

In this case, the time tag can also be changed if required. Access to the memory for updating purposes is random, in that any of the 256 memory addresses can be changed simply by specifying a particular 8-bit address configuration as one of the real time command words in the update sequence. In the case of an entirely new sequence, this should be located at the beginning of memory if the functions that were originally there have already been performed. Then, by using the real time command which causes the Computer and Sequcner to return to location zero and start over again, this new sequence can be entered. In cases where there is not enough room in the beginning of the memory for this sequence it can be entered at a latter portion of memory and carefully timed so that the new sequence will be entered into from the present sequence at the correct time.

To change a sequence stored in the memory where more than one command is involved it may be advantageous to store additional commands that were not in the sequence before. Because of this it is recommended that blank space be left in the memory in the sequence of words that are stored there originally so that these blank spaces can be used to store new words if necessary, in the updating process. The Computer and Sequencer will be configured such that a blank memory word will not affect the sequence and the Computer and Sequencer when decoding the fact that there is a blank memory word, will simply skip to the next instruction. The capability of the Computer and Sequencer to operate in special modes such as the "wait for discrete" mode and the "loop" mode, can be used by the flight controller to perform special functions, such as re-referencing the sequence to given events that are expected to occur, either as a prime mode of operation, or as a backup mode of operation, and performing fixed series of events that occur many times. It is felt that the capabilities afforded to the flight controller by the design of the Computer and Sequencer Subsystem are quite extensive and should fulfill all requirements operationally. The added complexity in hardware to provide for such features as looping, extension and discrete recognition are rather minor when compared to the capability that is added to the system.

5.5 ENVIRONMENTAL CONTROL SUBSYSTEM

5.5.1 LANDER THERMAL CONTROL DESIGN

The Thermal Control Subsystem maintains the Lander components within their allowable temperature range throughout the required three day mission lifetime. The thermal design for the configuration evolved from the parametric studies performed under Contract NAS 1-8098 with further studies conducted to evaluate the parameters common to the 1400 lb Capsule 3 day mission study. The Thermal Control Subsystem consists of an insulated payload utilizing the Lander honeycomb structure and additional free internal volume to insulate the temperature sensitive components from the extreme planet environments. Individual components are also provided with thermostatically controlled electric heaters and/or phase change materials to provide for maintenance of small temperature tolerances.

5.5.2 REQUIREMENTS AND CONSTRAINTS

The Martian surface and atmospheric temperature design criteria were taken from the 1968 NASA/LRC Mars Engineering Model Parameters for Mission and Design Studies. Fig. 5.5-1 shows the minimum and maximum design curves for Martian surface temperatures used in the analysis.

Based on the specified environments the major requirement is to design a thermal control system which has highly insulative characteristics thus minimizing the heater power required for thermal control during the continuous cold conditions with Mars cloud cover.

5.5.2.1 Equipment Temperatures

The operating temperature requirements of all on board electrical equipment are within the range of -40 to 160°F with the exception of the operational battery, which has a 65 ± 15°F temperature requirement. A separate compartment with increased thermal resistances will be provided to maintain the critical battery temperature specifications.

5.5.2.2 Equipment Power Levels

Thermal energy from equipment operation must be factored into the temperature response during surface lifetime. For the 3 day mission, peak thermal dissipation occurs once a day during the transmission periods and is as high as 258.7 watts during relay transmission immediately after impact. The nominal power profile is presented in Section 5.3.

5.5.2.3 Capsule Design Characteristics

Basic physical constraints on the subsystem are listed below:

1. Exterior surface coatings - Metal plating of exposed surfaces to achieve lowest possible emissivity (ϵ = 0.1).

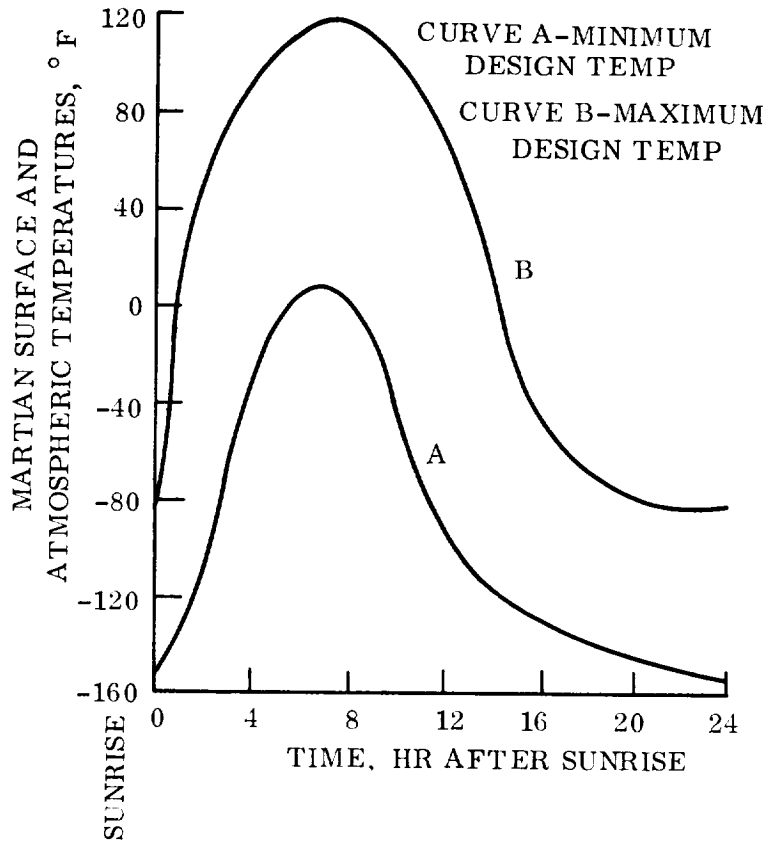

Figure 5.5-1. Atmospheric and Surface Temperatures vs Time on Surface After Sunrise

2. Insulation - The type of insulation selected must be compatible with the high impact shock, vibration, sterilization requirements, low thermal conductivity, and low density. A closed cell foam insulation, e.g., styrofoam or polyurethane satisfies these parameters and was therefore selected for application in the Lander. The 1.5 in. thick honeycomb container structure is ideally suited for mounting the insulation. A low thermal conductivity core material (phenolic glass) with foam insulation packed cells was utilized to control the Lander temperature response. Additional free internal space will be also taken advantage of for insulating purposes to minimize the heat leak.

3. Heat Sinks - Components such as transmitters, which have heat generation characteristics which result in unacceptable temperature rises will be protected from over exposure through the use of commonly used heat of storage methods which employ a heat of fusion technique for heat absorption.

5.5.3 DESIGN SOLUTION

5.5.3.1 Thermal Model

A thermal model describing the Lander configuration was constructed for the purpose of determining the temperature response of the Lander components in the Martian environment. The Lander subsystems were divided into a network of nodes comprised of the individual components, insulation, and structure, each thermally connected to the environment through their thermal capacitances and applicable node to node radiation and conduction couplings. Martian surface and atmospheric temperatures were specified as temperature-time dependent boundary nodes. The complex three dimensional heat transfer equations were solved through the use of a computer program especially designed to accommodate this type of heat transfer network. The program capabilities include the ability to specify an internal power profile for individual components as well as a heater power option which allows a particular component to be controlled at a desired minimum temperature. Transient analyses were computed for the three day mission lifetime requirement. Temperature responses were sampled every 10 min for the 72-hour mission.

5.5.3.2 Results

The detailed results of the study are presented in curve form in the subsequent figures. Initially temperature response was computed for the Lander components, assuming no component heat generation and no restriction on the lower temperature limit of the components. Typical transient component responses are shown in fig. 5.5-2 along with the temperature histories of the vehicle skin. Temperature at impact was assumed to be $40^{o}F$ for all cases. Results indicate that although the vehicle skin is fluctuating between $+80^{o}F$ and $-92^{o}F$, the temperature of the components within the insulated package continue to decrease, reaching the lowest value during the third diurnal cycle. All components except the battery ($50^{o}F$ min) remain within their specified $-40^{o}F$ allowable.

The study was then continued to determine the behavior of the components with the effects of internal heat generation caused by electrical power operation. Results of this phase of the study are shown in figs. 5.5-3 through -5. The outside environment continues to be the major influencing factor on skin temperatures. In comparing figs. 5.5-2 and 5.5-3 a hot side difference of approximately 4°F is shown versus a cold side change of -8°F. The components, however, are significantly affected by the operating power levels. The thermally enclosed nature of the Lander enhances the thermal control by thermal storage. The voltage regulator for example, operating at a 43.7 watt level, experiences a rapid peak rise of approximately 112°F during operation with a slow heat release feature, thus producing temperatures of near 25°F warmer in the night environments. A plot of the critical components show that excluding the battery all other components will remain within the -40 to 160°F temperature band without heater power.

Not shown in the figures are the S-band and UHF transmitter temperature histories. The high intermittent thermal dissipations will be absorbed by adjacent heat of fusion material whose upper temperature limit will not exceed the 110°F melt temperature characteristic. GE-RS has extensive experience in the use of this concept on various R/V hardware contracts, with excellent performance characteristics. The assembly of transmitters and thermal storage material is to be insulative mounted and radiative insulated by low emittance surfaces from the Lander exterior surfaces. The heat of fusion material will provide a reservoir of thermal energy at constant temperature to prevent excessive transmitter "soak down" during those passive periods following transmitter operation. See fig. 5.5-6 for weight estimates.

A trade-off of component allowable temperature as a function of heater power addition is provided in the final section of the study. Figs. 5.5-7 through -10 summarize the results of the study. Typical component temperature profiles for a -20 and +20°F temperature control are shown in figs. 5.5-7 and -8. As expected, controlling the lower temperature will have some effect on the peak rise, but only approximately 15°F. Fig. 5.5-9 shows the additional heater power requirements associated with an increase in the minimum allowable temperatures for the critical Lander components. At the -40°F level only the battery will require heater power to maintain the 50°F minimum temperature. A daily average of 1 watt will maintain this temperature specification. Fig. 5.5-10 shows the battery weight penalty associated with increasing the minimum temperature. Comparative results are shown for a 1 day and a 3 day mission. Weights were calculated based on battery design value of 30 watt-hr/lb. As shown on the curves, battery weight increases rapidly with an increase in allowable temperature and mission duration.

Fig. 5.5-11 shows the expected temperature profile for the S-band antenna due to environmental conditions. The mode of heat transfer effecting the antenna temperature will be almost entirely by radiation. Various combinations of solar absorptivity (α_S) and emissivity (ϵ) will yield different temperature profiles. For this study an $\alpha_S = 0.2$ and an $\epsilon = 0.15$ were selected. Results indicate that an acceptable 60°F gradient across the antenna could exist with skin temperatures fluctuating between -70 and 120°F.

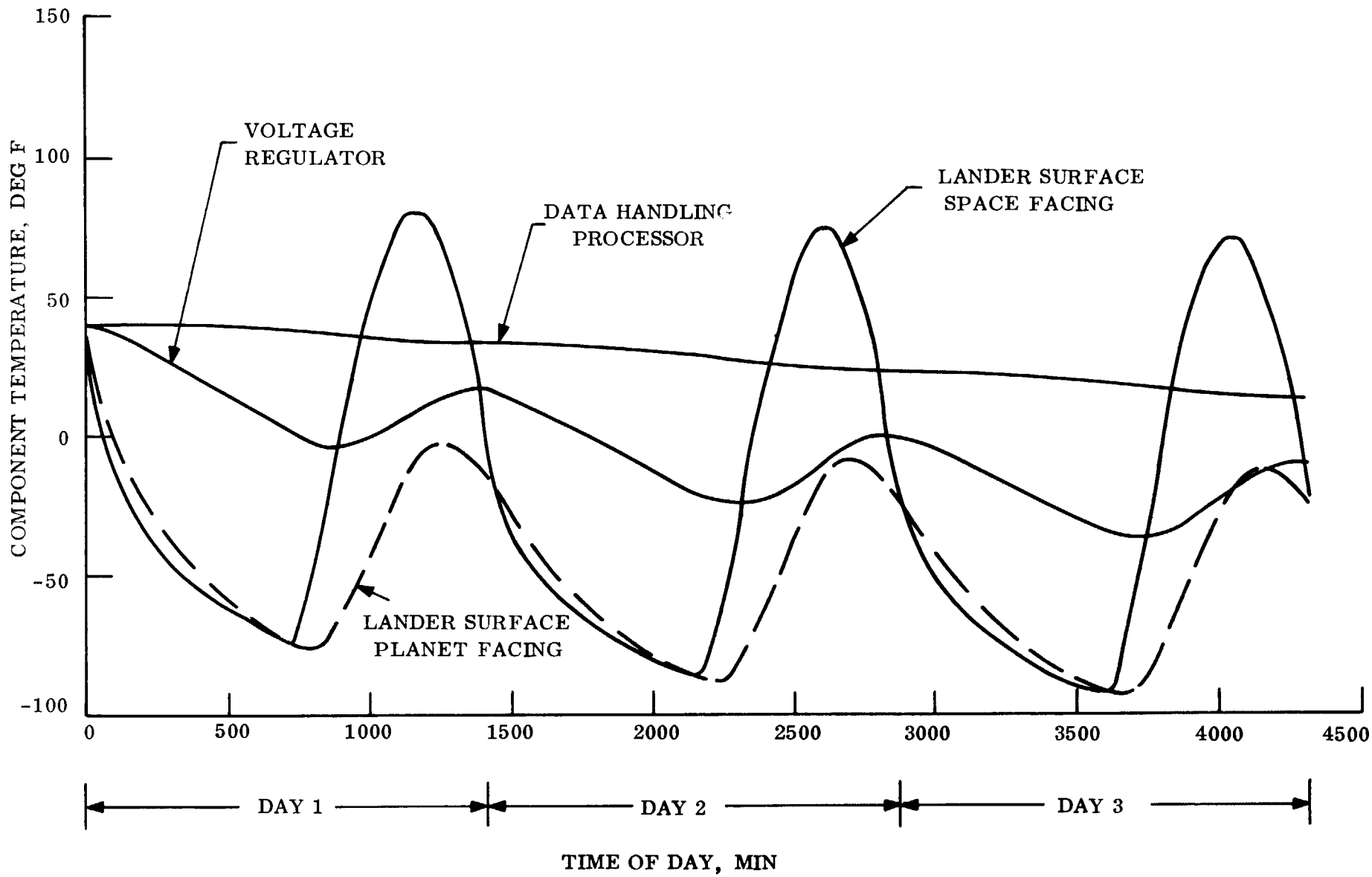

Figure 5.5-2. Equilibrium Component Temperature without Power Profile - without Heater Power Control (Voltage Regulator, Data Handling Processor)

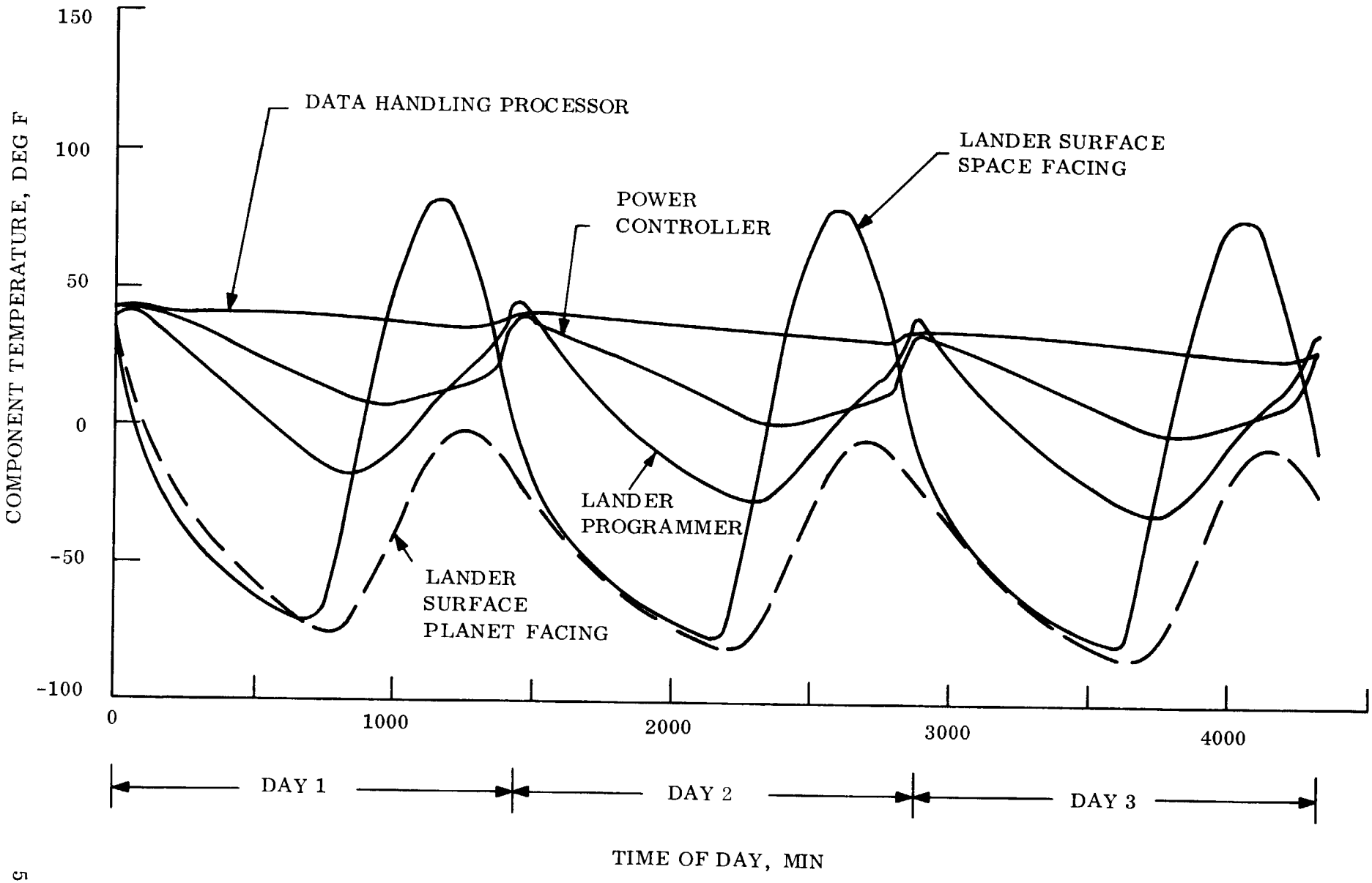

Figure 5.5-3. Equilibrium Component Temperature with Power Profile - without Heater Power Control (Data Handling Processor, Power Controller, Lander Programmer)

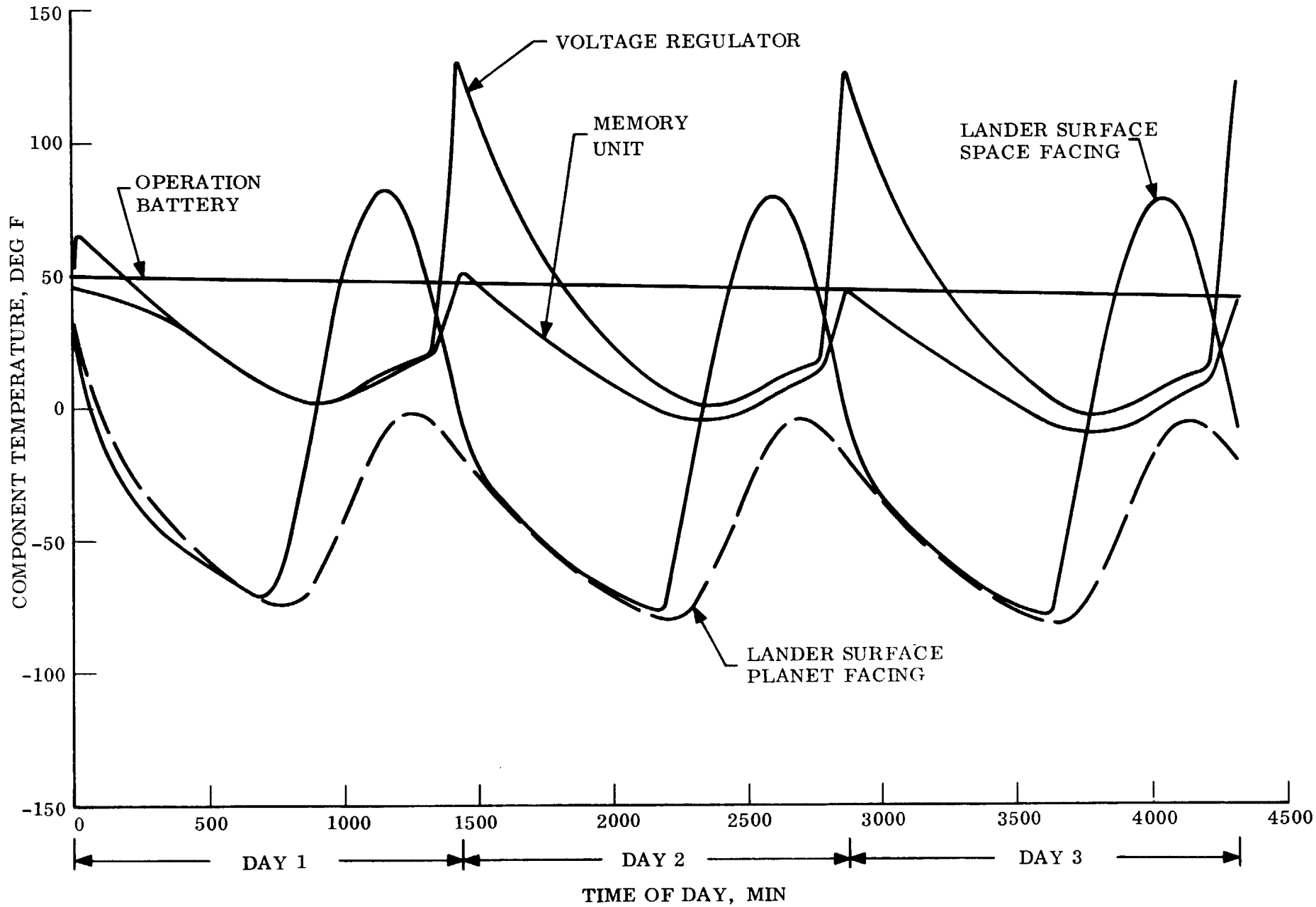

Figure 5.5-4. Equilibrium Component Temperature with Power Profile - without Heater Power Control (Operational Battery, Voltage Regulator, Memory Unit)

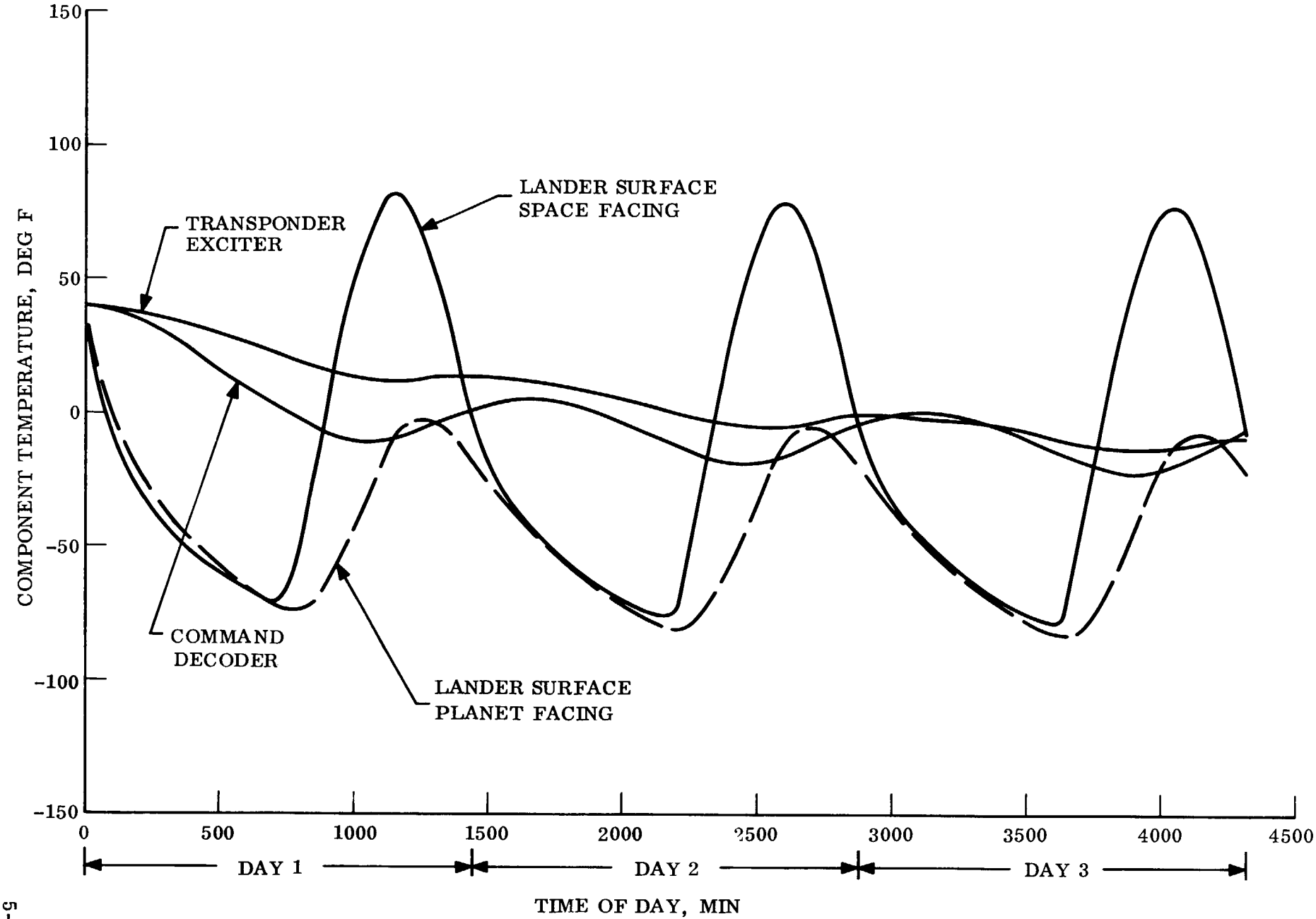

Figure 5.5-5. Equilibrium Component Temperature with Power Profile - without Heater Power Control (Transponder Exciter, Command Decoder)

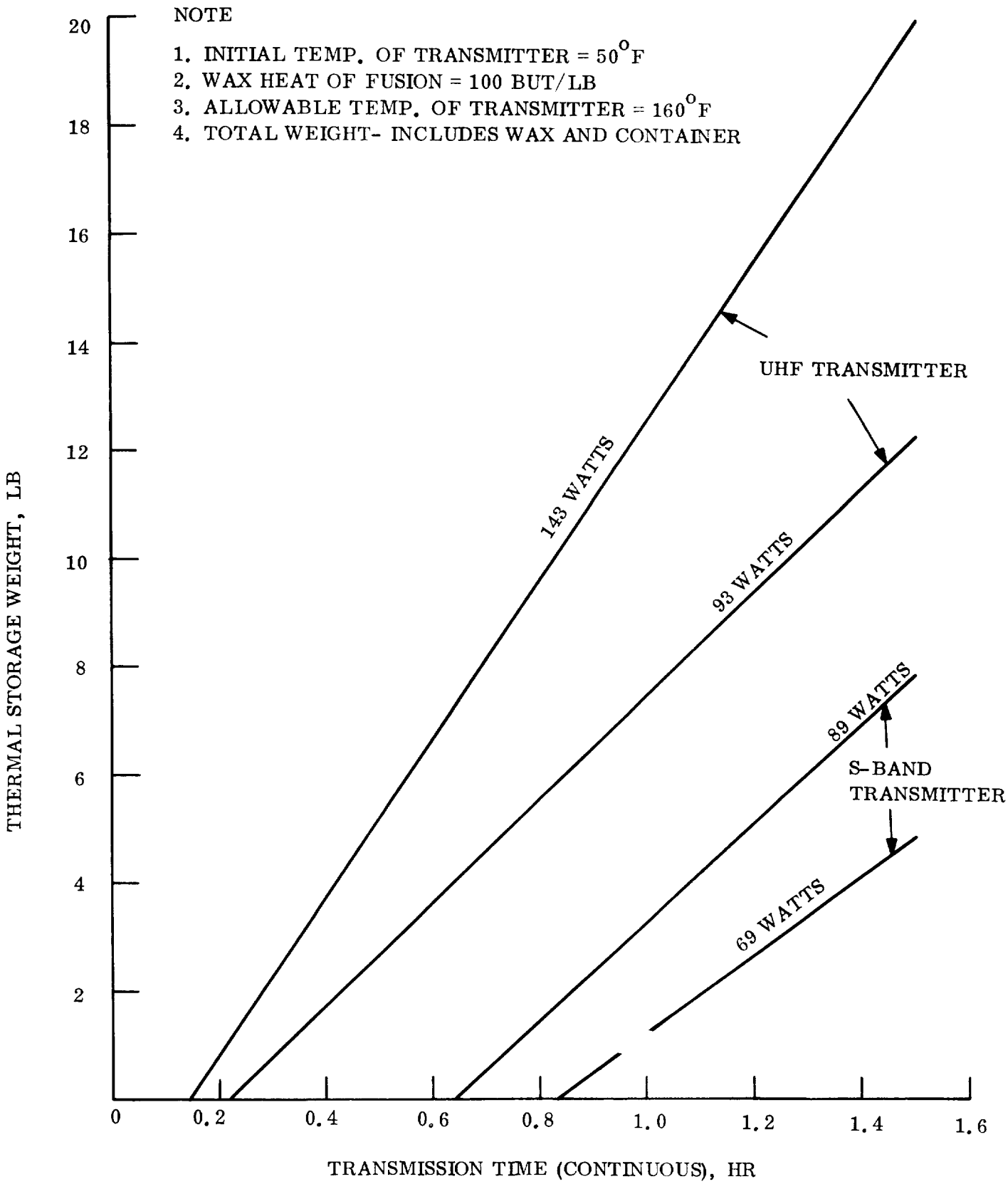

Figure 5.5-6. Transmitter Thermal Storage Weight vs Transmission Time

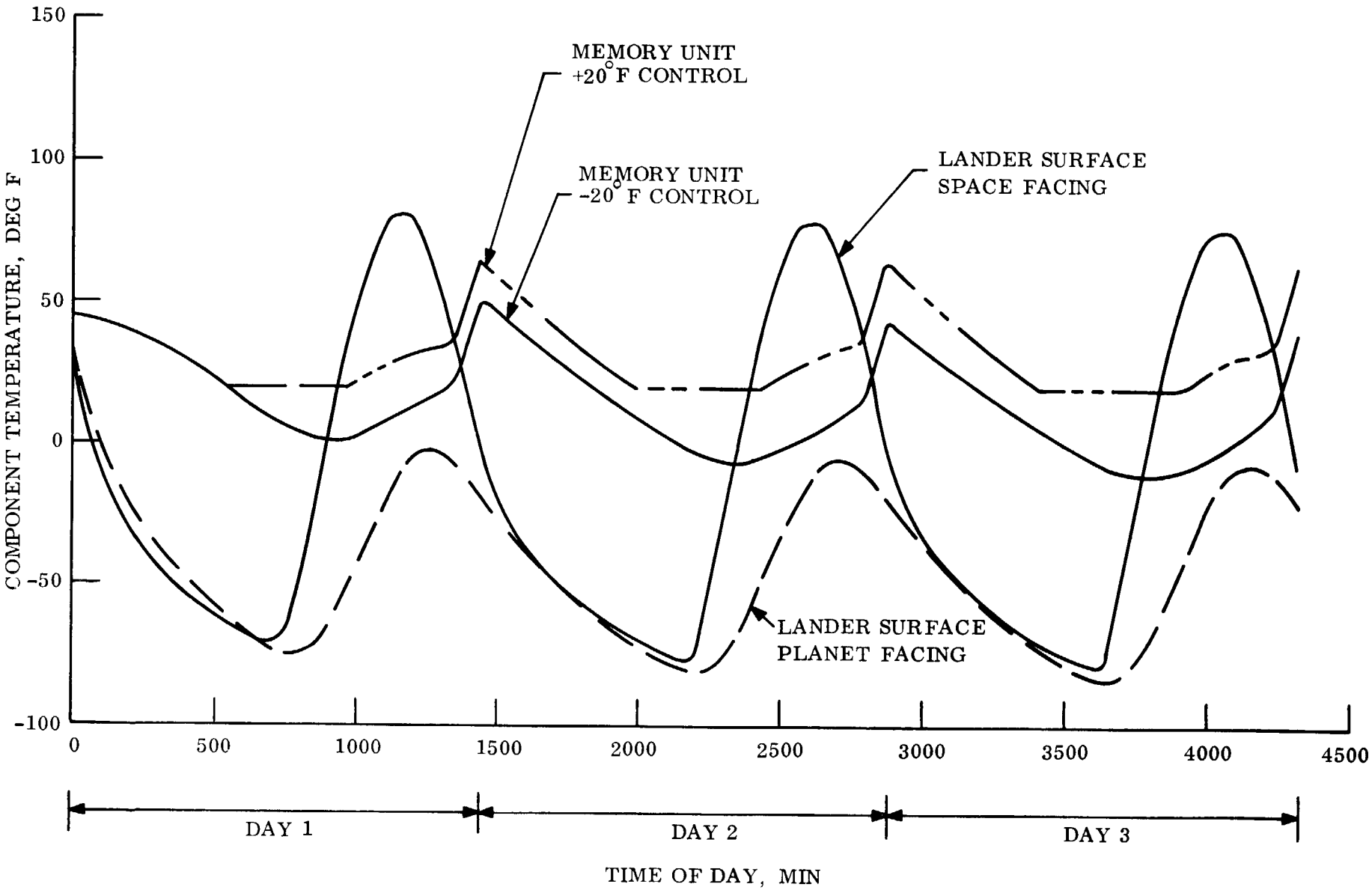

Figure 5.5-7. Equilibrium Component Temperature with Power Provile and Heater Power Control (Memory Unit)

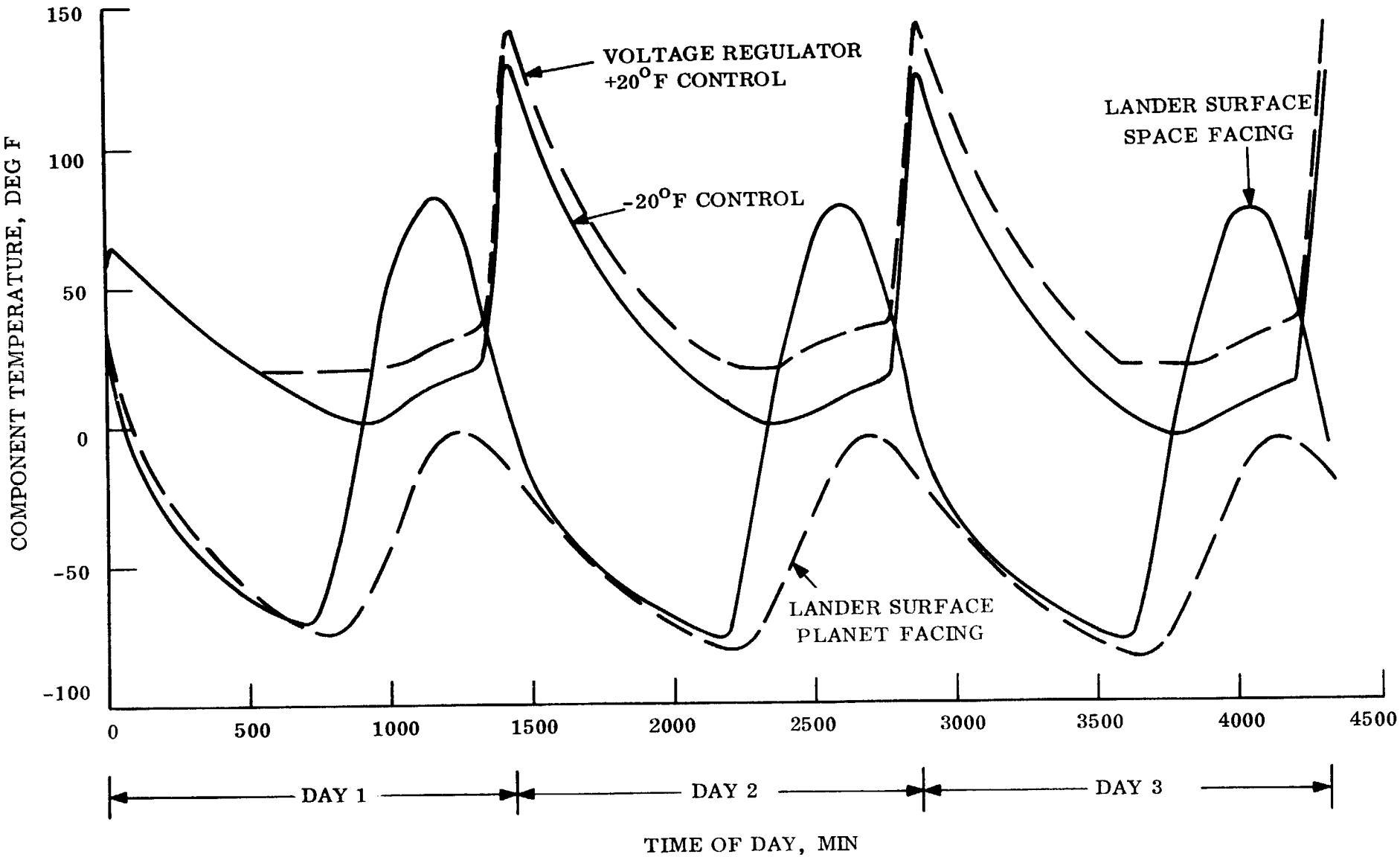

Figure 5.5-8. Equilibrium Component Temperature with Power Profile and Heater Power Control (Voltage Regulator)

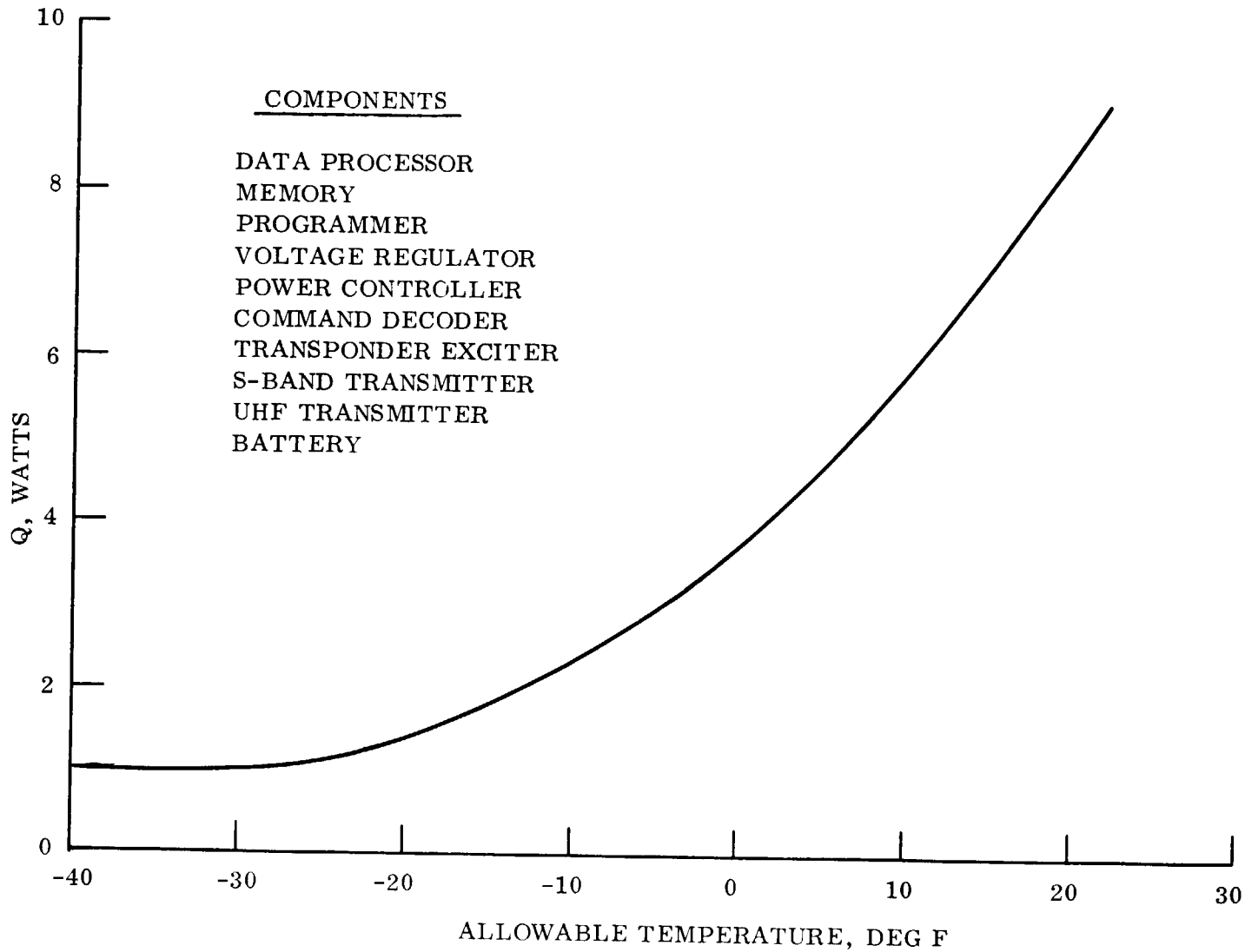

Figure 5.5-9. Daily Average Heater Power Requirements vs Allowable Temperature for Selected Group of Lander Components

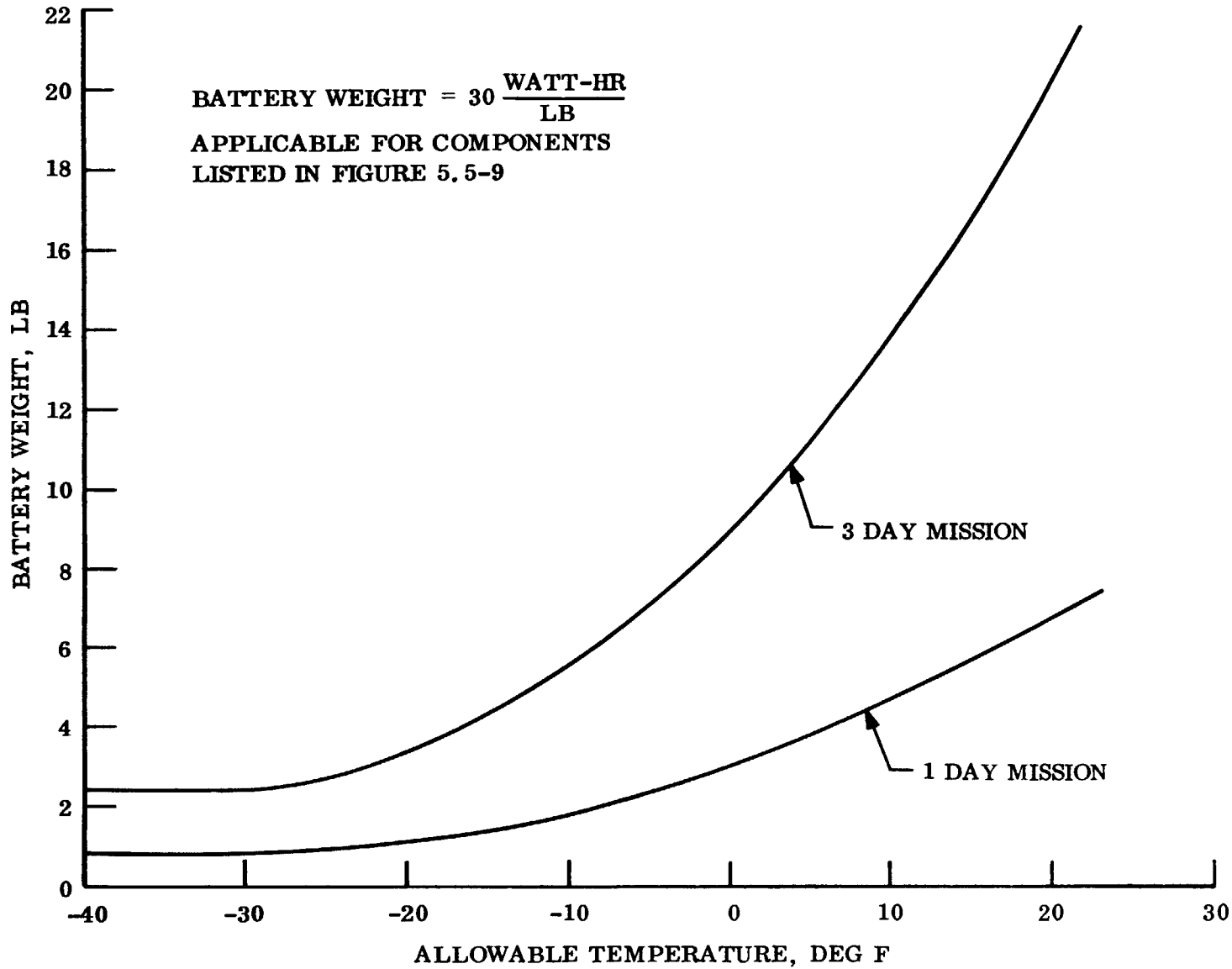

Figure 5.5-10. Battery Weight Allowances for Thermal Control vs Component Allowable Temperature

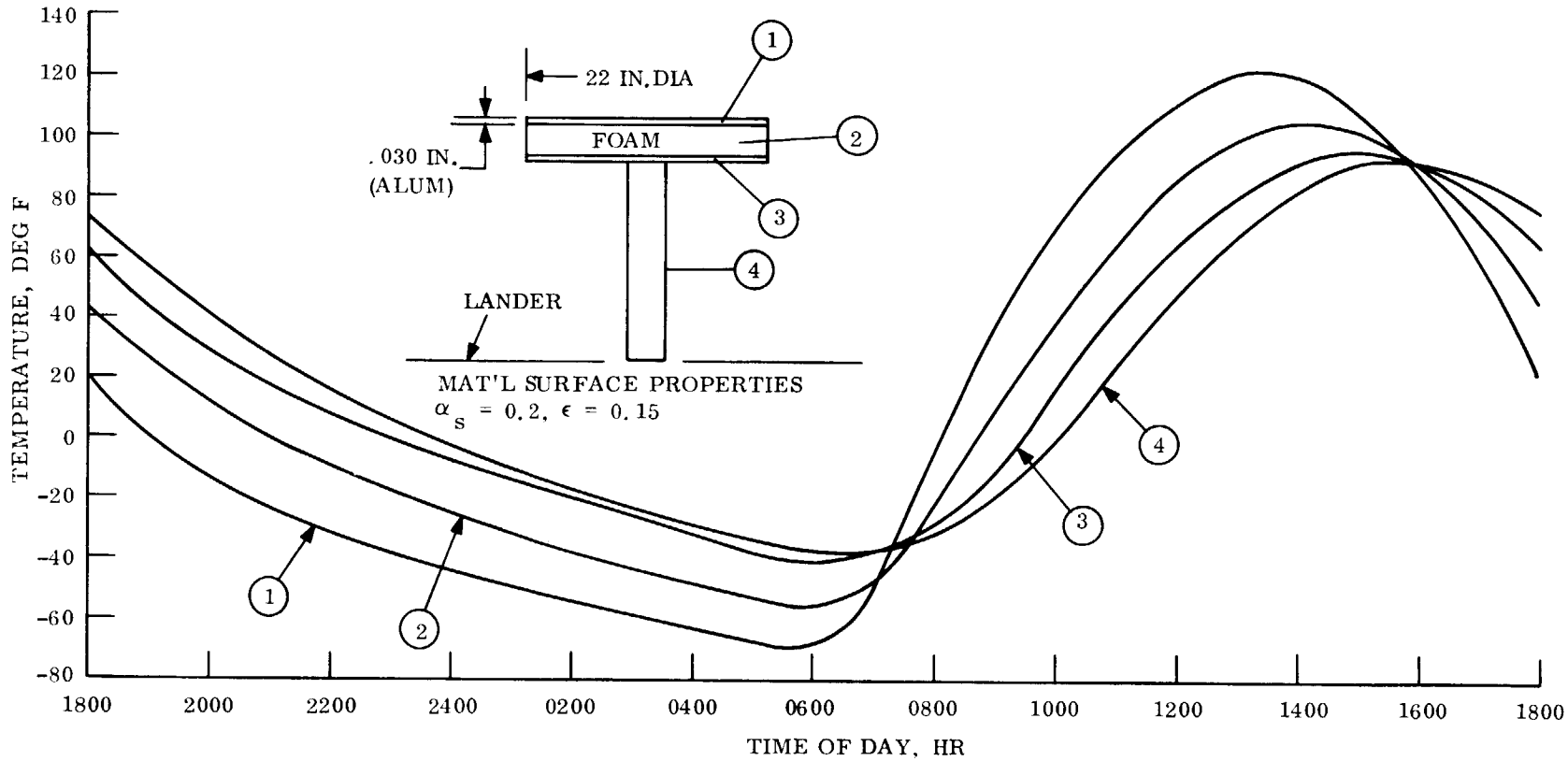

Figure 5.5-11. S-band Antenna Temperature Profile

5.5.4 PRE-ENTRY ENVIRONMENTAL CONTROL

5.5.4.7 Requirements

The thermal control objective is to establish an optimum system which includes the ideal combination of insulation, heater power, and surface emissivity. The design approach will be to insulate the surface Lander and aeroshell from the space environment through a multi-radiation barrier insulation blanket attached to the outside surface of the sterilization canister, supplemented with thermostatically controlled electric heaters to maintain acceptable temperatures. The heaters will be operated with power supplied from the Spacecraft solar cells. The attitude of the vehicle with respect to the Sun has minimum solar orientation effects. Solar heating effects were neglected, thereby achieving a design which is compatible with the worst case parameters. Minimum equipment temperature will be maintained throughout the cruise with all Lander components assumed non-operating.

5.5.4.2 System Performance

5.5.4.2.1 Design Criteria

1. Insulation - Within a vacuum environment, where gaseous conduction does not exist, the primary modes of heat transfer are radiation and conduction. It is within this environment where radiation barrier insulation finds application. A series of tests have been run at GE for the purpose of evaluating the effective thermal conductivity of this type of insulation. The thermal conductivity of the radiation barrier insulation as manufactured ranges from 2 to 4×10^{-5} Btu/hr-ft-^{o}F. However, when the insulation is applied to a structure, it is necessary to cut it and attach it with fasteners which compress the insulation and cause thermal shorts. This will have a significant effect on the effective thermal conductivity of the blanket as attached to the canister. Based on representative vehicle structure characteristics a value of 1×10^{-4}/Btu/hr-ft-^{o}F was used in the study.

2. Surface Coatings - The blanket is designed to have an initial surface emissivity value of $\epsilon = 0.1$. The study includes requirements for a possible degraded condition of $\epsilon = 0.4$.

3. Equipment temperatures - The study was performed for compartment temperatures between 0 and 40°F. Lander components are compatible with these values except for the battery which must be stored at 50°F minimum.

5.5.4.2.2 Results

The results of the study are presented in fig. 5.5-12. Interpreting the results it is seen that the heater power requirements become constant as insulation thickness is increased. Since the amount of heat loss from the surface is a function of the surface temperature of the canister which changes as a function of T_S^4. Results at the 0.8 in. thickness also indicate that only a 3 watt power penalty is paid when going from 0° F to 40°F compartment

temperature allowables. Therefore, the 1400 lb Capsule will utilize a 0.8 in. thick blanket (approximately 15 lb) with a 40°F compartment temperature specification resulting in a 30 watt power requirement initially which could increase to 36 watts if degradation in the surface coatings takes place.

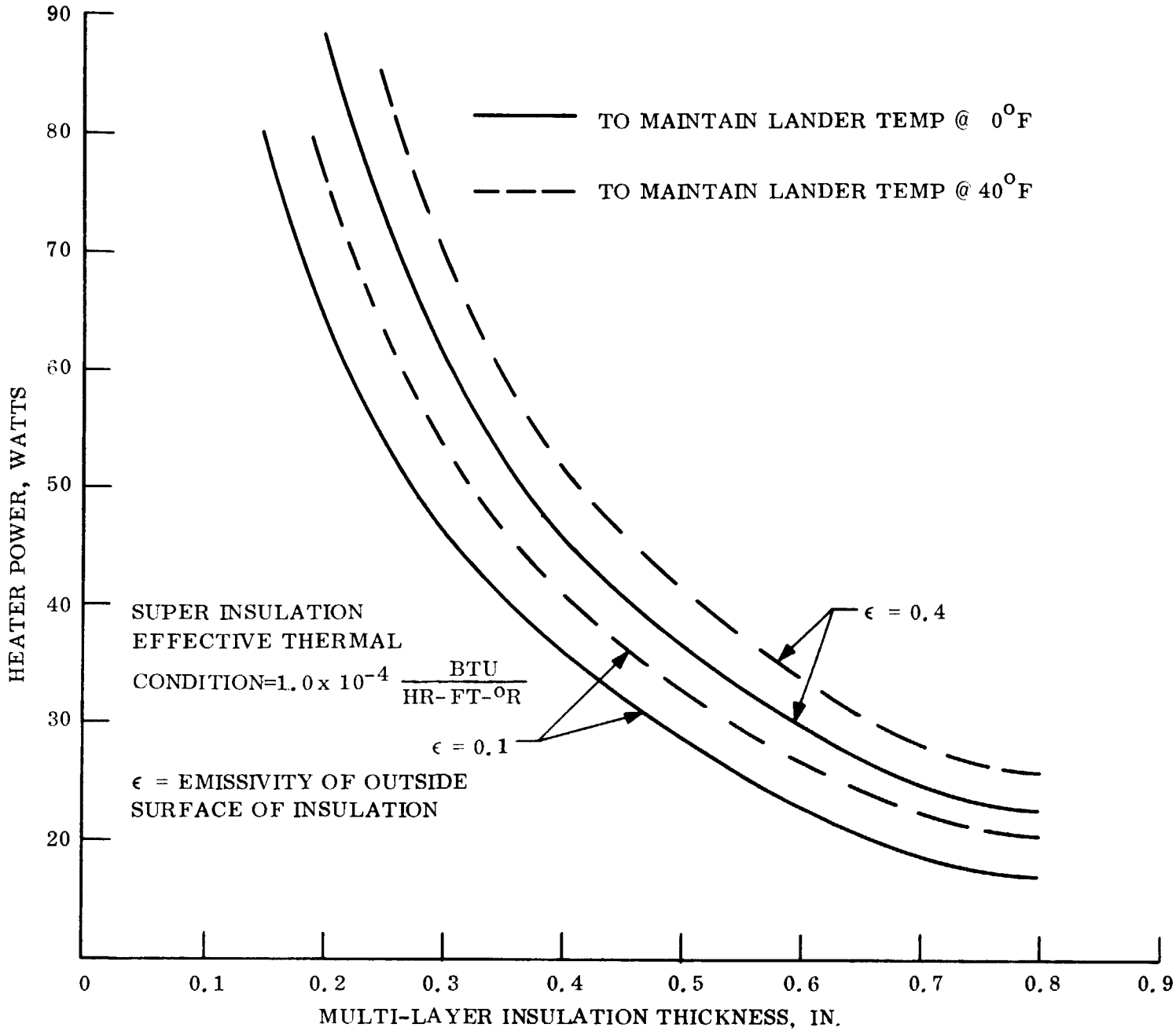

Figure 5.5-12. 1400 lb Cruise Module Heater Power vs Insulation Thickness

5.6 LANDED EQUIPMENT CONTAINER

5.6.1 SUBSYSTEM DESCRIPTION

The landed equipment container (figs. 5.6-1 and 4.2-7) contains all of the science and supporting equipment for the 3-day surface operations and includes the mass spectrometer, 3-axis accelerometer, and the base temperature and pressure sensors used in entry atmospheric measurements. All of this equipment is contained within a 40-in. diameter, 19-in.-deep cylinder as shown in fig. 5.6-2. This cylinder is assembled, after final test and checkout, to the rim-stiffening D section to which the toroidal, deep ring phenolic fiberglass impact attenuator is attached. The deployment equipment (cameras, antennas, wind, pressure, and temperature sensors) are designed for operation in either a heads-or-tails landing position (see figs. 5.6-1 and 5.6-3).

5.6.2 STRUCTURAL DESIGN

The structural design of the Lander equipment container offers the best compromise between structural efficiency and all other constraints, including packaging. A stiffened aluminum cylinder, with toroidal edge structure, was selected as the basic configuration because of its inherent ability to withstand high impact loadings in any direction around the periphery.

The container consists of three elements: a D-shaped toroidal edge structure, an inner cylindrical space frame, and top and bottom covers and doors. See fig. 5.6-4 for details of the container structures. The complete structural assembly is designed to withstand forces generated by initial impact up to 1000 g's and forces due to subsequent impact from rebound.

The design criteria for the container are as follows:

1. Container design weight:

Structure and equipment	441 lb
Attenuation weight	220 lb
Landed weight	661 lb

2. Forces imposed on Lander due to impact up to 1000 g's

3. Limit condition design factor = 1.0

4. Ultimate load = 1.25 times limit load.

The structure is designed not to yield under limit loads and not to fail under ultimate loads.

With the deep ring phenolic glass impact attenuation system, the D-shaped edge structure of the container acts as a primary load distribution path. The outer shell of the torus structure is tied to the cylinder wall with radial aluminum nose ribs, suitably stiffened so they will buckle under locally excessive loadings and redistribute the loading around the toroidal

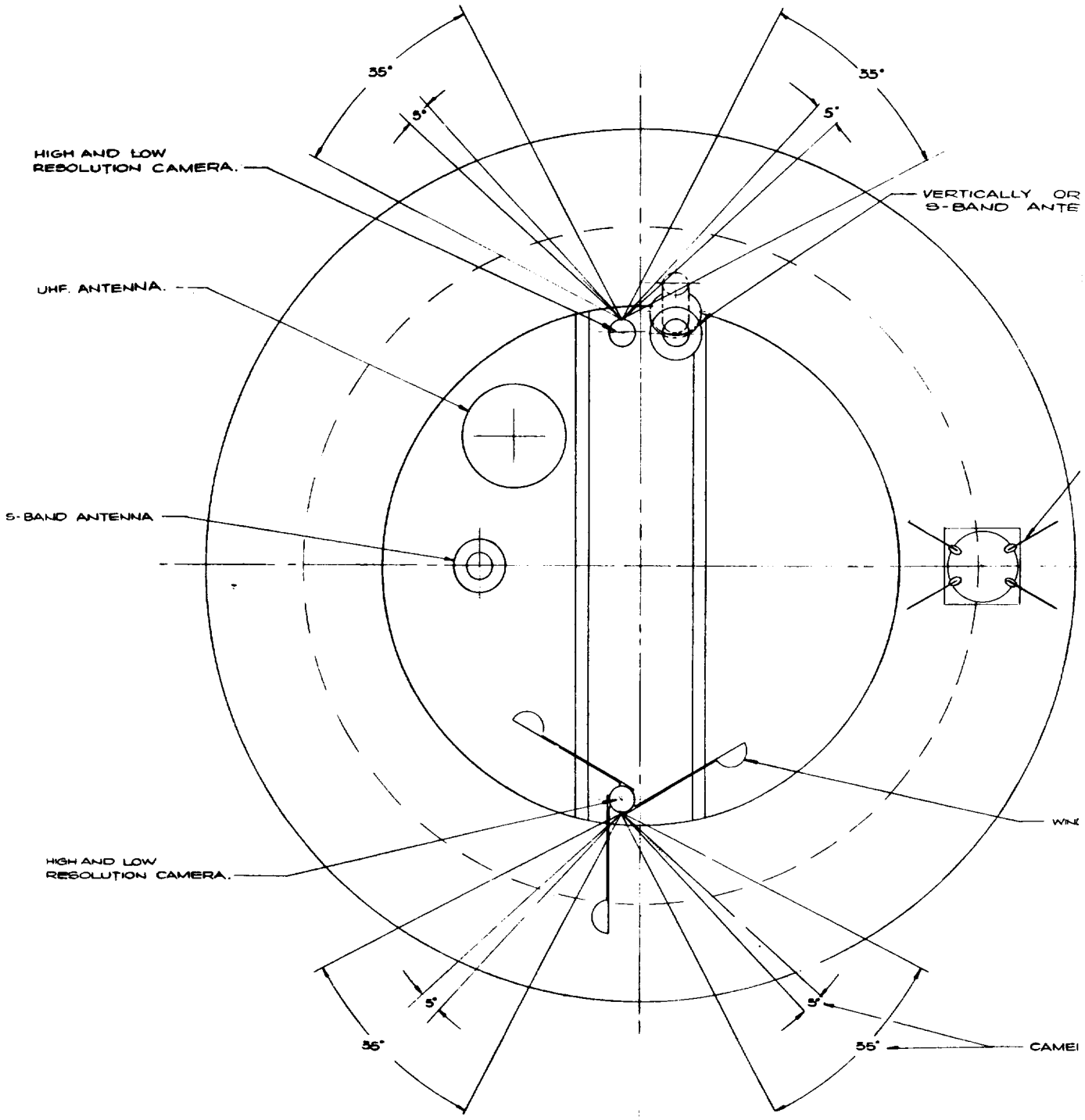

FOLDOUT FRAME 1

IENTED
NNA.

UHF. RELAY ANTENNA.

D VELOCITY TRANSDUCER.

RA FIELDS OF VIEW
(AZIMUTH)

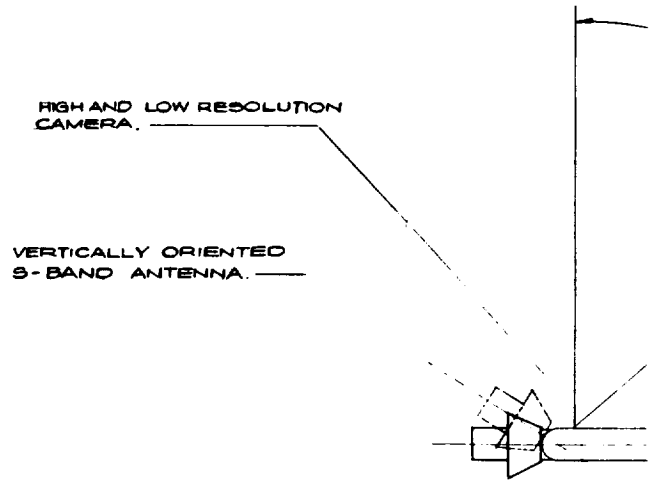

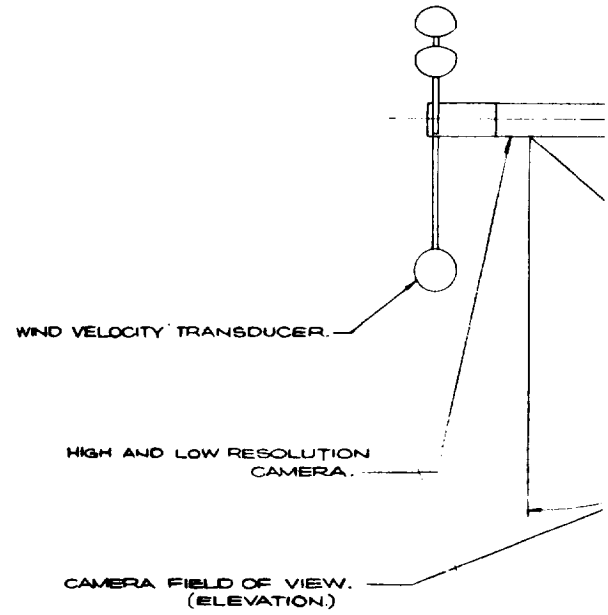

FOLDOUT FRAME 2

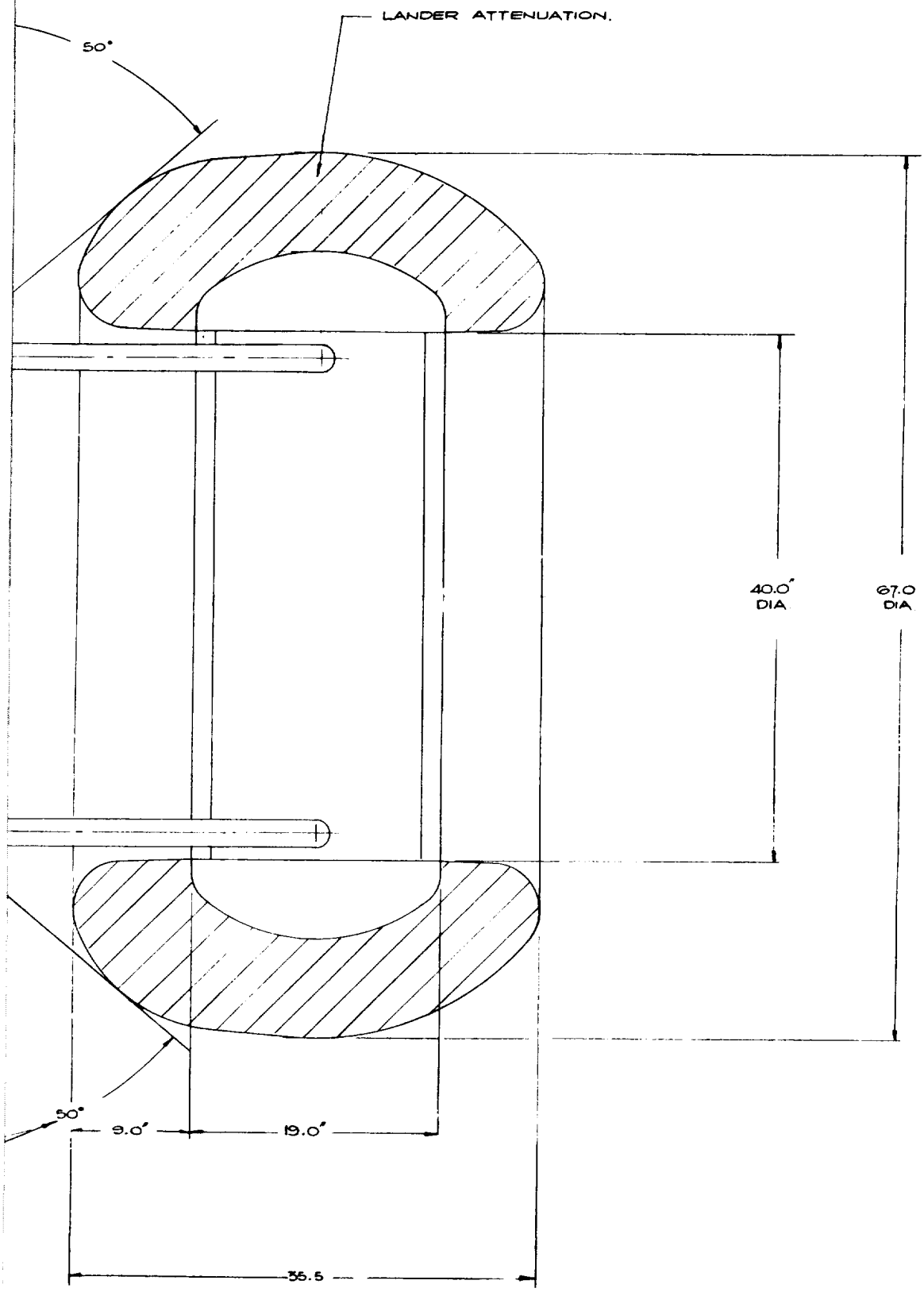

Figure 5.6-1. Lander Assembly

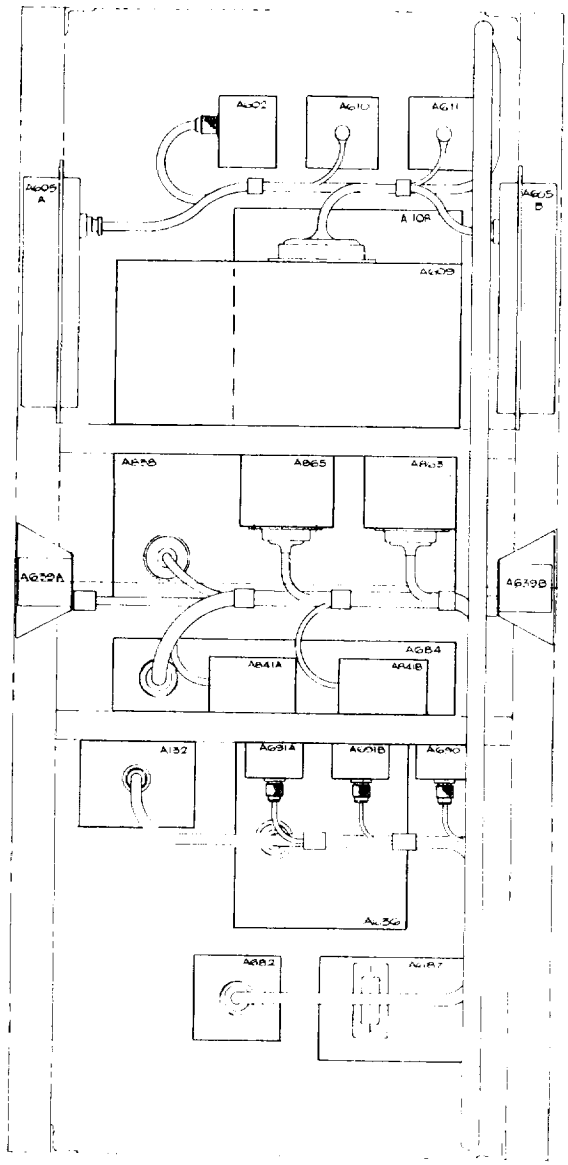

FOLDOUT FRAME

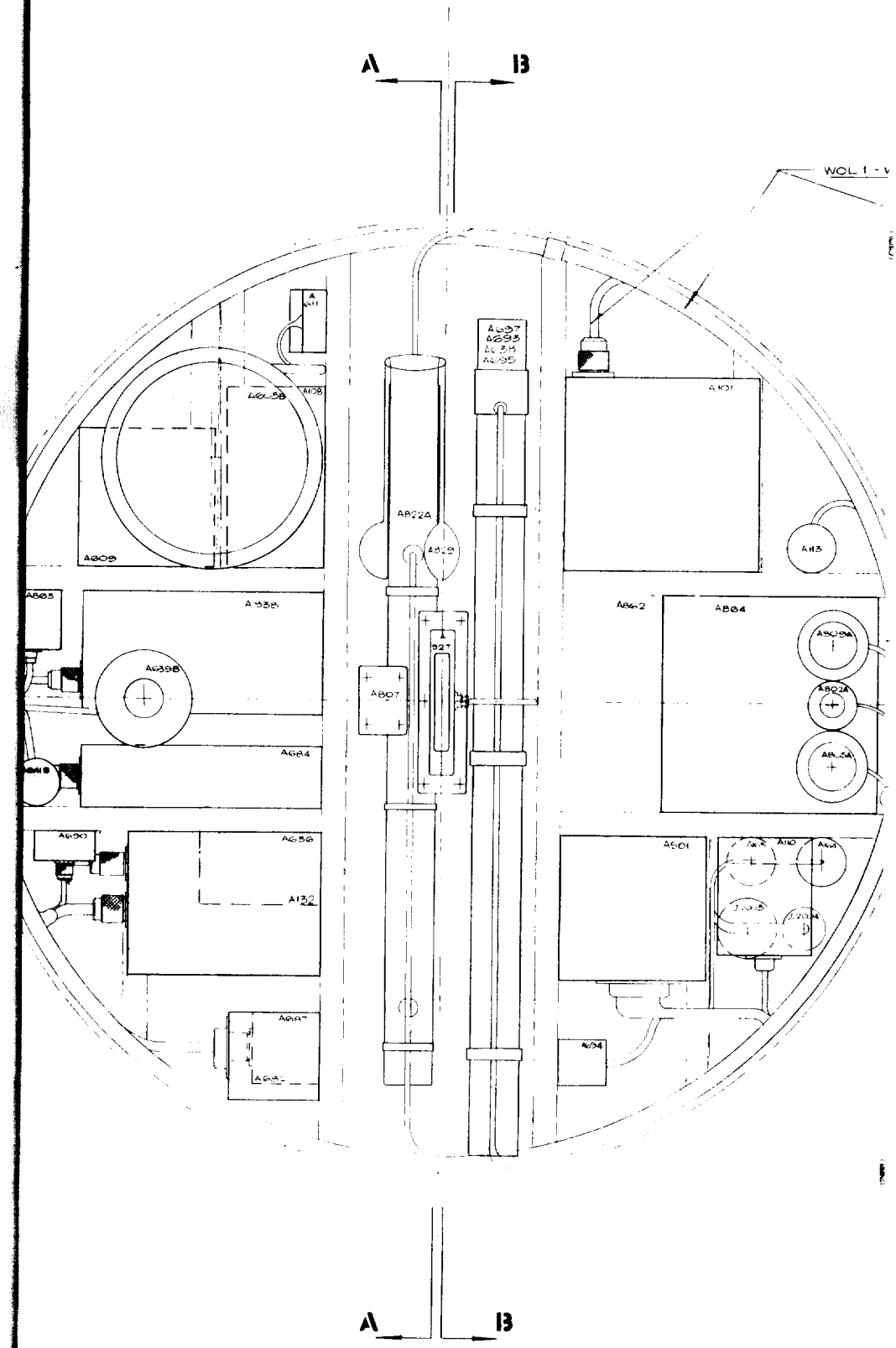

FOLDOUT FRAME 2

VOL 9

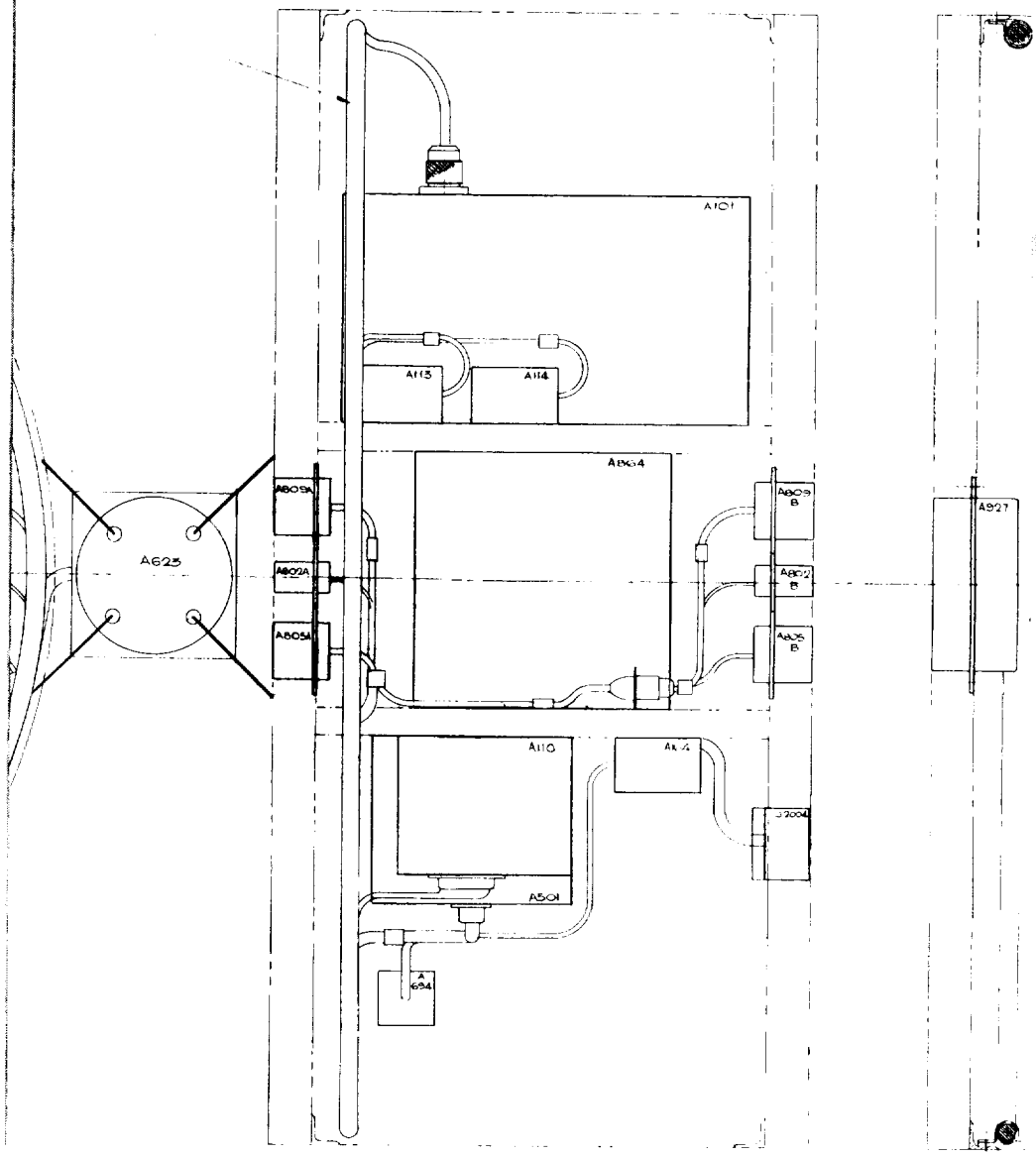

FOLDOUT FRAME 3

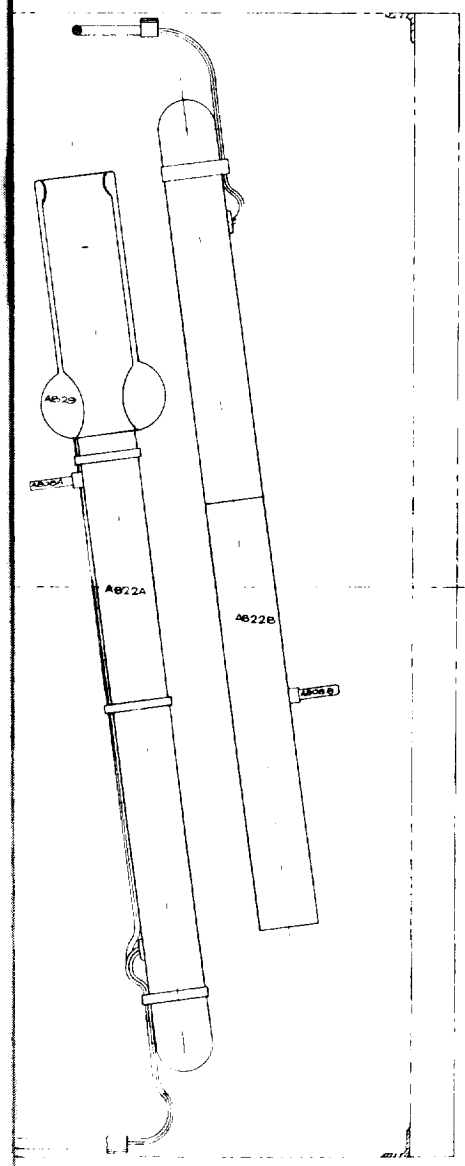

SECTION A-A

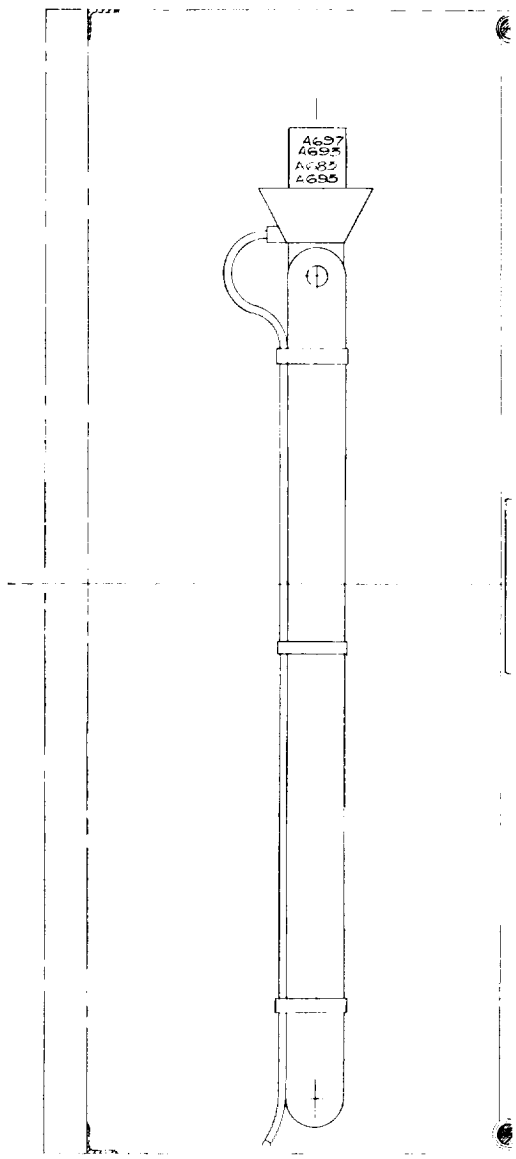

SECTION B-B

FOLDOUT FRAME 4

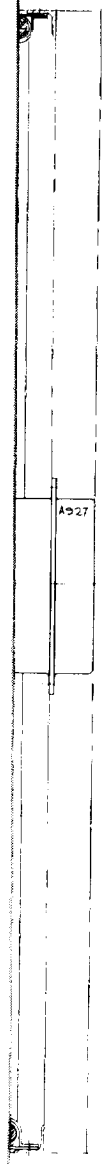

REF Nº	COMPONENT
ELECTRICAL POWER EQUIPMENT	
A101	BATTERY OPERATIONAL
A108	REGULATOR VOLTAGE A
A110	CONTROLLER POWER
A113	BATTERY, SET UP A
A114	BATTERY, SET UP B
A132	UNIT BRKER. & LIMITER
A163	BATTERY ENTRY A
A164	BATTERY ENTRY B
COMPUTER & SEQUENCING	
A501	PROCESSOR & SEQUENCER
A927	ANTENNA ALTIMETER
TELECOMMUNICATIONS	
A602	UHF TRANSMITTER
A608A, A608B	UHF ANTENNA
A609	DATA HANDLING UNIT
A610	UHF CIRCULATOR
A611	UHF CIRCULATOR
A623	UHF ANTENNA
A636	TRANSPONDER
A638	S-BAND ANTENNA
A638A	S-BAND ANTENNA
A638B	S-BAND ANTENNA
A682	IMPACT MEAS.
A684	S-BAND P/A
A687	COMMAND DETECTOR
A690	CIRCULATOR
A691A	CIRCULATOR
A691B	CIRCULATOR
A693	UNIT GRAVITY
A694	UNIT CONTROL
A695	MOTOR STEPPING
A697	SWITCH UMT.

REF Nº	COMPONENT
ENTRY SCIENCE	
A802A	TEMPERATURE TRANSDUCER
A802B	TEMPERATURE TRANSDUCER
A805A	PRESS TRANSDUCER
A805B	PRESS TRANSDUCER
A807	TRI-AXIAL ACCELEROMETER
SURFACE SCIENCE	
A808A	TEMPERATURE TRANSDUCER
A808B	TEMPERATURE TRANSDUCER
A809A	PRESSURE TRANSDUCER
A809B	PRESSURE TRANSDUCER
A822A	CAMERA
A822B	CAMERA
A823	WIND VELOCITY CUP ANEMOMETER
A838	GAS CHROMATOGRAPH MASS SPEC
A841A	CLINOMETER
A841B	CLINOMETER
A862	SOIL SAMPLER
A863	HYGROMETER SURFACE
A864	WOLF TRAP, LIFE DETECTOR
A865	HYGROMETER ATMOSPHERIC
ELECTRICAL INTERFACE EQUIPMENT	
A2003	IFD TC-LANDER
A2004	IFD AS-LANDER
HARNESSES	
WOL1	CABLE ASSY CMMD
WOL2	CABLE ASSY CMMD
WOL3	CABLE ASSY POWER
WOL4	CABLE ASSY INSTRUM.
WOL5	CABLE ASSY INSTRUM
WOL6	CABLE ASSY SHIELD
WOL7	CABLE ASSY POWER
WOL8	CABLE ASSY COAXIAL
WOL9	CABLE COAXIAL

Figure 5.6-2. Lander Component Arrangement

FOLDOUT FRAME 5

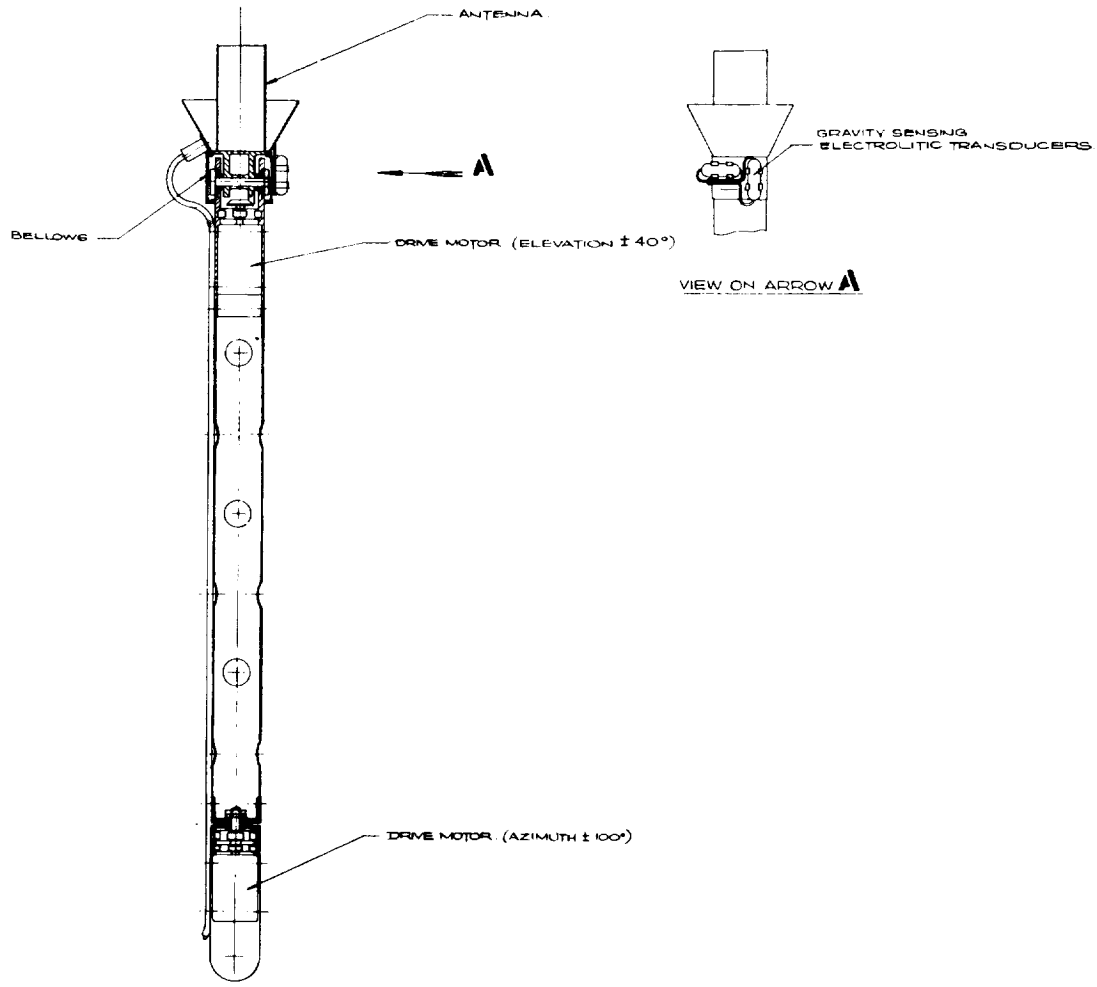

GRAVITY OF

VIEW SHOWING MOTOR DRIVEN S-BAND ANTENNA
(PREFERRED DESIGN.)

FOLDOUT FRAME 1

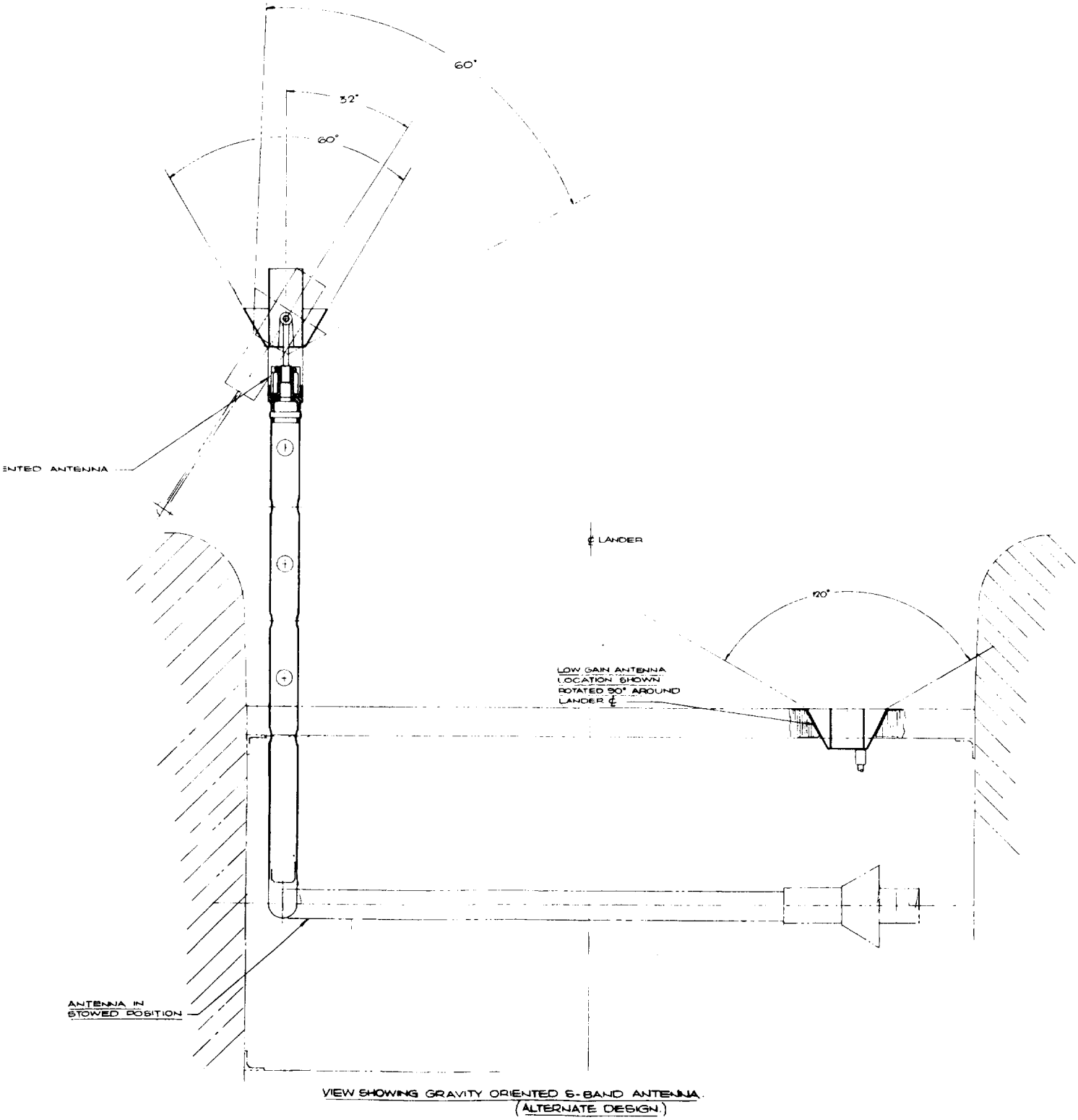

Figure 5.6-3. S-band Vertical Antenna

FOLDOUT FRAME 2

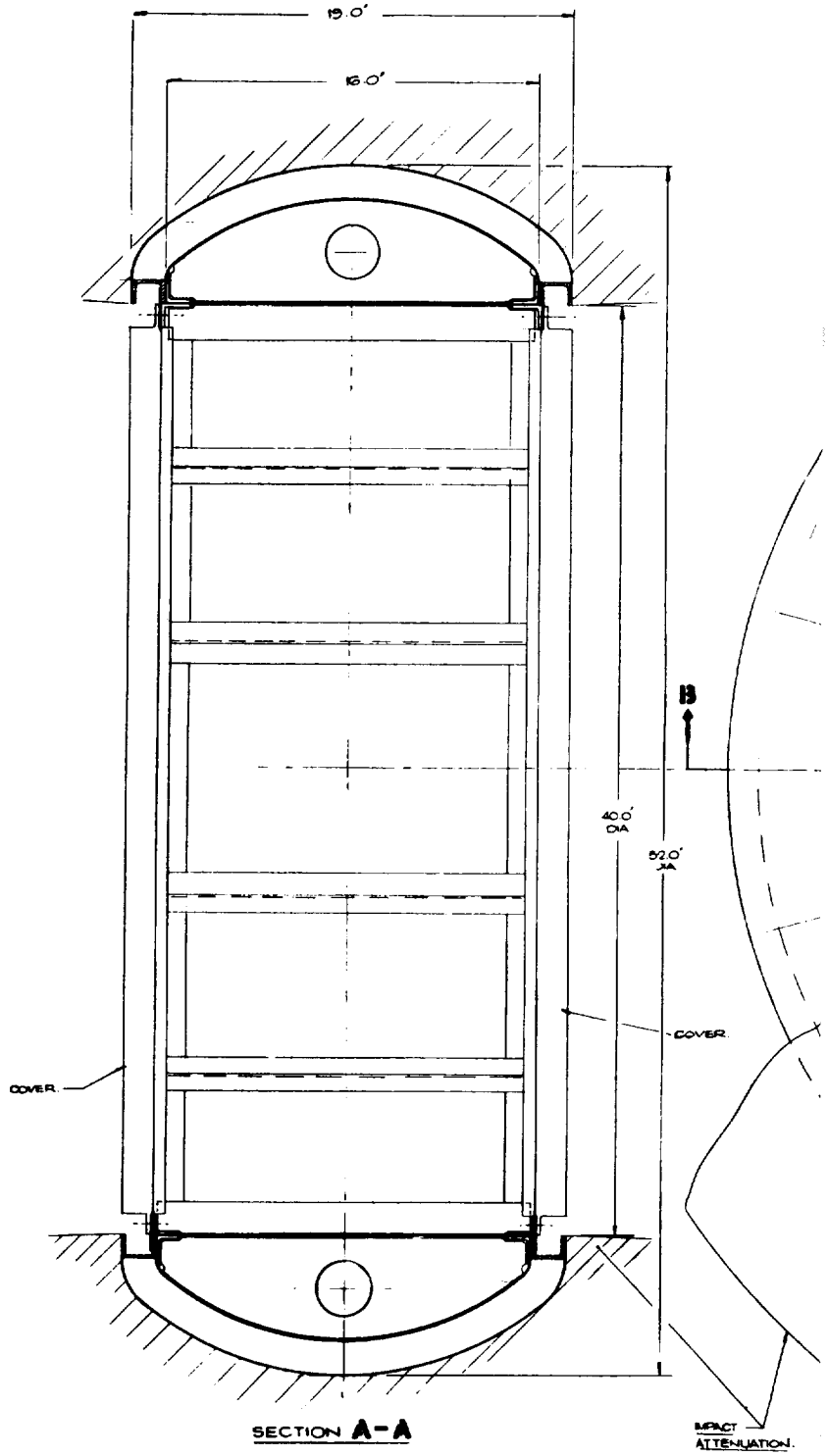

FOLDOUT FRAME 1

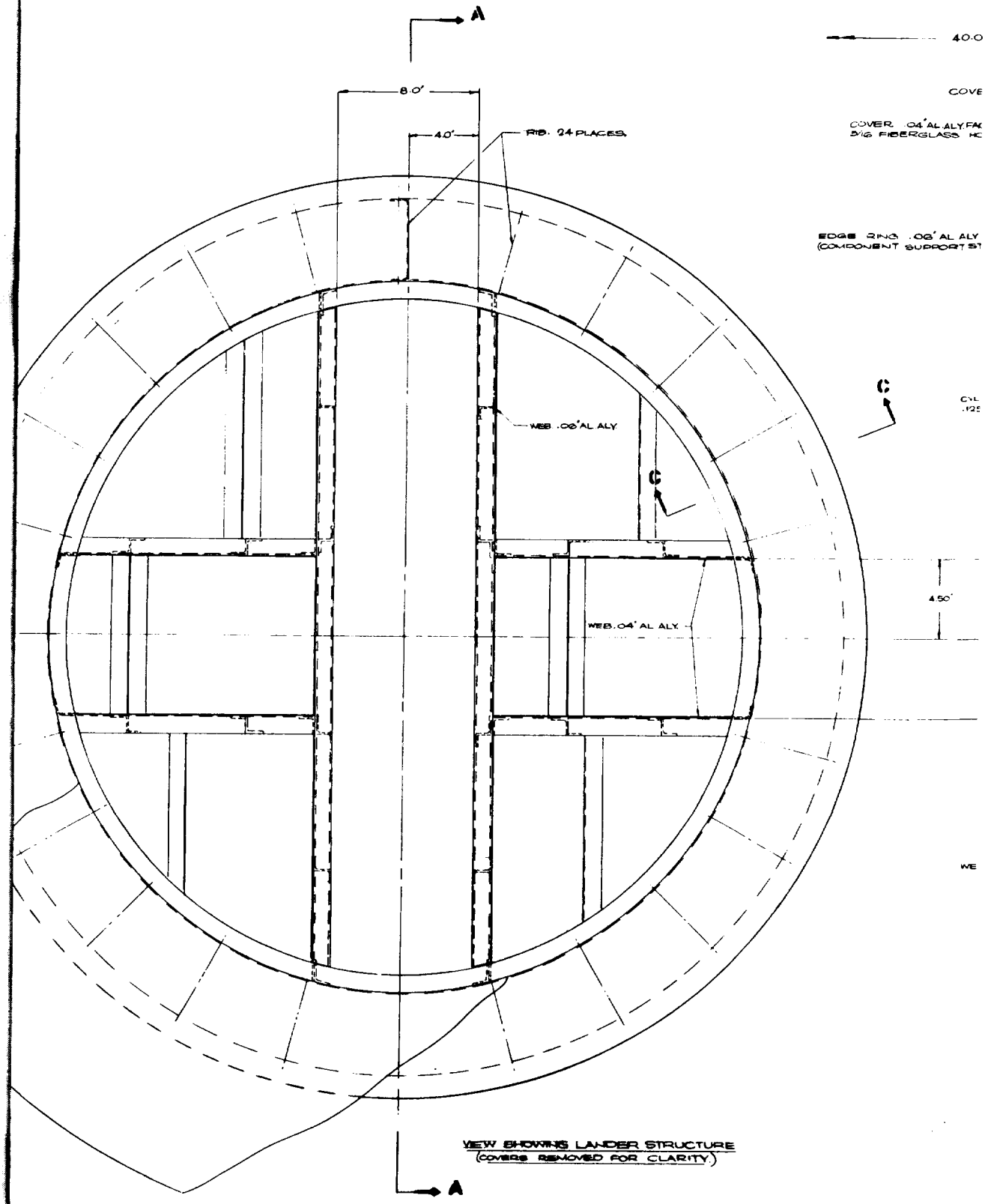

VIEW SHOWING LANDER STRUCTURE
(COVERS REMOVED FOR CLARITY)

FOLDOUT FRAME 2

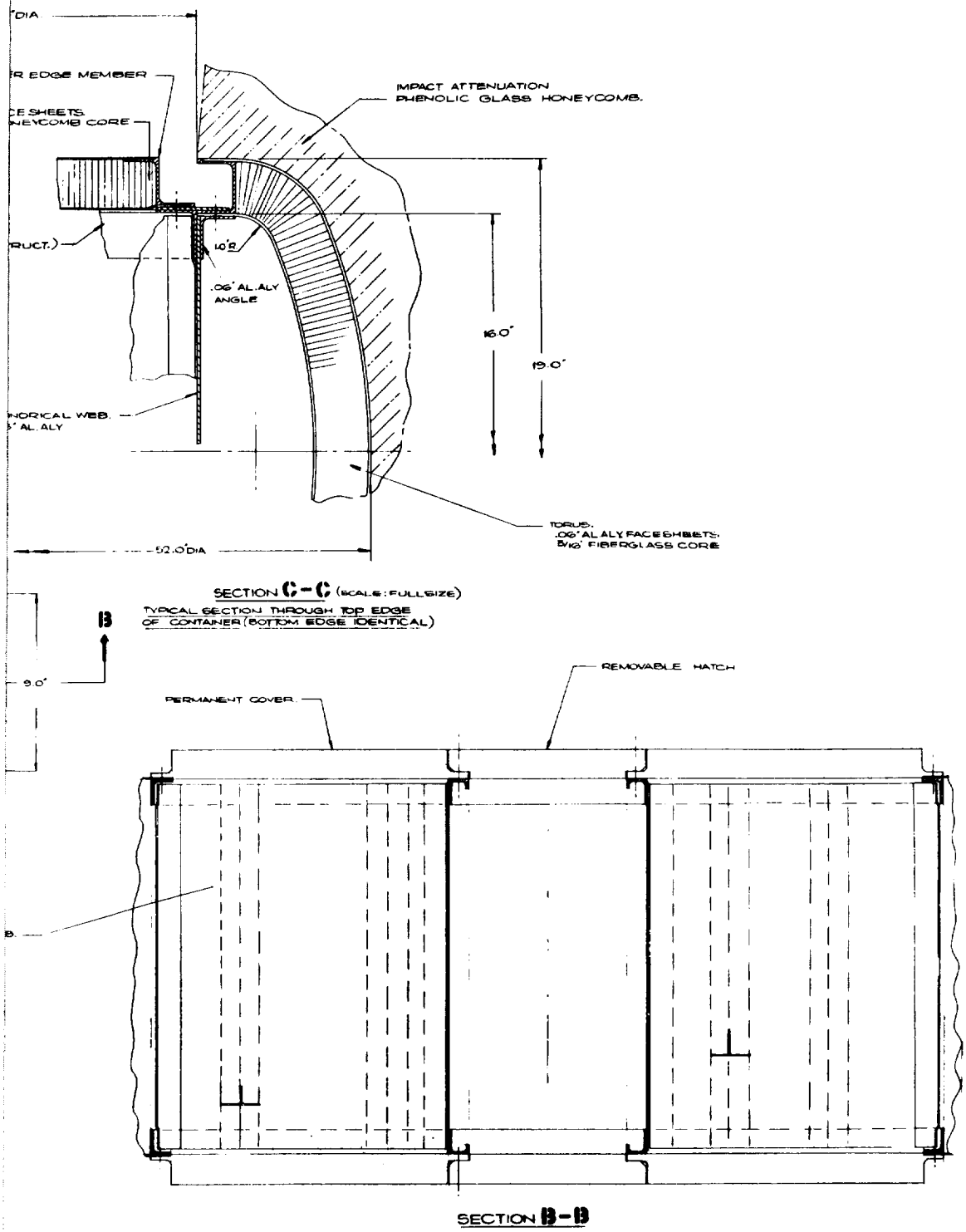

Figure 5.6-4. Lander Structure Detail

FOLDOUT FRAME 3

structure such that the inner cylindrical structure will not be overloaded. These radial nose stiffeners are spaced at approximately 5.0 in. around the circumference and are designed to transfer 50 percent of the total design loading to the internal cylindrical web. This critical design load is the 780 psi pressure load at the interface of the attenuator material and the outer facing of the D-shaped toroidal honeycomb. This 780 psi is due to a 1000 g impact where the Lander makes an angle of 60° with the Martian surface and the velocity vector passes through the point of impact. The toroidal D-shaped honeycomb structure has 0.060-in. 7075-T6 aluminum facings with a core thickness of 1.25 in. This compares with the basic container cylinder wall thickness of .125-in. aluminum. The two 0.060 in. honeycomb facings have the same hoop restraint as the single 0.125 in. cylinder wall and each absorbs approximately 50 percent of the 780 psi pressure loading. The limiter glass honeycomb has a density of 7.3 lb/ft^3 and a crushing strength of 795 psi. The 795 psi is the maximum stress in the attenuator material and is redistributed to the torodial surface to give a peak local interface pressure of 780 psi. If the interface pressure exceeds this value locally, the radial nose ribs will buckle in this local area and the loads will be redistributed through the attenuator material to load a larger area of the torus structure to the tolerable level of 780 psi. For the flat impact condition, the radial nose ribs transfer shear from the torus to the cylinder. At intermediate loading conditions between 60° and flat impact, the nose ribs and D-shaped section structure act to provide combined compression and shear transfer. The 1.25-in. deep honeycomb outer shell of the D-shaped edge structure is designed to withstand 390 psi in hoop restraint and 390 psi in bending from one nose rib to the next.

The full depth cross members of the inner space frame stiffen the overall container against deformation from the cylindrical shape and resists bending of the flat pack, as well as providing support for individual components and distributing their applied loads. Covers are considered secondary structure. The maximum bending of the flat pack occurs when the Lander has an angle of approximately 30° with the Martian surface and the velocity vector is normal to the surface. This impact condition results in high rotational inertia loadings resulting in high bending and shear loadings. (See figs. 5.6-5 and -6.)

The D-shaped section edge structure, which is made as a structural subassembly and acts as a heavy ring frame with the phenolic glass impact attenuation bonded to it, is based on an 0.125 in. thick cylindrical web, suitably stiffened, with circular top and bottom angle frames. The enclosing toroidal structure of the D-shaped section is made of 1-1/4 in. thick honeycomb panels with 0.06 in. thick aluminum face sheets, 3/16 in. fiberglass core and channel section edge attachments. Aluminum alloy sheet nose ribs are included in the edge structure spaced around the periphery at 5 in. intervals. The inner space frame is designed for insertion into or removal from the flat pack, as a bench subassembly complete with the majority of the Lander instrumentation and subsystems. Individual components can also be added or removed from the top or bottom of the container. This space frame consists of a top and bottom angle ring and a series of full depth web cross beams, the two main ones forming the camera bay and four secondary ones at right-angles to the main beam. The top and bottom circular edge angles are o.06 in. thick aluminum alloy. The main cross beams have 0.06 in. aluminum alloy webs, extruded alloy channel beams, and Z section vertical stiffeners. Secondary cross beams are of similar but lighter construction in aluminum alloy. The space frame assembly is completed with vertical angles at junctions of the main and secondary cross beams and at the free ends of these beams between the top and bottom circular edge angles. Where necessary, additional angles or T-shaped section members are

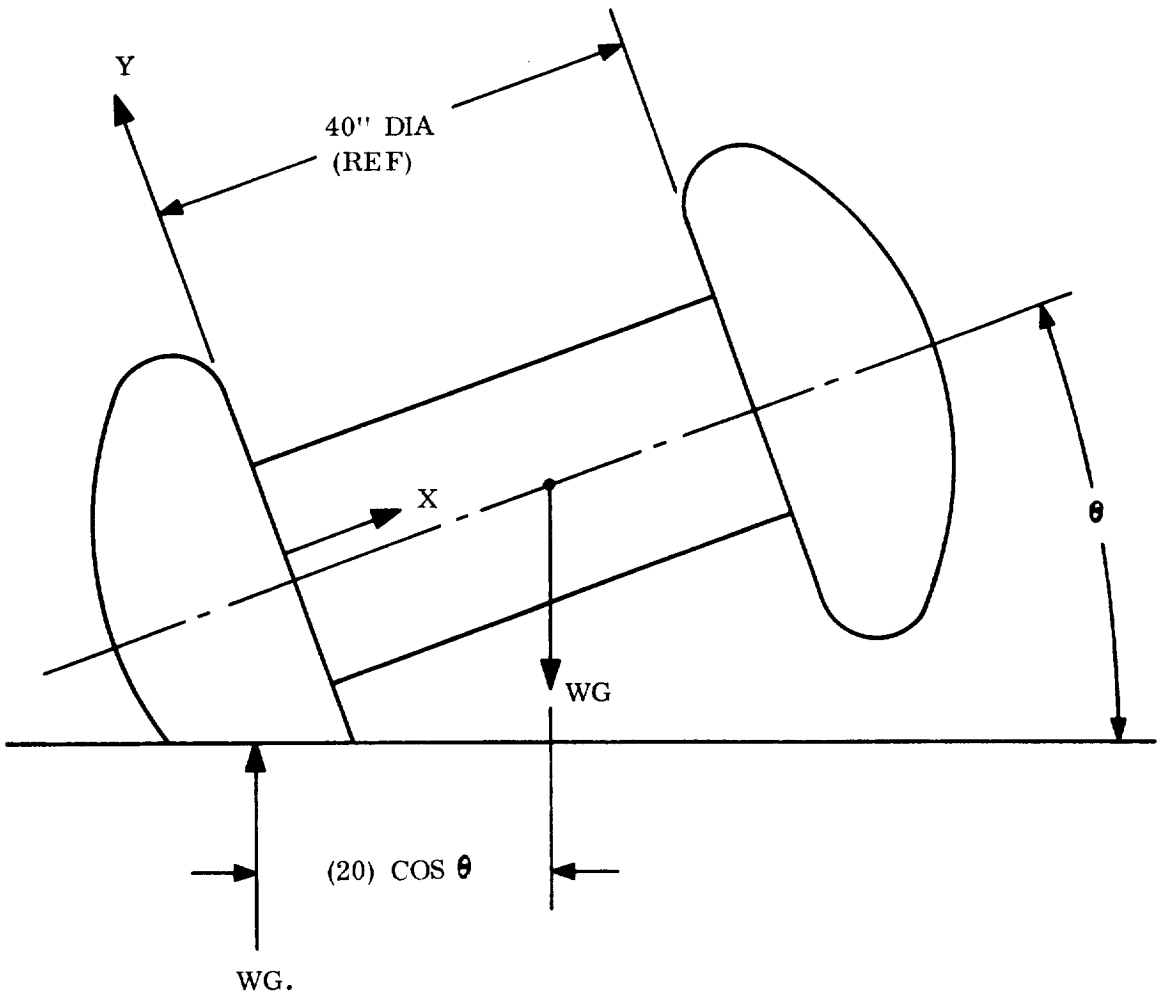

Figure 5.6-5. Lander Impact Angle

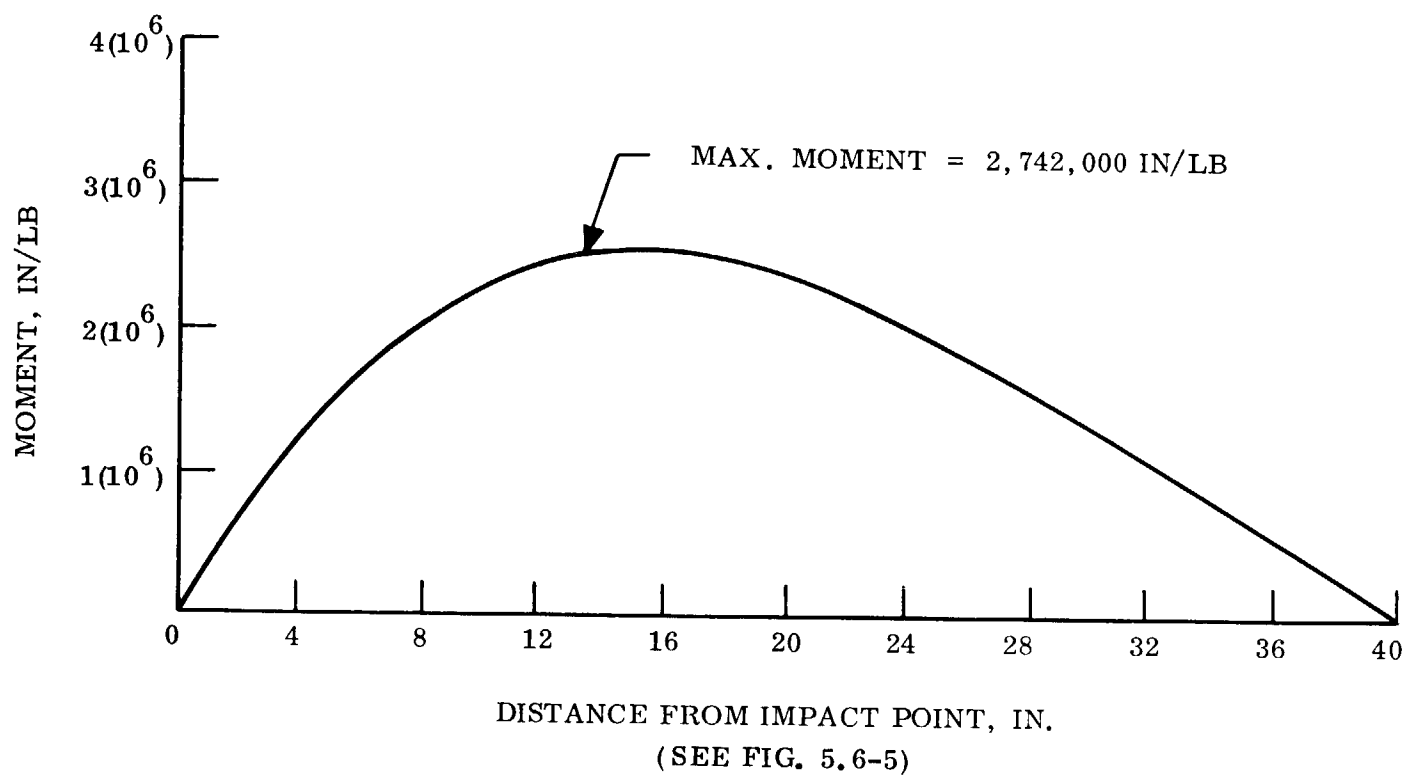

Figure 5.6-6. Bending Moment for Container Structure at $\theta = 30^{\circ}$

inserted horizontally between the full depth cross beams, for additional support of individual components. A primary attachment of the inner space frame to the toroidal edge structure is made through the vertical flanges of the top and bottom edge angles.

The Lander container top and bottom fixed covers are 1.35 in. thick honeycomb panels with 0.04 in. aluminum face sheets and 3/16 in. hexagonal cell fiberglass core material. A channel section is inserted in the edge between the face sheets for attachment purposes. The edge members of the D-shaped section cylindrical torus, the inner space frame and covers, when bolted together, form strong rings at the top and bottom surfaces of the Lander container and a primary load path.

Jettisonable doors are provided in each of the camera bays to permit deployment of these instruments. These doors are not considered primary structure but add to the stiffness and strength of the complete Lander and are consequently designed as honeycomb panels, but of reduced thickness relative to the fixed covers.

Thick honeycomb panels with fiberglass core have been selected for the construction of the outer shell of the container as a means of satisfying both structural and thermal requirements. Surfaces of the full depth cross beams, which are exposed when the camera bay doors are jettisoned, are thermally insulated with a layer of foam at least to the full depth of the beam vertical stiffeners. The foam is covered with plastic coating to maintain integrity on landing impact.

It was determined by energy considerations that for impact angles other than zero, up to 60°, from 15 to 24 percent of the total kinetic energy is used in angular acceleration of the Lander. In the design, this was considered to be equivalent to a 10 percent reduction in the rigid body deceleration at the center of gravity for θ from 30° to 60° as illustrated in fig. 5.6-5. A 900 g-load was considered for these conditions.

5.6.2.1 Container Bending Analysis

The critical load for bending of the flat pack cylinder/D-ring structure is the condition where the Lander angle at impact is 30° to the surface and the velocity vector is normal to the surface as shown in fig. 5.6-5. The rigid body acceleration in the X and Y directions and about the center of gravity are as shown in fig. 5.6-5 and summarized in table 5.6-1.

With the mass moment of inertia about the center of gravity (I_o) of 937 ft^2-lb; G = 900 g's, and the Lander weight of 661 lb; the accelerations listed in table 5.6.2-1 were determined.

The most severe bending occurs at $\theta = 30^\circ$. The bending moment diagram is shown in fig. 5.6-6.

Associated with this moment there is a compressive load in the "X" direction due to the 450 g's in this direction. At the minimum container cross-section, at X = 20 in., this compressive load is 148,000 lb.

TABLE 5.6-1. ACCELERATIONS

$\theta = 30^\circ$, $G_X = 450$ g		$\theta = 45^\circ$, $G_X = 635$ g		$\theta = 60^\circ$, $G_X = 780$ g	
X	G_y	X	G_y	X	G_y
0	1970	0	1610	0	868
20	750	20	635	20	450
40	423	40	345	40	245

The minimum cross-section of the container structure is shown in fig. 5.6-7. The maximum stress due to combined bending and compression is as follows:

Moment = 2,742,000 in.-lb

Compression load = 148,000 lb

Moment of inertia = 526.4 in.^{4}

Area of minimum section = 15.78 in.^{4}

The maximum compression stress is -57,000 psi and tensile stress is 38,000 psi.

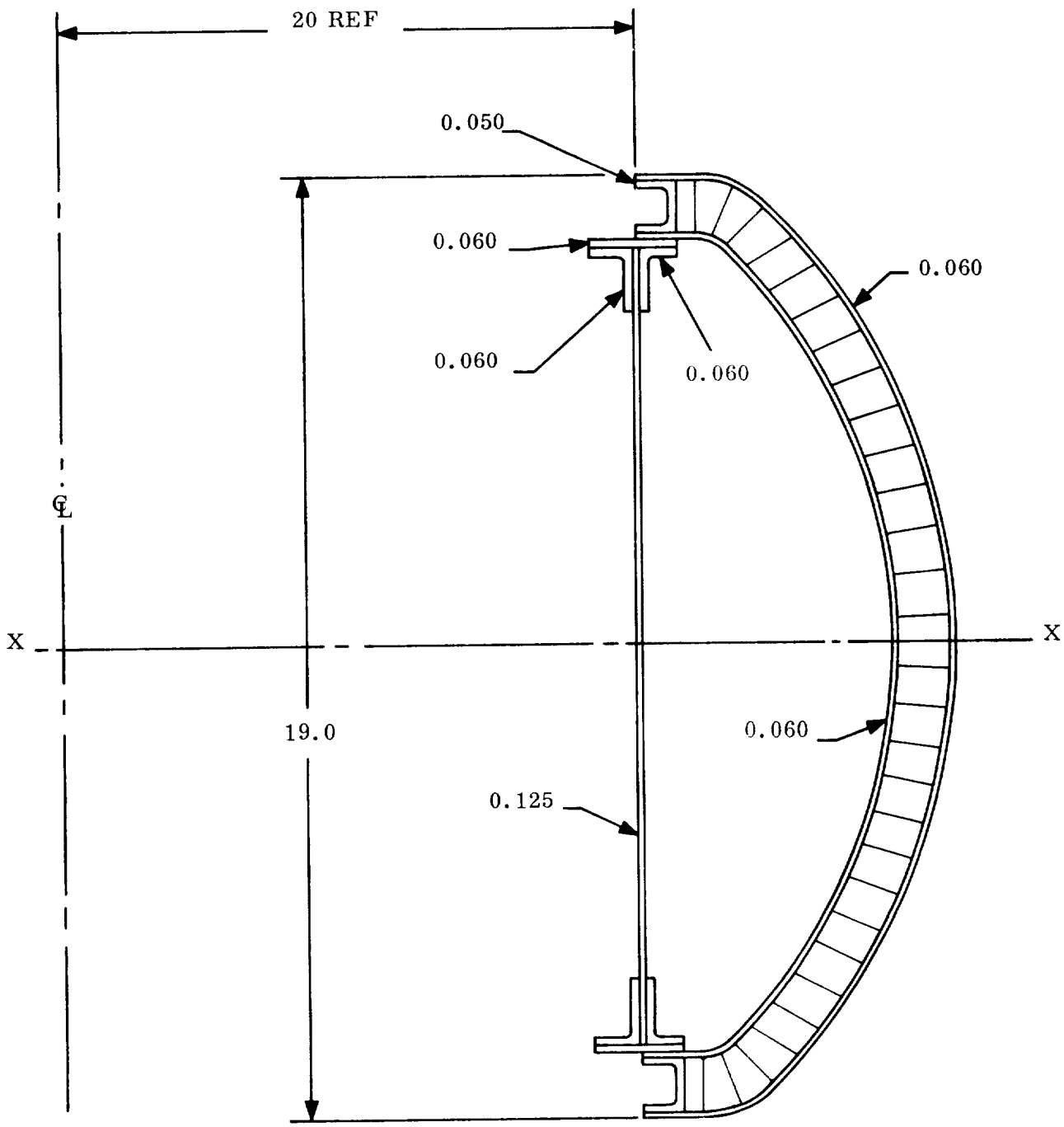

$I_{xx} = 526.4\ in^4$

$A = 15.78\ in^2$

ALL DIMENSIONS ARE IN INCHES

Figure 5.6-7. Minimum Container Cross Section

5.6.3 LANDER PACKAGING STUDIES

Lander packaging studies have been made based on two design approaches. The fundamental studies have covered the installation of conventional support subsystem components, together with scientific equipment as shown in fig. 5.6-2. For comparison, parallel investigations have been made on alternative packaging concepts for support subsystem components employing modular techniques. This is typically illustrated in figs. 5.6-8, 5.6-9 and 4.2-9. Because the payload container contains different classes of equipment, namely the scientific instruments and their supporting subsystem equipment, the flat pack Lander has been developed for either case on a zoning basis, which is divided broadly into three categories. A relatively high density packaged zone for support subsystem components, and two lower density packaged zones for scientific instrumentation and associated hardware. The zones are shown on fig. 5.6-10 (conventional packaged scheme) and fig. 5.6-11 (alternative packaged scheme) together with information on their packaging densities. This zoning approach with compartments of varying density is consistent with the fact that the characteristics of the support subsystems equipment are well established and have been through design development cycles and flight programs; therefore, packing density can be confidently predicted. However, the scientific instrumentation is new equipment and relatively undeveloped; therefore, low packaging densities are appropriate. In general, consistent with the constraints of achieving reasonable vehicle weight and good hardening capability, packaging densities selected provide adequate margins for growth and component change. In all component categories, the installed densities are less than those determined by past program experience as shown in table 5.6-2.

TABLE 5.6-2. COMPARISON OF INSTALLED GROSS PACKAGING DENSITIES

	Predicted Values (lb/ft^3)	1400 lb Design Values (Conventional Packaging) lb/ft^3	1400 lb Design Values (Alt. Concepts) lb/ft^3
Science	25 (Bios)	20	12
Support Subsystems Equipment	40	35	35
Deployables	--	6.5	6.5

The numbers given in table 5.6-2 are to some extent generalized, however, regarding the support subsystem equipment it is reasonable to assume that densities higher than the predicted value of 40 lb/ft^3 can be achieved. The low figure of 6.5 lb/ft^3 for the deployable equipment in the central bay can be readily appreciated by reference to fig. 5.6-12.

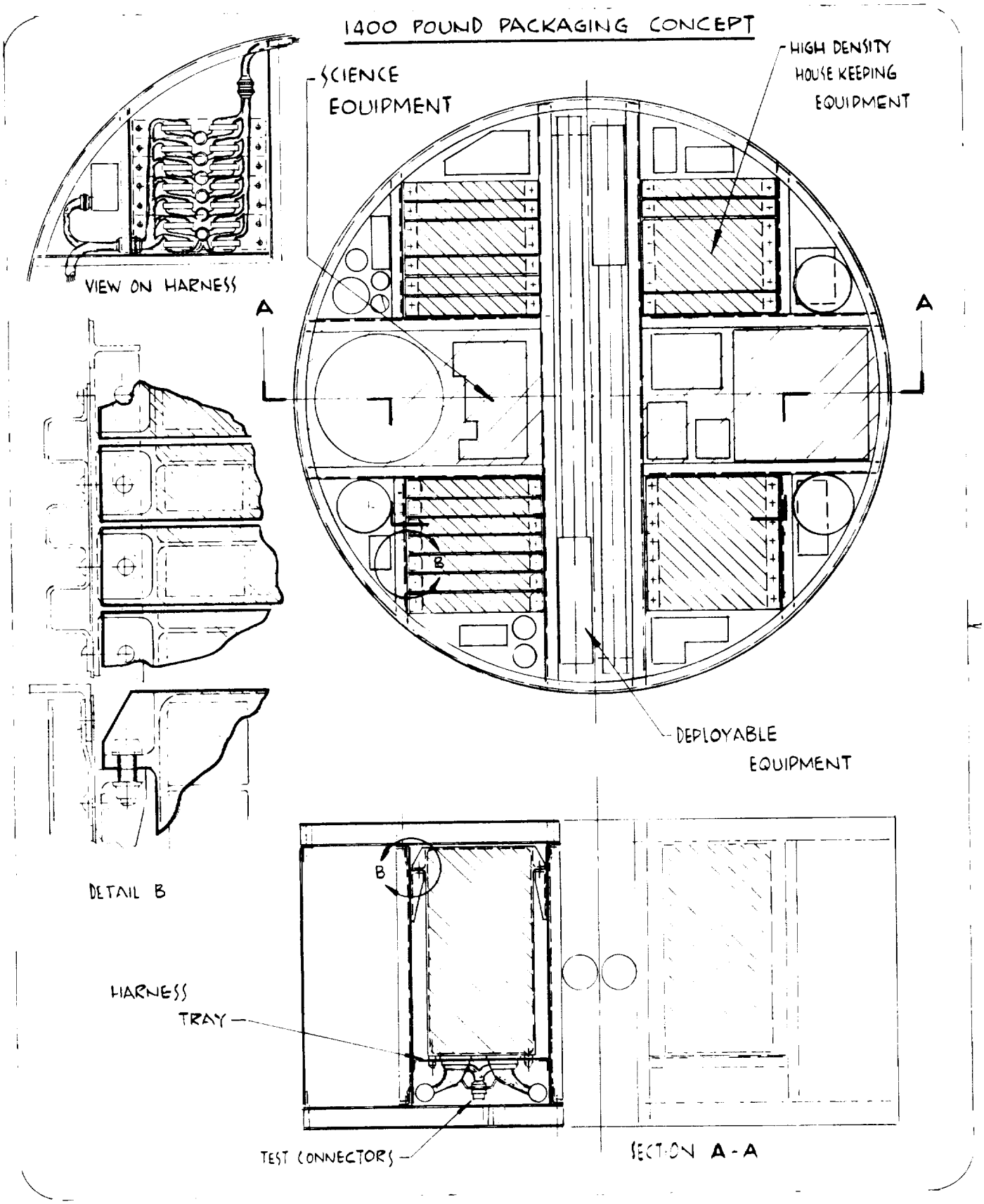

Figure 5.6-8. Lander Packaging Concept

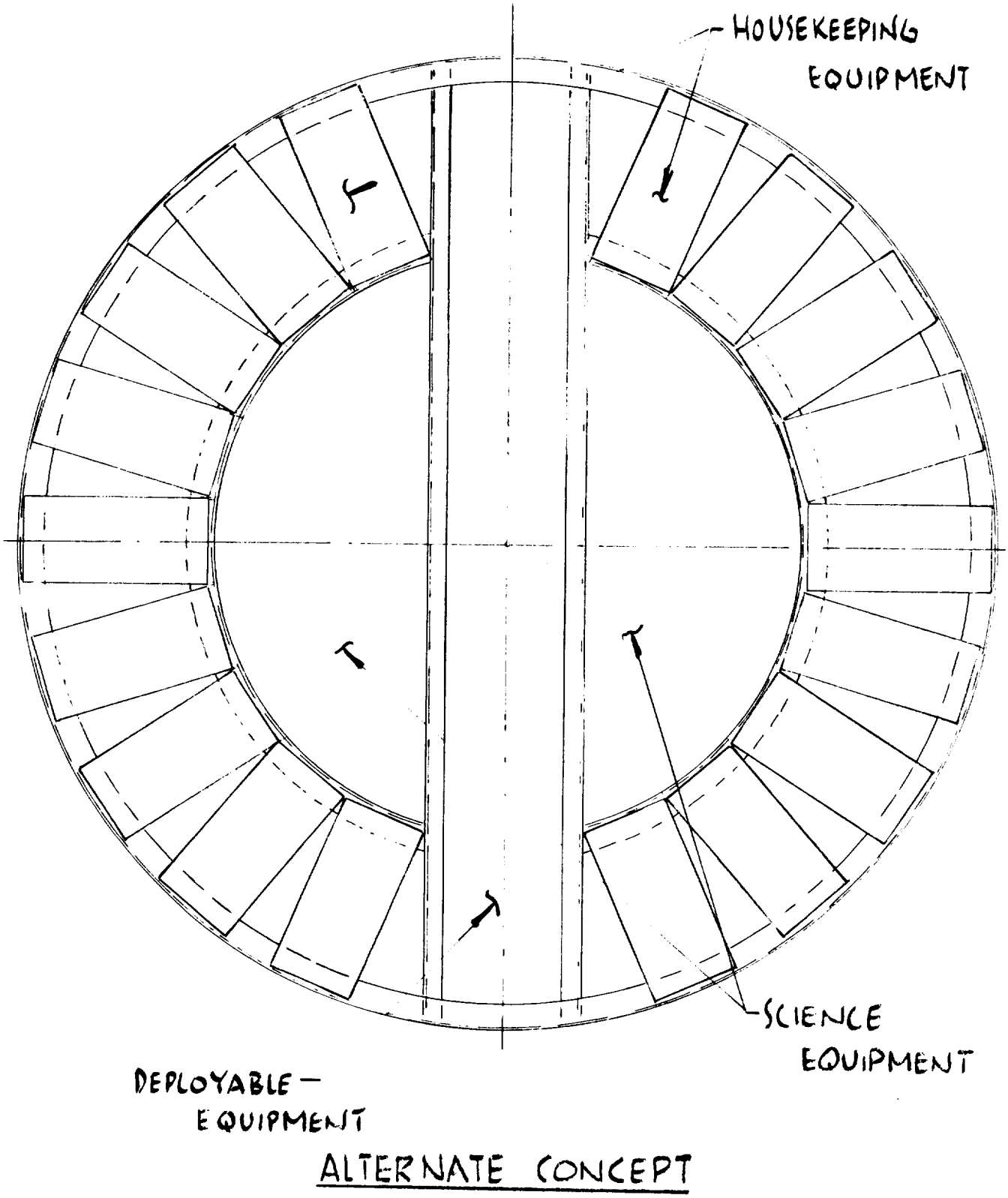

Figure 5.6-9. Alternate Packaging Concept

CLASSES OF COMPONENTS	DENSITY LB / FT ^{3}
I VEHICLE SUB SYSTEMS	35
II SCIENCE INSTRUMENTS WITH SAMPLERS	20
III DEPLOYABLES, CAMERAS ENV. SENSORS	6.5

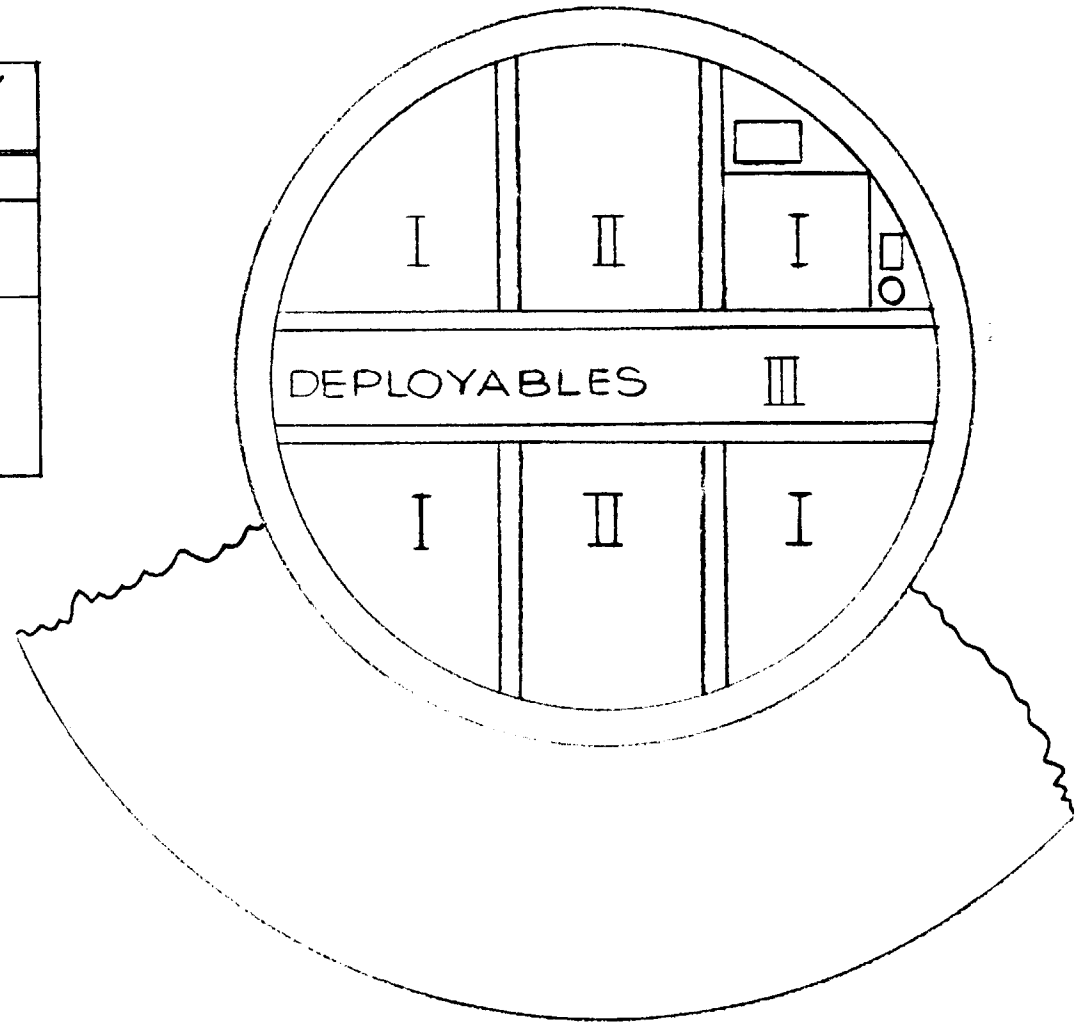

Figure 5.6-10. Conventional Packaged Scheme, Zones and Packing Densities

CLASSES OF COMPONENTS	DENSITY LB / FT³	
I VEHICLE SUB SYSTEMS	60-70	35
II VEHICLE SUB SYSTEMS	8	
III SCIENCE INSTRUMENTS WITH SAMPLERS	12	
IV DEPLOYABLES, CAMERAS ENV. SENSORS	6.5	

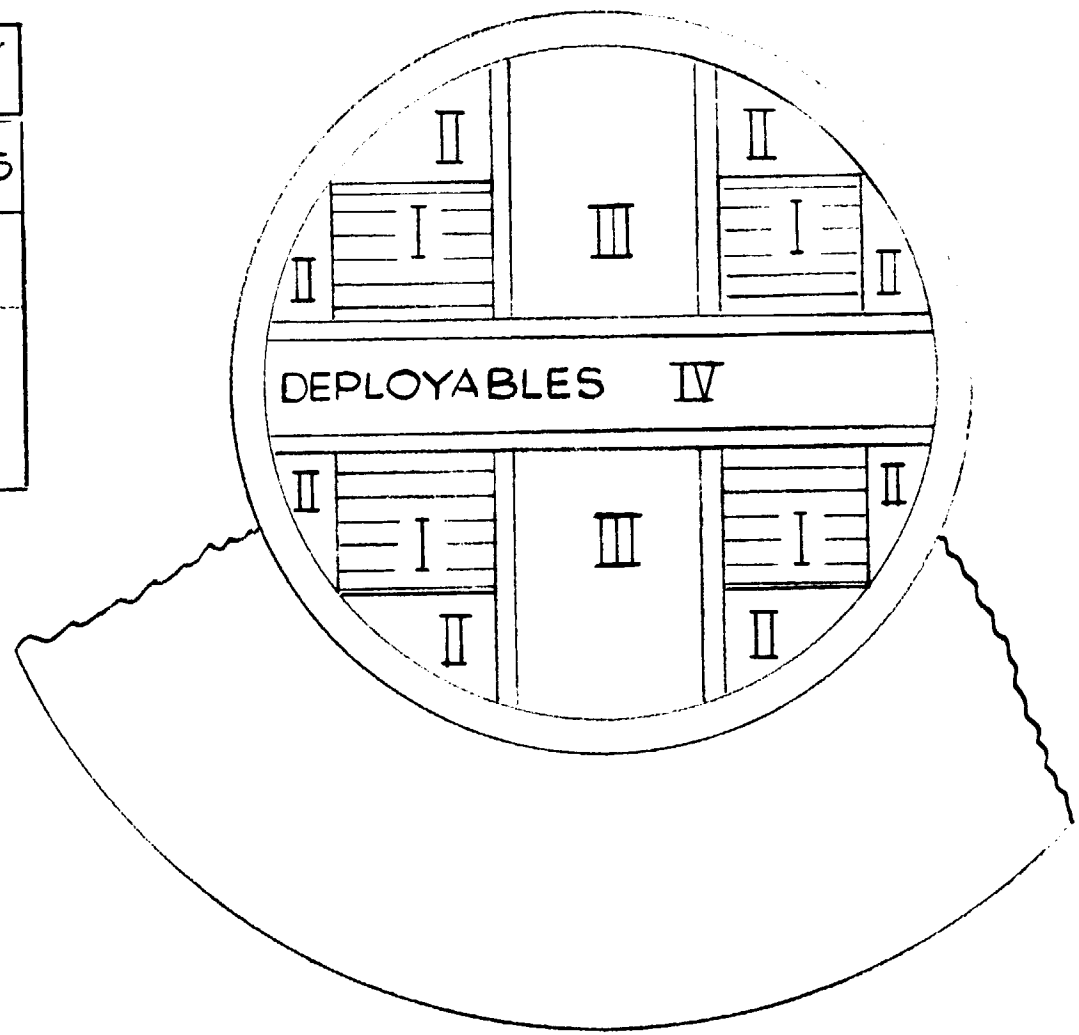

Figure 5.6-11. Alternative Packaged Scheme, Zones and Packaging Densities

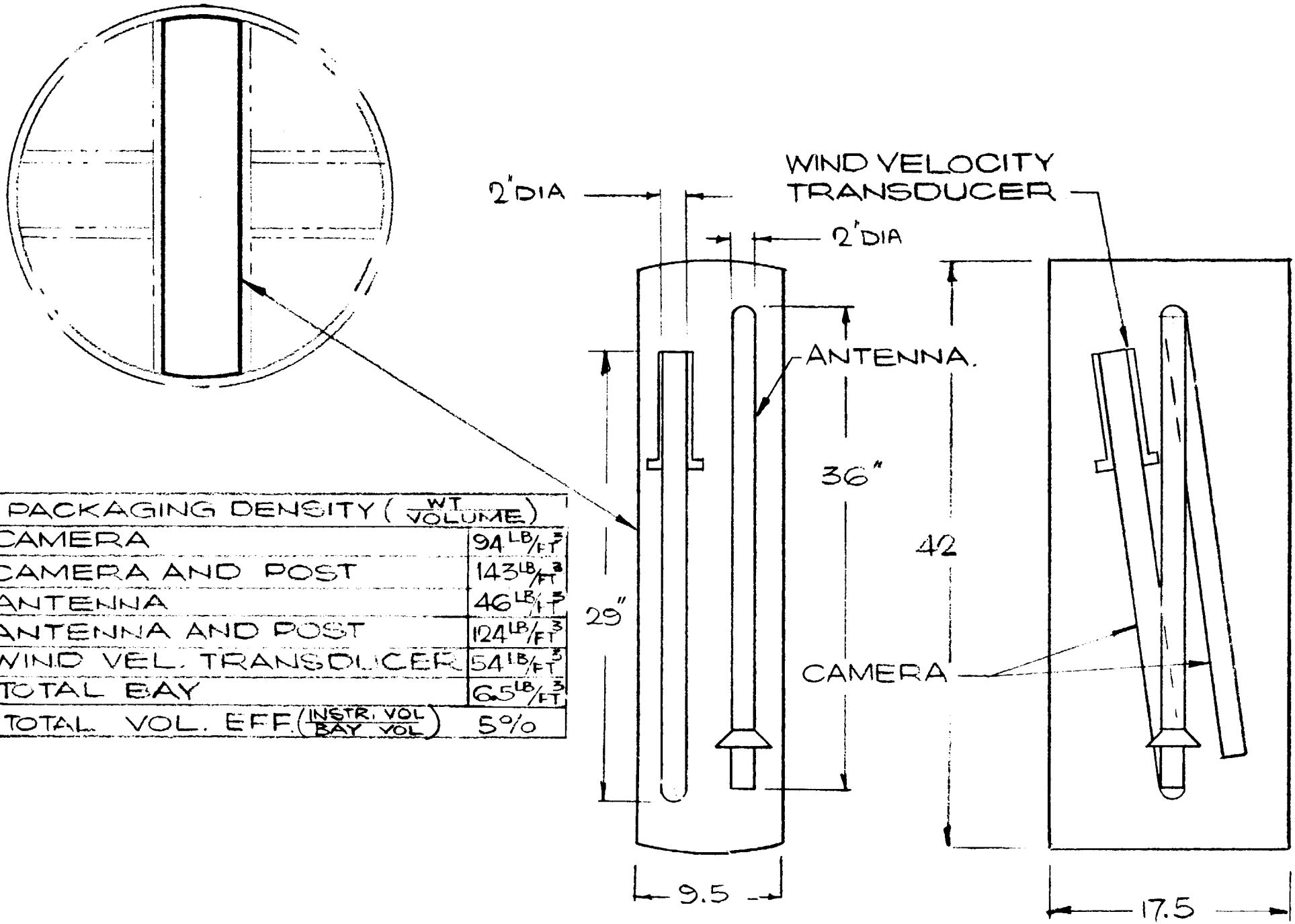

PACKAGING DENSITY (WT / VOLUME)	
CAMERA	94 LB/FT³
CAMERA AND POST	143 LB/FT³
ANTENNA	46 LB/FT³
ANTENNA AND POST	124 LB/FT³
WIND VEL. TRANSDUCER	54 LB/FT³
TOTAL BAY	6.5 LB/FT³
TOTAL VOL. EFF. (INSTR. VOL / BAY VOL)	5%

Figure 5.6-12. Central Bay

5.6.3.1 "Conventional" Packaging Concept

The scheme is illustrated in fig. 5.6-2. As previously discussed in Section 5.6.2 on the Lander container design, all components are installed on an inner Lander space frame which can be removed as a complete assembly from the container and impact attenuator or alternatively access is available in sites for the majority of individual components. Most of the wiring between components and the harnesses are incorporated in the inner space frame resulting in a substantially self-contained assembly.

The components are mounted on the five full depth webs which sub-divide the Lander space frame into discrete bays. Four corner bays are used exclusively to house the support subsystem components; the central full width bay is used for deployable items, the cameras, wind velocity and temperature transducers, and the S-band antenna. The two remaining side bays are generally reserved to house scientific equipment which requires the installation of sampling devices to operate. Adequate provision has been made for access to individual components, electrical harnesses and connections and as previously stated the initial packaging densities provide good margin for growth.

5.6.3.2 Description of Alternative Concept (Modular)

Figs. 5.6-8 and 4.2-9 illustrate a preliminary Lander packaging concept which reflects a support subsystem modular packaging design and improves the design objectives of providing design flexibility and payload growth capability.

The science equipment with associated hardware is located and packaged in bays in a similar manner to that of the conventional concept. However, increased volume is made available in a container of identical dimensions for this equipment due to the decrease in volume required for the modularized support subsystems. It will be seen that the payload container is compartmented in a similar manner to that of the conventional concept. The corner bays are again utilized for support subsystem equipment, but the modular packaging approach has been applied; the majority of this equipment is integrated into the standardized equipment modules, and the technique leaves spare volume available in the corner bays.

The modularized equipment installation is amenable to hardening, and its location close to the outer main structural ring is advantageous from the point of view of inertia and hence lower secondary G loadings. As previously stated, gross packaging densities are of the order of 35 lb/ft^3 compared with the 60-70 lb/ft^3 for the modularized equipment volume in the corner bays.

This lower gross density, or conversely this spare bay volume available, illustrates a major advantage of the modular design.

The figure of 60-70 lb/ft^3 for modular packaging itself reflects adequate margin for growth.

Table 5.6-3 shows the past, hardware program experience available for predicting the weight growth history of space vehicles. By providing allowances for growth in the housekeeping equipment bays and in the modular packaging of this equipment, the probability of a form factor change for true science zones is minimal.

TABLE 5.6-3. WEIGHT GROWTH HISTORY - FROM DESIGN CONFIGURATION FREEZE TO FLIGHT DATE

Space Vehicle Program	Percent Growth in Weight
NERV	9.5
SARV MK II	10.0
MK VI	8.0
A 45 H 30	7.5
30-Day Biosatellite	8.0
MK III	7.0
MBRV	6.6
RVTO	6.5
SARV MK IV	5.0
TVX 30	4.0
RVX 2A	3.0
MK I	3.0
MM II R/V	7.5
MM III R/V	2.0

Fig. 5.6-9 illustrates another possible variation of the modular packaging concept. The housekeeping equipment is packaged in modules around the periphery of the Lander structure with the science mounted in the remaining volume inside.

5.6.3.3 Description of Modular Equipment Packaging

The approach shown is similar to design concepts developed for Mariner and Voyager (Tasks A through D) where electronic components such as resistors, capacitors, etc., modules such as flip flops, gates, etc. and printed circuit boards are assembled to a subchassis such as the one shown in fig. 5.6-13. These subassemblies are structurally rigid and capable of sustaining the loads imposed.

Each subsystem is assembled in these subassemblies which have constant cross section heights and widths, the thickness being variable to suit individual components. Male connectors are located on the end of the subassemblies which engage floating female connectors attached to a rigid subharness tray, which is attached in the vehicle structure. The subharness has connectors which then attach to the main harness. In this way, the harness is fixed in the vehicle and is not subjected to handling, but may be removed for rework. The

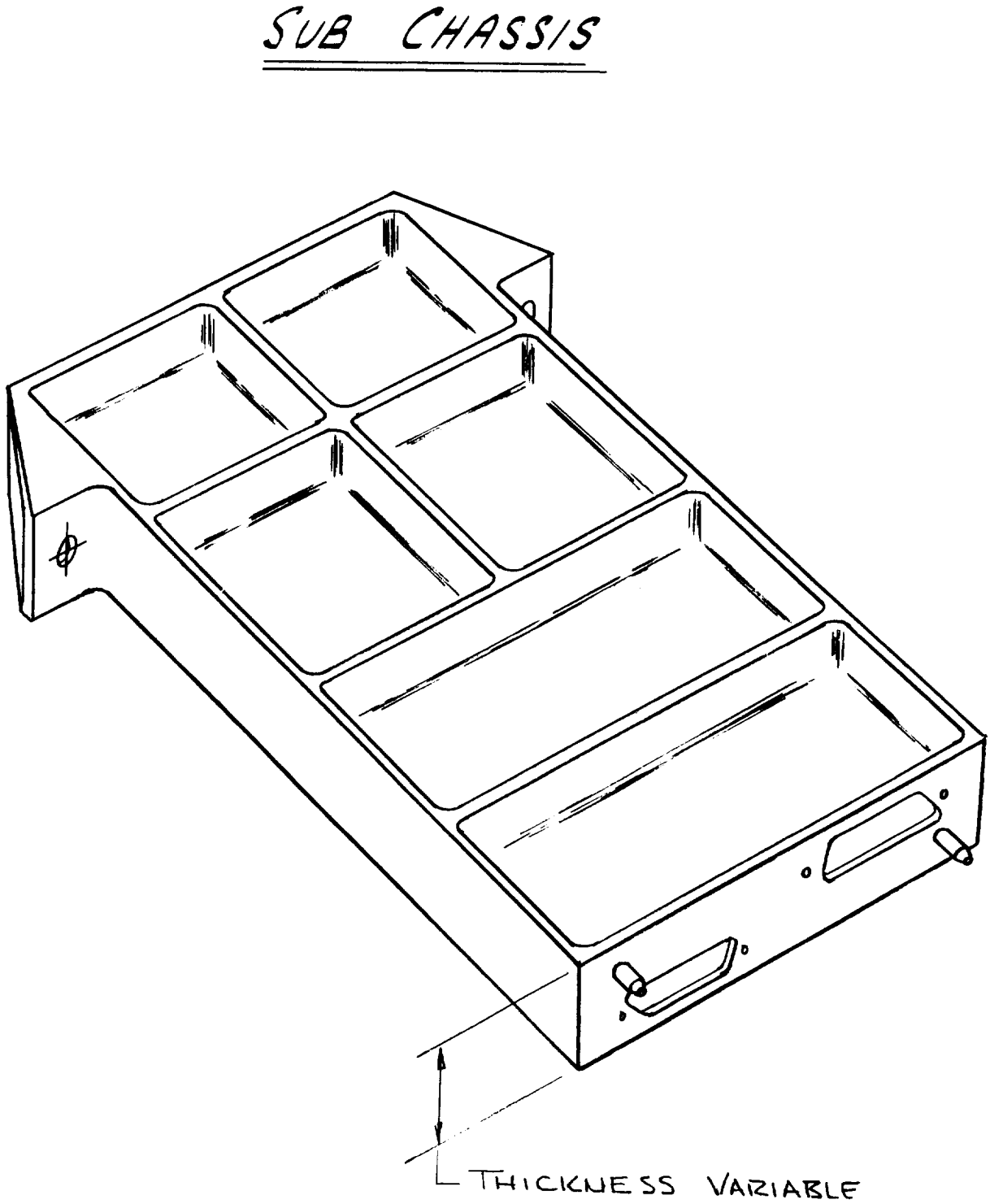

Figure 5.6-13. Component Sub-Chassis

subassemblies are rigidly assembled to the structure with minimum attachments and may be arranged to suit system requirements, such as thermal balance, weight, RF noise, etc. Payload flexibility is achieved by the ability to change the arrangement of the subassemblies without a major perturbation to the vehicle design.

5.6.3.4 Other Program Advantages

In addition to the advantages cited above, this Lander packaging concept provides other program advantages.

The standardized, modular packaging will greatly reduce the number of mountings, responses, etc. so that the overall design is simplified and more predictable. This enhances confidence in the analyses conducted and the initial design of the Lander will be improved. Thus test results obtained from the impact tests on the development system will be representative even though changes may be required within the zones. This provides schedule flexibility in that work can be done in parallel rather than in series.

Modular packaging also lends itself to an integrated harness system which is preferable from an assembly, test, maintenance and reliability viewpoint.

5.6.4 DEPLOYMENT STUDIES

In the landed position, either surface of the vehicle may be uppermost, so provision has been made for the deployment of instruments and equipment from either surface of the flat pack container. However, to avoid unnecessary duplication of instruments, the actuating mechanisms have been designed for two-way operation. A 'g' sensing device will determine the direction of deployment.

Instruments deployed from the flat pack container of the 1400 lb Capsule are the following: two cameras, one antenna, two temperature transducers, a wind velocity instrument, and a soil sampler. Except for the soil sample, all of these instruments are deployed from the central bay of the flat pack container.

5.6.4.1 Camera Installation

Each of the two cameras is a combined high resolution-low resolution instrument mounted on the free end of a pivoted tubular boom. Each boom is fabricated from aluminum alloy material with an approximate length of 30 in. and an outside diameter of 2 in. (see fig. 4.3-5). In the stowed position the two booms lie in an almost-horizontal position in the central bay in an over-and-under arrangement and are supported in this position by aluminum honeycomb saddles placed between the booms and the container covers and, in addition, between the two booms. These supports clamp the booms securely to resist the impact loads experienced by the booms during landing. Deployment is automatically initiated by a torsion spring at the hinged end of the boom when the uppermost central bay door is released and jettisoned pyrotechnically. The deployment sequence is as follows. When the upper door is removed, it takes the boom support saddles with it. This permits the upper boom to rotate about its hinge. Once the saddle on the back of the upper boom clears the lower boom, the lower boom

in turn rotates. In the final deployed condition, the two booms are vertical and spaced at opposite ends of the central bay. In this position the booms are latched against further movement.

This arrangement of relatively short swinging booms, with the capability to erect two cameras on either side of the Lander and take pictures over the edge of the Lander in segments, was selected as the most satisfactory compromise between the need for simple and stable erection devices and the requirement for adequate azimuth and vertical angles of uninterrupted vision. Studies were made of telescoping (not hinged) tubes as an alternate design, but the resulting designs proved to be unsatisfactory. Telescoping tubes cannot easily be made to extend in two directions, as required for two-way deployment capability. In addition, it was found that unless the number of cameras was doubled, the telescopes had to be many feet in length in order to provide adequate vertical angles of vision over the edge of the Lander's impact attenuator. Also, booms of such length pose serious problems regarding camera stability.

The central bay door(s) of the flat pack container are secured with bolts incorporating a hot-wire release and jettisoned by springs with sufficient force to ensure that they fall clear of the Lander.

5.6.4.2 Wind Velocity and Temperature Transducers

The wind measuring device consists of three arms 120° apart mounted on one of the camera booms with a wind cup at the end of each arm. In the stowed position these arms are parallel to the long axis of the boom. After boom ejection the three arms rotate through 90°, actuated by torsion springs. The arms are attached to a bearing which can rotate about the central axis of the boom. The temperature transducers are mounted on the camera booms, one on each boom.

5.6.4.3 Direct Link Telecommunication Antenna

A deployable S-band antenna, with local vertical orientation capability is incorporated in the Lander. It is mounted on a swinging boom, similar in design to the camera booms but with an overall length of antenna boom of approximately 36 in. The installation is illustrated in fig. 5.6-3.

The subassembly is stowed in the central equipment bay alongside the camera installation. The deployment principal is the same as that for the camera booms, namely, initiation by a two-way torsion spring, automatically actuated by the removal of the bay cover door. The boom rotates through 90° to a position alongside one of the deployed camera booms.

Erection of the antenna boom normal to the Lander automatically completes the circuit which provides power to the electro/mechanical local vertical orientation system. Two electric motors are incorporated in this system. One at the base rotates the boom in azimuth, or about its vertical axis, through $\pm 100^{o}$. The other at the top of the boom levels the antenna in the horizontal plane through $\pm 40^{o}$. The combined movement in two planes ensures that the antenna can be orientated to the local vertical for all defined Lander attitudes. Suitable gearing is incorporated so that both motors are kept to a minimum size.

Gravity sensors in conjunction with electronic logic circuitry and limit switches control the operation of the antenna to the local vertical. A block diagram of the vertical orientation sensing, control and driving mechanism is shown in fig. 5.6-14.

The antenna can be orientated and locked to the local vertical with a total position error significantly less than 5°. The design of the electro/mechanical deployment and orientation system is conventional and components can be readily selected or developed. As an illustration, the Stepping Motors required for vertically orienting the antenna can be the same as those used on the Surveyor antenna drive mechanism. Their physical and operational parameters are tabulated below.

Parameter	Value
Weight	1.2 lb
Length	2.53 in.
Diameter	1.81 in.
Step Length	40°
Temperature Range	-225°F to +260°F
Life	120,000 steps
Torque rating	27 in.-oz
Pulse length	45 msec
Coil resistance	0.66 ohm
Duty Cycle at 2 pulses/sec	15 min. on/15 min. off
Maximum pulse rate	11 pulses/sec
Current (nominal)	10.5 amp

The gravity sensor, another important element of the vertical orientation system is also a conventional component. It is proposed that dual axis gravity sensing units be installed on the antenna and typical physical characteristics are shown in fig. 5.6-15. Each unit is constructed as shown in fig. 5.6-16. The electrolytic transducer is sufficiently immune to vibration and shudder to eliminate the effects of wind gusts on the antenna, however its principal of proportional output as the horizontal position is approached provides close control and keeps hunting to a minimum. The unit weight is approximately 14 grams. It requires an a-c voltage reference source at a frequency in the range from 25 to 400 cps. The unit can operate satisfactorily at temperatures in the range -20°F to 280°F. Suitable choice of electrolyte for the sensor will enable it to meet sterilization requirements.

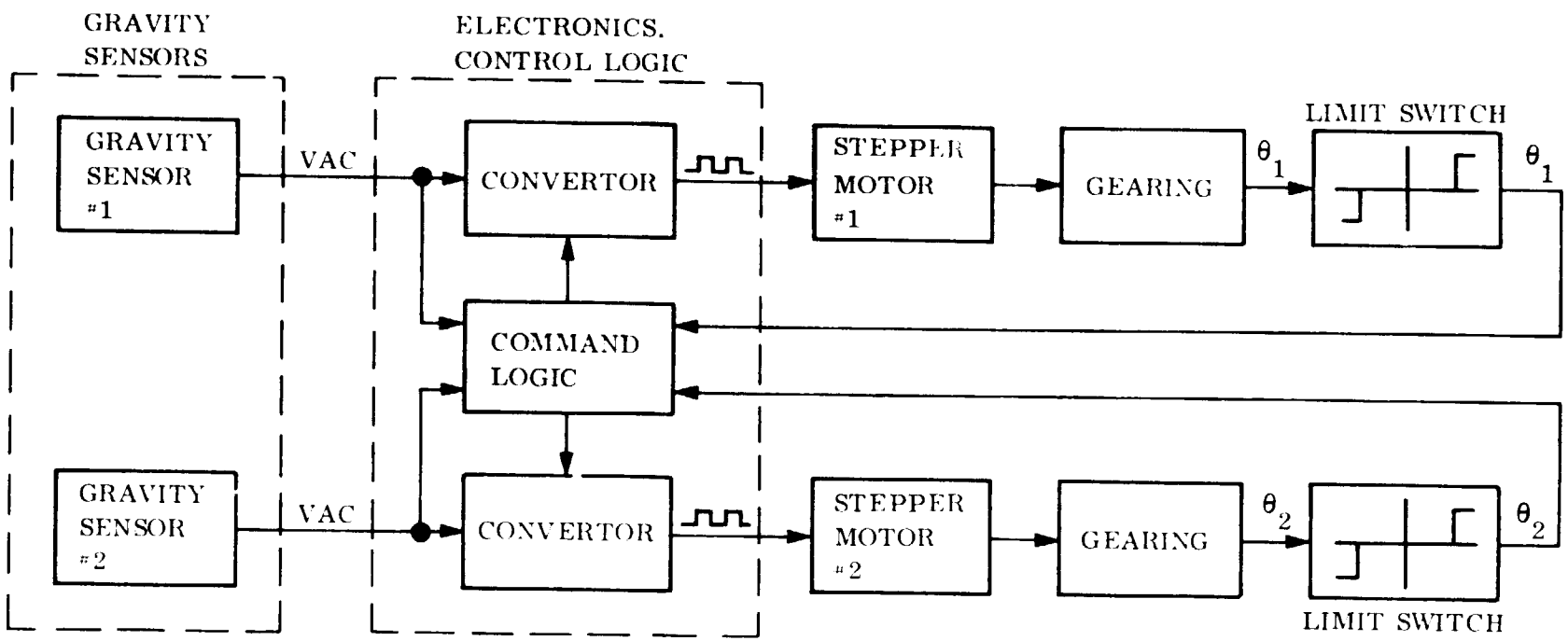

Figure 5.6-14. Block Diagram - Vertically Oriented Antenna

5.7 IMPACT LIMITER

The Lander System is designed to attenuate the landing impact loads by the mechanical crush-up of phenolic glass honeycomb. In this design concept, all of the equipment to conduct the surface operations and the major portion of the entry science mission is assembled within a cylindrical container that is surrounded by a torroidal, deep ring of phenolic glass honeycomb material. The ring of crush-up structure is bonded to a D-ring structure that provides stiffening to the cylinder rim and a load transfer path from the crush-up to the payload container.

The depth of crush-up material is a function of the square of the impact velocity, the surface slope, and the chute sway, and varies inversely with the selected deceleration rate at which the impact energy is dissipated in bringing the Lander to rest. The total depth of crush-up material is determined by adding the amount for rock clearance to the stroke required for decelerating the body to rest. The shape of the impact limiter profile is determined by the depth and area of crush-up required at the various impact conditions and potential surface contact angles.

5.7.1 REQUIREMENTS AND DESIGN CONSTRAINTS

In this Lander design, the crush-up material is determined for the following conditions. It is presumed that the surface impacted is infinitely rigid as the limit on surface bearing strength and that 100 percent of the kinetic energy at impact is dissipated in the honeycomb material actively crushed during the impact. This material is sized to bring the Lander to rest within a 1000 g's rigid body deceleration limit. Preliminary analysis indicates that rebound may occur with subsequent impacts at up to 100 ft/sec. Adequate crush-up material is provided all around the Lander to decelerate the Lander for a second time at 1000 g's. The conditions of impact are illustrated in figure 5.7-1 and are based on the following requirements:

1. 118 ft/sec horizontal velocity due to wind
2. slopes up to 20°
3. rocks of 5 in. diameter
4. maximum deceleration of 1000 g's in any direction at the impact limiter/structure interface.

In addition, the following constraints have been placed on the limiter design on the basis of system trade-offs and preliminary dynamic analysis:

1. vertical velocity at impact of 100 ft/sec
2. parachute sway angles of up to 40°
3. secondary impact in any direction (except the exact spot of primary impact) at 100 ft/sec.

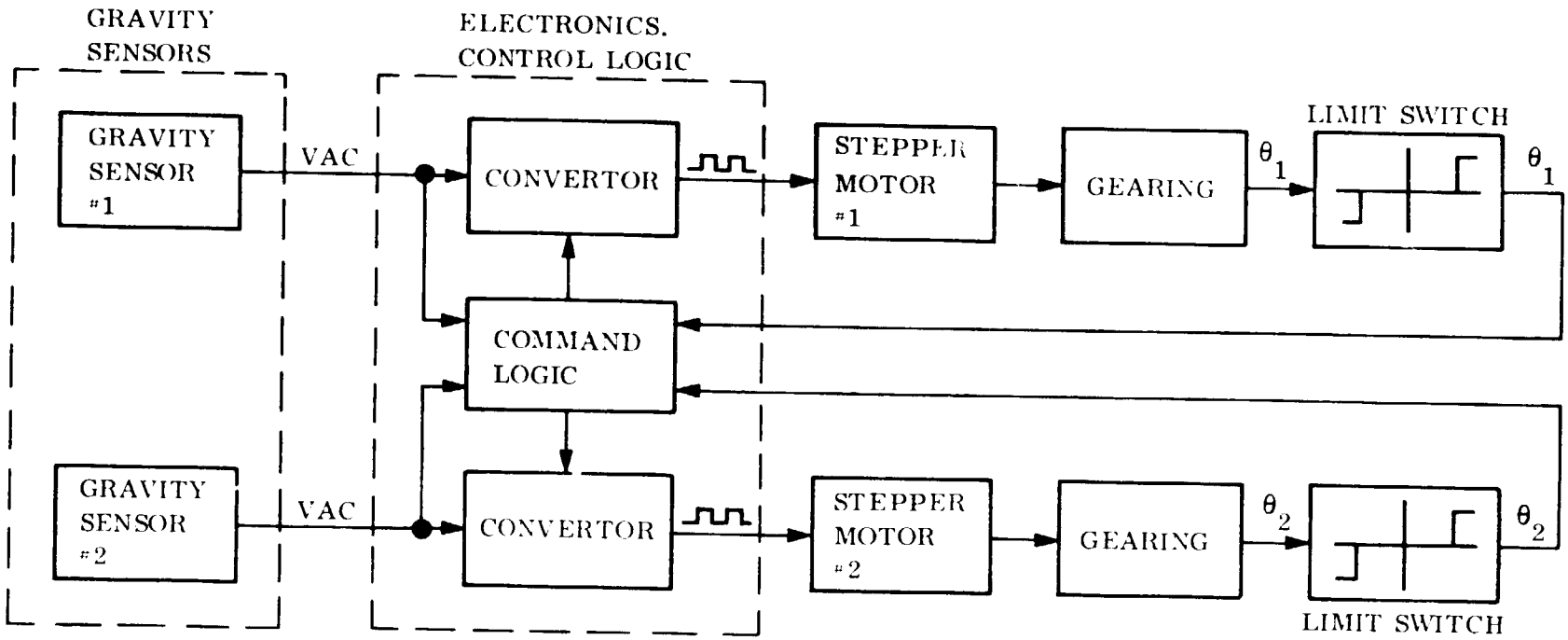

Figure 5.6-14. Block Diagram - Vertically Oriented Antenna

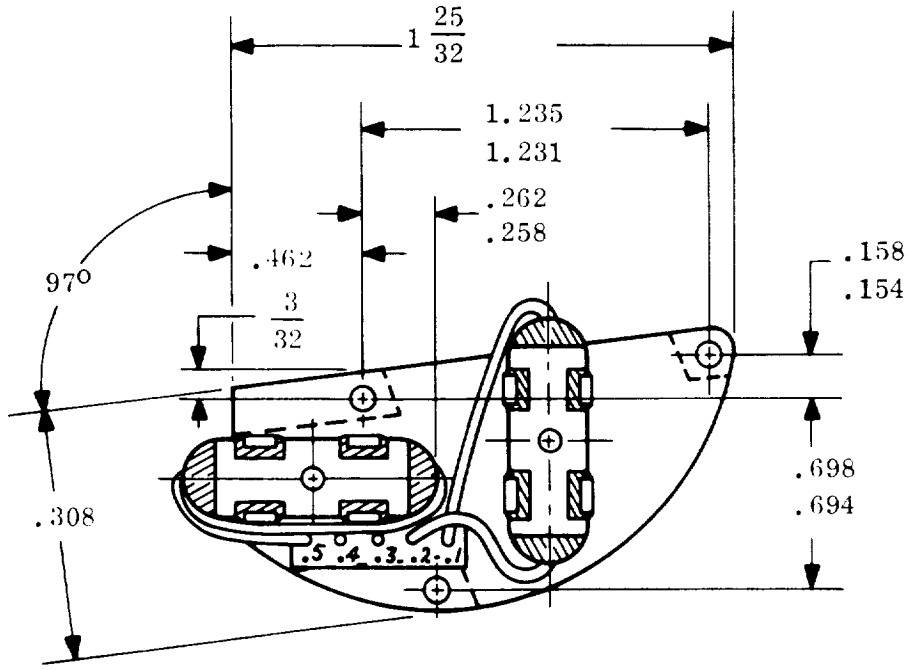

TOP VIEW

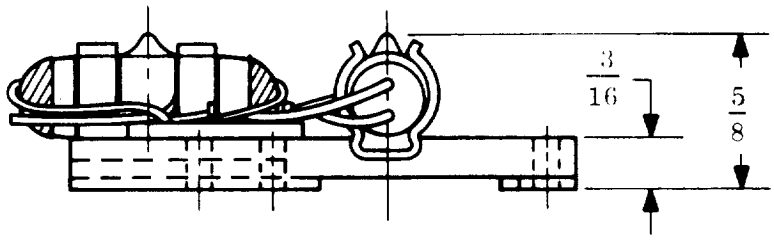

FRONT VIEW

ALL DIMENSIONS ARE IN INCHES

Figure 5.6-15. Dual Axis Gravity Sensing Unit

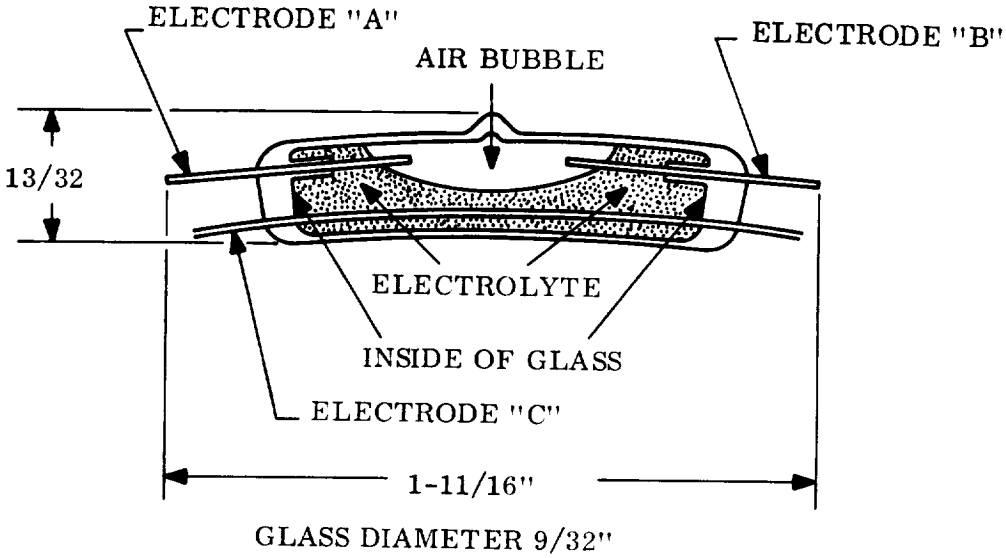

Figure 5.6-16. Gravity Sensing Electrolitic Transducer

An antenna design which is oriented to the local vertical using gravitational force only can be developed. A preliminary version of this design approach is illustrated as an alternative concept in fig. 5.6-3.

5.7 IMPACT LIMITER

The Lander System is designed to attenuate the landing impact loads by the mechanical crush-up of phenolic glass honeycomb. In this design concept, all of the equipment to conduct the surface operations and the major portion of the entry science mission is assembled within a cylindrical container that is surrounded by a torroidal, deep ring of phenolic glass honeycomb material. The ring of crush-up structure is bonded to a D-ring structure that provides stiffening to the cylinder rim and a load transfer path from the crush-up to the payload container.

The depth of crush-up material is a function of the square of the impact velocity, the surface slope, and the chute sway, and varies inversely with the selected deceleration rate at which the impact energy is dissipated in bringing the Lander to rest. The total depth of crush-up material is determined by adding the amount for rock clearance to the stroke required for decelerating the body to rest. The shape of the impact limiter profile is determined by the depth and area of crush-up required at the various impact conditions and potential surface contact angles.

5.7.1 REQUIREMENTS AND DESIGN CONSTRAINTS

In this Lander design, the crush-up material is determined for the following conditions. It is presumed that the surface impacted is infinitely rigid as the limit on surface bearing strength and that 100 percent of the kinetic energy at impact is dissipated in the honeycomb material actively crushed during the impact. This material is sized to bring the Lander to rest within a 1000 g's rigid body deceleration limit. Preliminary analysis indicates that rebound may occur with subsequent impacts at up to 100 ft/sec. Adequate crush-up material is provided all around the Lander to decelerate the Lander for a second time at 1000 g's. The conditions of impact are illustrated in figure 5.7-1 and are based on the following requirements:

1. 118 ft/sec horizontal velocity due to wind
2. slopes up to 20°
3. rocks of 5 in. diameter
4. maximum deceleration of 1000 g's in any direction at the impact limiter/structure interface.

In addition, the following constraints have been placed on the limiter design on the basis of system trade-offs and preliminary dynamic analysis:

1. vertical velocity at impact of 100 ft/sec
2. parachute sway angles of up to 40°
3. secondary impact in any direction (except the exact spot of primary impact) at 100 ft/sec.

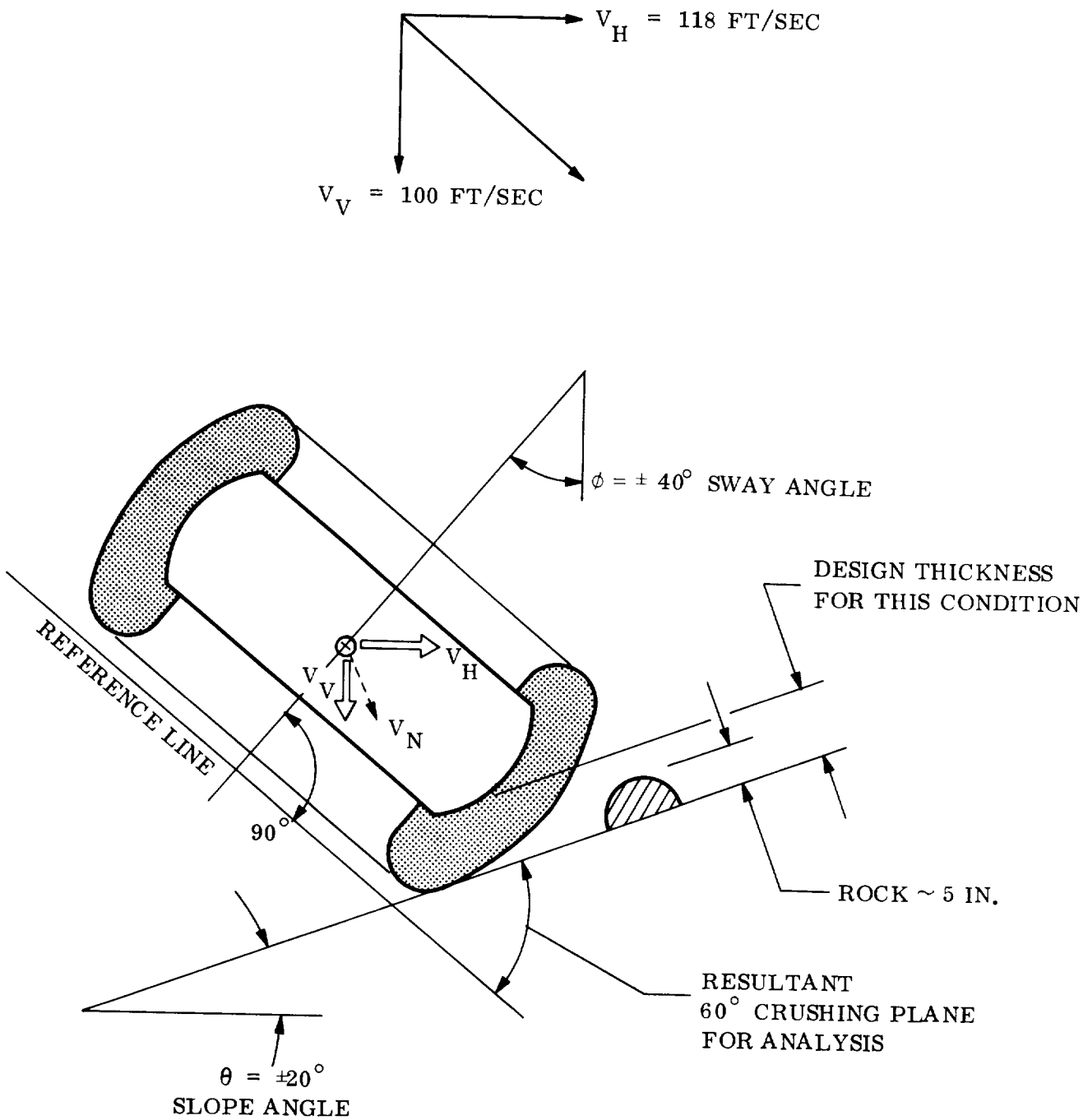

Figure 5.7-1. Design Conditions

Effects of variation of the above design conditions are discussed in Section 5.7.3.

5.7.2 IMPACT LIMITER DESCRIPTION

Although all of the point design effort was based on parametric analytical information, a preliminary design of the impact limiter has been prepared to identify problem areas and illustrate construction details.

Fig. 5.7-2 shows the design dimension for the phenolic glass crush-up material surrounding the 40 in. diameter by 19 in. deep payload cylinder of the 1400 lb Capsule. Five in. of crush-up are provided as a rock protection barrier between the structure of the cylinder and the crush-up material needed for stroke purposes. The amount of crush-up for primary impacts is 4-1/2 in. with 2-1/2 in. required for the secondary rebounds. This limiter material amounts to 30 ft^3 and the material density, determined on the basis of the maximum crushing stress computed in the 1000 g deceleration stroke, is 7.3 lb/ft^3 giving a limiter allocation of 220 lb. Fig. 5.7-2 shows that the material cross-section provides a minimum of 7-1/2 in. in all directions and 9-1/2 in. in the region of prime impacts at angles up to 60°, i.e. 20° slopes plus 40° sway.

The variation of crushed material area, as the stroke increases to the depth required to bring the 661 lb Lander to rest, is shown in fig. 5.7-3 for impacts at 20°, 40°, and 60° and horizontal at 0°. Horizontal landings after a rebound and 180° flip-over are shown as a 180° condition. The areas shown in fig. 5.7-3 are gross areas in that they do not account for the crush-up stress level reduction due to honeycomb cell orientation with respect to the load direction. The net effective area is determined by reducing the gross area by 2 percent for each degree off normal between the impacted surface and the honeycomb cell axis.

The limiter assembly as shown in fig. 5.7-2 is composed of blocks of honeycomb core arranged in 24 segments of 15° each in the circumferential direction and 11 pieces in the radial profile section. Each block is cut to the required compound angles and curvature on the inner face before assembly to the substructure. The bonds between blocks and to the structure are formed by a film type adhesive which foams during curing to fill the open cells and provide a bond stronger than the honeycomb basic material. This bond process has been proven by combined shear and bending impact tests where the foamed bond joint survived and the honeycomb failed. These tests were performed as part of GE-RS Contract No. 951172 with the Jet Propulsion Laboratory (subcontract under NASA Contract NAS 7-100)(ref. 5.7-10).

The optimization of the block sizes and orientations in the radial profile section involves an iterative design, analysis, and test cycle to obtain progressively more efficient and exact designs. The design layout portion involves the determination of required stroke, block size and cell orientation, maximum g-level based on final area, net area and stress level based on reduction of strength due to off normal orientation of honeycomb cell axes, honeycomb density, and summation of kinetic energy absorbed

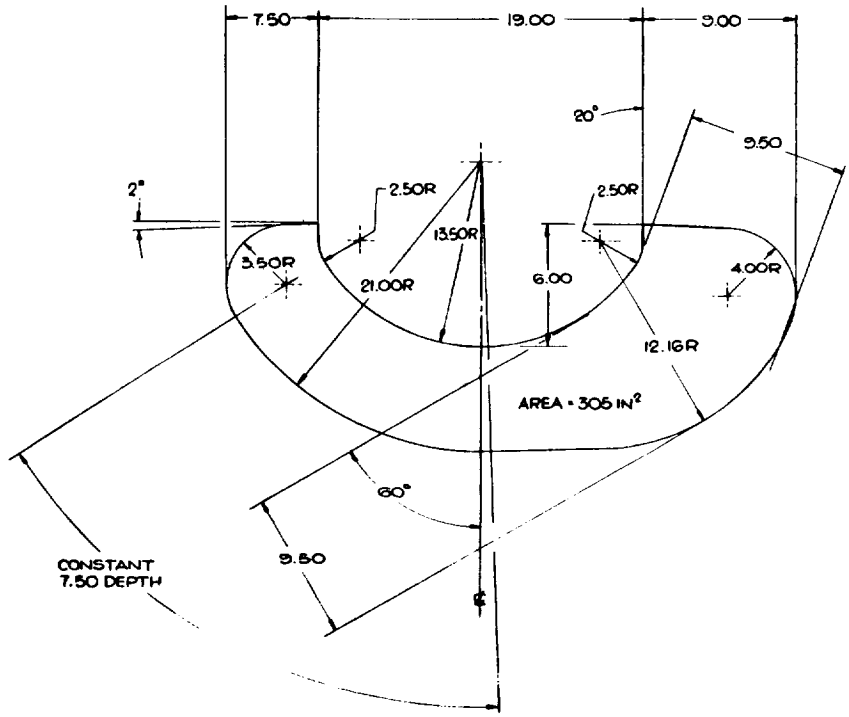

ATTENUATOR GEOMETRY

FOLDOUT FRAME

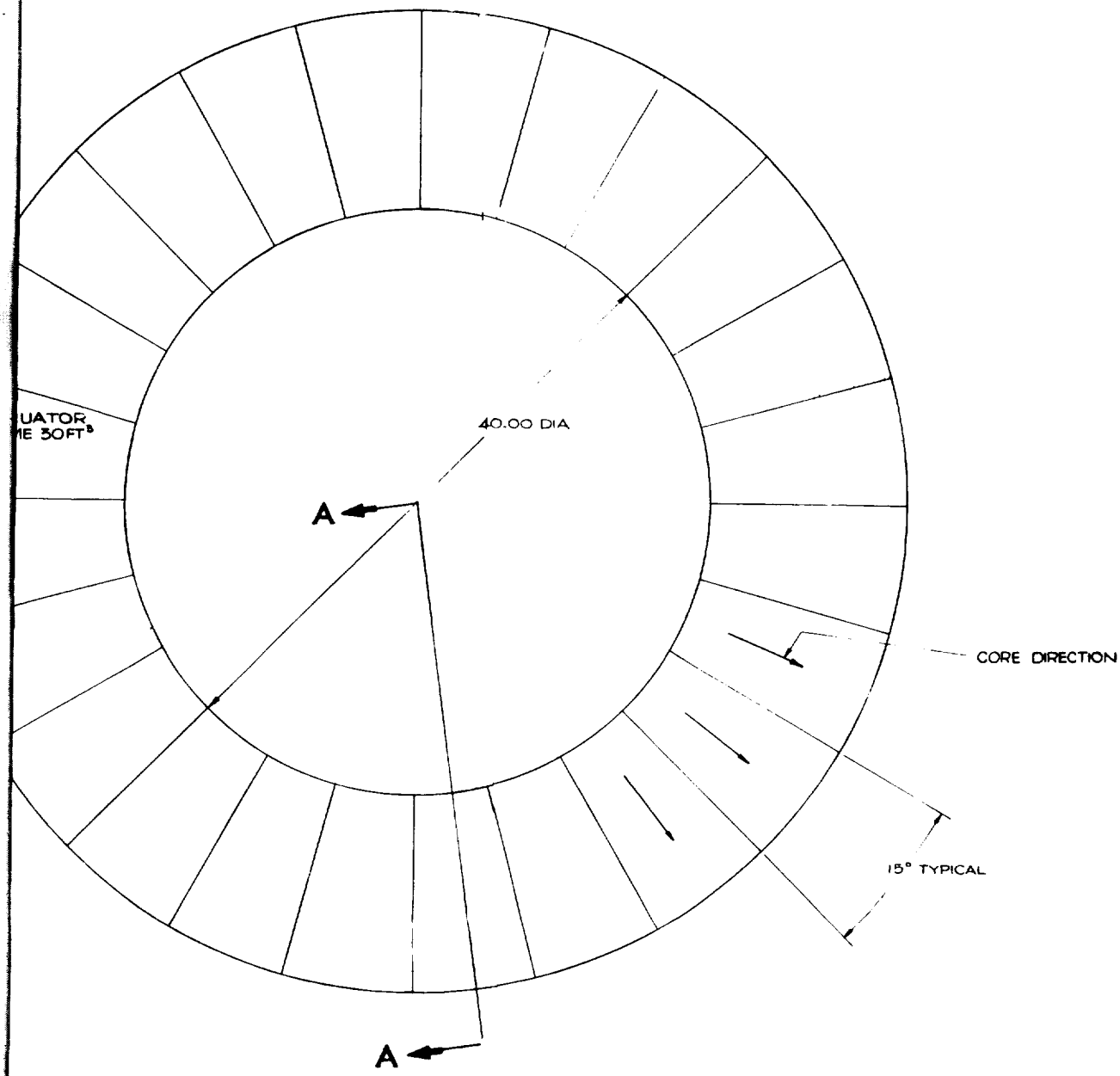

OLDOUT FRAME 2

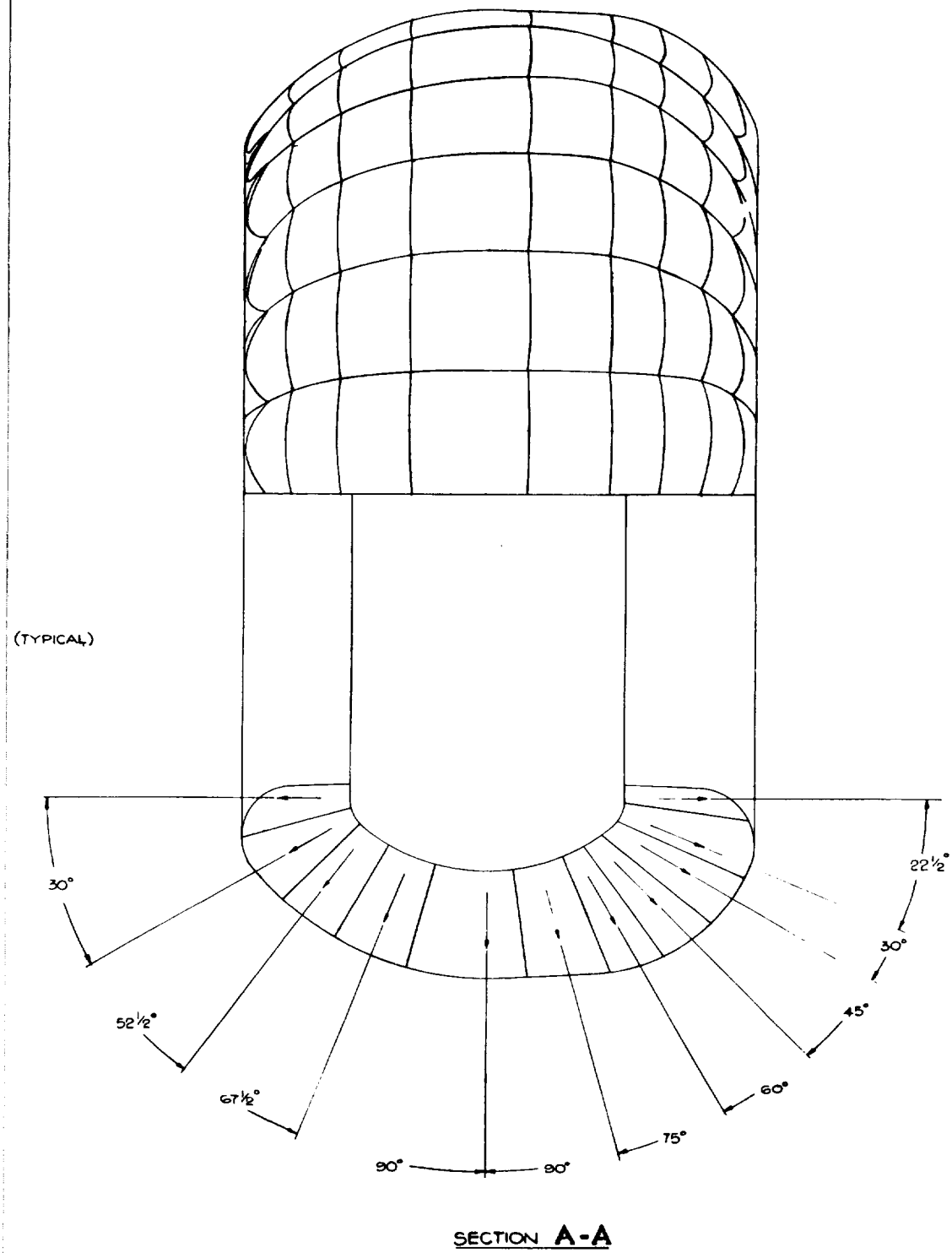

Figure 5.7-2. Impact Limiter Details

FOLDOUT FRAME 3

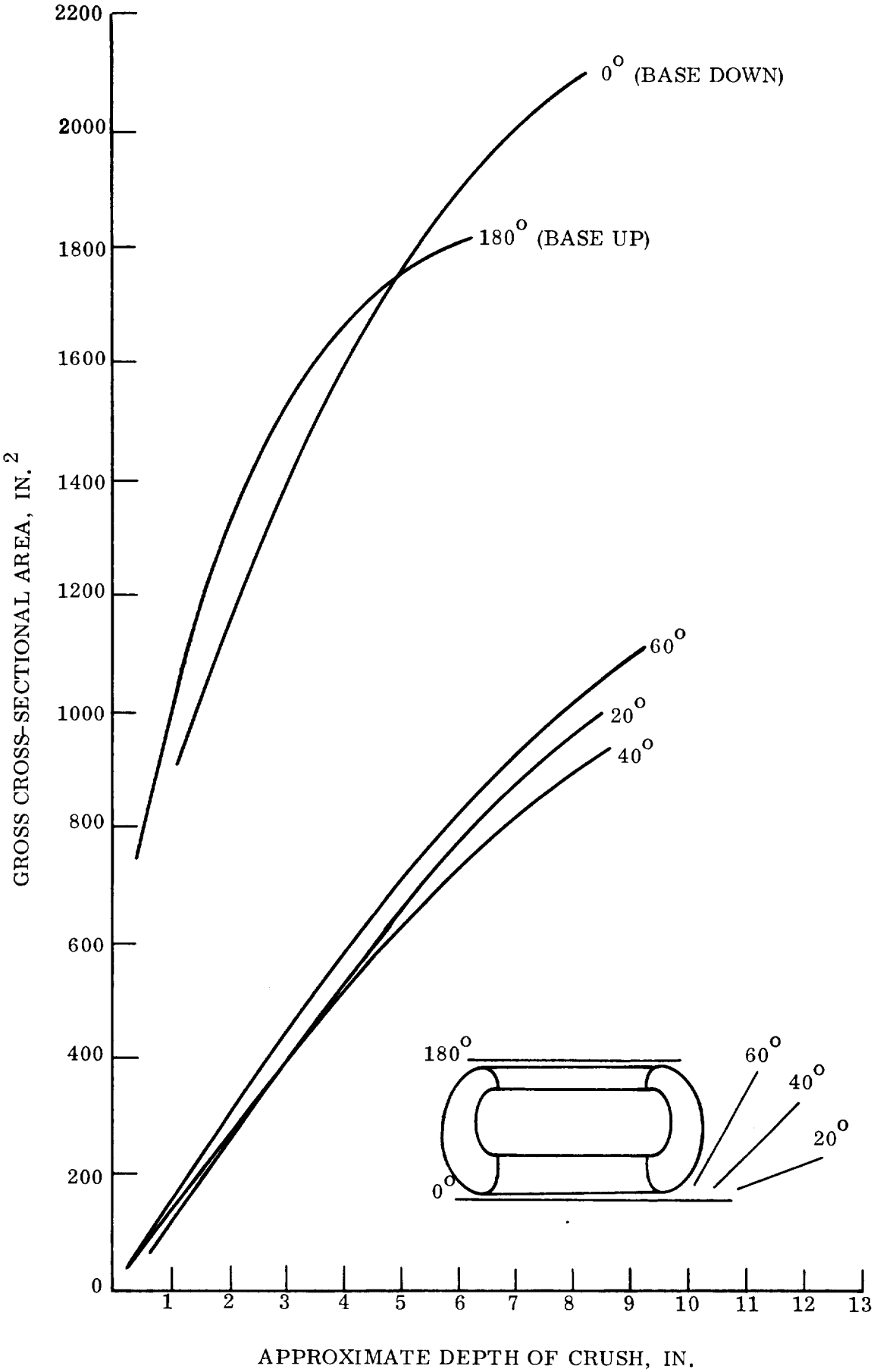

Figure 5.7-3. Area Variation with Stroke

for each of several critical contact angles between the limiter and the impacted surface. Each cycle of this process in the arrangement of the blocks is largely based on engineering judgment and the trends learned in earlier cycles. After a complete analysis of any selected arrangement, test verification is then necessary to confirm predicted load levels and energy absorbed.

A preliminary arrangement of blocks is shown in fig. 5.7-2 to illustrate the design procedure. Here 264 blocks have been arranged to minimize the volume and weight of the impact limiter. The arrangement has been evaluated for impact at angles of 0°, 20°, 40°, and 60° from horizontal for primary impact and 180° for secondary impact leading to the weight allocation noted previously. To reiterate, the following parameters must be varied and optimized to obtain a minimum weight limiter:

1. Block size and shape
2. Cell orientation within block
3. Honeycomb density including use of different densities
4. Maximum g-level for different impact angles.

In summary, the shape and weight of the impact limiter for the 1400 lb Capsule has been derived on a conservative basis. The adverse conditions of wind speed, surface slopes, parachute induced sway angle and rock outcrop have been combined simultaneously (reference discussion in Section 3.3.2). In addition, energy-absorbing rotational motion during impact has not been included; none of the initial or rebound impact energy is assumed to be dissipated in either the Martian surface or Lander structure.

5.7.3 EFFECTS ON DESIGN DUE TO VARIATIONS IN DESIGN CONDITIONS

Although the impact limiter described above for the 1400 lb Lander is based on the specific design conditions of Section 5.7.1, it is of value to examine the trends identified in varying some of the key conditions.

5.7.3.1 Effect of Rocks on Crush-Up Weight

The rock specification is a critical parameter for the limiter design. In general, protection against rock penetration of the container requires a thickness of honeycomb material over and above that required for impact on a smooth surface. The exact magnitude of this penalty (in volume and weight) depends upon the particular impact conditions considered. This is true because the touchdown conditions govern the honeycomb density selection as well as the attenuator thicknesses required for deceleration at the desired g-level. In fig. 5.7-4 the increase in impact limiter weight, as a percent of the weight required with no rock protection is plotted against the specified design rock size in inches. Three significant features are shown in this figure.

First, the thickness design procedure used in allowing for stroke efficiency of approximately 80 percent inherently includes some rock protection capability. By dividing the

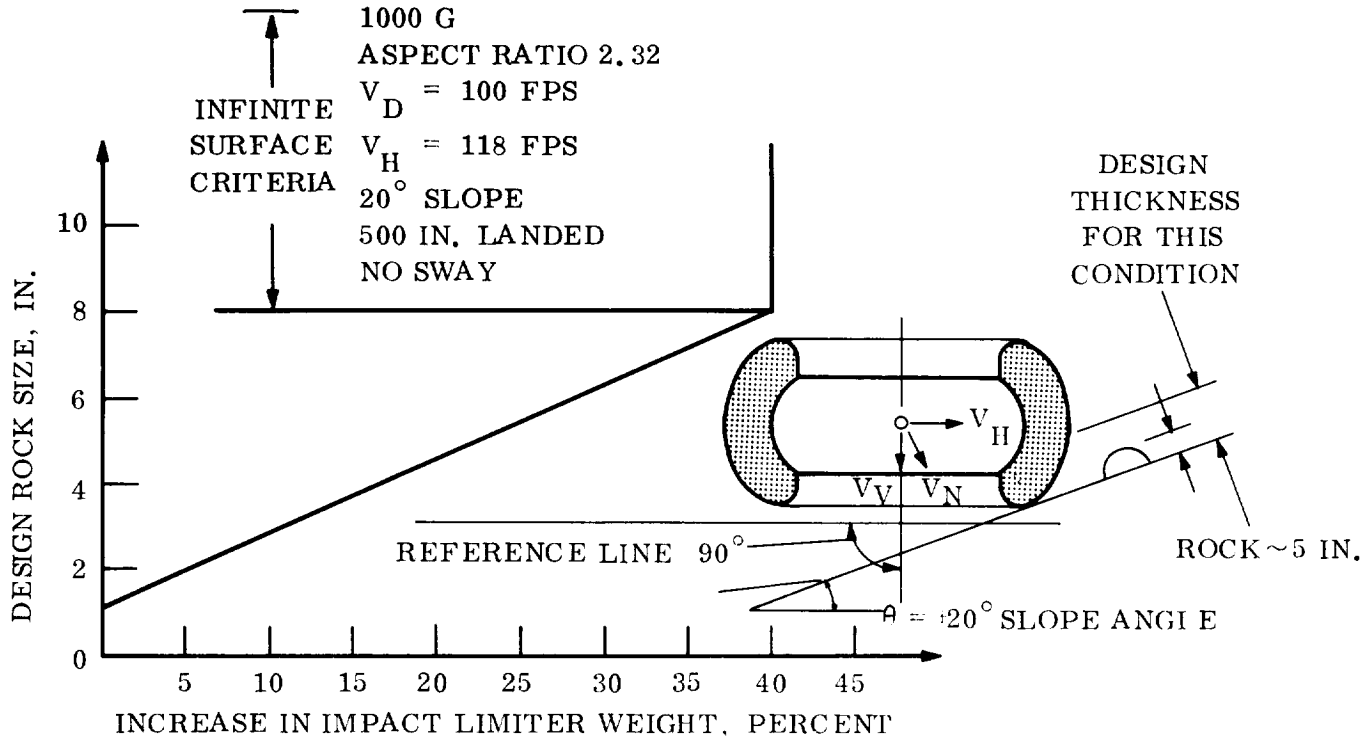

Figure 5.7-4. Limiter Weight Due to Rock Clearance

required stroke by 0.8 and using this thickness for design an increment of about 1.11 in. is available. This means a rock of less than this size may be impacted without excessive loading and no increase in impact limiter weight is required. This margin is subject to test verification on the specific impact limiter and rock parameters to be selected.

Second, with increasing rock size an increasing weight penalty may be expected. This is plotted, for the specific conditions shown in fig. 5.7-4.

Third, there is an upper limit to the applicability of this rock criteria. Based upon geological analysis true rocks do not exceed certain proportions. This implies that as the rock size becomes larger there is a marked tendency for a rounding of the rock with an attendant decrease in the sliver-piercing characteristics. With this effect accounted for, there is a size of rock above which low load penetration of the honeycomb does not occur and the Lander is effectively impacting a smooth surface of infinite strength.

5.7.3.2 Effects of Sway on Crush-Up Weight

Detailed design activity when compared to baseline parametric data indicates that an increasing weight penalty is associated with sway angle effects on the Lander. This arises due to the interaction of sway angle and the ground slope specified for the Lander. In effect, with no sway, cutting planes up to and including 20° above the horizontal must

be investigated in the limiter analysis. With a sway angle of 40° as used for the 1400 lb Lander, cutting planes up to and including 60° above the Lander baseline must now be checked. Added crush-up material will be necessitated by the Lander experiencing sway than will be the case with no sway effect on touchdown attitude. A second effect produced by sway is that the maximum normal velocity component, which would otherwise be experienced in only one direction, can now be experienced in several directions. This adds material to a portion of the Lander that would be thinner if there were no sway. Because of the interaction of parachute-induced sway angle with the other touchdown characteristics and limiter design parameters, a general design rule for the weight penalties caused by sway is not at hand.

Fig. 5.7-5 shows the increment in attenuation weight in designing for 40° sway compared to 0° sway as a function of the vertical velocity component for the specific conditions of wind, g-level, slopes and weight stated on the figure.

5.7.3.3 Effects of g-Level Variation

Additional design studies were performed on the basic impact limiter design (fig. 5.7-2) in order to test the interrelationship of stroke and deceleration level with the net, effective area, and weight of crush-up. Results of this study are discussed below.

It was found that the weight of the impact attenuation material is relatively insensitive to g-level. This is shown in fig. 5.7-6 where for a specific set of conditions, impact attenuation system weight is plotted as a function of g-level, for different values of V_N, V_N is the component of velocity normal to the surface of impact and is a function of descent velocity, wind velocity, and slope. The curves show that there is a small decrease in attenuator weight with increasing g-level and as the velocity, V_N, decreases there is a major decrease in attenuator weight, as one would expect. However, as V_N decreases, the change in attenuator weight with g-level also decreases. At the lowest velocity shown there is almost no change with g's. In fact, some detailed design studies have shown that the slope of these curves changes at the lower velocities and the weight actually decreases slightly with decreasing g-level.

Although the parameter on this figure is V_N, the real implication is that lower descent velocities, lower wind velocities and smaller slopes, i.e., generally less severe impact conditions, are all in the direction of decreasing the weight sensitivity to g-level.

5.7.3.4 Effects of Payload Container Shape Variation

Design layouts were made, and the parametric data for design and performance analyzed to determine the sensitivity of the weight of crush-up material to variations in the diameter and depth of the payload container. The studies showed that considerable latitude is available to the designer in selecting the preferred cylinder aspect ratio for packaging arrangement because diameter/depth relationships could be varied without affecting the limiter material weight. Three payload containers at 10 lb/ft^3 each with diameters of 36, 40, and 44 in. were studied for the impact conditions of this 1400 lb Capsule Lander design. For 1000 g maximum deceleration the weight of impact limiter for each cylinder was 255, 256, and 256 lb, respectively. The constant weight resulting is due to the product of material density (varies directly with net crushed area) and material volume remaining constant.

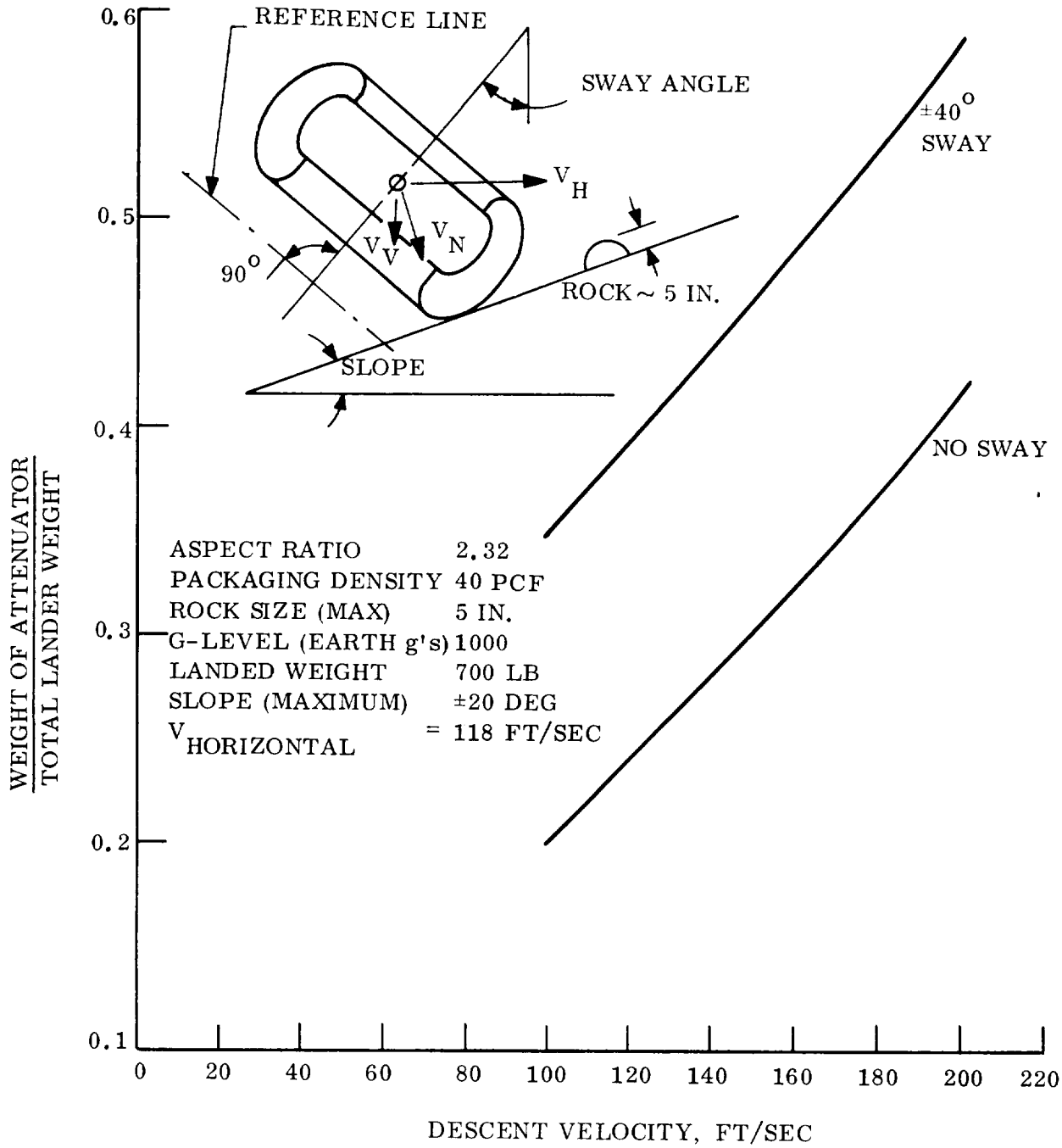

Figure 5.7-5. Effect of Sway on Limiter Weight

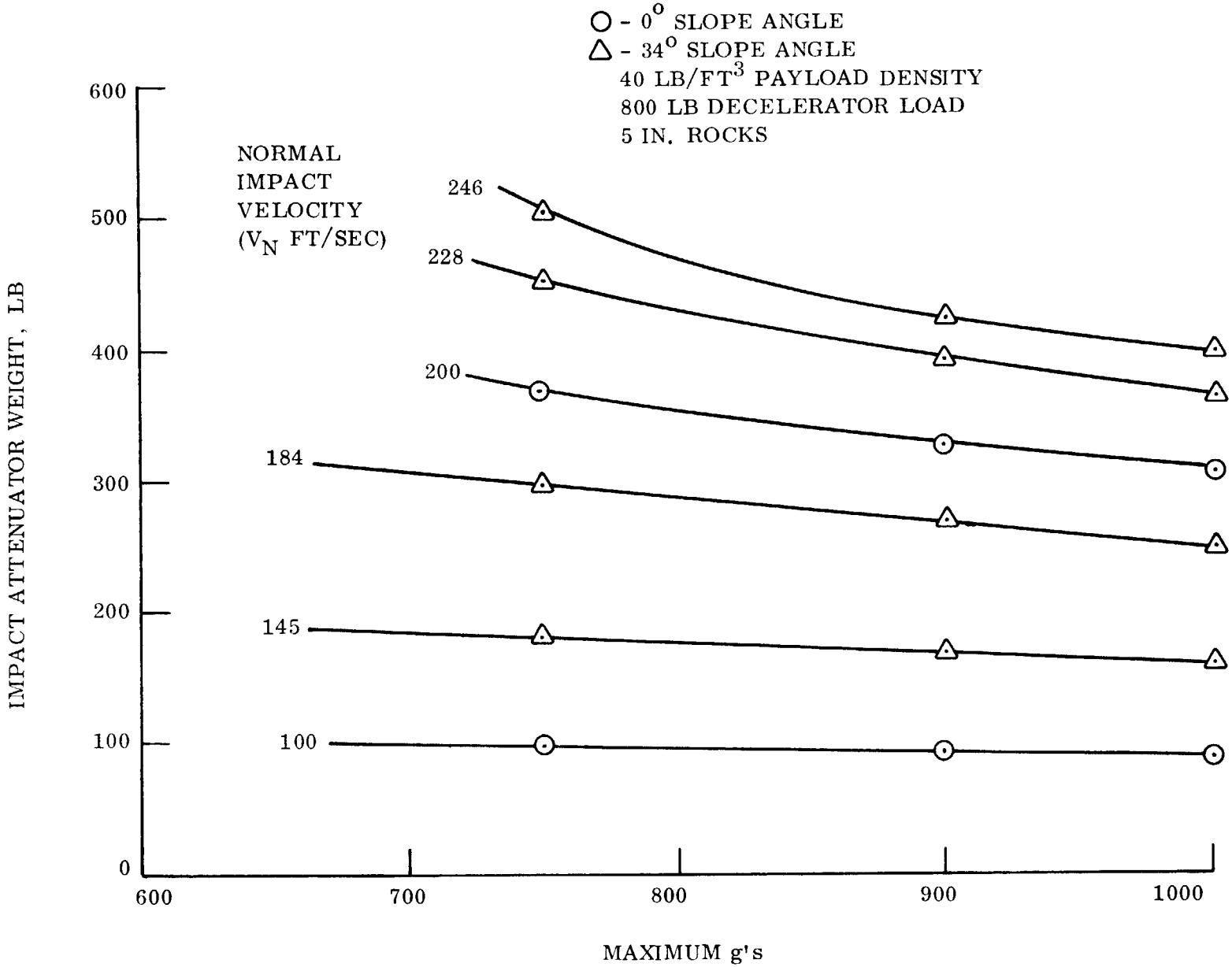

Figure 5.7-6. Effect of g-Level Variation

5.7.4 MATERIALS CONSIDERATIONS, BALSA VS HONEYCOMB

Phenolic honeycomb was selected as the reference material for this Capsule design study although both balsa wood and honeycomb are feasible materials for the size and weight vehicles being examined. Both materials can function at the operating g-levels anticipated with the Hard Lander System.

In studying both candidate materials, a comparison of the mechanical properties can be drawn by examining crushing stress vs material density, specific energy vs material density, and material effectiveness as a function of obliquity of impact.

This data is shown in figs. 5.7-7 through -9 for phenolic fiberglass honeycomb and corresponding information, from various sources (ref. 5.7-1 through -5) for balsa wood in the figures. In fig. 5.7-7 the specific energies of the materials are compared on both a gross volume and net volume (ft-lb/lb crushed) basis. By examining curves E and B it can be seen that for densities from 8 to 11 pcf the material specific energy is very similar for both balsa wood and phenolic honeycomb. On either side of this density regime the balsa wood appears superior based on this average curve for balsa (ref. 5.7-1). Comparison of curves A and B indicates that from 8 to 11 pcf density, the phenolic honeycomb is preferrable from a specific energy basis. The subtle but highly significant factor which must be introduced is the variation in balsa mechanical properties. This is seen from the inset to fig. 5.7-7, in which the ratio of the maximum crushing stress to the minimum crushing stress for various balsa densities is presented (ref. 5.7-1). From this plot, it is recognized that balsa wood material properties have been known to vary from ± 15 to ± 50 percent. This is significant since balsa, being a natural material, cannot be further developed to a significant extent. The variation in crushing stress introduces a corresponding variation in specific energy for balsa wood. This is the reasoning underlying the construction of curve C for minimum balsa properties and curve F for the most optimistic balsa properties. Review of these two curves indicates that balsa wood can be significantly better than phenolic honeycomb but may be considerably lower in specific energy. Moreover, phenolic honeycomb, being a manufactured product, shows a low measurable scatter in performance indicators. The material has been chemically improved in the past and this trend can be expected to continue.

For design purposes it is useful to have the relation between crushing stress and material density. The data in fig. 5.7-7 are repeated in fig. 5.7-8 on a crushing stress basis. Curves F, E, C correspond to the upper, normalized mean, and minimum properties curves for balsa wood on a gross volume basis. Curve G is for balsa wood and is taken from ref. 5.7-5. This reference does not state whether the curve is on a gross or net volume basis; the curve is presented for information value only. Curves D and B present crushing stress data for phenolic honeycomb on both net volume (curve D) and gross volume bases (curve B).

A comparison of the curves reveals that the normalized mean values (curve E) for the balsa wood are higher than those of curve B for phenolic honeycomb. Once again, however, when the scatter in balsa properties is introduced, (curve C) the phenolic honeycomb is the superior material.

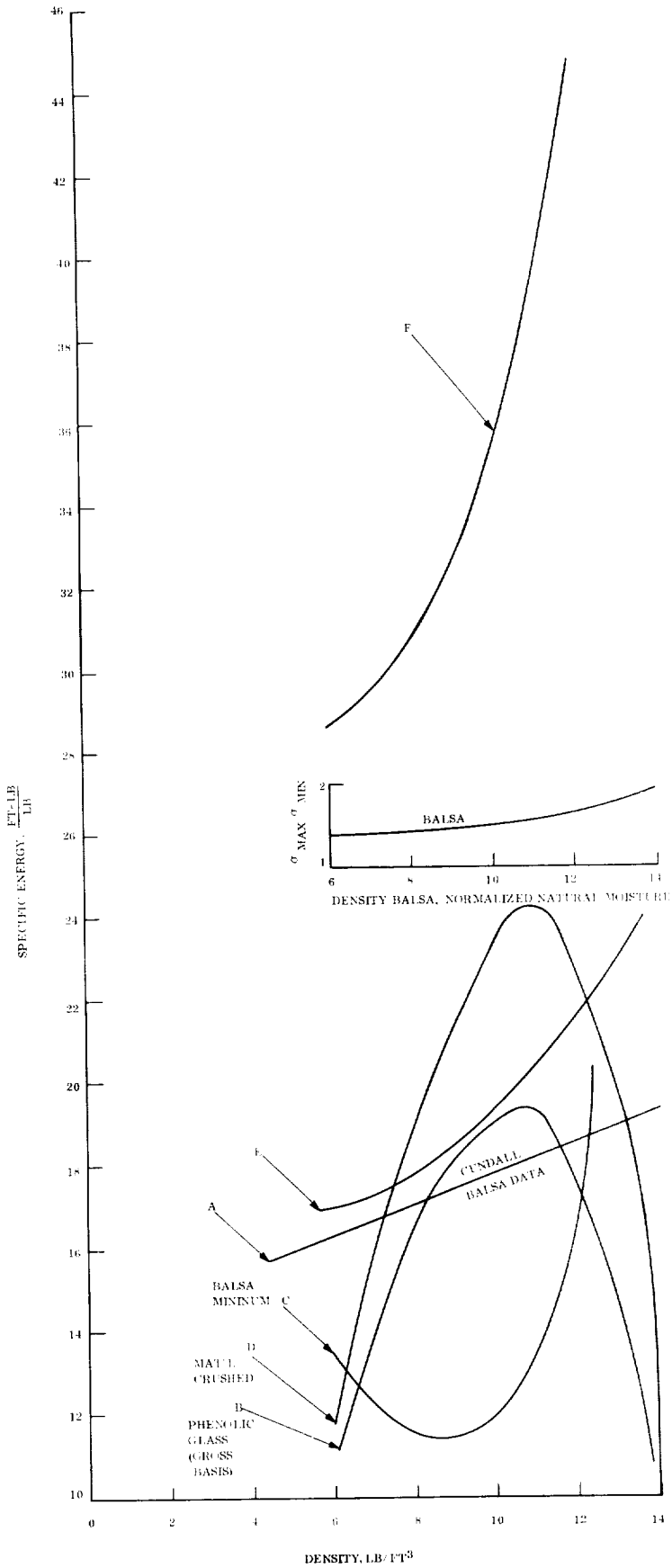

Figure 5.7-7. Materials Specific Energy

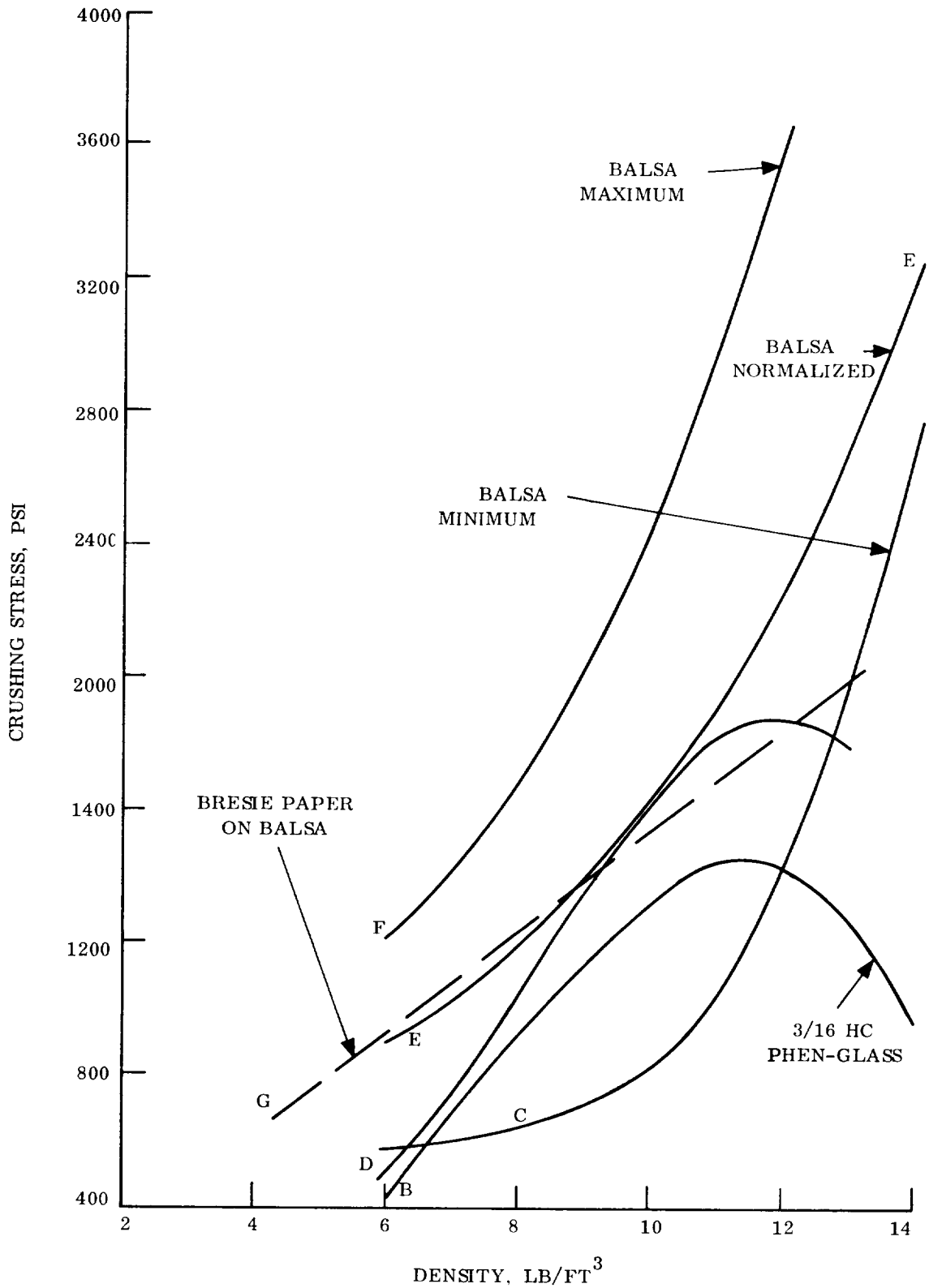

Figure 5.7-8. Materials Crushing Stress

From the above analysis, it appears that until further data on both materials is available, balsa and phenolic honeycomb are almost equal in energy-absorbing capability. Improved procedures for selective procurement of balsa will enhance its status; chemical improvement of the phenolic material will favor its adoption for attenuation purposes.

To extend the comparisons to material thickness efficiency, and obliquity effects figs. 5.7-9 and -10 were generated. In fig. 5.7-9 material thickness efficiency for balsa and phenolic honeycomb is plotted as a function of density. For the densities of interest (4 through 11 pcf), the thickness efficiency of phenolic honeycomb ranges from 0.9 down to 0.8. For balsa wood of these densities, the efficiency is practically constant and equal to 0.8. It is reasonable to conclude that the materials are practically identical in this aspect of their behavior.

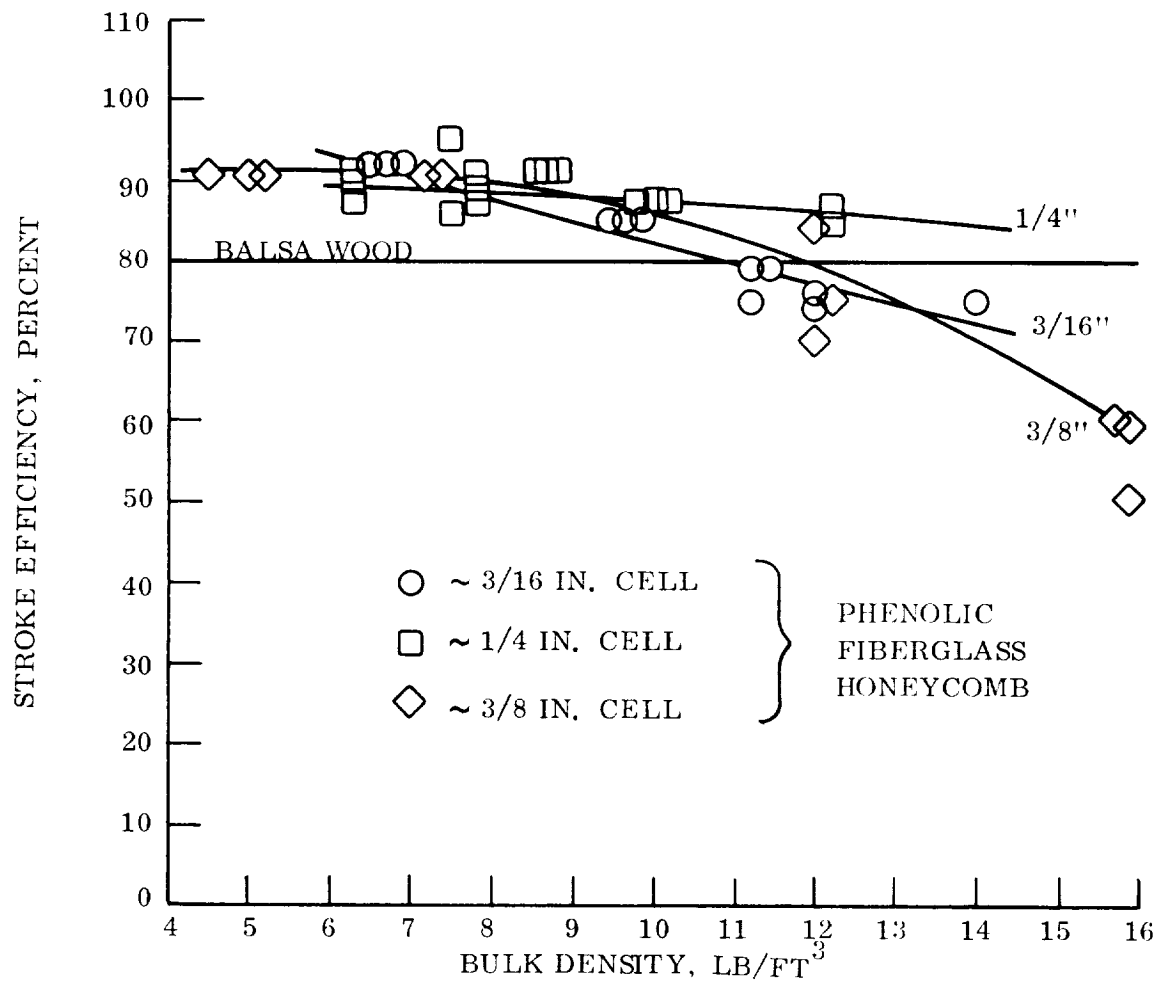

Figure 5.7-9. Materials Thickness (Stroke) Efficiency

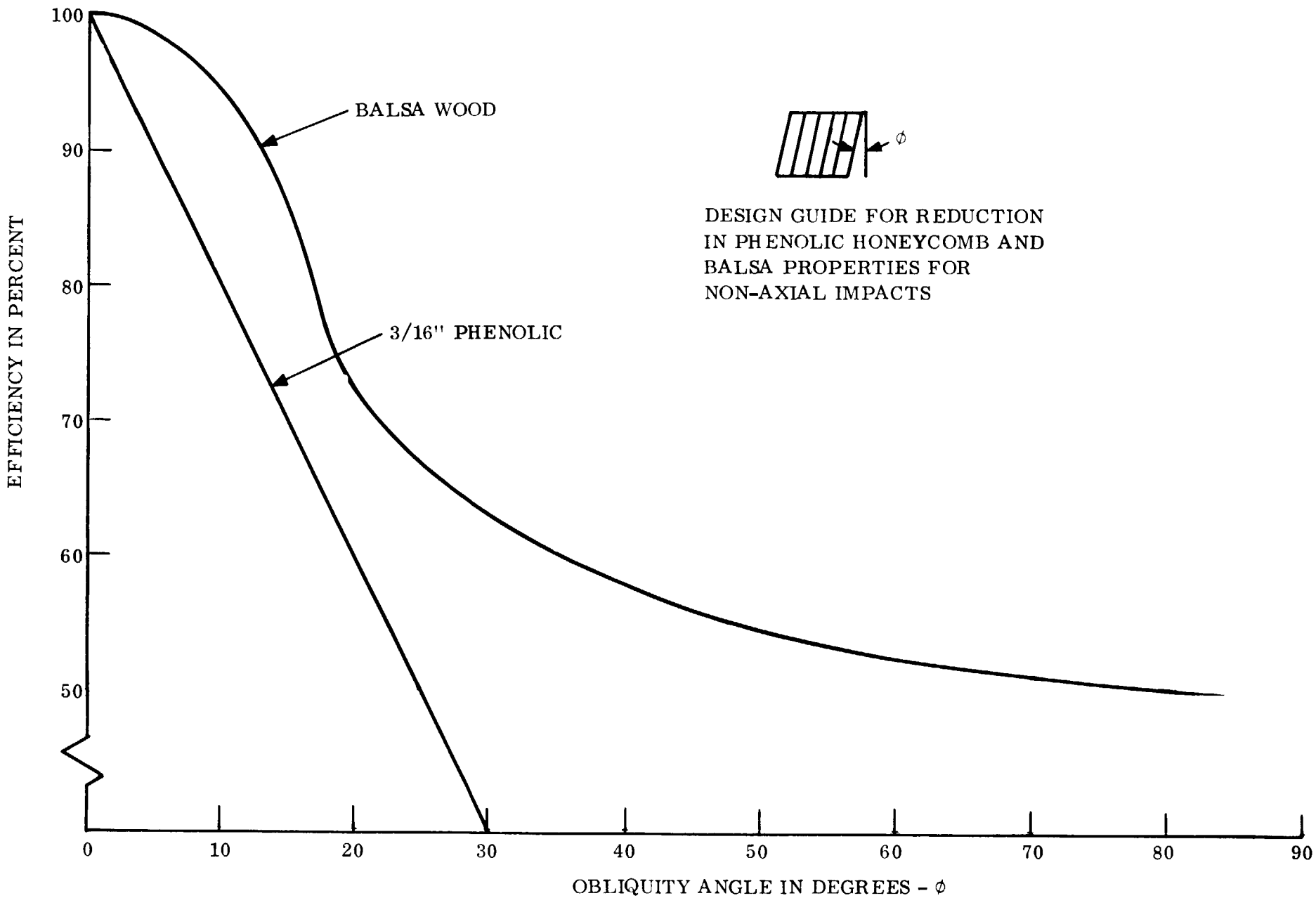

Figure 5.7-10. Materials Obliquity Effects

In fig. 5.7-10 the material efficiency as a function of obliquity angle is presented. It is recognized that the capability to absorb energy is reduced when the material is crushed at some angle other than along the wood grain (or along the honeycomb cell axis). For phenolic honeycomb this reduction amounts to a linear 2 percent/degree effect. For balsa wood the reduction is non-linear and not as severe.

In addition, balsa has a lower limit of 50 percent of maximum at 90° to the grain and consequently has an advantage in this factor. While no quantitative evaluation on a weight basis is available this factor could be of value in the shaping for minimum weight as discussed below.

5.7.5 SHAPING APPROACH FOR A MINIMUM WEIGHT IMPACT LIMITER

Fig. 5.7-6 showed the insensitivity of limiter weight, for a given impact condition, to the rate at which the energy of impact is dissipated, i.e., the maximum deceleration experienced in bringing the body to rest. Design studies have found that further weight reductions are possible by reducing the deceleration level in certain zones with increased stroke and thickness of lower density material. For example, the 36 in. diameter cylinder attentuation material was increased in the prime impact area to limit deceleration to 700 g's maximum while the remaining material was sized for 1000 g. The weight of attenuation material was reduced from 255 to 220 lb.

This capacity to reduce weight and tailor the deceleration encountered to various levels in different zones of the attenuator is useful for design conditions where instrument or equipment tolerance to impact is different in the vertical and lateral directions. This feature is also compatible with tailoring or varying the deceleration level to conform with results of probabilistic analyses of the impact and environmental conditions.

5.7.6 FABRICATION

The steps and techniques of fabrication of a honeycomb impact limiter model have been developed and demonstrated by GE on Contract No. 951172 to the Jet Propulsion Laboratory (subcontract under NASA Contract NAS 7-100), a Development of Energy-Dissipating Plastic Honeycomb, and are fully reported in ref. 5.7-10. A complete model, approximately 22 in. in diameter, which was designed, fabricated and successfully tested on that program, is shown in fig. 5.7-11.

A brief summary of the fabrication and assembly steps involved in this process is given below:

1. The payload container structure is prepared including finishing to dimensional requirements and the special treatment of apertures and holes as required.

The structure is given a surface treatment such as Alodine 1200 to assure good adhesive bonding.

2. The raw honeycomb crush-up material is then rough cut to size with proper attention to the design lay-up and resultant cell wall orientation.

3. The rough cut surface is then checked for dimensional accuracy and secondary trimming or sanding is performed.

4. A preliminary fit-up of the honeycomb to the payload container is made. This is done by using shims to allow for adhesive bond thicknesses.

5. The epoxy adhesive for bonding the crush-up material is then prepared according to the manufacturer's specifications.

6. The bonding of the honeycomb segments to the container structure and to one another is then begun. For this purpose, a rotation spit device is used to hold the container, along with the associated jigs and fixtures for temporary support during curing. Rotation during curing is necessary to prevent bond sagging due to gravity. The exact fixture details must be determined during the manufacturing development period. However, in general, wooden forms which can be snapped in and out of position are sufficient.

7. The assembly, which is now fully mated, is given the proper cure cycle determined by the adhesive and also the specified strength level to be attained.

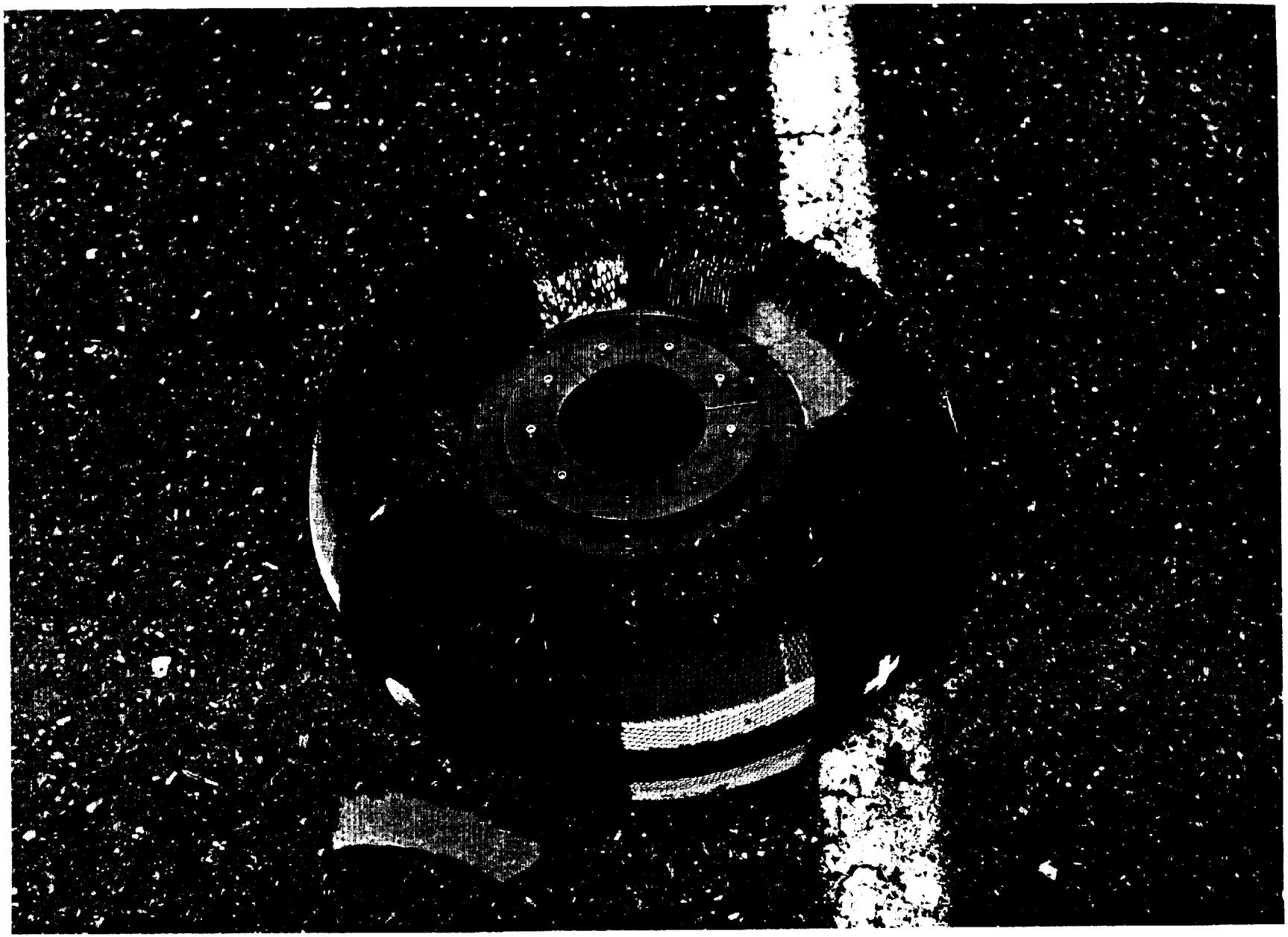

Figure 5.7-11. Post Test Photograph of GE-RS Phenolic Fiberglass Honeycomb Impact Limiter Model

5.7.7 IMPACT LIMITER CONFIGURATION STUDIES

The six point designs reported in the earlier Hard Lander contractor documents and the Autonomous and Flyby Landers have all utilized an impact limiter of crushable fiberglass honeycomb at a maximum deceleration level of 1000 g's. This approach was selected since analytical tools were available for the parametric study and the deceleration level is representative of the range associated with a Hard Lander. No attempt has been made to show that the approach taken represents the optimum impact limiter or decleration level.

5.7.7.1 Potential Range of Impact Limiter Designs

It is possible to design useful Lander configurations having different deceleration levels both within the general design constraints of the deep-ring crushable configuration and also utilizing many other configurations. If a Hard Lander may be defined as having energy dissipation means inactive up to the moment of touchdown, the decleration range may include values of 100 g to 10,000 g. Some general observations from past and current studies may be drawn on the applications of the various portions of this range.

1. The 10,000 g level resembles the artillery shell application and probably is of interest only on 'one instrument', one signal, type devices.

2. The 2000 to 5000 g level is most applicable for a small (probably under 100 lb) probe type system having very limited instrumentation and lifetime.

3. The 700 to 1500 g range is typified by the parametric studies and represents a very useful regime for relatively complex Landers.

4. The 100 to 300 g level will be more accommodating to the requirements of a sophisticated payload but can only be achieved by the use of pneumatic or hybrid impact limiter at a cost of some increase in complexity.

The deep-ring crushable design has been analyzed to show its application down to g-levels of 600 g's at a very modest weight increase above minimum. Since impact limiters in the greater than 1200 g range have limited application, it was decided to focus the study of alternate configurations on the lower end of the potential range of deceleration level, 100 to 300 g's.

5.7.7.2 Low 'g' Lander Configuration Study

This study was undertaken with the broad objectives of identifying potential low 'g' configurations and defining the penalties and advantages attendant to each.

Several candidate concepts were chosen for consideration, some of which were quickly eliminated due to significant weaknesses or disadvantages. The remaining ones were

studied through design layout stage to define specific details and select the most desirable approach. Limiter design conditions for the study were as follows:

Vertical Velocity	100 fps
Horizontal Velocity	118 fps
Slopes	$\pm 20^{o}$
Rocks	5 in.
g-Level	200 - 300
Parachute Sway	$\pm 40^{o}$
Payload Weight	336 lb

Preliminary results of the study are summarized below and reported in ref. 5.7-11. Dynamic testing of both crushable and pneumatic systems is in progress to confirm analytical results. Test results will be combined with additional preliminary design effort to permit selection and recommendation of a best impact limiter configuration considering all program factors in January 1969.

5.7.7.3 Pneumatic Impact Limiter Preliminary Design

As an example of a high stroke (low g) impact limiter a pneumatic, omni-directional concept was studied by Goodyear Aerospace Corp. based on General Electric specifications very similar to those above. A preliminary design of this approach was prepared and is reported in ref. 5.7-12. The configuration is a variation of the sphero-toroid concept which is under test at GE. The study resulted in an impact limiter system weight of 148 lb including attachments and inflation system, for a landed weight of 786 lb at a maximum deceleration of 155 g's.

Various arrangements of 2 main pneumatic bag spheres with 2 or 4 smaller spheres in a plane at 90° to and between the main spheres were investigated and found to be a realistic way of limiting impact loads with a good feasibility of being a lightweight system. Orientation and access to the surface environment is provided by sequential deflation of the bags. The conclusions must necessarily be treated as preliminary data because more detailed design and analysis is required to determine and select the best combination of payload container and pneumatic attenuator and integration of the Lander within the aeroshell. The study shows the technical feasibility of the inflatable attenuator for less than 250 g limit design but the study results are not yet in the detail required for comparisons with other design approaches.

5.7.7.4 Preliminary Impact Limiter Study Results

Although present results are insufficient to be conclusive several significant results are evident for the pneumatic and hybrid systems being studied.

1. Realistic impact limiters can be built in the 100 to 300 g range.

2. These limiters may be weight competitive with a minor increase in complexity and cost. In addition to the advantages of a lower deceleration level, other apparent features which may result include:

   a. Lower density payload packaging

   b. Better aeroshell packaging

   c. Single directional sensor deployment

   d. Simple addition of solar cells

   e. High payload flexibility and accommodation

   f. Broad growth potential both within a specific design and for other opportunities and applications.

5.7.8 REFERENCES

5.7-1 Knoll, A.C., Environmental and Physical Effects on the Response of Balsa Wood as An Energy Dissipator, Tech. Rept. #32-944, FPL, Pasadena, California.

5.7-2 Hess, T.E., Comments on Comparison of Balsa Wood and Phenolic Honeycomb for Impact Absorbing Systems, PIR U-9335-PE-0032.

5.7-3 Cundall, D.R., Balsa-Wood Impact Limiters for Hard Landing on the Surface of Mars, Philco-Ford Aeronutronic Div., c.1965.

5.7-4 Meyers, W.M., Coppa, A.P., Lorsch, H.G., "A Radio Frequency Transparent, Impact Energy Absorbing Material," TIS 65SD257, GE-MSD, 5/17/65.

5.7-5 Bresie, Don, Practical Limits for Balsa Impact Limiters, NASA-S-65-7287, Manned Spacecraft Center, Houston, Texas.

5.7-6 Meyers, Wm. M., Development of Energy Dissipating Plastic Honeycomb Final Report, GE-Doc. No. 68SD4264, 14 June 1968.

5.7-7 Kornhauser, M., "Structural Effects of Impact,: Spartan Books, 1964.

5.7-8 Young, C.W., "The Development of Empirical Equations for Predicting Depth of an Earth-Penetrating Projectile," Sandia Laboratory SC-DR-67-60, May 1967.

5.7-9 NASA-Langley Research Center, Mars Engineering Model Parameters for Mission and Design Studies, May 1968. (Preliminary Draft)

5.7-10 General Electric Report #66SD4390, "Development of Energy Dissipating Plastic Honeycomb Final Report, 14 June 1968.

5.7-11 Merz, E.J., PIR 9329-MARS-018, Preliminary Evaluation of Low g Impact Limiter, November 1968.

5.7-12 Goodyear Aerospace Corp. Report RSE-81104-3, Preliminary Analysis and Design of Pneumatic Landing System, 4 November 1968.

5.8 PARACHUTE SUBSYSTEM

5.8.1 SUBSYSTEM REQUIREMENTS

The parachute subsystem provides the final deceleration of the Lander prior to impacting the Mars surface. A parachute decelerator has been selected for the Hard Lander application because of its high drag-to-weight efficiency, extensive past experience, ability to readily adapt to an unknown environment, and relatively simple operation, which is in keeping with the passive nature of a Hard Lander. The parachute provides one of the three deceleration stages (aeroshell, parachute, impact limiter) for the Lander. To determine the design requirements for the Parachute Subsystem, trade-offs between the aeroshell, parachute and impact limiter are required as discussed in Section 3.3. The results of these trade-offs have resulted in a parachute designed to provide a maximum descent velocity of 100 fps at 6000 ft altitude in the NASA/LRC minimum atmosphere. Deployment of this parachute at a Mach number of 2.0 or less at an altitude of 10,000 ft or greater has been established so that the descent velocity of 100 fps can be achieved by 6000 ft altitude. The aeroshell β of 11.5 psf does satisfy this Mach/altitude requirement.

Parachute design requirements have resulted from definition of desired performance in the low density Mars atmosphere. Specifically, a canopy type having good stability characteristics, high drag efficiency, previous experience and an ability to absorb punishment. Based on the NASA/LRC PEPP tests both the Disc-gap band and modified Ringsail satisfy these requirements. The modified Ringsail has been selected, however, because of the extensive experience with large sizes of the closely related regular Ringsail design and the potential increased drag efficiency that can be obtained by decreasing the geometric porosity of modified Ringsail and moving toward the design of the normal Ringsail canopy.

5.8.2 DESIGN TRADE-OFFS

In order to establish the retardation system components and the system concepts to be used in the Hard Lander application, studies of numerous recovery system techniques used in past programs were conducted. The primary concern in this review is the selection of a retardation system which will perform reliably in the most severe anticipated deployment environment and be minimally affected by variations in the deployment environment.

The most significant recovery system conceptual techniques are listed in table 5.8.2-1. It is apparent from the problem areas listed therein that a single parachute, reefed, and deployed by means of a pilot parachute represents the most efficient and hence, reliable recovery system concept.

A serious drawback to the use of a non-reefed main canopy (in addition to the inherent weight penalty) is the additional weight penalty which must be included to account for variations in filling time and in deployment dynamic pressure.

TABLE 5.8.2-1. PARACHUTE RECOVERY SYSTEM TECHNIQUES

Technique	Data/Status/Application		Problem Areas
	Supersonic	Subsonic	
1. Clustering	Limited-small parachutes (low supersonic designs)	Extensive-common technique cargo and manned systems	Manned systems: non-synchronous filling
2. Reefing	Extensive-ground and flight tests-low supersonic designs ($M \leq 2.0$)	Extensive-common technique to accomplish orderly deployment of large parachutes and efficient designs of all sizes	Minor to none
3. Deployment	Extensive-mortared pilot or decelerator stage extracts main canopy	Extensive-mortared pilot or decelerated stage extracts main canopy	None
4. Use of large canopies	Limited - PEPP tests. $D_o \leq 85$ ft	Extensive - over 100 ft D_o.	Minor to none
5. Large parachute deployment, unreefed	Limited - high altitude sounding applications - PEPP tests, low q.	Limited - high altitude sounding applications - low q.	1 Opening load variation with filling time 2 Weight penalty at high deployment q.

Since the opening time of a parachute is difficult to predict analytically, test data are used where possible and in addition adequate latitude is allowed to predict parachute "performance" and "design" conditions. For parachutes of the "geometric porosity" type, the filling time follows a variation shown in fig. 5.8.2-1 (ref. 5.8-1). A short filling time will result in a large opening shock load, hence the design curve of fig. 5.8.2-1 is used to predict parachute strength requirements. Alternately, a longer filling time will result in a lower opening load, but will result in a greater loss of altitude during filling. For such predictions, the "performance" curve is used. Parachute weights resulting from the use of filling time extremes of fig. 5.8.2-1 are shown in table 5.8.2-2 for the 1400 lb Capsule when no reefing is used. When reefing is used, variations in filling times are not significant, since near infinite mass conditions occur in the present application as shown in table 5.8.2-2.

The independence of the reefed parachute weight on the accurate prediction of filling time had a strong influence on the selection of this concept for the present application. Since filling time for a reefed parachute primarily affects the performance of the system, the conservative "performance" filling time is used in all trajectory computations.

TABLE 5.8.2-2. PARACHUTE WEIGHTS - 1400 LB CAPSULE

System	Filling Time	Weight of Parachute and Lines (lb)
Mortared pilot deploys reefed main	Performance	52.2
Mortared pilot deploys reefed main	Mean	52.2
Mortared pilot deploys reefed main	Design	52.2
Pilot deployed main, no reefing	Performance	57.6
Pilot deployed main, no reefing	Mean	82.3
Pilot deployed main, no reefing	Design	104.7

In addition to the weight penalty of the unreefed system paid for uncertainties in filling time, the parachute weight requirements are highly reliant upon the deployment dynamic pressure. This is shown in fig. 5.8.2-2, where the effects of both filling time and dynamic pressure are demonstrated for the 1400 lb Capsule. The reefed parachute weight is seen to be independent of dynamic pressure as well as filling time since the opening loads (reefed and disreef) are less than the limit load for "minimum" gauge materials.

Errors, or deviations in the reefing ratio, do not significantly affect the parachute weight, as shown in fig. 5.8.2-3 for ratios in the range used in the current design analyses. Here, opening force variation is interpreted as weight variation if materials lighter than the "minimum" gauge had been used in the designs. Deviations in the design reefing ratio (8 to 12 percent) will not result in opening loads exceeding the allowable value for the minimum gauge materials assumed (375 lb lines and 1.1 oz/yd^2 cloth).

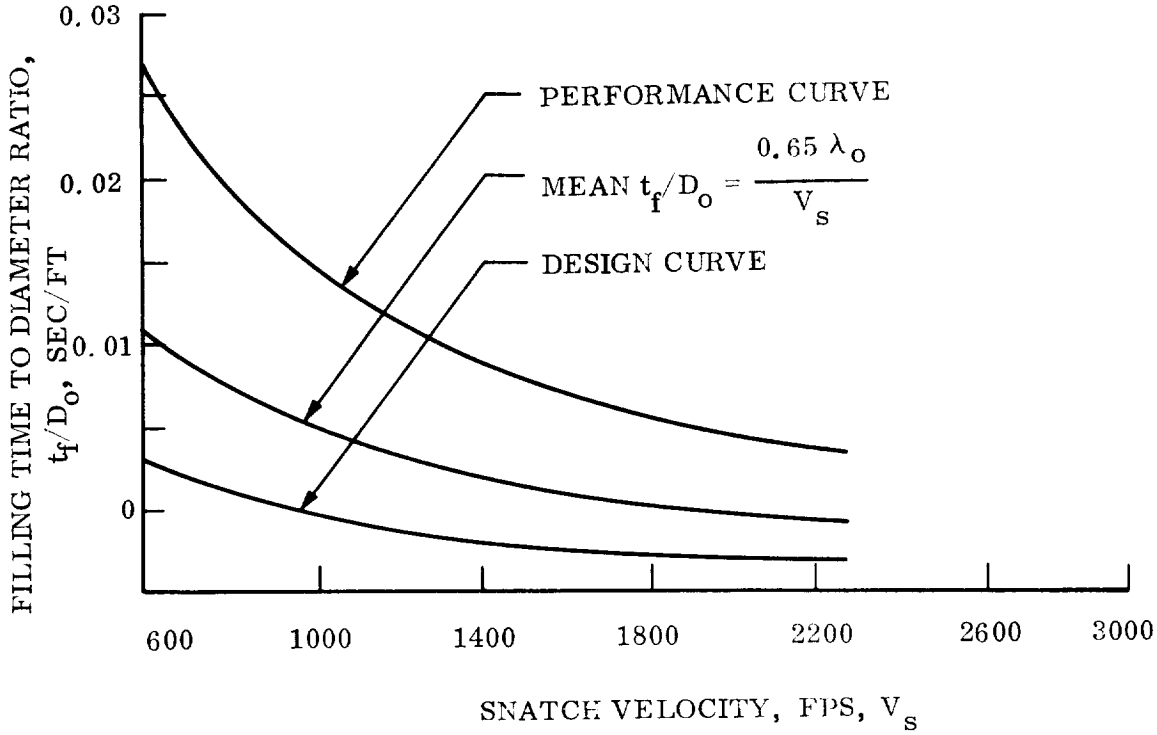

Figure 5.8.2-1. Variation of Ratio of Filling Time to Diameter with Snatch Velocity

Since opening loads are not an important constraint on a reefed parachute for this application, at least for the range of reefing ratios being considered, the only critical parameter is to insure sufficient drag during the reefed interval to provide at least the predicted Lander deceleration. While drag estimates are not highly accurate for reefed parachutes, it can be seen from fig. 5.8.2-3 that sufficient conservation can be built into the reefing ratio design, without a penalty in weight, that a minimum reefed drag area can be virtually guaranteed before a development test program is conducted and optimized as a result of the normal test program that must be conducted independent of whether or not reefing is used.

5.8.3 SUBSYSTEM DESCRIPTION

The subsystem design selected for the 1400 lb Capsule consists of two parachutes of the modified Ringsail type with the large (D_o = 67 ft) main descent parachute providing two stages of aerodynamic drag. The smaller parachute (D_o = 8.3 ft) serves as a pilot to deploy the main parachute and provides no deceleration for the Lander. A mortar is used to deploy the 8.3 ft pilot parachute. The signal to mortar out the pilot parachute is provided by a radar altimeter described in Section 5.2. The Parachute Subsystem deployment events are described below and shown pictorially in fig. 5.8.3-1.

On receipt of the signal, initiated by the radar altimeter for parachute system deployment, power from the vehicle power supply will be applied to the mortar pyro initiation. Mortar firing will release and deploy the pilot parachute thermal cover and the pilot parachute. After stripping off the pilot parachute, the pilot parachute deployment bag and attached thermal cover free-fall away.

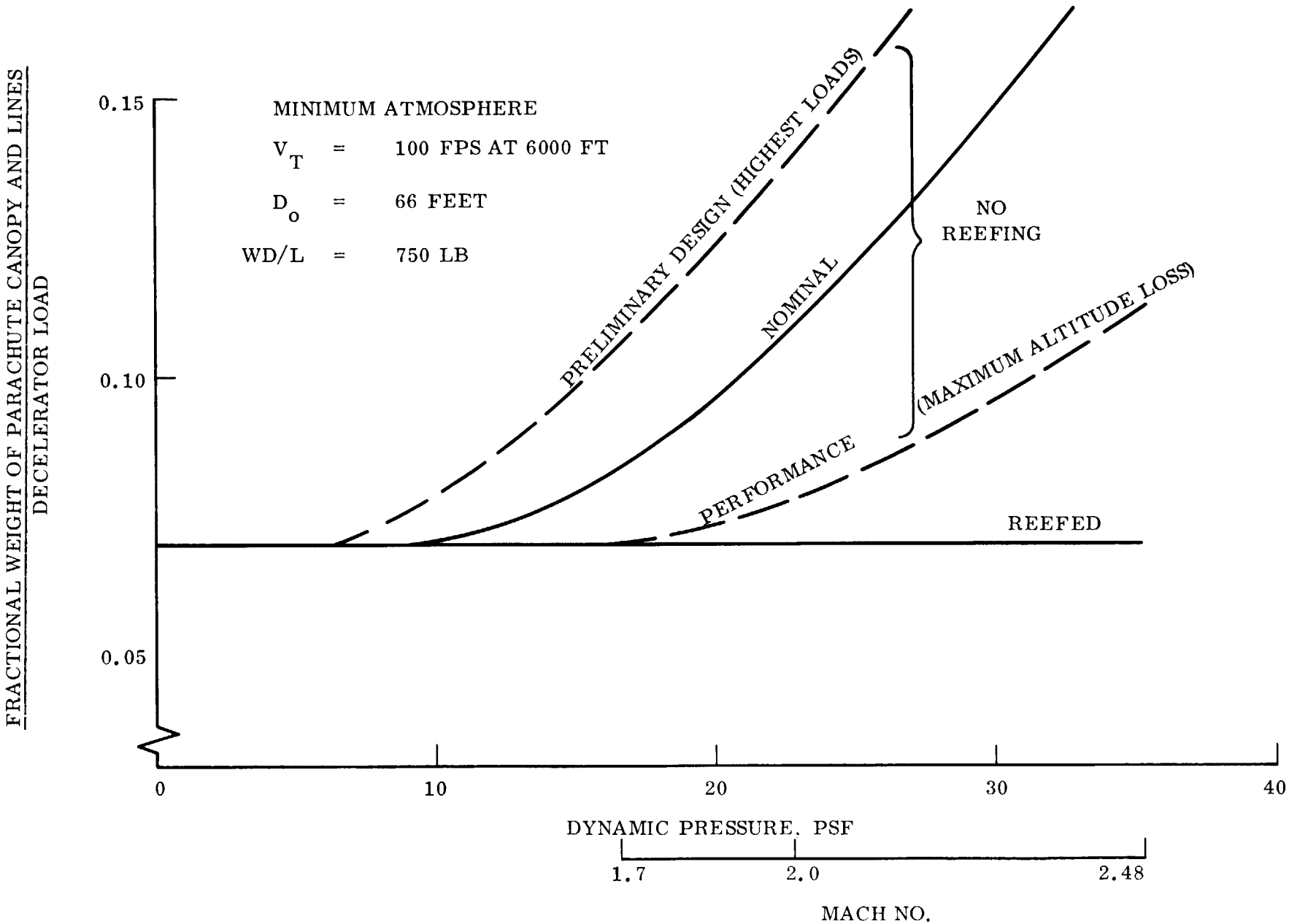

Figure 5.8.2-2. Parachute Weight Variation with Dynamic Pressure

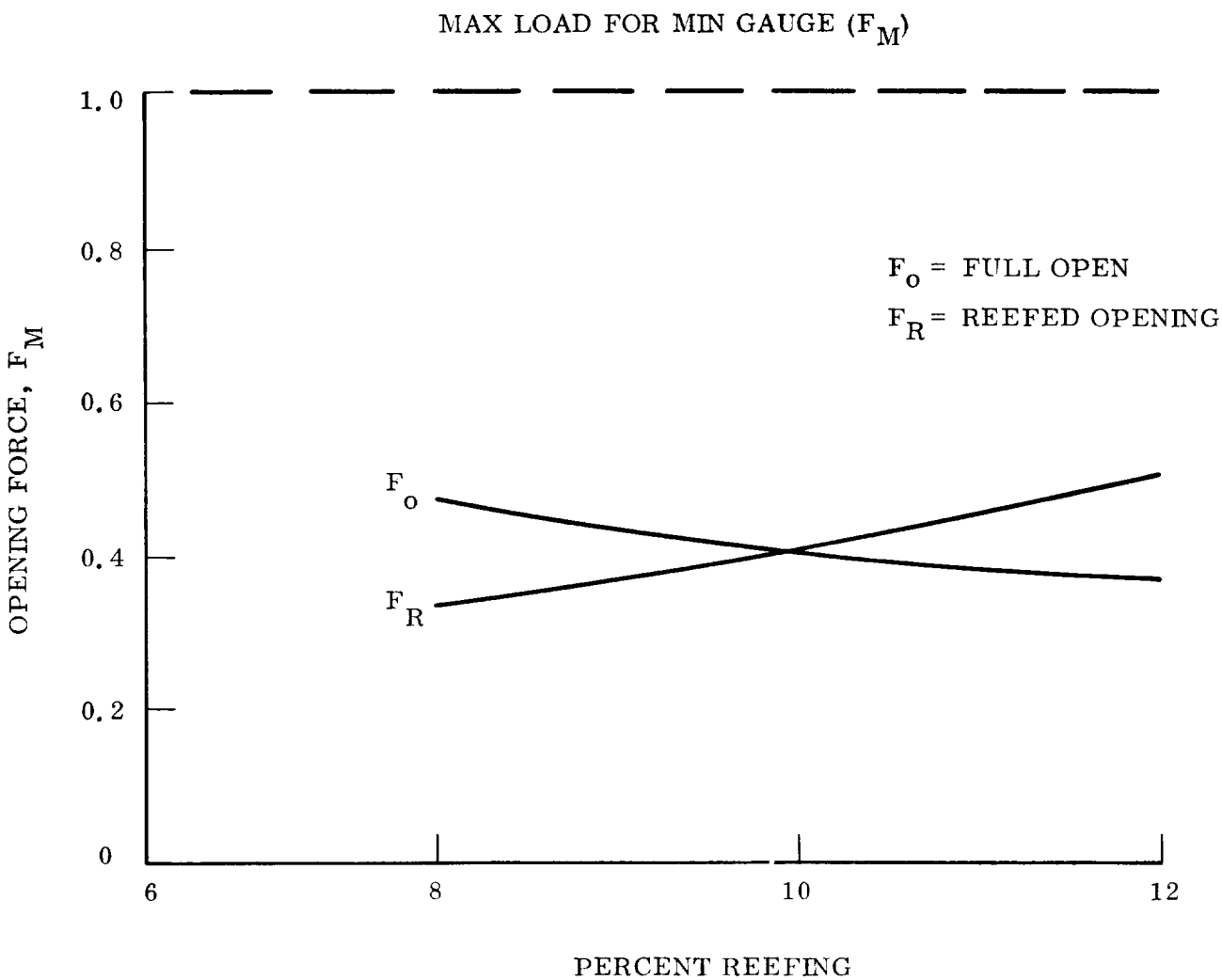

Figure 5.8.2-3. Opening Force for Reefed Parachute

As the pilot parachute is being deployed, the main compartment thermal cover will be deployed by the snatch force of the pilot parachute. One end of the main thermal cover is released by the pilot parachute cover separation. The main cover is attached to the pilot parachute riser at two points for deployment and retention to the riser.

As the cover is rotated out by the pull from the pilot parachute, the hold-down tang on the edge of the cover opposite the mortar will rotate out of a slot in the main parachute compartment, completely releasing the cover (see fig. 5.8.6-1 for details of cover and component arrangement).

The snatch force of the main compartment thermal cover on the pilot parachute riser will pull out the tuck bight securing the main parachute tie-down straps. This releases the main parachute pack for deployment. Further pull force on the pilot parachute riser will be applied to the main parachute bag handles for main parachute extraction and deployment.

The main parachute is extracted and deployed in a reefed condition by the pilot parachute. During this deployment, the mechanically initiated pyrotechnic time delay reefing line cutters are actuated. After time-out of the redundant reefing line cutters, the cutters actuate, severing the reefing line. This event permits main parachute full open deployment. As the drag of the full open main parachute develops, the aeroshell is released and allowed to free-fall away.

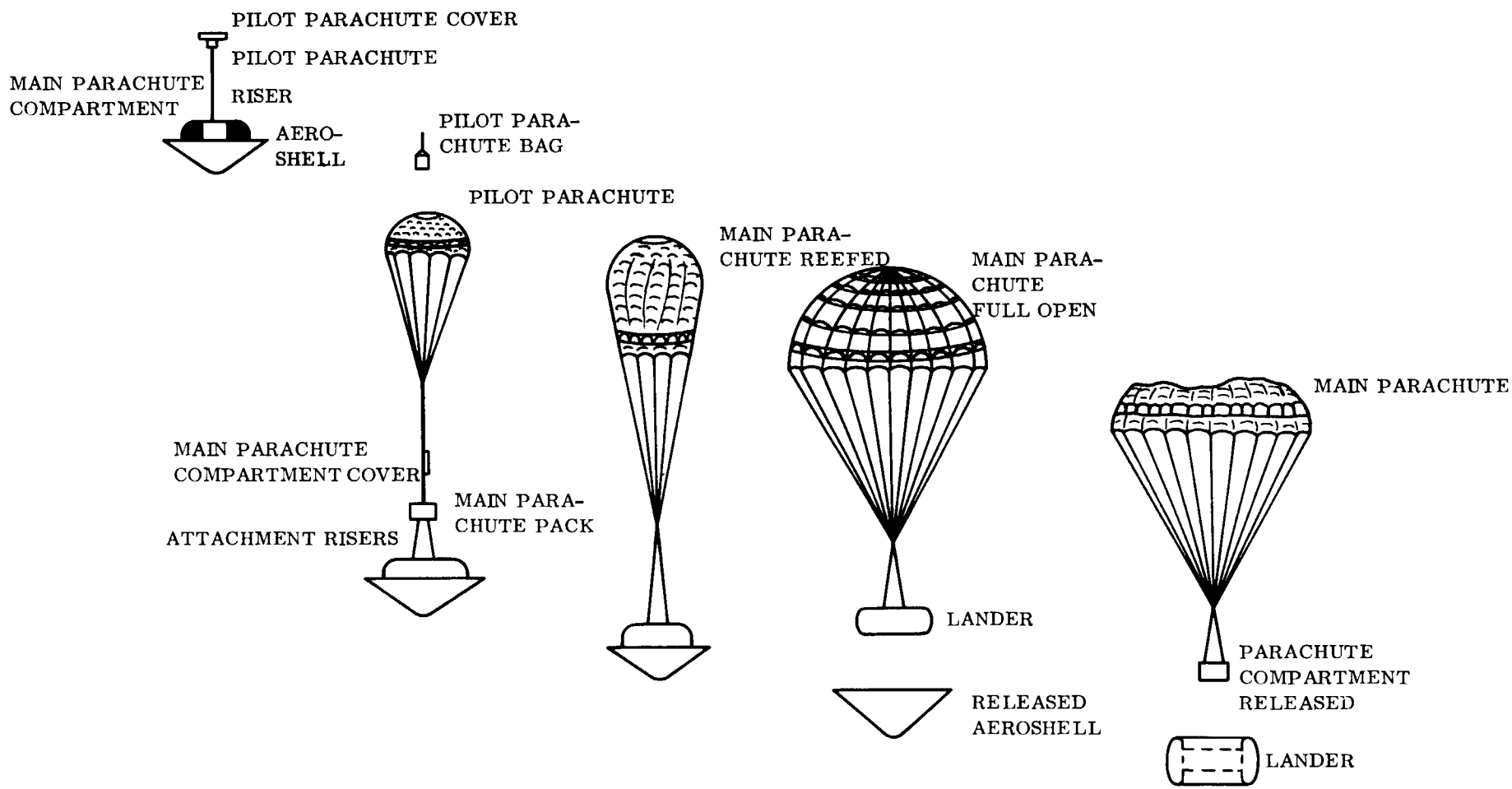

Figure 5.8.3-1. Parachute Subsystem Deployment Sequence

The radar altimeter is used to sense the distance above the touchdown surface. When this distance is 150 ± 50 ft a firing signal is given to release the hot-wire nuts, which in turn causes separation of the parachute compartment/mortar assembly from the Lander; the Lander will free-fall to surface impact. The jettisoned main parachute will collapse due to the sudden release of the loading from the suspension lines. Based on previous experience with Earth recovery systems the parachute can be expected to spill to one side as a result of the collapse. Even so, a finite probability exists where with little or no winds the parachute could fall on the Lander. For earth recoveries this probability is on the order of one or two envelopments for 50 chances. A direct comparison with the Mars environment is not possible; however, release of the parachute above the surface is felt to provide a reduced probability. Semi-active and active concepts are currently being investigated which will increase the probability that the parachute will not drape over the Lander.

5.8.4 SUBSYSTEM DESIGN

Parachute designs, including the sizing, staging, and selection of canopy types which are optimum for a given application are performed by the GE Recovery System Selection Program (RESSEP). A summary of the parachute characteristics is given in table 5.8.4-1. The modified Ringsail main descent parachute has a D_o = 67 ft with a predicated drag area of 1830 ft^2.

TABLE 5.8.4-1. PARACHUTE DESCRIPTION, 1400 LB CAPSULE

Component	Drag Area ($C_{D_o} S_o$)	Area (S_o)	Diameter D_o	Weight (lb) (Canopy, Lines, and Riser)	Fabric (T_c) (lb/in.)	Specific Drag Area* (ft^2/lb)
Main Parachute Modified Ringsail	1830	3520	67	53.34	14.3	35.0
Pilot Parachute Modified Ringsail	28.3	54.3	8.3	3.01	4.5	13.0

$$* \frac{C_{D_o} S_o}{\text{Weight of canopy and lines}}$$

In accordance with the results of studies involving the comparison of various recovery system techniques and system components discussed previously, both components types and system sequencing methods selected for the present application are compatible with past recovery system practice and experience. This, coupled with results of the PEPP test program, adequately enable the preliminary design and analysis of a retardation system for the present application. A mortared pilot parachute extracts the main canopy which is deployed reefed. After a short reefed period, the main canopy is disreefed and allowed to fully open.

The pilot parachute is sized to extract and extend the main canopy to line stretch in approximately 1 sec at maximum dynamic pressure. The pilot strips the bag from the main canopy, which is then free to inflate. The use of a deployment bag prevents the opening shock and snatch load from occurring simultaneously. As shown previously the selection of this retardation system technique and components results in a low weight system which is minimally sensitive to atmospheric deployment environments and parachute filling time variations.

In sizing the pilot parachute, drag effectiveness in the supersonic wake of the aeroshell has been taken into account. As a preliminary estimate of the reduced drag effectiveness of the pilot parachute in the wake of the blunt aeroshell, data from ref. 5.8-1, (shown in fig. 5.8.4-1) are used. At Mach 2, the drag in the wake is about 0.6 of the freestream value. Negligible variation in this ratio exists as a function of x/d (up to 10) as shown in fig. 5.8.4-1. The use of the drag effectiveness values shown in fig. 5.8.4-1 for an Apollo-shaped vehicle appears warranted by the data in fig. 5.8.4-2 (ref. 5.8-1). These and numerous other past data demonstrate that the drag effectiveness of trailing bodies in the wake of a forebody is dependent upon the forebody drag, and the diameter of the trailing body compared to the forebody (d/D). Since the aeroshell drag coefficient in the present design is approximately the same as the P-shape at Mach 2, and since the pilot diameter is in the same general relative size ratio to the forebody, these data appear readily applicable to the present analysis for preliminary design purposes.

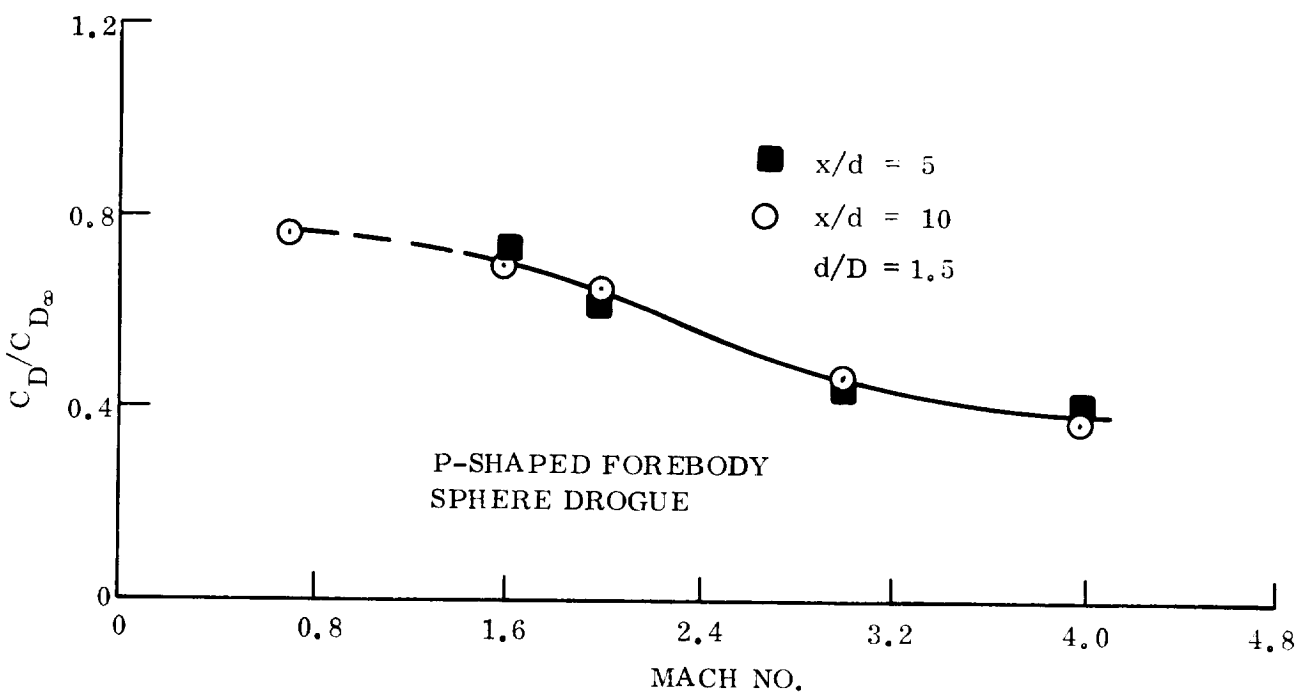

Figure 5.8.4-1. Effect of Mach No. on Trailing Drogue Drag

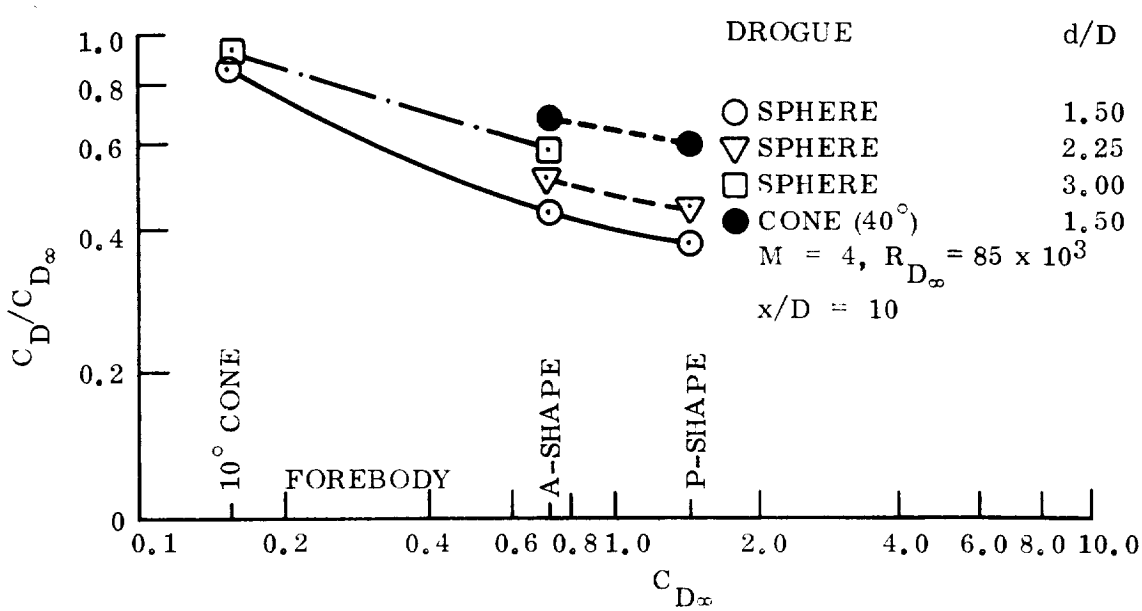

Figure 5.8.4-2. Effect of Forebody Drag on Trailing Drogue Drag

In order to establish the ejection velocity of the pilot parachute-mortar thermal cover required to overcome the adverse wake reverse flow region upstream of the rear stagnation point, and the vehicle deceleration at the time of pilot deployment, the GE Cover Ejection Computer Program is used. The pilot parachute pack and cover geometry are shown in the following sketch:

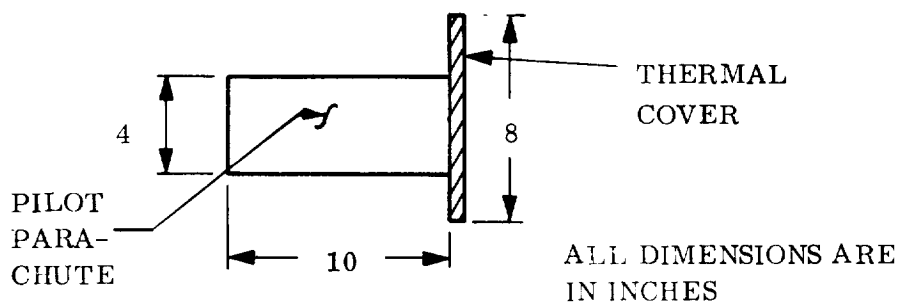

The cover size has been selected to reflect a favorable ballistic coefficient for the cover and pilot bag after stripping off the pilot parachute. This ballistic coefficient will be less than that of the vehicle and reefed main parachute.

In fig. 5.8.4-3 results of the pilot-cover ejection studies are shown where several ejection velocities are evaluated. It is apparent that the minimum ejection velocity required for positive separation from the vehicle is between 50 and 75 fps.

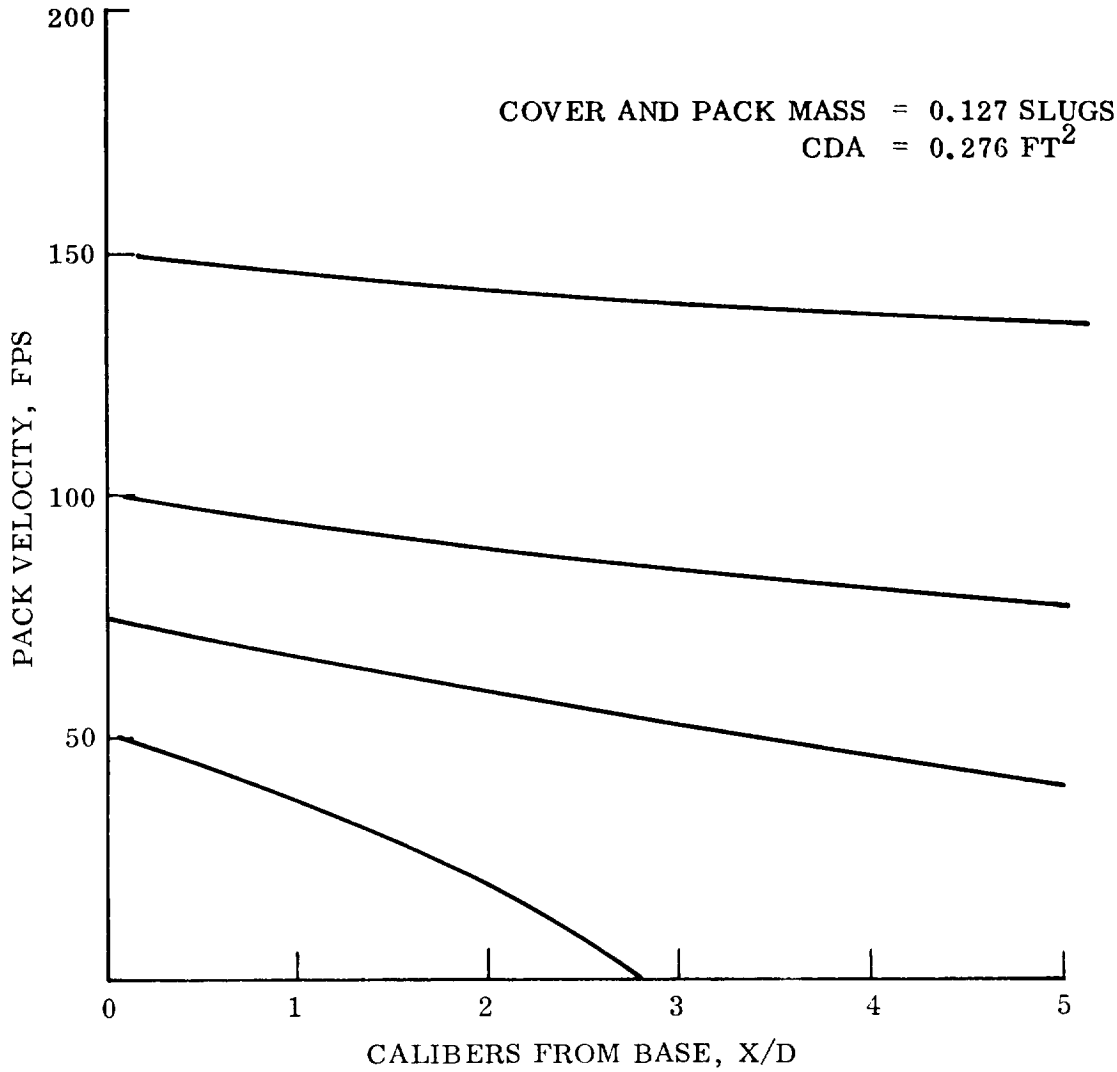

Figure 5.8.4-3. Pilot Thermal Cover Ejection Study - Mach 2, 10 kft, q = 20 psf

5.8.5 SUBSYSTEM PERFORMANCE

A trajectory study was performed to verify that the selected design could perform under the 1400 lb Capsule deployment conditions, meet the design requirements of parachute deployment at Mach 2 and reach a terminal velocity of 100 fps by 6 kft altitude.

The worst trajectory conditions for the parachute occur in the rarest NASA/LRC minimum density atmosphere. Trajectory studies indicate that the β = 11.5 psf vehicle will decelerate to Mach 2 at approximately 11 kft altitude. For mean and maximum atmospheres, Mach 2 occurs at a higher altitude. Parachute performance was designed to meet the worst case deployment conditions of the minimum atmosphere deployment. The study included the extraction and deployment of the main parachute by the pilot parachute.

For the re-entry vehicle trajectory used, mortar firing occurred at 12 kft, Mach 2.2, and q = 25.4 psf. The trajectory of the pilot parachute extracting the main parachute was examined and compared to the trajectory of the vehicle now minus the weight of parachutes. This study was used to determine the point of start of main parachute reefed inflation (at M = 2) where the main parachute skirt has been deployed. The results of this study are shown in fig. 5.8.5-1 and the parameters used are listed in table 5.8.5-1.

TABLE 5.8.5-1. PILOT PARACHUTE DEPLOYMENT TRAJECTORY STUDY PARAMETERS

Atmosphere = LRC minimum density
Initial deployment altitude = 11,770 ft
Weight being decelerated by pilot parachute = 60 lb
Vehicle weight minus the parachutes = 962 lb
Path angle below horizontal = 24.2°
Pilot parachute fill time = 0.12 sec
Linear pilot parachute inflation with time assumed
Pilot parachute D_o = 8.3 ft
Pilot parachute C_D = 0.52
Pilot parachute $C_D S$ = 28.3 ft^2
Pilot parachute opening shock factor = 2.0 (conservative selection)
Aeroshell D_o = 9.0 ft
Aeroshell C_D = 1.46

Parachute reefing and duration of the reefed stage were optimized to produce equal opening loads for both main parachute stages within the strength capability of the suspension lines, and to minimize altitude loss during deployment. The parameters selected for the staging optimization study are shown in table 5.8.5-2. The parachute/vehicle trajectories were calculated by computer, using the initial conditions and calculated parameter listed in table 5.8.5-3.

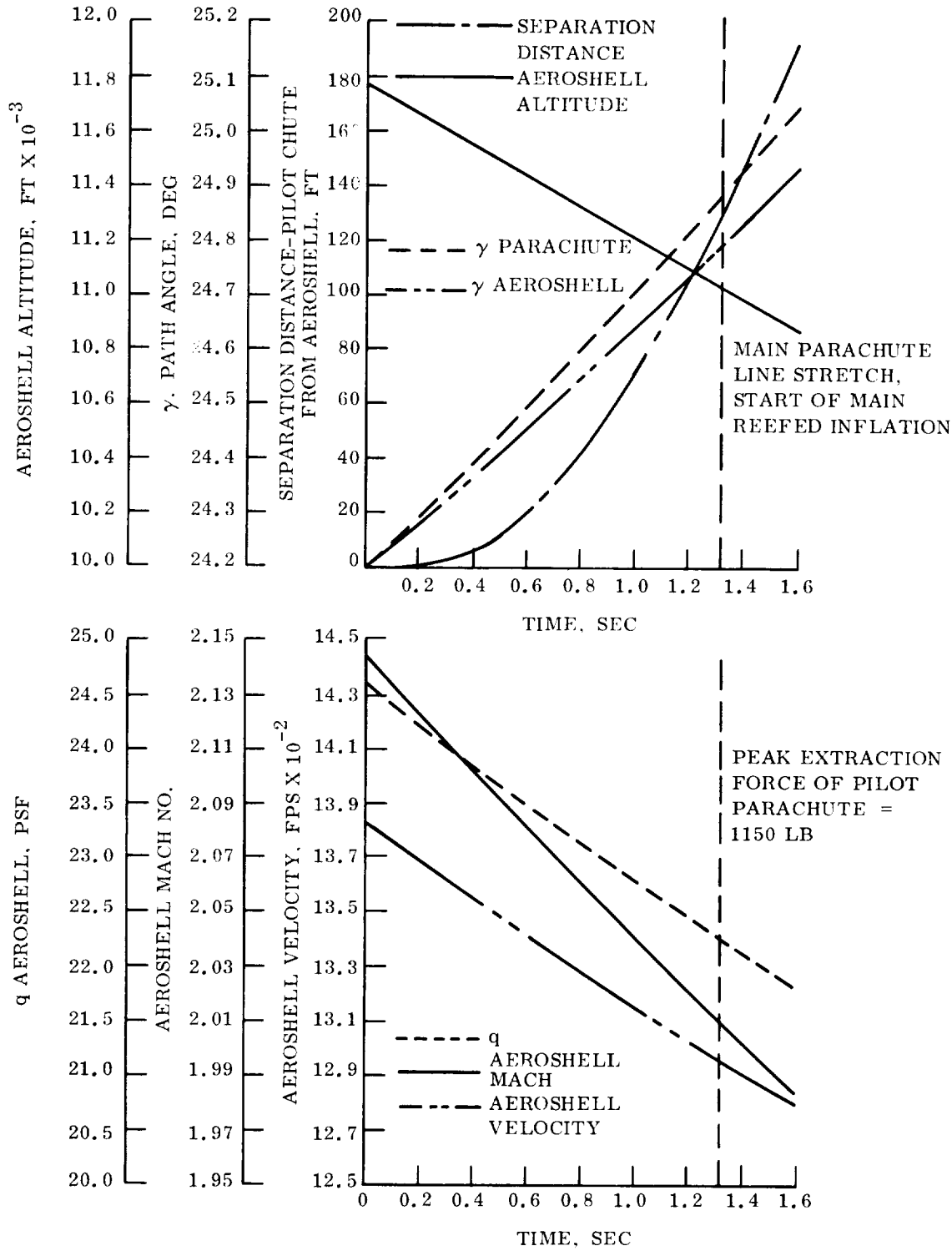

Figure 5.8.5-1. Pilot Deployment Trajectory in Minimum Density Atmosphere

TABLE 5.8.5-2. MAIN PARACHUTE REEFING OPTIMIZATION DESIGN PARAMETERS

Main parachute full open $C_D S$ = 1830 ft^2
Initial reefed deployment q = 22.25 psf
Reefed stage opening shock factor = 2.0 (conservative selection)
Disreef opening shock factor = 0.42 (conservative selection)
Axial deceleration at disreef ~ 9 g's, Martian
Total weight being decelerated = 1014 lb (at time of reefed opening)
Main parachute C_D = 0.52
Aeroshell $C_D A$ = 91.5 ft^2

TABLE 5.8.5-3. PARACHUTE TRAJECTORY PARAMETERS 1400 LB CAPSULE

Atmosphere = NASA/LRC minimum density
Total weight being decelerated = 1014 lb
Initial deployment altitude = 11,034 ft
Initial velocity, reefed deployment = 1296 fps
Initial path angle = 24.8° (down from horizontal)
Linear reefed opening inflation with time assumed
Effective reefing ratio = 11.2 percent
Reefed filling time = 0.10 sec
Total time of reefed stage = 2.6 sec
Main parachute D_o = 67 ft
Main parachute C_D = 0.52
Main parachute full open $C_D S$ = 1830
Main parachute full open fill time = 1.1 sec
Linear full opening inflation with time assumed

The results of this trajectory study are shown on fig. 5.8.5-2. These calculations are conservative inasmuch as Lander drag area is not considered as part of retardation drag area after main parachute full open deployment.

Based on a final entry trajectory, Section 3, Mach 2.0 occurs at an altitude of 11,034 ft in the minimum atmosphere for an aeroshell ballistic coefficient of 11.5 psf. This altitude is slightly higher than the 10 kft minimum established earlier. Trajectory studies show that with mortar firing at 12 kft, pilot parachute inflation starts at 11,770 ft. In turn the main parachute reaches line stretch and starts inflation at M = 2.0 at the 11,034 foot altitude. By balancing the parachute opening loads and minimizing reefing time (2.6 sec) main parachute disreef begins at an altitude of 9,800 ft. With disreef at this altitude a velocity of 99.7 fps is obtained at 8 kft altitude which is 2 kft above the design value of 6 kft. The fact that the velocity is less than 100 fps at 8 kft altitude results from a flight path angle less than 90° at the 8 kft altitude. Thus it can be seen that based on the latest entry trajectory the parachute subsystem surpasses the terminal velocity/altitude requirements. This capability is desirable since entry vehicle weight growth or decreased parachute deployment environment can be accommodated. These results also indicate that a larger aeroshell β or Lander weight could possibly be incorporated through more detailed trajectory and optimization analysis.

5.8.6 COMPONENT SELECTION

The basic hardware concepts selected have been previously used, tested, and proven in other programs. The mortared parachute deployment is a commonly used technique and the thermal cover concept and deployment arrangement has been used by GE on the 698 BJ program and the Maneuvering Ballistic Re-entry Vehicle (MBRV) program.

The parachute designs selected are based on the designs and results to date of the NASA PEPP program. The aeroshell release and fallaway is similar to the re-entry heat shield separation used by GE in the A-45 program and other recovery Capsule programs.

Pilot parachute extraction and deployment of the main parachute was selected to ensure orderly deployment of the large diameter main parachute. The use of the pilot parachute also reduces the size of mortar required for deployment compared to directly mortaring the main parachute. The mortar reaction forces are also greatly reduced by mortaring the smaller parachute. The reaction force shock of a large mortar capable of direct deployment of the main parachute could possibly impose a limiting shock design requirement on the Lander science payload. The pilot parachute mortar will be angled so that the reaction force passes through the vehicle c.g.

The hardware components of the retardation subsystem are described in the following paragraphs. Fig. 5.8.6-1 shows mounting location and the interrelations of the various components in an exploded isometric view.

The pilot parachute mortar thermal cover provides the means for securing the pilot extraction parachute in the mortar prior to mortar deployment. It also anchors one end of the main parachute thermal cover and provides thermal protection from wake heating to the pilot parachute, mortar gas source, and the electrical cable cutter. The cover will be secured to the mortar

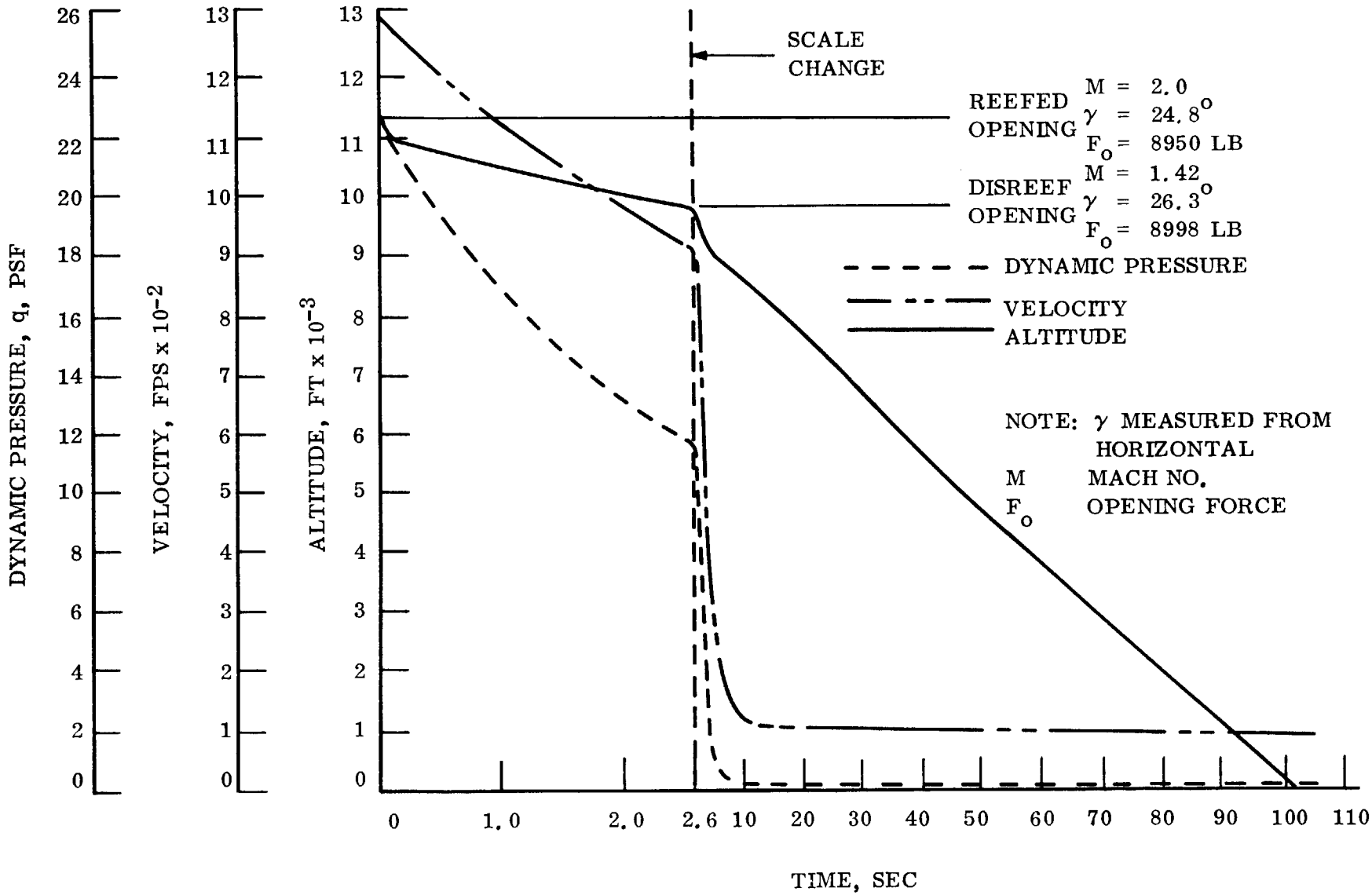

Figure 5.8.5-2. Main Parachute Trajectory in Minimum Density Atmosphere

tube by shear pins until mortar firing. A bag handle on the pilot parachute deployment bag will be secured to the thermal cover in a recess within the cover. Thus, the thermal cover will also provide a mass to assist in stripping the deployment bag from the pilot parachute during deployment.

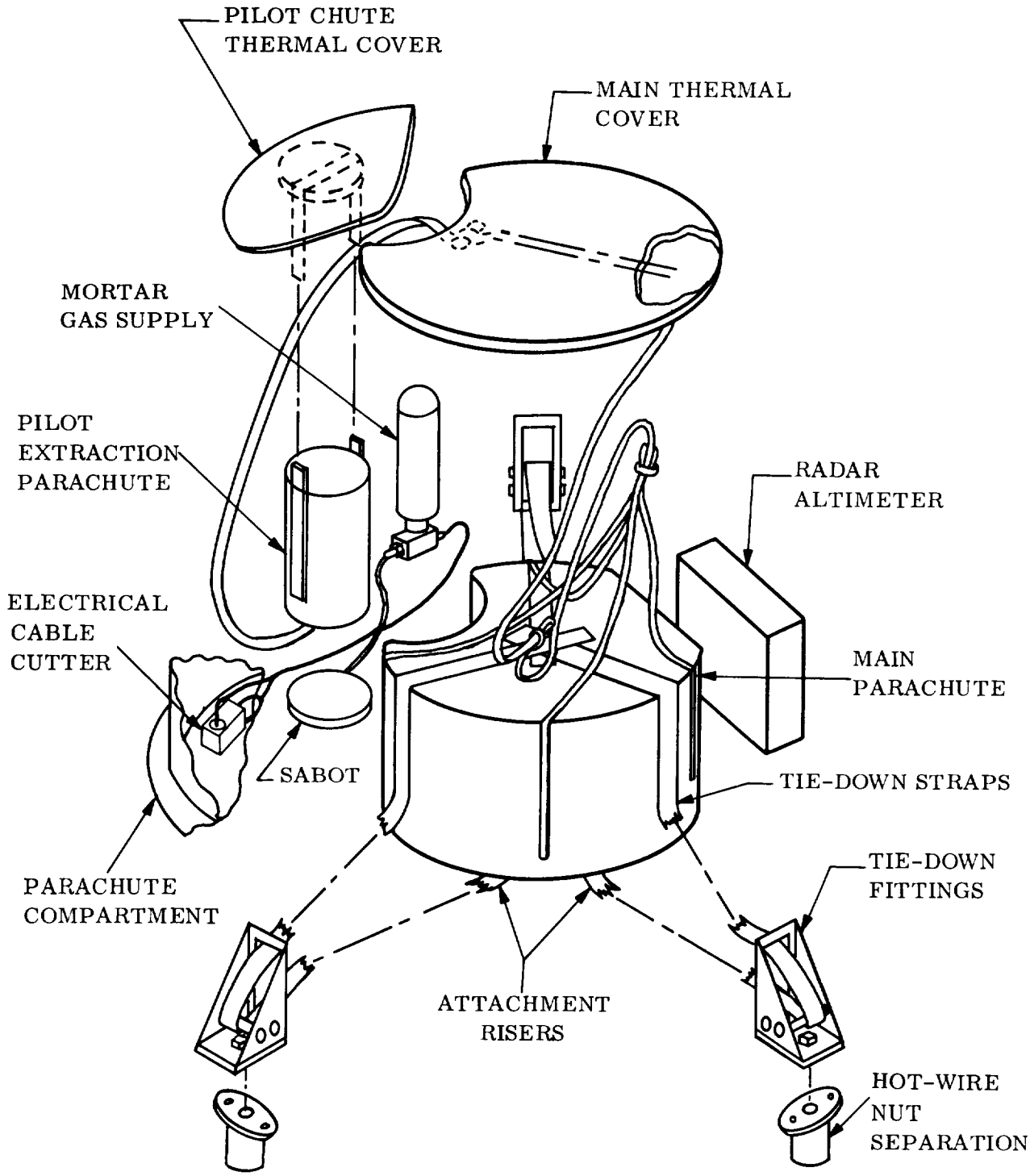

Figure 5.8.6-1. Retardation Subsystem Hardware Arrangement

The 8.3 ft pilot extraction parachute will be similar in design to modified Ringsails tested in the NASA PEPP program. All parachute lines and material will be sterilizable dacron, and lightweight construction is envisioned, using 1.1 oz cloth and 375 lb suspension lines. The pilot parachute will be pressure packed to a 40 lb/ft^3 density or slightly higher. The pilot extraction parachute will be provided with a riser line to provide a minimum length of six aeroshell base diameters to the skirt at parachute inflation. This line will also be used to provide a mouth lock for the pilot parachute bag and to extract the main parachute bag for main deployment. It will attach to two fittings, one at each end of the main parachute thermal cover, for extraction and deployment of this cover. The end of this line, at the main parachute bag, will be used to form a tuck bight through a locking loop of the three tie-down straps securing the main parachute in its compartment.

The main parachute compartment thermal cover is deployed by the pilot extraction parachute and permanently attached to the pilot parachute riser.

The cover will be aluminum with necessary reinforcement to sustain the loads of deployment. All edges will be well rounded to prevent damage to the pilot parachute riser line. The outside surface is covered with thermal protective coating to preserve the cover's structure and control main parachute temperature during entry wake heating.

The main parachute will be a single large diameter modified Ringsail parachute with one stage of reefing. Existing design hermetically sealed reefing line cutters, manufactured by Technical Ordnance Products Co. will be used. The parachute will be made of sterilizable dacron material, in lightweight construction similar to the constructions tested in the NASA PEPP program. At present the parachute would be made of 1.1 oz cloth with 375 lb suspension lines since maximum deployment q will be 22.25 psi or less. The main parachute will be pressure packed to 38 to 40 lb/ft^3 density. The attachment risers will connect the main parachute at the suspension line confluence to the three tie-down fittings at the base of the parachute compartment. At main parachute release, the parachute compartment including the mortar will remain with the main parachute attached by the main parachute risers.

The parachute compartment will be an aluminum sheet metal fabrication to confine the parachute and provide thermal protection from re-entry wake heating. The outside surface of the compartment will be provided with the required thermal protective coating. The attachment and tie-down fittings will be attached to the rim at the base of the compartment. The pilot parachute mortar will be built into one side of the compartment. It will consist of a mortar tube and a sabot for the pilot parachute to seat against. The gas for mortar ejection will enter through tubing at the bottom of the mortar under the sabot. The area on each side of the mortar will be used for mounting the gas source for mortaring and the electrical cable cutter to separate the power supply from the mortar pyrotechnic. The side of the parachute compartment opposite the mortar will provide a slotted recess to receive the tang on the main thermal cover that secures that end of the thermal cover. The radar altimeter will be mounted on the outside of the compartment to allow its weight to be jettisioned at main parachute release.

Three parachute attachment and tie-down fittings, one for each of the three risers, are attached to the parachute compartment at the bottom flange and will be provided with two pins for webbing attachment. One pin will attach the main parachute risers (3), and the second pin will attach tie-down straps (3) that secure the main parachute in a position such that it

does not put a load on the main parachute thermal cover by pressing against it. The three tie-down straps will secure the main parachute using a locking loop and a tuck bight formed by the pilot parachute riser. They will carry most of the powered flight loads of the main parachute.

The gas for mortar ejection can be provided by either a pyro gas generator or a compressed gas supply. The compressed gas supply can be provided at a slight weight increase over the gas generator. Standard components are available from Conax Corporation (Conax Eager Paks) for the compressed gas supply. It would consist of a small hermetic cylinder (10 to 15 in.^{3} capacity) containing compressed nitrogen at 3000 psi and a pyro valve that fires, piercing the cylinder allowing flow out through a connecting tube. This arrangement offers several advantages. There is no hot gas that could damage fabrics or components used for mortaring. There will be less problem of pyro development for the Mars mission in that the valve uses a standard squib and does not need the special gas generating materials. Reaction forces and performance will be more predictable. The compressed gas can be sterilized readily where this may be a problem with the gas generator materials.

The parachute compartment will be secured to the payload by three hot-wire nuts, attached to bolts passing through the attachment and tie-down fittings. These will be similar to the hot-wire nuts used for Capsule separation. To sever the electrical cable connection between the Lander and parachute equipment, an electrical cable cutter is used. At parachute release the three hot-wire nuts and the cable cutter are initiated, allowing the parachute to extract the parachute compartment from the Lander.

5.8.7 REFERENCE

ASD-TR-61-579, "Performance of and Design Criteria for Deployable Aerodynamic Decelerators", December 1963.

5.9 AEROSHELL

This section describes the design of structure and heat shield to satisfy the mission and system requirements of the 1400 lb Flight Capsule.

5.9.1 REQUIREMENTS AND CONSTRAINTS

The maximum path angle and minimum terminal velocity constraints determine the Entry Capsule ballistic coefficient (β = 11.5 psf). These conditions were described in Section 3.0. For a fixed β and a maximum decelerator load, a minimum aeroshell diameter is established which is consistent with the Lander packaging problem, Entry Capsule stability, and other similar system design constraints. (These trade-offs are described in great detail in Section 3.1.2 of NASA CR-66678-3, Vol III, Hard Lander Capsule Study).

The maximum decelerator load for the 1400 lb Capsule is provided for in this flyby mission with an aeroshell 108 in. in diameter, having a cone half angle of 60° and bluntness of 0.5. The maximum deceleration trajectory (γ = 24.75° - MIN atmosphere) and the maximum heating trajectory (γ = 16.5° - MAX atmosphere) override all other powered flight, cruise, and ground handling load conditions for the aeroshell design.

5.9.2 STRUCTURAL DESIGN

In order to determine the critical entry loads and heating on the aeroshell, nine entry trajectories which bound the total design corridor were evaluated and are shown in table 5.9-1. With these nine combinations of trajectory and atmospheres there is a considerable variation in maximum deceleration loadings.

TABLE 5.9-1. MAXIMUM ENTRY DECELERATION LOADS

Entry Condition	Entry Path Angle	Atmosphere	Maximum G_x	Time From 244 kft (sec)
1	16° 27'	MIN	8.1	214
2	16° 27'	MEAN	7.6	184
3	16° 27'	MAX	8.2	156
4	21°	MIN	22.0	132
5	21°	MEAN	15.6	122
6	21°	MAX	14.2	110
7	24° 45.5'	MIN	29.5	108
8	24° 45.5'	MEAN	20.4	100
9	24° 45.5'	MAX	18.2	90

The maximum loads occur for Entry Condition No. 7 in the Mars MIN atmosphere. The maximum total heating trajectory is Entry Condition No. 3.

Due to the large size, light weight, and high-angle conical shape, stability for collapsing pressure is an area of major concern in the aeroshell design. It was recognized that a honeycomb design reduced the hoop compressive buckling loads in the outer ring because of its inherent increased shell bending stiffness and increased hoop load capability of a honeycomb shell. The outer ring loading is reduced because a greater percentage of the total hoop load is carried by the honeycomb facings. A second advantage of honeycomb construction over ring stiffened construction is that the inertia loads from the payload can be distributed into the shell more efficiently. The local shell shear loads and bending moments where the payload bears against the shell are easily distributed into the honeycomb structure. With ring stiffened structure, local meridional stiffening is required to distribute these loads into more than one ring, and the skins locally must be increased in thickness. As shown later in this section, a detailed design comparison of a ring stiffened and a honeycomb aeroshell using the MULTISHELL computer program results in a heavier ring stiffened aeroshell weight.

With the honeycomb design, when the core thickness is made large enough to withstand the local shell bending mements and the local shear loads, the shell is no longer stability critical. The only stability problem is in the outer ring box that must be stable for out-of-plane buckling. In the ring stiffened design, every ring must be designed for ring stability.

Four facing materials were compared for use on the honeycomb configuration and unit weight comparison are shown in table 5.9-2.

TABLE 5.9-2. HONEYCOMB FACING MATERIAL COMPARISON

	Facing Thickness (in.)	Core Thickness (in.)	Core Density (lb/ft^3)	Unit Weight (lb/ft^2)
Aluminum	0.012	1.00	3.1	0.663
Titanium	0.006	1.00	3.1	0.564
Stainless Steel	0.006	1.00	3.1	0.788
Phenolic Glass	0.020	1.00	3.1	0.693

5.9.2.1 Loads Analysis

The detailed analysis of the aeroshell structure to withstand the entry inertial loads, aerodynamic pressure loadings, and temperature gradient loadings is performed by "MULTISHELL", a GE computer program. The inputs to this program consist of the entire aeroshell configuration, upon which are imposed the inertia loads, the pressure loads, and the temperature. Output from the program consists of the shell internal stresses, moments, shear, in-plane shell loads and complete shell deformations. Figs. 5.9-1 through -5 present deflection, moment, shear, in-plane load and facing stress distributions for typical Capsule entry

conditions. From this type of MULTISHELL analysis, empirical equations were developed to determine the maximum moments, in-plane meridional tensile load, and the maximum shear load in the region where the Lander subsystem bears against the aeroshell. This location is a radial location of 29 in. in figs. 5.9-1 through -5.

These equations were used to: (1) determine the maximum shell loads as a function of the aeroshell configuration, (2) determine the location where the Lander subsystem bears on the aeroshell, and (3) determine the optimum honeycomb configuration for the axial deceleration and external pressure loading. Fig. 5.9-6 shows the parameters required to obtain these internal loads.

The bending stress in the honeycomb facings is:

$$S_{fb} = \pm \frac{0.0275\ WG_x}{t_f\,(t_f + t_c)} \left[1 - \frac{R_o^2}{a^2}\right] \left[1 - \frac{a + Ro}{2R}^{\ 2}\right]$$

This equation gives the meridional stresses in the facings, compression in the inner facing and tension in the outer facing at the radial distance R_o. This is due to the maximum moment as shown in fig. 5.9-2. It should be noted that the moment results in the same stress levels outboard and inboard of the bearing point.

The meridional tension stress in the facing outboard of the radius R_o is:

$$f_{fN_1} = \frac{WG_x}{\pi t_f} \left[\frac{1}{a + R_o} - \frac{a + R_o}{4R^2}\right]$$

The meridional tension facing stress inboard of the radius R_o is:

$$f_{fN_2} = \frac{1}{2}\ f_{fN_1}$$

The core shear stress at the radius R_o is:

$$\tau = \frac{p}{2R_o\,(t_f + t_c)} \left[R^2 - \left(\frac{a + Ro}{2}\right)^2\right]$$

These equations are used to size the aeroshell honeycomb structure. The final configuration is then checked using the MULTISHELL computer program.

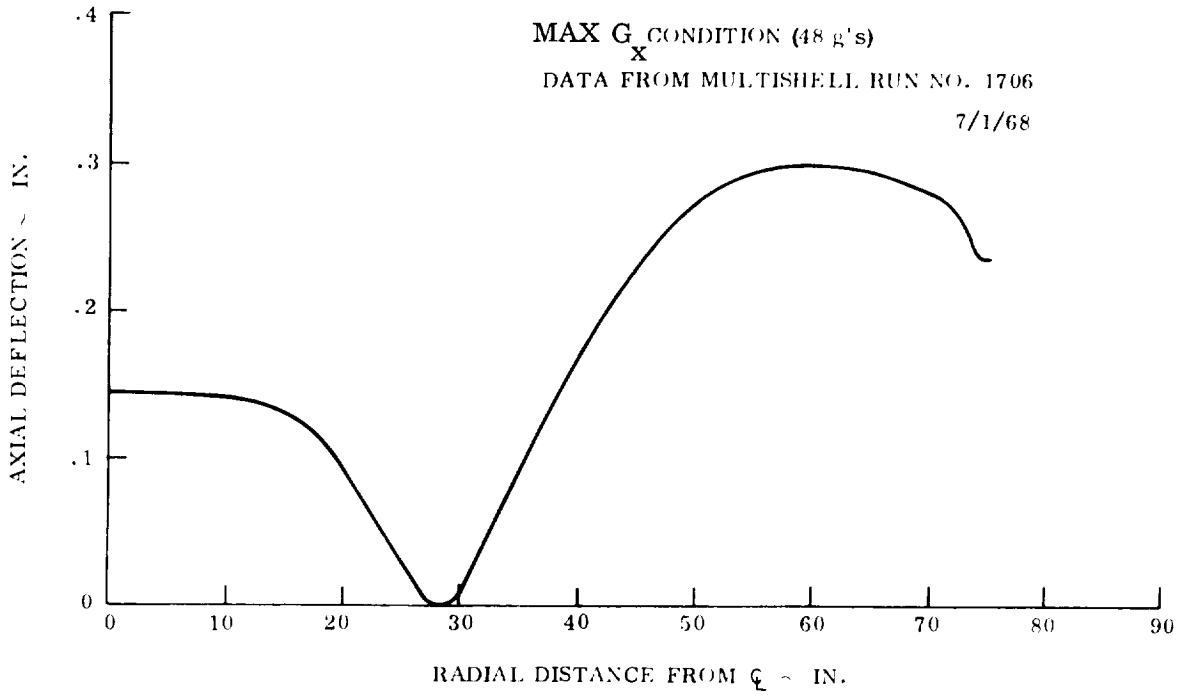

Figure 5.9-1. Axial Deflection vs Radial Distance

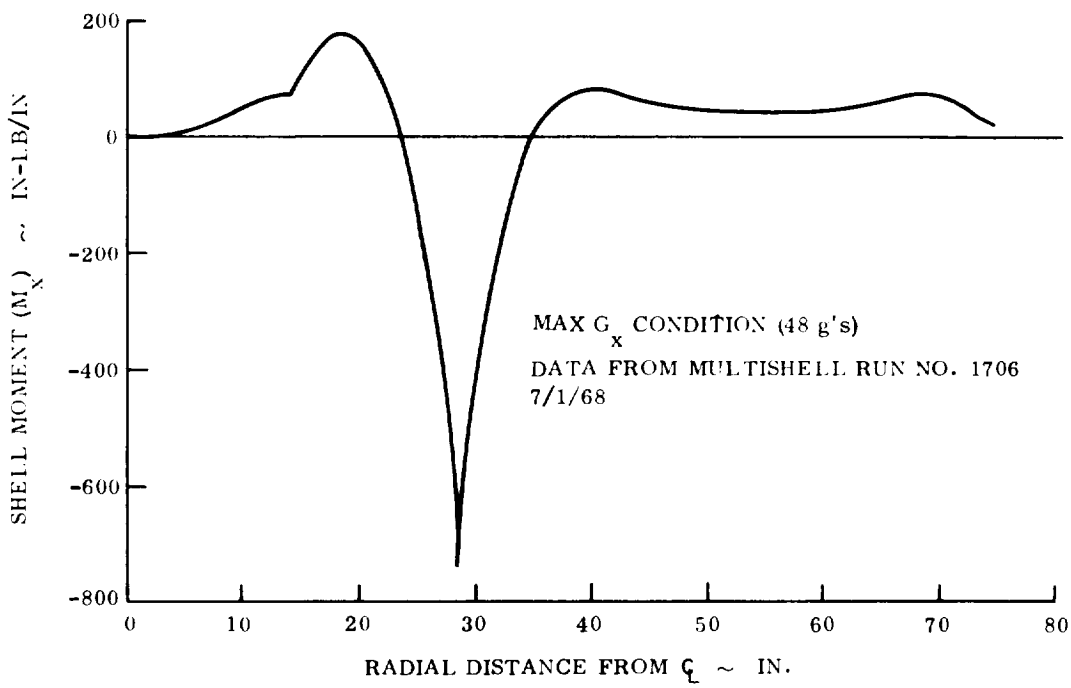

Figure 5.9-2. Axial Bending Moment (M_X) vs Radial Distance

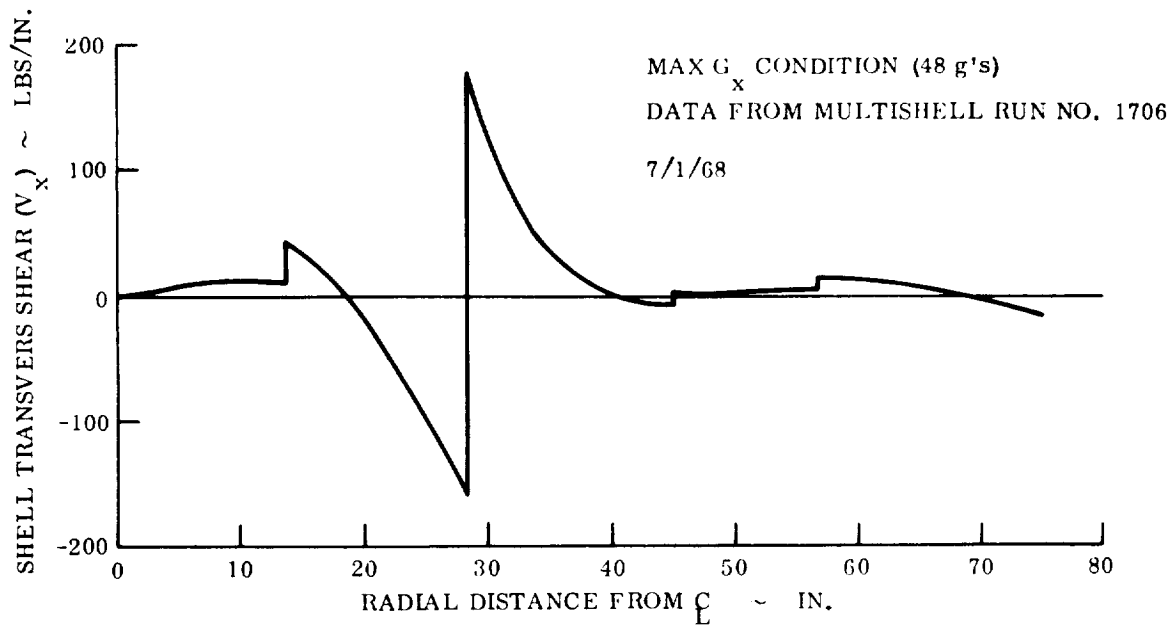

Figure 5.9-3. Shell Transverse Shear vs Radial Distance

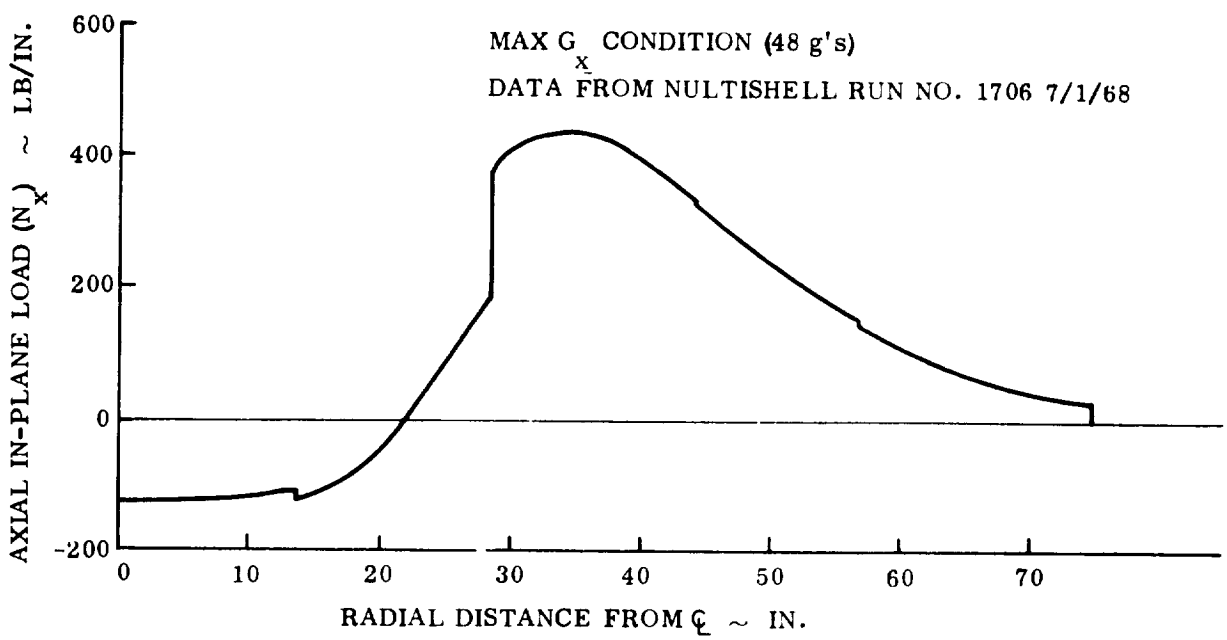

Figure 5.9-4. Meridional In-plane Load vs Radial Distance

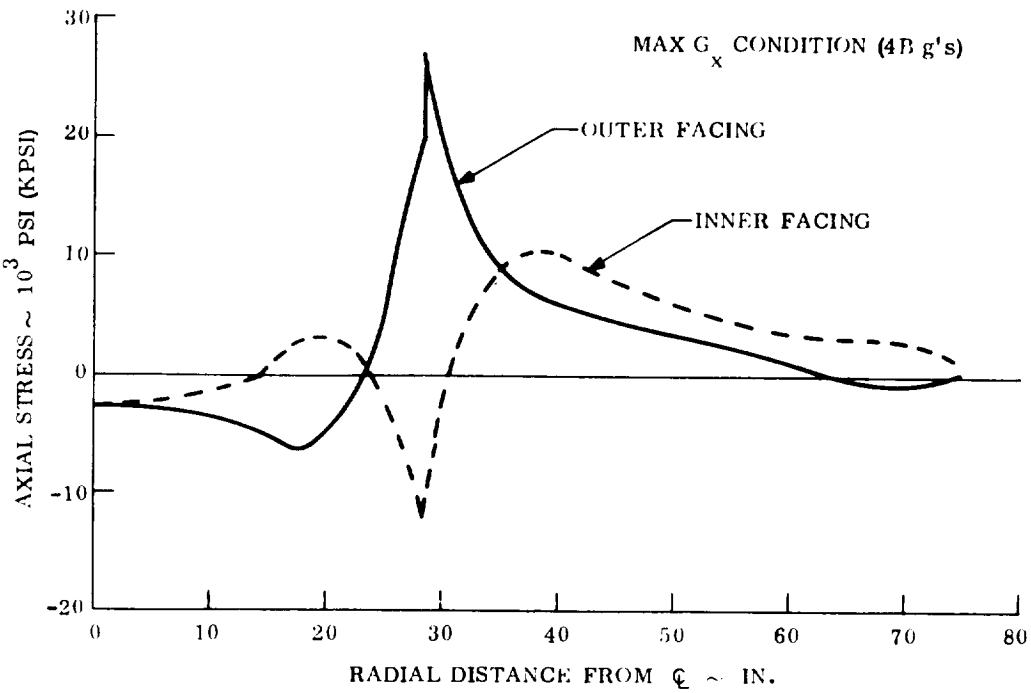

Figure 5.9-5. Axial Honeycomb Facing Stress vs Radial Distance

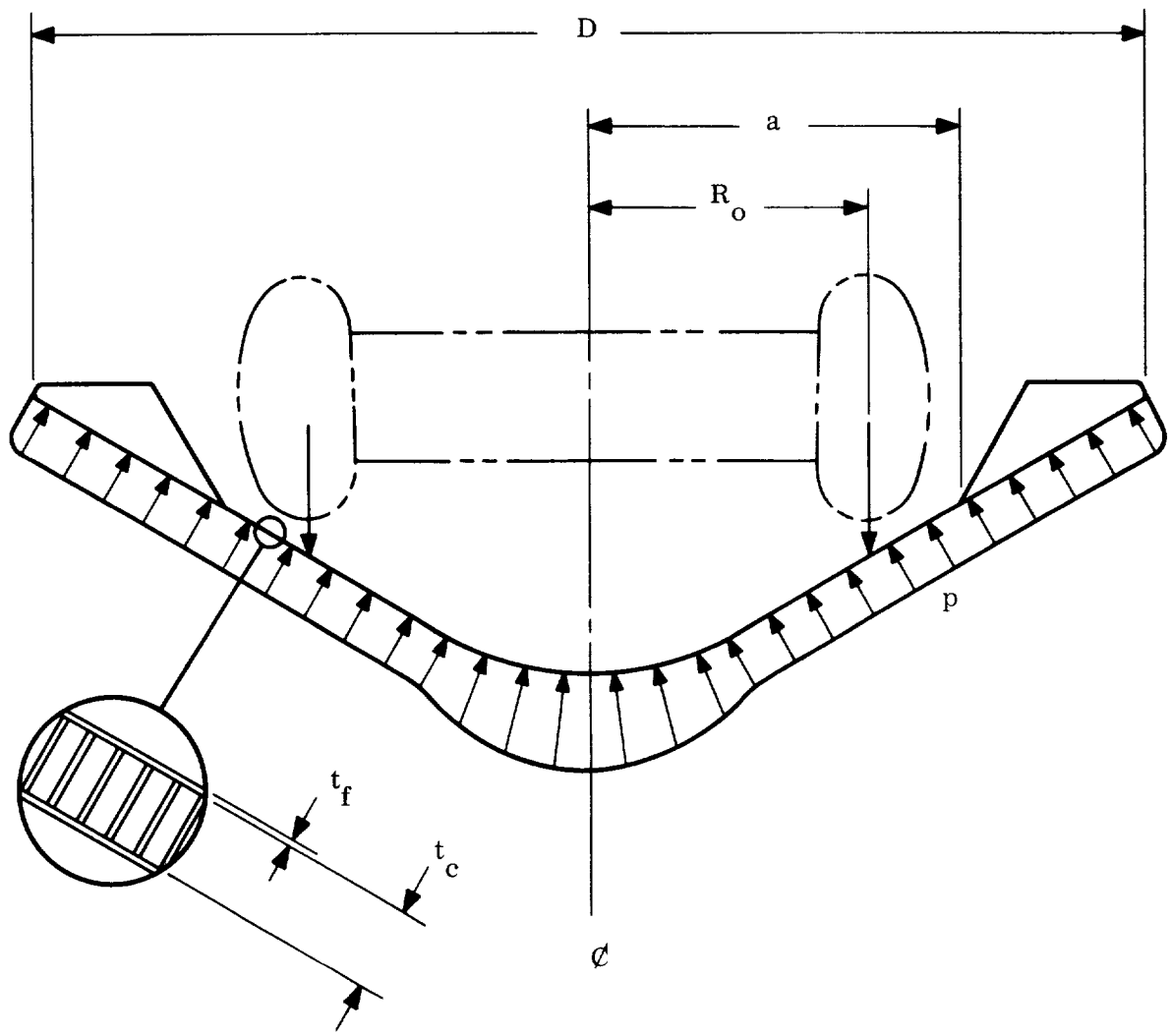

R = AEROSHELL RADIUS

t_f = HONEYCOMB FACING THICKNESS

t_c = HONEYCOMB CORE THICKNESS

D = AEROSHELL DIAMETER

a = RADIUS TO INBOARD EDGE OF BOX STRUCTURE

R_o = RADIUS TO POINT WHERE LANDER INERTIA LOAD ACTS ON SHELL

p = EXTERNAL PRESSURE LOADING

W = ENTRY WEIGHT

G_x = DECELERATION

Figure 5.9-6. Critical Aeroshell Dimensions

5.9.2.2 Thermal Stress Analysis

After designing the aeroshell for the maximum entry deceleration of 29.5 g's (Entry Condition No. 7), a thermal stress analysis was performed as a function of time during entry. The stresses due to a temperature differential between the outer and inner facing were superimposed on the mechanical loadings to obtain the minimum margins of safety versus time. The point on the aeroshell that was evaluated was in the area of the Lander bearing pad. Two critical trajectories were evaluated; the maximum deceleration trajectory, (Entry Condition No. 7 in table 5.9-1) and the maximum heating trajectory (Entry Condition No. 3). The temperature-time history, the load-time history, and the minimum margin of safety-time history is shown in fig. 5.9-7 and fig. 5.9-8 for Entry Condition No. 7 and No. 3, respectively. The important conclusion of this analysis is that there is essentially no structural temperature rise for the steep trajectory, Entry Condition No. 7, where the 29.5 g's maximum deceleration load occurs. In the maximum heating trajectory, Entry Condition No. 3, the temperature rise is considerable but the maximum deceleration is only 8.2 g's.

This entry analysis is based on 7075-T6 properties that were reduced because of the 300°F sterilization temperature. The room temperature properties were reduced by an amount equivalent to a total soak time of 500 hr at 300°F. Subsequently, the properties were further reduced to give the allowable strength shown in fig. 5.9-9. With these allowable strengths, the temperature versus time, and the deceleration vs time as shown in figs. 5.9-7 and -8, the thermal and mechanical facing stresses versus time were calculated.

The thermal stresses were determined by the following equation:

$$\sigma_T = \pm \frac{\alpha \left(T_o - T_i \right)}{(1 - \nu) \left(\frac{1}{E_o} + \frac{1}{E_i} \right)}$$

where:

α = facing thermal expansion coefficient

T_o = outer facing temperature

T_i = inner facing temperature

E_o = outer facing Young's Modulus

E_i = inner facing Young's Modulus

ν = Poisson's Ratio

The thermal stresses in the outer facing is compression and the inner facing is tension throughout entry because the outer facing is always at a higher temperature than the inner facing.

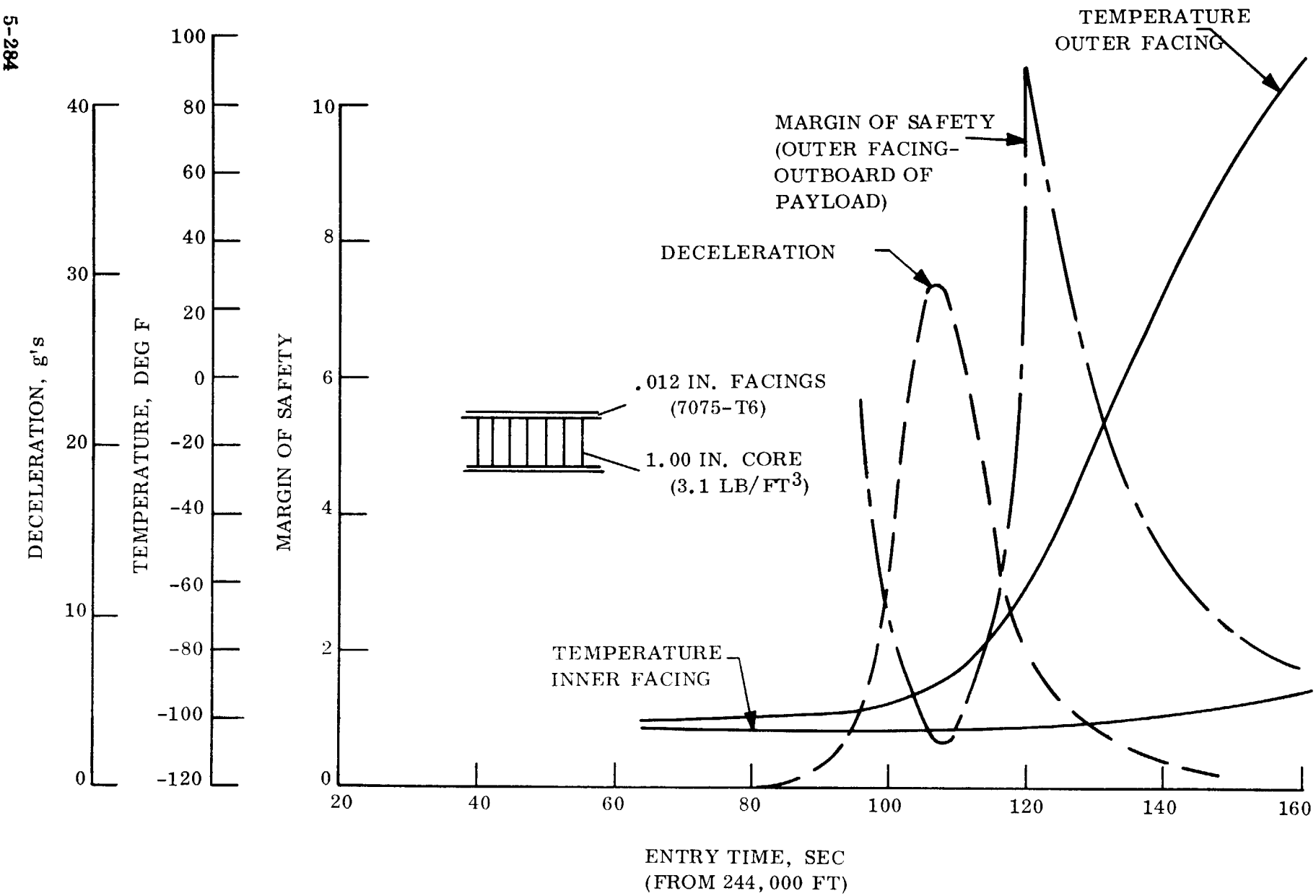

Figure 5.9-7. Aeroshell Entry Loads, Temperature, and Margin of Safety - Entry Condition No. 7

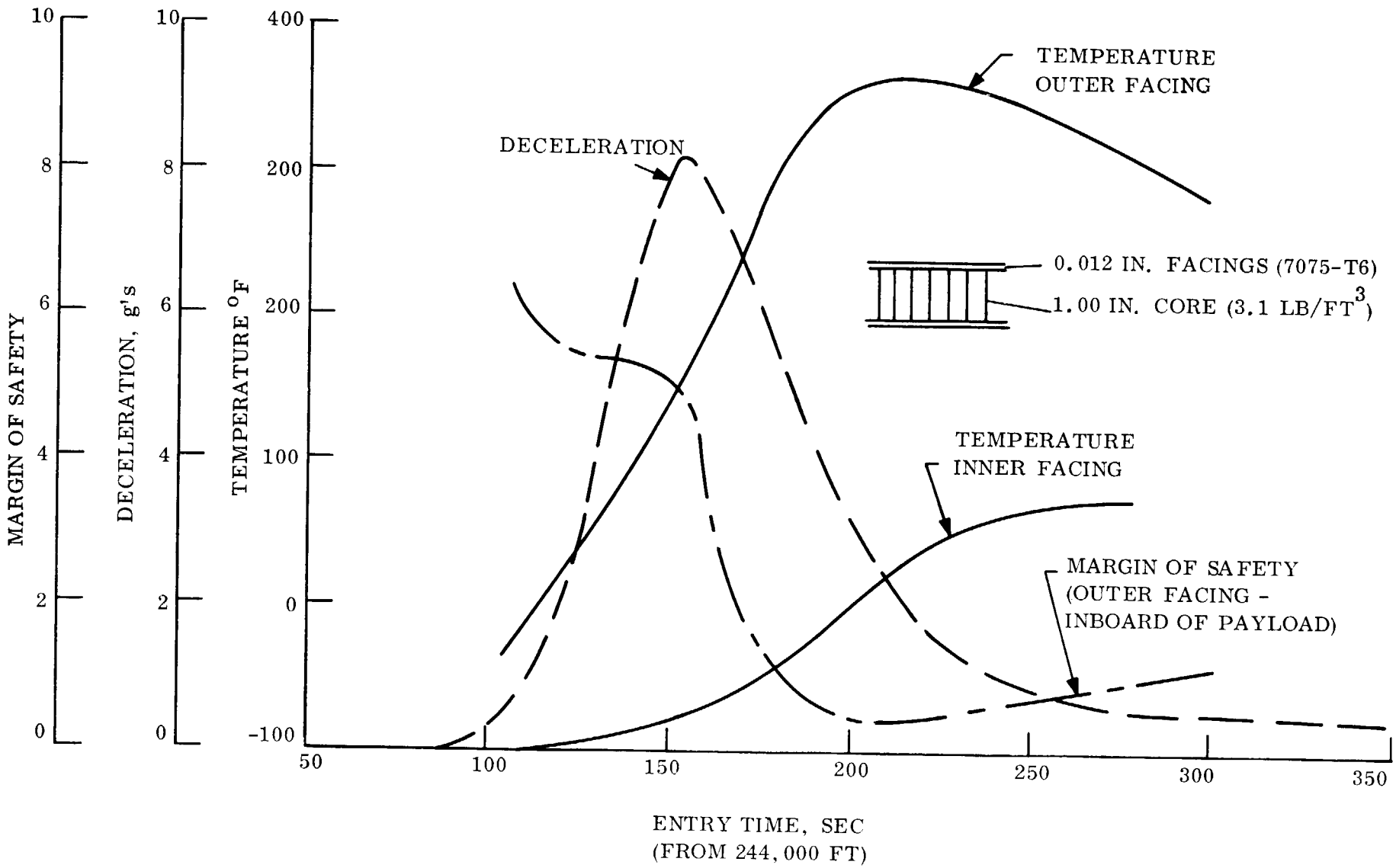

Figure 5.9-8. Aeroshell Entry Loads, Temperature, and Margin of Safety - Entry Condition No. 3

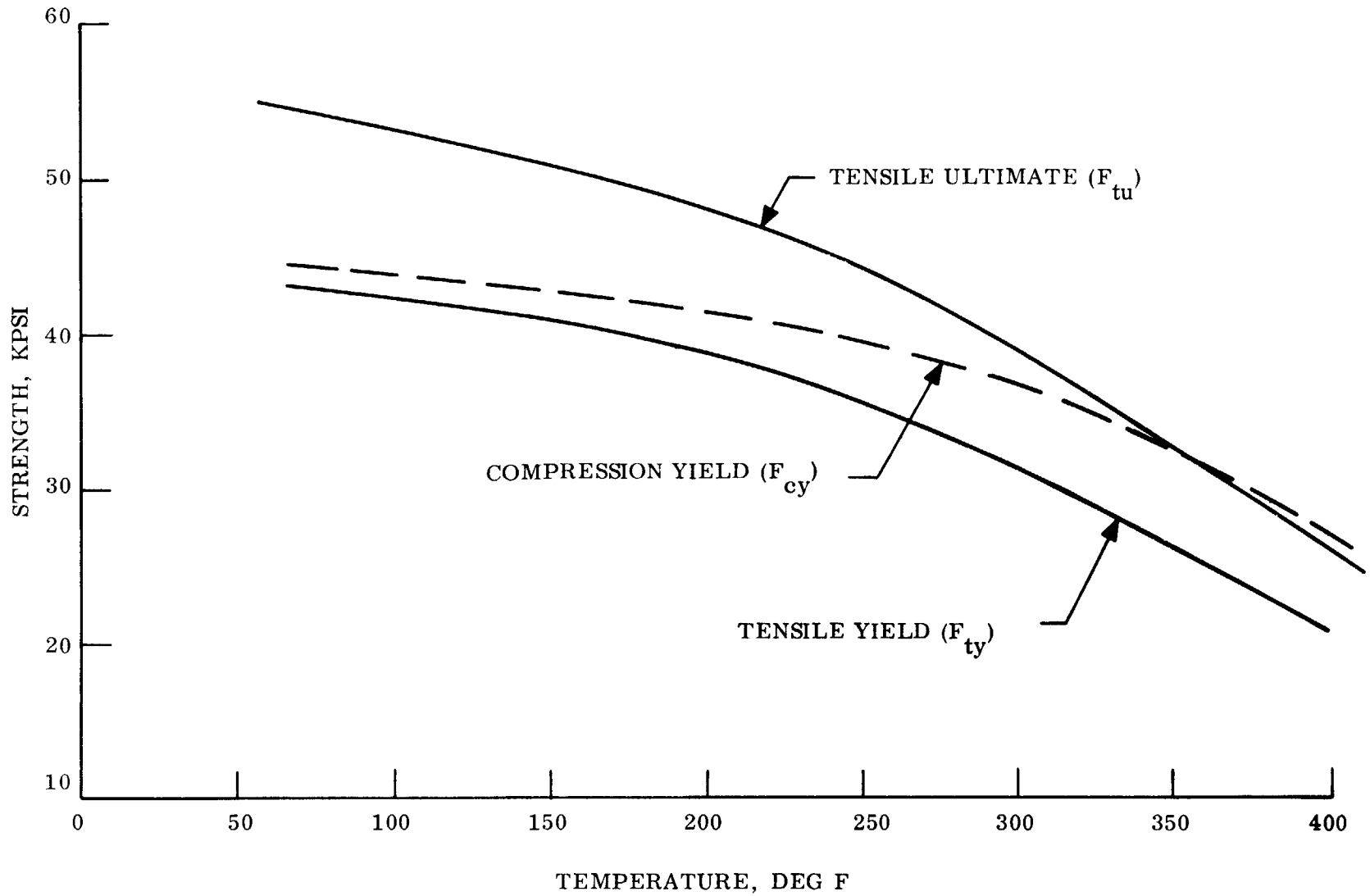

Figure 5.9-9. Allowable Strength of 7075-T6 After 500 hr at 300°F (Sterilization)

The mechanical stresses in the facings were calculated using the equations previously shown in this section. Figs. 5.9-10 through -17 show the resulting stresses in the 0.012 in. facings. Four discrete points were evaluated:

1. Outer facing - outboard of payload

2. Inner facing - outboard of payload

3. Outer facing - inboard of payload

4. Inner facing - inboard of payload.

These four locations were evaluated for the two trajectories, making a total of eight figures. The first four are for the maximum deceleration condition (No. 7) while the last four are for the maximum heating trajectory (No. 3).

5.9.2.3 Results

In comparing the stress levels, the steep trajectory results in maximum stresses at time of maximum deceleration while the shallow trajectory results in maximum stresses at the time of maximum differential temperature between the outer and inner facing as shown in figs. 5.9-7 and -8.

Finally, the margin of safety was calculated versus time by one of the following equations:

$$M.S. = \frac{F_{ty}}{\sigma} - 1$$

$$M.S. = \frac{F_{tu}}{1.25\sigma} - 1$$

$$M.S. = \frac{F_{cy}}{\sigma} - 1$$

The margin of safety vs time is plotted in figs. 5.9-18 and -19.

Analysis of this design indicated that the shell bending is critical, that aluminum honeycomb is just as efficient as titanium honeycomb, lighter than stainless steel honeycomb and easier to fabricate than both materials. The aluminum honeycomb is as efficient as the titanium or steel honeycomb because local shell bending is the critical loading condition and the minimum gage is no longer the controlling factor. This local shell bending, fig. 5.9-2, is induced by the loading of the aeroshell internally by the Lander and the aerodynamic loading externally.

The heat shield structure interface temperature is very low at the time of maximum loading (29.5 g's limit) and the mechanical loadings are small at time of higher temperature gradients.

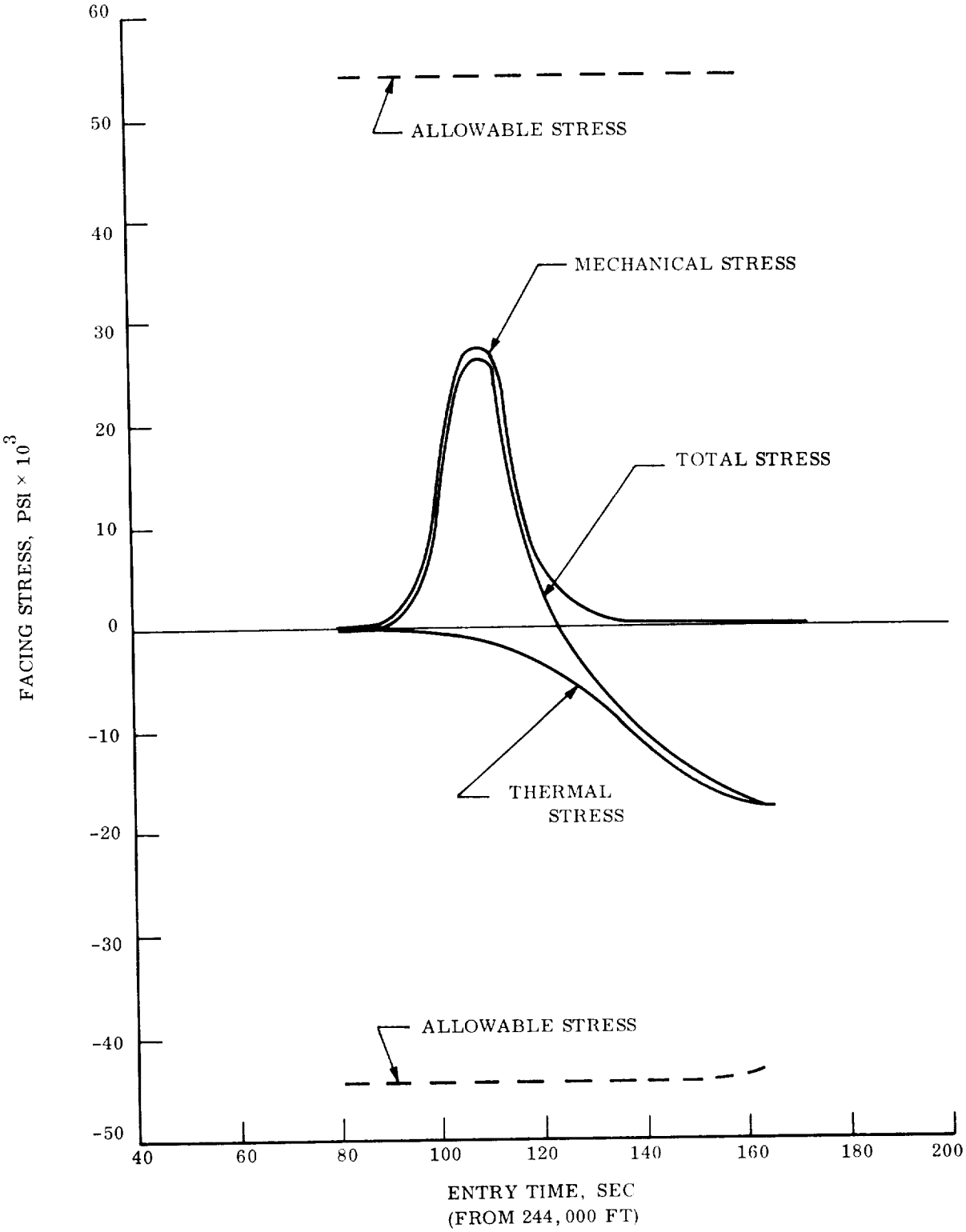

Figure 5.9-10. Aeroshell Entry Stresses, Entry Condition No. 7, Outer Facing, Outboard of Payload

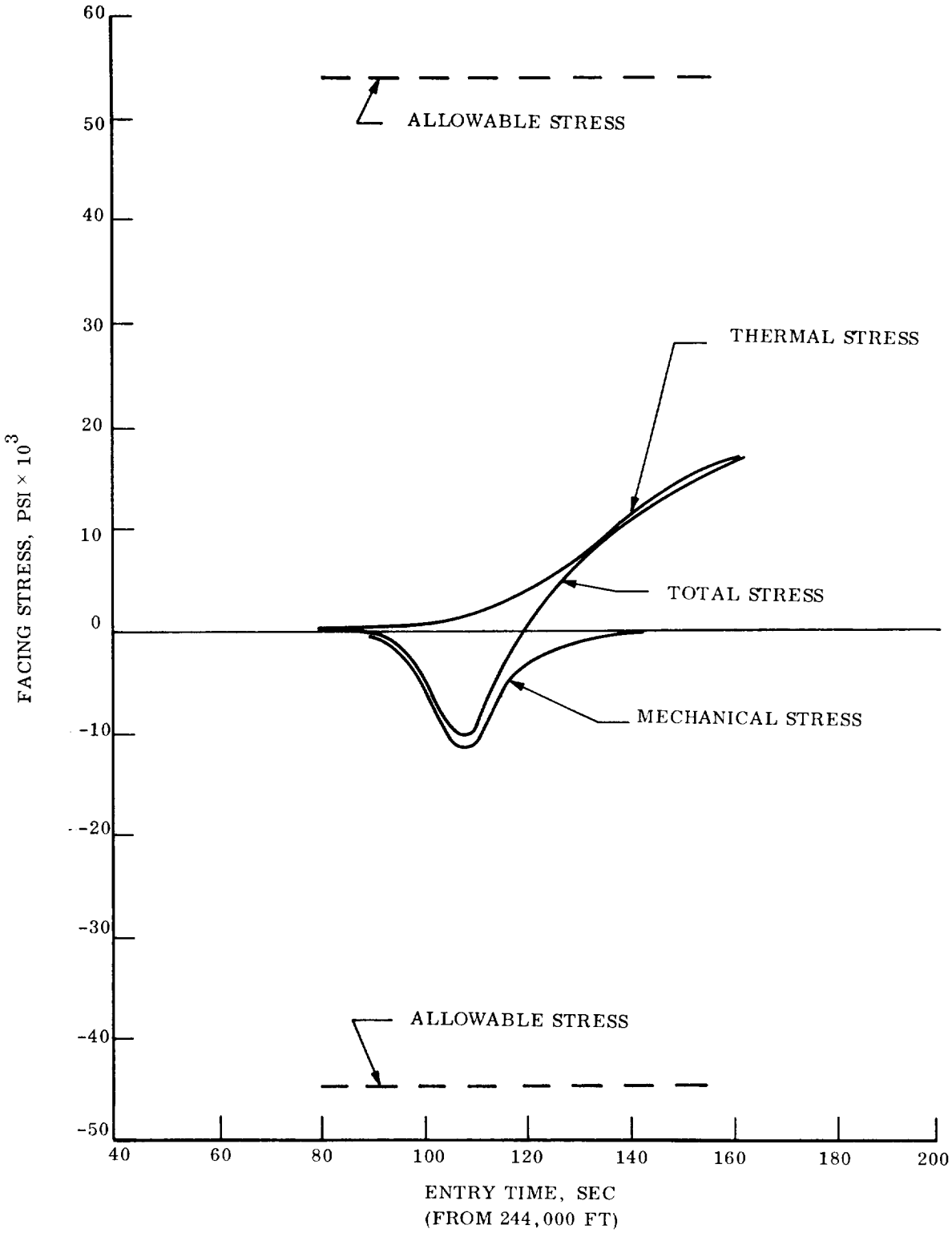

Figure 5.9-11. Aeroshell Entry Stresses, Entry Condition No. 7, Inner Facing, Outboard of Payload

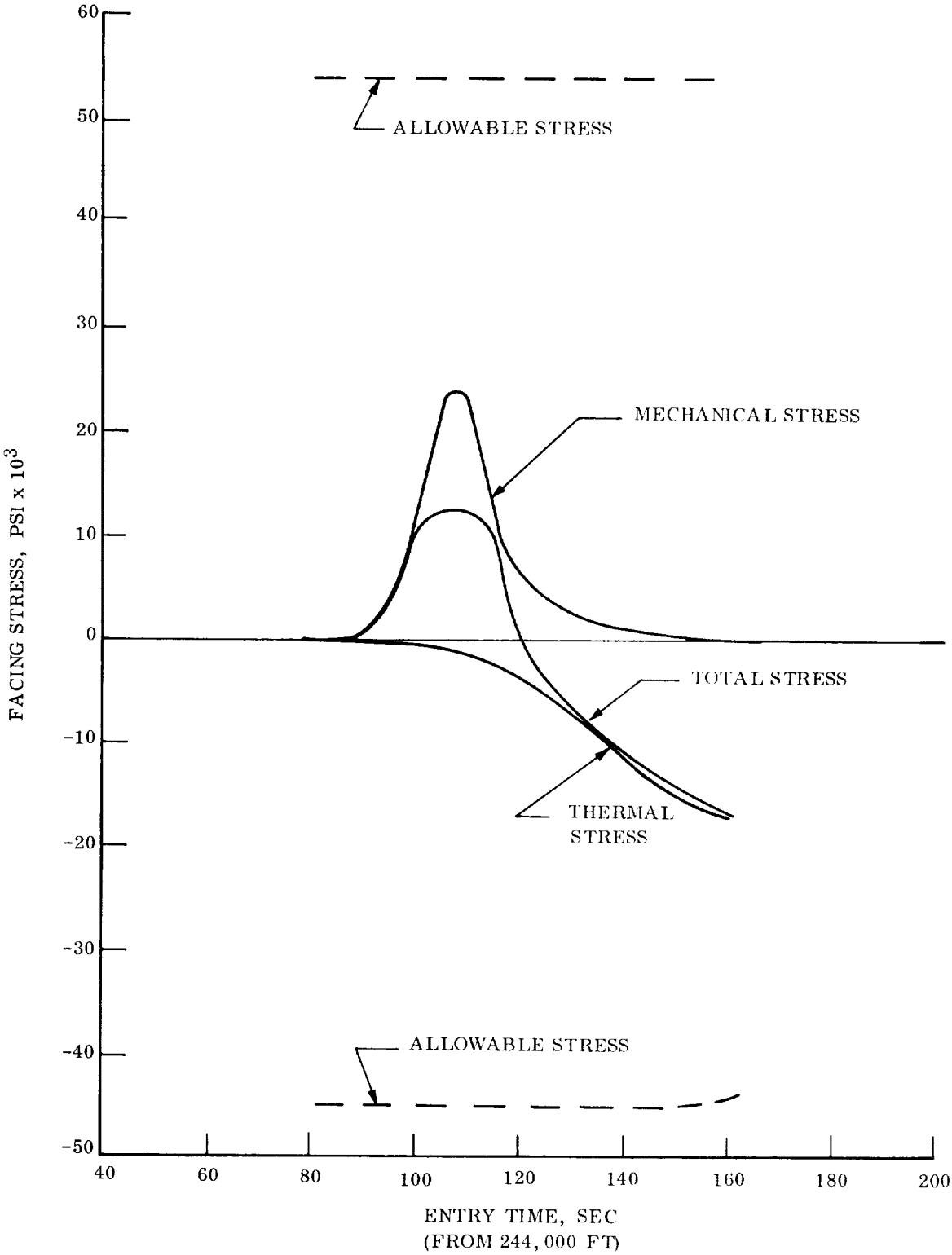

Figure 5.9-12. Aeroshell Entry Stresses, Entry Condition No. 7, Outer Facing, Inboard of Payload

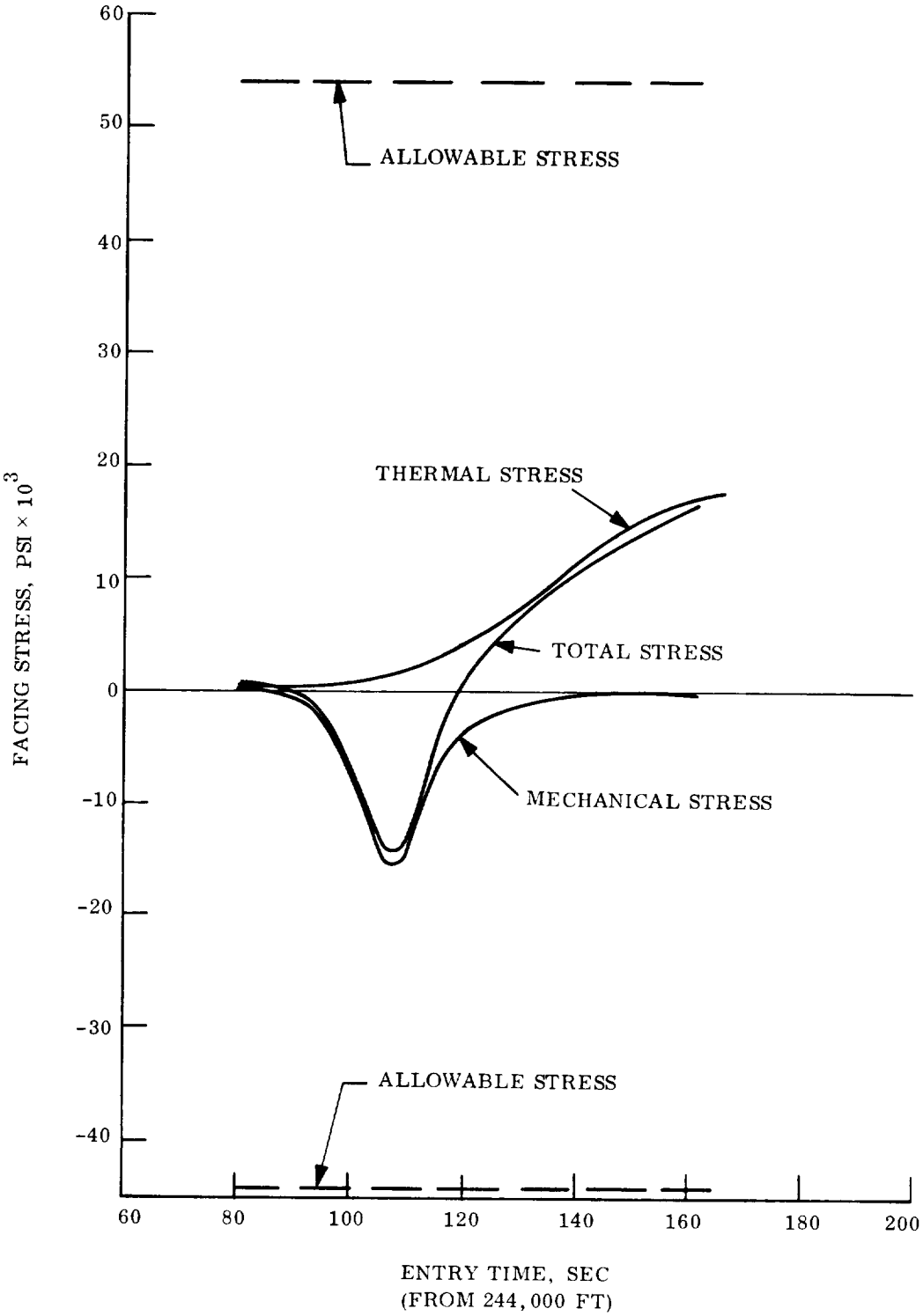

Figure 5.9-13. Aeroshell Entry Stresses, Entry Condition No. 7, Inner Facing, Inboard of Payload

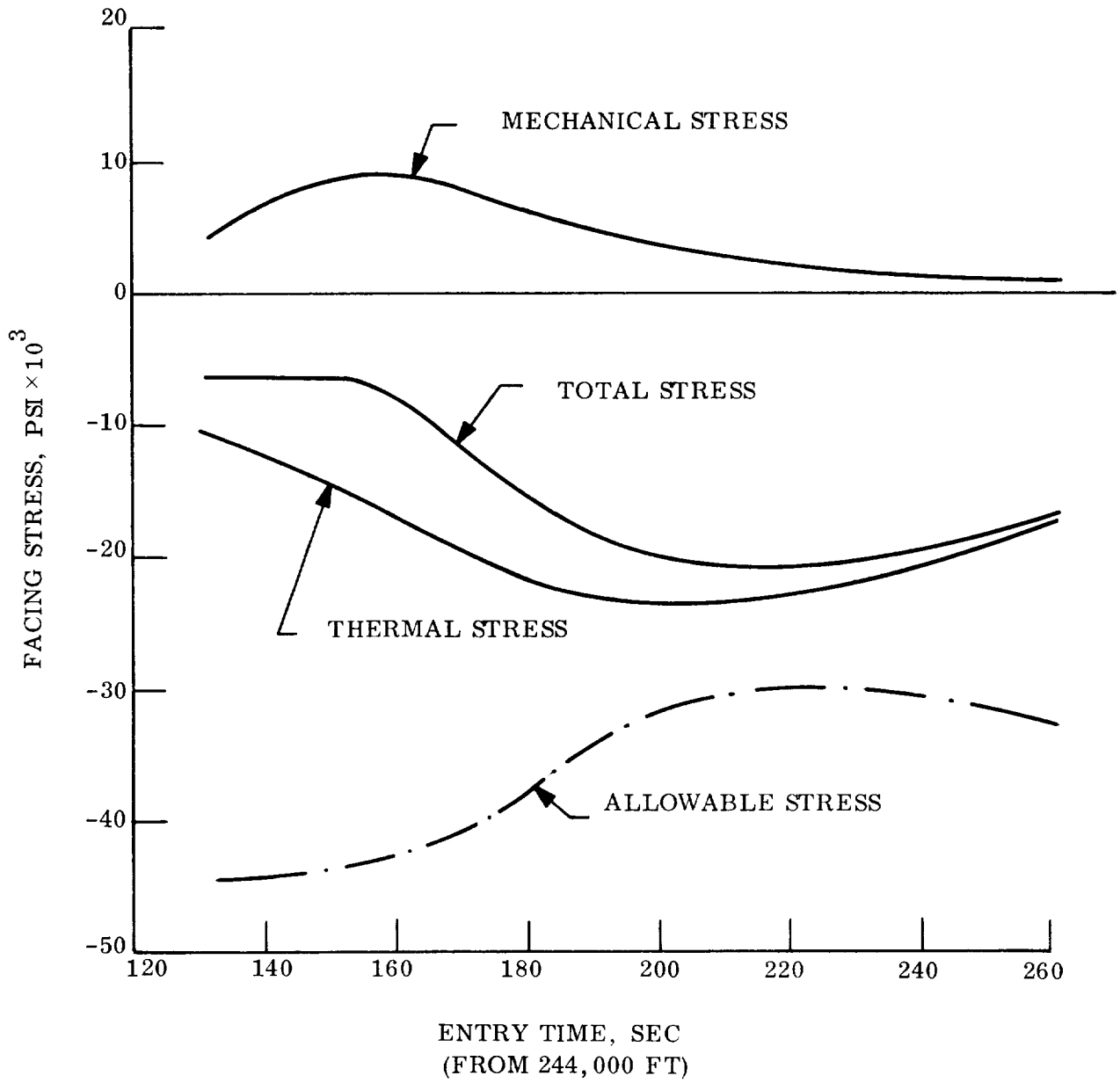

Figure 5.9-14. Aeroshell Entry Stresses, Entry Condition No. 3, Outer Facing, Outboard of Payload

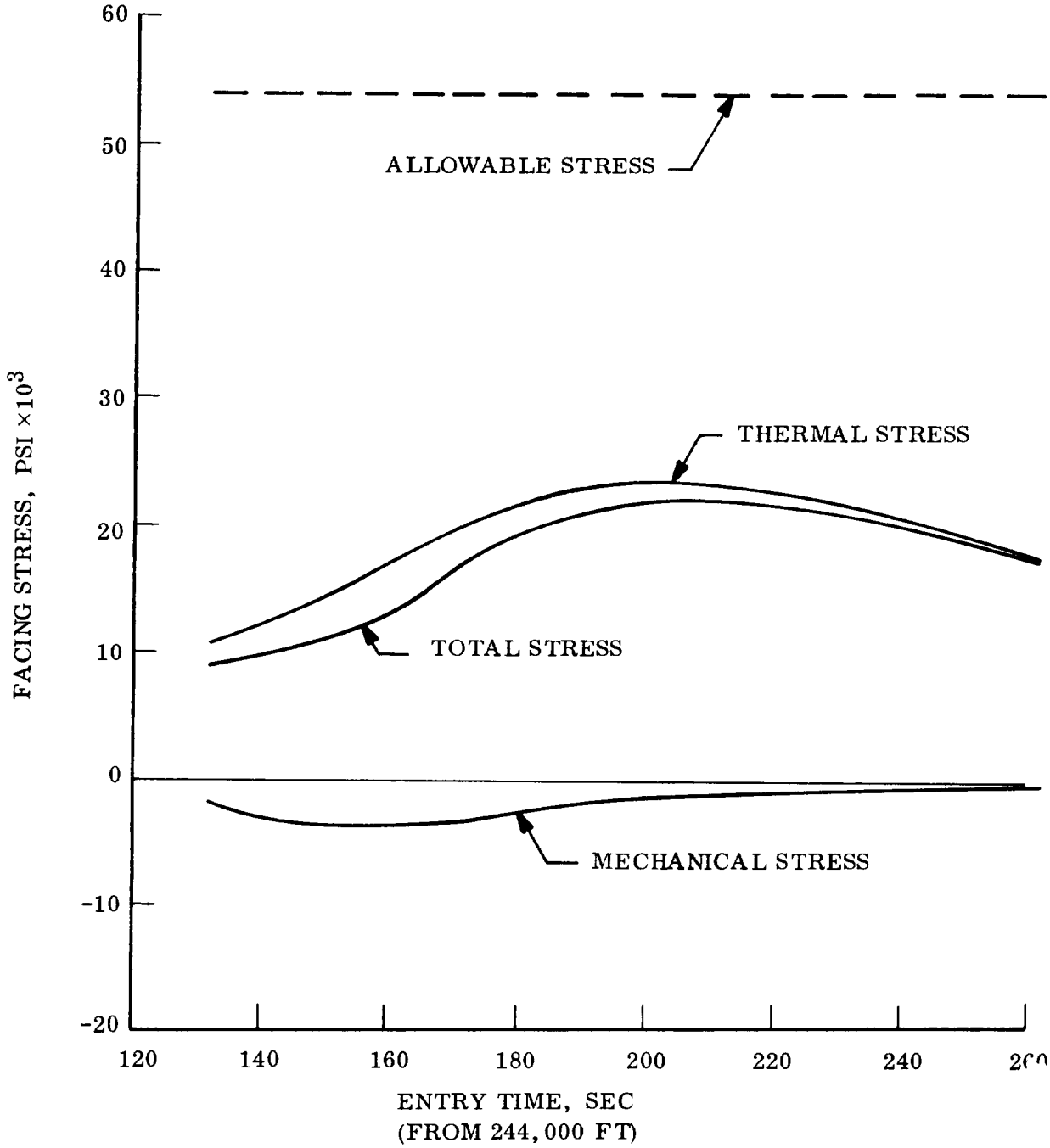

Figure 5.9-15. Aeroshell Entry Stresses, Entry Condition No. 3, Inner Facing, Outboard of Payload

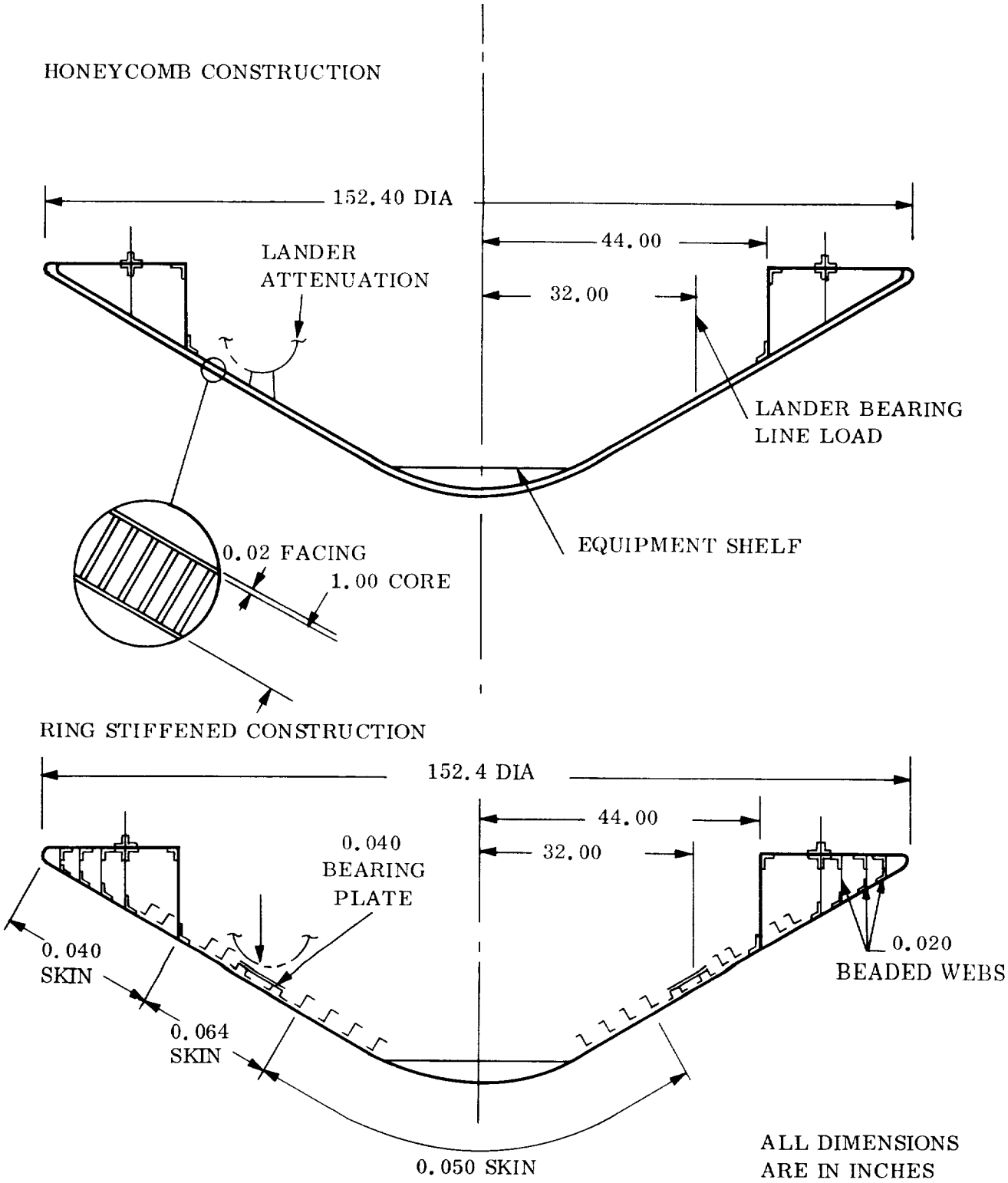

STRUCTURE ADDED FOR STABILITY

- 6 - 0.040 Z-RINGS 3/4 × 1-1/2 × 3/4
- 2 - 0.040 HAT RINGS 3/4 × 3/4 × 1 × 3/4 × 3/4
- 6 - 0.032 ANGLE RINGS 1 × 1
- 3 - 0.020 BEADED CYLINDRICAL WEBS IN OUTER BOX
- 1 - 0.040 BEARING PLATE

Figure 5.9-21. Aeroshell Alternate Designs

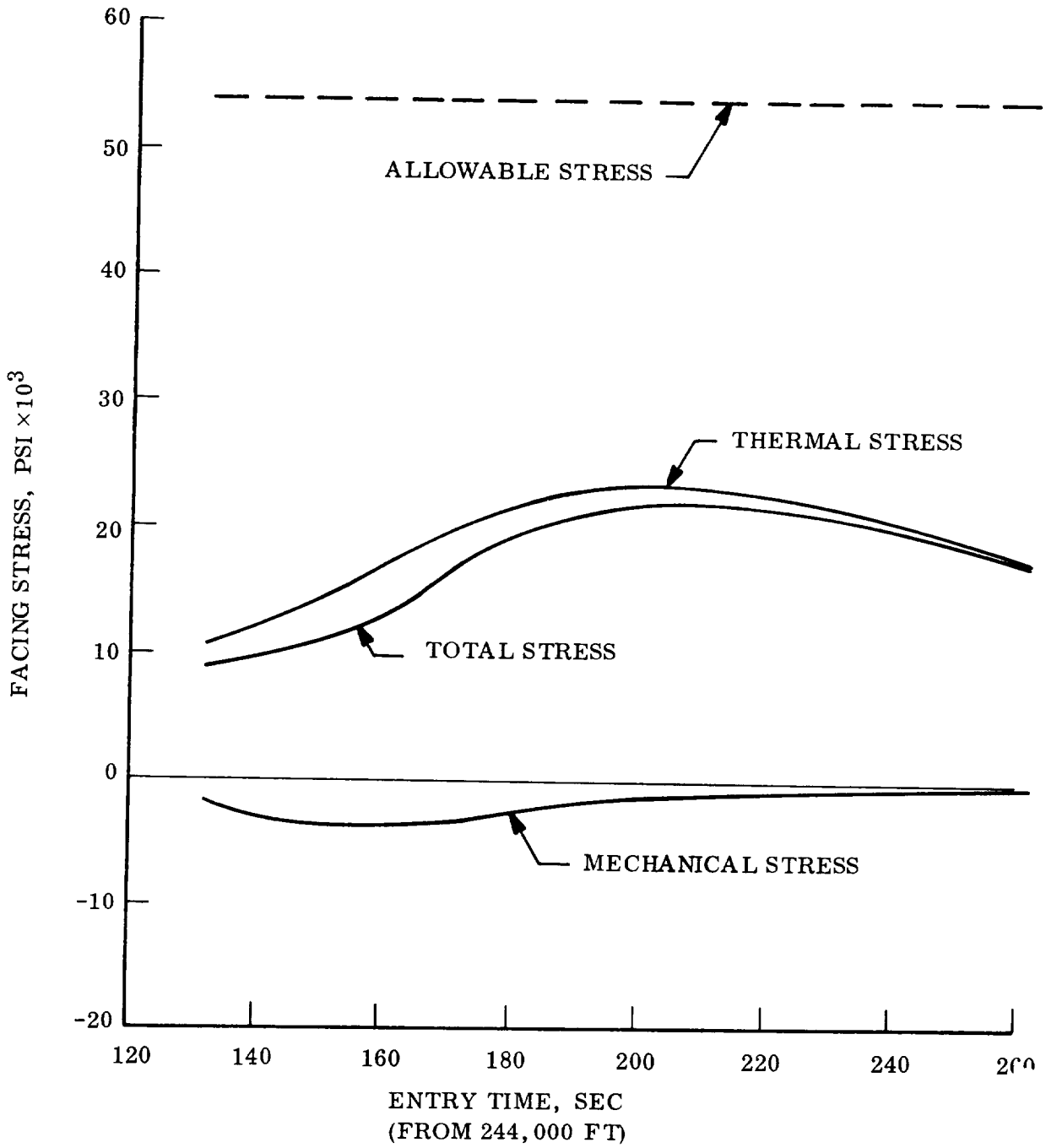

Figure 5.9-15. Aeroshell Entry Stresses, Entry Condition No. 3, Inner Facing, Outboard of Payload

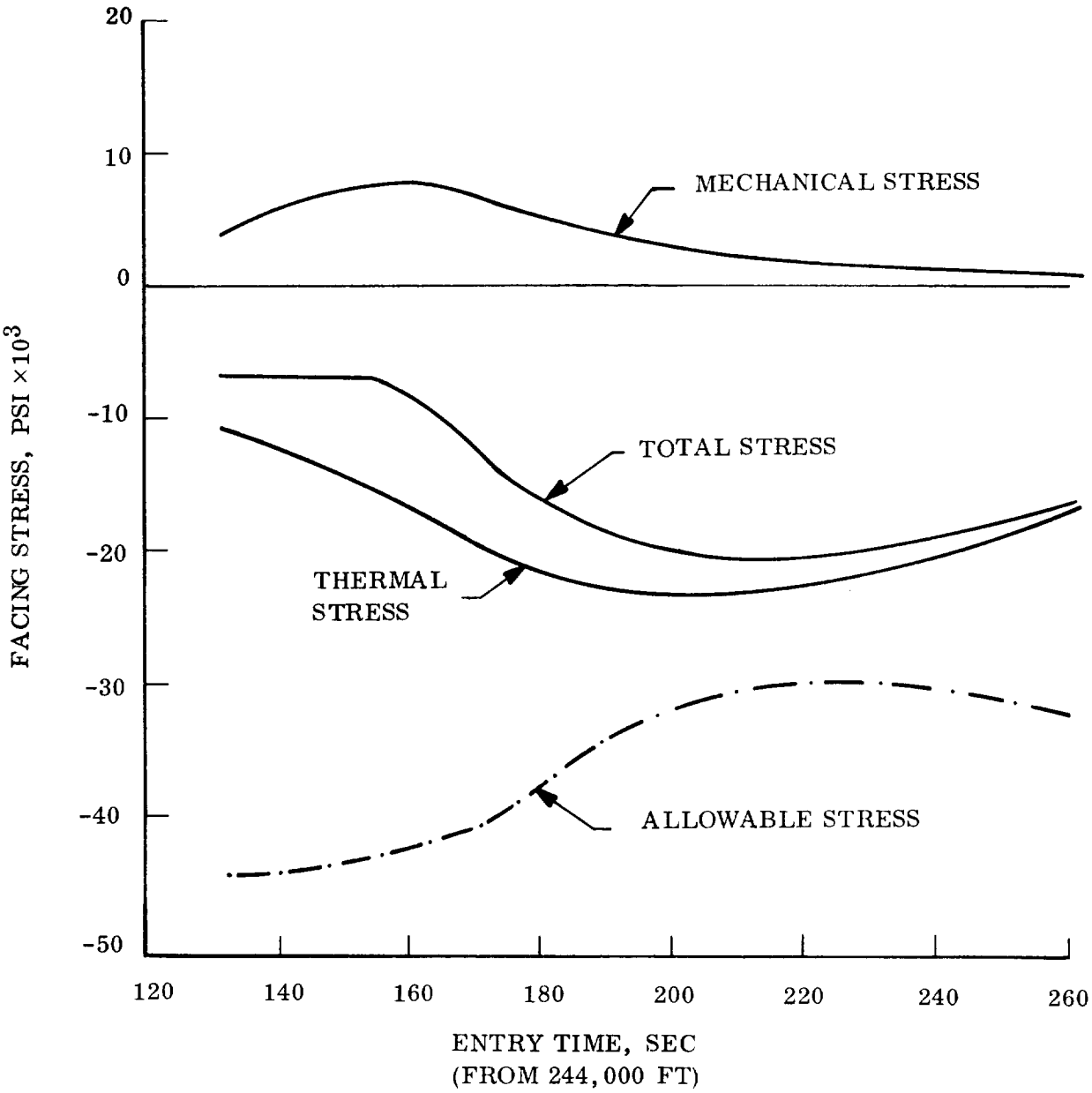

Figure 5.9-16. Aeroshell Entry Stresses, Entry Condition No. 3, Outer Facing, Inboard of Payload

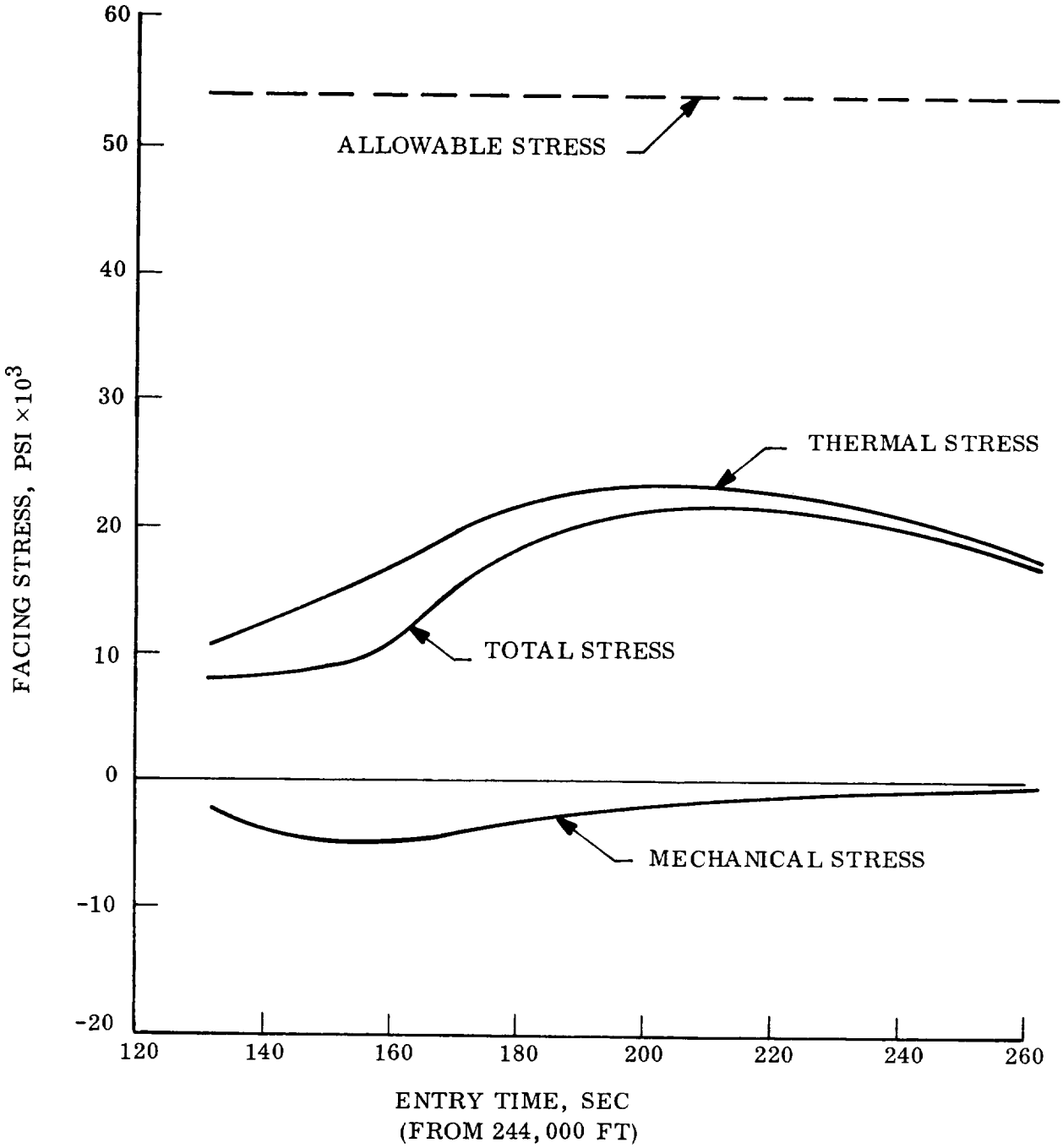

Figure 5.9-17. Aeroshell Entry Stresses, Entry Condition No. 3, Inboard Facing, Inboard of Payload

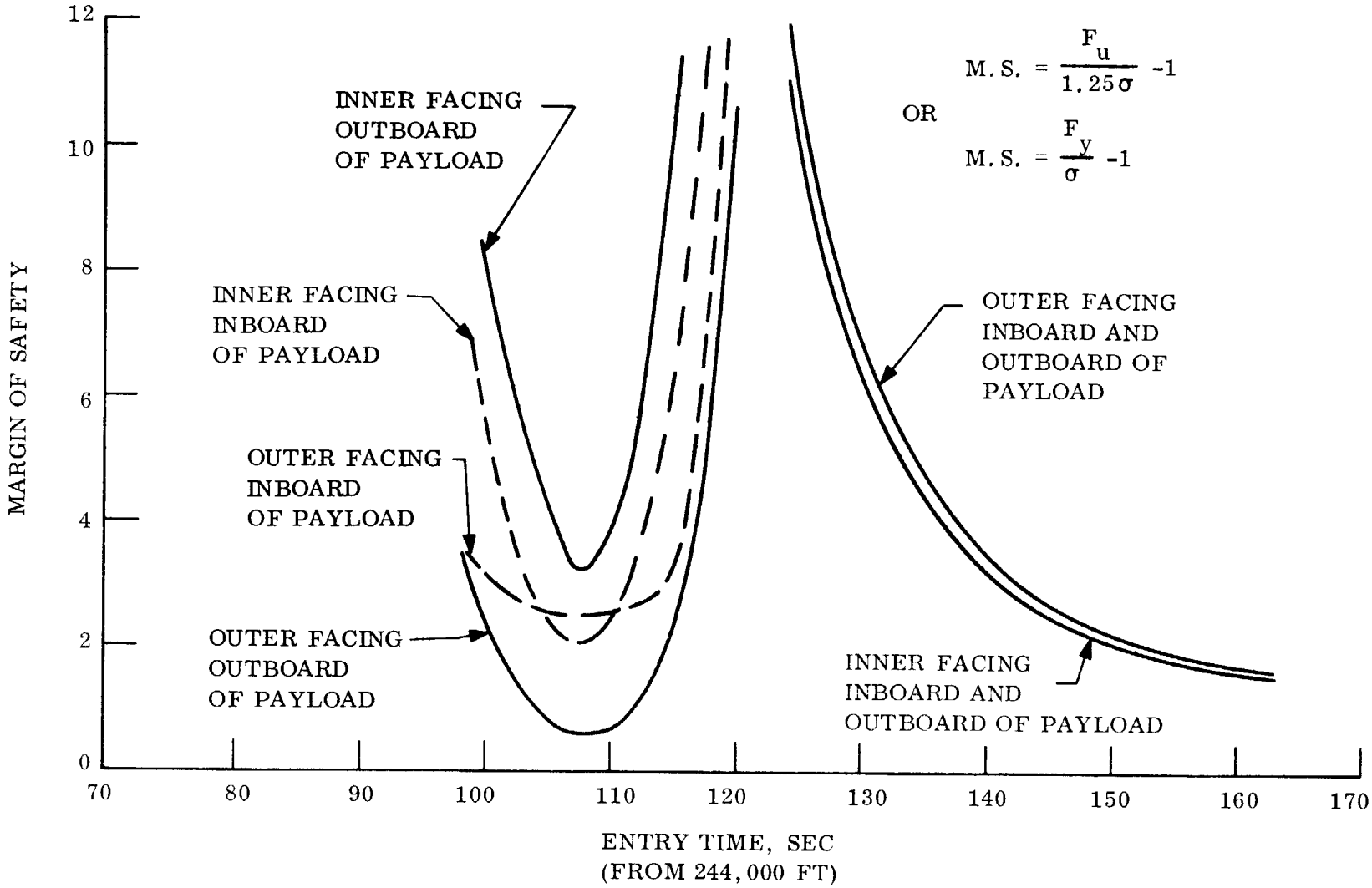

Figure 5.9-18. Aeroshell Entry Margin of Safety, Entry Condition No. 7

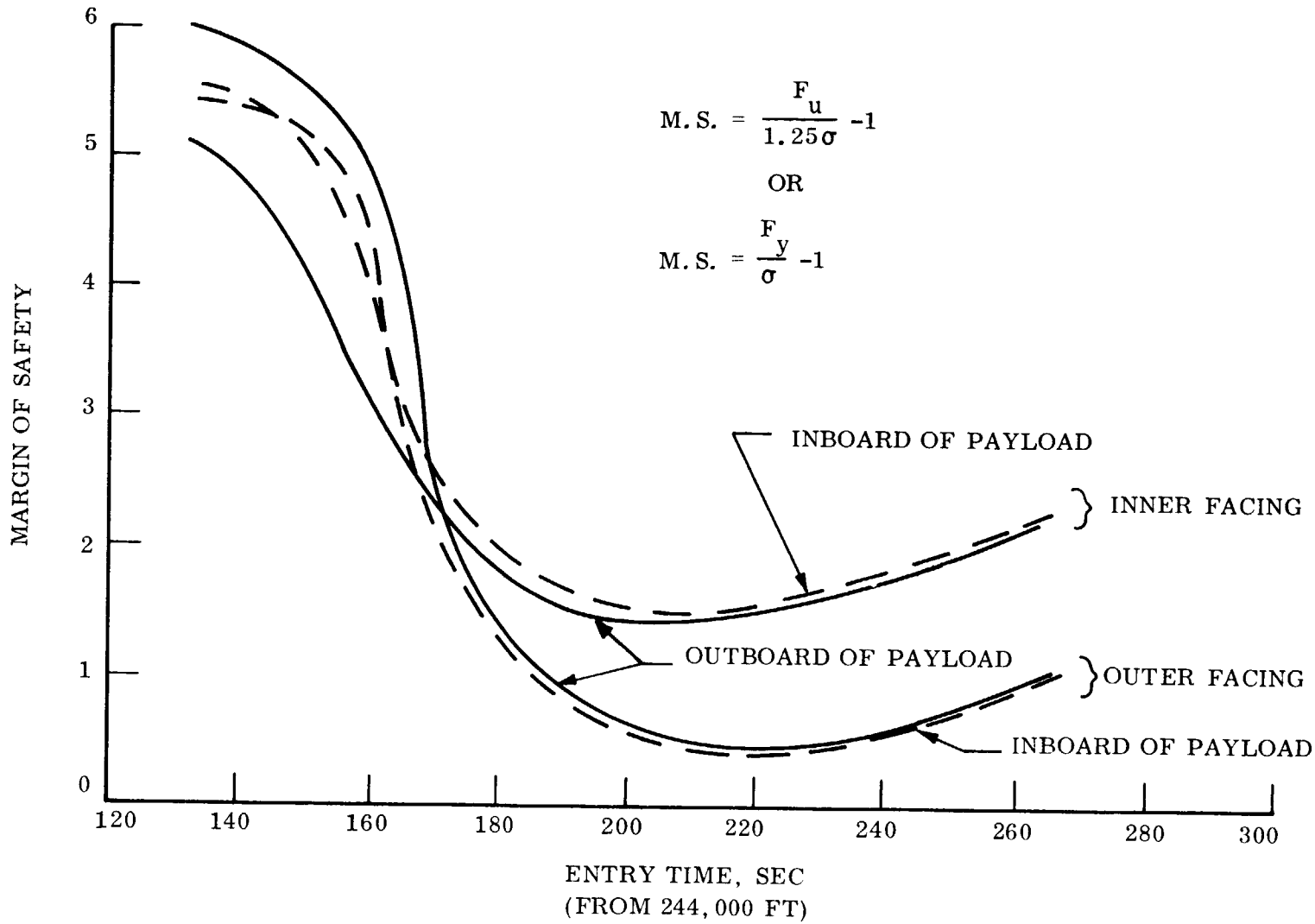

Figure 5.9-19. Aeroshell Entry Margin of Safety, Entry Condition No. 3

The temperature and gradient at parachute deployment can be high since at this time the mechanical loading on the aeroshell is negligible.

The box-like outer structure of the aeroshell acts as a torque box (ref. figs. 4.2-1 and -4) to restrain rotation and acts as a ring section to obtain sufficient ring bending stiffness for ring stability.

The construction of this torque box structure and the radial distance from the point of application of the load due to the payload bearing against the honeycomb shell, determines the magnitude of the shell bending loads. The magnitude of the bending load can be reduced by moving the bearing load outboard as far as possible.

A comparison was made between an all aluminum ring stiffened aeroshell and an all aluminum honeycomb aeroshell. This comparison was made using the MULTISHELL computer program. The basic configuration was that of Point Design 2A of the Mars Hard Lander Capsule Study with an entry weight of 1556 lb. Both were designed to a maximum deceleration of 48 g's and the associated pressure distribution. Fig 5.9-21 shows the two configurations and the difference in structural requirements. Two MULTISHELL runs were made on the ring stiffened configuration. The first run was made with three Z-ring stiffeners in place of the 0.020 beaded webs and six angle rings as well as an 0.040 external skin over the entire surface. Alterations were made as shown in the lower part of fig. 5.9-21 and a second computer run was made. The final weight comparisons are shown in table 5.9-3.

The basic external ring stiffened shell is 36.6 lb, or 28.9 percent heavier than the equivalent honeycomb stiffened configuration. This large difference is reduced when the local filler weight of the honeycomb at ring attachments points and the ring fastener weights are included. The delta weight is only 18.8 lb, or the ring stiffened structure is only 12 percent heavier than the honeycomb design. When the additional structural weight common to both designs is included (the shelf structure and the box structure) the ring stiffened aeroshell is 9.4 percent heavier. The other point of interest is the relative unit weight of the aeroshells based on the surface area of 145 ft^2. The basic honeycomb shell is only 0.88 lb/ft^2 of surface area compared with 1.25 lb/ft^2 for the ring stiffened design. However, the difference is not so great if the shelf and box ring structure is included in the comparison.

The reason for the added structure in the outer box section of the ring stiffened configuration was because the outer ring section required a higher moment of inertia to prevent out-of-plane ring instability. The stiffener Z-rings were used because the hoop compression loads and internal stresses were low such that ring instability and local flang crippling did not occur. Because of this design, more of the hoop compression load was transferred to the outer box structure. With hat sections replacing all of the Z-rings, the loads on the outer ring might be reduced to result in a slightly lighter ring stiffened design.

A point of interest in the ring stiffened design is that the aft portion of the stiffener Z-rings were in hoop tension and only half of the outstanding legs were in hoop compression as shown in fig. 5.9-20.

From this study, it was concluded that for overall simplicity of design of the honeycomb configuration and due to the fact that this configuration is lighter in weight, that honeycomb construction is preferred over a ring stiffened configuration.

TABLE 5.9-3. WEIGHT COMPARISON OF HONEYCOMB VS RING STIFFENED AEROSHELL

	Honeycomb Configuration		Ring Stiffened Configuration		Δ Weight Ring-Honeycomb (lb)	Increase of Ring Structure Weight over Honeycomb (%)
	Weight (lb)	Unit Weight (lb/ft^2)	Weight (lb)	Unit Weight (lb/ft^2)		
Basic Shell	127	0.88	163.6	1.25	36.6	28.9
Fasteners and filler materials	29.8		12.0			
	156.8	1.08	175.6	1.21	18.8	12.0
Shelf and box structure	44.3		44.3			
	201.1	1.39	219.9	1.51	18.8	9.4

Note: Total surface area - 145 ft^2.

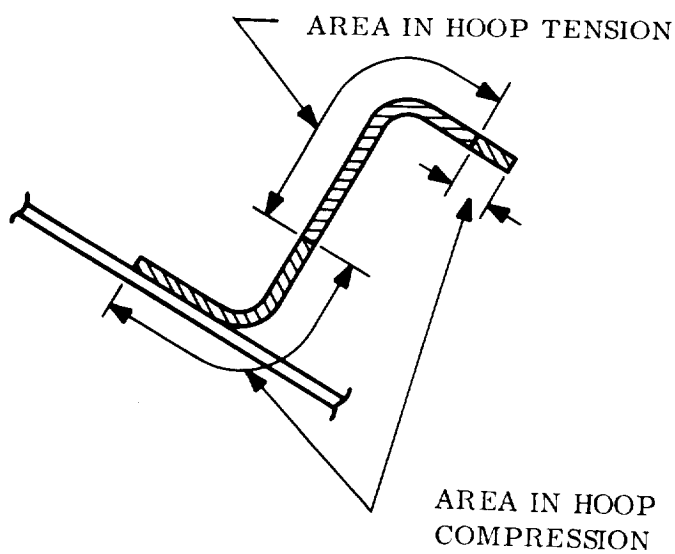

Figure 5.9-20. Typical Stress Distribution in Z-type Stiffener Rings

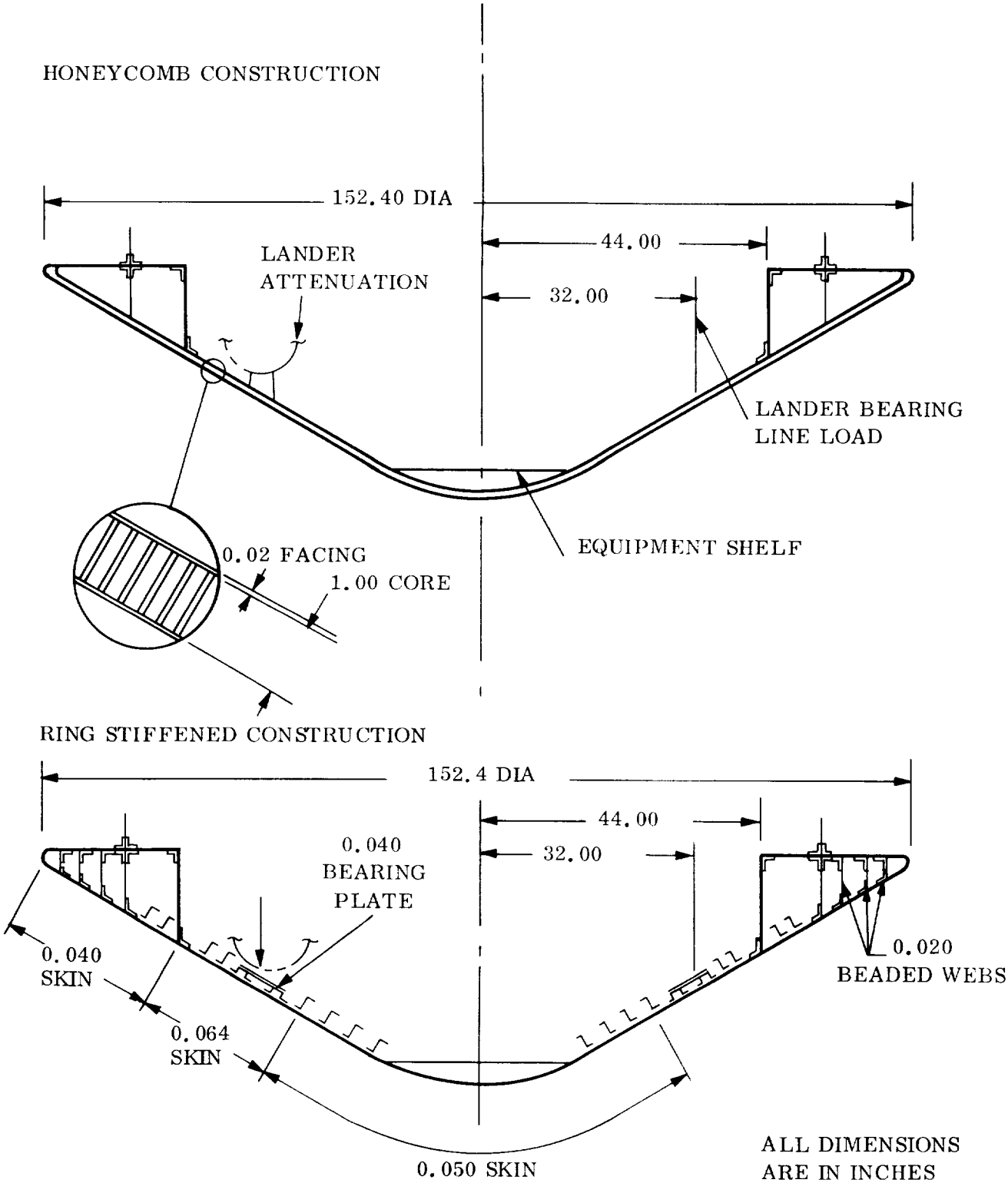

STRUCTURE ADDED FOR STABILITY

6 - 0.040 Z-RINGS 3/4 × 1-1/2 × 3/4
2 - 0.040 HAT RINGS 3/4 × 3/4 × 1 × 3/4 × 3/4
6 - 0.032 ANGLE RINGS 1 × 1
3 - 0.020 BEADED CYLINDRICAL WEBS IN OUTER BOX
1 - 0.040 BEARING PLATE

Figure 5.9-21. Aeroshell Alternate Designs

5.9.3 STRUCTURAL AEROSHELL DEVELOPMENT STATUS

5.9.3.1 Structural Development

Analytical methods exist to design a large, lightweight aeroshell with a half cone angle as large as 60°, but as indicated below, additional development work is required in order to establish confidence in these methods.

5.9.3.1.1 Shell Stability

For homogeneous aeroshell configuration the critical buckling pressure for a conical frustum under rotationally symmetric pressure is given by Weingarten and Seide (ref. 5.9-1) by the following formula:

$$P_{cr} = \frac{0.684\ E\ (1-\nu^2)^{3/4}}{\frac{L}{R_{AVE}}\left(\frac{R_{AVE}}{t}\right)^{5/2}}, \tag{1}$$

where

E = Young's modulus of the shell

L = slant length of conical frustum

R_{AVE} = average radius of curvature of conical frustum

t = shell thickness, and

ν = Poisson's ratio

Equation (1) can also be used for honeycomb construction, provided that modulus (E) is replaced by the equivalent modulus (E_e), and that the thickness (t) is replaced by the equivalent thickness (t_e), defined below:

$$E_e = 2\ E_f t_f / t_e \tag{2}$$

$$t_e = \sqrt{3}\ (t_f + t_c), \tag{3}$$

where

t_f = facing thickness,

t_c = core thickness, and

E_f = Young's modulus of facing.

These equivalent quantities are obtained by introducing the concepts of equivalent bending and extensional rigidities into the derivation for the buckling pressure. Weingarten and Seide have considerable test data to verify that this method is adequate provided that the edge ring is stiff enough to preclude ring instability.

5.9.3.1.2 Design of Intermediate Rings

An analysis by Cheney (ref. 5.9-2) predicts the buckling strength of rings restrained to displace normal to the shell surface. The expression for the lowest buckling mode (n = 2) and, neglecting torsional, in-plane, and tangential restraint by the shell, is:

$$P_{cr} = \frac{9}{R^3 (4 \sec^2 \alpha - 1)} \left[EI_y + \frac{EI_x \tan^2 \alpha \left(JG + \frac{4E\Gamma}{R^2} \right)}{\left(JG \frac{4E\Gamma}{R^2} \right) + \frac{EI_x}{4}} \right] , \qquad (4)$$

where

P_{cr} = critical radial load, lb/in

R = radius, in.

α = half cone angle, °

EI_y = in-plane flexural rigidity, lb/in.^{2}

EI_x = out-of-plane flexural rigidity, lb/in.^{2}

JG = torsional rigidity, lb/in.^{2}

Γ = warping constant, in.^{6}

$\Gamma = \frac{1}{144} \Sigma (bt)^3$

b = length of each ring element, in.

t = thickness of each ring element, in.

Cheney's expression reduces to the classical in-plane buckling equation when $\alpha = 0$:

$$P_{cr} = \frac{3EI}{R^3} \qquad (5)$$

When the conical shell has a 60° half cone angle and I_x equals I_y, equation (4) reduces to:

$$P_{cr} = 1.96 \frac{EI}{R^3} \qquad (6)$$

In the 60° aeroshell, if I_x is approximately equal to I_y, equation (6) is used to design the ring but if there is a large differential between I_x and I_y, the basic equation (4) is used.

5.9.3.1.3 Design of Outer Ring

Work has been performed by G. A. Cohen (ref. 5.9-3) on the effect of edge constraint on the buckling of sandwich and ring-stiffened 120° conical shells subjected to external pressure. In this work, the critical shell buckling pressure was determined using Novozhilov shell and ring theory. A honeycomb shell was evaluated with outer rings of different bending stiffnesses (EI). The critical shell buckling pressure was obtained as a function of the EI of the outer ring.

From these data in ref. 5.9-3, it was determined that the value of critical ring loading was about one half of the value using equation (6). If expression (6) is replaced by

$$P_{cr} = K \frac{EI}{R^3} , \tag{7}$$

the value of K calculated for the three rings in ref. 5.9-3 were as follows:

smallest ring $K = 0.94$

medium ring $K = 0.715$

largest ring $K = 0.745$.

Because no test data were available to support the analysis, the edge rings for the 1400 lb Capsule design were designed with a value of K equal to 0.98 or one-half of the 1.96 value in equation (6). If I_x and I_y were not very close to each other, the critical ring load was obtained by using one-half of the value obtained from equation (4).

5.9.3.1.4 Development Work Required

As previously stated, there is substantial test data on homogeneous frustum sections where the aft ring is very stiff, providing confidence in the basic honeycomb shell buckling capability. However, the buckling of a honeycomb shell with an efficient-weight aft ring requires test data to verify that a high ring bending stiffness predicted by Cohen (ref. 5.9-3) is required. The theory of Cohen appears to be in conflict with the theory of Cheney (ref. 5.9-2). Therefore, structural testing of frustum sections with 60° half cone angles should be made with various stiffness edge rings. If it can be shown that the theory of Cheney is adequate, the aft ring weights can be reduced and more efficient aeroshell designs can be made.

5.9.4 HEAT SHIELD DESIGN

The primary function of the heat protection system is to shield the aeroshell structure and Lander from the heating loads encountered during entry into the Martian atmosphere. Studies were directed toward selection of a single shield material for the entire Capsule. This approach resulted in the selection of the low density charring ablator ESM 1004 AP (35 lb/ft^3 density) due to the relatively mild Martian entry environment, where total surface recession is small in most cases and thermal insulation is of prime importance.

Based on previous studies, the criteria for selection of ESM 1004 AP as the heat shield material were:

1. Minimum system weight.

2. Maximum flexibility to accommodate non-design conditions.

3. Fewer anticipated fabrication and development problems than with other approaches

4. Sensitivity to the sterilization/decontamination and low temperature hard vacuum environments has been circumvented by proper material formulation.

5. Free of low molecular weight volatiles when post cured at high temperature under vacuum, or when manufactured from an RTV silicone from which low molecular weight volatiles have been previously removed.

For the direct entry mode where steep path angle entry into the MIN atmosphere (25°) results is ESM surface melting, ESM 1004 AP (35 lb/ft^3 density) is the preferred approach due to its good performance in relatively mild melting regimes.

The design of the heat protection system is based on the anticipated range of entry conditions, with the maximum heat shield thickness requirement dictated by the shallowest path angle attainable into the MAX atmosphere; however, the design must consider all environmental conditions experienced prior to entry. These environments include ground handling; chemical decontamination with gaseous ethylene oxide and Freon 12; dry heat sterilization; loads and vibrations during both powered flight and insertion into the interplanetary trajectory; cold soak and hard vacuum for 6 to 9 months during transit; loads and vibrations during midcourse maneuvers and de-orbit periods; solar exposure during the descent period to provide temperature control; and exposure to the meteoroid environment.

The entry heating environment is quite mild compared to Earth entry for comparable entry conditions. A comparison between the VM-3 and VM-8 model atmospheres and the postulated NASA/LRC model atmospheres was made in ref. 5.9-4. It was found

that the total time integrated heating (which designs the heat shield thickness requirements) predicted for entry into the VM-3 and NASA/LRC maximum model atmospheres was very similar. Consequently, design calculations were made for entry into the VM-3 atmosphere. The flow regime in the low density region of the entry was determined using the Knudsen number as the criterion. This technique indicated that the Knudsen number was less than 0.01, and thus continuum flow theory is applicable in calculating the convective heating.

The entry heating histories for the shallow entry path angle ($\gamma_E = 16^\circ$) into the VM-3 model atmosphere for both convective and equilibrium and non-equilibrium radiative heating are shown in fig. 5.9-22 for the stagnation point and end of skirt locations. These were obtained using the Planetary Aerodynamic Heating Program (PAHP) and Hot Gas Radiation Program (HGRP) described in ref 5.9-4. Fig. 5.9-23 shows a breakdown of the heat flux components of the heat balance equation at the material-boundary layer interface.

Employing the thermo-physical properties described in table 5.9-4 and the convective and radiative heat flux histories shown in fig. 5.9-22, the heat shield thickness requirements were determined (fig. 5.9-24) using the test calibrated mathematical model, Reaction Kinetics Ablation Program (REKAP). Fig. 5.9-25 shows a comparison of REKAP predictions with test data for ESM 1004 AP in a simulation of a typical Martian atmosphere (28 percent CO_2 -- 72 percent N_2 by mass) reported in ref. 5.9-5.

The shield thickness requirements are those required to hold the design bondline temperature to 600° F. In lieu of a detailed evaluation to justify a statistical safety margin, a safety factor of 1.2 is applied to the shield thickness requirements presented for vehicle design layouts. This would result in a margin of about 200° F on the backface temperature. Analysis has shown that one of the most significant factors that affects the estimation of the shield thickness is the tolerance on the entry path angle. Designing the heat shield thickness to the lower limit on entry angle results in a safety margin of about 10 percent when compared to the nominal entry condition.

Figs. 5.9-26 and -27 show typical backface and frontface temperature histories and thermal gradients at selected times during entry for the Mars Flyby mission. These results are presented for entry into the VM-3 atmosphere. Entry into the VM-8 model atmosphere for the same nominal stagnation point design thickness results in a bondline temperature rise of approximately 300°F.

Corner heating effects were taken into consideration at the base of the entry vehicle and a peripheral edge protection of ESM 1004 AP is provided at the base of the aeroshell. To protect against the possibility of backface heating around the edge of the entry vehicle, the exposed aeroshell structure at the base and inboard on the vehicle is coated with ESM 1004 AP. A theoretical analysis, based on flight test data on a sphere cone configuration similar to the current design, shows that the total heat load on the afterbody is small compared to that experienced by the forebody, (i.e., $\dot{q}_{s_B} < 0.01\ \dot{q}_s$ -- ref. 5.9-6)

TABLE 5.9-4. THERMOPHYSICAL PROPERTIES OF ESM MATERIAL

		ESM 1004AP
Virgin Density (ρ_v lb/ft^3)		35.0
Char Density (ρ_c lb/ft^3)		14.0
Pyrolysis Gas Specific Heat (Cpg Btu/lb° F)		0.384
Molecular Weight of Injected Species (Mg)		24.5
Order of Reaction (N)		2
Pre-exponential Factor (A sec^{-1})		30000
Activation Energy (E Btu/lb mole)		47500
Heat Decomposition (HGF) (Btu/lb gas generated)	1335° R	50
	1460° R	450
	1710° R	1000
	1960° R	2610
Specific Heat (Cp) (Btu/lb° R)	600° R	0.305
	710° R	0.360
	1210° R	0.44
	2075° R	0.44
Conductivity (k) Virgin (Btu/ft - sec° R)	610° R	0.0000237
	800° R	0.0000220
	1335° R	0.0000210
	1710° R	0.0000231
Char	1335° R	0.0000777
	1710° R	0.0000855
	2210° R	0.000104

For the decomposition reaction described by the following Arrhenius type equation:

$$\frac{1}{W_o} \frac{dw}{dt} = \frac{(W-Wf)^N}{(Wo)} Ae^{-\delta E/RT}$$

Surface Recession for $T_{WALL} > 3400°R$

$$\dot{S} = 38.56\, e^{\frac{-43800}{T_W}} \text{ ft/sec}$$

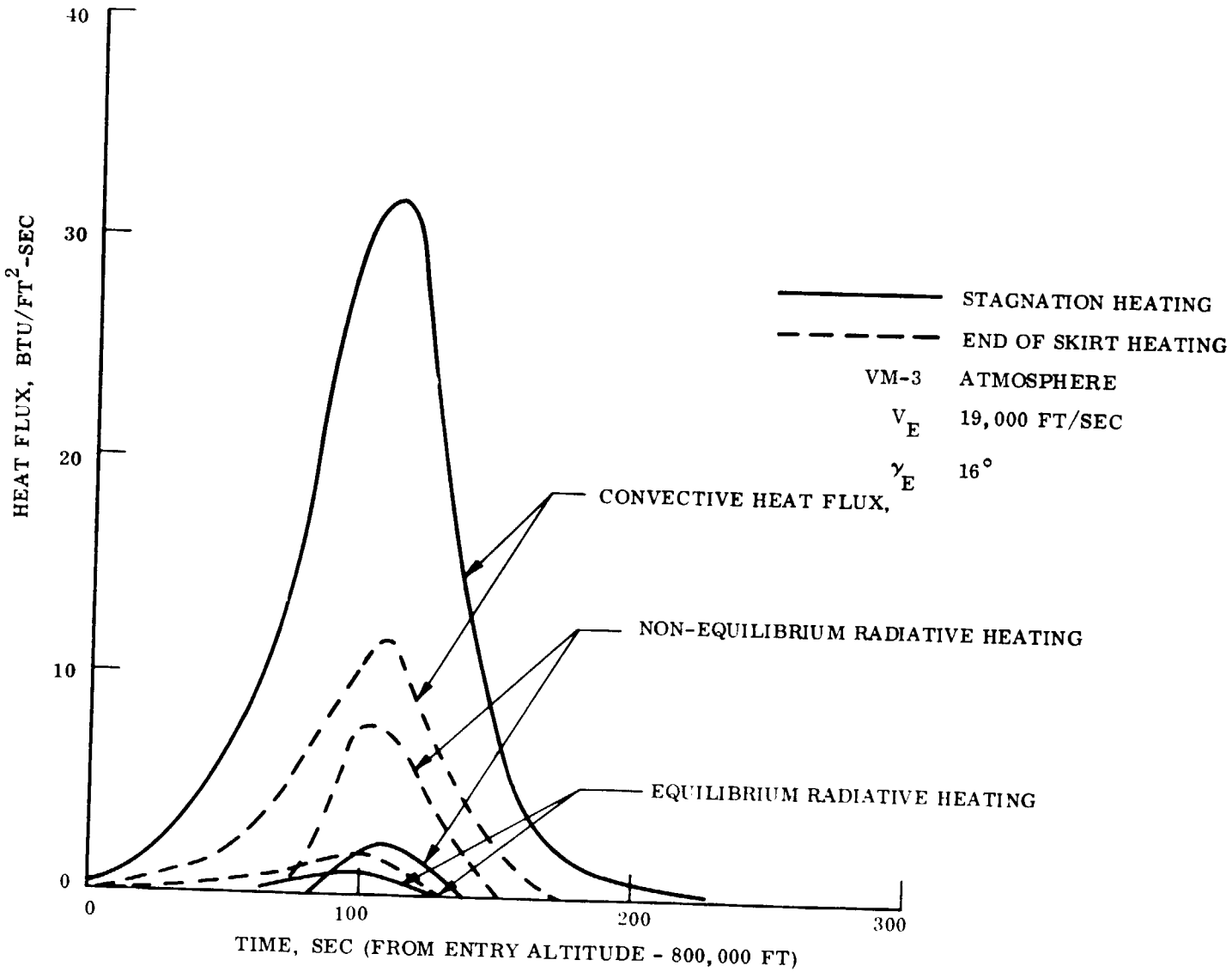

Figure 5.9-22. Cold Wall Convective and Radiative Heat Flux Histories for Thermal Design Trajectory

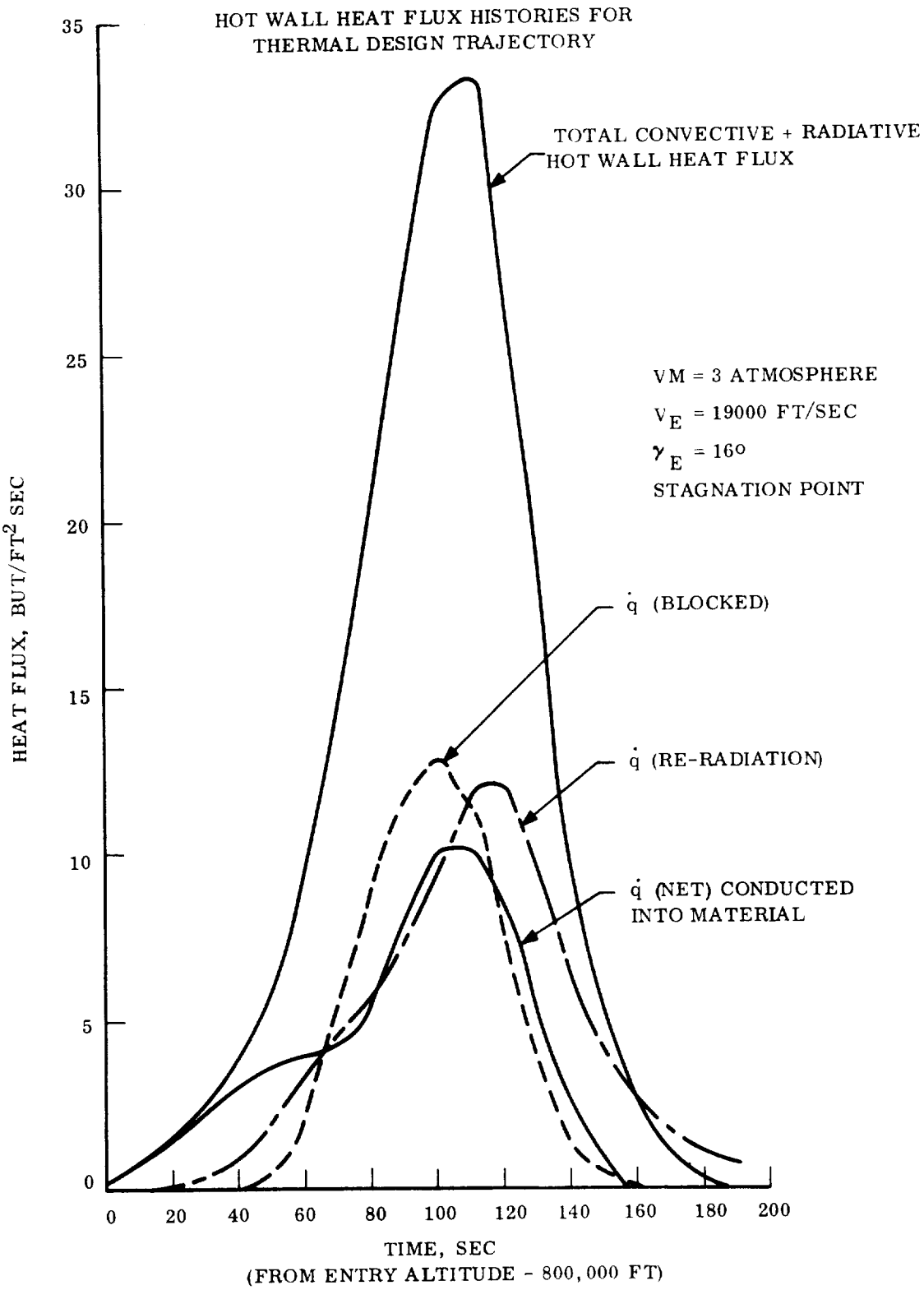

Figure 5.9-23. Hot Wall Heat Flux Histories for Thermal Design Trajectory

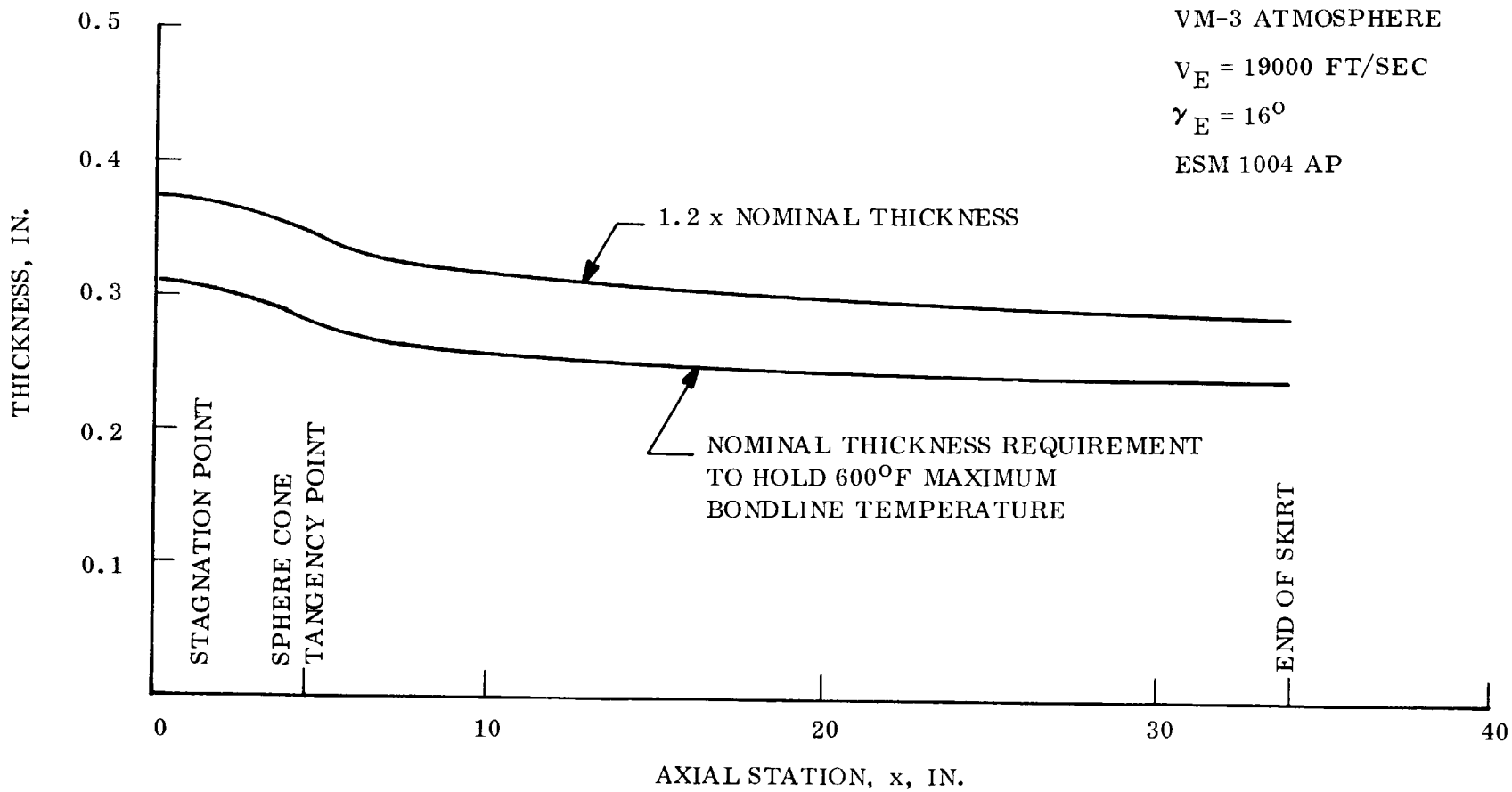

Figure 5.9-24. Heat Shield Thickness Requirements

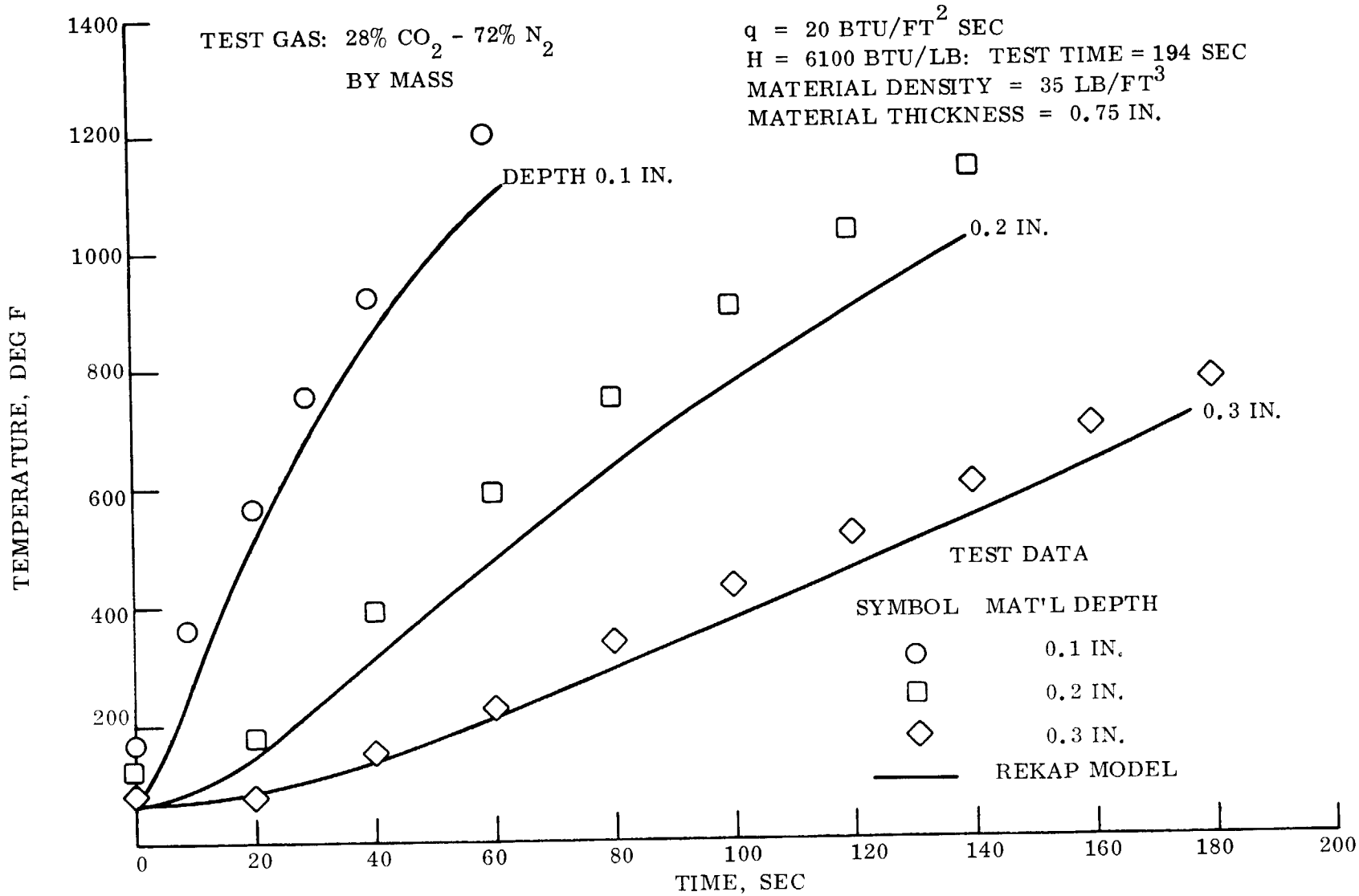

Figure 5.9-25. Hyperthermal Arc Test - ESM 1004 AP

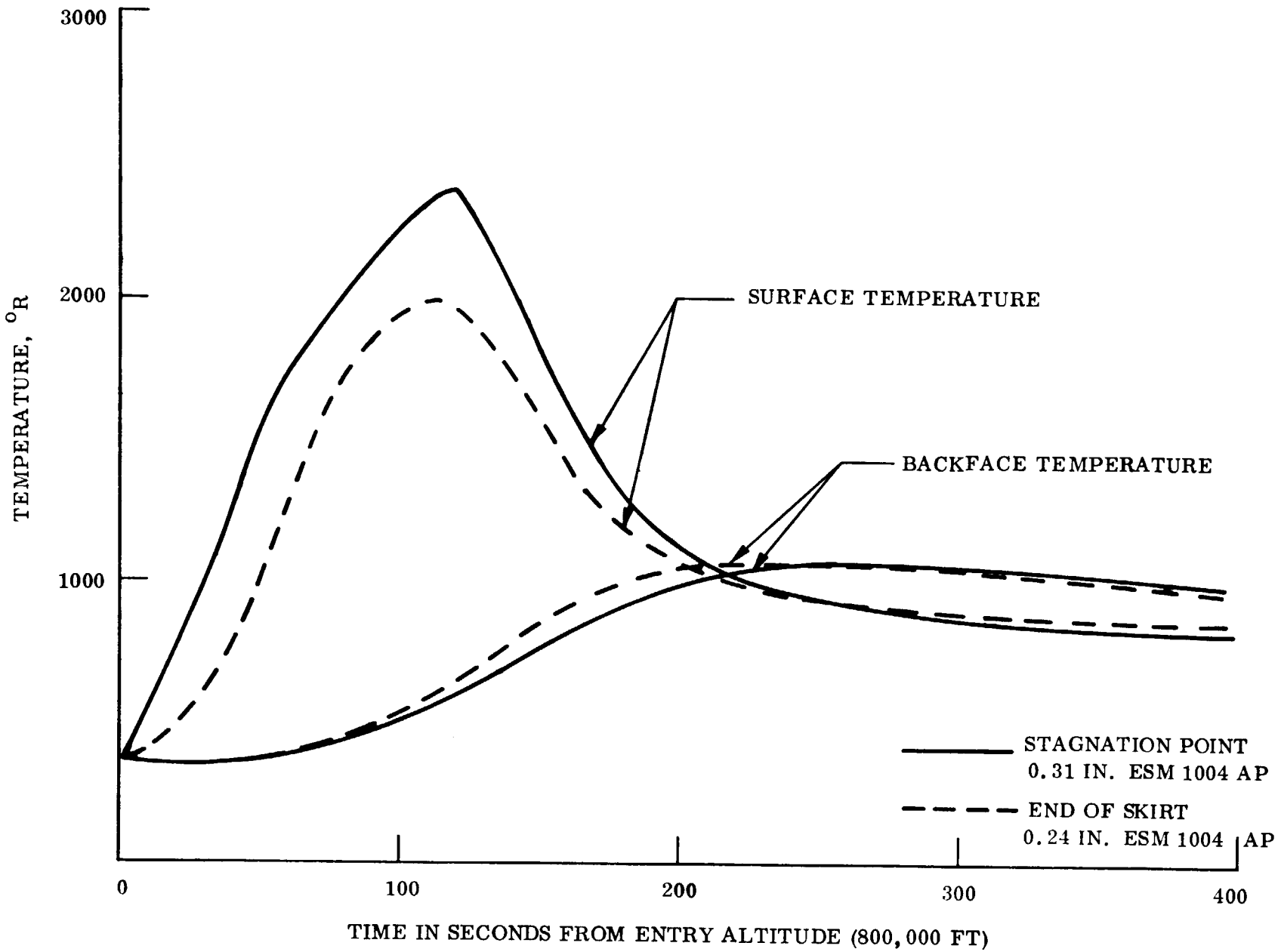

Figure 5.9-26. Surface and Backface Temperature Histories

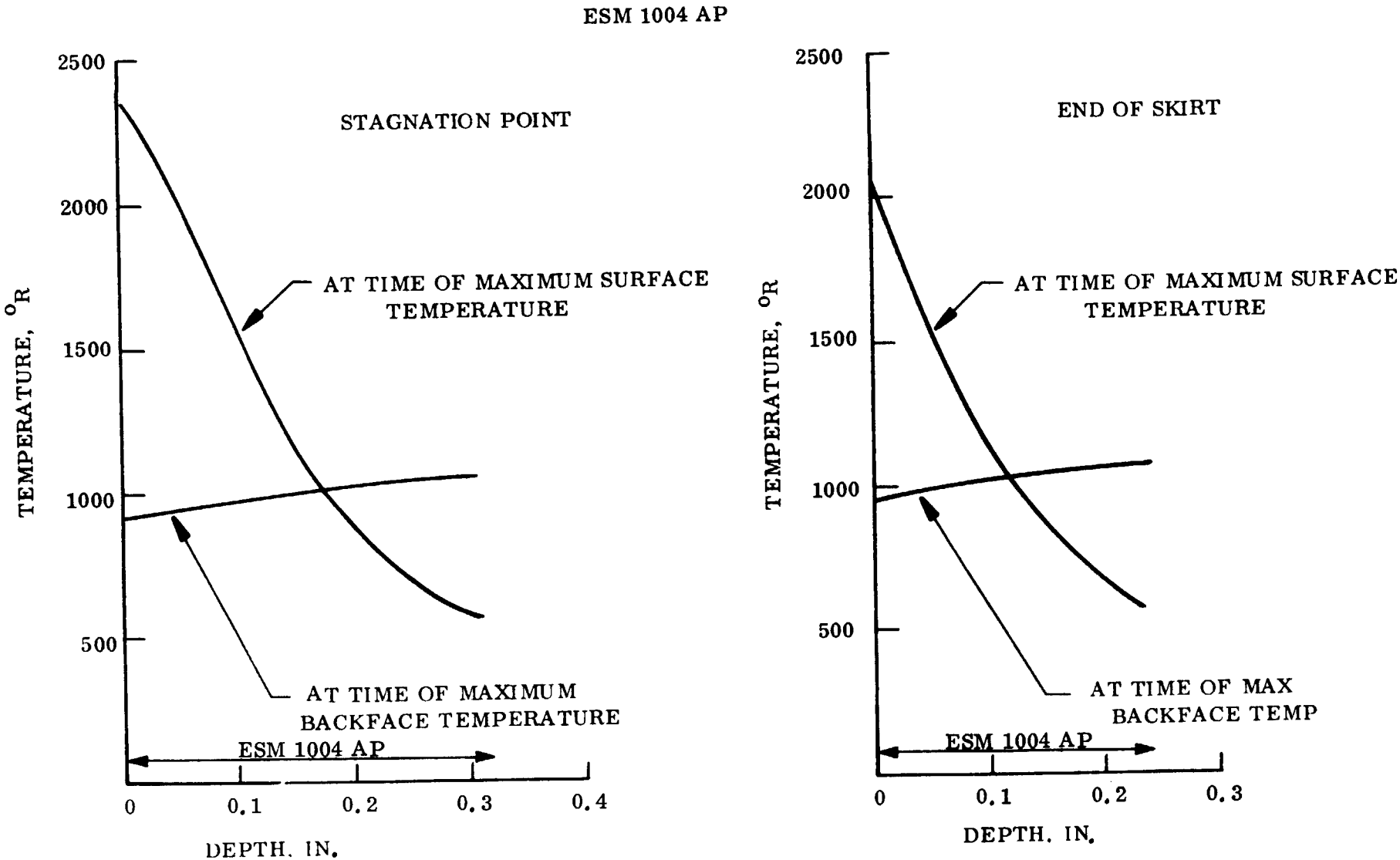

Figure 5.9-27. Temperature Gradients Through the Shield

even for the maximum angle-of-attack condition, since no separated flow re-attachment occurs in the afterbody region. An ablating material for thermal protection is unnecessary, and a high emissivity coating would be adequate protection. The analysis showed that the maximum temperature rise on the afterbody is only 240° F. Consequently, the maximum attainable afterbody temperature is less than the maximum temperature of 760° R imposed on the vehicle for the sterilization process.

A beryllium plug is utilized in the nose cap of the ESM 1004 AP heat shield. It was desirable to use a different material, (a non-ablator) to prevent any of the ablation products from entering the temperature and pressure sensors at the forward stagnation region. As a result of the lightweight structure of the Capsule, there will be inherent surface waviness due to fabrication techniques, and surface irregularities, such as steps, will exist due to panel joints. The effect of these surface irregularities have been examined to determine whether any severe local hot spots will occur during entry. The results obtained indicate that within the tolerances specified for manufacturing the heat shield, no severe local heating will occur.

The current design for the ESM 1004 AP heat shield allows for ease of fabrication, handling and final assembly. The heat shield material is designed to be fabricated in panel sections of approximately 10 ft^2. Additional advantages of the segmented shield are that it allows for 100 percent inspection, does not require the aeroshell during shield manufacturing operations, and allows for finish machining prior to its being bonded to the aeroshell. The heat shield material ESM 1004 AP is soft bonded to the structure with 10 mils RTV -560 being adequate bond for the 35 lb/ft^3 ESM material.

Design considerations were also taken into account for the steps developed between the segmented panels both longitudinally and circumferentially. These steps were determined by both the bond and heat shield thickness tolerances. A test program has been conducted to determine the thermal effect on seams of ESM 1004 AP (ref. 5.9-7). The test data indicates that the best performance is obtained with a circumferential scarf joint (the seam line is on a 45° angle to the surface), with a thermal control coating. It is recommended that a 45° scarfed seam be employed on this design, and that longitudinal seams be avoided, by having the panel seams at 45° to the longitudinal axis.

5.9.5 HEAT SHIELD DEVELOPMENT

The thermal performance of the heat shield material ESM 1004 AP (density -35 lb/ft^3) proposed for this mission has been characterized and a mathematical model has been well calibrated with test data for the environment anticipated for Mars entry. The mathematical model Reaction Kinetics Ablation Program (REKAP) enables confident predictions of the thermal performance to be made for the mild Martian environment postulated for this mission.

However, further development studies are required in the following areas:

1. Develop and define the scale up techniques for fabricating full scale thermal shields for the Hard Lander configuration.

2. Laboratory studies should be performed to compare the properties of ESM 1004 AP prepared with low volatile reactants with those of standard ESM 1004 AP from which volatiles have been removed by post-cure thermal treatment.

3. Thermo-physical and mechanical property tests at selected representative conditions should be conducted for the low volatile ESM 1004 AP formulation to compare with the available high volatile ESM 1004 AP data, and thus verify the thermal performance of the proposed heat shield.

5.9.6 REFERENCES

5.9-1 Weingarton, V.I. and Seide, P., "Elastic Stability of Thin-Walled Cylindrical and Conical Shells Under Combined External Pressure and Axial Compression", AIAA Journal, Vol. 3, No. 5, May 1965.

5.9-2 Cheney, J.A., "Buckling of Shell Supported Rings", Journal of Aircraft, Vol. 1, No. 4 (July-August 1964).

5.9-3 Cohen, Gerald A., "The Effect of Edge Constraint on the Buckling of Sandwich and Ring-Stiffened 120 Degree Conical Shells Subjected to External Pressure", NASA CR-795, May 1967.

5.9-4 "Mars Hard Lander Capsule Study", NASA CR-66678-3, July 1968.

5.9-5 Brewer, R.A. and Charlino, R.J., "Thermal Performance of Ceramic Insulating Materials", GE TTDM #122, March 1968.

5.9-6 Brewer, R.A., "Mars Hard Lander-Afterbody Heating", GE PIR 9151-ARSTA-032, October 10, 1968.

5.9-7 Kohr, J., "Evaluation of ESM 1004 AP Prototype Heat Shield, Hyperthermal Arc Test Results", GE TDM-9151-014, July 1968.

5.10 DE-ORBIT PROPULSION

5.10.1 SUMMARY AND REQUIREMENTS

The function of the Propulsion Subsystem is to provide the impulse for the separated Capsule path deflection. This function consists of providing impulse to change the velocity of a 1000 lb Capsule by 25 meters/sec. This weight does not include the weight of propulsion. The velocity change is required to an accuracy of 0.75 percent (3σ).

To allow for some mission design flexibility the present system design provides propellant to permit 30 mps. The tanks are large enough, if filled to capacity to impart a velocity of about 42 mps. It is desirable that the Propulsion Subsystem be capable of terminal heat sterilization in the fully loaded condition. Aseptic loading of the propellant, however, is acceptable.

Two systems were considered for performing the mission: the Mariner '69 liquid propellant system and a solid propellant rocket motor. These were compared in their respective ability to satisfy the requirements. As is subsequently shown, both can meet performance requirements but the liquid system is expected to be significantly less expensive and is therefore selected.

5.10.2 SYSTEM DESCRIPTION

5.10.2.1 Liquid Propulsion Subsystem

The Liquid Propulsion Subsystem evaluated is the one used on the Mariner '69 Spacecraft with two relatively minor modifications. The first change stems from the heat sterilization requirement which was non-existent on Mariner. The second stems from the method of achieving attitude control during rocket engine operation. Mariner employs thrust vectoring by means of jet vanes. These are no longer needed since the Hard Lander is spin stabilized.

The Mariner '69 Propulsion Subsystem provides 50 lb of vacuum thrust and employs anhydrous hydrazine as the liquid monopropellant. As shown on the schematic diagram in fig. 5.10.2-1, high pressure nitrogen regulated to 308 psia feeds propellant from the propellant storage tank to the rocket engine. Propellant and pressurant on/off flow control is accomplished with multiple start and stop explosive valves. The propellant tank contains a butyl rubber bladder for positive expulsion in a gravity free environment. The rocket engine contains Shell 405 catalyst for spontaneous ignition and sustained decomposition of the hydrazine.

The weight breakdown on the Propulsion Subsystem is presented in table 5.10.2-1 and a nominal performance summary is listed in table 5.10.2-2.

Several changes are required to accommodate the terminal heat sterilization requirement. First, the existing butyl rubber bladder in the propellant tank is not compatible with hydrazine at elevated temperatures; therefore, a new bladder must be developed and qualified, should sterilization in the loaded condition be desired. Even if sterilization in the loaded condition is not required, the effect of heat on the bladder must be evaluated. Teflon/aluminum laminates are promising but have yet to be fabricated and qualified. If aseptic loading of propellants is selected, remote loading microorganism rejecting methods must be designed.

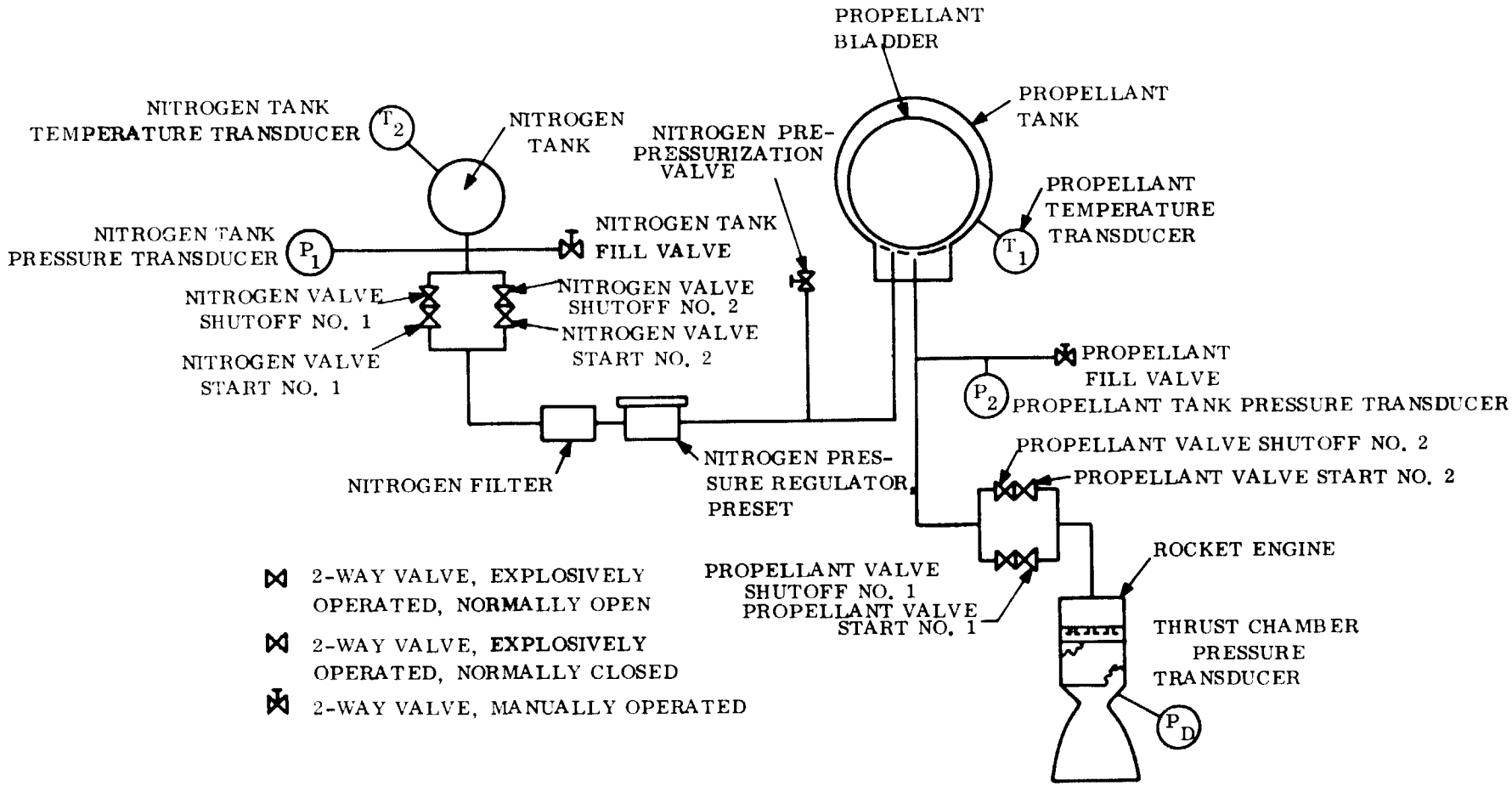

Figure 5.10.2-1. MM '69 Propulsion Subsystem Schematic

Secondly, the nitrogen tank will have to be strengthened to allow for the higher nitrogen pressures and lower tank material strength at the 275° F necessary for sterilization. Other components that possibly will be affected are the pressure regulator, the electrical harness, and the tank support liners.

TABLE 5.10.2-1. SUBSYSTEM DETAILED WEIGHT BREAKDOWN

Equipment	Weight (lbm)
Thrust Plate and Engine Assembly	7.7
Transducer - Thrust Chamber Pressure	0.1
Engine Insulation	0.3
Rocket Engine Assembly	1.9
Propellant Tank Assembly	3.8
Support Structure - Propellant Tank	1.0
Propellant Valve Assembly	1.5
Tank - Nitrogen	3.8*
Nitrogen Equipment Assembly	
Nitrogen Valve Assembly	1.0
Nitrogen Pressure Regulator Assembly	1.2
Tubing, Fitting, etc.	3.0
Transducer - Nitrogen Pressure	.3
Propellant - N2H4 (for 30 MPS, 1100 lb Capsule)	15.0
Nitrogen Gas	1.0
Transducer - Temperature, Propellant Tank	1.1
Transducer - Temperature, Propulsion N2 Tank	1.1
Total Subsystem Weight	43.8

*Increased 2.0 lb over MM'69 due to sterilization requirements.

TABLE 5.10.2-2. NOMINAL PERFORMANCE SUMMARY

Vacuum Specific Impulse	$231 \frac{lb_f - sec}{lb_m}$
Vacuum Thrust	50.71 lb_f
Vacuum Thrust Coefficient	1.71
Characteristic Velocity	4,352 ft/sec
Propellant Flow Rate	0.224 lb/sec
Throat Area	0.15 in^2
Chamber Pressure	198 psia
Nozzle Expansion Ratio	44:1
Nitrogen Tank Pressure (initial)	3015 psia @ 70°F
Propellant Tank Pressure (operating)	308 psia @ 70°F
Injector Inlet Pressure (operating)	295 psia @ 70°F
Thrust Chamber Temperature (operating)	1800°F

The subsystem was designed by JPL as a completely modular unit. This modular approach allows the subsystem to be simply installed in the Capsule. The system has the following features which lead to mission reliability and long term storage:

1. Gaseous nitrogen pressurant was selected over helium to minimize leakage.

2. Welded and brazed tubing and fittings were used wherever possible.

3. In places where mechanical joints were required to facilitate component removal and replacement, all-metal seals (aluminum crush gaskets) were chosen in place of elastomeric seals to eliminate the possibility of damage from the effects of radiation, and long storage.

4. Explosive valves were chosen for system startup and shutdown.

5.10.2.2 Solid Propellant Rocket Motor

In selecting the Mariner '69 liquid Propulsion Subsystem, solid propellant rocket motors were also evaluated.

The solid propellant propulsion system considered is shown in fig. 5.10.2-2. It was designed by Aerojet-General and is believed to be representative of applicable solid systems in general. The major components are: the titanium alloy case, the semi-submerged nozzle, insulation, and the BPN pellet igniter. A shaped charge unit to separate the nozzle may also be included if thrust termination should be required. This feature, however, is not expected to be required.

The propellant, designated ANB-3289-2, is an 85 percent solid loaded propellant with a saturated hydrocarbon binder and stabilized ammonium perchlorate oxidizer recently developed by Aerojet-General for use in sterilizable motors. In a test program, several 3 x 5 in. blocks of this propellant were exposed to six successive 53 hr exposures at 275°F in air. Only minor changes in mechanical properties were detected in the samples after the sterilization cycle.

The SD-850-2 liner has undergone heat sterilization tests. It has been demonstrated that the bond strength was not degraded by heat sterilization.

The motor case will be insulated with IBT insulation, a filled epoxy-cured, saturated, polybutadiene insulation system, developed by Aerojet-General to withstand sterilization. The propellant release boots are made of the same material.

The case is made of 6A1-4V titanium alloy, spun in halves and welded together at the centerline. An increased thickness is provided in the weld area to compensate for reduced strength. A single aft opening is provided for attaching the nozzle and tabs are located at the equator for mounting the motor.

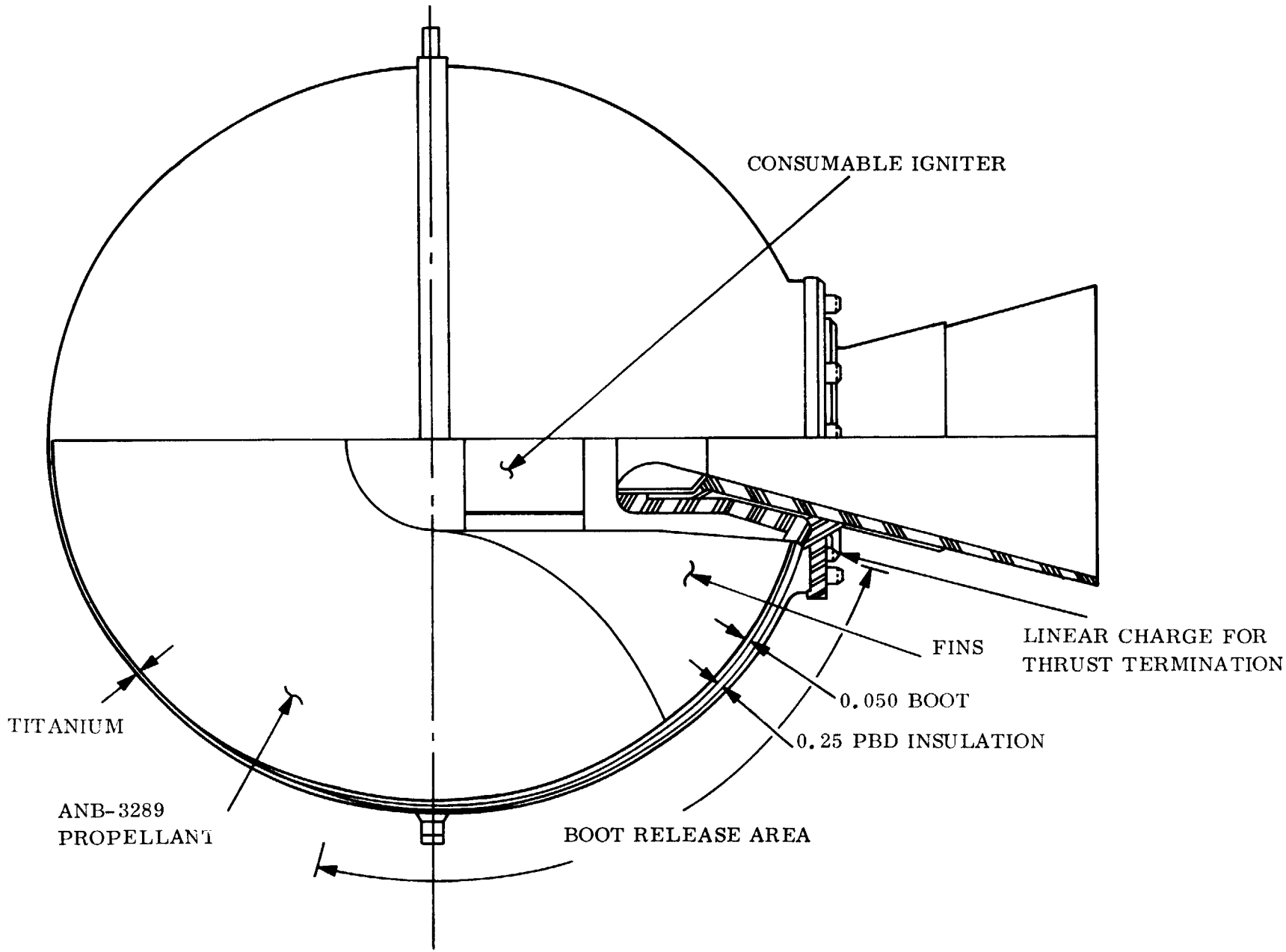

Figure 5.10.2-2. Solid Propellant System

The nozzle consists of a forged titanium housing, graphite throat insert, silica phenolic exit cone and IBT insulation on the outside of the submerged portion of the expansion cone. A circular shaped charge is mounted on the nozzle flange to release the nozzle should thrust termination be desired.

A consumable BPN pellet igniter is used. The igniter inserted in the bore of the propellant grain and bonded in place before the nozzle is installed, consists of a BPN pellet charge and an initiator in a foamed plastic housing.

The performance, weight, and basic envelope data is presented in table 5.10.2-3.

TABLE 5.10.2-3. SOLID PROPELLANT MOTOR DATA

Thrust (lbf)	220
Total impulse (lbf-sec)	4540
Burn time (sec)	20.5
Isp vac (lbf-sec/lbm)	285
Expansion ratio	40:1
Throat area (in.^{2})	0.17
Case diameter (spherical) (in.)	8.3
Total subsystem weight (lbm)	16.4
Propellant (lbm)	12.0
Inert (lbm)	4.4
Nozzle (lbm)	
Case (lbm)	
Insulation and Liner (lbm)	
Igniter (lbm)	
Thrust Termination (lbm)	
Mass Fraction	0.73

5.10.3 SYSTEM COMPARISON

The two systems were compared by evaluating cost, probability of successful operation, schedule, performance, and flexibility. These are discussed in the following paragraphs.

5.10.3.1 Cost

Table 5.10.3-1 summarizes the cost of the two systems. These figures were estimated by the manufacturers. As budgetary estimates of cost are not in general accurate the relative costs of the two systems, shown on table 5.10.3-1, are plausible for the following reasons.

The liquid system has been developed and is being qualified on the Mariner '69 Program. This system meets all performance required by the Hard Lander Capsule System including impulse capability. The sterilization environment is the only potential area of concern. Its effect on the system has been discussed in para 5.10.2.1 and the design, development and qualification costs shown include effects of the required sterilization.

The solid propellant rocket motor, on the other hand, has not been designed. There is not an available motor which fits this application; hence, one must be designed. Sterilization of a solid propellant rocket motor using ANB 3289-2 propellant has not yet been demonstrated. Tests on samples of this sterilized propellant appear promising but a total motor has not been cast, subjected to environments, and fired. A rocket employing UTC's UTREZ has been successfully sterilized, but this propellant has lower performance characteristics.

5.10.3.2 Probability of Successful Operation

Insufficient meaningful data exists to obtain a quantitative comparison of reliability of the two systems. The Solid Propellant System, because of its relative simplicity, is expected to be more reliable than the Liquid System. The latter is nevertheless highly reliable as demonstrated by the performance on the Mariner Mars '64 and Mariner Venus '67 missions. The Mariner Mars '69 mission may offer further evidence of satisfactory performance. Neither propulsion system should be a significant factor in limiting mission success.

5.10.3.3 Schedule

As with cost, the already designed Liquid System provides a greater confidence in meeting a defined program schedule.

TABLE 5.10.3-1. COST COMPARISON

(in millions of dollars)

	Liquid (MM '69)	Solid
Design and Development	0.94	4.36
Qualification	0.82	2.04
Subtotal	1.76	6.40
Flight Hardware (3 copies)	0.72	0.54
	2.48	6.94

5.10.3.4 Performance

Both systems have an acceptable thrust level, and are capable of delivering impulse to the desired accuracy. The liquid system weighs 44 lb, or 2.7 times the 16.4 lb of the solid. Although this is an advantage for the solid system it is not too significant when it is considered that the weight difference represents about 1.2 percent of total Capsule weight. Further, since this weight does not enter or land, the penalty of employing the liquid system is about 3.5 lb of landed payload.

The impulse accuracy of 0.75 percent can be met by both systems, but in different ways. The solid propellant rocket can meet such accuracies by precise weight loading of propellants. The liquid system requires an integrating accelerometer to effect thrust termination.

5.10.3.5 Flexibility

In general, propellant systems permit mission flexibility more readily than solid propellant systems. In this application, however, ample flexibility is available from the solid system by varying the direction and time at which the impulse is applied. If this is not sufficient, thrust termination of the solid could be added. This, however, results in a complexity penalty. In general then both systems have adequate flexibility for the current mission.

5.10.3.6 Summary

Both systems are comparable by all criteria except cost, which favors the liquid systems rather significantly. Moreover, minimizing total program costs is important. The preceding considerations have led to the selection of the Mariner Mars '69 Propulsion Subsystem.

5.11 ATTITUDE CONTROL

5.11.1 SYSTEM REQUIREMENTS

The control requirements of the Flight Capsule Attitude Control Subsystem (ACS) are:

1. Provide control of the Flight Capsule attitude during the firing of the deflection propulsion subsystem. It is necessary to limit the pointing error such that the entry path angle is within mission requirements. Reference mission studies establish the allowable pointing error to be 0.6°, 1σ.

2. Provide control of the Flight Capsule attitude during pre-entry such that the angle-of-attack at entry is acceptable. The angle-of-attack must lie in the range $-40^{\circ} < \alpha < 40^{\circ}$ to meet entry requirements.

3. Provide control of the Flight Capsule roll rate during entry to assure attitude stability. The roll rate is to be controlled to below a limiting value which could produce a divergence of the trim angle-of-attack.

The vehicle characteristics and the factors which influence the design of the ACS are shown in table 5.11.1-1.

TABLE 5.11.1-1. VEHICLE CHARACTERISTICS AND DESIGN

	@ Separation	@ Entry
Capsule Weight	1250 lb	1180 lb
Inertias Roll	199 sl-ft^2	≈ Same
Pitch	120 sl-ft^2	
Yaw	121 sl-ft^2	
ΔV Thrust	50 lb	
C. M. Offset	< 0.2 in.	
Nozzle Alignment Error	< 0.5°	
Separation Angular Rate	< 0.3°/sec	
Velocity Increment	25 mps	
Moment Arm	5 ft	
Time, Separation to Entry	24 hr	
Maximum Entry Roll Torque	90 ft-lb	
Entry Roll Angular Momentum	720 ft-lb-sec	
Entry Angle-of-Attack	$-40^{\circ} \leq \alpha \leq +40^{\circ}$	

5.11.2 SYSTEM PERFORMANCE

5.11.2.1 Summary: Selection of ACS

5.11.2.1.1 Control Concept

The selected control concept for use on the Mars Hard Lander ACS is a spin control system rather than a three-axis control system. The spin control system, which is mounted on the aeroshell, will spin-up the Capsule immediately after separation. The spin stabilization of the spinning Capsule will control the orientation of the attitude of the Capsule during deflection thruster firing and during the pre-entry period. The Capsule will de-spin at the start of entry to allow convergence of the Capsule angle-of-attack and will maintain roll rate control throughout entry.

The three-axis ACS would consist of three body-mounted precision integrating rate gyros and the associated electronics to provide pitch, yaw, and roll control. The three-axis ACS would operate from separation through entry. A comparison of the two control concepts was made during the Mars Hard Lander Capsule Study and is discussed in the Final Report, NASA CR 66678-4, dated July 31, 1968. Both systems give adequate performance. Even though the three-axis system is slightly better in achieving pointing accuracy and better angle-of-attack control, the resulting improvement in mission performance is not sufficient to justify the additional system complexity and reduced reliability.

5.11.2.1.2 Reaction Control System

The two reaction control systems which merit serious consideration and review are (a) the cold gas (nitrogen) system and (b) the liquid monopropellant (hydrazine) propulsion system. Several factors used for comparison of the two systems are given below.

A. Cost. A primary factor influencing the selection of the reaction control system is cost. A 10 to 1 difference is expected in the costs required for the design, development and qualification of the systems. The estimated cost of the cold gas system is $0.1M while the hydrazine cost is $1.1M. The cost difference arises because of the differences in the development status of the two systems. A subcontract would be required for the development of the hydrazine system. The combustion process of the hydrazine system requires relatively extensive testing with a significant cost for test facilities.

B. Performance. Both systems adequately meet the specified requirements.

C. Reliability. The cold gas system, because of its system simplicity and its extensive use on past space vehicles, can be expected to have the higher reliability.

D. Weight, Size and Power. The hydrazine system has one major advantage over the cold gas system. The weight of the hydrazine system would be approximately 11.5 lb while the weight of the cold gas reaction control system would be approximately twice that value, (22.6 lb). Since the system is carried only through entry and is not landed, the landed penalty is only about 5 lb. The size and power required are similar.

E. Sterilization. It has been demonstrated that both systems can be sterilized; however, fewer problems areas are anticipated with the cold gas system. For the cold gas system, it is necessary to increase the tank weight to accommodate the increased gas pressure and decreased material strength. For the hydrazine system it is also necessary to use the same considerations for the pressurant tank. In addition, the high sterilization temperatures can create problems due to the chemical interaction of the hydrazine with metallic parts such as tubing which are not titanium (the tank is to be titanium) as well as interaction with the expulsion bladder in the propellant tank.

F. Schedules, Development Time. The cold gas system has a significant advantage as a result of system simplicity and extensive use for previous applications. A minimum of new development work would be required for the cold gas system.

G. Handling and Test. Because a cold gas (nitrogen) system is inert, whereas liquid monopropellant system obtains its thrust by means of combustion of the hydrazine, the nitrogen system will significantly ease handling and test procedures.

The advantages derived from the use of a cold system are sufficient to offset the fact that it is not the minimum weight system.

5.11.2.2 Attitude Control Subsystem Description

The schematic diagram of the ACS is shown in fig. 5.11.2-1.

A tabulation of significant parameters of the selected ACS and of the weight, size and power requirement of the components of the subsystem are given in table 5.11.2-1.

The schematic diagram on fig. 5.11.2-1 shows the basic elements of the cold gas reaction control propulsion system, the single rate gyro, the associated electronics and the primary signal paths from the computer-sequencer and the EP&D sections. The rate gyro shown measures the Capsule roll rate and yields an output which is compared with an analog voltage reference level. The threshold detectors, whose inputs are the error signal produced by the difference between the reference level and the rate gyro output, activate the solenoid power switches to turn on either the +roll or the -roll nozzles. The power for operation of the rate gyro and the spin electronics, for firing the squib valve, and for operating the solenoid valves is obtained from the EP&D section but is controlled by the Computer-Sequencer.

5.11.2.3 Sequence of Operation

The operational sequence of the Capsule ACS is as follows:

1. At the start of the pre-entry phase of flight, the Spacecraft orients the Capsule in the proper direction for the firing of the ΔV propulsion engine. This Capsule orientation establishes the direction of the Capsule spin vector, (roll axis), which is to be maintained until the entry phase of flight. The selection of the direction of the spin vector and the time of imparting the

deflection velocity are determined to result in a desired entry flight path angle. The resulting entry angle-of-attack is sufficiently small to be acceptable. The entry flight path angle requirement is relatively stringent ($\gamma = 21^{o} \pm {}^{4^{o}}_{5^{o}}$) while the entry angle-of-attack requirement is quite broad. The aerodynamic design of the Capsule can tolerate an initial angle-of-attack of $\pm 40^{o}$.

2. A minimum of 30 sec prior to separation, "Gyro Power - ON" command is issued by the Computer-Sequencer.

3. At 0.5 sec after separation, commands are given by the Computer-Sequencer to (a) fire the explosive squib valve, (b) establish the spin rate reference level equivalent to 25 rpm, and (c) provide power to the solenoid power switches. This will initiate spin-up by activating the +roll nozzles.

4. A spin rate of 25 rpm is reached at 12.5 sec after spin-up is started. The spin system then operates to maintain this roll rate within a threshold level of ±2.5 rpm from the commanded 25 rpm.

5. At 30 sec after initiation of spin-up, the computer sequencer issues a discrete command to turn off the power to the solenoid power switches and to the gyro and spin electronics to conserve power.

6. After a 28 min delay (prior to deflection propulsion firing) the computer-sequencer issues a discrete command to turn on power to the gyro and spin electronics. Power is not applied to the solenoid power switches. The spin rate is monitored during deflection propulsion firing. The gyroscopic stability obtained by spinning the Capsule at 25 rpm is sufficient to maintain the ΔV orientation accuracy during the firing of the 50 lb thruster of the propulsion Subsystem. By this method the first primary control requirement of the ACS is met.

7. At 2 min after separation of the thrust cone, the gyro power is again turned off to conserve power during the long free flight phase prior to entry. The spin rate is allowed to remain at approximately 25 rpm so that gyroscopic stability can act to maintain the inertial attitude of the Capsule until the beginning of entry. By maintaining the inertial attitude of the Capsule as established by the Spacecraft prior to separation, the ACS meets the second of the primary control requirements.

8. Just prior to entry, the computer-sequencer will activate the ACS to prepare for roll rate control. The commands issued will (a) turn on the gyro power and (b) set the commanded spin rate to zero.

9. At the sensing of 0.1g of axial drag on the Capsule, (with a timer back-up on the command) a discrete command from the computer-sequencer is issued to the EP&D section to provide power to the solenoid power switches. Since the Capsule spin rate is approximately 25 rpm and the commanded rate is zero, the solenoid valve for -roll will be opened to de-spin the vehicle. The -roll nozzles will operate until the spin rate is reduced to a value within the deadband set in the threshold detectors. This deadband is presently set at ±2.5 rpm. Roll rate control about this band is to be maintained throughout the entry phase of flight.

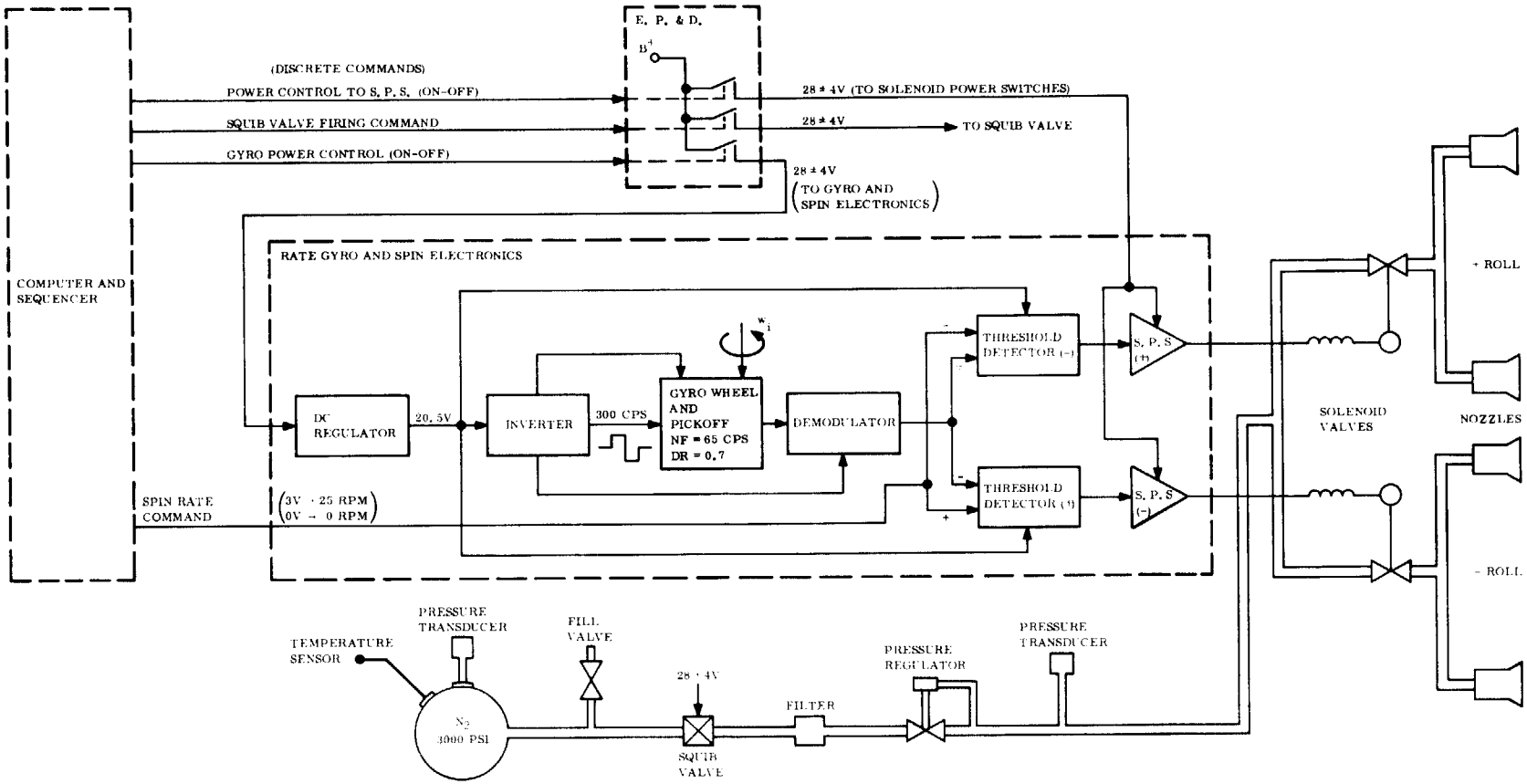

Figure 5.11.2-1. Spin, De-spin, Roll Rate Control Subsystem (Propulsion - Cold Gas Reaction Control)

TABLE 5.11.2-1. SIGNIFICANT PARAMETERS

PERFORMANCE CHARACTERISTICS	
Time, Separation to Spin-up Command	0.5 sec
Spin Rate during Pre-entry	25 rpm
Spin-up Time	12.5 sec
Roll Thrust per Nozzle	4.2 lb
Maximum Roll Control Torque	42 ft-lb
Impulse Requirements:	
Spin/De-spin	208 lb-sec
Entry Roll Rate Control	145 lb-sec
Maximum Allowable Entry Roll Rate	17 rpm

COMPONENT CHARACTERISTICS

	Weight (lb)	Size (in.)	Power
Cold Gas (N_2)	5.43	—	
N_2 Tank	10.50	10.8 diameter	
Fill Valve	0.20	0.875 diameter x 1.5 long	
Squib Valve	0.50	1 x 1.5 x 2.5	28V - 3 amp
Filter	0.25	1 diameter x 3 long	
Pressure Regulator	1.50	4 x 3 x 3	
Pressure Sensors (2) @ 0.5 lb	1.00	1 diameter x 1.6 long	
Temperature Sensor	0.25	0.25 diameter x 0.12 long	
Solenoid Valves (2) @ 0.5 lb	1.00	1.2 diameter x 2.5 long	28V - 1 amp
Nozzles (4) @ 0.2 lb	0.80	2 diameter x 2.5 long	
Tubing and Fittings	1.20	—	
Rate Gyro and Spin Electronics	1.40	3.25 x 4.5 x 2	5 watts
Total Weight	24.03		

10. Roll rate control is terminated at the time of parachute deployment by turning off the power to the solenoid power switches and the gyro.

5.11.2.4 System Design for Initial Spin-up

The first primary performance requirement of the ACS is to limit the pointing errors during deflection propulsion firing such that the entry path angle is within mission requirements. The pointing accuracy of the Spin Control Subsystem is, of course, directly dependent on the accuracy with which the Spacecraft orients the Capsule prior to separation. Two major additional errors are introduced by the Capsule Separation Subsystem and the Spin Control Subsystem. These errors are the tip-off error and the coning error during deflection propulsion firing.

The tip-off error is caused by asymmetry in the force causing separation from the Support Module. This results in a rate which produces an attitude deviation from the separation Spacecraft attitude proportional to the time interval from separation to spin-up command. It is estimated that the separation tip-off rate can be held to less than 0.3°/sec. It is advantageous to begin spin-up at the earliest possible time following separation. It is proposed that the time interval between separation and initiation of spin-up be set at 0.5 sec to reduce the pure tip-off error to less than 0.15°.

The coning error is caused by the upsetting torque created by the deflection propulsion thrust not acting through the Capsule center-of-mass. Gyroscopic action of the spinning Capsule reacts to the torque by producing a spiraling increase in the attitude error during the burn time of the engine. The spin rate selected must be sufficiently high to minimize the ΔV orientation error and yet minimized so that the required total impulse for the spin-up and de-spin is not unnecessarily increased. The magnitude of the spin rate required is a function of the path deflection propulsion thrust level, Capsule mass characteristics and ΔV orientation accuracy required.

A parametric set of data has been computed using a six degree-of-freedom computer program to simulate the Capsule motion histories. A nomograph of the results for the ΔV orientation error is shown on fig. 5.11.2-2. The curves are valid in this case where the deflection propulsion thrust acts sufficiently long to allow averaging over several cycles of motion, since a relatively low thrust level (50 lb) is used.

The ratio of the pitch and roll inertias of the Capsule is:

$$\frac{I_{pitch}}{I_{roll}} = \frac{120 \text{ slug-ft}^2}{199 \text{ slug-ft}^2} \approx 0.6$$

The ratio of the thrust, T, and the effective c.g. offset, C_2, (which includes the effect of thrust misalignment), to the pitch inertia may take a value as high as:

$$\frac{TC_2}{I_{pitch}} = \frac{[50\ \text{lb}]\ [0.5\ \text{in.}]}{120\ \text{sl-ft}^2} = 0.21$$

Use of these values and the nomograph on fig. 5.11.2-2 show that the allowable errors in attitude greater than 0.5°, the spin rate required is approximately 15 rpm. The spin rate has been selected to be 25 rpm which is equivalent to an allowable error of less than 0.25°.

A summary of all expected error sources is shown in table 5.11.2-2. All the errors shown are, in general, random with the exception of the Spacecraft control deadband which has uniform probability of occurrence within the deadband. The values shown are 3σ errors except for the control deadband which is a maximum error. The overall error was obtained by root sum squaring the random errors and adding the control deadband directly.

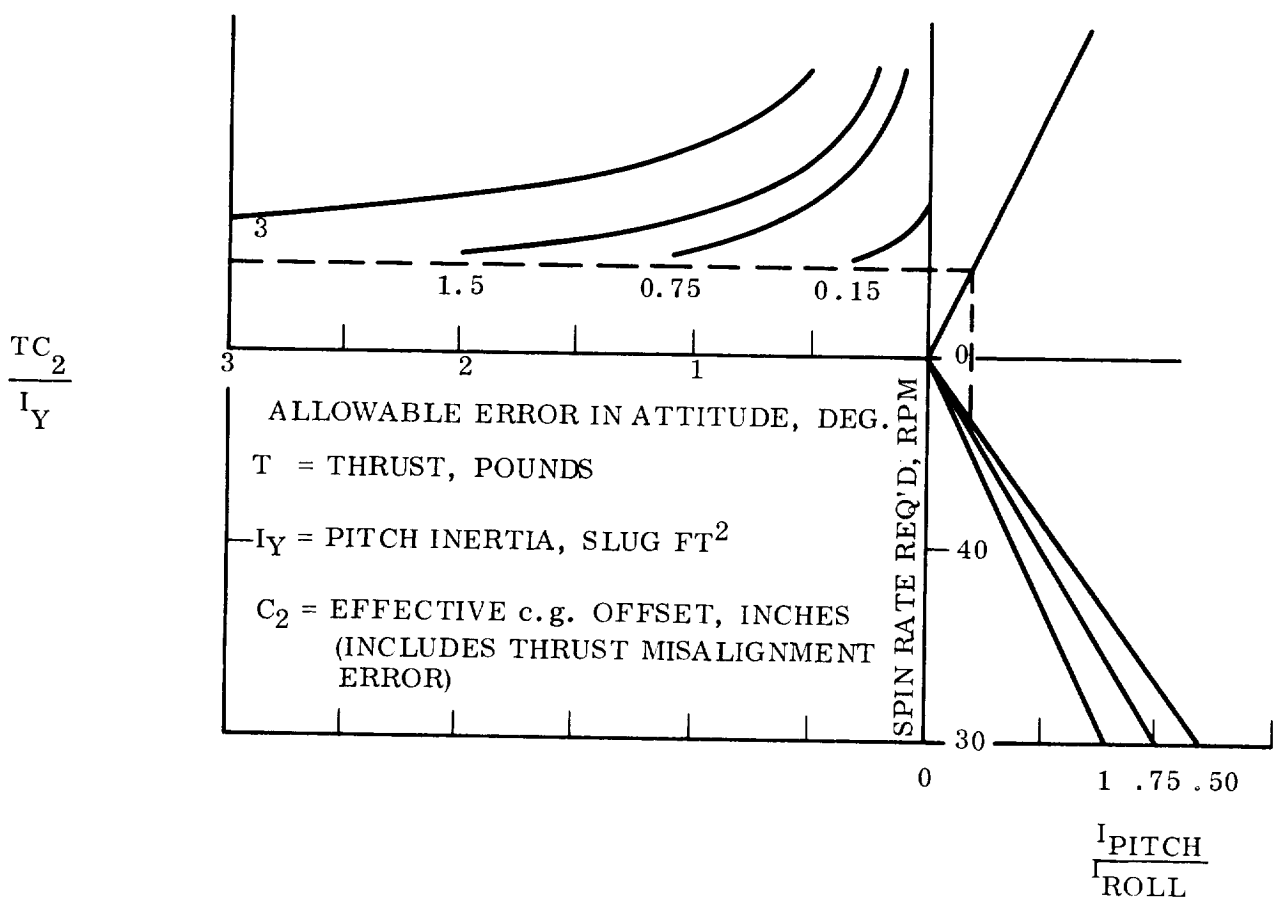

Figure 5.11.2-2. ΔV Orientation Error

TABLE 5.11.2-2. EXPECTED ERROR SOURCES

No.	Error Source	
	Spacecraft	
1.	Control Deadband	0.25°
2.	Sensor Alignment/Repeatability	0.15°
3.	Electronic Drift Error	0.05°
4.	Maneuver Error	0.20°
5.	Gyro Drift	0.15°
	Capsule	
6.	Capsule Alignment Error	0.30°
7.	Tip-off Error	0.15°
8.	Spin-up Coning Error	0.20°
9.	ΔV Coning Error	0.25°
	TOTAL ERROR	0.82°

The impulse required from the Reaction Control System for spin-up is a function of the roll inertia and selected spin rate.

$$tT = I_{roll} \Delta W$$

where T = torque acting to increase roll rate

t = time duration for the application of T

I_{roll} = roll inertia = 199 slug-ft^2

ΔW = change in roll rate = 25 rpm

$$tT = \frac{(199)\ (25)\ (2\pi)}{(60)} = 520 \text{ ft-lb-sec}$$

Since the moment arm for each roll nozzle is 5 ft, the impulse requirement is 104 lb-sec.

Since the thrust per nozzle has been set at 4.2 lb/nozzle (based on entry roll rate control requirements), the time required for spin-up to 25 rpm is:

$$t = \frac{104 \text{ lb-sec}}{(2 \text{ nozzles})\ \frac{4.2 \text{ lb}}{\text{nozzle}}} = 12.4 \text{ sec}$$

5.11.2.5 System Design for Free Flight Attitude Control

The second control requirement of the ACS is to provide control of the Capsule attitude during the extended time period between deflection propulsion firing and entry so that the angle-of-attack at entry meets entry requirements. The angle-of-attack at entry must lie in the range $-40° < \alpha < +40°$. Since the spin attitude for propulsion firing is within 40° of the inertial direction of the entry angle, continued Capsule spin will satisfy the angle-of-attack requirement.

Two factors that could affect spin axis pointing accuracy are long term precessional torques and energy dissipation. The only identifiable torque is solar pressure whose magnitude acting for 24 hr is not sufficient to perceptibly precess the axis. With respect to the effect of energy dissipation, the problem of attitude divergence due to energy dissipation will not arise because of the inertial characteristics of the Capsule. The roll (spin) inertia of the Capsule is $I_x = 199$ sl-ft^2 while the pitch and yaw inertias are both approximately 120 sl-ft^2.

Near the end of the period of free flight just prior to entry it will be necessary to de-spin the Capsule. This will allow more rapid convergence of the Capsule angle-of-attack during the early part of entry. The Capsule is de-spun to a value within the threshold deadband of ±2.5 rpm, which is the spin control level to be used for controlled roll rate during entry. The impulse required to de-spin the Capsule will be approximately the same as that required for spin-up.

5.11.2.6 System Design for Entry Roll Rate Control

The need for attitude stability during entry requires that a roll rate control capability be provided. The Capsule may tend to spin-up during entry under the action of aerodynamic torques. At low dynamic pressures, blunt bodies (such as the Capsule with its 60° half cone angle) can be made unstable at zero angle-of-attack by spin. This phenomenon occurs after peak pressure where the pressure is decreasing with time. The effect is that in the terminal steady state condition the vehicle will diverge to a trim angle-of-attack (dependent upon configuration, spin rate, ballistic coefficient and inertia properties) and follow a helical flight path. Specific items that would be affected by this divergence are base pressure measurements, radar altimeter measurements, vehicle ballistic coefficient and communication aspect angle.

In order to insure stability during entry, a maximum roll rate limit must not be exceeded. The roll rate limit, P_{Lim}, for the vehicle is a function of the Capsule aerodynamic characteristics and vehicle properties. The roll rate during entry should be held below the value given by:

$$P < 8\, T_1 \left(\frac{I_y}{I_x} \right) \sqrt{\frac{-g\, C_{m_\alpha}}{2\ell\, C_D\, C_{m_q}\, C_{L_\alpha}}}$$

where

$$T_1 = \frac{m\ell^2}{8 I_y} C_{m_q} - \frac{C_{L_\alpha}}{4}$$

m = 37.4 slug = Capsule mass

ℓ = 11 ft = reference length

I_x = 199 slug-ft^2 = roll moment of inertia

I_y = 120 slug-ft^2 = pitch moment of inertia

$g_{Mars} \approx$ 12.6 ft/sec^2 = Mars gravitational constant

C_{m_α} = -0.08/rad

C_{m_q} = -0.34/rad

C_{L_α} = -1.15/rad

C_D = 1.40

Substitution of these values into the above expressions yields a roll rate limit value of approximately 17 rpm. It is to be noted there is a strong dependence on the value of the aerodynamic derivative, C_{m_q}, which seldom is a well defined value.

The sizing of the reaction control system must be such that sufficient roll control torque and impulse be available to prevent the Capsule roll rate from reaching the roll rate limit, P_{Lim}. The maximum aerodynamic roll torque acting on the Capsule is estimated to be 90 ft-lb. It is not necessary that the control roll torque be equal to or greater than the peak disturbance torque (which occurs for a very short period) as long as the integrated effect on Capsule roll rate due to the net difference between the disturbance torque and the control torque does not cause the Capsule to spin-up near the roll rate limit.

A total roll control torque of 42 ft-lb is available by use of two nozzles, each having a thrust of 4.2 lb and acting through a moment arm of 5 ft. Therefore, during the time periods where the aerodynamic roll torque is less than the control roll torque capability the ACS will maintain roll rate control to Capsule roll rates near the threshold level of either ±2.5 rpm. However, when the aero-torque, T_a, exceeds the control torque capability, T_c, there will be an increase in the Capsule roll rate even though the nozzles remain full on. This approximate change in roll rate is expressible as:

$$\Delta P = \int \frac{T_a - T_c}{I_{Roll}} \, dt \approx \frac{T_a - T_c}{I_{Roll}} \Delta t$$

For an average torque difference of $T_a - T_c = 25$ ft-lb, the approximate change in roll rate as a function of time would be:

$$\Delta P \approx \frac{25}{199} \Delta t$$

Assuming the initial controlled roll rate was +2.5 rpm, the existence of the above condition for a period of time $\Delta t = 5$ sec would produce a roll rate of $P = 2.5 + 6.3 = 8.8$ rpm, which is well below the P_{Lim} value of 17 rpm. A careful review of sizing of the roll control nozzles will need to be made as changes are defined to the vehicle aerodynamic characteristics, the vehicle mass properties, and the entry dynamic flight conditions.

For purposes of sizing the reaction control system, the impulse requirements during entry requires approximately 104 lb-sec for initial de-spin of the Capsule and 145 lb-sec for roll rate control during entry.

5.11.3 COMPONENT SELECTION

The schematic diagram of the proposed attitude control subsystem (ACS) was shown on fig. 5.11.2-1. The selection of the components of the cold gas reaction control system is dependent upon the subsystem requirements given in the previous sections. The total impulse required is the summation of the requirements for spin-up, de-spin, and entry roll rate control. This value is 353 lb-sec.

The weight of the cold gas (nitrogen) needed to provide the total impulse of 353 lb-sec is 5.43 lb based on a specific impulse of 65 sec.

The weight of the tank used to contain the cold gas is a function of the volume and pressure of the stored gas and the thickness and material of the tank wall. The volume of the gas is approximately 655 in.^{3}, which therefore yields a tank diameter of 10.8 in. The tank material will be titanium. Considering safety factor and sterilization requirements, the weight of the tank and its associated mounting structure and hardware is 10.5 lb.

The weight of the fixed hardware components of the cold gas reaction control system (table 5.11.2-1) is 6.7 lb.

The total weight of the reaction control system is:

Fixed Hardware	6.70 lb
Cold Gas (N_2)	5.43 lb
Tank	10.50 lb
	22.63 lb

The gyro and electronics assembly is 3 1/4 × 4 1/2 × 2 in. and weighs 1.4 lb. The assembly requires 8 watts of power during a 30 sec warm up period and 5 watts for normal operation.

A tabulation of the weight, size and power requirements of the components of the ACS was shown on table 5.11.2-1.

5.11.4 DEVELOPMENT STATUS

No problem is expected with developing a pneumatic system which can withstand the sterilization environment of six cycles of 92 hr at 130°C. The two critical components, the pressure regulator and solenoid valve, have successfully passed these environments. The components are manufactured by the Sterer Engineering Company and the tests were conducted for The Martin Company (Denver). The regulator has all metal parts and has successfully flown on the Ranger Program. The solenoid valve requires O-rings; however the Viton "A" O-rings successfully performed during the tests. Similar configurations of this valve have flown on the OAO/698 and BIOS programs. It is expected that utilization of a Viton "A" O-ring on the filter will similarly perform well especially since it is a static O-ring application. Similar filters have flown on the OAO, Nimbus, MK2, MK3CTP, MBRV, RMV and BIOS programs. It is expected that all the pneumatic components can be obtained in 90 days. However, if operability assurance tests and qualification tests are required, the delivery time will be extended accordingly. Usually 2 weeks can be added for operability assurance tests and 8 weeks for qualification tests.

Minor development work will be required to adapt the Aeroquip brazing system which has successfully been used on such programs as Mercury, Gemini, and Apollo. The brazed system will eliminate tubing connectors and greatly enhance the pressure integrity of the system during operation since the squib valve will seal the system prior to operation.

A bread-board system shall be fabricated to verify the brazing techniques and the pneumatic subsystem performance.

5.12 CANISTER AND ADAPTER

5.12.1 CANISTER DESIGN REQUIREMENTS

The canister is the container which provides a biological barrier around the sterilized Flight Capsule and permits separation of the Capsule near Mars. System requirements described below are those for achieving and maintaining sterility and those associated with the functional and structural adequacy of the canister.

5.12.1.1 Sterilization Requirements

Since a scientific objective for the exploration of Mars is the study of extraterrestrial life that may have evolved there, adequate measures are required to limit the possibility of contaminating Mars by Earth life forms. Sterility of the Mars Hard Lander will be achieved by heat sterilization in a dry nitrogen atmosphere. This sterility will be maintained by enclosing the Flight Capsule within the canister from the start of the heat sterilization cycle until shortly before Capsule separation.

The microbial integrity of the canister will be assured by maintenance of a differential pressure between 0.5 and 1.0 psid within the canister from the start of the heat soak cycle of terminal sterilization to Earth orbit altitude. Gas flow from inside the canister through the relief valve will prevent microbial penetration of the bio-barrier. Failure of the relief valve in the open position will result in premature loss of the differential pressure. Therefore, a filter capable of filtration of 0.3 micron size particles is required in series with the relief valve to protect against microbial penetration in event of a relief valve failure, or due to backflow during venting, or during vent valve opening.

5.12.1.2 Canister Structural Design Requirements

The canister structural design requirements were as follows:

1. Withstand an internal pressure up to 1.0 psid, with lightest weight construction.

2. Withstand dynamic and inertial loads of Titan IIIC launch and powered flight.

3. Provide adequate clearance between the aeroshell heat shield and the canister.

4. Provide a canister separation joint and field joint.

5. Provide support for the entry system.

6. Act as a load transfer medium from the entry system to both the Spacecraft and the Support Module.

The structural design analysis performed to confirm meeting these requirements is given in the following paragraph.

5.12.2 CANISTER STRUCTURAL DESIGN ANALYSIS

The canister consists of three parts. As shown in fig. 5.12-1 these parts are designated as (1) forward canister, (2) the midsection and (3) the aft canister. As a unit these three sections comprise the container structure, which must meet all the design requirements.

All structures were designed such that there will be no yielding under design load conditions and no failure under ultimate design load conditions. This includes the transient and steady state loads encountered under the conditions of handling, transportation, sterilization, preflight, powered flight, transit, and separation.

The critical conditions for this structure are shown in table 5.12-1. The critical loading condition for most of this structure is a combined axial acceleration of 6 g's and 2 g's lateral or in 3 g's axial combined with 2 g's lateral (conditions E and F), in addition to the internal pressure loadings (conditions H and I). Inertial loading conditions were determined to be less severe than the internally pressurized condition in the design of the canister and the field joint ring. This can be seen in table 5.12-2 where the running loads on the interface ring are tabulated for both inertial and pressure loading conditions. As a result, the pressure loading condition determined the desired construction, material, and thicknesses to be used in the structural design of both the forward and aft canister.

Minimum sheet gages were the overriding constraint on the thicknesses selected for the canister design. Stiffeners to rigidize the shell for dynamic and ground handling loads may be required. The limit pressure condition for the canister is 1.0 psid internal pressure, and the structure is designed to withstand a 1.7 psid burst pressure, which results in a safety factor of 1.7 on the limit pressure.

The forward canister is a hemispherically-shaped minimum gauge aluminum shell making a tangent at its maximum diameter through a quarter torus section. This structure has been designed to act as a pressure vessel, and the torus section is provided to eliminate the inboard kick loads and minimize shell bending at the field joint ring due to the internal pressure. The minimum gauge, 0.020 in., aluminum material is more than adequate to withstand the pressurization and inertial loads imposed on it. The hemispherical shape has been shown in previous analyses (Voyager Phase B Study) to be considerably stiffer from a dynamic standpoint than a conical shape.

Due to the requirement to maintain biological integrity within the internal portion of the canister, it was necessary to evaluate the effects of an internal pressure on the shape, material and construction of both the forward and aft canisters. Inertial loading of the canister during flight and handling conditions, including equipment loadings on the aft canister, was compared to the differential pressure to determine the more severe loading environment for the aft canister structure.

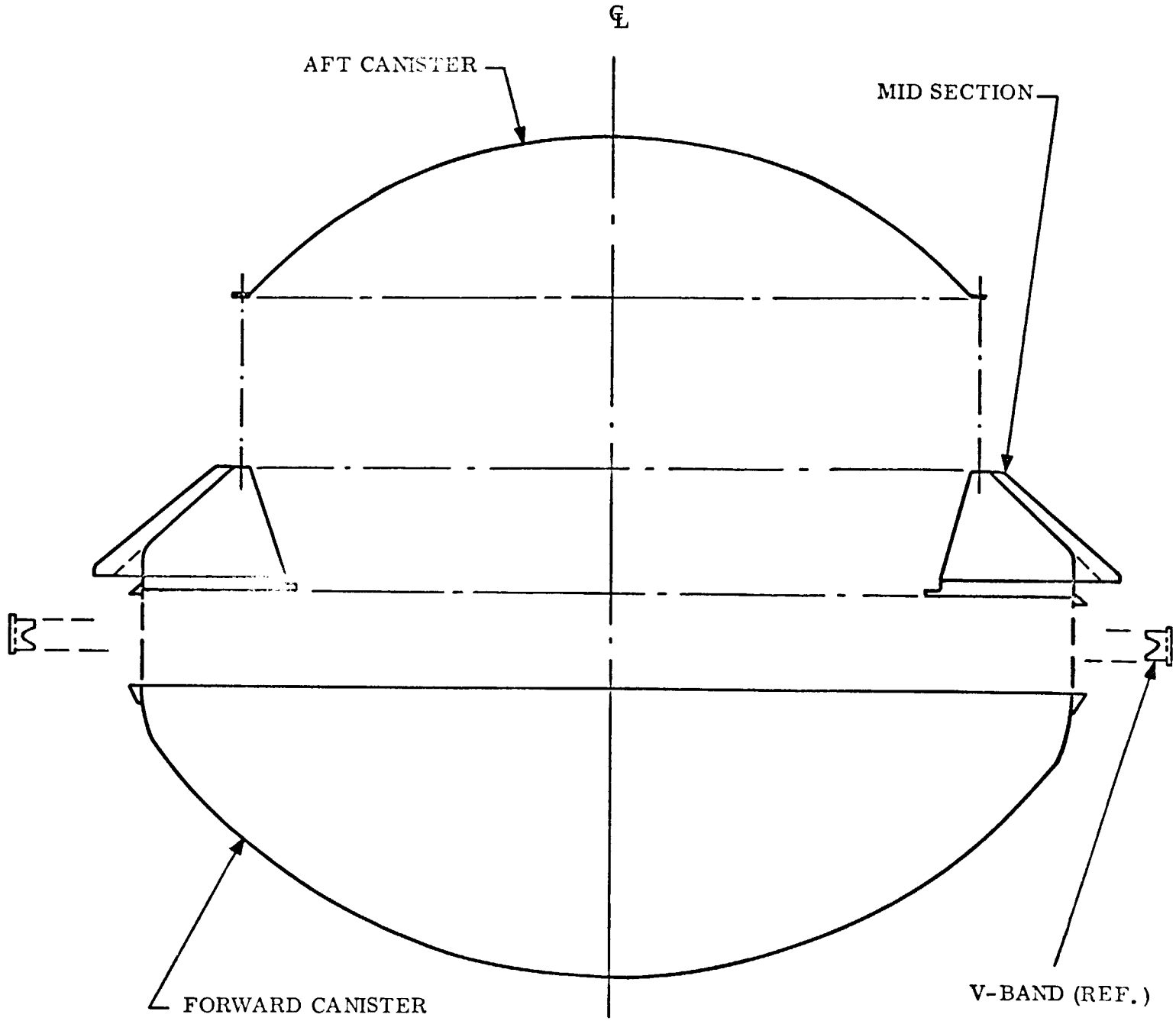

Figure 5.12-1. Sterilization Canister

TABLE 5.12-1. CANISTER/ADAPTER LIMIT DESIGN LOADS

Loading Condition	Accelerations		Notes
	G_X	G_N	
A. Ground Handling	2.0	2.0	
B. Band Clamp	N/A	N/A	48 lb/in.
C. First Stage Burnout	5.2	2.0	
D. Second Stage Burnout	4.0	2.0	
E. Axial Vibration	+6.0 -3.0	—	
F. Lateral Vibration	—	±2.0	
G. Canister Separations	Negligible	Negligible	
H. Canister Pressure	N/A	N/A	ΔP = 0.5 psi at 300°F
I. Canister Pressure	N/A	N/A	ΔP = 1.0 psi maximum at ambient
J. Sterilization	N/A	N/A	300°F soak and 0.5 psi internal pressure in canister (6 cycle-24 hr +3 cycle-96 hr)

A driving influence on the forward canister size was the allowance necessary for clearance between the entry system and canister. The minimum clearance required to allow for Capsule System dynamic excursions has been estimated to be 1.9 in. As shown in fig. 5.12-2, a 2 in. aeroshell/canister clearance was provided.

The field joint rings for the forward canister and the midsection provide a seat for the band clamp, which holds the forward canister to the midsection, resist the loads imposed by the internal pressure and the band clamp, and provide for the pressure tight sealing of the canister assembly. The alternate canister separation joints are discussed in Section 5.13 and the preferred type is shown in fig. 5.12-3.

TABLE 5.12-2. STRUCTURAL ANALYSIS OF FORWARD CANISTER LOADS

Load Condition	N_X Axial Load (lb/in.)
C. First stage burnout	0.94
E. Axial vibration	1.62
H. 0.5 psid pressure 300°F	24.5
I. 1.0 psid pressure 75°F	49.0

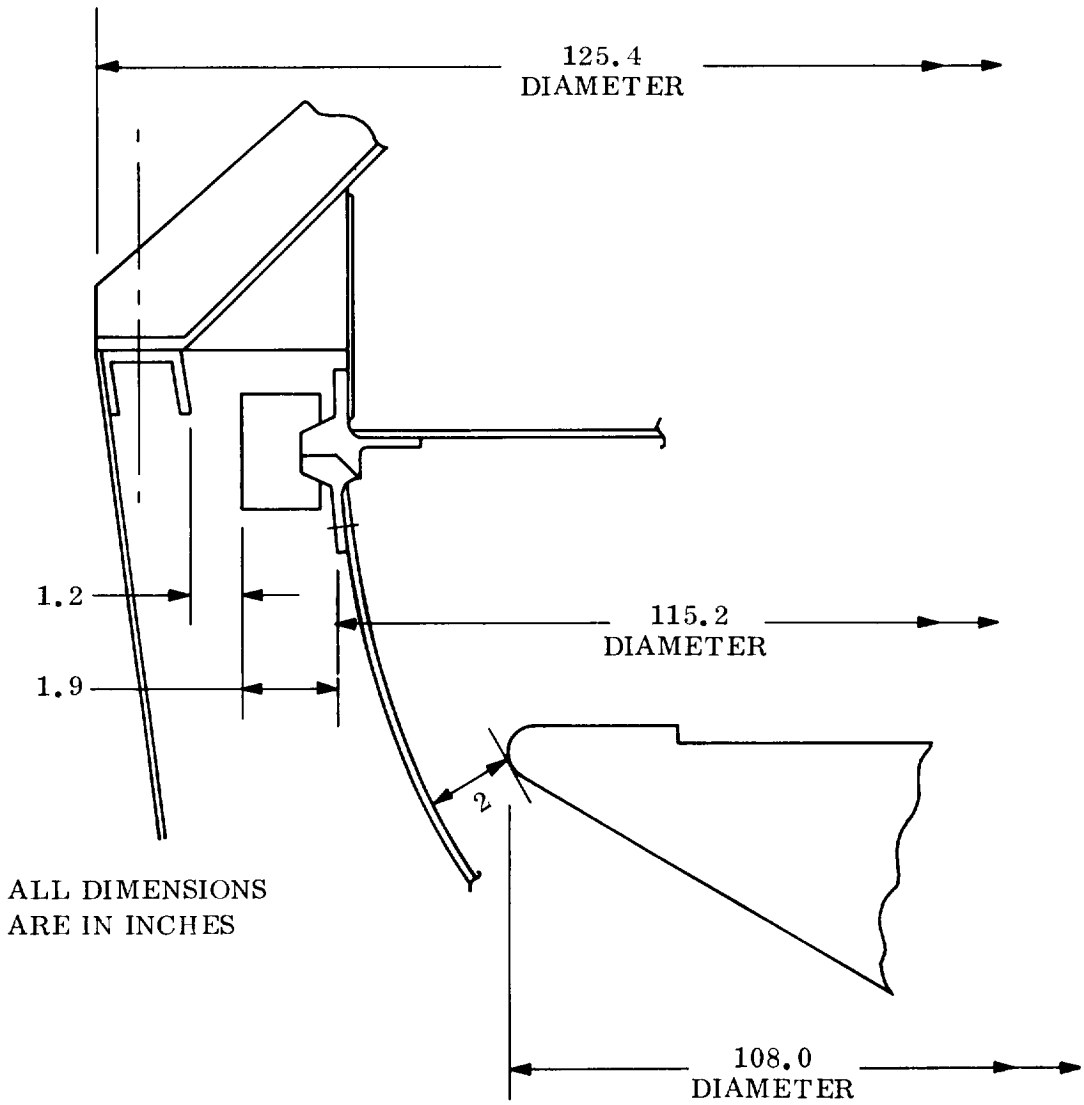

Figure 5.12-2. Aeroshell/Canister Dynamic Excursion Clearance

The combined inertia of the forward ring, aft rings and bulkhead is more than adequate to insure structural stability of the field joint under the critical load condition. Fig. 5.12-4 shows a plot of the required inertias for ring stability as a function of critical load in lb/in.

Structurally, the aft canister is sized for the internal pressure which dictates the same minimum sheet gage, 0.020 in. aluminum, as the forward canister. The aft canister is essentially hemispherically shaped.

The midsection box structure serves both as part of the canister container and, as the load transfer structure between the entry system and the two adapters (Support Module and Transtage). This box structure is so arranged that it has four rings, the aft box ring, the inboard box ring, the outboard box ring and the forward canister separation rings. The canister separation rings act as a single ring in this box structure. The webs between these rings are made of 0.020 in. beaded aluminum construction. Under maximum loading of 6 g's axial and 2 g's lateral, the box structure rotates only 0.2°. The centroid of this box is 2.95 in. aft of the forward surface. The only ring that experiences compressive loads of any magnitude is the aft ring, which develops 7,050 psi compressive stress due to rotation of the box

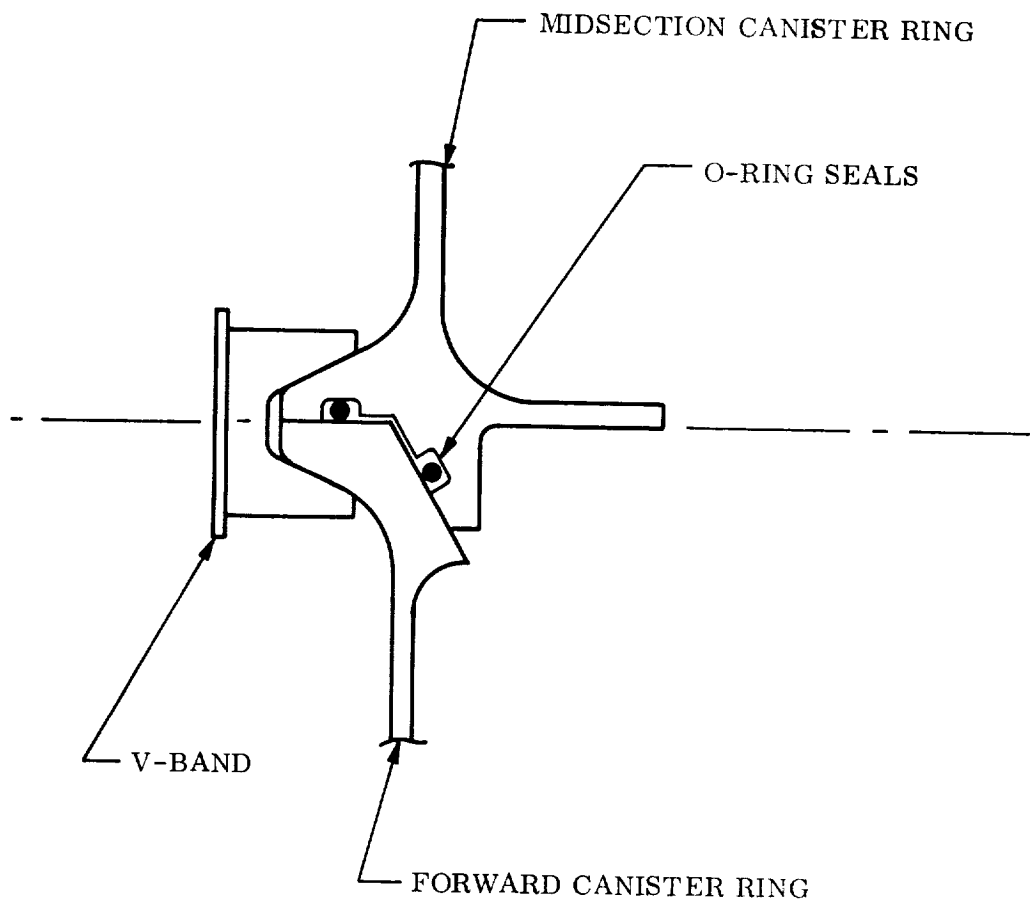

Figure 5.12-3. Canister Separation Joint

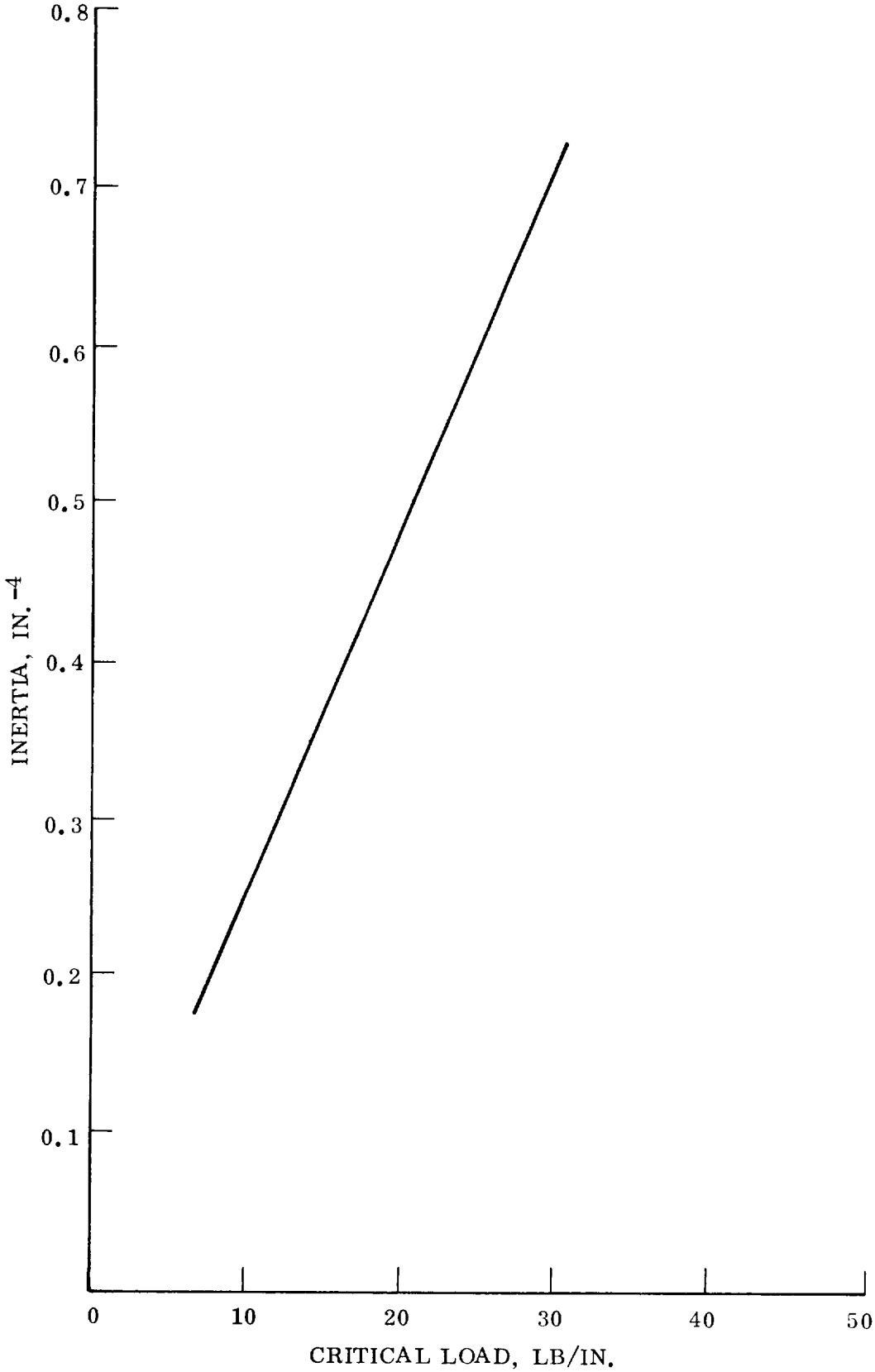

Figure 5.12-4. Required Ring Inertia for Stability as a Function of Critical Load

structure. The box structure is interrupted by eight closing fittings that connect to the entry system and the Support Module adapter. The loads from the aeroshell, the forward canister and the aft canister are transferred through these fittings and all kick loads due to offset are resisted by rotation of this box ring structure. The lateral loads from the entry system tending to induce unsymmetrical twisting of this box structure are very small because the c.g. of the entry system in the axial direction is very close to the adapter/Spacecraft separation plane. This box ring stiffened structure acts as a large ring to help redistribute the lateral loadings from the Support Module adapter into the aft ring of the Spacecraft-to-Transtage Adapter. This ring is tied to the box structure at eight places so they both act to redistribute this loading.

5.12.3 PRESSURE AND VENTING SUBSYSTEM REQUIREMENTS

The basic function of the canister's Pressure and Venting (P&V) Subsystem is to maintain a positive pressure of sterilized gas within the canister, as a deterrent to biological recontamination of the Lander and entry systems from unsterile system elements. The pressurization is designed to be active from Capsule sterilization until final venting prior to canister separation.

A secondary function of the P&V Subsystem, in conjunction with sterilized, ground based make up gas, is amelioration of thermal effects on the Capsule system by reducing the time needed to achieve thermal equilibrium at both the start and finish of sterilization.

During the thermal sterilization process, the P&V Subsystem is required to circulate dry nitrogen gas through the canister. The source of the gas, its input lines to the canister and output lines from the canister, are not part of the P&V Subsystem, but are Operational Support Equipment (OSE). A flow of gas sufficient to provide four changes/hr, at a pressure of 1.0 psig maximum, and at the sterilization temperature, is assumed. (After sterilization, this same sterile gas flows through the canister at a reduced temperature to assist in bringing the canister and its enclosed systems to thermal equilibrium at a lower temperature).

Starting with the sealing of the canister prior to sterilization, the P&V Subsystem is required to maintain a differential positive pressure of gas within the canister of 0.5 psig to 1.0 psig throughout the temperature ranges seen by the canister; ambient, sterilizing temperature, and post sterilization ambient. The sterile gas provided by OSE during sterilization continues to be required after the completion of sterilization to maintain the positive pressure regardless of temperature variations.

The 1.0 psid maximum pressure requirement is set by the canister separation seal design limit. The 0.5 psid minimum pressure requirement is set by the need for a substantial minimum positive pressure to maintain sterility.

After completion of sterilization, the P&V Subsystem is required to maintain the internal canister pressure during Capsule to Support Module mating, incorporation of the shroud, transfer to the launch pad area, booster mating, and pre-launch operations. During this process, the flight system would normally expect to see substantial temperature variations which would result in venting and reduction of gas quantity and pressure. The OSE sterile gas makeup supply should therefore remain connected to the P&V Subsystem throughout this phase of ground operations. This would require that the shroud accommodate the gas umbilical, without breaking the connection. The OSE gas lines would also have to include a shroud-to-Capsule in-flight disconnect which would be incorporated into the shroud-to-Capsule interface. The alternative to this approach is shroud cooling during the pre-launch phase of ground operations, starting with disconnect of the makeup gas prior to shroud installation. The allowable temperature range within the canister would be required to be controlled to a value determined by the temperature of the gas at the final vent valve closure, and corresponding gas pressure. Greater temperature excursions would result in undesirable gas venting from the canister during pre-launch.

During the launch phase, from liftoff until an altitude marked by a substantial vacuum environment, the P&V Subsystem is required to vent the canister gas, maintaining a pressure differential of 0.5 psi to 1.0 psi while the ambient pressure drops from 1.0 atmosphere to 0.0 atmospheres. This is required to be accomplished without auxiliary gas reservoirs.

5.12.4 PRESSURE AND VENTING SUBSYSTEM DESCRIPTION

Fig. 5.12-5 is a functional schematic of the P&V Subsystem in the sterilization configuration. It assumes that the canister would have been purged by placing it in a vacuum chamber and pulling a vacuum. The OSE makeup gas supply shown in the illustration would bring the canister up to 0.5 to 1.0 differential pressure as the vacuum chamber starts to refill, and maintain that differential pressure.

The makeup gas supply and associated OSE are then placed in the sterilization chamber with the canister, the connection being maintained.

The vent valve is used as the exit port during both purge and sterilization. It normally will vent with increase in pressure, but can also be controlled electrically by OSE. This control option permits a greater gas mass flow during both heat up and cool down parts of the sterilization cycle.

The exit port is shaped as a convergent nozzle in order to prevent nozzle flow separation, and thereby minimize the chances of recontamination through the nozzle.

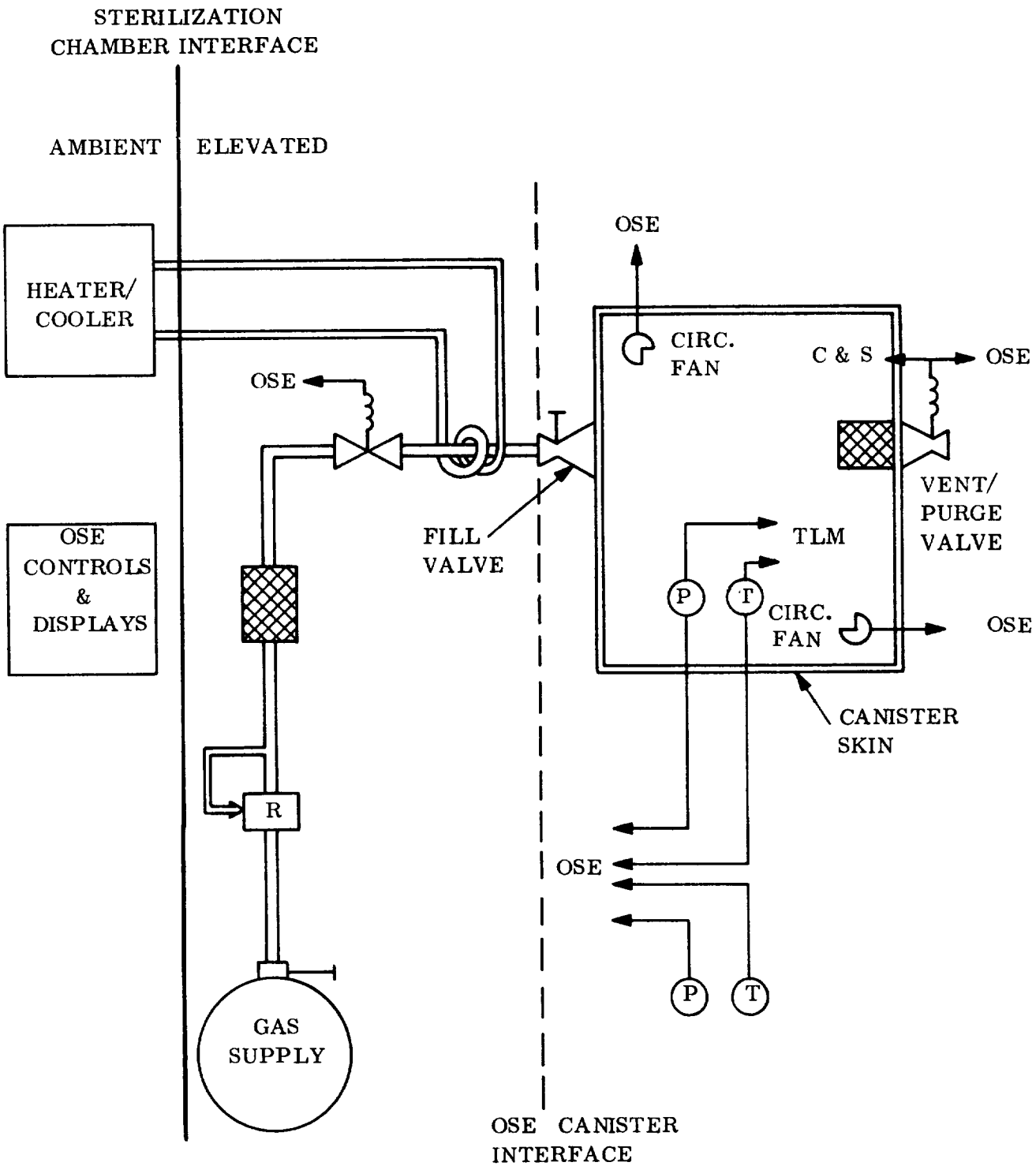

Figure 5.12-5. Pressure and Venting Subsystem, Functional Schematic, Sterilization Configuration

This design, together with the use of biological filters, makes the possibility of recontamination through the nozzle almost nil.

Two fans, which operate only during the sterilization process, are shown. These fans assist in the circulation of hot (or cold) gas within the canister, to decrease the time required to reach thermal equilibrium, and avoid undesirable thermal overstressing of components. An alternate to the fans is internal baffling, within the canister, to direct gas flow. The detailed design configuration of the Lander will determine whether fans or baffles, ducts, etc. will be more efficient.

During the post sterilization ground cycle at the launch site, the canister will be subject to temperature and pressure variations. Some of the major events in this cycle are:

1. Canister/Support Module mating
2. Shroud installation
3. Transport, sterilization facility to Launch Area
4. Mating of Flight Vehicle to Booster
5. Pre-launch and Launch operations.

If the shroud is installed over the mated Support Module and canister in the above sequence, there may be several days during which ambient temperatures and/or pressure variations would cause gas venting, and possibly even negative differential pressure within the canister. Excluding flyaway makeup gas, which is incompatible with a lightweight design, the alternative preventative approaches are:

1. Continued dependence upon an OSE makeup supply of sterilized gas
2. Shroud temperature control
3. Combinations of makeup supply and shroud temperature control.

The approach favored at this time is the combination. The OSE makeup supply of sterilized gas would remain connected to the canister for as long as access remained practicable. This access will probably end with installation and closure of the shroud. Shroud temperature control, which will be highly desirable for the Support Module system, and which may be a Support Module requirement, will be required to prevent canister venting or canister overpressure.

If the canister internal positive pressure is built up to nominal pressure and temperature, shroud thermal control to a $\pm 5^{o}F$ range should prevent reduction of positive pressure during the rest of the ground cycle. Depending upon the internal shroud temperature profile, there may be some canister venting, but little chance that canister positive pressure differential will fall below 0.5 psi. The length of time

during which canister pressure would be maintained by shroud thermal control is dependent upon the closeness to launch of shroud installation and booster mating.

After liftoff, the canister will vent so as to maintain the 0.5 to 1.0 positive pressure, as the external atmospheric pressure falls essentially to zero. This occurs within 2 min. The valve sizing is determined by this time and by the enclosed free gas volume within the canister. Fig. 5.12-6 shows the results of some computed pressure - time profiles for the P&V Subsystem. They are based upon the nominal characteristics of the Titan IIIC vehicle with a 2000 lb payload. The computer program opens the vent on increasing internal pressure and closes it on decreasing internal pressure. Dry nitrogen gas (R = 55.2, K = 1.4, and a volume of 300 ft^3) was used in the computation.

These pressure profiles show that several venting cycles will occur during the first 10 to 12 sec after liftoff. Continuous venting occurs until 90 to 100 sec after liftoff, at which time a final closure of the valve would occur. The profiles indicate that initial canister pressure, and the setting of the valve levels for closing and opening, have little effect on the systems performance after about 10 sec. The number of cycles of operation during the early flight are sensitive to these parameters, and to the actual ambient pressure-time profile.

The pressure profiles show undershoots (below 0.5 psi) at the final valve closing. They also show a pressure fluctuation cycle during the final venting. Neither of these characteristics are expected to occur in the actual flight. The curve fitting technique used to program the Titan IIIC flight characteristics, and other attributes of the computer program, give rise to these indications, which are spurious.

Prior to canister separation, the remaining positive pressure (0.5 to 1.0 psid of N_2 plus outgassing and less leakage) is vented. This is accomplished by command from either the command system or the Computer-Sequencer system, which causes the valve's solenoid to override the springs and hold the valve in the open position.

5.12.4.1 Pressure and Venting Subsystem Components

1. Vent Valve - The preferred design is the use of a single vent valve sized to meet the requirement of 1.0 to 0.5 psi pressure differential. Its required vent area is in the order of 4.0 in^2, set by canister volume, resulting in a 5.72 in^2 circular orifice. The valve is a spring-loaded relief valve with a latching override solenoid and a position indicating switch.

2. Filter - The biological filter prevents bacteria migration into the canister by back flow through the vent valve. The selected filter uses Pall Corporation "Ultipor 0.9" medium. It is sized to entrap 0.3 micron particles and not have a greater pressure drop than 0.1 psi at a flow of 0.53 lb/sec (425 scfm). Its catalog rating is 100 percent removal of 0.08 micron particles from dry air.

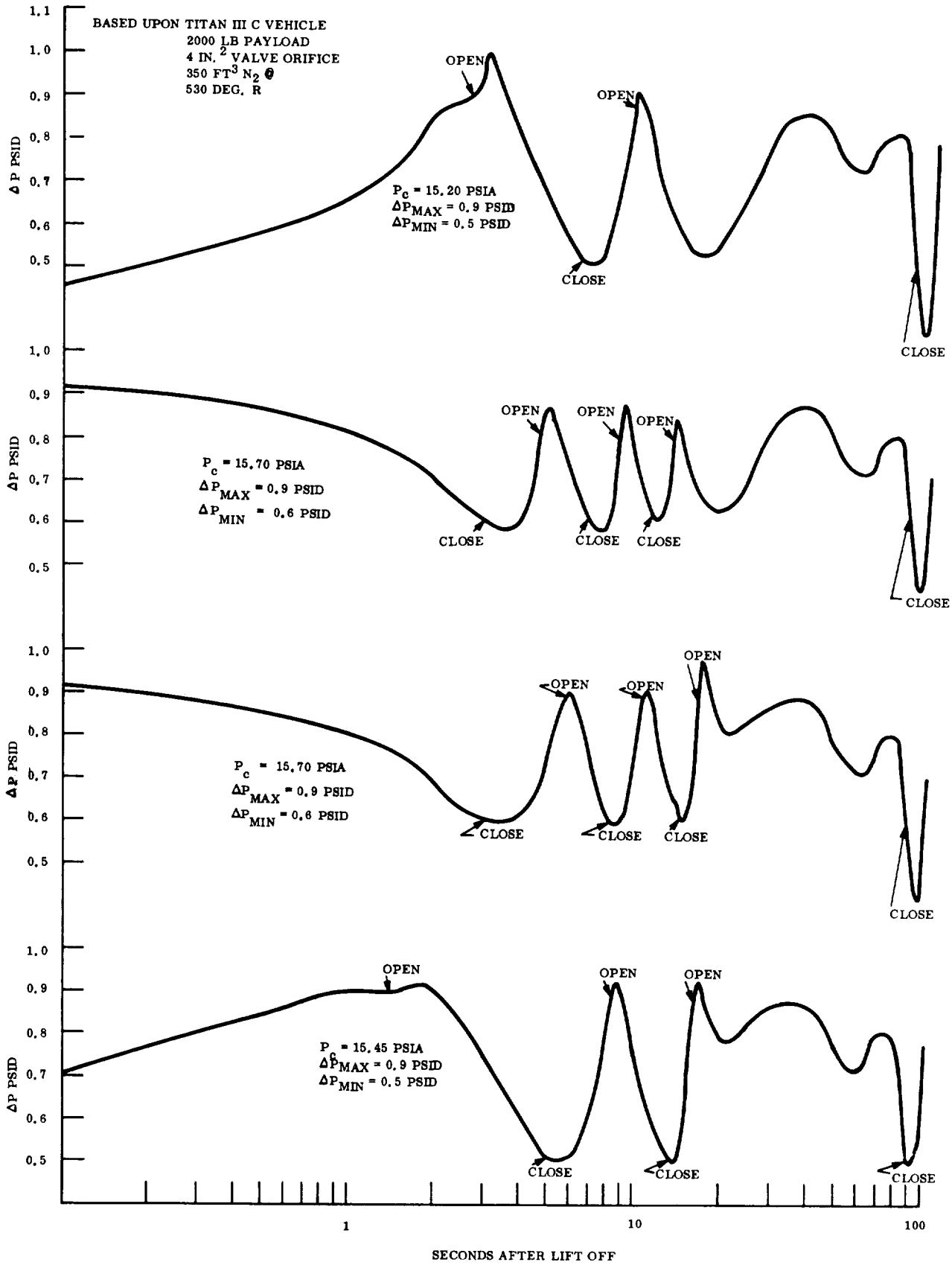

Figure 5.12-6. Pressure-Time Profiles for P&V Subsystem

3. Purge-Fill Valve - The purge-fill valve is a manually operated valve, sized to be compatible with the flow rates and vent valves. It is operated only for the purging and sterilization process. When the OSE makeup gas supply is removed, the valve is closed and remains closed throughout the rest of the mission.

4. Fans - If fans are used, instead of baffles and ducting, for increased circulation during heating up and cooling down operations, two fans, powered and controlled by OSE are expected to provide substantial thermal equalization assistance.

Table 5.12-3 gives the significant parameters of the selected P&V Subsystem components.

TABLE 5.12-3. P&V SUBSYSTEM COMPONENT SUMMARY

Component	No. Required	Baseline	Weight (lb)	Volume (in.^{3})	Power
Vent Valve	1	Sterer P/N 19260	6	84	1.5A, 30 vdc 1/2 sec
Biological Filter	1	Ultipor 0.9	4	45	—
Fill Valve	1	—	2.5	—	—
Fan	2	Rotron Aximax 3	0.8	16.3	400 ~ OSE
Tubing	AR	—	1	—	—
Total			15.3		

5.12.4.2 P&V Subsystem OSE

In addition to the makeup gas supply and associated gas makeup components, a gas heating/cooling system must be kept in the configuration shown in fig. 5.12-5. Its heat exchange must provide direct heating or cooling to the fill line. The heat generator and refrigerator need not be placed within the sterilization chamber.

A panel or rack of OSE components are needed, and should remain connected to the canister's umbilical until the mating with the Support Module. The functions it is required to perform include:

1. Control of vent valve solenoid and indication of its position

2. Pressure and temperature monitoring, inside and outside the canister

3. Gas supply fill valve (OSE) control

4. Power for circulating fans, if used.

The quantity of makeup gas which the OSE would have to provide during the heat up and cool down parts of the sterilization cycle will be dependent upon the thermal characteristics of the Capsule and the heat up/cool down characteristics of the sterilization chamber. It is anticipated that a large quantity of gas will be required.

The quantity of makeup gas needed between the end of sterilization and the installation of a thermally controlled shroud can be estimated:

1. 350 ft^3 gas @ 15.45 ± 0.25 psi, weight = 27.6 lb @ 70°F.

2. Vent valve opens at 1.0 psi, closes at 0.5 psi

3. For a 40°F daily temperature variation, 2.3 lb of gas escape, per day

4. For a daily ambient pressure increase of 1.0 psi, gas must be added, 1.8 lb/cycle.

5.12.5 ADAPTER STRUCTURAL DESIGN REQUIREMENTS

The basic roles of the adapter structure are to:

1. Provide mechanical support for the Spacecraft flight modules.

2. Transmit structural loading from Spacecraft flight modules to the launch vehicle during critical (liftoff and powered) loading conditions.

3. Impart sufficient rigidity to flight modules to preclude both excessive deflection and interaction.

The structural design of the adapters is primarily constrained by flight operation and requirements.

The adapter also provides structural support for testing, shipping and handling of the assembled spacecraft.

5.12.6 ADAPTER STRUCTURAL DESIGN

Spacecraft configuration studies so far have indicated that there will be three basic adapter sections.

1. Spacecraft to Launch Vehicle

2. Flight Capsule to Support Module

3. Entry system to sterilization canister.

Item 3 for this report is considered to be part of the sterilization canister and is discussed in para. 5.12.2.

The selected Capsule Adapter system shown in fig. 5.12-1 requires that part of the sterilization canister be load carrying for the complete Spacecraft.

This load carrying portion of the canister is 14 in. high and is a triangular-shaped torque box structure, supporting the entry Lander system from its inside edge and transmitting the load through torsional restraint to the eight support fittings mounted on the outer surface. This restraint is provided by hoop tension and compression loads in the box rings. The torodial-shaped section is then capped forward and aft by dome-type covers to complete the sterilization canister.

Three adapter concepts for the mounting of the Flight Capsule to the Support Module were considered:

1. The independent canister adapter

2. The fully integrated canister adapter

3. The partially integrated canister adapter.

The partially integrated canister concept was selected, primarily based on the ease of assembly associated with the concept of a separate domed cover (aft portion of the canister), which attaches to a box ring structure which, in turn, interfaces with the spacecraft-to-Launch Vehicle adapter. This domed section can be removed during testing, allowing free access to the complete Lander system.

5.12.6.1 Support Module Adapter

The Support Module adapter is a lightweight "W" truss, extending from the interface ring of the reinforced sterilization ring up to the lower face of the Support Module. It functions to transmit the boost loads from the Support Module to the Flight Capsule support section and to provide mechanical support between the Support Module and Flight Capsule during mission cruise.

The vertical height is approximately 22 in., depending on the final dome height of the aft sterilization canister. The 16 truss tubes of 1-1/2 in. diameter, 0.035 wall aluminum alloy tubes, interface with the Support Module octagon longerons and with the eight "bath tub" fittings, mounted externally around the reinforced sterilization canister. Attachment at each end would be by eight tension shear bolts. If required by a change in mission requirements, a separation joint, similar to the Mariner '69, could be readily incorporated at the Support Module interface.

5.12.6.2 Spacecraft Support Adapter

The adapter functions to transmit boost phase loads from the Spacecraft proper to the launch vehicle (Titan IIIC).

The adapter is a semimonocoque conical frustum, consisting of aluminum alloy skins, two interface rings and an intermediate ring, with eight major longerons running from the transtage interface to the spacecraft separation plane. Electrical and mechanical interfaces are provided at each end of the adapter. The adapter also contains the launch vehicle separation devices.

5.13 SEPARATION

The separation devices and functions can be regarded as a subsystem which accomplishes the sequence of separations shown in fig. 5.13-1. The major separation events in this sequence are:

1. Separation of the two halves of the canister or biobarrier, which have contained the Capsule throughout interplanetary cruise, in a sterile environment.

2. Separation of the Capsule from the aft biobarrier, retained by the Spacecraft, prior to Capsule insertion into a landing trajectory.

3. Separation of the thrust cone, with its used propulsion components, from the entry system, after it has entered into a landing trajectory.

4. Separation of the aeroshell at that point in the entry sequence when the parachute is the principal mode of deceleration.

5. Separation of the Lander system from the parachute, for the final free fall phase of landing.

5.13.1 CANISTER SEPARATION

The selection of the separation design for the canister is governed by the requirements of assembly and sterilization of a large, flexible structure which must maintain a pressure seal. The separation joint must be one that can apply a continuous, distributed force. The candidate separation mechanisms for this type of joint included MDC, primer cord, V-bands, close spaced bolted joints, pyro fuse joint and thermal heat pad.

The canister separation mechanism and the canister seal are a single design problem, and are considered together.

The two halves of the canister constitute a large, awkward body with considerable flexibility. To seal the body and maintain internal pressure, inflatable seal configurations appeared attractive, because of their capability to accomodate mismatch in sealing surfaces, flexure, etc. Inflatable seals were not selected however, as their flexability is obtained through the use of thin membrane cross sections which lose large volumes of gas. Maintenance of the seal, and of canister internal pressure, would require an in-flight gas resevoir.

The use of redundant O-ring seals was selected as the preferred seal. Two silicone O-rings, one forming a face seal, the other a gland seal, with both being contained by a V-band clamp, constitute the preferred seal. The O-rings must be maintained at temperatures above -150°F.

The V-band, in addition to sealing, is part of the canister separation mechanism.

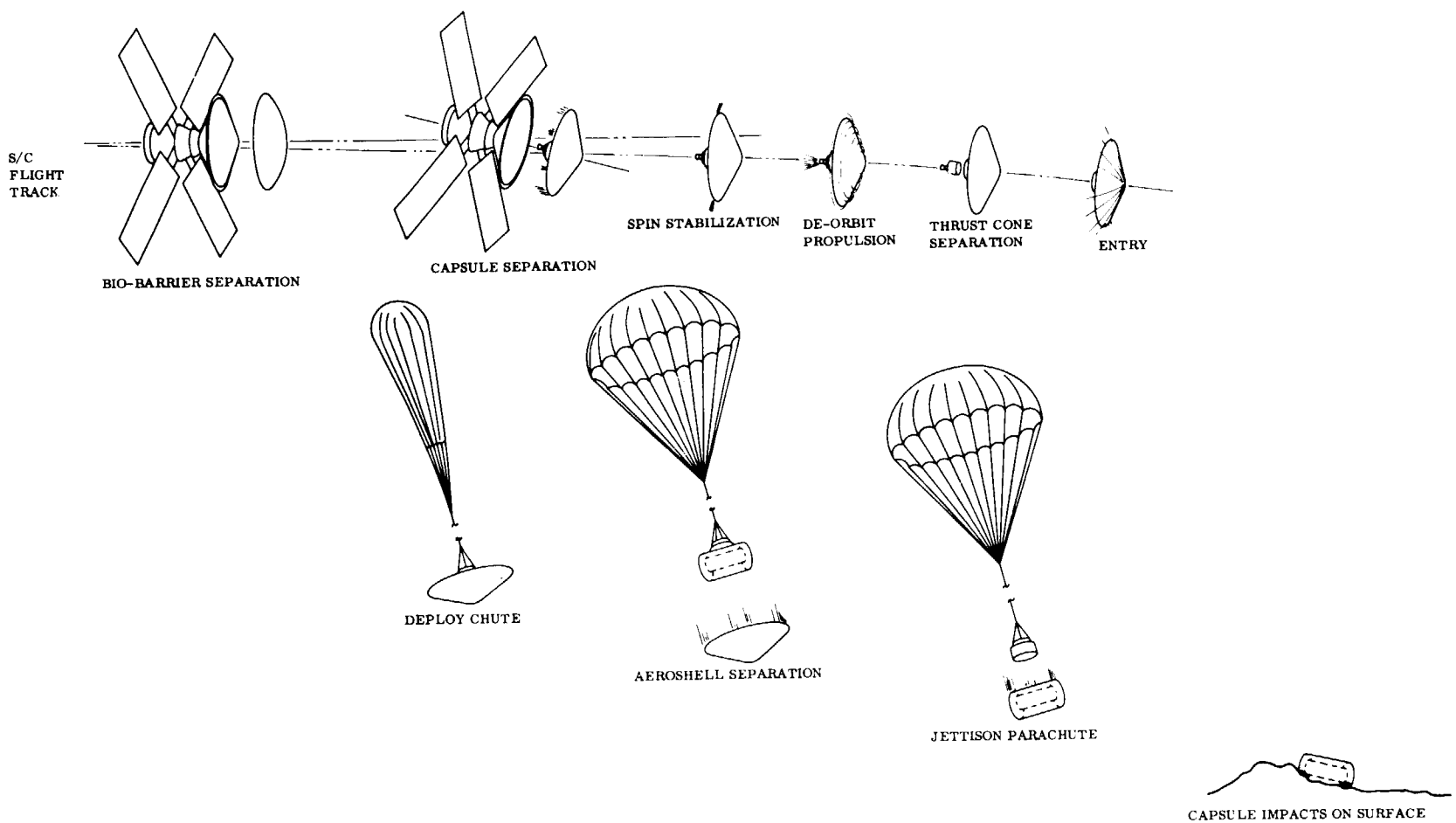

Figure 5.13-1. Sequence of Separation Events

The V-band assembly is made in four segments, with the strap material being 2024T86 Aluminum, 1 in. wide × 0.102 in. thick. The slippers, which are attached to the band by clips, are made of 7075T73 aluminum. The band is preloaded to 3400 lb ± 10 percent in order to sustain all loads, allow for creep during cruise, and allow for tension variations during assembly.

The design of the V-band clamp is determined by canister internal pressure, diameter, O-ring loads, dynamic loads and the ejection springs.

The normal load due to internal pressurization, based upon a 1.0 psid and a 16 ft diameter, is 48 lb/in. of circumference. The force required to compress the O-rings and bring the canister rings into contact is approximately 17 lb/in. circumference, based upon 0.01 in. maximum flatness of the forward canister ring. The dynamic load on the forward canister is given by

$$F_N = \frac{A_x W_c}{\pi D} + \frac{2A_y W_c h}{D^2}$$

where A_x, A_y are booster accelerations, h = vertical height from c.g. of forward canister, W_c = weight of forward canister. It is assumed that the moment load is carried over an arc equal to 1/2 diameter in length.

For $A_x = 5g$, $A_g = 2g$, h = 12 in., W_c = 100 lb and D = 16 ft, $F_N \simeq 1$ lb/in. circumference, which is negligible.

The spring load is also negligible, approximately 0.1 lb/in., making the total load approximately 68 lb/in. of circumference. This normal load, with allowance made for creep, indicates that the band can be fabricated from 0.102 in. stock, which is a standard stock.

The V-band segments are held in tension by four hot-wire bolt assemblies. The choice of four points for attaching and torquing was made to maintain nearly uniform tension on the entire band and to facilitate band disengagement. When the hot-wire bolts separate (a single bolt separation will suffice) the four V-band segments will release, allowing springs to separate the canister. The clamp segments remain tethered to the aft canister, as the forward canister is ejected.

The hot-wire separation devices, nuts or bolts, are a GE-RS development.

A sketch of a hot-wire separation nut is given in fig. 5.1.3.1-1. The two separable bodies are held together in tension by segmented tension links. These are double cross-hatched in the figure. The tension segments are held to the two studs (one for each of the bodies which will separate) by several turns of wire. When a high level current is applied, the wire burns free and the segmented tension links fly outward. The two bodies are then free to separate. Springs can then force body "A" and body "B" apart, with a predetermined force.

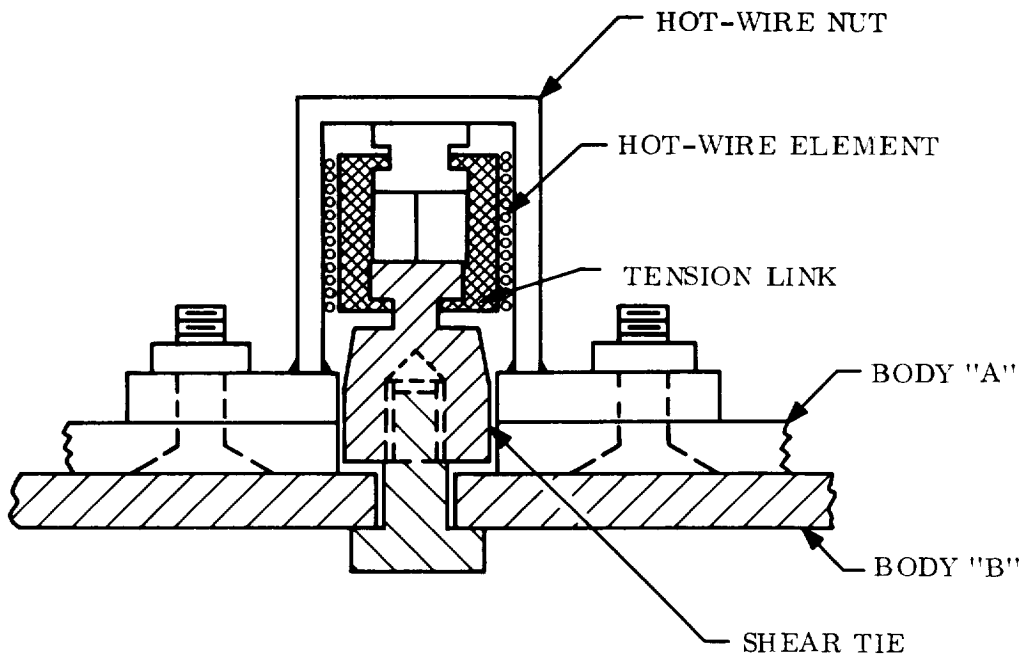

-CROSS HATCHED PARTS REMAIN TOGETHER AT SEPARATION

-SHEAR TIE ADAPTER IS PART OF NUT ASSEMBLY INITIALLY

Figure 5.13.1-1. Hot-wire Separation Nut

This method of separation is preferred to electro explosive devices because of its ease of test and fabrication oriented handling. The response times of these hot-wire nuts are short, 5 msec being the nominal duration of firing current. No debris is involved in the operation, as the tension segments are retained.

The bolt configuration of the device, used to separate the V-band, has the outlines shown in fig. 5.13.1-2.

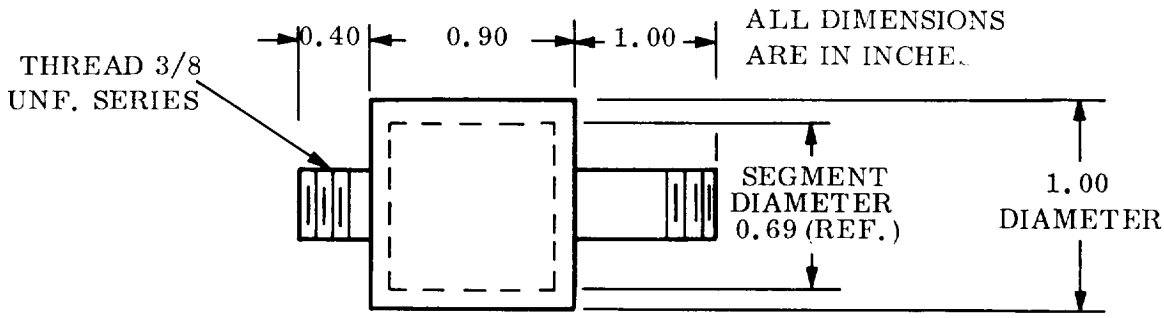

Figure 5.13.1-2. Hot-wire Tension Bolt

The debris from the hot-wire, and the released tension segments are contained within the bolt body, after separation. The hot-wire element consists of nine turns of 0.014 in. diameter 302 stainless. The ultimate load capacity, in tension, in 8,000 lb.

The canister is ejected by two helical coil compression spring assemblies, retained in the aft canister. They provide a force of 35 lb to the forward canister, imparting a velocity of 2.5 ± 0.25 fps, at a tip-off rate of less than 2°/sec.

5.13.2 CAPSULE SEPARATION

The Capsule is retained by the aft canister, through use of eight captive hot-wire nuts. One nut was chosen for each of the eight structure pickup points.

Ejection of the Capsule is accomplished by four spring assemblies. The most significant design requirement of this separation is the confinement of Capsule tip-off rate to an acceptable value. The worst case tip-off rate has been calculated to be 0.29°/sec about any transverse axis. This worst case calculation is compatable with the 0.5°/sec maximum tolerable tip-off rate imposed by the analysis of the mission.

A worst case spring eccentricity error and c.g. offset of 0.12 in. is assumed. Then

$Tt = IW$ where $t = \frac{\pi}{2 \quad K/M}$ and $T = 0.7\ T_{max}$.

$F_{max} = 100$ lb, $F_{min} = 96$ lb, $K = 75$ lb/in. per spring

$M_c = 1100$ lb, $I_c = 106$ slug-ft^2

$M_o = 810$ lb, $I_o = 131$ slug-ft^2

For four springs on an 88 in. circle, opposed pairs loaded to ± 2 lb, with spring constant of 75 lb/in., the maximum tip-off rate is 0.52°/sec, total, of which 0.29°/sec is imparted to the Capsule.

Fig. 5.13.2-1 shows the correction factor to be applied to tip-off rate, as Support Module to Capsule mass ratio is changed. Tip-off to the Capsule also varies inversely as the transverse moment of inertia.

5.13.3 THRUST CONE SEPARATION

The thrust cone is separated from the entry system by the actuation of three hot-wire bolts which hold it to the entry system. It is ejected by two captive spring assemblies which impart a relative velocity of the order of 2.5 fps.

5.13.4 AEROSHELL SEPARATION

The aeroshell is separated from the Lander (parachute deployed) by actuation of three hot-wire bolts which hold it to the Lander. The tension and spring of the parachute shroud lines will assure that the aeroshell falls away from the descending Lander and parachute.

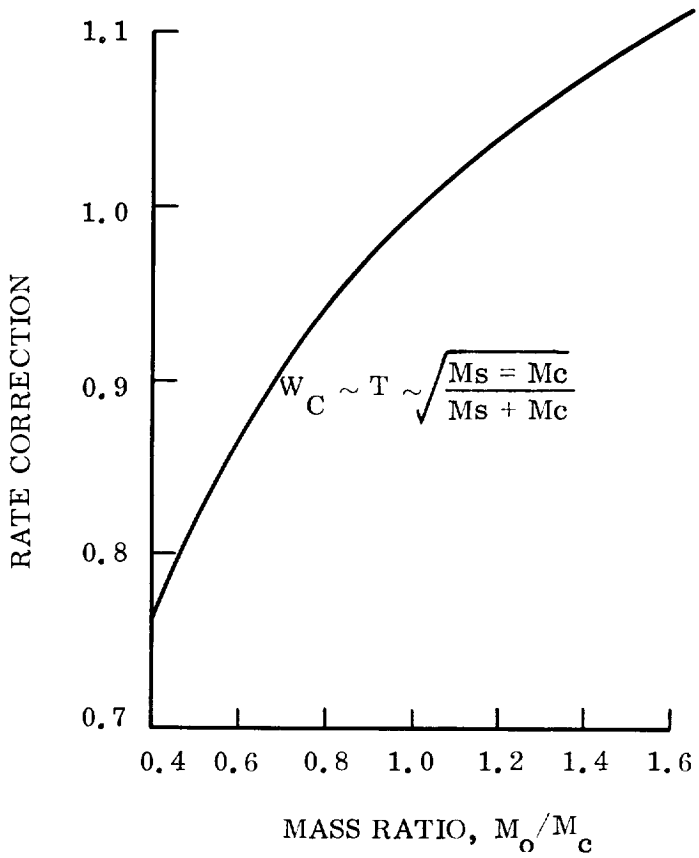

Figure 5.13.2-1. Correction to Capsule Tip-off Rate as a Function of Support Module to Capsule Mass Ratio

5.13.5 PARACHUTE SEPARATION

The parachute is separated from the Lander by actuating the three hot-wire nuts by which it is affixed to the Lander. Gravity pulls the Lander away from the separated parachute assembly.

5.13.6 SEPARATION COMPONENTS

Table 5.13.6-1 summarizes the components used to effect the separations. Weights are given in the weight summary section of this report.

5.13.6.1 Hot-Wire Bolts and Hot-Wire Nuts

These are based on Bruceton sensitivity analysis performed on the pin pullers described below, where 6 amps give a 0.995 probability with a 90% confidence of firing within 10 msec at room temperature. A firing pulse of 6 amps minimum for 30 msec provides a safety margin. Where simultaneous function is critical, such as Capsule and parachute separation, a firing current of twice the A.F. current is estimated to give simultaneity within 0.002 msec.

The hot-wire design is based on a miniature pin puller (20-200 lb capacity) used to operate electrical, inflight disconnects. The pin puller has been qualified and flown by GE-RS. The proposed tension bolt uses the same hot-wire, with identical break point configuration as the flight qualified pin puller.

TABLE 5.13.6-1. SEPARATION MECHANISM SUMMARY

Separating	Components	Retention Elements	Initiation Elements	Propulsive Elements	Remarks
Aft Canister	Forward Canister	V-band clamp and double O-ring seal	Hot-wire bolts (4) 24A, 30 msec	Springs (2) V = 2.5 ± 0.3 fps	Clamp remains with aft canister and flyby
Capsule	Aft canister and Support Module	Hot-wire nuts (8) 96A, 30 msec	-	Spring assemblies (4) V = 1.5 ± 2.5 fps	IFD's between Capsule and Support Module
Entry System	Thrust Cone	Hot-wire bolts (3) 24A, 30 msec	-	Spring assemblies (2) V = 1.0 fps minimum	IFD between thrust cone and entry system
Lander (Parachute deployed)	Aeroshell	(8) Hot-wire bolts (3) 18A, 30 msec	-	Parachute drag and shroud line tension	IFD Lander to aeroshell
Lander	Parachute Assembly	Hot-wire nuts (3) 12A, 30 msec	-	Gravity	-

5.13.6.2 Spring Assemblies

The spring assemblies used for ejection are adjustable, captive assemblies. In the case of Capsule ejection, each of the four assemblies exert a 98 lb force, with a working stroke of 1 in. This assembly is shown in fig. 5.13.6-1

The spring assembly provides for adjustment of initial load; for adjustment of total stroke, retains the spring at the end of the stroke and provides a locating pilot. The inner sleeve is coated with teflon on both inner and outer surfaces to reduce friction. Operation of the spring over the inner 80 percent of its total possible stroke assures nearly constant spring rate.

Table 5.13.6-2 summarizes the spring assembly data for each of the separations using springs for ejection.

TABLE 5.13.6-2. SPRING DATA

	Canister Separation	Capsule Separation	Thrust Cone Separation
Wire diameter (in.)	0.107	0.143	0.107
Mean coil diameter (in.)	1.07	1.034	1.07
Number of springs	2	4	2
Compressed length (in.)	1.29	2.49	1.29
Solid height (in.)	1.09	2.19	1.09
Free length (in.)	3.29	3.79	3.29
Total weight (lb)	0.17	0.80	0.17
Number of active coils	8.4	12.7	8.4
Stress (lb/in.^{2})	90,000	110,000	90,000
Nominal ΔV (fps)	2.5	1.5	2.5

The inflight disconnects will be electrically actuated rather than mechanically actuated. The IFD will be timed to disconnect prior to actuating the separation device. This eliminates tip-off from electrical disconnects.

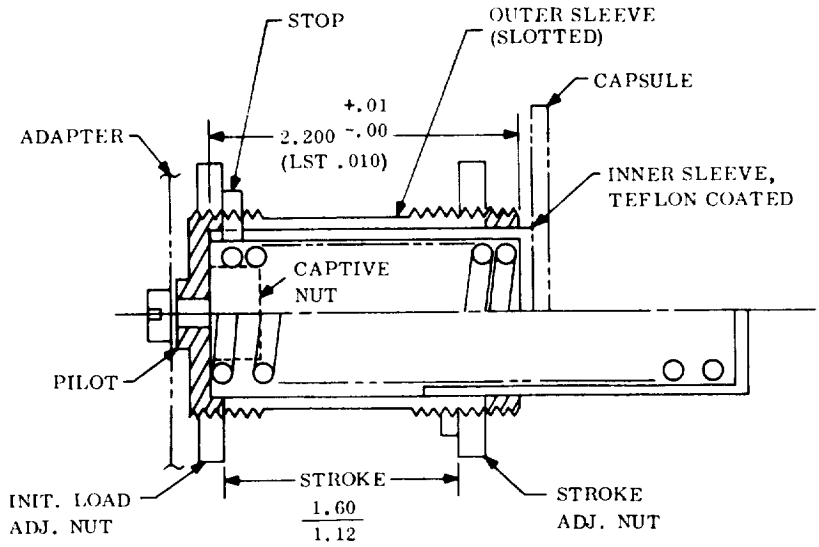

SPRING DATA

WIRE DIA	-	.148"
O. D.	-	1.034"
SPS. CONST	-	75 #/IN
TOT. TURNS	-	14.7
MAX. LOAD	-	120 #
NOM. LOAD	-	108 #
LS	-	2.19 #
LF	-	3.79"
NOM. STROKE	-	1.00"

MAT. - AL-AL WT. - SPRING - .20 #
MECH. - .35 #

Figure 5.13.6-1. Spring Assembly

6. SUPPORT MODULE SUBSYSTEMS

6. SUPPORT MODULE SUBSYSTEMS

The Support Module for the '73 Mars Mission was described in summary form in Section 4. This section describes in further detail the significant subsystems contained in the Support Module with emphasis on the changes required to the Mariner Spacecraft to satisfy the Support Module function.

6.1 ENGINEERING MECHANICS

The Support Module Engineering Mechanics consists of five subsystems which are: Structure, Temperature Control, Mechanical Devices, Pyrotechnic, and Cabling. Each of these subsystems is briefly described using the respective Mariner '69 Subsystem as a baseline. The descriptions include modifications or changes, including weights, required for either a flyby or orbiting mode Support Module.

6.1.1 STRUCTURE SUBSYSTEM

The basic requirements of the Structure Subsystem are:

1. To structurally integrate, within its allocated weight, those subsystems which comprise a functioning spacecraft;

2. To provide mechanical support and alignment for all flight equipment;

3. To transmit structural loadings on flight equipment to the launch vehicle during critical loading conditions;

4. To provide Spacecraft compatibility both with the allowable space envelope and with the launch vehicle;

5. To impart sufficient rigidity to deployed appendage structures (e.g., maneuver and low gain antennas) to preclude both excessive deflection and deleterious interactions with the Spacecraft Control Subsystem.

The structural design of the Spacecraft is primarily controlled by flight operations and mission requirements. The Structure Subsystem also provides a means for testing, shipping, and handling the assembled vehicle. The mechanical configuration for the Support Module is shown in fig. 4.1-1.

The primary structure is the Mariner '69 structure which requires some modification. It consists of an octagonal compartment approximately 54.5 in. across the diagonal and 18 in. high. Of the eight electronic bays available, three will not be used because of deletion of the science package, planet scan experiment, and remounting the Propulsion Subsystem on the roll axis. The planet scan platform and its structure has been removed from the lower side of the octagon. The Propulsion Subsystem is mounted on the roll axis and is supported by a series of struts attached to the upper and lower rings of the octagon in 16 places, 8 on the

upper ring and 8 on the lower ring. The deployable solar array can be replaced by a fixed solar array consisting of 12 panels. It would provide the 50 ft^2 of solar array required and cover approximately 270°. The other 90° is cut out for the high gain antenna. The two attitude control gas assemblies have their gas supply and regulators mounted on the top ring of the octagon with the gas jets mounted on the outer edge of the solar array. The required plumbing between the jets and manifolds attaches to the octagon and solar array structure.

The high gain antenna is mounted in a fixed position on the outside of the octagon by a superstructure. The low gain and maneuvering antennas are deployable and are so mounted as to clear the solar array when deployed.

The V-band separation joint used on Mariner '69 has been replaced in favor of an 8-point bolt attachment at the Capsule to Support Module adapter interface.

The anticipated weight savings for the above modifications amount to 44 lb, or from 203 down to 159 lb. The same structure will be used for both the flyby and orbital modes.

6.1.2 TEMPERATURE CONTROL SUBSYSTEM

The prime function of the Temperature Control Subsystem is to maintain all Support Module equipment within specified temperature limits for the life of the mission. Its purpose is to enhance and maintain operational reliability. Thermal control is accomplished through the use of thermally actuated louver assemblies, thermal blanket, selected surface coatings and finishes, and electric heaters.

Thermal design of the Support Module is based on the concept of temperature control by regulating the quantity of rejected heat from an insulated enclosure. The insulated vehicle surface serves as the enclosure while the active control louver system provides the regulated heat rejection. Power systems will be in operation throughout the flight. A portion of the dissipated power will be used to maintain internal equipment at their desirable operating temperatures. Excess heat will be rejected from the Spacecraft primarily through the louver systems.

The Temperature Control Subsystem is the same as that on Mariner '69 with the exception of planet scan and science subsystems, which have been eliminated. The weight of the subsystem is therefore reduced 3 lb, down to 26 lb.

6.1.3 MECHANICAL DEVICES SUBSYSTEM

The Support Module Mechanical Devices Subsystem is similar to Mariner '69 but, because of a reduction in the deployable appendages, the quantity of devices required is reduced. The subsystem includes provisions for spacecraft-to-booster separation, separation-initiated switching functions such as pyro-arming and sequencer time initialization, maneuvering antenna deployment, and low gain antenna deployment. These devices are required for both the flyby and orbiting modes of the Support Module.

The orbiting mode, in addition to the devices already listed, requires separation mechanics for jettisoning the canister afterbody and Support Module adapter from the Support Module prior to orbit insertion, and requires two linear electromechanical actuators for engine gimballing.

The weight of the Mechanical Devices Subsystem for the flyby Support Module is reduced from a Mariner '69 weight of 63.1 lb to approximately 11.1 lb with the deletion of deployable solar panels, the deployable high gain antenna, and the planet scan platform. The orbital mode Support Module devices will weigh approximately 16.3 lb.

6.1.4 PYROTECHNIC SUBSYSTEM

The Pyrotechnic Subsystem is involved in the performance of the Spacecraft separation maneuver, the Capsule separation maneuver, and the propulsion maneuvers. It consists of squib actuation release devices for separation, squib actuated normally open and normally closed valves in the Propulsion Subsystem, and two identical pyrotechnic controllers.

The two identical electronic controllers redundantly perform the functions of energy storage, command control, and energy switching to fire squibs. The pyrotechnic mechanical devices initiated by the pyrotechnic controllers have two redundant single bridgewire squibs (pin pullers) or a single squib with two redundant bridgewires (valves). The pyrotechnic controllers redundantly initiate all pyromechanical devices.

The Pyrotechnic Subsystem differs from the Mariner '69 as follows:

1. Pin pullers are not required for deployable solar panels.

2. Pyrotechnics associated with the planet scan system are deleted.

3. Separation pyrotechnics are added due to the additional requirement for Capsule separation.

4. Additional squib actuated valves are required in the Orbiting Support Module for the bi-propellant Propulsion Subsystem.

These changes result in no weight change to the 11 lb Mariner '69 Pyrotechnic Subsystem for the orbital mode and a 1 lb reduction to 10 lb for the flyby mode.

6.1.5 CABLING SUBSYSTEM

The Cabling Subsystem electrically interconnects the various electronic assemblies and subsystems of the Support Module. The weight of cabling required is reduced approximately 10 lb over that required for Mariner '69. The reason, of course, is the deletion of all science, the planet scan system, and the deployable solar panels. The new weight for the Cabling Subsystem is 57.9 lb.

6.2 PROPULSION SUBSYSTEM

6.2.1 REQUIREMENTS

The Propulsion Subsystem must provide the impulse for imparting velocity increments to the vehicle for maneuvers as follows:

1. 50 meters/sec to the vehicle initially weighing 2500 lb (including propulsion) for mid-course trajectory corrections. This requirement is for both the flyby and orbital modes.

2. 1300 meters/sec to a 500 lb payload (less propulsion) for orbit insertion and 100 meters/sec for orbit trim for the orbital model only.

6.2.2 FUNCTIONAL DESCRIPTION

6.2.2.1 Flyby Mode

The Propulsion Subsystem for the Flyby Support Module is the same as the Mariner '69 Propulsion Subsystem except for increased tankage requirements and the structural arrangement. The mission described here requires two approximately 12-in. diameter tanks to contain 53 lb of hydrazine propellant, an increase of about 31 lb over the propellant required for Mariner'69. The Mariner '69 Propulsion Subsystem was designed by JPL as a completely modular unit; however, due to the requirements of the Support Module, structural and mounting provisions will change.

The Mariner '69 Propulsion Subsystem, as modified for this mission, is schematically shown in fig. 6.2.2-1. High pressure nitrogen is regulated down to 308 psia feeding propellant from the propellant tanks to the rocket engine. Propellant and pressurant on/off flow control is accomplished with multiple start and stop explosive valves. The propellant tanks contain butyl rubber bladders for positive expulsion. The thrust chamber assembly contains Shell 405 catalyst for spontaneous ignition and sustained decomposition of the hydrazine. Four jet vanes included in the thrust vector control assembly are located at the exit plane of the nozzle and are used to provide roll, pitch, and yaw control during the engine burn sequence. A weight breakdown is presented in table 6.2.2-1.

6.2.2.2 Orbital Mode

The Orbital Support Module Propulsion Subsystem is a modular assembly consisting of the following subassemblies: pressurant storage, pressurant control, propellant storage, propellant control, thrust chamber, and structure. A schematic diagram is shown in fig. 6.2.2-2 and a weight breakdown is presented in table 6.2.2-1.

The helium pressurant is stored in two spherical 6 Al-4V tanks. Pressurant control is provided by explosive valves for the operation and isolation functions, respectively. Redundant regulators connected via a pressure sensing and switching network are used to provide pressurant gas to the propellant tanks at constant pressure.

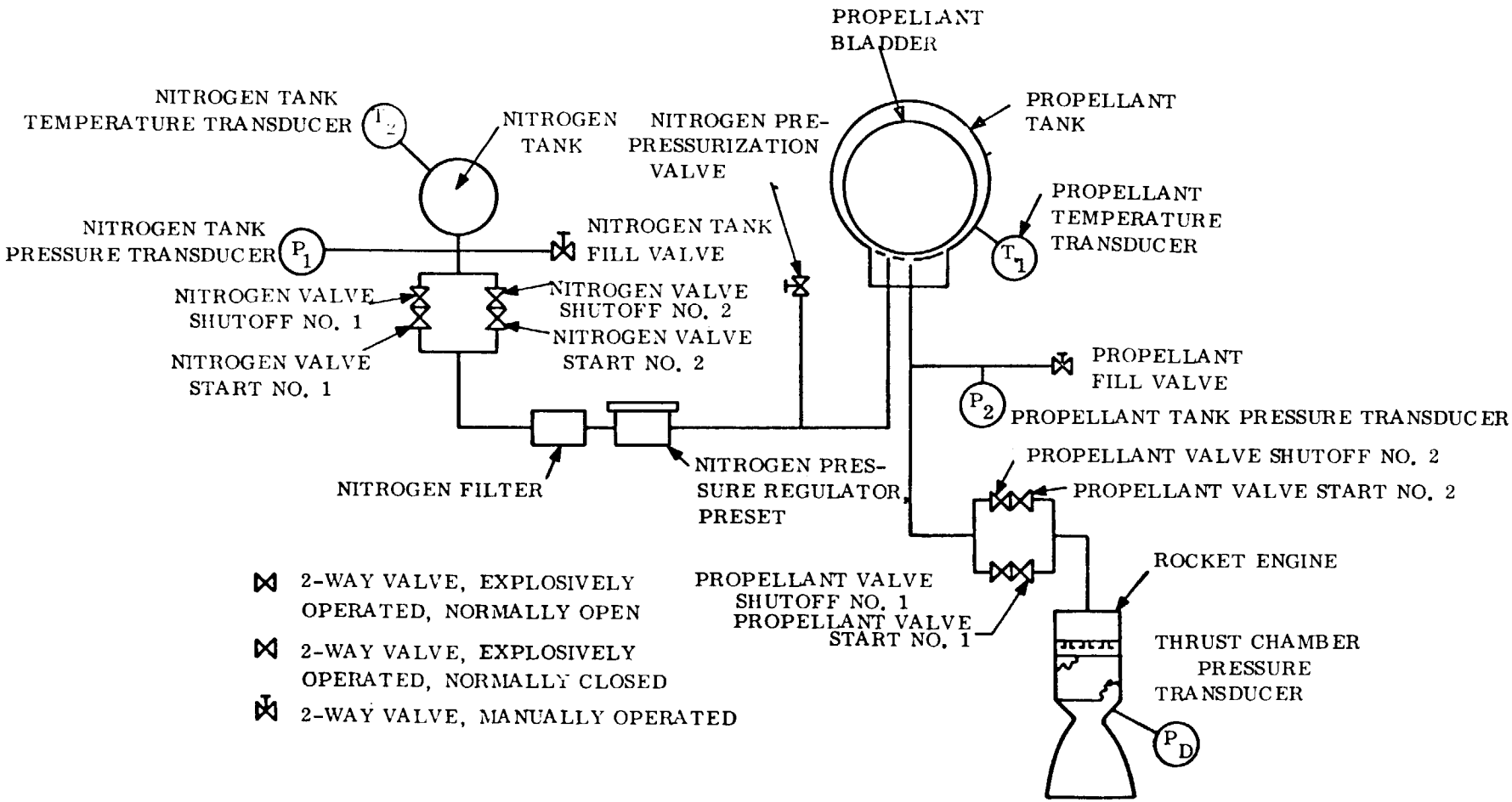

Figure 6.2.2-1. MM '69 Propulsion Subsystem Schematic

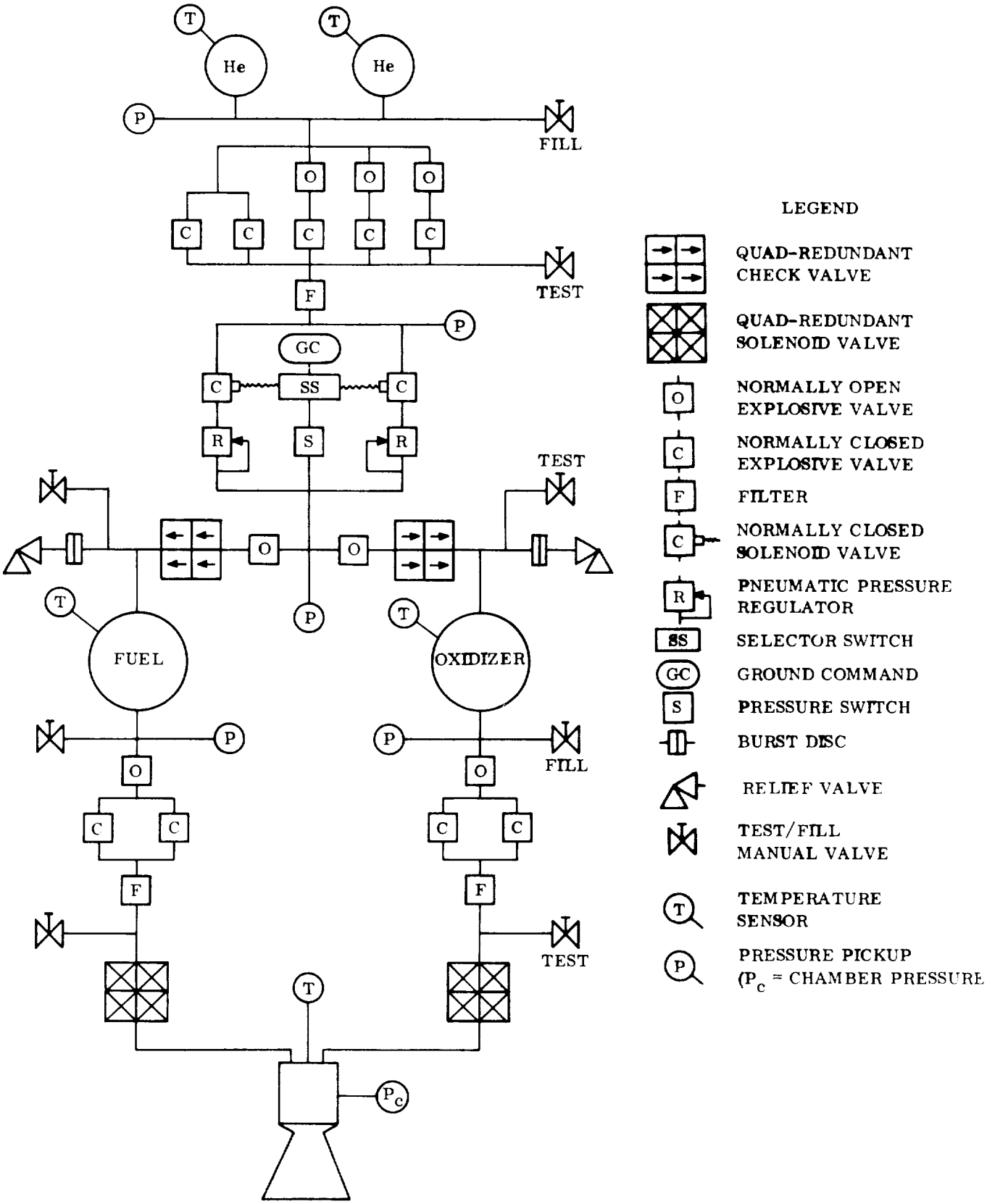

Figure 6.2.2-2. Orbiting Support Module Propulsion Subsystem Schematic

TABLE 6.2.2-1. PROPULSION SUBSYSTEM WEIGHT BREAKDOWN

	Flyby Mode		Orbital Mode	
Propellant Weight, lbm		53		428
Mid-course	53		44	
Orbit Insertion	—		364	
Orbit Trim	—		20	
Inert Weight, lbm		29		137
Structure	3.8		17.8	
Propellant Tanks	4.2		22.8	
Pressurant Tanks	5.1		31.6	
Fixed Weight (1)	14.1		49.1	
Residuals (2)	2.1		15.8	
Total Propulsion Subsystem Weight, lbm		82		565

(1) Includes thrust chamber, valves, regulators, etc.
(2) Both pressurant and propellant

The Propellant Storage Subassembly consists of two spherical 6A14V titanium tanks, one fuel and one oxidizer, each containing a teflon/aluminum laminate bladder for propellant expulsion and propellant-pressurization gas separation. Propellant control is provided by solenoid and explosive valves for the operation and isolation functions. Use of series-parallel and quad-redundant networks provides assurance of valve opening or isolation of the pressurant or propellant control subassemblies as desired.

The thrust chamber assembly is the Rocketdyne RS 14 bi-propellant engine providing a thrust of 316 lbf. It uses the space storable propellants nitrogen tetroxide (N_2O_4) and mono-methylhydrazine (MMH). Performance data for the RS 14 engine is summarized in table 6.2.2-2. The RS 14 is gimballed to provide pitch and yaw control during engine burn sequences.

The Propulsion Subsystem structure supports all elements of the subsystem in a modular assembly.

6.2.3 COMPARISON TO MARINER '69

6.2.3.1 Flyby Mode

The Flyby Mode Propulsion Subsystem was compared to the Mariner '69 earlier in this section of the report.

TABLE 6.2.2-2. RS 14 ENGINE DATA SUMMARY

Thrust, lbf	316
Specific Impulse, lbf-sec/lbm	288
Minimum Impulse Bit, lbf-sec	12.6
Chamber Pressure, psia	125
Mixture Ratio (oxidizer/fuel)	1.6:1
Propellants (oxidizer/fuel)	N_2O_4/MMH
Expansion Ratio	30:1

6.2.3.2 Orbital Mode

The Propulsion Subsystem for the Orbiting Support Module described above is essentially the same as described in GE report "Mariner Mars '71 Baseline Description", document 68SD4238, dated 1 April 1968 and revised 15 June 1968. The major difference is in the selection of the RS 14 engine for this system rather than the Marquardt 100 lb thrust R4D engine. The referenced report also summarizes the differences between the Mariner '69 and '71 Propulsion Subsystems, or in other words, the Mariner '69 and the subsystem described herein. It is very evident that little similarity exists between the two because of the orbital capability requirement.

The RS 14 engine was chosen for this application because:

1. The total impulse requirement for this mission is more than 23 times that required for Mariner '69, i.e., 5000 lbf-sec to 117,000 lbf-sec.

2. The referenced report indicated a thrust level in excess of 200 lb was required to accommodate gravity losses.

3. The engine will be flight proven on the Mariner '71 vehicle.

6.3 GUIDANCE AND CONTROL SUBSYSTEM

6.3.1 CENTRAL COMPUTER AND SEQUENCER

6.3.1.1 Functional Description

The Support Module is capable of a high degree of automatic control. Supplemental control by ground command is included as necessary for some functions, and in others it is provided as a backup alternative to automatic control. The Central Computer and Sequencer (CC&S) described in this section provides the automatic control.

The CC&S is a cycled, special purpose, digital data processor, which generates and distributes the on-board commands necessary for the Spacecraft to perform its mission automatically. Except for certain optional functions described herein, the CC&S obviates the need for ground command provided that (1) the flight is nominal (all systems are functioning as expected), and (2) trajectory corrections, instrument calibration, and alteration of time dependent or trajectory dependent sequences are not required. All commands from the CC&S to using subsystems are timed discrete digital states.

Any normal loading of the CC&S is accomplished using the Mariner '69 coded command (CC) formats CC-1 through CC-5 shown in fig. 6.3.1-1. Ground commands to the CC&S during the mission are accommodated via the command subsystem. Sufficient command capacity is included both for normal CC commands to the CC&S, as well as backup of CC&S functions by direct (DC) commands.

All of the '73 mission requirements can be fulfilled by the basic Mariner '69 CC&S hardware. A functional block diagram of the '73 CC&S is shown in fig. 6.3.1-2 within the dashed outline. It is shown to interface with a large number of subsystems. The CC&S is a memory-oriented device consisting of two main portions. The upper portion is called the computer and contains a 128-word magnetic core storage device. The lower portion is called the sequencer and is directed to the most critical commands related to maneuvers. Memory is applied in the form of separate pseudonoise (PN) type, shift register counters.

Each of the two portions of the CC&S have output actuators which provide the distribution to using subsystems. The computer has an output matrix to decode user addresses. Each portion can be loaded via OSE or by the flight command subsystem. Each portion also gives indications of state to the flight telemetry subsystem. Clock and power signals of 2.4 kHz are supplied to each portion from the power subsystem.

With its processor and memory, the computer portion of the CC&S is the most flexible. A single memory word contains data to enable a discrete command to a coded user on the occasion of the elapse of a pre-established increment of time (Δt). There are 128 such memory locations organized in sequential order of occurrence. Memory addresses normally step one at a time. It is possible for the memory to command itself forward or backward in large jumps to other addresses and return to normal step sequence operation. In this manner, sequences used before can be reused and the actual number of possible commands can exceed 128. The '73 Orbiter uses this feature extensively for the repeated maneuvers.

		WORD FORMAT																									
COMMAND BIT NUMBER		1	2	3	4	5	6	7	8	9	10	11	12	13	14	15	16	17	18	19	20	21	22	23	24	25	26
CC&S BIT NUMBER										1	2	3	4	5	6	7	8	9	10	11	12	13	14	15	16	17	18
BIT VALUE	CC-1 COMPUTER LOAD	1	1	0	0	1	1	1	1	0	1	0	PROGRAM														PARITY P
	CC-2 COMPUTER LOAD	1	1	0	0	1	1	1	1	0	1		PROGRAM														
	CC-3 WORD INTERROGATE	1	1	0	0	1	1	1	1	0	0	1	MEMORY ADDRESS					ALL ZEROS									
	CC-4 SEQUENCER LOAD	1	1	0	0	1	1	1	1	0	0	0	REG. ADDR.		P	TIME DURATION											
	CC-5 TOLERANCE DETECTOR DISABLE	1	1	0	0	1	1	1	1	0	1	1	ALL ZEROS													P	

NOTES:

1) COMMAND BIT 9 IS SHIFTED TO CC USERS WITH BALANCE OF VARIABLE DATA.
2) WHEN PROGRAMMING THE COMPUTER PORTION OF THE CC&S GROUND COMMAND:
   A) CC-1 AND CC-2 MUST BE SENT IN ORDER TO INSERT ONE COMPUTER WORD OF PROGRAM INTO THE CC&S. THE TIME BETWEEN THE START OF CC&S BIT NO. 1 OF CC-1 AND THE END OF CC&S BIT NO. 18 OF CC-2 MUST BE LESS THAN FOUR MINUTES, OR THE PROGRAM INFORMATION CONTAINED IN THEM WILL BE REJECTED.
3) WHEN PROGRAMMING THE CC&S FIXED SEQUENCER (CC-4):
   A) CC&S BITS NO. 4 AND 5 DESIGNATE THE REGISTER INTO WHICH THE TIME DURATION PORTION (CC&S BITS NO. 7 TO 17) IS TO BE PLACED "01" FOR THE ROLL REGISTER, AND"11" FOR THE MOTOR BURN REGISTER.
   B) CC&S BIT NO. 18 SPECIFIES POLARITY FOR BURNS: "1" = POSITIVE, "0" = NEGATIVE. FOR MOTOR BURN, CC&S BIT NO. 18 IS "1".
4) CC-3 CONTAINS THE ADDRESS OF THE MEMORY WORD TO BE READ OUT IN THE SINGLE WORD READOUT MODE, CC&S BIT 10 CONTAINS THE MOST SIGNIFICANT BIT.
5) PARITY BITS ADJUST CC&S BITS 1 THROUGH 18 TO HAVE ODD PARITY.

Figure 6.3.1-1. Coded Command Word Formats

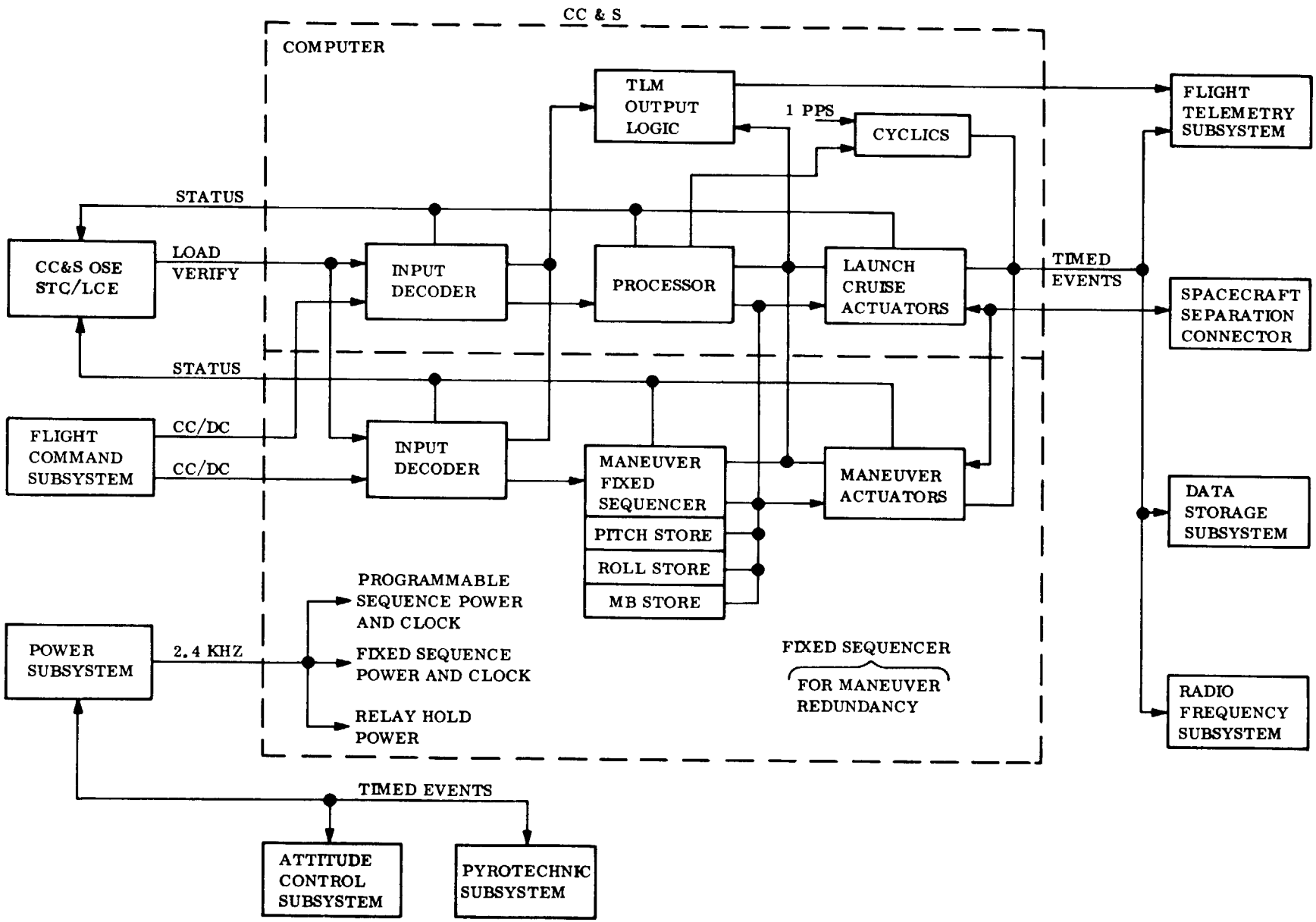

Figure 6.3.1-2. CC&S Functional Block Diagram - Mars '73

Repetitious commands are required at 1 hr and 24 hr intervals throughout the mission. The cyclic commands are derived directly by countdown of the clock frequency supplied to the CC&S.

6.3.1.2 Modifications for '73

The Mariner '69 CC&S contains considerable redundancy. The programmable section is backed up by the command system such that its memory can be changed in Flight and/or any event can be ground commanded to occur in the event of CC&S program failure. During the critical maneuver sequence of reorientation and engine firing when ground command may be too slow, the fixed sequencer portion of the CC&S provides redundant information about magnitude of turns and burn time, which is compared against the programmed section. Earlier Mariners (such as Venus '67) did not contain the programmable section. Occurrence of events were preset before launch, and were not changeable in flight. The command system was used as back up; however, the maneuver sequencer was not backed up and was critically necessary for mission success. Using a CC&S comparable to these earlier models could result in a saving of about 12 lb and 8 watts.

This alternative was not selected for three reasons. First, the aiming requirements are much more critical during this mission so that the maneuver sequencer failure might result in an inability to deliver the Capsule to Mars atmosphere. Secondly, the Capsule separation attitude must be completed in an accurate and timely manner if separation is to occur at the proper time and direction. In previous flyby missions, the maneuver sequencer was last used several days before encounter. A third reason was the difficulty experienced during Mariner '69 hardware procurement in trying to obtain Mariner '64 or '67 parts. . . . they were no longer being manufactured. A stripped down version of the '69 CC&S might negate this latter reason, but the first two still remain.

6.3.1.3 Subsystem Characteristics

The estimated weight, power and size of the CC&S are 24 lb, 17 watts and 600 in^3, respectively.

Some of the principal performance parameters are as follows:

Memory Capacity:	128 words of 22 bits each	
Basic Clock Rate:	1 pulse/sec	
Input Form:	Mariner '69 Coded Commands:	26 bit block including 9 bit address

Output command timing resolution:

Programmer:	1 sec
Attitude Control Fixed Sequencer:	1 sec
Motor Burn Fixed Sequencer:	1/20 sec
CC&S Timing Reference Accuracy:	From Power Subsystem ± 0.01%

6.3.2 ATTITUDE CONTROL

There are three broad requirements for the Support Module Attitude Control Subsystem. First, control of the Spacecraft attitude is required during the heliocentric cruise phase to provide a satisfactory communications link to the earth and efficient solar power collection by the solar array. Second, reorientation of the Spacecraft attitude to any arbitrary special attitude is required to point the fixed midcourse thruster for trajectory corrections during the cruise phase. Finally, attitude hold during firing of the propulsion system is required to control Spacecraft attitude and therefore the direction of velocity change to the Spacecraft.

The Attitude Control Subsystem (A/C) acquires and stabilizes the Spacecraft to the Sun and the star Canopus. It then maintains the Spacecraft attitude relative to these references during the heliocentric cruise and Mars encounter phases. Upon receipt of commands from the Central Computer and Sequencer (CC&S), the A/C maneuvers the Spacecraft by sequential rotations about its axes to any arbitrary spatial attitude where velocity changes are performed by the propulsion system for trajectory corrections. During engine firing, the A/C changes the thrust vector direction by controlling vanes in the engine exhaust to maintain vehicle attitude and stability. At a signal from the CC&S at the ends of the maneuver sequence, the A/C reacquires the Sun and Canopus.

During launch ascent, all parts of the A/C are unpowered except the gyros. Following separation from the launch vehicle, power is applied to the rest of the A/C. Sun sensors are used in pitch and yaw and rate signals are provided by the gyros; the Canopus sensor output is not used. The initial rates are reduced to a low value and the A/C operates to acquire the Sun. Then, a sun gate operates to enable the Canopus sensor and to roll the vehicle about the sunline until the sensor acquires and locks onto the star Canopus. The system discriminates against stars other than Canopus by brightness gate settings in the Canopus sensor acquisition logic. At the completion of Sun and Canopus acquisition, the gyros are turned off. The system switches to the cruise mode, in which the Sun sensors control pitch and yaw attitude, and the Canopus sensor controls roll during the heliocentric cruise phase. The gyros are off and control loop damping is obtained by derived rate. The A/C is capable of automatic reacquisition of Sun and Canopus references if either is lost.

When a velocity correction maneuver is commanded, the optical sensor outputs are not used. The gyros, operating in their position mode, establish an inertial reference. The gyros are torqued in sequence to produce a constant Spacecraft turning rate about the desired axis. The time the gyros are torqued is controlled to yield the desired rotation. The attitude is then controlled by the position signals from the three single axis gyros. At the completion of the commanded turn sequence, the Propulsion Subsystem is initiated to supply the velocity correction. The autopilot maintains the inertial attitude of the Spacecraft by positioning jet vanes to control the thrust vector direction. The gyros generate position error signals, which are processed by the autopilot electronics, to drive the vane actuators. Upon completion of the velocity correction, the CC&S commands the A/C to reacquire the Sun and Canopus and return to cruise mode.

Prior to Capsule separation, the Spacecraft maneuvers to the Capsule separation attitude, and holds this attitude until separation is completed.

During Capsule pre-entry, entry, and post impact relay phase, no action is required of the Support Module A/C Subsystem other than maintenance of its normal Sun/Canopus orientation.

6.3.2.1 Modifications for '73

The Mariner '69 A/C system consists of six independent assemblies whose interconnections are shown in fig. 6.3.2-1.

1. Sun Sensor System
   a. Four assemblies making up the secondary Sun sensor
   b. Two assemblies making up the primary Sun sensor
   c. Sun gate
2. Canopus sensor
3. Gyro control subassembly
   a. Three rate integrating gyros
   b. Electronics
   c. Integrating capacitors
4. A/C electronics
   a. Attitude control electronics
   b. Autopilot electronics
   c. Power supply
   d. Control system logic

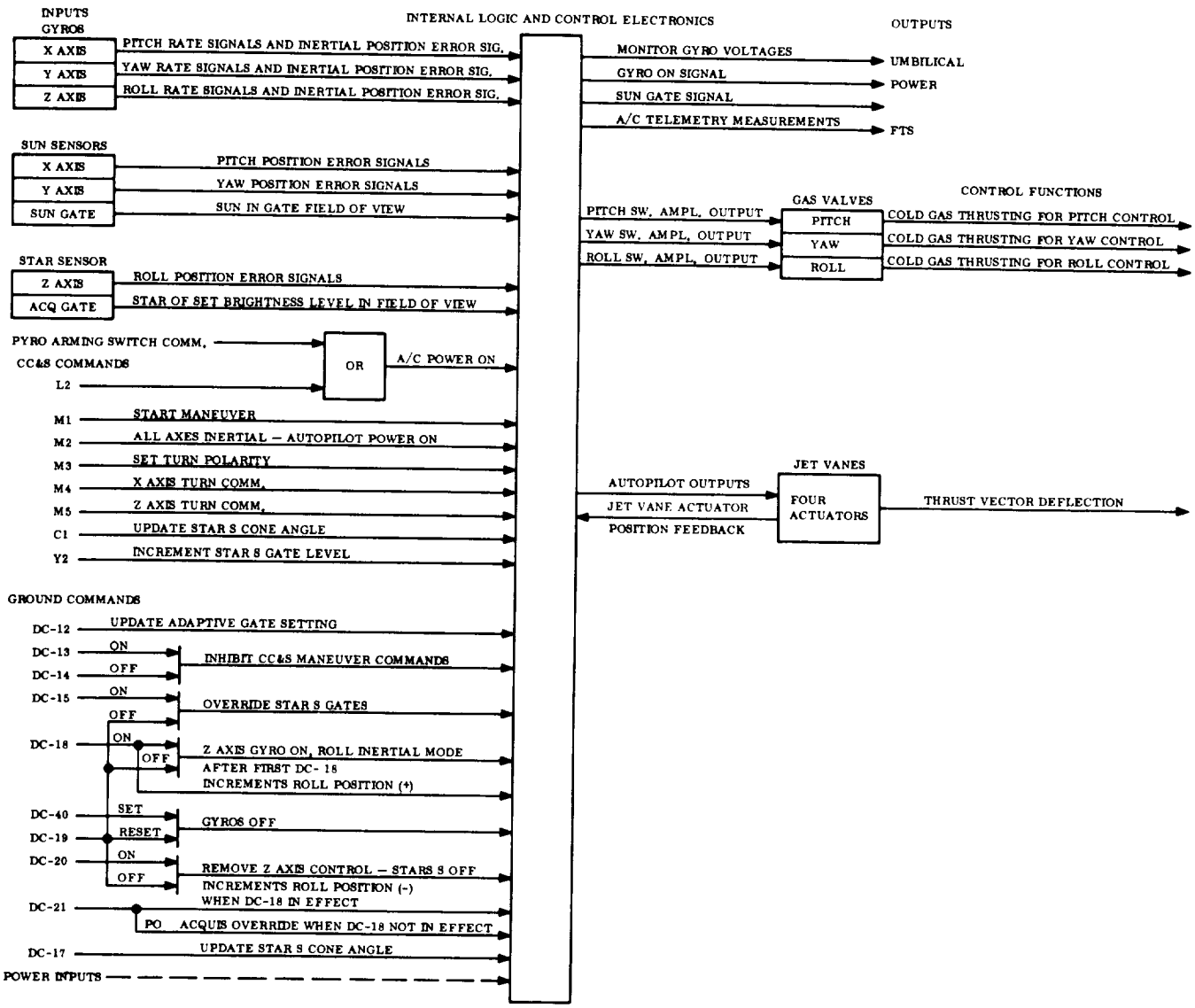

Figure 6.3.2-1. Attitude Control Functional Block Diagram

5. Jet vane assembly

6. Gas jet assembly (reaction control system)

6.3.2.1.1 Sun Sensors

The Mariner '69 Sun sensors can be used in Mars '73 mission. For the '73 mission the four assemblies of the secondary Sun sensor must be relocated since the Capsule will be in their fields of view. Relocation to provide necessary field of view is expected to be a minor change.

6.3.2.1.2 Canopus Sensor

The JPL Canopus sensor, which performed the 1964 Mars mission adequately, has undergone significant redesign for the 1969 mission to improve its performance. Most of the effort has been to reduce the effect of stray light and false objects. Automatic operation has been increased, and roll angle control range has been doubled to permit higher search rates. The stray light baffle, which is attached to the sensor in front of the lens, provides unwanted light rejection due to reflections from surfaces of the Spacecraft and from the surface of Mars. The Mars '73 Spacecraft will probably require redesign of the light shield to reject Spacecraft and Capsule reflected light.

6.3.2.1.3 Attitude Control Electronics

Changes to the attitude control electronics will occur only in the autopilot section. The power supply and control logic are expected to be unchanged or at most to undergo minor changes. The function of the autopilot is the same for the MM'69 and '73 missions, i.e., stabilization of the Spacecraft during engine thrusting. However, the electronic gains and compensation of the autopilot are dependent upon the geometric and dynamic characteristics of the Spacecraft which are different in the '73 mission. The Mariner '69 engine was not aligned with the vehicle axis, and three-axis vehicle control was obtained from a single engine by resolving sensor signals by means of electrical networks to yield the correct signal for each vane. In '73, the engine is on the roll axis, and no resolution of signals is required. Mathematically, or electrically, these changes may be significant. Physically the change is not expected to be significant, so that volume and weight should remain essentially unchanged.

6.3.2.1.4 Jet Vane Assembly

No changes are required for the flyby Support Module since the MM'69 engine is retained. The orbiting Support Module, however, employs a bipropellant rocket which, by virtue of high exhaust gas temperature, precludes the use of jet vanes. The entire engine will be gimballed in two axes. Roll control will be achieved with the cruise attitude control system using cold gas jets. If additional roll torque is required (considered unlikely), the thrusters may be increased in size, but this will not require electronic changes other than perhaps addition to the logic. A two-axis gimballed engine will require only two drive amplifiers instead of four drive amplifiers required for the vanes.

6.3.2.1.5 Gas Jet Assembly (Reaction Control System)

Nitrogen gas is stored at high pressure in tanks. The pressure is reduced thr ugh a pressure regulator and distributed to four locations on the Spacecraft. At these four locations, the gas is further manifolded and expanded through a nozzle to generate a thrust, and hence, a torque in the appropriate direction. Gas flow is controlled by solenoid valves which are operated by the respective attitude control channel.

Functionally, the gas jet systems for the two missions are identical. Physically, they are very similar. Despite the larger size and smaller moment arms of the '73 Spacecraft, no increase in gas is required since MM'69 gas budget was very conservative. The new Spacecraft configuration requires new tubing runs, new nozzle designs, and relocation of the nozzles; but these changes are relatively minor. Active components such as regulators and solenoid valves, as well as fill valves and filters, remain unchanged.

6.3.2.2 Subsystem Characteristics

The estimated weight, power and volume of the A/C Subsystem are as follows:

Weight	-	62 lb (including 5 lb N_2)
Power	-	5.6 watts in cruise mode; 43 watts in maneuver mode
Volume	-	2500 in.^{3} (including 1200 in.^{3} for gas storage bottles).

The A/C can orient the Spacecraft to the Sun and Canopus from any initial orientation; and with the initial rates as high as 3°/sec about each axis. Orientation to the Sun takes place in less than 30 min, followed by a Canopus search and lock-on in less than 70 min additional time. During acquisition, the initial rates are quickly reduced, and they are limited to 0.25^o/sec as the position error is reduced. Roll rate during Canopus search is 0.1^o/sec.

During cruise and orbit modes of operation, the limit cycle rate is 0.2×10^{-3} deg/sec. The deadband is $\pm 0.25^o$ for each axis. The combined effects of all errors such as those due to deadband, alignment, null shifts and drifts, noise, and other random errors are less than 0.5^o/axis (3σ).

During command turns, the turning rate is 0.18^o/sec. The turn magnitude is controlled by allowing this rate to continue for a predetermined interval of time. The error between the resulting orientation and the commanded orientation depends on the magnitude of the specific turns involved, and on the total time interval. Specifically, the cruise orientation error, gyro drift errors over the turning interval, gyro rate calibration, and capacitor leakage errors are the most significant. The resulting error for a 90° turn is 0.85^o (3σ).

An error analysis of the autopilot has not been made, nor have requirements been established. As noted previously, the autopilot requires redesign due to changes in Spacecraft dynamics. Errors in attitude hold during autopilot operation (i.e., while engine is firing) are affected by Spacecraft center-of-mass offset and thrust misalignment. The allowable error is a function of the velocity increment to be given the Spacecraft. The steady state autopilot error can be held to less than 0.5^o. Transient errors have not been evaluated.

6.4 POWER SUBSYSTEM

6.4.1 FUNCTIONAL DESCRIPTION

The Power Subsystem provides electrical power to operate the Spacecraft electrical equipment. It also provides switching and control functions to manage and distribute that power and provides timing and synchronizing signals.

The simplified functional block diagram of the Support Module Power Subsystem is shown in fig. 6.4.1-1. Primary power is generated by the solar array and is used to power the Spacecraft and recharge the battery. Power from the array or battery is supplied to some users directly, and the remainder is conditioned to a-c and distributed to the Spacecraft subsystems.

Raw power from the Support Module is also used to supply the following functions on the Capsule:

1. Thermal control power

2. Charging the battery prior to separation

3. Checkout of Capsule prior to separation.

Power is distributed to the loads in the following forms:

1. Unregulated d-c, 25 to 50 volts, to the radio subsystem, battery charger, heaters, and to the Propulsion Subsystem and autopilot servos.

2. 2.4 kHz, single-phase, square-wave a-c at 50 vrms, + 2 to -3 percent to the majority of the Spacecraft loads.

3. 400 Hz, three-phase, stepped square-wave a-c to 27.2 vrms, ± 5 percent, to the gyro motors.

The main booster regulates the unregulated dc to 56 vdc, ± 1 percent for use by the inverters. This regulated d-c is not distributed.

Redundancy is provided in both the main boost regulator and the 2.4 kHz inverter. If the boost regulator, the inverter, or the clock (one is incorporated in each 2.4 kHz inverter) should fail, a new boost regulator and inverter are substituted as a pair. On-board failure detection is provided for this function.

The boost mode sensing and control unit is provided to eliminate undesired array/battery load-sharing. When the Spacecraft is oriented to the Sun, as indicated by a Sun-gate signal from the Attitude Control Subsystem, an unregulated bus voltage of less than 31.5 volts will result in a pulse output from the booster converter sufficient to drive the array/battery voltage higher than the array maximum power output voltage, and force the array out of the load-sharing mode with the battery.

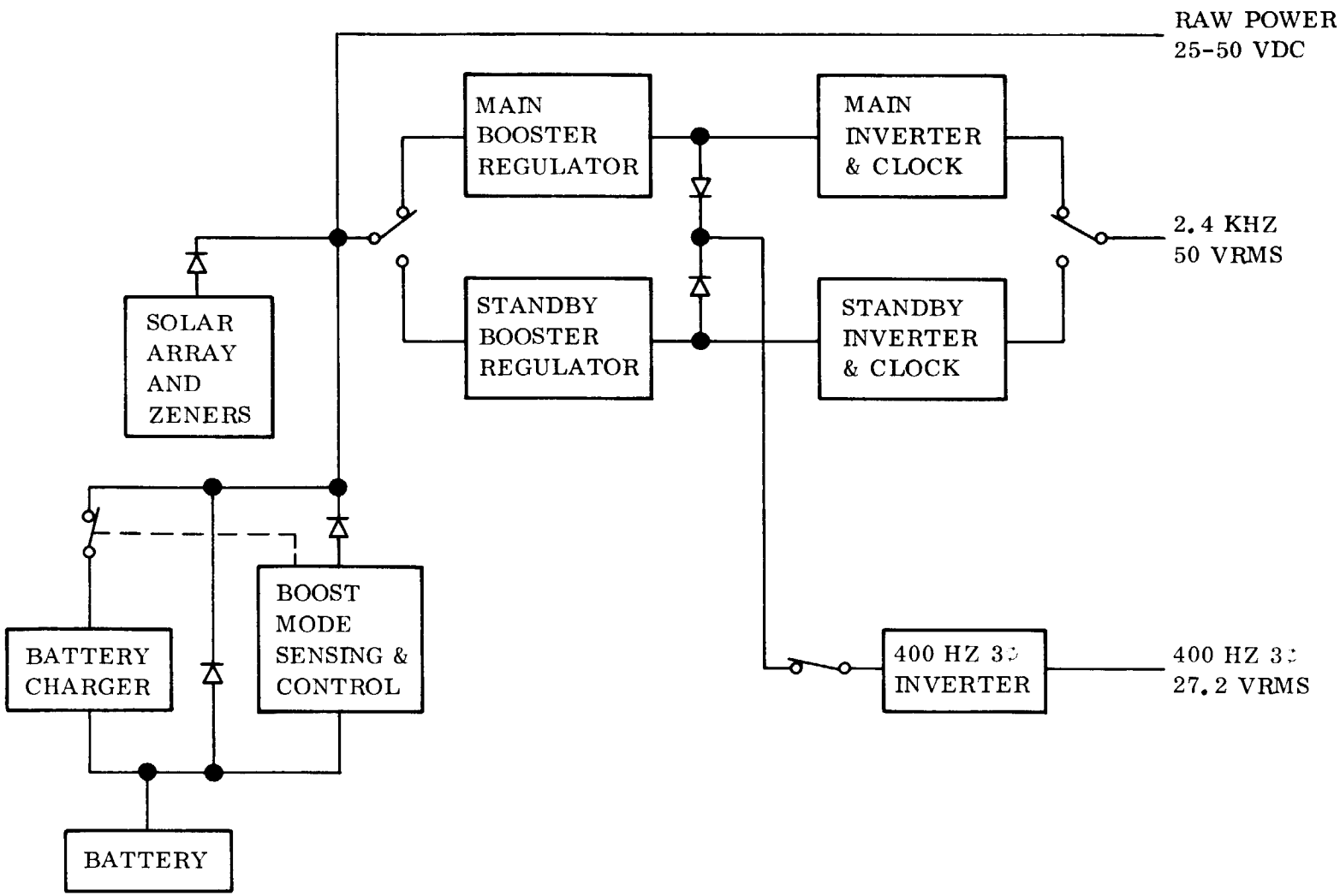

Figure 6.4.1-1. Power Subsystem Functional Block Diagram

6.4.2 MODIFICATIONS TO '73

The solar array is decreased to 50 ft^2. This is possible due to the lower loads resulting from the deletion of Scan Platform Subsystem and science, and the reduction of the data storage subsystem capacity. The smaller array area allows the use of a fixed array rather than the Mariner '69 deployable array. Based on the solar cell data listed below, the '73 array will have a unit power output of about 4.8 watts/ft^2 at 1.55 AU. The required array areas have been calculated based on the loads specified in table 6.4.3-3.

The single phase 400 cycle inverter can be eliminated since the science and Scan Control Subsystem are not used during '73 mission.

The size of the Mariner '69 battery can be reduced to reflect the reduced demands for stored power in the Support Module. The maximum battery drain occurs during a maneuver when the Spacecraft is not Sun oriented. At that time, the power demand is about 310 watts for about 70 min, or about 364 whr. The Mariner '69 battery is rated at 1200 whr when new and about 900 whr at the time of the final maneuver. A battery rated at 600 whr was considered. The Mariner '69 design would be retained but the cell area would be reduced; a new case or the Mariner '69 case packed with potting could be used. A weight savings of 12 lb is possible. Such a battery does not now exist, so that flight qualification would be required. It was decided that the potential weight savings did not warrant the added costs of qualification.

6.4.3 POWER PROFILES AND ALLOCATIONS

Table 6.4.3-1 lists the Power Subsystem demands for each mission phase. At the bottom of each of these tables the raw power demands for the Capsule have been listed. These demands include the heater power required for thermal control, the power required to monitor the status of the Capsule, and the power necessary to charge the Capsule battery prior to separation.

Table 6.4.3-2 lists the abbreviations used for the user subsystem and power conversion equipment.

The gross power requirements are shown in table 6.4.3-3. These gross requirements have been reflected to the power source using power conditioning unit efficiencies based on the Mariner '69 data. The cruise phase has been used to size the solar array. Note that higher power demands do occur in the mission (e.g., during Lander preparation checkout), but these are of short duration and can be accommodated by solar array/battery load sharing, if necessary.

TABLE 6.4.3-1. SUBSYSTEM POWER ALLOCATION

Power Supply	Subsystem	Launch	Sun Acquisition	Cruise	Capsule Checkout	Maneuver	Record	Playback
2400 Hz	FTS	12	12	12	12	12	12	12
	FCS	3.2	3.2	3.2	3.2	3.2	3.2	3.2
	CC&S	17	17	17	17	17	17	17
	DSS	21					42	20
	A/C1	13	25	5.6	5.6	5.6	5.6	5.6
	A/C2					29		
	RFS	31.4	31.4	31.4	31.4	31.4	31.4	31.4
	GYRE	8	8			8		
	PYRO		1	1	1	1	1	1
	PWRD	2.2	2.2	2.2	2.2	2.2	2.2	2.2
	T/C1	27	27	27	27	27	27	27
2400 Hz (Total)		134.8	126.8	99.4	99.4	136.4	141.4	119.4
400 Hz, 3φ	GYRO	9	9			9		
28V DC	VALV					60		
Raw Power	TWT	60	60	60	60	60	60	60
	BTCG	0.5	0.5	0.5		0.5	0.5	0.5
	CAPH			28				
	CAPS			5	75			
	CAPBC			10				
Raw Total		60.5	60.5	103.5	135	60.5	60.5	60.5

TABLE 6.4.3-2. ABBREVIATIONS

FTS	Flight Telemetry Subsystem
FCS	Flight Command Subsystem
CC&S	Central Computer & Sequencer
DSS	Data Storage Subsystem
A/C1	Attitude Control
A/C2	Autopilot
RFS	Radio Frequency Subsystem
GYRE	Gyro Electronics
T/C1	Cruise a-c heater
PYRO	Pyrotechnics
PWRD	Power Distribution Unit
GYRO	Gyro Motor
TWT	TWT Amplifier
VALV	Solenoid Valves
BTCG	Battery Charger
BRFS	Boost Regulator Failure Detector
CAPH	Capsule Heater Power
CAPS	Capsule Status
CAPBC	Capsule Battery Charging

TABLE 6.4.3-3. NOMINAL FLIGHT PHASES AND GROSS POWER REQUIREMENTS

Phase	Duration (min)	Power Requirements	
		Array (watts)	Battery (watt-hrs)
1. Launch	20.3		87
2. Sun Acquisition	30 (max)		135
3. Cruise		241	
4. Maneuver	70		310
5. Lander Pre-separation Checkout	30	273	
6. Record		252	
7. Relay Playback		225	

6.4.4 SUBSYSTEM CHARACTERISTICS

The power subsystem weighs 101 lb including 50 ft^2 of cells weighing 28 lb.

Performance Characteristics

Solar Cell Performance

Type:	Heliotek 8-mil, 2 ohm-cm, N/P cells
Nominal efficiency:	11% at 28°C, AMO
Current Loss Factors:	
Radiation	0.946 (10 mil. glass, 9 months)
Uncertainties	0.900
Voltage Loss Factors:	
Radiation	0.968
JPL Fit Factor	0.977

Uncertainties include manufacturing losses, measurement uncertainties, UV losses, micrometeoroid erosion, and random cell failures. The fit factor enables the curves obtained by our computer program to fit JPL data derived from measurements made on the Mariner '69 solar panel at Table Mt., California. No other factors are needed, apparently, to account for filter transmission or other preflight losses.

Other Power Subsystem parameters are shown in table 6.4.4-1.

TABLE 6.4.4-1. POWER SUBSYSTEM PARAMETERS

Unit	Voltage Output	Rated Power Output (watts)	Rated Energy Capacity (w-hr)
Solar Array	50 (max)		
Ag-Zn Battery	25-36		1200 New 900 Encounter
Boost Regulator	56 ± 1%	250	
2.4 kHz inverter	50 rms, +2 to -3%	210	
400 Hz, Three-Phase Inverter	27.2 rms, ± 5%		
Battery Charge	34.6, ± 0.2	21	
Load Share Booster Converter	0.5 sec pulse	1 amp (max)	

6.5 TELECOMMUNICATIONS SUBSYSTEM

6.5.1 RADIO FREQUENCY SUBSYSTEM

6.5.1.1 Functional Description

The Mars '73 Radio Subsystem performs the following functions:

1. Receives the r-f signal transmitted to the Spacecraft from the DSIF.

2. Coherently translates the frequency of the received r-f signal by a fixed ratio of 240/221.

3. Demodulates the received r-f signal and sends a composite command signal to the command subsystem.

4. Detects the ranging signal transmitted to the Spacecraft by the DSIF.

5. Modulates the transmitted signal with a composite telemetry signal.

6. Modulates the transmitted signal with a ranging signal.

7. Transmits to the DSIF a modulated r-f signal that is phase coherent with either the received signal or with an internally generated r-f source.

In performing these functions, the subsystem is further constrained by the availability of only one 210 ft DSIF antenna with an acceptable viewing time of approximately 8 hr. Command capability must be maintained through a low gain antenna throughout the mission.

6.5.1.1.1 Subsystem Description

A block diagram of the Radio Subsystem is shown in fig. 6.5.1-1. The configuration combines two exciters and two TWT power amplifiers in a redundant manner with selection based on either onboard failure sensing circuits or command from the ground. One receiver is used throughout the mission and is connected to either the maneuver antenna (MA) or the low gain antenna (LGA). Three antennas (MA, LGA, and HGA) are connected to the bay components by circulator switches, a coaxial switch, and a diplexer. The subsystem can transmit on any antenna and can receive on either the LGA or the MA. The power output level is either 20 watts or 10 watts at 2295 MHz, and the receiver threshold for an unmodulated carrier applied at the preselector inputs is -151 dBm. All components with the exception of the antennas and the coaxial switch are identical to the Mariner '69 Radio Subsystem.

The receiver is a double superheterodyne, narrowband, automatic phase tracking type and operates at a nominal frequency of 2113 MHz. The spacecraft receiver recovers command and ranging information from the uplink signal. Command data is sent to the Command Subsystem.

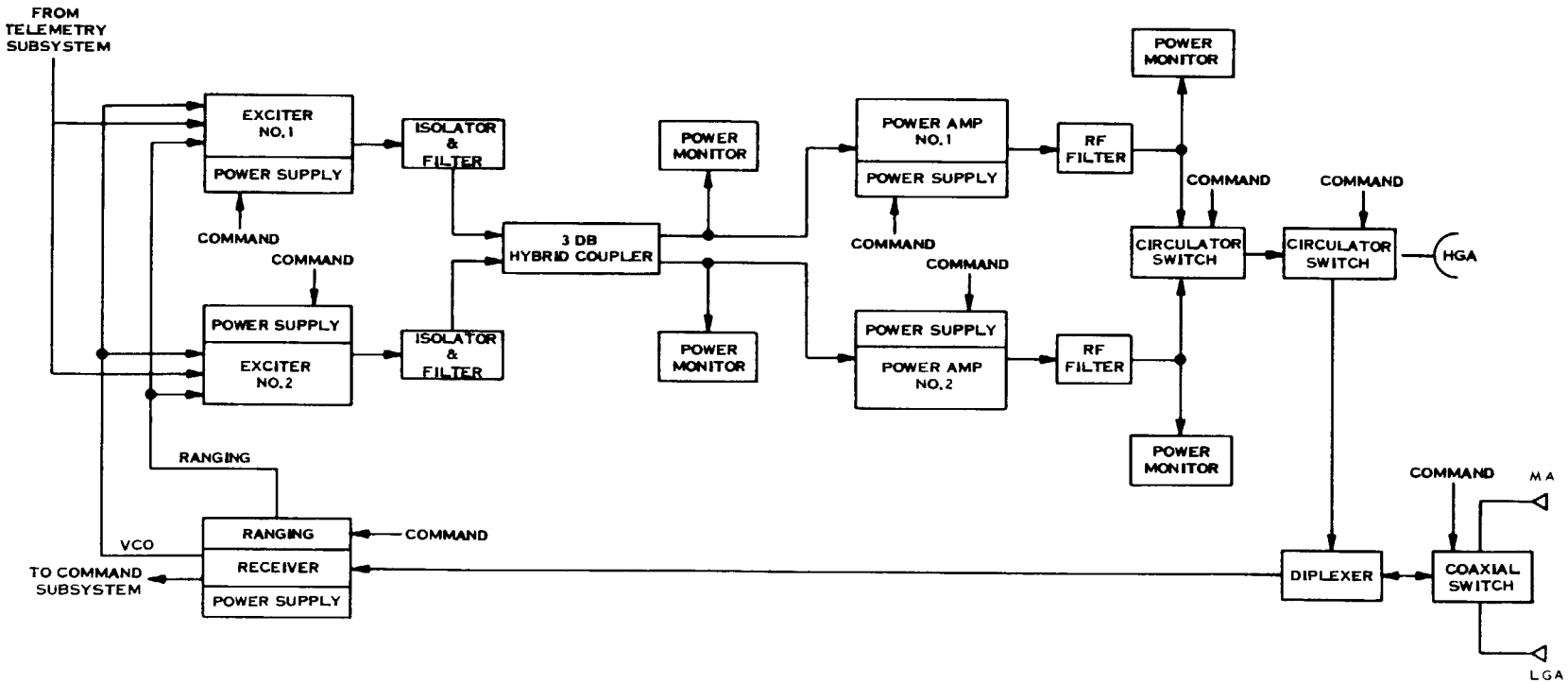

Figure 6.5.1-1. Mariner Mars '71 Radio Subsystem Block Diagram

Ranging data from the uplink signal is sent to the exciters to modulate the Spacecraft transmitter in order to support the turnaround ranging function. The ranging function can be commanded on or off. The VCO output is sent to the exciters whenever the uplink signal is present, thus providing a downlink carrier frequency which is 240/221 times the uplink frequency and is phase coherent.

The two exciters are identical and can be turned on either by command or by onboard failure sensing circuits. The exciters contain their own crystal oscillator source, which is used when the uplink signal is not present. The purpose of the exciter is to provide a means of phase modulating the composite telemetry or ranging signals onto the carrier and to multiply this signal up to the desired S-band frequency. The exciters and power amplifiers are coupled together by a 3 dB hybrid coupler such that either exciter can drive either power amplifier. A 20 watt power level is obtained by the use of traveling wave tube amplifiers (TWTA) in two identical power amplifier packages, which are activated by command or onboard failure sensing circuits. The TWTA's can be operated to a 10 watt level by changing the operating voltages. During the mission, it is planned to operate the TWTA's in their 10 watt mode only in order to conserve power and, therefore, to reduce solar array area and battery capacity. The 20 watt mode is still available, but the additional power must be supplied by the battery if it is used.

The high gain antenna (HGA), low gain antenna (LGA), and maneuver antenna (MA) have the following functions:

1. Provide adequate downlink support to permit attainment of data rates which are compatible with the storage capability and the scientific mission requirements

2. Support a data link for purposes of maneuver attitude verification

3. Support the command link throughout the mission

4. Support a downlink during cruise

5. Support an r-f link during prelaunch operations.

The HGA is a prime focus paraboloid whose nominal diameter and gain are 40 in. and 25.5 dB, respectively. The antenna will be fixed at a clock and cone angle of about 275° and 40°, respectively.

The LGA with a peak gain of 7.5 dB and 3 dB beam width of 80° is the same antenna that is used for Mariner '69. The pattern is pointed along the Z-axis and is symmetrical about this line. With transmitted power of 10 watts, this antenna can support the 33-1/3 bps engineering link to the 210 ft dish to approximately 180 x 10^6 km, and the 8-1/3 bps link to 280 x 10^6 km. Communications to the 85 ft DSNA can be maintained only to 92 x 10^6 km, and then only at the 8-1/3 bps rate.

The maneuver antenna (MA) has a toroidal shaped beam which is aligned so that its major radiation is in a plane parallel to the ecliptic. The gain is 4.5 dB, and the HPBW in the XY

plane is 50°. The primary purpose of this antenna is to support the downlink during maneuver attitudes but it can also be used in place of the HGA at long range. Maneuver verification is accomplished by rolling the Spacecraft about the Z-axis for any thrust orientation, until the Earth is in the pattern. Maneuver attitude verification can be accomplished through the 210 ft DSNA to a range beyond 210 x 10^6 km with transmitted power of 10 watts. Maintenance of the link through the 85 ft DSNA, however, is only good to a distance of about 60 x 10^6 km. It is assumed that all maneuvers will be in view of the 210 ft antenna at Goldstone.

The two circulator switches provide the same function as in the Mariner '69 vehicle. An additional switch (single-pole, double-throw coaxial) enables selection of the LGA or the MA. The diplexer is a two bandpass filter, which provides attenuation of the power amplifier noise spectrum in the vicinity of 2115 MHz to prevent significant degradation of the receiver noise figure, and attenuates any power amplifier spurious outputs.

6.5.1.1.2 Radio Modes

The modes of operation from launch to encounter are given in table 6.5.1-1.

TABLE 6.5.1-1. RADIO MODES

Mode	Power (watts)	Antenna	Reception Mode	Data Rate (bps)	Greyout Range (10^6 KM)
Cruise	10	LGA	210 85	33.3/8.33 8.33	180/280 92
Maneuver	10	MA	210 85	8.33 8.33	210 60
Relay record	-	Relay	NA	1100 70,000	NA
Relay playback	10	HGA	210	4050	225
Capsule checkout	10	HGA	210	1100	350
Command	100 KW	LGA	85	1	770
Command	100 KW	MA	85	1	485

6.5.1.2 Modifications for '73

The only differences between the Radio Subsystems of the Mariner '69 and the '73 vehicles are in the antennas' r-f switching components.

6.5.1.2.1 Coaxial Switch

One additional switch (a single-pole, double-throw coaxial type), is added to connect either the MA or the LGA to the diplexer. This change is necessary to support the mission requirement of maneuver attitude verification from launch through encounter.

6.5.1.2.2 Maneuver Antenna

The maneuver antenna has a toroidal shaped beam oriented in a plane parallel to the XZ plane. It is a slot fed, bi-conical antenna, deployed on a 5 ft boom. Its gain is 4.5 dB with a HPBW of 50° normal to the toroidal plane.

6.5.1.2.3 Low Gain Antenna

The LGA is the same antenna as that of Mariner '69 but with a shortened circular wave guide section to avoid the engine plume.

6.5.1.3 Subsystem Characteristics

6.5.1.3.1 Physical Characteristics

The weight and power requirements for the low power mode of operation is 65.9 lb and 92 watts, respectively. The 20 watt mode requires 131 watts. A volume of 1200 in.^{3} is required for the subsystem, exclusive of the antennas.

6.5.1.3.2 Performance Characteristics

Table 6.5.1-1 shows the various radio links for telemetry and command. For the command links, the 85 ft, 100 kw range corresponds to approximately 75 percent spherical coverage at the encounter range of 180 x 10^6 km. Utilizing the 210 ft DSNA for command increases that coverage to approximately 81 percent. Both of these estimates are based on the Mariner C low gain antenna, which has a similar pattern to the '69 antenna, and the proposed LGA. The design of the radio link for the '73 mission assumes that no commands will be sent via the 210 ft dish. This permits realization of a lower ground receiver noise temperature by not requiring that the antenna be in the diplexed configuration.

6.5.2 COMMAND SUBSYSTEM

6.5.2.1 Functional Description

The Command Subsystem accepts the composite command sync and command data subcarriers from the Radio Frequency Subsystem, demodulates the subcarriers, and with a matched filter, detects the command data. The data signal is decoded, and direct (DC), coded (CC), and quantitative (QC) commands are distributed to the subsystems addressed by the received commands. The '69 subsystem provides 49 DC, 5CC and 4QC words. No changes are required although the QC commands will not be used.

The command detector is shown in fig. 6.5.2-1. The data subcarrier at f_s is bi-phase modulated by the data (D) at 1 bps, and by a 1/2 cps square wave which enables the detection ambiguity to be resolved. The data subcarrier is separated from the PN sync subcarrier by filtering and is processed to provide the reference for the subcarrier phase lock loop. The VCO is used as the reference for detecting the data and for driving the PN generator. The phase of the PN generator is stepped until the output reaches synchronism with the received PN sequence, and then sync search is stopped and decoding is enabled. The PN generator state is decoded to provide bit sync signals for the data channel matched filter and for the decoding operations.

The basic direct command word format is shown below:

Bit No.	1	2	3	4	5	6	7	8	9	10	11	12	13	14	15	16	17	18	19	20	21	22	23	24	25	26
Function	Word Start			Sub-Address																DC Address						
Value	1	1	0	0	0	0	0	1	1	All Zeros										Variable						

Before the Decoder Program Control Unit will recognize a command, 26 consecutive zeros must be received. Decoding of the command begins upon receipt of the word start sequence, 110. Bits 4 through 9 denote whether the succeeding command is a DC, CC or QC. The allowed combinations of bits 4 through 9 are restricted in order to prevent single errors in detection from leading to a false command either from a false word start signal or from errors in the command bits themselves. The particular sequence of bits 4 through 9 shown above denotes that a DC is being sent. For this case, bits 10 through 19 are zeros and 20 through 26 define the specific DC. Other selected sequences of bits 4 through 9 denote CC's and QC's. After the Program Control Unit recognizes a DC subaddress, the bits which follow are shifted out to the decoding matrix. After all 26 bits have been received, the matrix is interrogated and a specific isolated switch is closed, completing the decoding operation. If a CC or QC is received, the bits following the subaddress are routed to the CC&S. QC commands will not be used in '73. They were used in Mariner '69 to stop the scan control subsystem which has been deleted for the '73 mission.

6.5.2.2 Subsystem Characteristics

6.5.2.2.1 Physical Characteristics

Size: 275 in.^{3}

Weight: 8.0 lb

Power: 3.2 watts standby
3.9 watts command execution

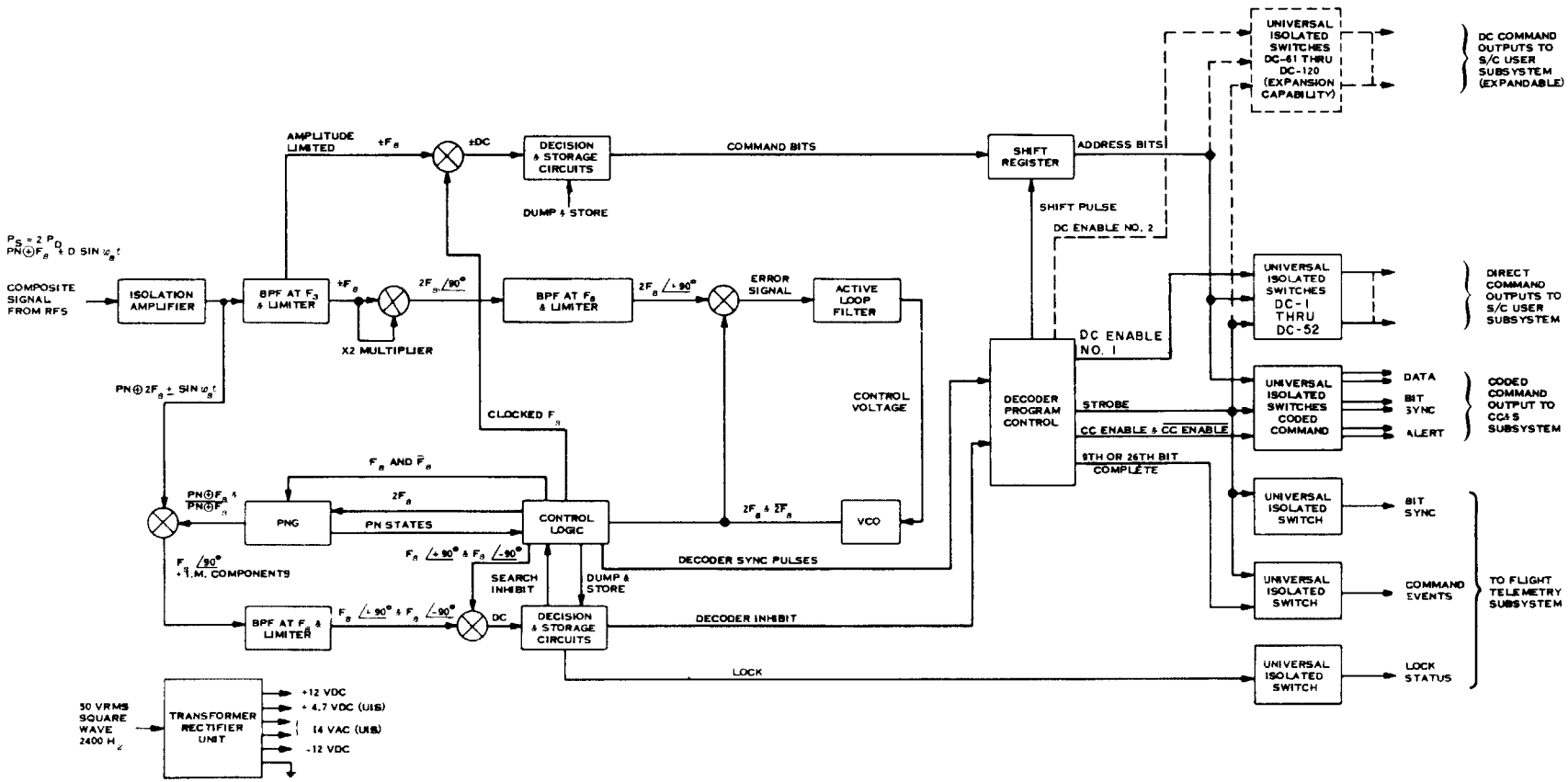

Figure 6.5.2-1. Mars '73 FCS Block Diagram

6.5.2.2.2 Performance Characteristics

1. The threshold input composite subcarrier power to noise density ratio is 16.5 ± 1 dB for a bit error probability of 10^{-5}.

2. The threshold command word error probability is less than 10^{-6}.

3. The probability of no response at threshold is less than 10^{-2}.

4. The command bit rate is 1 bps.

6.5.3 FLIGHT TELEMETRY SUBSYSTEM

6.5.3.1 Functional Description

The Flight Telemetry Subsystem (FTS) provides signal conditioning, encoding and time multiplexing of the Spacecraft engineering data and coding of the digital science data. The engineering and science data channels are modulated onto subcarriers, frequency multiplexed, and outputted to the r-f exciters. In addition, the FTS provides for mode and data rate switching depending on the requirements of the mission phase.

A block diagram of the FTS is shown in fig. 6.5.3-1. The engineering measurements are commutated in ten decks sampled at four rates, as in Mariner '69. Analog data is conditioned to a 3v standard range, converted to a digital number by the analog-to-digital converter and multiplexed with serial digital engineering data and event data. When commanded, the CC&S memory can be read out through the digital multiplexer.

The 32/6 block coder encodes the stored serial bit stream from the data storage subsystem containing capsule relay data.

Table 6.5.1-1 shows data rates versus mission phase. There is a low rate and a high rate channel for engineering and relay data respectively. The low rate channel is placed on high frequency subcarrier compatible with the DSN multimission telemetry demodulator (MMTD). The high rate channel coded data is modulated on a subcarrier using three cycles of subcarrier per coded bit, which allows the use of ground decoding hardware built for Mariner '69 by the High Data Rate Project. The uncoded data on the high rate channel (1100 bps) is split-phase modulated.

During cruise and maneuver phases, Support Module and Capsule engineering data are collected and transmitted at 33-1/3 or 8-1/3 bps. The Capsule engineering data is multiplexed within the Capsule Data Handling Subsystem and is read out to the Support Module Telemetry Subsystem.

During Capsule checkout, Support Module engineering data at 8-1/3 bps is transmitted over the low rate channel, while the high rate channel handles the Capsule checkout data at 1100 bps. The Capsule data is not coded but is routed directly to the modulator for transmission in real time.

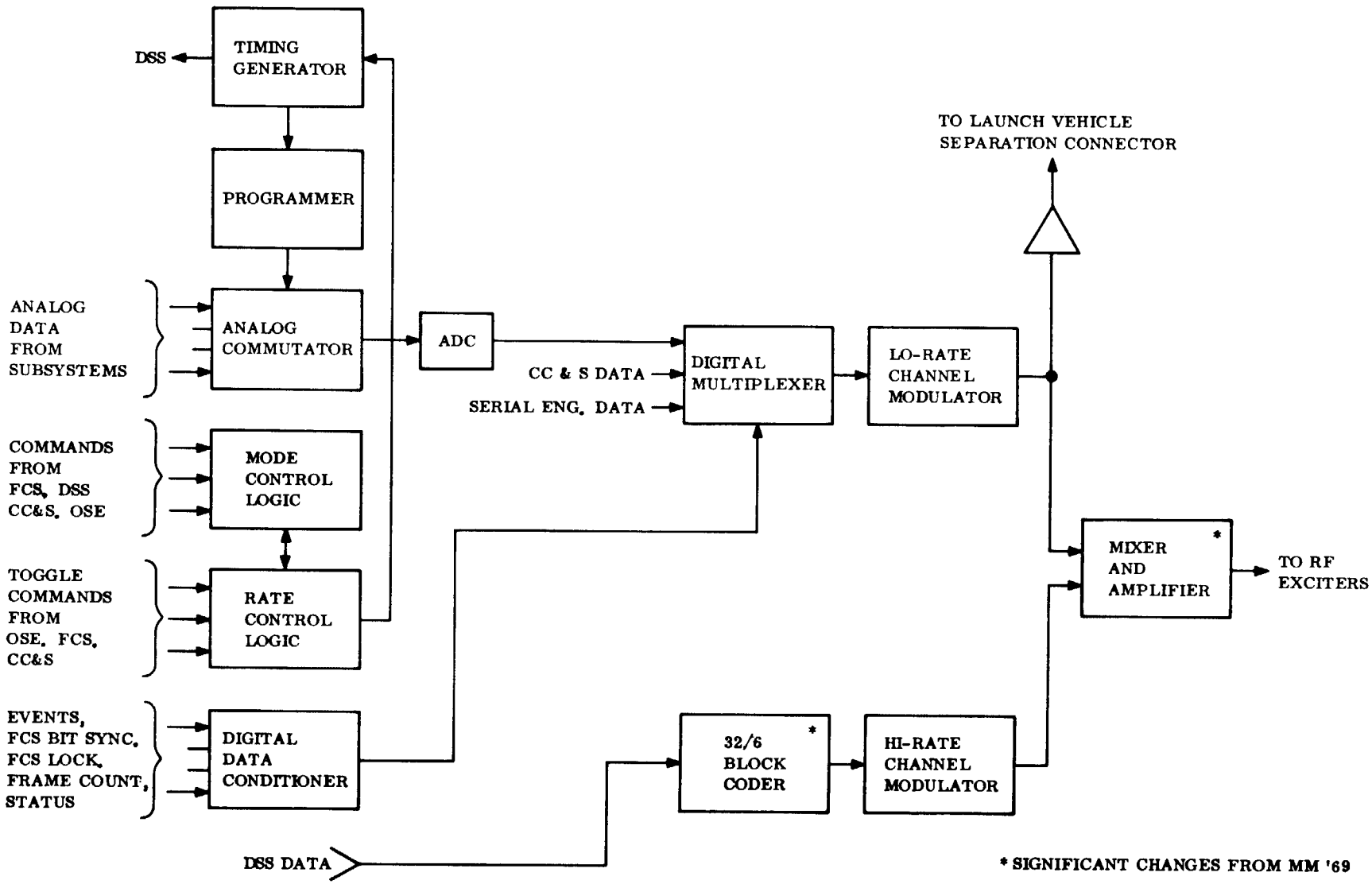

Figure 6.5.3-1. Flight Telemetry Subsystem Block Diagram

During Capsule pre-entry cruise phase, Capsule data, which occurs once per hr in two min bursts, is relayed in real time at 1100 bps on the high data rate channel and is also stored for later transmission. The low rate channel continues to transmit engineering data.

During entry, Capsule data is stored for later transmission and is also relayed in real time at 1100 bps.

After impact, Lander imagery data is relayed to the Support Module at 70 kbps and is stored on the digital tape recorders for later transmission over the high rate channel with coding. During playback, the stored data is transmitted to Earth at 4050 bps, when in view of the 210 ft antenna at Goldstone.

6.5.3.2 Modification for '73

The asterisks in fig. 6.5.3-1 indicate the functional blocks of the FTS that require significant changes to the existing Mariner '69 design. All changes required can use Mariner '69 circuits, with the exception of a new master oscillator and a change in the resistors performing the mixing of the science and engineering data channels.

The timing generator must be changed to reflect the changes in data rates and subcarriers.

The mixer and amplifier must be modified to accommodate changes in modulation indices.

6.5.3.3 Subsystem Characteristics

Estimated weight, power, and size are 24 lb, 12 watts and 785 in.^{3}, respectively.

6.5.3.3.1 Performance Characteristics

Data rates and data modes are presented in table 6.5.1-1. The accuracy of the analog-to-digital conversion is ± 1 percent of full scale for 0-3v, and ± 1.5v signals and ± 3 percent for the 0-100 mv signals. Sampling times are given in table 6.5.3-1.

TABLE 6.5.3-1. TIME BETWEEN SAMPLES (SEC)

Rate (bps)	Deck			
	High	Medium	Low	Low-Low
8-1/3	16.8	168.0	1680.0	3360.0
33-1/3	4.2	42.0	420.0	840.0

6.5.4 DATA STORAGE SUBSYSTEM

6.5.4.1 Functional Description

The Data Storage Subsystem provides buffering between Capsule high rate video and entry data via the relay subsystem, and the lower transmission rates to Earth. A total equivalent storage capacity of 2.9×10^7 bits is provided by the digital tape recorder. Two recorders are provided to yield degraded mode redundancy.

During Capsule pre-entry and entry phases, the Digital Tape Recorder (DTR) receives and stores data at the rate of 1100 bps. Two to five min after impact on Mars, the DTR receives and stores data at the rate of 70,000 bps. The DTR is read out while in view of the 210 ft antenna. Bit sync from the FTS is used as the reference for the phase lock loop servo control.

6.5.4.2 Modification for '73

Changes in the record and playback speeds are required to reflect the data rate requirements of a flyby relay mission. These changes are significant enough to require a new tape recorder.

6.5.4.3 Subsystem Characteristics

Recorder designs have not been evaluated but it is expected that weight, power and size will be similar to Mariner '69 digital tape recorder. These were 17 lb, 22 watts and 420 in.^{3}

6.5.5 RELAY SUBSYSTEM

6.5.5.1 Description

The Relay Subsystem performs the following:

a) Receives the r-f signal transmitted to the Support Module from the Capsule during cruise, entry and post-impact.

b) Demodulates the received r-f signal and sends it to the Data Storage Subsystem of the Support Module.

The Relay Subsystem consists of two separate antennas and receivers to receive and demodulate the high and low rate signals. Fig. 6.5.5-1 is a block diagram of the subsystem. The low rate receiver/antenna is utilized to receive entry data at a rate of 1100 bps from the Capsule during cruise and entry. The high rate receiver/antenna accepts post-impact data at a rate of 70,000 bps for a minimum of 7 min enabling the accumulation of at least 2.9×10^7 bits.

Receivers

The receivers are superheterodyne, wideband, FSK devices with a 4-dB noise figures. The signal, after RF amplification, is translated to a wideband 1.5 MHz i-f amplifier. From this, it is separated into two channels centered 700 kHz apart each having a bandwidth of 300 kHz in the high rate receiver and 25 kHz in the low rate receiver.

The outputs of the two envelope detectors are differenced, and the result is combined with a square wave at the bit rate frequency, converting the split-phase signal to NRZ. Bit sync is used to match filter detect the data.

Two synchronization loops, one for each rate, are mechanized as shown in fig. 6.5.5-2. The input is squared and filtered to generate a frequency component at the data rate frequency, R_b. A phase lock loop acquires and tracks the phase of this signal. Signal presence is determined by a quadrature detector for each loop.

Antennas

The antenna gain required for the post-impact relay link is 0 dB. This gain can be achieved over an angle of 130° by using a turnstile over a ground plane with a dipole-to-reflector electrical spacing of 130°. Fig. 6.5.5-3 shows the antenna, and fig. 6.5.5-4 shows the pattern. The two crossed dipoles are fed by a coaxial split balun transformer. One dipole is slightly longer than a half wavelength, the other slightly shorter to obtain circular polarization on axis. The antenna provides +4 dB gain on its axis and +3 dB at ±55°, including polarization loss. The antenna is fed by type RG-442 coaxial transmission line with type N terminals.

To provide the required coverage during the cruise and entry phases without sacrificing post-impact performance, a separate entry antenna is required. The one provided is identical to that described above, and it is oriented to achieve 3 dB minimum gain during entry.

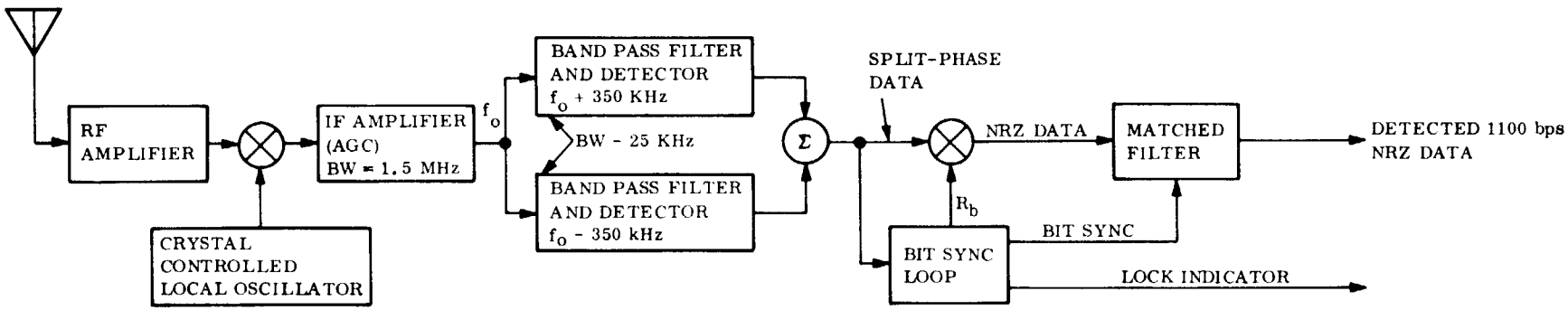

(a) LOW RATE ANTENNA/RECEIVER

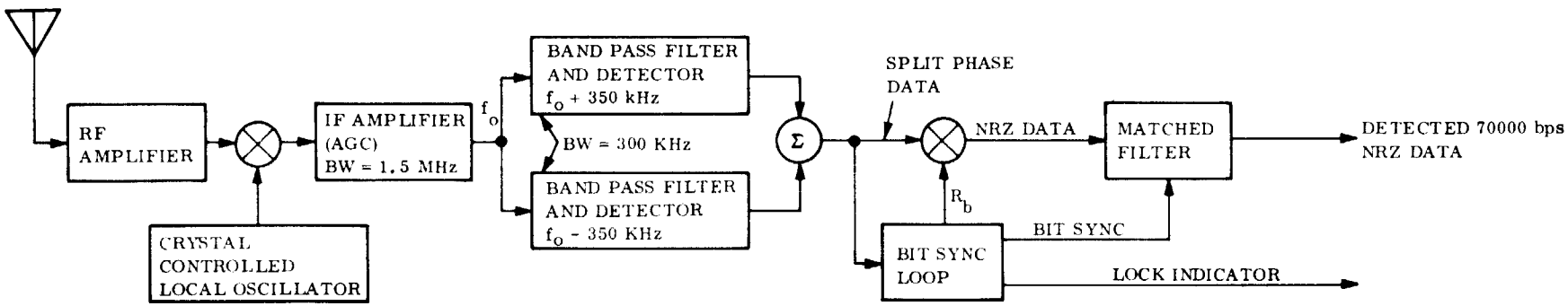

(b) HIGH RATE ANTENNA/RECEIVER

Figure 6.5.5-1. Relay Subsystem Block Diagram

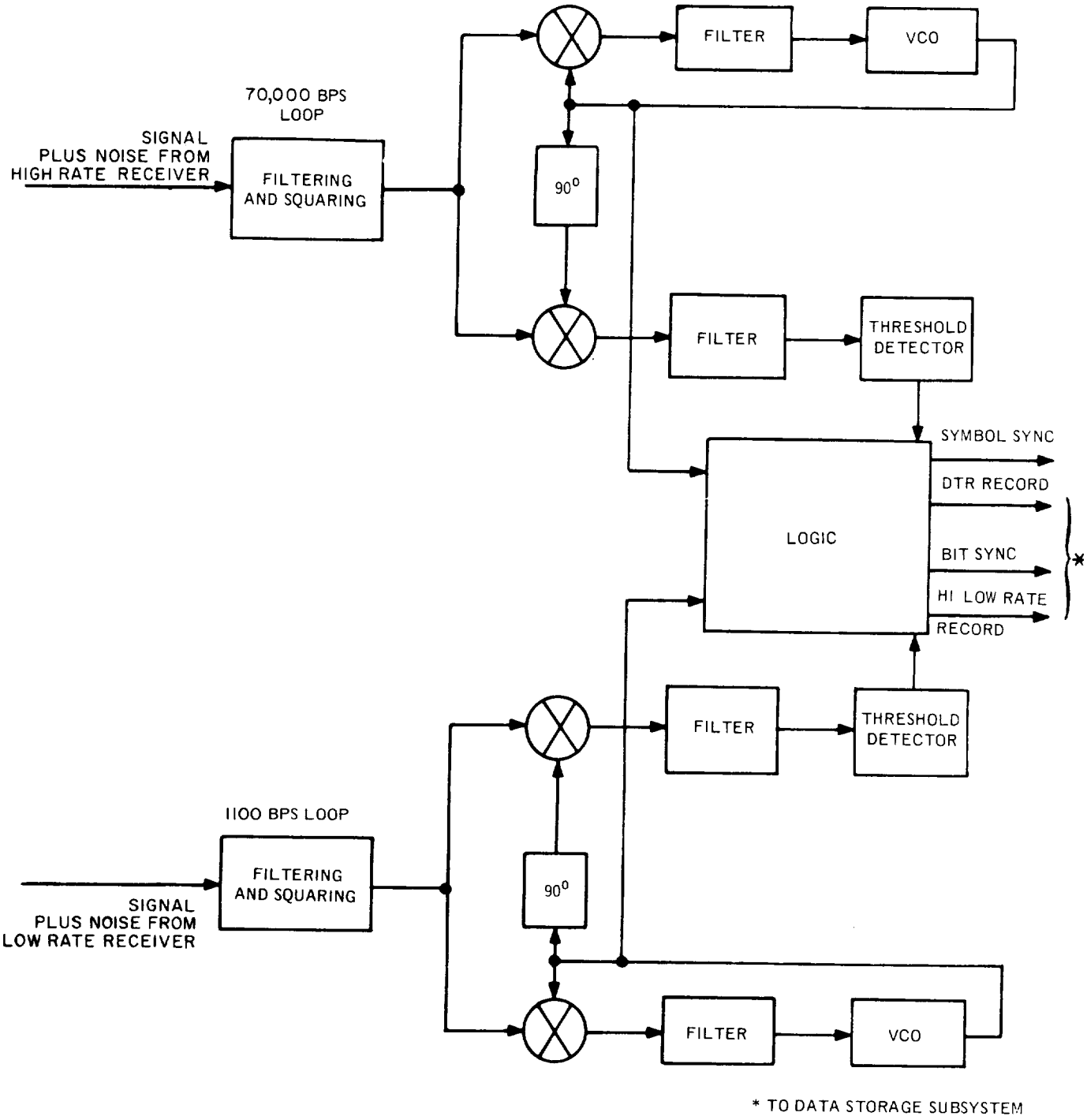

Figure 6.5.5-2. Synchronization Loops, 70 kbps and 1.1 kbps

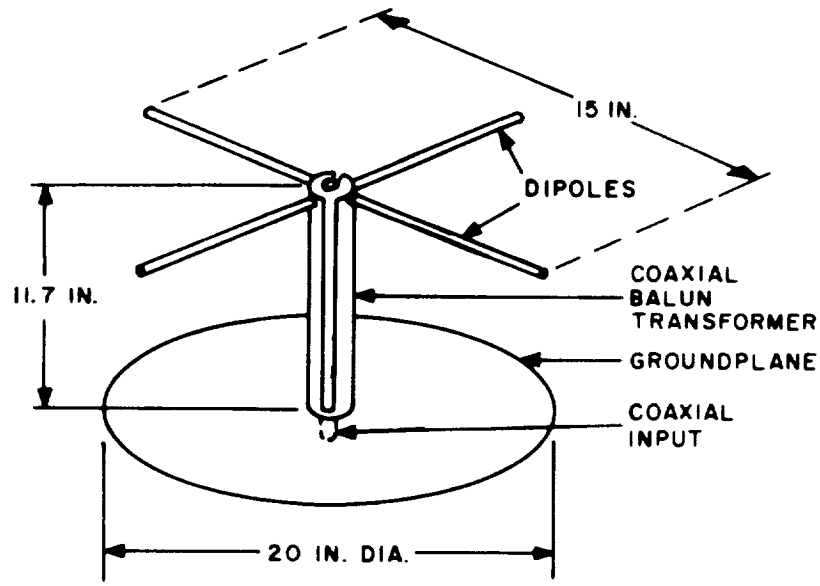

Figure 6.5.5-3. Relay Antenna - Turnstile Over Ground Plane

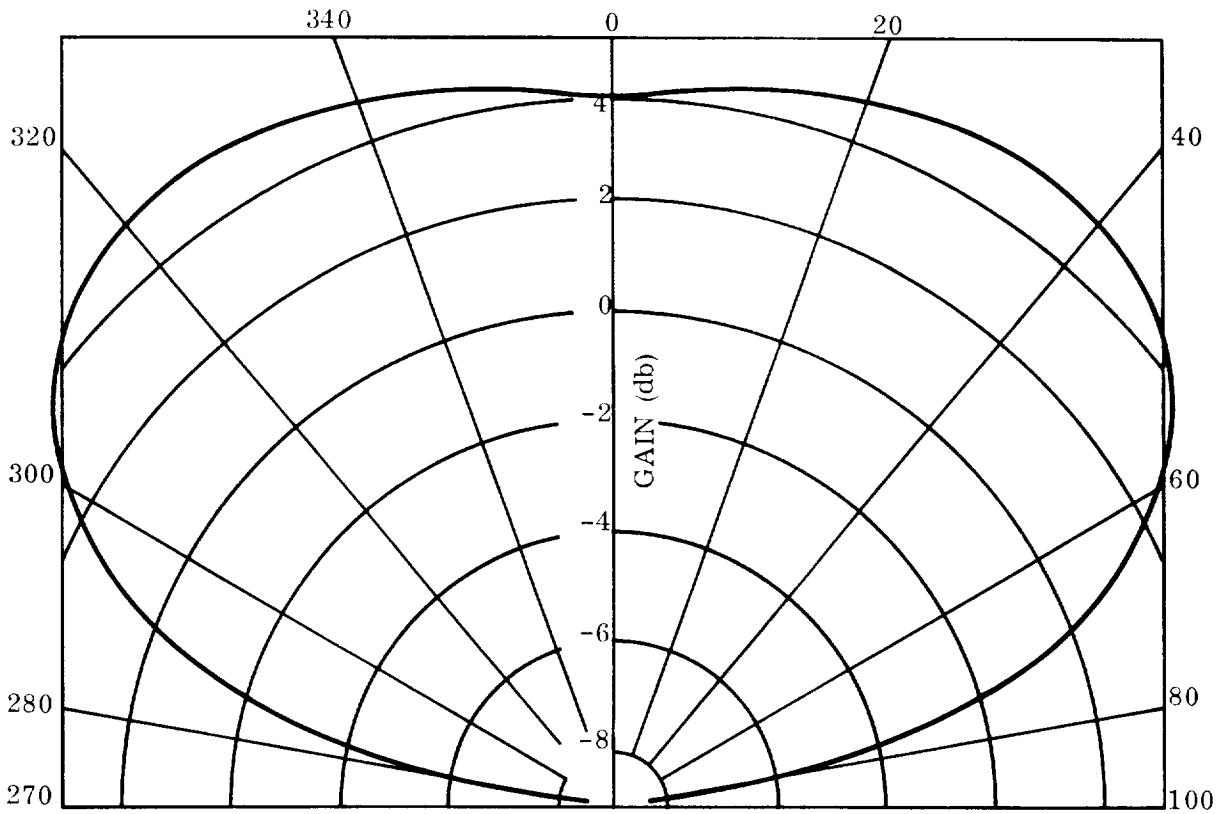

F = 400 MHz, CIRCULAR POLARIZATION
TURNSTILE OVER A GROUND PLANE
130° SPACING BETWEEN DIPOLES AND REFLECTOR
INCLUDES POLARIZATION LOSS OFF AXIS
EFFICIENCY = 90% (-0.5 db)

Figure 6.5.5-4. Relay Antenna Pattern

7. MISSION ASSURANCE

7. MISSION ASSURANCE

Mission assurance has two different, but interrelated connotations in this study. First, there is the probability of performing the mission considering the large uncertainties in the Mars environments, assuming that the reliability of the system is perfect. Secondly, there is the probability that the hardware will perform satisfactorily assuming the mission and its related environments are adequately defined.

There are large uncertainties associated with the Mars environments. Examples are the atmosphere, local surface elevations, winds, surface slopes, rock sizes, local surface hardness, etc. A set of design environments could be chosen which would compound margins of safety to the point that a useful mission could not be performed. An initial attempt to treat these environments probabilistically to arrive at design requirements is discussed in Section 3.3, which deals with the design of the Retardation System. This statistical approach must be extended to arrive at an assessment of the probability that the system can perform the mission, but the preliminary indications is that the present design may be conservative.

The second aspect of mission assurance is concerned with the selection and application of specific hardware to implement the system design. This involves reliability analyses, criticality analyses, failure modes, redundancy, etc. and the program which will be implemented to demonstrate hardware capability.

This section deals with this second aspect of mission assurance and illustrates the approach for applying GE-RS Failure Effect Management System (FEMS) to achieve reliable hardware. The numbers presented herein do not reflect the combined probability of mission success considering both aspects of mission assurance.

7.1 CRITICALITY AND RISK

In lieu of performing failure effects predictions, analysis and determining a course of action based upon mission risk and other trade factors, a preliminary assessment has been made of those aspects of the design which entail highest risk to the mission.

The concept of risk, as used here, is the product of mission criticality and failure probability. Mission criticality is that fraction of mission value lost as a result of nonperformance.

By assigning a numerical value to each of the mission outcomes, the loss of an outcome(s) caused by the failure of an element will be proportional to the element criticality. In other words, the criticality of an element is equal to the ratio of the mission value lost to the total mission value. For example, if the operational battery of 1400 lb Lander failed at impact, 50 percent of the total mission value would be lost. Hence, the criticality of the battery for the landed phase of the mission would be 0.5.

Accordingly, a mission value profile (fig. 7.1-1) was prepared. A numerical value was assigned to each of the major mission functions. The values are in the nature of tentative, and would require NASA/LRC approval in an early phase of design activity.

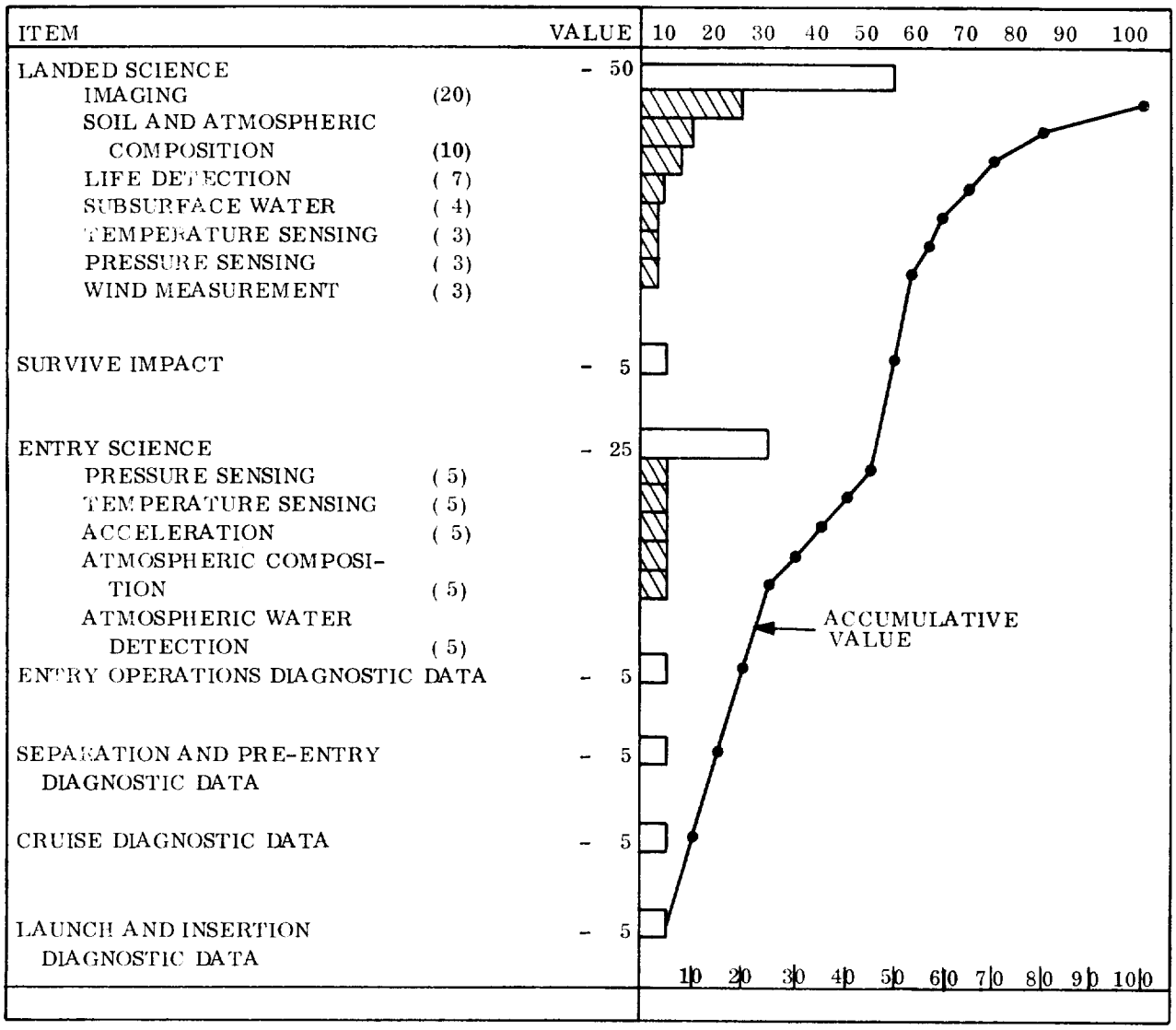

Figure 7.1-1. Mission Value Profile 1400 lb Capsule Mission

Utilizing the mission sequence of events and Mission Value Profile (MVP) a Mission Function Flow Diagram (MFFD) was constructed. See fig. 7.1-2. This diagram depicts the sequence of functions that must be accomplished to attain the mission value specified in the MVP. Each succeeding level of the flow diagram provides a more detailed breakout of each function of the preceding level. The number within the diamond shaped symbols indicates the mission value attained by successfully reaching that point in the mission.

The criticality of each function shown in the second level of the MFFD was first determined. This function criticality was then assigned to all components required to perform that function. In many cases, the same component will have different criticalities in different phases of the mission. For example, the operational battery has a criticality of 0.85 for the entry phase as opposed to 0.5 for the landed operation phase.

The Criticality Analysis conducted for this study considered only the effects of the failure of a component on mission success. A more detailed Failure Mode, Effects and Criticality Analysis would be performed during detail design stages.

7.2 RISK

On the basis of Criticality Analysis and Reliability Analysis, a Risk Analysis is possible.

The Risk Factor of an element is defined as the probabilistic loss in mission performance associated with the non-performance of the element. Thus, if criticality is the proportional loss of mission value on the hypothesis of the failure of the element, then the product of criticality and the probability of failure is identified as the risk factor. In mathematical form,

$$RF_i = C_i Q_i$$

where:

RF_i = Risk Factor of the ith element

C_i = Criticality of the ith element

Q_i = Failure Probability of the ith element

This is illustrated by the following table:

Element	Criticality	Failure Probability	Risk
A	0.90	0.01	0.0090
B	0.25	0.03	0.0075

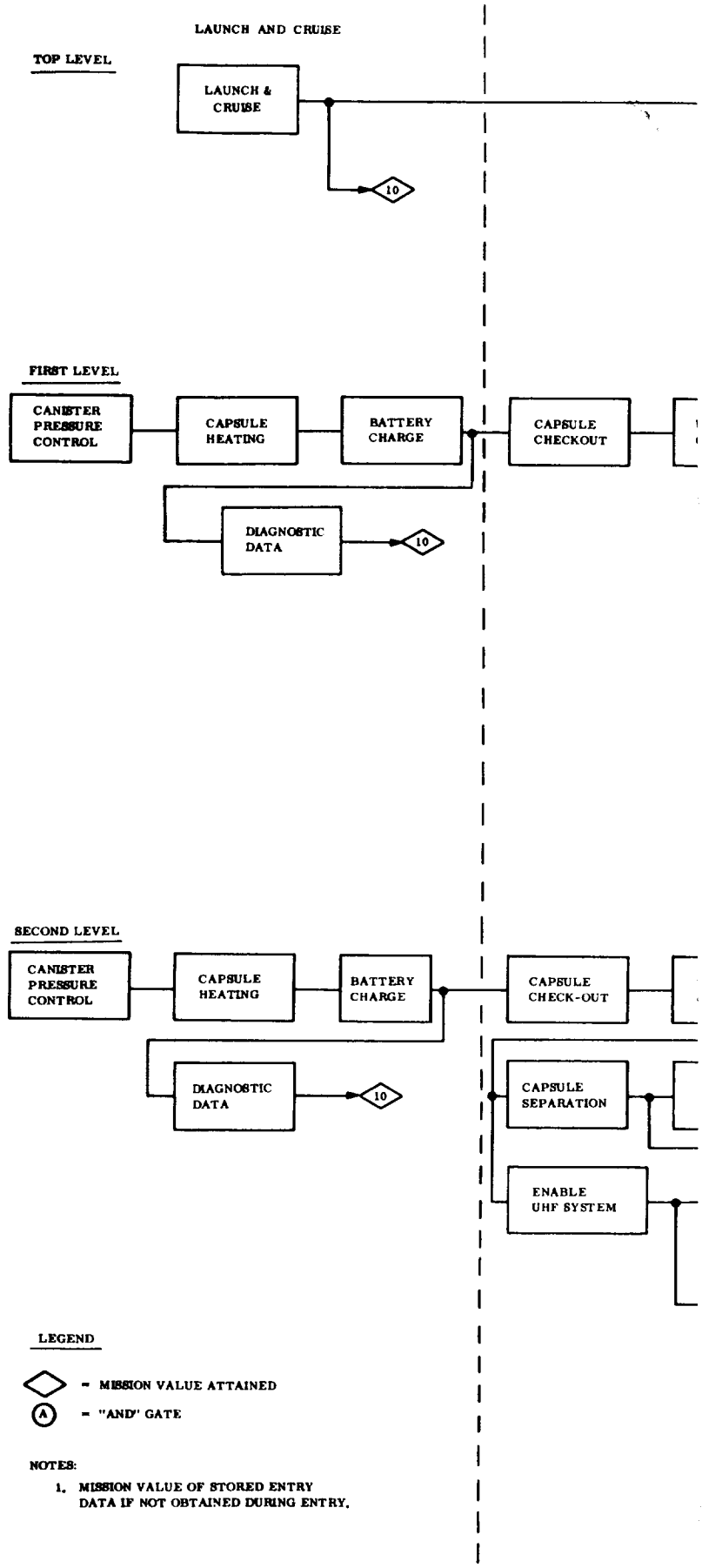

LEGEND

◇ = MISSION VALUE ATTAINED

Ⓐ = "AND" GATE

NOTES:

1. MISSION VALUE OF STORED ENTRY DATA IF NOT OBTAINED DURING ENTRY.

FOLDOUT FRAME 1

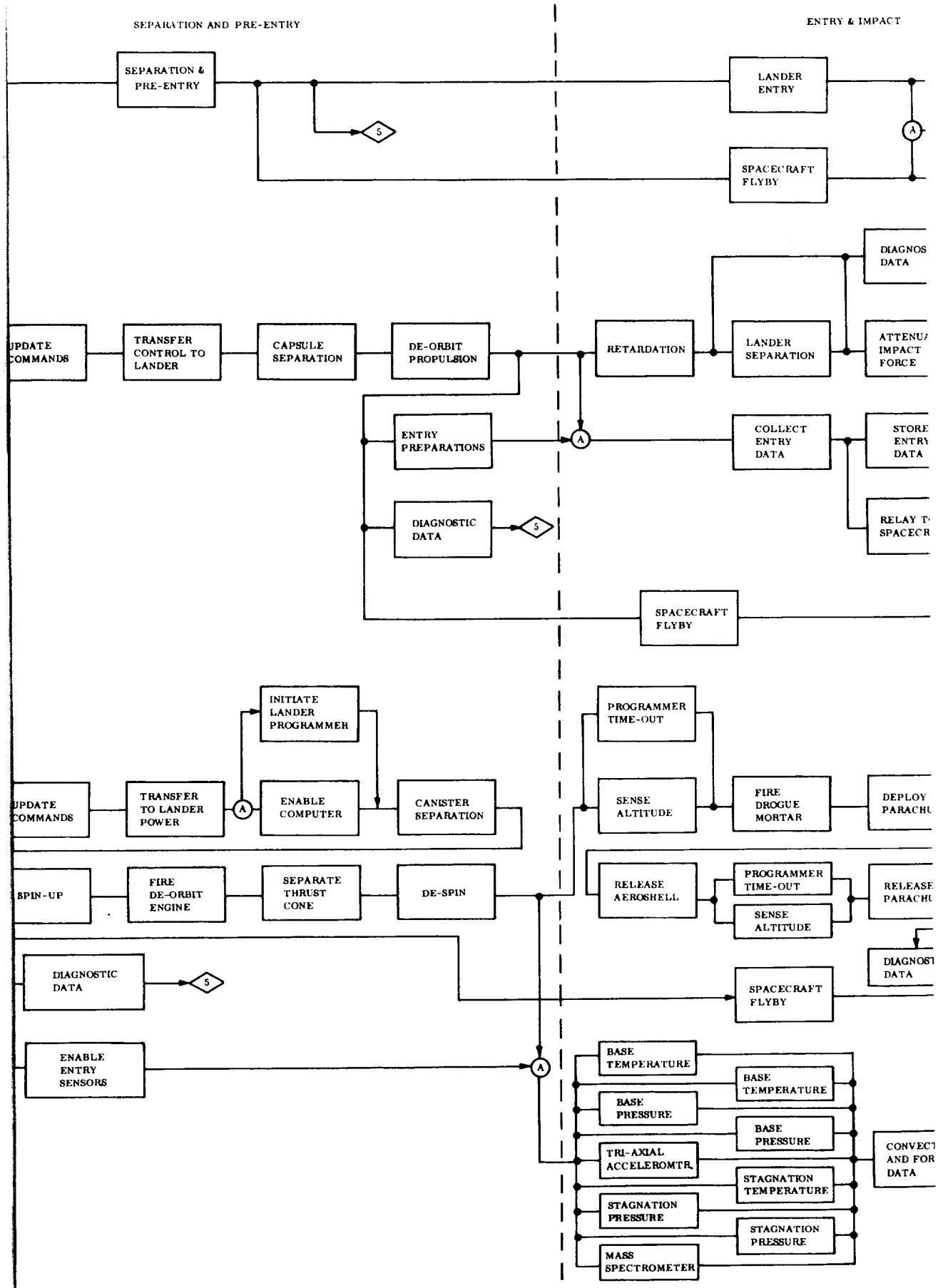

FOLDOUT FRAME 2

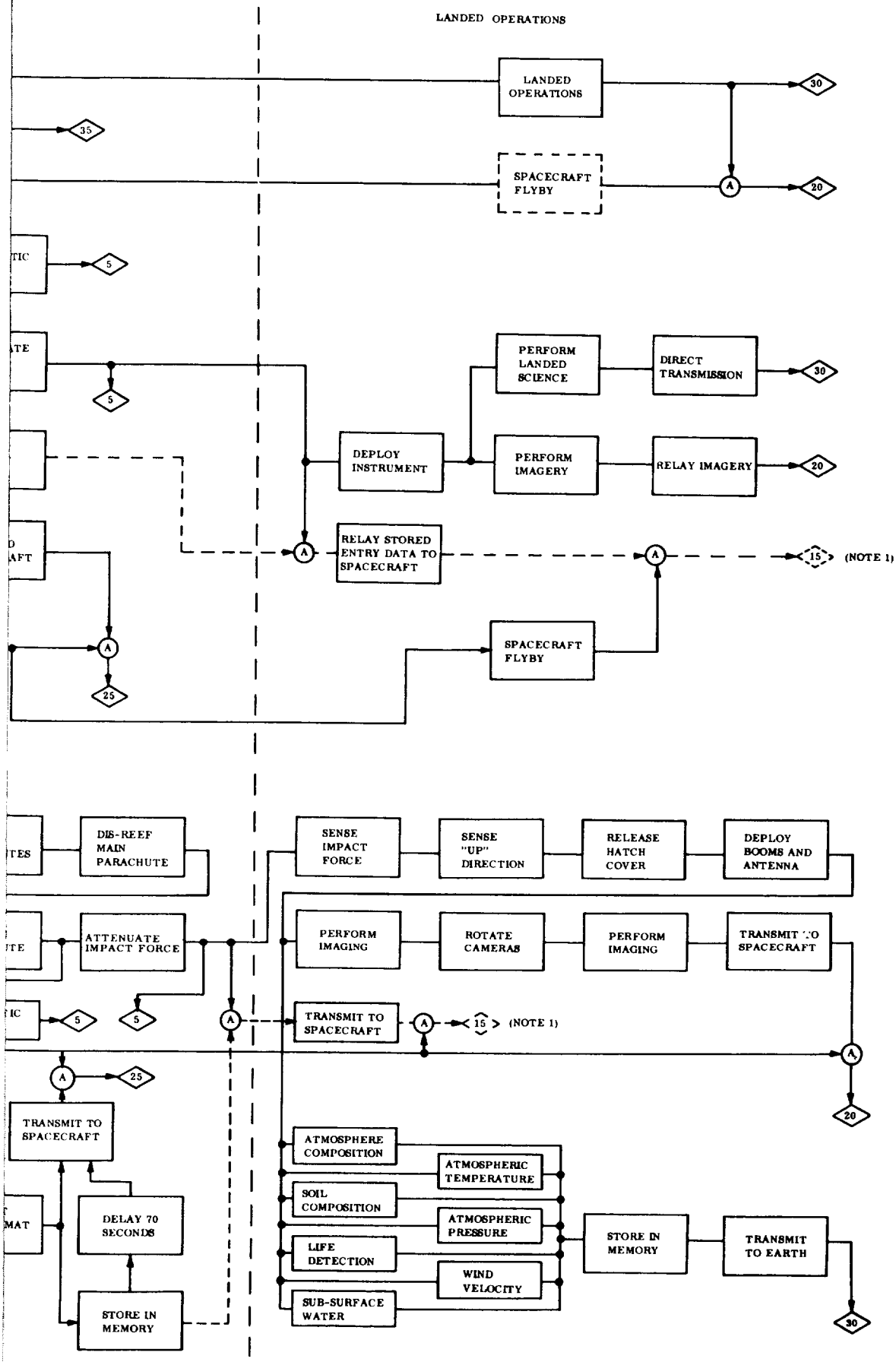

Figure 7.1-2. Mission Functional Flow Diagram

FOLDOUT FRAME 3

The probability of element B failing is three times as great as element A. However, element A has a greater risk to mission success since its failure would result in a greater loss of the mission's value.

Risk factors were computed for each component of the Mars Hard Lander System using the above equation. The highest criticality and total reliability were substituted into the equation of the overall risk factor.

The ten items which were determined as having the greatest risk factor values are listed in table 7.2-1. The highest single item is the Lander Power Controller. This is a single unit which handles the transfer of all power and signals in the Capsule after separation from the Support Module. It consists of numerous switching relays as well as diode and thermal relay blocking modules and a line contactor. Failure of this unit could result in the loss of all mission functions thereafter.

Table 7.2-2 lists the ten items with the highest probability of failure values. The difference between this index of potential problem items and the risk method is shown by the last column. The Lander Computer has the greatest probability of failure but is ranked third by risk due to the fact that many of the mission functions can be accomplished even if this unit fails. The same is true of the gas chromatograph/mass spectrometer which ranks fourth in probability of failure but only ninth by risk.

These tables illustrate how this procedure provides design engineers and program management with a means to objectively assess potential problem areas at any stage of a design so that corrective actions may be taken to reduce the risk and improve the mission probability of success.

Since the overall reliability requirement has not been specified for the Capsule System, no specific recommendations for reducing component risk have been made at this time. In the actual design phase, however, the Risk Analysis would be extended to include balancing the component risk factors to the overall system reliability requirement. The purpose of balancing (equating) risk factors is twofold; it results in each component contributing the same degree of risk to mission success, while providing realistic reliability requirements for the components. Risk factor balancing may involve increasing (or decreasing) component reliability requirements, alterations of the system topology or the inclusion of redundancies, stand-by provisions and/or alternate mode operations.

7.3 RELIABILITY ESTIMATE ANALYSES (REA)

A REA is an analytical procedure for predicting the reliability of a system through synthesis from elements, parts, components, and/or subsystems and for prescribing reliability improvement methods which will assist in evolving a design to meet the reliability requirements.

A tentative reliability estimate analysis was performed on the conceptual design of the Mars Hard Lander Capsule System using standard techniques and as described in previous Capsule Study Reports. A summary of the mission success probabilities by mission phase is shown in table 7.3-1. These reliability estimates represent the probability of success with zero

TABLE 7.2-1. HIGH RISK COMPONENTS

Component	Criticality (percent)	Failure Probability	Risk Factor (percent)
Power Controller (Lander)	90	0.0071	0.6390
Lander Programmer	55	0.0049	0.2695
Computer	35	0.0076	0.2660
Power Controller (Canister)	90	0.0029	0.2610
Transponder/Exciter	30	0.0060	0.1800
Voltage Regulator	90	0.0013	0.1170
Memory Unit	70	0.0015	0.1050
Data Handling Unit	75	0.0013	0.0975
Gas Chromatograph	16	0.0052	0.0832
Vent Valve	95	0.0008	0.0760

TABLE 7.2-2. COMPONENT PROBABILITY OF FAILURE

Component	Probability of Failure	Rank by Risk
1. Computer	0.0076	3
2. Power Controller (Lander)	0.0071	1
3. Transponder/Exciter	0.0060	5
4. Gas Chromatograph/Mass Spectrometer	0.0052	9
5. Lander Programmer	0.0049	2
6. Power Controller (Canister)	0.0029	4
7. Memory Unit	0.0015	6
8. Data Handling Unit	0.0013	8
9. Voltage Regulator	0.0013	7
10. Command Decoder	0.0012	—

TABLE 7.3-1. MISSION SUCCESS PROBABILITY

Subsystem \ Mission Phase	Launch/ Cruise	Separation/ Pre-entry	Entry	Landed Operations	Total
EP&D and I/F	0.991	0.984	0.994	0.981	0.950
Computer and Sequencer	—	0.994	0.997	0.988	0.979
Attitude Control	0.997	0.992	0.996	—	0.985
Propulsion	0.999	0.994	—	—	0.993
Pressure and Venting	0.999	0.999	—	—	0.998
Separation	—	0.991	0.994	0.998	0.983
Telecommunications	0.998	0.995	0.996	0.987	0.976
Thermal Control	0.998	0.999	—	—	0.997
Scientific and Diagnostic Data	0.995	0.998	0.993	0.962	0.948
Retardation	—	—	0.993	—	0.993
Launch Vehicle and Spacecraft	0.822	0.999	0.999	0.999	0.819
Total (Single Mission)	0.803	0.945	0.962	0.917	0.669
Probability of one success out of two missions					0.890

functional failures. In this analysis no attempt has been made at this time to assess the risks due to design errors. GE's experience with L^2S^2* studies has shown that these can be a significant factor. Efforts to isolate and eliminate this type of failure effect will be made at later design stages.

Failure rate data for the various components were obtained from the sources listed in table 7.3-2. Standard reliability growth modifiers have been incorporated as applicable. Since there is no defensible standard modifier established for dormant conditions in space, the non-operating faulure rate for the components was assumed to be negligible.

7.4 SUMMARY

Mission assurance study efforts to date have determined technical feasibility of a 1400 lb Hard Lander Capsule. Furthermore, they have identified areas of highest criticality and risk so that further efforts can be exerted in the most effective manner to reduce the risks and improve the probabilities of mission success.

*GE Missile and Space Division Study Effort - "Long Life System Study".

TABLE 7.3-2. FAILURE RATE DATA SOURCES

1.	MIL-HDBK-217A
2.	FARADA
3.	Voyager Study
4.	Equipment Reliability Status Report — Mark 12 Program
5.	Equipment Reliability Status Report — TT Program
6.	MBRV Reliability Analysis

The design as described in this report is basically a Single String System. Further analysis will be conducted to determine where redundancies can most effectively be applied on reduction of risk per pound or per cost bases.